NBSIR 83-2742 (R)

Photonuclear Data - Abstract Sheets 1955 - 1982 Volume XIV (Lead - Actinium)

E. G. Fuller, Henry Gerstenberg

U.S. DEPARTMENT OF COMMERCE
National Bureau of Standards
National Measurement Laboratory
Center for Radiation Research
Gaithersburg, MD 20899

January 1986

U.S. DEPARTMENT OF COMMERCE

NATIONAL BUREAU OF STANDARDS

NBSIR 83-2742

PHOTONUCLEAR DATA - ABSTRACT SHEETS 1955 - 1982 VOLUME XIV (LEAD - ACTINIUM)

E. G. Fuller, Henry Gerstenberg

U.S. DEPARTMENT OF COMMERCE
National Bureau of Standards
National Measurement Laboratory
Center for Radiation Research
Gaithersburg, MD 20899

January 1986

U.S. DEPARTMENT OF COMMERCE, Malcolm Baldrige, *Secretary*
NATIONAL BUREAU OF STANDARDS, Ernest Ambler, *Director*

TABLE OF CONTENTS

Photonuclear Data-Abstract Sheets
1955-1982

I. Introduction

As used in connection with this collection of data-abstract sheets, the term photonuclear data is taken to mean any data leading to information on the electromagnetic matrix element between the ground state and excited states of a given nuclide. The most common types of reactions included in this compilation are: (e,e'), (γ,γ), (γ,γ'), (γ,n), (γ,p), etc. as well as ground-state particle capture reactions, e.g. (α,γ_0). Two reactions which fit the matrix element criterion are not included in the compilation because of their rather special nature. These are heavy particle Coulomb excitation and the thermal neutron capture reaction (n,γ_0). While the energy region of particular interest extends from 0 to 150 MeV, papers are indexed which report measurements in the region from 150 MeV to 4 GeV. Most of the experiments listed are concerned with the excitation energy range from 8 to 30 MeV, the region of the photonuclear giant resonance.

The hierarchical grouping of the photonuclear data-abstract sheets within the file is by: 1. Target Element, 2. Target Isotope, and 3. by the Bibliographic Reference Code assigned to the paper from which the data on the sheet were abstracted. In this file, colored pages are used to mark the beginning and end of the sheets for each chemical element. A brief historical sketch of the element is given on the divider sheet marking the start of each section; the information for this sketch was derived from references such as the Encyclopaedia Britannica. In those cases where the sheets for a given element make up a major part of a volume, colored pages are also used to delineate sections pertaining to the individual isotopes of the element. Each of the sections of the file, as delineated by two colored divider sheets, represents a 27 year history of the study of electromagnetic interactions in either a specific nuclide or a specifc element.

The data-abstract sheets are filed under the element and/or isotope in which the ground-state electromagnetic transition takes place. For example, the abstract sheet for a total neutron yield measurement for a naturally occurring copper sample would appear in the elemental section of the copper file. On the other hand, a measurement of the ^{62}Cu 9.73 minute positron activity produced in the same sample by photons with energies below the three-neutron separation energy for ^{65}Cu (28.68 MeV) would be filed with the sheets for ^{63}Cu. Similarly a measurement of the ground-state neutron capture cross section in ^{12}C would be filed under ^{13}C while the corresponding ground-state alpha-particle capture cross section would be filed under ^{16}O.

At the end of this volume there is a master list of the abbreviations that have been used in the index section of the abstract sheets. The listings are those used in the final published index, Photonuclear Data Index, 1973-1981, NBSIR 82-2543, issued in August 1982 by the U. S. Department of Commerce, National Bureau of Standards, Washington, DC 20234. In some cases two notations are entered for the same quantity. The second entry is the abbreviation that was used in one or more of the earlier published editions of the index.

PB

LEAD
Z=82

Knowledge of the metallic element, lead antedates recorded history. Egyptian ruins contained coins or medallions of lead. It seems probable that the extraction of lead from its ores by smelting was the first such practice recognized by man. The lead ores are widely distributed in nature and are easily smelted. Babylonian inscriptions were found engraved on thin plates of metallic lead. The Romans used it for water pipes, writing tablets, and coins. They also used it for cooking utensils with lead poisoning as a frequent result. Marcus Vitruvius, an architect and engineer under the Emperor Augustus, was familiar with the toxicity of lead and observed that the laborers in the smelter have pale complexions because of their prolonged exposure to lead dust and vapor.[1]

PB

[1]Darmstaedter, Ludwig, "Handbuck zur Geschichte der Naturwissenschaften und der Technik," J. Springer, Berlin, 1908, 2nd ed., p30.

PB

P. S. Baranov, V. I. Gol'danskii
Zhur. Eksp. i Teoret. Fiz. 28, 746 (1955)
Soviet Phys. JETP. 1, 613 (1955)

ELEM. SYM. A

Pb 82

METHOD

Synchrotron; ion chamber monitor; ^{12}(n,2n) threshold detector

REF. NO.

55 Ba 5 EGF

REACTION	RESULT	EXCITATION ENERGY	SOURCE		DETECTOR		ANGLE
			TYPE	RANGE	TYPE	RANGE	
G,XN	ABY	30 - 200	C	150-250	THR	30-	DST

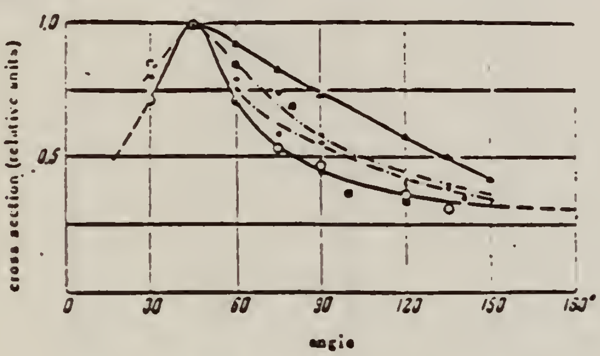

FIG. 2. Angular distribution of photoneutrons with energies higher than 30 mev. o – C_{250}, + – C_{200}; ▲ – Be_{250}; O – Al_{250}; • – Pb_{250}; ■ – data of work[5].

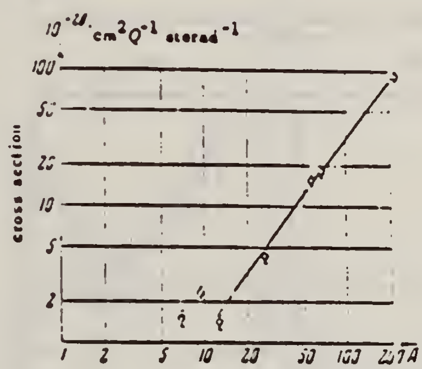

FIG. 4. The dependence of the yield of photoneutrons with energies higher than 30 mev at an angle of 90° (in units 10^{-28}cm^2 per eff. quant steradian on the mass number A).

REF.	ELEM. SYM.	A	Z
J. L. Burkhardt Phys. Rev. <u>100</u>, 192 (1955)	Pb		82

METHOD	REF. NO.	
	55 Bu 1	JOC

REACTION	RESULT	EXCITATION ENERGY	SOURCE TYPE	SOURCE RANGE	DETECTOR TYPE	DETECTOR RANGE	ANGLE
G,G	RLX	0 - 3	C	3	NAI-D		90

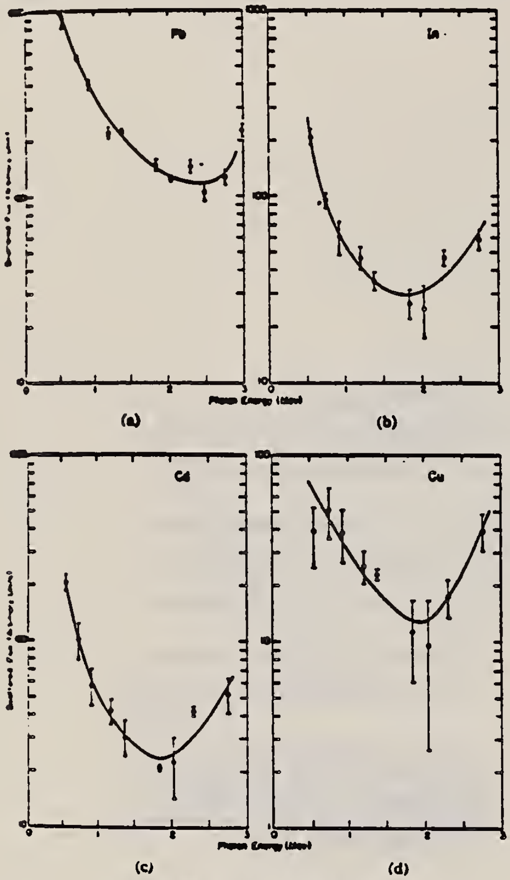

FIG. 3. Scattered photon flux.

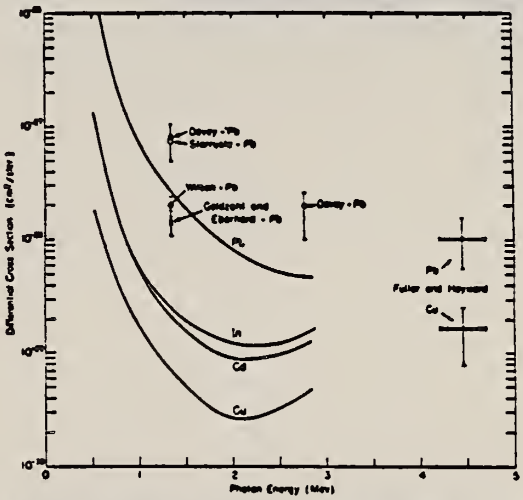

FIG. 4. Differential photon scattering cross sections at 90°. The points shown on the graph are taken from references 3, 5, 7, 8, and 22.

Ref.		Elem. Sym.	A	Z
W.R. Dixon Can. J. Phys. 33, 785 (1955)		Pb		82

Method	Ref. No.	
Synchrotron; neutron spectrum, angular distribution; nuclear emulsion; scintillator; ion chamber	55 Di 1	NVB

Reaction	E or ΔE	E_o	Γ	$\int \sigma dE$	Jπ	Notes
Pb(γ,xn)	70					Used scintillator for angular distributions; curves fitted to $a + b \sin^2\theta$.
Pb(γ,xn)		E_n = 0.5-8				Used emulsion for spectra.

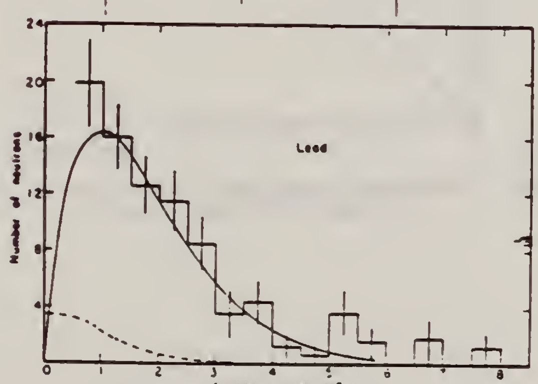

FIG. 3. The energy distribution of photoneutrons from lead. The solid and dashed curves are calculated for the evaporation of first and second neutrons, respectively.

TABLE II

EXPERIMENTAL VALUES FOR b/a

Target	Correction factor for self-scattering	Corrected b/a
Lead	1.10	−0.08±0.08
Tin	1.08	0.12±0.17
Copper	1.48	0.23±0.15
Iron	1.35	0.09±0.25
Aluminum	1.17	0.36±0.29
Carbon	1.8	1.6 ±0.8
Beryllium (1)	2.6	1.2 ±0.4
Beryllium (2)	1.35	

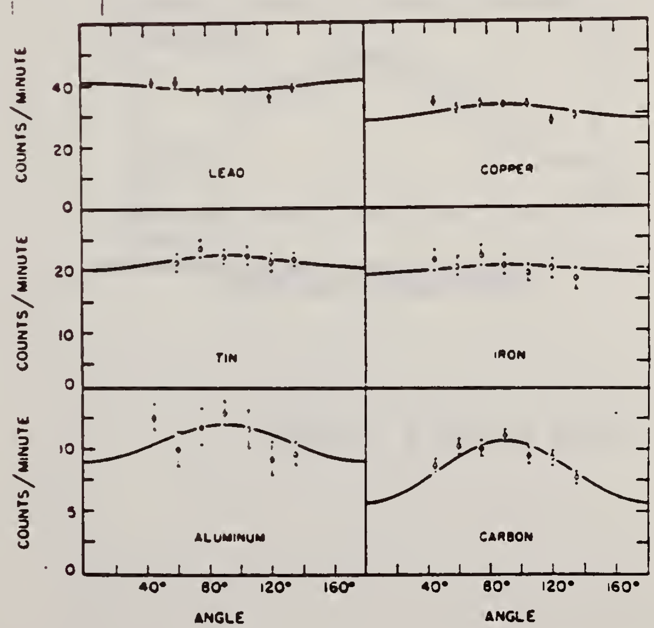

FIG. 2. The angular distributions of photoneutrons as measured with the zinc sulphide [illegible]

REF.	ELEM. SYM.	A	Z
Sven A. E. Johansson Phys. Rev. 97, 434-43 (1955)	Pb		82
METHOD	REF. NO.		
Synchrotron; ZnS counter; ion chamber	55 Jo 1		NVB

REACTION	RESULT	EXCITATION ENERGY	SOURCE TYPE	SOURCE RANGE	DETECTOR TYPE	DETECTOR RANGE	ANGLE
G,N	RLY	THR - 65	C 65		SCI-D	5 - +	DST
G,N	RLY	THR - 65	C 65		SCI-D	10 - +	DST

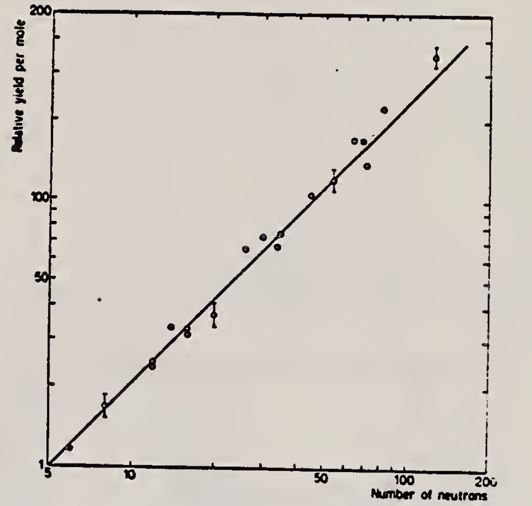

FIG. 11. The relative yield per mole for neutrons above 7 5 Mev as a function of the neutron number.

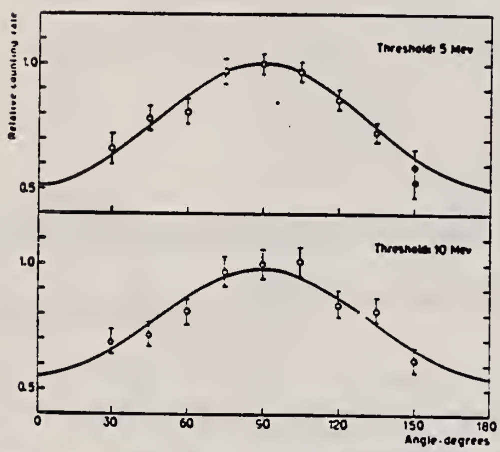

FIG. 9. The angular distributions of the neutrons from lead. Counter thresholds at 5 and 10 Mev.

Curves of form $a + b \sin^2\theta$

REF.	ELEM. SYM.	A	Z
K. G. McNeill Phil. Mag. 46, 321 (1955)	Pb		82
METHOD	REF. NO. 55 Mc 1		EGF

REACTION	RESULT	EXCITATION ENERGY	SOURCE TYPE	SOURCE RANGE	DETECTOR TYPE	DETECTOR RANGE	ANGLE
G,XN	RLY	THR - 22	C	22	NAI-I		90

Target element	Counts in 30 minutes per 1000 monitor counts	22 Mev yield/mol/r relative to copper	Yield/mol/r $\times 10^{-4}$
Cu	288 ± 15	1·0	3·2
Cd	647 ± 28	$4·1 \pm 0·3$	13
Hg	661 ± 26	$9·5 \pm 0·9$	30
Pb	470 ± 17	$8·4 \pm 0·5$	27

Ref. E.G. Fuller, E. Hayward Phys. Rev. 101, 692 (1956)	Elem. Sym. Pb	A	Z 82
Method: Betatron; photon scattering; NaI spectrometer	Ref. No. 56 Fu 1		NVB

Reaction	E or ΔE	E_o	Γ	$\int \sigma dE$	Jπ	Notes
Pb(γ,γ)	Bremss. 4-40					Detector at 120°. Cross sections given here are 13% too high due to erroneous cos θ factor in denominator of Eq. 5. [See footnote 8 in Phys. Rev. 106, 993 (1957)].

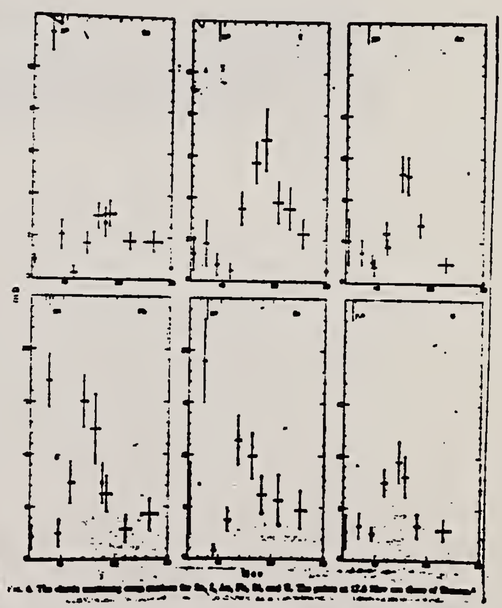

[4] E. R. Gaerttner and G. L. Yeater, Phys. Rev. 76, 363 (1949).
[5] Dressel, Goldhaber, and Hanson, Phys. Rev. 77, 754 (1950).
[6] M. B. Stearns, Phys. Rev. 87, 706 (1952).

Ref. W.H. Hartley, W.E. Stephens, E.J. Winhold Phys. Rev. 104, 178 (1956)	Elem. Sym. Pb	A	Z 82
Method Li (p,γ) source, 480 kev protons.	Ref. No. 56 Ha 1		EGF

Reaction	E or ΔE	E_o	Γ	$\int \sigma dE$	$J\pi$	Notes
(γ,xn)						Average Li cross section is 310 mb; cross section with detector response weighted for low energy neutrons, 295 mb. Assumed ratio 17.6/14.8 = 1.7. Calculated cross section at 14.8 and 17.6 MeV assuming cross section curves measured at Pennsylvania and Saskatchewan (refer Table I).
		13.75	4.5			$\sigma^o = \frac{310}{.42} = 735$ mb.

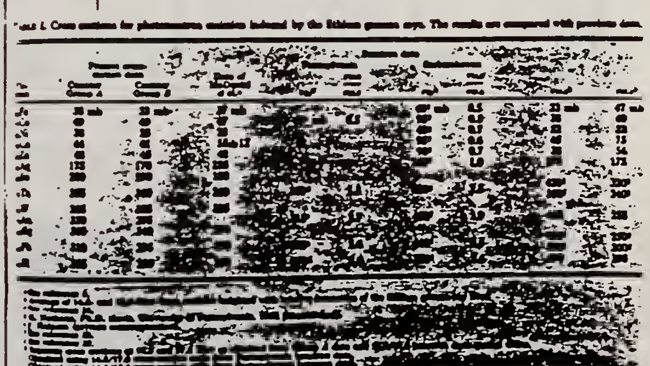

Ref. M.E. Toms, W.E. Stephens Phys. Rev. 108, 77 (1957)	Elem. Sym. Pb	A	Z 82
Method Plates; 23MeV Bremss.; BF_3 neutron counters.	Ref. No. 57 To 1		EGF

Reaction	E or ΔE	E_0	Γ	$\int \sigma dE$	Jπ	Notes
(γ,xn)	~ 8-22	13.8	2.4			σ_{max} = 55 barns. Proton yield of 1.42×10^7 n's/mole r is low compared to Price and Kerst [Phys. Rev. 77, 806 (1950)] value of 2.3×10^7 n/mole r and Montalbetti, Katz and Goldemberg [Pnys. Rev. 91, 659 (1953)] value of 2.7×10^7 n/mole r. Neutron spectron measured for 23 MeV Bremsstrahlung.

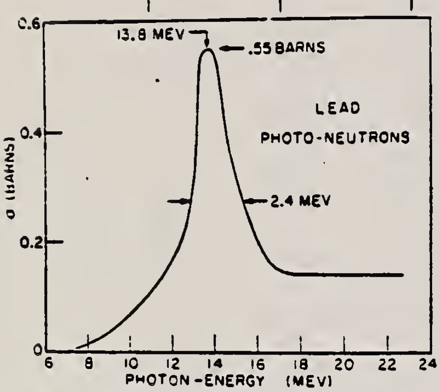

FIG. 3. Photoneutron cross section of lead as a function of photon energy.

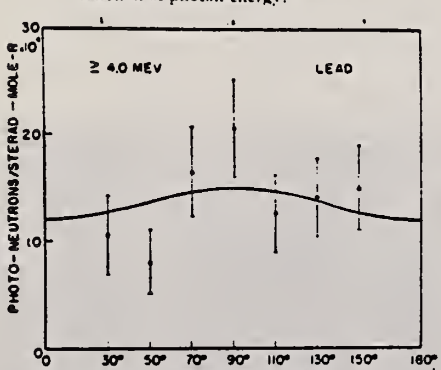

FIG. 4. Angular distribution of photoneutrons from lead having energies ≥4.0 Mev. The curve is of the form $a-b \sin^2\theta$, with a b/a ratio of 0.23.

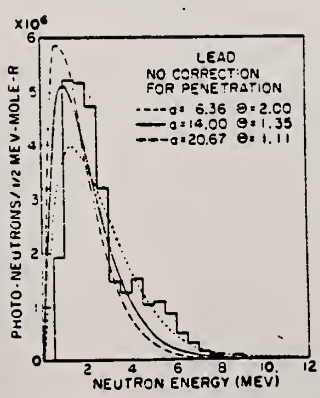

FIG. 5. Energy distribution of photoneutrons from lead with curves calculated for "evaporation" with residual nuclear temperatures, Θ=1.11 Mev (dashed), 1.35 Mev (solid), and 2.00 Mev (dotted), and no correction for neutron transmission through the centrifugal barrier.*

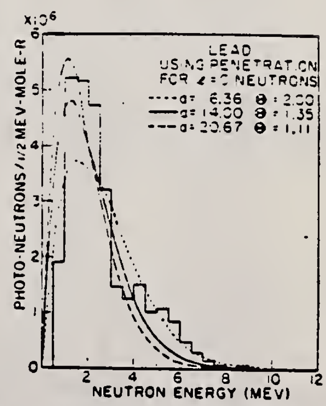

FIG. 6. Energy distribution of photoneutrons from lead with curves calculated for "evaporation" with residual-nuclear temperatures, Θ=1.11 Mev (dashed), 1.35 Mev (solid), and 2.0 Mev (dotted), and with the correction for $l=0$ neutron transmission through the centrifugal barrier.*

Ref.		Elem. Sym.	A	Z
T. Asada, M. Masuda, M. Okumura, J. Okuma J. Phys. Soc. Japan 13, 1 (1958)		Pb		82
Method	Betatron; angular distribution; scintillator; ionization chamber	Ref. No. 58 As 1		EH

Reaction	E or ΔE	E_0	Γ	$\int \sigma dE$	$J\pi$	Notes
Pb (γ,n)	Bremss. 17					Angular distribution is of the form, $a + b \sin^2\theta$ where $b/a = 0.30\pm0.11$

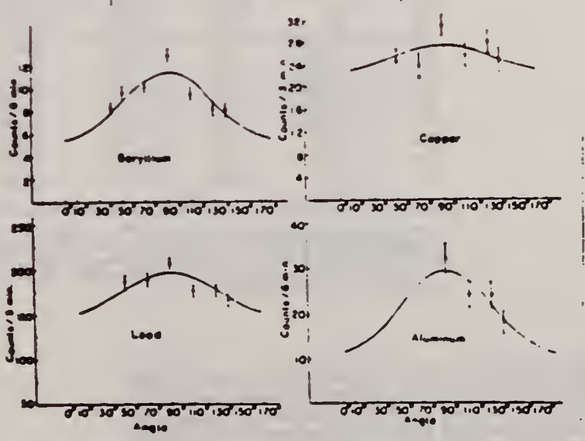

Fig. 6. The angular distributions of photo-neutrons as measured with Emmerich button type scintillation detector.

Table I. The values of b a.

Energy		Target Al	nucleus Cu	Pb	Be	Detector
Present	(17 Mev)	1.6 ± 0.8	0 17 ± 0.06	0.30 ± 0.11	1.29 ± 0.53	Emmerich[a]
Dixon	(70 Mev)	0.36 ± 0.29	0 23 ± 0.15	uniform	1 2 ± 0.4	Hornyak[b]
Halpern	(70 Mev)				1.26 ± 0.11	Emmerich[a]
Price	(22 Mev)		0.33	0.84	uniform	Al (n, p)[c]
Johansson	(65 Mev)	1		0.8	1 5	Hornyak[b]

a) A scintillation detector with a ZnS paraffin-Lucite light guide

b) A scintillation detector with a ZnS-Lucite.

c) A fast neutron detector by measuring the beta activity of Al^{27} (n, p) Mg^{27} reaction

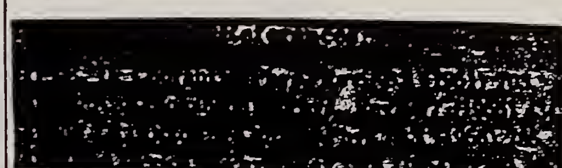

:.G. Fuller, B. Petree, M.S. Weiss
'hys. Rev. 112, 554 (1958)

ELEM. SYM.	A	Z
Pb		82

Betatron; ion chamber

REF. NO.	
58 Fu 1	NVB

REACTION	RESULT	EXCITATION ENERGY	SOURCE TYPE	SOURCE RANGE	DETECTOR TYPE	DETECTOR RANGE	ANGLE
G,XN	RLX	7-40	C	7-40	BF3-I		4PI

CF DANØS THEØRY

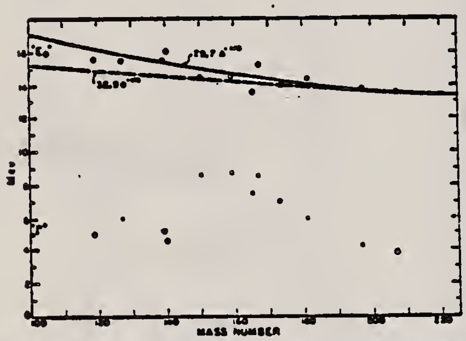

FIG. 6. Mean energy and width of giant resonances. "E_0" and "Γ" are the mean energy for photon absorption and the full width at half maximum of the giant resonance obtained from dashed histograms as in Fig. 5. No attempt was made to fit data with resonance curves to obtain these parameters.

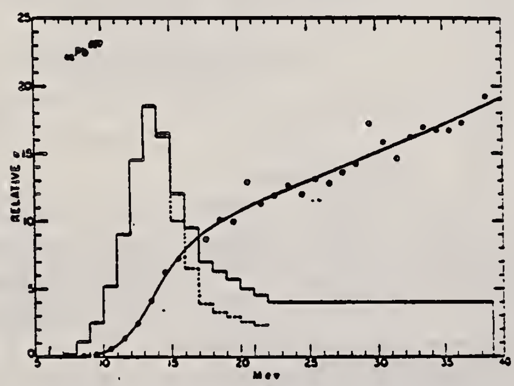

(b)

TABLE I. Target properties and results.

Element	Form used	Weight grams	$\sigma^0(\gamma,n)$[a] barns	$\frac{S\sigma dE}{NZ/A}$[b] Mev-b	"Γ"[a] Mev
Sn	Sn	4.81	0.30	0.064	5.0
I	I	8.55	0.36	0.085	6.0
La	La	10.43	0.34	0.063	5.2
Ce	Ce	4.99	0.45	0.080	4.5
Sm	Sm_2O_3	2.90	0.26	0.073	8.6
Tb	Tb_4O_7	3.04	0.39	0.087	8.7
Ho	Ho_2O_3	1.87	0.41	0.079	7.5
Er	Er_2O_3	5.41	0.50	0.100	8.5
Yb	Yb_2O_3	5.57	0.50	0.090	7.0
Ta	Ta	8.41	0.49	0.077	6.0
Au	Au	3.16	0.68	0.085	4.2
Pb	Pb	8.05	0.75	0.081	3.8

[a] $\sigma^0(\gamma,n)$ is the maximum value and "Γ" the full width at $\sigma^0(\gamma,n)/2$ of the neutron production cross section corrected for multiple neutron emission. Data were not fitted with resonance lines to determine these values.
[b] Integrated neutron production cross sections corrected for multiple neutrons above $(\gamma,2n)$ threshold.

FIG. 5. Relative photoneutron production cross sections for tin, iodine, samarium, holmium, erbium, and lead. The points and smooth curves represent the integral neutron-production cross section defined by $\int_0^E \sigma_{Tn}(E)dE$, where $\sigma_{Tn}(E)=\sigma(\gamma,n)+2\sigma(\gamma,2n)+\sigma(\gamma,pn)+3\sigma(\gamma,3n)+\ldots$. The scales are normalized to give approximately the same total neutron yield at 40 Mev. The errors indicated were obtained by propagating the statistical uncertainties, $(\sqrt{n})$, in the original activation curve data through the integral cross section matrix. Solid histograms represent first differences of integral cross section curves. Dashed histograms show result of correcting for neutron multiplicity above the $(\gamma,2n)$ threshold.

REF.	ELEM. SYM.	A	Z
W. C. Barber and W. D. George Phys. Rev. 116, 1551 (1959)	Pb		82

METHOD	REF. NO.	
	59 Ba 3	EGF

REACTION	RESULT	EXCITATION ENERGY	SOURCE TYPE	SOURCE RANGE	DETECTOR TYPE	DETECTOR RANGE	ANGLE
E,N	ABY	THR - 36	D	10 - 36	BF3-I		4PI

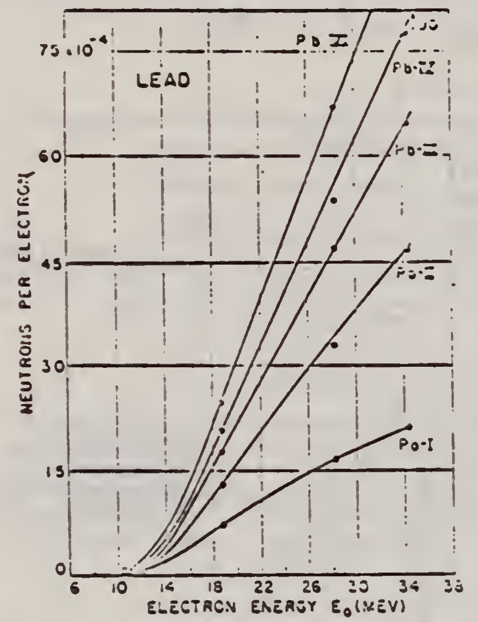

Fig. 8. Yield of neutrons per incident electron as a function of initial electron energy for the natural lead targets of various thicknesses. The number 90 refers to the value of the VI curve at the indicated energy.

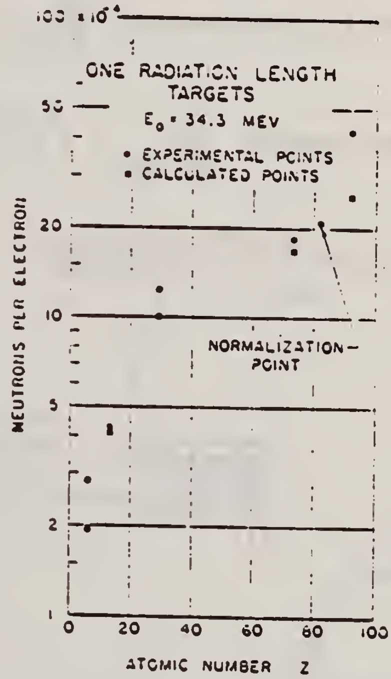

Fig. 14. Experimental and expected yields of neutrons per incident electron for 1-radiation-length targets at 34.3 Mev, as a function of atomic number Z. The experimental yields were obtained by dividing the measured yields from the targets listed in Table I by the actual target thicknesses listed in Table I. The expected yields were calculated from expression (8).

Table I. Thicknesses of the targets used in the experiment. With the exception of heavy water, all targets contained isotopes in their naturally-occurring proportions.

Target	Thickness (g/cm²)	Thickness (radiation lengths)
Heavy water	0.698	"thin"
Be	0.559	0.00567
C-I	38.91	0.88
Al-I	24.19	1.00
Cu-A	1.372	0.108
Cu-I	13.26	1.04
Cu-II	26.50	2.08
Cu-III	39.86	3.13
Cu-IV	53.13	4.17
Ta-I	6.21	0.98
Pb-I	5.88	[illegible]
Pb-II	11.42	1.97
Pb-III	17.30	2.95
Pb-IV	22.89	3.94
Pb-VI	34.42	5.93
U-I	6.17	1.14
U-II	12.42	2.30
U-III	18.61	3.46
Concrete	28.5	1.19

REF.

S. G. Cohen
Nuovo Cimento, 14, 931-37 (1959)

ELEM. SYM.	A	Z
Pb		82

METHOD

$^{19}F(p,\alpha)^{16}O$ reaction

REF. NO.	
59 Co 6	NVB

REACTION	RESULT	EXCITATION ENERGY	SOURCE TYPE	SOURCE RANGE	DETECTOR TYPE	DETECTOR RANGE	ANGLE
G,G	ABX	6,7	D	6,7	NAI-D		30
		(6.14, 6.91,		(6.14, 6.91			
		and 7.12)		and 7.12)			

Average elastic cross section $\left.\frac{d\sigma}{d\Omega}\right|_{30^\circ} = 5 \times 10^{-28}$ $\frac{cm^2}{steradian}$, at $E_\gamma = 7$ MeV.

Elastic cross section $\left.\frac{d\sigma}{d\Omega}\right|_{30^\circ} > 3 \times 10^{-29}$ $\frac{cm^2}{steradian}$, at $E_\gamma = 6.14$ MeV.

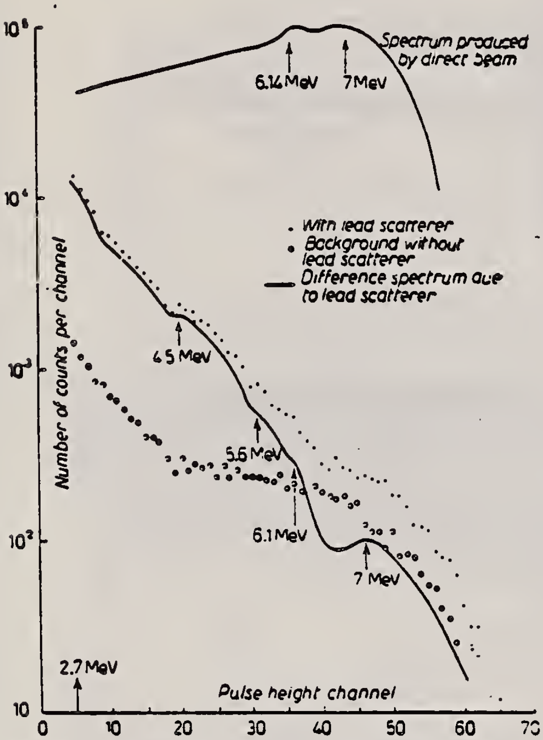

Fig. 2. – Spectrum of γ-rays scattered from lead. Primary γ-rays mostly around 7.0 MeV. Proton energy 2.9 MeV. Mean angle of scattering 30°.

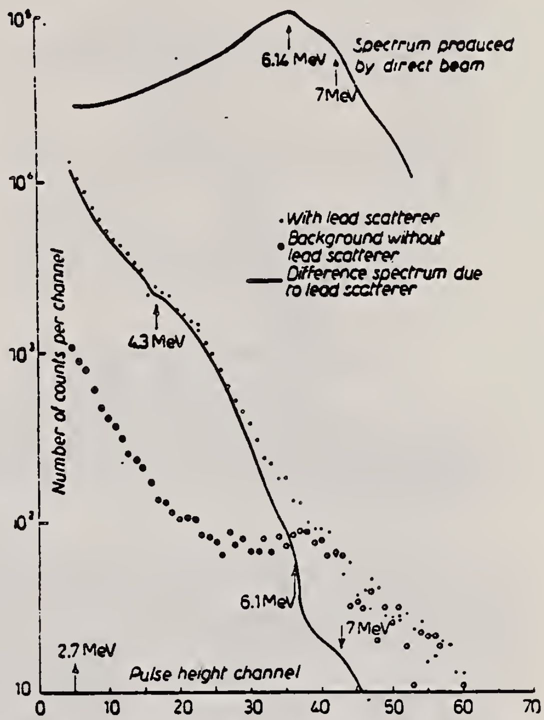

Fig. 3. – Spectrum of γ-rays scattered from lead. Primary γ-rays mostly 6.14 MeV. Proton energy 1.5 MeV. Mean angle of scattering 30°.

Energy of primary γ-rays (MeV)	Energy of scattered γ-rays (MeV)	Approximate energy of excited levels of Pb nuclei produced after inelastic scattering (MeV)
7.0 (average)	7.0	
	6.1	0.9
	5.6 ?	1.4 ?
	4.5	2.5

REF.

P. Paul and U. Stierlin
Nucl. Physics 13, 576 (1959)

ELEM. SYM.	A	Z
Pb		82

METHOD

REF. NO.	
59 Pa 3	EGF

REACTION	RESULT	EXCITATION ENERGY	SOURCE		DETECTOR		ANGLE
			TYPE	RANGE	TYPE	RANGE	
G, G	ABX	17	D	15,18	NAI-D	17	90

Source Li(p,γ) with E_p = 500 keV.

TABELLE 1

Die gemessenen totalen Streuquerschnitte in cm^2 unter Annahme von E1- und E2-Streuung

Element	eigene Werte	Fuller und Hayward [13])	Stearns [6])
Pb	$(5.6 \pm 1) \times 10^{-27}$	$(4-8) \times 10^{-27}$	$(6-9) \times 10^{-27}$
Al	$(2 \pm 1) \times 10^{-29}$	$(2-6) \times 10^{-29}$	
0	$(1 - 5) \times 10^{-30}$		
C	$(5.8 \pm 2) \times 10^{-30}$		

Durch die Wahl der Meßgeometrie ergibt sich für eine E1- wie eine E2-Winkelverteilung innerhalb der Fehlergrenzen der numerischen Rechnung der gleiche Wert für den totalen Streuquerschnitt. Die angegebenen Fehler enthalten nur den Fehler in der Bestimmung des primären γ-Flusses und die statistischen Fehler der Streuraten. Zum Vergleich sind die entsprechenden Ergebnisse von Fuller und Hayward [13]) und Stearns [6]) gegenübergestellt. Die angegebenen Werte gehören jeweils zu den Fehlergrenzen.

Ref.	Elem. Sym.	A	Z
V.M. Grizhko, D.I. Sikora, V.A. Shkoda-Ul'yanov, A.D. Abromenkov, B.I. Shramenko, A.N. Fisun Zhur. Eksp. i Teoret. Fiz. 38, 1370 (1960) Soviet Phys. JETP 11, 987 (1960)	Pb		82

Method	Ref. No.	
Electrons from 30 MeV linac; Pb block serves as electron-to-photon converter, Faraday cup moniter and reaction target	60 Gr 1	JH

Reaction	E or ΔE	E_o	Γ	$\int \sigma dE$	Jπ	Notes
(γ,n)	10.5-20.5			$2.6 \Big\vert_{10.5}^{20.5}$ barns-MeV		Integral cross section estimated assuming a peak-energy at 13.8 MeV. Thick lead target bombarded with electron 10.5-20.5 MeV.

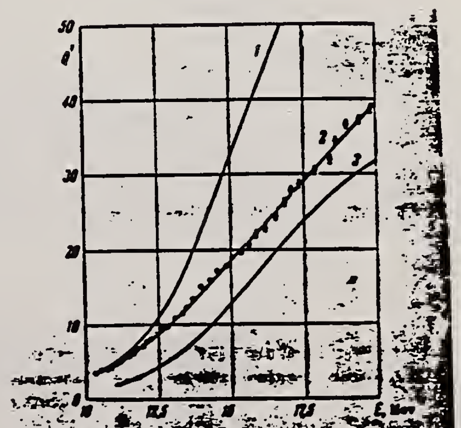

FIG. 2. Photoneutron yield (Q') as a function of the [illegible]tron-beam energy. To determine the absolute value of the [illegible] (per electron), Q' must be multiplied by 10^{-6}.

Ref. K. Reibel, A.K. Mann
Phys. Rev. 118, 701 (1960)

Elem. Sym.	A	Z
Pb		82

Method
γ's from $F^{19}(p,\alpha\gamma)$ reaction; protons from VandeGraaff; NaI

Ref. No.	
60 Re 1	JHH

Reaction	E or ΔE	E_o	Γ	$\int \sigma dE$	Jπ	Notes
(γ,γ)	$E_p = 2.05$					$\langle\bar{\sigma}\rangle = 15 \pm 2.2$ mb
					1	D(average level spacing based on J): 3.4 ± 2.2 kev
						$\bar{\Gamma}_{\gamma o}/\bar{\Gamma}_{\gamma} = 0.6 \pm 0.3$
						$\bar{\Gamma}_{\gamma} = 0.6 \pm 0.3$ eV
						$\bar{\Gamma}_{\gamma o} = 0.36 \pm 0.15$ eV
	$E_p = 2.40$					$\langle\bar{\sigma}\rangle = 7.4 \pm 1.2$ mb
					1	D(average level spacing based on J): 1.3 ± 1.0 kev
						$\bar{\Gamma}_{\gamma o}/\bar{\Gamma}_{\gamma} = 0.2 \pm 0.1$
						$\bar{\Gamma}_{\gamma} = 1.0 \pm 0.5$ eV
						$\bar{\Gamma}_{\gamma o} = 0.2 \pm 0.1$ eV
	$E_\gamma = 6.9$					$\langle\bar{\sigma}\rangle = 4.8 \pm 1.1$ mb
	$E_\gamma = 7.1$					$\langle\bar{\sigma}\rangle = 18 \pm 4$ mb

R.G. Baker, K.G. McNeill
Can. J. Phys. 39, 1158(1961)

ELEM. SYM.	A	Z
Pb		82

METHOD betatron; fast neutron yield; angular distribution; Al and Si threshold detectors; ion chamber

REF. NO.	
61 Ba 2	NVB

REACTION	RESULT	EXCITATION ENERGY	SOURCE TYPE	SOURCE RANGE	DETECTOR TYPE	DETECTOR RANGE *	ANGLE
G,XN	ABY	THR-22	C	22	THR-I	3-+	DST
G,XN	ABY	THR-22	C	22	THR-I	5-+	DST

In Tables 2 and 4:

$\bar{\sigma}$ = average cross section of detector weighted with neutron spectrum

Φ = neutrons/100 roentgen/mole

$$W(\theta) = a_0 \sum_{n=1}^{\infty} [1 + A_n P_n (\cos\theta)]$$

* "3-+" is the detector range of Aluminum and "5-+" of Silicon.

TABLE II

Normalized yields for aluminum detectors

Element	Al(n,γ) reaction 30°	90°	150°	a_0	Al(n,p) reactions 30°	60°	90°	a_0	a_1	a_2	$(\bar{\sigma}\Phi)^* \times 10^6$
Bismuth	399	567±130	620	541±85	3632	5139±290	3168	4306±185	0.06±0.06	−0.35±0.1	17.76
	478	423±130	641	484±85	2562	5353±290	2955	4144±185	−0.05±0.06	−0.53±0.1	16.87
Lead	426	312±120	725	429±77	3123	5754±260	3154	4591±166	−0.004±0.05	−0.51±0.07	18.68
Tantalum	378	367±190	688	441±122	2757	3024±425	2088	2757±275	0.14±0.14	−0.19±0.17	11.22
Lanthanum	208	222±110	330	243±70	2139	3371±250	1891	2768±160	0.05±0.07	−0.43±0.10	11.27
Arsenic	77	100±50	108	97±32	788	937±115	764	865±74	0.02±0.11	−0.16±0.14	3.52
Copper	13	65±30	70	55±20	710	748±70	569	700±45	0.11±0.08	−0.14±0.11	2.85

*$(\bar{\sigma}\Phi) = 4.07\times10^6$ cc millibarn-neutron.

TABLE IV

I Element	II a_0	III a_1	IV a_2	V $(\bar{\sigma}\Phi)\times10^{6*}$	VI Φ_{total} (22 Mev)$\times10^9$	VII Φ_{fast}/Φ_{total}
Vanadium	245 (1±0.06)	0.01±0.08	−0.00±0.10	6.05	0.21	0.12
Chromium	164 (1±0.03)	0.04±0.04	−0.05±0.05	4.05	0.17	0.10
Manganese	308 (1±0.02)	0.07±0.03	−0.09±0.04	7.61	0.25	0.12
Iron	200 (1±0.03)	0.05±0.04	−0.17±0.05	4.94	0.18	0.11
Cobalt	390 (1±0.02)	0.08±0.03	−0.22±0.04	9.63	0.26	0.15
Nickel	145 (1±0.05)	0.07±0.07	−0.23±0.09	3.58	0.12	0.12
Copper	347 (1±0.02)	0.05±0.03	−0.29±0.04	8.57	0.30	0.12
Arsenic	482 (1±0.03)	0.11±0.04	−0.24±0.05	11.91	0.33	0.15
Rubidium	638 (1±0.05)	0.13±0.06	−0.14±0.08	15.76		
Strontium	409 (1±0.05)	0.10±0.06	−0.17±0.08	10.10		
Yttrium	290 (1±0.10)	0.08±0.12	−0.12±0.15	7.16		
Silver	590 (1±0.04)	0:10±0.06	−0.22±0.08	14.57	0.87	0.07
Cadmium	905 (1±0.02)	0.02±0.02	−0.26±0.03	22.35		
Iodine	1133 (1±0.03)	0.04±0.04	−0.20±0.05	27.99	1.42	0.08
Barium	1048 (1±0.04)	0.10±0.06	−0.38±0.08	25.89		
Lanthanum	1595 (1±0.02)	0.02±0.03	−0.42±0.04	39.40	1.04	0.15
Cerium	1316 (1±0.05)	0.05±0.06	−0.39±0.08	32.50		
Dysprosium	1652 (1±0.08)	0.04±0.10	−0.34±0.13	40.80		
Tantalum	1558 (1±0.02)	0.04±0.03	−0.22±0.04	38.48	2.50	0.06
Tungsten	1365 (1±0.02)	−0.07±0.03	−0.24±0.04	33.71		
Mercury	1345 (1±0.02)	0.04±0.03	−0.31±0.04	33.22		
Lead	2274 (1±0.01)	0.02±0.02	−0.42±0.03	56.17	2.72	0.08
Bismuth	2162 (1±0.02)	0.05±0.03	−0.45±0.04	53.40	3.36	0.06
Thorium	3031 (1±0.04)	0.06±0.05	−0.32±0.07	74.87		
Uranium	4630 (1±0.02)	0.05±0.03	−0.17±0.04	114.36		

*$(\bar{\sigma}\Phi) = 2.47\times10^7$ cc millibarn-neutron. Errors are standard errors due to counting statistics only.

REF.	ELEM. SYM.	A	Z
J. Miller, C. Schuhl, C. Tzara J. Phys. Radium 22, 529 (1961)	Pb		82

METHOD	REF. NO.	
Positron annihilation; neutron cross section; BF_3 counter; ion chamber	61 Mi 1	NVB

REACTION	RESULT	EXCITATION ENERGY	SOURCE TYPE	SOURCE RANGE	DETECTOR TYPE	DETECTOR RANGE	ANGLE
G,G	ABX	10-22	D	10-22	NAI-D	10-22	DST
G,XN 470	ABX	8-20	D	8-20	BF3-I		4PI

470

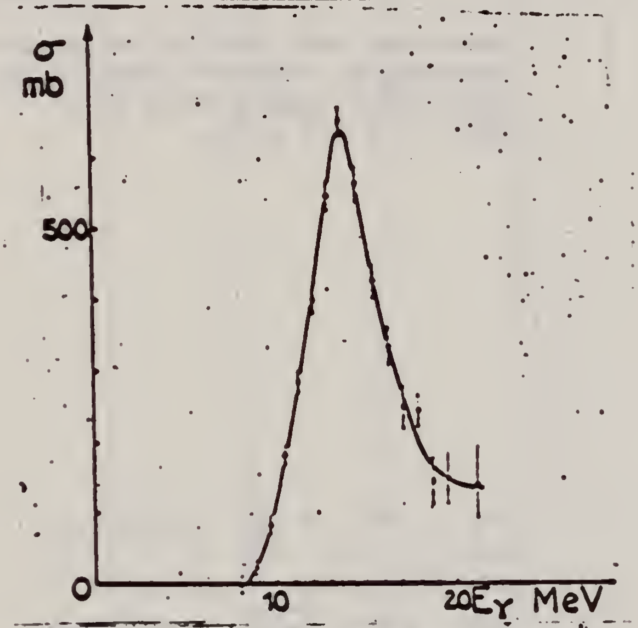

FIG. 26. — Plomb, $\sigma(\gamma, n) + 2\sigma(\gamma, 2n) + \sigma(\gamma, np) + \dots$

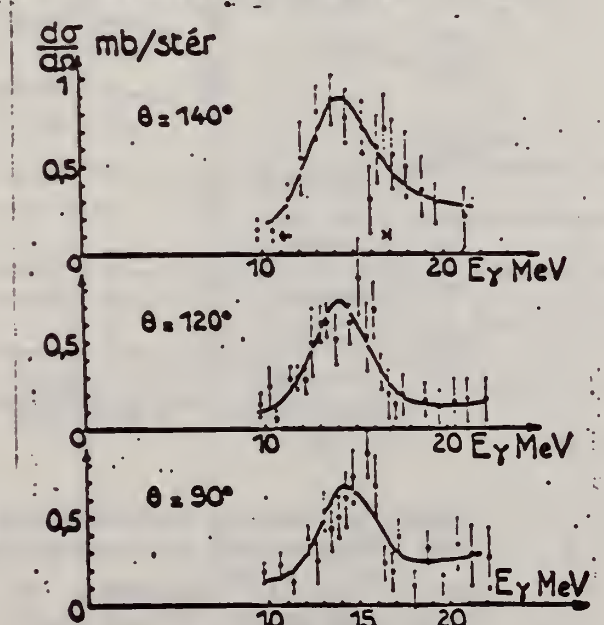

FIG. 7. — Distribution angulaire des photons diffusés élastiquement sur Pb.

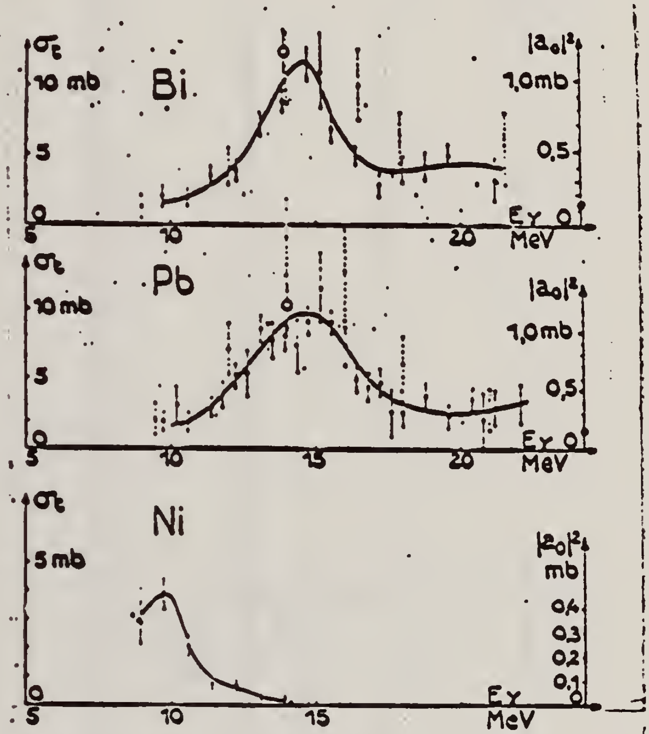

FIG. 8. — Section efficace totale de diffusion élastique et module au carré de l'amplitude de diffusion vers l'avant. Cas de Ni, Pb et Bi.

Cercles vides : module au carré des amplitudes de diffusion absorptive calculées à partir des sections efficaces $\sigma(\gamma, n) + 2\sigma(\gamma, 2n) + \sigma(\gamma, np) + \dots$ (seule la première réaction intervient vers (14 MeV).

Cercles pleins : limites $(Ze^2/Mc^2)^2$ de la section efficace de diffusion à haute énergie. En réalité, à cause des interactions mésoniques des nucléons et de l'incertitude sur la limite à haute énergie de la diffusion, il vaudrait mieux parler de la section efficace de diffusion vers l'avant au delà de la résonance géante et avant le seuil photomésonique ; on peut montrer que l'expression

$$(Ze^2/Mc^2)^2 (1 + 0{,}8x)^2$$

où x est la fraction de force d'échange entre nucléons, est mieux appropriée.

En pointillés : résultats de Fuller et Hayward.

Ref.	F. Tagliabue, J. Goldemberg Nuclear Phys. 23, 144 (1961)	Elem. Sym. Pb	A	Z 82
Method	22 MeV betatron; $Si^{28}(n,p)Al^{28}$ threshold detector.	Ref. No. 61 Ta 1		JHH

Reaction	E or ΔE	E_o	Γ	$\int \sigma dE$	Jπ	Notes
(γ,n)	Bremss. 22					$E_n > 6$ MeV. $W(\theta_n) = A + B \sin^2\theta$ where B/A = 1.0±0.45 Consistent with detailed calculation according to Wilkinson [Physica 22, 1039 (1956)] model, which gives $W(\theta) = 1 + 0.7 \sin^2\theta$.

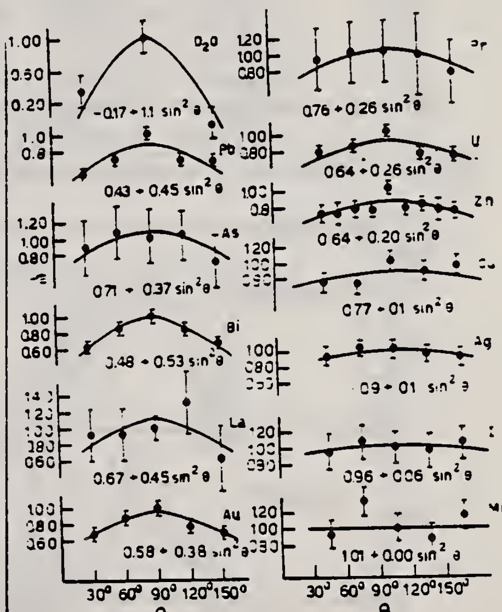

Figure 4: Angular distributions of fast photoneutrons as observed with the $Si^{28}(n,p)Al^{28}$ detector. Data normalized at 90° in each case.

Ref.	T. Tohei, M. Sugawara, S. Mori, M. Kimura J. Phys. Soc. Japan 16, 1657 (1961)	Elem. Sym.	A	Z
		Pb		82
Method	25 MeV betatron; photon scattering; NaI(Tℓ) spectrometer; ion chamber	Ref. No.	61 To 1 cS	NVB

Reaction	E or ΔE	E_o	Γ	$\int \sigma dE$	Jπ	Notes
Pb(γ,γ)	Bremss. 5-12	7.2				Detector at 120° Table II from J. Phys. Soc. Japan 18, 17-22 (1963)

References

1) E. G. Fuller and E. Hayward: Phys. Rev. **101** (1956) 692.
2) see E. Segre: *Experimental Nuclear Physics*, vol. 1, p. 346.
3) J. S. Levin and D. J. Hughes: Phys. Rev. **101** (1956) 1328.
4) K. Reibel and A. K. Mann: Phys. Rev. **118** (1960) 701.

Table II. The correction of the energy scale

Energy in Ref. 1	should be read
4.0 Mev	[illegible] Mev
6.0	5.5
8.0	[illegible]
10.0	[illegible]
12.0	[illegible]
14.0	[illegible]

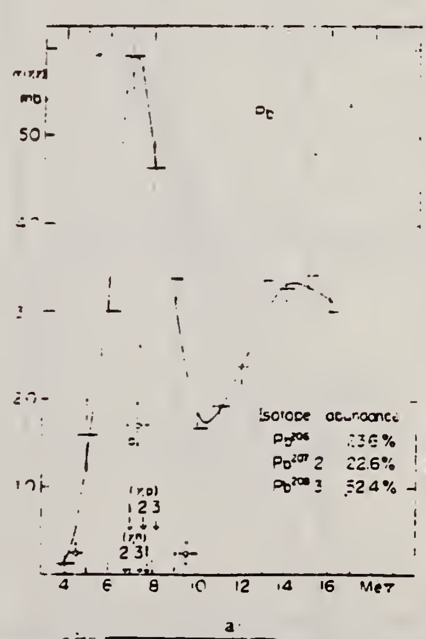

Fig. 9. The elastic scattering cross sections of photons. [illegible]: data from Fuller and Hayward[1], [illegible]: data from monochromatic γ-rays[a]. a: σ(γ,γ) by Pb. The arrows indicate the positions of (γ,p) and (γ,n) threshold energies of isotopes. Numbers 1, 2 and 3 correspond to Pb206, Pb207 and Pb208 [illegible]

Ref.		Elem. Sym.	A	Z
G.Ben-David (Davis); B.Huebschmann Phys.Letters 3, 87 (1962)		Pb		82
Method		Ref. No.		
(n,γ) reaction - NaI(Tl)		62Be2		BG

Reaction	E or ΔE	E_o	Γ	$\int \sigma dE$	Jπ	Notes	
(γ,γ)	discrete energies in the range 5.44 - 8.997	7.261 7.28				σ_s(total)(mb) 6 800	γ source Mn FE

NBS-418
3)
MM-DC 18886-P63

U.S. DEPARTMENT OF COMMERCE
NATIONAL BUREAU OF STANDARDS

REF.	ELEM. SYM.	A	Z
H. Breuer Z. Naturforsh. 17a, 584 (1962)	Pb		82

METHOD	REF. NO.	
Betatron; neutron spectrum; LiI spectrometer; ion chamber	62 Br 4	NVB

REACTION	RESULT	EXCITATION ENERGY	SOURCE		DETECTOR		ANGLE
			TYPE	RANGE	TYPE	RANGE	
G,N	SPC	8-33	C	33	SCI-D	0-11	90
				(32.5)			

Figure 8 is figure 7 minus the statistical part.

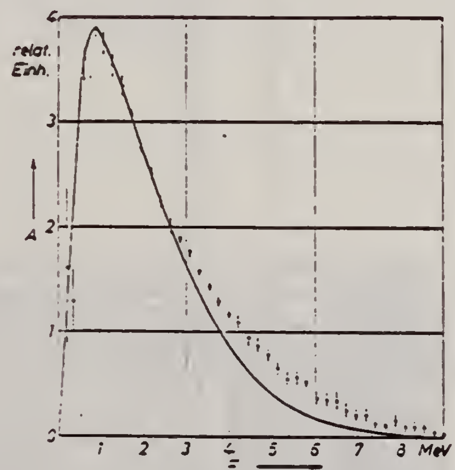

Abb. 7. Spektrum der Photoneutronen aus Pb. Die ausgezogene Linie stellt die Emission nach der statistischen Theorie dar.

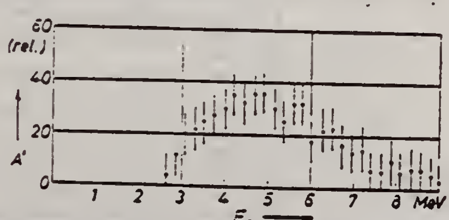

Abb. 8. Spektrum der „direkt" emittierten Photoneutronen.

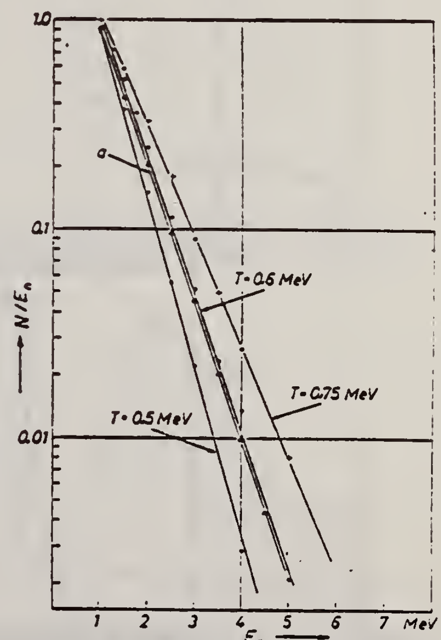

Abb. 11. ln N/E_n als Funktion der Neutronenenergie E_n.

Ref. J. Miller, C. Schuhl, C. Tzara
Nuclear Phys. 32, 236 (1962)

Elem. Sym.	A	Z
Pb		82

Method: Linac; monoergic photons by e^+ annihilation in flight; NaI

Ref. No.	
62 Mi 3	JHH

Reaction	E or ΔE	E_0	Γ	$\int \sigma dE$	Jπ	Notes
Pb (γ,xn)	6.5-22	13.8±0.5		$\int_0^{22} = 4.10\pm0.06$ MeV-b		

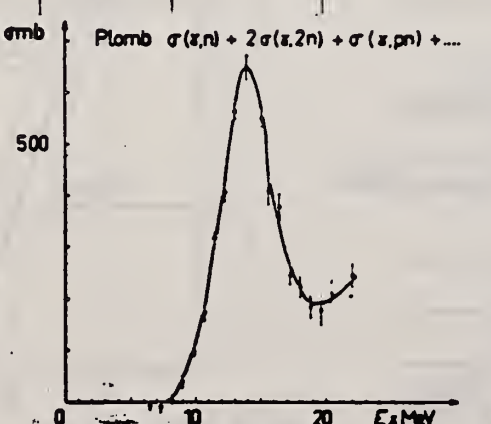

Fig. 11. Section efficace $\sigma = \sigma(\gamma, n) + \sigma(\gamma, np) + 2\sigma(\gamma, 2n) + \ldots$ pour le plomb.

Tableau 5

Résultats expérimentaux

Eléments	Fig. No	E_m (MeV)	σ_{int} (MeV · b) [a]	σ_{int} / 0.06 NZ/A	Seuils γ, n	Seuils γ, p	Seuils γ, 2n	Seuils γ, np
Cu	6	17 ±0.5	0.45 ± 0.015	0.47 ± 0.015				
La	7	13.6 ± 0.5	1.91 ± 0.03	0.94 ± 0.015	8.80 [19]		14.25 [19]	14.90 [19]
Ce 140	8	15.6 ± 0.5	1.88 ± 0.03	0.92 ± 0.015	9.05 [16]	8.50 [16]	14.1 [16]	
Ce 142					7.15 [16]	9.50 [16]	14.3 [16]	
Ta 181	9	13 ± 0.5 16.5 ± 0.5	2.97 ± 0.03	1.13 ± 0.02	7.55 [19]		13.84 [19]	13.47 [19]
Au 197	10	14.2 ± 0.5	3.00 ± 0.05	1.06 ± 0.02	7.90 [19]		13.71 [19]	12.94 [19]
Pb 206	11	13.8 ± 0.5	4.10 ± 0.06	1.38 ± 0.02	10.8 [19]	7.1 [19]	14.3 [19]	14.5 [19]
Pb 207					7.2 [19]	8.2 [19]	14.3 [19]	17.9 [19]
Pb 208					6.9 [19]	8.4 [19]	15.0 [19]	14.2 [19]
Bi 209	12	14.0 ± 0.5	3.73 ± 0.06	1.24 ± 0.02	7.44 [16]	3.76 [16]	10.4 [19]	

[a] L'intégrale $\int_0^x \sigma dE$ est prise jusqu'à x égal à 19.6 MeV pour Cu, à 21.2 MeV pour La et Ce et à 22 MeV pour Ta, Au, Pb et Bi. D'autre part, les erreurs indiquées sont les erreurs statistiques.

Ref. V.G.Shevchenko, B.A.Yur'ev Zhur.Eksptl. i Teoret.Fiz. 42, 707 (1962) Soviet Phys.JETP 15, 492 (1962)	Elem. Sym. Pb	A	Z 82
Method: 35 MeV Betatron	Ref. No. 62Sh2		BG

Reaction	E or ΔE	E_o	Γ	$\int \sigma dE$	Jπ	Notes
(γ,p)	$E_{\gamma\ max}$ = 22.5 33.5					Angular distribution of photoprotons fitted to $a + b\sin^2\theta(1 + p\cos\theta)^2$ where a, b and p are given in the article.

FIG. 4. Energy distribution of photoprotons from Pb for $E_{\gamma max}$ = 22.5 MeV. The smooth curve was calculated for the direct photoeffect.

Table I. Parameters of curves of $a + b\sin^2\theta(1 + p\cos\theta)^2$ and estimated contributions of E2 transitions

Element	Z	$E_{\gamma max}$, MeV	E_p, MeV	[illegible]	[illegible]	[illegible]	[illegible]
[illegible]	[illegible]	22.5	5.25–10.25	[illegible]	[illegible]	[illegible]	[illegible]
			>10.25	[illegible]	[illegible]	[illegible]	[illegible]
[illegible]	[illegible]	33.5	5.25–10.25	[illegible]	[illegible]	[illegible]	[illegible]
			>10.25	14.5	[illegible]	[illegible]	[illegible]
[illegible]	[illegible]	33.5	[illegible]	[illegible]	[illegible]	[illegible]	[illegible]
			>14.25	[illegible]	[illegible]	[illegible]	[illegible]
Pb	[illegible]	22.5	>5.25	[illegible]	[illegible]	[illegible]	[illegible]
			>10.25	[illegible]	[illegible]	[illegible]	[illegible]

Table II. Measured yields Y of photoprotons from Rh, Pt, and Pb and estimates based on the evaporation model and on the direct photoeffect

Element	Rh		Pt	Pb
$E_{\gamma max}$, MeV	22.5	33.5	33.5	22.5
Y_{exp}, protons/mole-roentgen	[illegible]	[illegible]	$9.6 \cdot 10^4$	$2.9 \cdot 10^4$
Y_{exp}/Y_{evap}	~[illegible]	~[illegible]	~2000	~1500
Y_{exp}/Y_{direct}	~[illegible]	~[illegible]	~20	~11

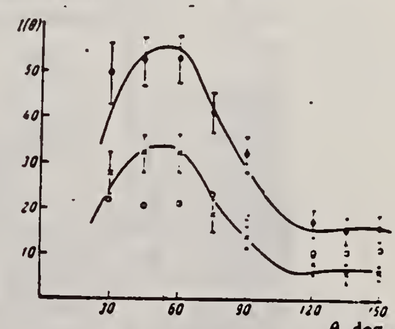

FIG. 8. Angular distributions of photoprotons from Pb for $E_{\gamma max}$ = 22.5 MeV. o–E_p = 5.25–10.25 MeV; ●–E_p > 5.25 MeV; x–E_p > 10.25 MeV.

Ref. V.G. Shevchenko, B.A. Yurev
Nuclear Phys. 37, 495 (1962)

Elem. Sym.	A	Z
Pb		82

Method: 35 MeV betatron; emulsions

Ref. No.	
62 Sh 4	JHH

Reaction	E or ΔE	E_o	Γ	$\int \sigma dE$	Jπ	Notes
Pb (γ,p)	Bremss. 22.5 33.5					Parameters a, b and p for $\omega(\theta_p) = a + b \sin^2\theta\,(1 + p\,co\theta)^2$ in Table I.

TABLE 1

Coefficients of expressions of type (1) for approximate angular distributions and estimates of the [illegible] contribution from E2 transitions [illegible]

Element	Z	$E_{\gamma max}$ (MeV)	E_p (MeV)	[illegible]	[illegible]	[illegible]	[illegible] (%)
Rh	45	22.5	6.25-9.25	[illegible]	[illegible]	[illegible]	[illegible]
			> 9.25	2.6	1.9	[illegible]	[illegible]
		33.5	3.25-9.25	[illegible]	[illegible]	[illegible]	[illegible]
			> 9.25	[illegible]	0.7	1.2	≈20
[illegible]	50	22.5	4.5-7.25	1.4	0.2	0.42	2
			7.25-11.25	2.9	4.4	0.29	3
			> 11.25	1.5	2.4	0.44	4
		33.5	4.5-7.25	2.2	1.2	2.0	≈15
			7.25-11.25	3.3	1.16	2.2	≈50
			> 11.25	0.8	1.2	1.0	≈40
W	74	22.5	4.25-8.75	[illegible]	[illegible]	[illegible]	[illegible]
			8.75-12.75	2.6	1.0	1.6	≈25
			> 12.75	1.5	0.5	2.6	≈65
		33.5	4.25-8.75	1.2	0.96	0.44	6
			8.75-12.75	1.3	0.25	2.6	≈55
			> 12.75	[illegible]	0.5	3.4	≈70
Pt	78	22.5	6.25-8.75	0.6	1.0	0.4	3
			8.75-11.75	2.8	1.9	1.2	≈20
			> 11.75	1.4	0.50	2.6	≈35
		33.5	7.25-14.25	2.1	1.1	2.6	≈55
			> 14.25	0.5	0.6	3.4	≈70
Pb	92	22.5	5.25-10.25	1.05	0.75	0.8	≈10
			> 10.25	0.75	0.75	2.2	≈50
		33.5	3.25-10.25	1.9	1.2	1.2	≈20
			10.25-14.25	1.15	0.65	3.0	≈65
			> 14.25	1.5	1.0	3.3	≈70

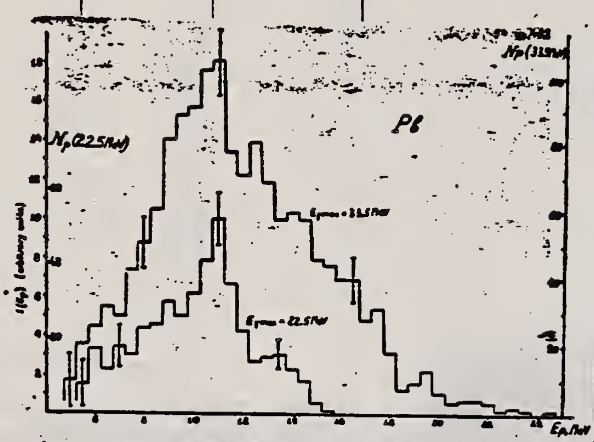

Fig. 6. Energy distributions of photoprotons from Pb.

TABLE 3

Measured photoproton yields and comparison with estimates by the models of evaporation and [illegible] direct photoeffect *)

Element	$E_{\gamma max}$ (MeV)	Y_{exp} *)	Y_{ev}/Y_{exp}	Y_{ex}/Y_{exp}
Rh	22.5	1.3×10[illegible]	≈ 3	≈ 3
	33.5	2.8×10[illegible]	≈ 6	≈ 4.5
[illegible]	22.5	6.7×10[illegible]	≈ 16	≈ 4.5
	33.5	1.3×10[illegible]	≈ 25	≈ 6
W	22.5	2.8×10[illegible]	≈ 1.8×10[illegible]	≈ 6
	33.5	8.8×10[illegible]	≈ 3 ×10[illegible]	≈ 11
Pt	22.5	2.4×10[illegible]	≈ 5 ×10[illegible]	≈ 5
	33.5	8.8×10[illegible]	≈ 3 ×10[illegible]	≈ 20
Pb	22.5	2.8×10[illegible]	≈ 1.8×10[illegible]	≈ 11
	33.5	9.2×10[illegible]	≈ 4 ×10[illegible]	≈ 25

*) The yield Y_{exp} is expressed in protons per mol per Roentgen.

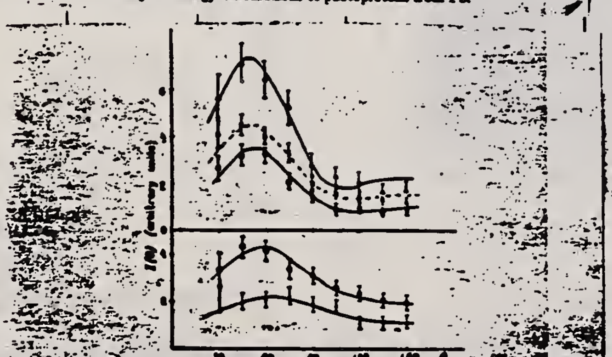

Fig. 11. Angular distributions of photoprotons from Pb. The experimental points for $E_{\gamma max}$ = 22.5 MeV are denoted by solid dots for E_p = 5.25-10.25 MeV and solid squares for E_p > 10.25 MeV. In the case of $E_{\gamma max}$ = 33.5 MeV centred circles denote E_p = 3.25-10.25 MeV, crosses denote E_p = 10.25-14.25 MeV and solid triangles denote E_p > 14.25 MeV.

References

1) M. E. Toms and W. E. Stephens, Phys. Rev. 98 (1955) 626
2) M. M. Hoffman and A. G. W. Cameron, Phys. Rev. 92 (1953) 1184
3) W. C. Barber and V. J. Vanhuyse, Nuclear Physics 16 (1960) 381
4) M. E. Toms and W. E. Stephens, Phys. Rev. 92 (1953) 362
5) E. D. Makhnovsky, JETP 38 (1960) 96
6) R. B. Taylor, Nuclear Physics 19 (1960) 468
7) A. G. W. Cameron, W. Harms and L. Katz, Phys. Rev. 83 (1951) 1264
8) V. G. Neudachin, V. G. Shevchenko and N. P. Yudin, Report of the Second All-Union Conf. for Nuclear Reactions at Low and Medium Energies, Moscow, 1960
9) E. D. Courant, Phys. Rev. 82 (1951) 703
10) V. V. Balashov, V. G. Shevchenko and N. P. Yudin, JETP 41 [illegible]

R. Bosch, J. Lang, R. Muller, W. Wolfli
Helva. Phys. Acta 36, 625 (1963)

Pb		82

METHOD

n capture source; photon scattering; NaI spectrometer

REF. NO.	
63 Bo 2	NVB

REACTION	RESULT	EXCITATION ENERGY	SOURCE		DETECTOR		ANGLE
			TYPE	RANGE	TYPE	RANGE	
G,G	ABX	9	D	9	NAI - D		DST

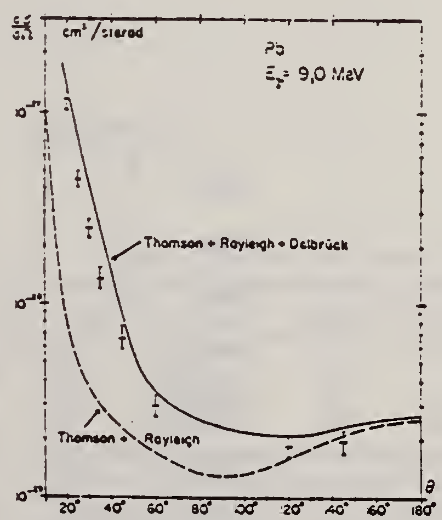

Fig. 10.

Experimentell bestimmte Wirkungsquerschnitte für die Streuung von 9-MeV-Quanten an Blei. Die gestrichelte Kurve gibt den theoretischen Wert für Thomson- und Rayleighstreuung (nach Bethe); in der ausgezogenen Kurve ist zudem der Delbrückeffekt (nach einer Extrapolation aus den Werten Zerniks) mit einbezogen.

H.H. Fleischmann
Ann. Physik 12, 133 (1963)

Pb		82

METHOD

Radioactive source; photon scattering; NaI spectrometer

REF. NO. 63 Fℓ 1 — NVB

REACTION	RESULT	EXCITATION ENERGY	SOURCE TYPE	SOURCE RANGE	DETECTOR TYPE	DETECTOR RANGE	ANGLE
G,G	LFT	2-6	D	2-6	NAI-D		

Peak at 5.2 MeV

$\Gamma_o = 0.9 \pm 0.4$ eV

G-WDTH

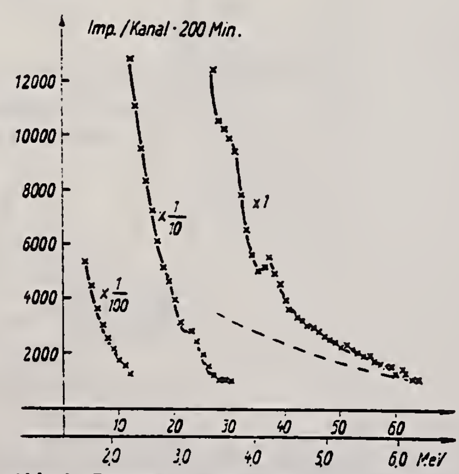

Abb. 6. Pb-Streuspektrum mit Cd-Quelle (gestrichelt ungefährer nicht streukörperbedingter Untergrund)

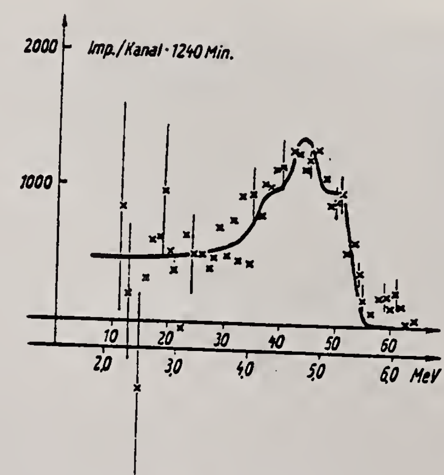

Abb. 7. Resonanz der Cd-Strahlung in Blei. Differenz der Spektren bei Hg- und Pb-Absorbern (Summation aller Messungen)

Ref.	Elem. Sym.	A	Z
C.S. Young, D.J. Donahue Phys. Rev. <u>132</u>, 1724 (1963)	Pb		82

Method	Ref. No.	
200 kW pool reactor; monoergic γ's from (n,γ) in Ti, Mn, Fe and Cu; NaI	63 Yo 1	JHH

Reaction	E or ΔE	E_0	Γ	$\int \sigma dE$	$J\pi$	Notes
(γ,γ)	5.0-8.2					Measure σ (elastic scattering) values in Table II; interpolated to 7 MeV in Table V.
	7.285	~ 7.285	$0.1 \le \Gamma_0 \le 4$ ev			7.285 MeV angular distribution fits $W(\theta) = 1+(0.94\pm0.1)\cos^2\theta$ [see figure 5].

TABLE II. Total elastic scattering cross sections (mb).

Source element	Energy interval (MeV)	Source energy (MeV)	Target (thickness in cm) Ta(1.3)	Hg(3)	Pb(0.6)	Bi(1.3)
Tl	5.0–7.0	6.41 6.75			0.6 ± 0.4	
Mn	6.0–7.5	7.26 7.15 7.05	<0.3	0.5 ±0.3	0.9 ± 0.5	0.8 ±0.4
Fe	6.0–7.6	7.64 7.28	0.7 ±0.4	2.4 ±1.3	125 ±20[a]	2.0 ±1.1
Cu	7.6–8.2	7.91.	<0.2	<0.4	<0.2	<0.2

[a] Calculated using the intensity of 7.64-MeV γ rays produced by neutron capture in iron.

TABLE V. Cross sections at about 7 MeV (mb).

	This work	Ref. 2	Ref. 1[a]	Ref. 3	Ref. 4[b]
Ta	<0.3		2		
Hg	0.5±0.3	3.5			
Pb	0.9±0.5	15	17	60	55
Bi	0.8±0.4	17.5	19	35	17

[a] See also E. G. Fuller and Evans Hayward, Phys. Rev. Letters 1, 465 (1958).
[b] Differential cross sections at 135° were multiplied by 11.2.

[1] E. G. Fuller and Evans Hayward, Phys. Rev. 101, 692 (1956); Nucl. Phys. 33, 431 (1962).
[2] K. Riebal and A. K. Mann, Phys. Rev. 118, 701 (1960).
[3] Tsutomu Tohei, Masumi Sugawara, Shigeki Mori, and Motohara Kimara, J. Phys. Soc. Japan 16, 1657 (1961).
[4] P. Axel, K. Min, N. Stein, and D. C. Sutton, Phys. Rev. Letters 10, 299 (1963).

REF.	ELEM. SYM.	A	Z
F.R. Allum, T.W. Quirk, B.M. Spicer Aust. J. Phys. 17, 420 (1964)	Pb		82

METHOD	REF. NO.	
Synchrotron; r-chamber	64 Al 4	NVB

REACTION	RESULT	EXCITATION ENERGY	SOURCE		DETECTOR		ANGLE
			TYPE	RANGE	TYPE	RANGE	
G,N	NØX	THR-18	C	18	SCI-I	4-	DST
				(17.5)		(4.5-)	

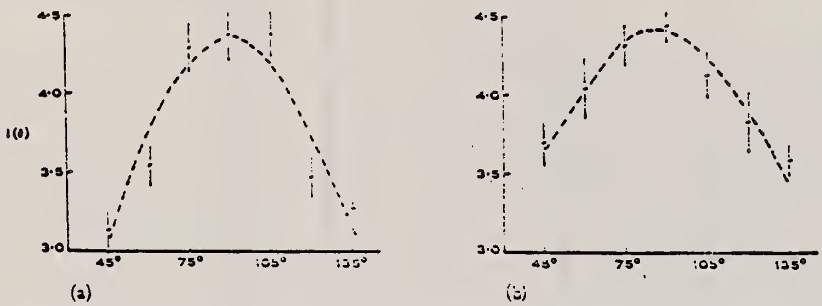

Fig. 1.—Fast photoneutron (>4·5 MeV) angular distributions from bismuth and lead. (a) Bismuth, $I(\theta) = 4\cdot50-0\cdot04\cos\theta-2\cdot52\cos^2\theta$ (dotted line); (b) lead, $I(\theta) = 4\cdot40+0\cdot14\cos\theta-1\cdot71\cos^2\theta$ (dotted line).

No asymmetry about 90°.

REF.	ELEM. SYM.	A	Z
F.R. Allum, T.W. Quirk, and B.M. Spicer Nucl. Phys. 53, 545 (1964)	Pb		82
METHOD	REF. NO. 64 Al 5		JOC

REACTION	RESULT	EXCITATION ENERGY	SOURCE		DETECTOR		ANGLE
			TYPE	RANGE	TYPE	RANGE	
G,XN	NØX	THR-34	C	34	THR-I	6-	DST

TABLE 1

Summary of present experimental data at 34 MeV bremsstrahlung

Element		$-\frac{a_2}{a_0}$	$\frac{a_1}{a_0}$
$_{4}$Be		0.43 ± 0.02	0.05 ± 0.01
$_{6}$C		0.61 ± 0.04	0.09 ± 0.0[illegible]
$_{13}$Al		0.39 ± 0.03	0.05 ± 0.01
$_{22}$Ti		0.34 ± 0.02	0.06 ± 0.01
$_{24}$Cr	34 MeV	0.33 ± 0.02	0.02 ± 0.0[illegible]
	22 MeV	0.13 ± 0.07	-0.02 ± 0.0[illegible]
$_{29}$Cu		0.36 ± 0.02	0.10 ± 0.0[illegible]
$_{50}$Sn		0.38 ± 0.02	0.11 ± 0.0[illegible]
$_{56}$Ba		0.39 ± 0.03	0.11 ± 0.0[illegible]
$_{73}$Ta	Before installation of iron shielding	0.26 ± 0.04	0.13 ± 0.0[illegible]
	After installation of iron shielding	0.27 ± 0.02	0.12 ± 0.0[illegible]
$_{82}$Pb	target diameter 3.0 cm	0.39 ± 0.03	0.15 ± 0.0[illegible]
	target diameter 1.5 cm	0.40 ± 0.03	0.19 ± 0.0[illegible]
$_{83}$Bi		0.42 ± 0.03	0.17 ± 0.0[illegible]

$$Y = a_0 + a_1 \cos\theta + a_2 \cos^2\theta$$

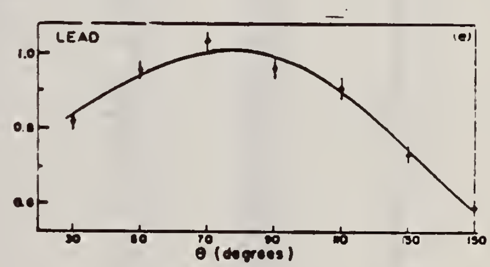

REF.	ELEM. SYM.	A	Z
B. Arad (Huebschmann), G. Ben-David (Davis), I. Pelah, Y. Schlesinger Phys. Rev. 133, B684-700 (1964)	Pb		82

METHOD	REF. NO.	
Reactor, (n,γ) reactions source	64 Ar 1	NVB

REACTION	RESULT	EXCITATION ENERGY	SOURCE TYPE	SOURCE RANGE	DETECTOR TYPE	DETECTOR RANGE	ANGLE
G,G	ABX	7,7	D	7,7	NAI-D		135
		(6.98, 7.32)		(6.98, 7.32)			

TABLE II. Capture gamma-ray sources and their properties.[a]

Source	Chemical composition	Mass kg	Principal γ rays (in MeV)
Al	Metal	1.640	7.73
Cl	polyvinyl Chloride	0.380	8.55, 7.78, 7.41, 6.96, 6.64, 6.12, 5.72
Co	CoO	0.250	7.49, 7.20, 6.98, 6.87, 6.68, 6.48, 5.97, 5.67
Cr	Metallic powder	0.480	9.72, 8.88, 8.49, 7.93, 7.09, 6.65, 5.60
Cu	Metal	1.860	7.91, 7.63, 7.29, 7.14, 7.00, 6.63
Fe	Metallic powder	0.440	9.30, 7.64, 7.28, 6.03
Hg	$Hg_2(NO_3)_2 \cdot 2H_2O$	0.310	6.44, 6.31, 5.99, 5.67, 5.44
Mn	MnO_2	0.240	7.26, 7.15, 7.04, 6.96, 6.79, 6.10, 5.76
Ni	Metal	0.900	9.00, 8.50, 8.10, 7.83, 7.58, 6.84, 6.64
Ti	TiO_2	0.210	6.75, 6.56, 6.42
V	V_2O_5	0.120	7.30, 7.16, 6.86, 6.51, 6.46, 5.87, 5.73
Y	Y_2O_3	0.200	6.07, 5.63

[a] For more detailed information, additional lines, intensities, etc., see Ref. 6.

TABLE III. Effective cross sections.

γ source	Energy (MeV)	Scatterer Element	Protons	Neutrons	$\langle\sigma_{\gamma\gamma}\rangle$ (mb)	Notes
Hg	5.44	Hg	80	116, 118, 119, 120, 121, 122, 124	128	
Cl	6.12	Pr^{141}	59	*82*	103	a
V	6.508	Sn	*50*	62, 64–70, 72	14	
Co	6.690	Pr^{141}	59	*82*	2.7	a
Co	6.867	Nd	60	82, 83, 84, 85, 86, 88	22	
Al	6.98	Pb^{208}	*82*	*126*	2900	b
Cl	6.98	Pb	*82*	124, 125, *126*	346	a
Ti	6.996	Bi^{209}	83	*126*	1560	b
Cu	7.01	Sn	*50*	62, 64–70, 72	1000	b
Ti	7.149	Pb^{208}	*82*	*126*	1000	b
Co	7.201	Pb^{208}	*82*	*126*	25	
Mn	7.261	Pb^{208}	*82*	*126*	25	a
Fe	7.285	Pb^{208}	*82*	*126*	4100	a
V	7.305	Pb^{208}	*82*	*126*	12.5	
Hg	7.32	Pb	*82*	124, 125, *126*	5500	c
Fe	7.639	Ni	28	30, 32, 34, 36	10.5	d
Fe	7.639	Pr^{141}	59	*82*	10	d
Cr	8.499	Cu	29	34, 36	24.4	
Cr	8.881	Pr^{141}	59	*82*	9.3	
Ni	8.997	Sm	62	*82*, 85–88, 90, 92	2.8	

[a] A large error could be introduced in the cross-section value [illegible] large differences in line intensities quoted by Bartholomew and Higgs and by Groshev *et al.* (Ref. 6).

[b] Because of the low counting rate, thick scatterers were [illegible] will introduce a systematic error in estimating $\langle\sigma_{\gamma\gamma}\rangle$ for resonances having a high nuclear cross section.

[c] The cross section was evaluated assuming the gamma [illegible] 0.02 photons per 100 captured neutrons (see text).

[d] Reference 6 gives the 7.639 line of iron capture [illegible] line. However, a recent paper by Fiebiger, Kand, and Segel [Phys. Rev. 125, 2031 (1962)] reports two different lines of equal inten[illegible] of 7.647 and 7.633 MeV. The present experiment cannot resolve an energy difference of 14 keV, therefore, there is no possibility [illegible] is responsible for the scattering.

REF.	ELEM. SYM.	A	Z
M.M. Dorosh, A.M. Parlag, V.A. Shkoda-Ul'Yanov, L.A. Shabalina Zhur. Eksp. i Teoret. Fiz. 46, 1540-44 (1964) Soviet Phys. JETP 19, 1042-44 (1964)	Pb		82
METHOD	**REF. NO.**		
Betatron; ion chamber monitor	64 Do 1		NVB

REACTION	RESULT	EXCITATION ENERGY	SOURCE		DETECTOR		ANGLE
			TYPE	RANGE	TYPE	RANGE	
G,N	ABX	8 - 20	C	8-20	BF3-I		4PI

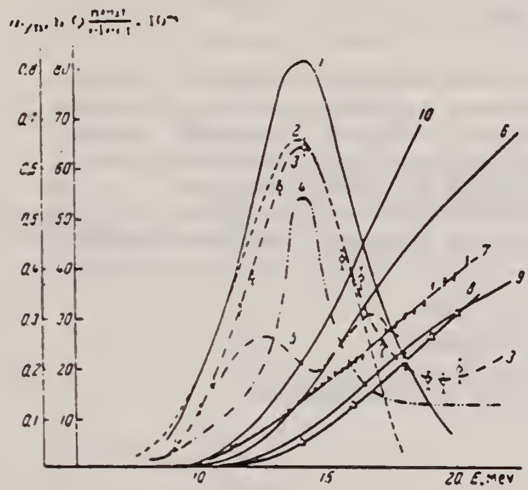

FIG. 1. Cross section of (γ, n) reaction in lead and photoneutron yield curves from an infinitely thick lead sample under the action of electrons. The ordinates on the left show the cross section of the (γ, n) reaction in barns, and on the right the absolute yield of neutrons in neutron/electron units; curve 2 shows the cross section of the (γ, n) reaction in lead, obtained in the present paper and calculated from the yield curve of Fig. 2.

REF.	ELEM. SYM.	A	Z
M. Giannini, P. Oliva, D. Prosperi and S. Sciuti Nuovo Cimento 34, 1116 (1964)	Pb		82

METHOD	REF. NO.	
Reactor; Fe(n,γ), Al(n,γ)	64 Gi 1	NVB

REACTION	RESULT	EXCITATION ENERGY	SOURCE		DETECTOR		ANGLE
			TYPE	RANGE	TYPE	RANGE	
G,G	NØX	7,8	D	7,8	NAI-D		135
		(6.98, 7.28)		(6.98, 7.28)			

WIDTH

TABLE I.

Source-scatterer	Energy (MeV)	$\langle\sigma_{rs}(300)\rangle$ (Barn)	$\bar{\sigma}_{rs}(300)$ (Barn)	$\frac{\langle\sigma_{rs}(100)\rangle}{\langle\sigma_{rs}(300)\rangle}$	$\Gamma_{\gamma 0}/\Gamma$	$\Gamma_{\gamma 0}$ (eV)	δ (eV)
^{57}Fe-^{208}Pb	7.28	5.62 ±0.15	17.5±1.5	1.004±0.006	0.84±0.08	0.73±0.05	4.8±0.3
^{57}Fe-$^{(60)}$Ni	7.64	0.375±0.006	≤5	0.838±0.011	0.71±0.07	0.15±0.02	11.0±0.5
^{57}Fe-$^{(114)}$Cd	7.64	0.287±0.006	4.1±1.8	1.116±0.015	0.11±0.06	0.22±0.02	≤1
^{28}Al-^{208}Pb	6.98	1.29 ±0.06	22.1±2.7	1.002±0.012	0.30±0.07	0.86±0.10	11.5±2.5

Cross sections based on assumed $1 + \cos^2\theta$ distribution.

REF.		ELEM. SYM.	A	Z
Yu.Ya. Glazunov, M.V. Savin, I.N. Safina, E.F. Fomushkin, Yu.A. Khokhlov Zhur. Eksp. i Teoret. Fiz. 46, 1906-08 (1964) Soviet Phys. JETP 19, 1284 (1964)		Pb		82
METHOD		REF. NO.		
Linac		64 Gl 1		NVB

REACTION	RESULT	EXCITATION ENERGY	SOURCE TYPE	SOURCE RANGE	DETECTOR TYPE	DETECTOR RANGE	ANGLE
G,N	SPC	16	D	16	TØF-D	0-5	90

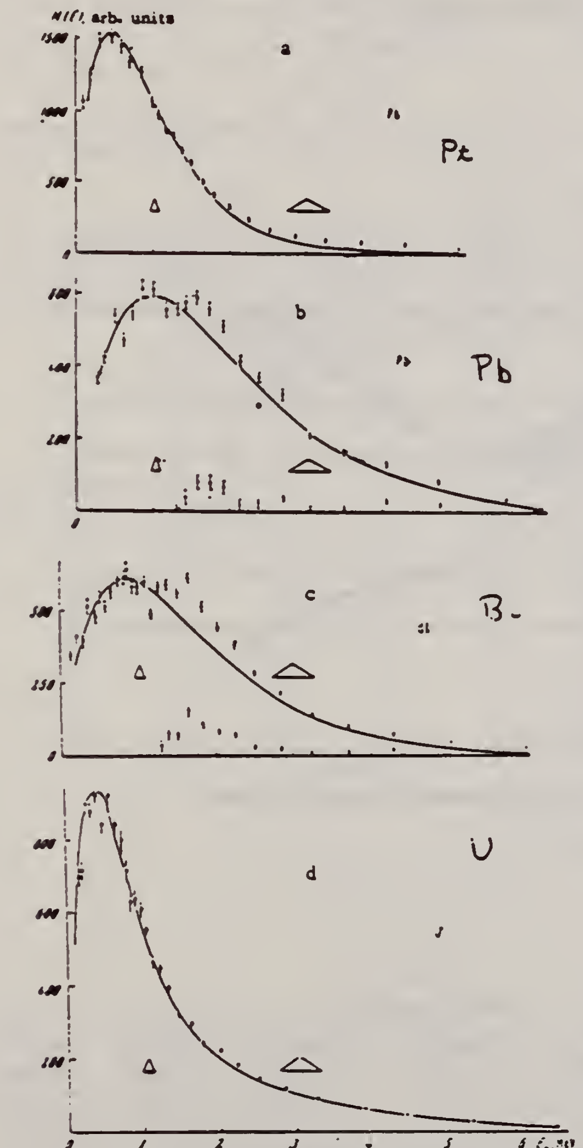

Photoneutron energy distributions.

shown in the figure. The solid curves a, b, and c are the evaporation spectra

$$N(E) \sim \frac{E}{T} \exp\left(-\frac{E}{T}\right)$$

with the temperature T = 0.48 ± 0.03 MeV for platinum, 0.84 ± 0.04 MeV for Bi, and 0.98 ± 0.04 MeV for lead.

The solid curve d is the sum of the evaporation spectrum and the fission spectrum of uranium:

$$N(E) = \alpha \frac{E}{T} \exp\left(-\frac{E}{T}\right) + (1-\alpha) \exp\left(-\frac{E}{T}\right) \times \frac{1}{\sqrt{\pi \omega T_f}} \exp\left(-\frac{E}{T_f}\right) \sinh \frac{\sqrt{\omega E}}{T_f}$$

with the parameters: T = 0.33 ± 0.03 MeV, T_f = 1.05 ± 0.04 MeV, ω = 0.5 MeV, α = 0.49 ± 0.01.

REF.

M. Giannini, P. Oliva, D. Prosperi and S. Sciuti
Nuclear Phys. 65, 344 (1965)

ELEM. SYM.	A	Z
Pb		82

METHOD

REF. NO.	
65 Gi 1	EGF

REACTION	RESULT	EXCITATION ENERGY	SOURCE		DETECTOR		ANGLE
			TYPE	RANGE	TYPE	RANGE	
G,G	LFT	5 - 8	D	5 - 8	NAI-D	3 - 8	135

Source n capture γ's from Fe and Al changed temperature from T_{eff} 150-400°K.

$$< \sigma_{rs} > = \int_0^\infty f(E)\sigma_{rs}(E)dE$$

$$\bar{\sigma}_{ra} = \frac{\Gamma}{\Gamma} \frac{\int_0^\infty f(E)\,\sigma_{rs}^2\,dE}{\int_0^\infty f(E)\,\sigma_{rs}(E)dE}$$

$f(E)$ source spectrum

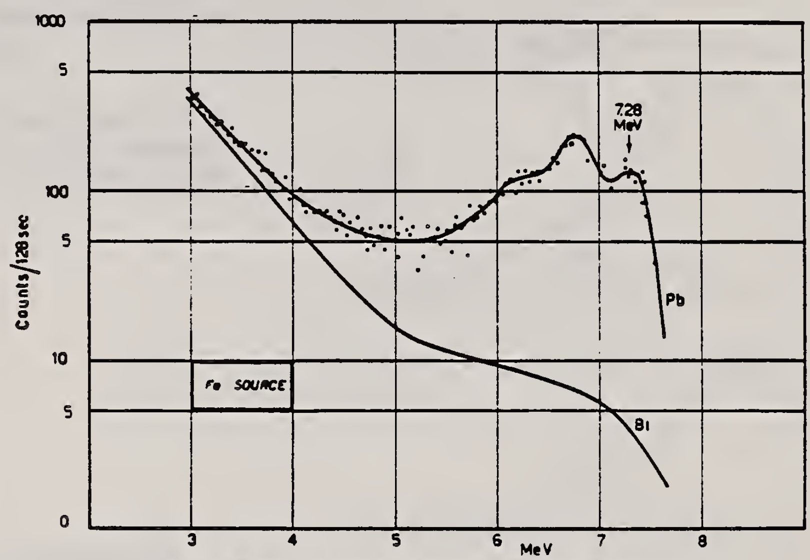

Fig. 2. Spectra of γ-rays scattered by Pb and Bi targets.

REF.

M. Giannini, P. Oliva, D. Prosperi and S. Sciuti
Nuclear Phys. 65, 344 (1965)

ELEM. SYM.	A	Z
Pb		82

METHOD

REF. NO.	
65 Gi 1	EGF

REACTION	RESULT	EXCITATION ENERGY	SOURCE TYPE	SOURCE RANGE	DETECTOR TYPE	DETECTOR RANGE	ANGLE

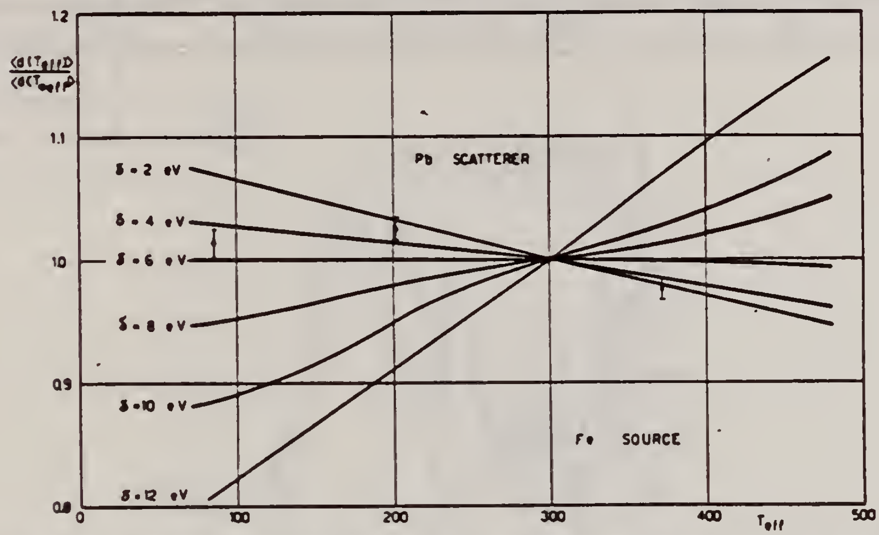

Fig. 6. Fe–Pb resonance. Calculated variation in resonant scattering cross section as a function of scatterer temperature, for different values of δ.

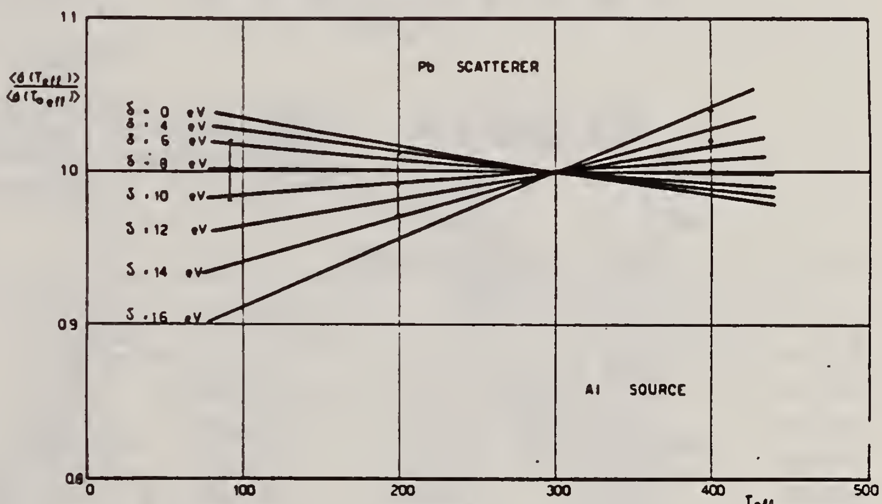

Fig. 9. Al–Pb resonance.

TABLE 1

Experimental results

Source scatterer	Energy (MeV)	$\langle\sigma_{rs}(300)\rangle$ (b)	$\bar{\sigma}_{rs}(300)$ (b)	Γ(eV)	$\Gamma_{\gamma 0}$(eV)	δ(eV)
Fe^{57}-Pb^{208}	7.28	5.62 ±0.15	17.5±1.5	1.2 ±0.2	0.86±0.06	5.0±0.5
Fe^{57}-$Ni^{(62)}$	7.64	0.375±0.006	4.4±2.6	3.0 ±1.5	0.63±0.17	12.5±0.5
Fe^{57}-$Cd^{(114)}$	7.64	0.287±0.006	4.1±1.8	1.6 ±0.5	0.22±0.05	≲1
Al^{28}-Pb^{208}	6.98	1.29 ±0.06	22.1±2.7	∽3.5	0.95±0.10	10 ±1

In columms 3 and 4, $\langle\sigma_{rs}(T_e)\rangle$ and $\langle\sigma_{rs}(T_e)\rangle$ are cross sections measured at temperature T_e(°K).

REF.	ELEM. SYM.	A	Z
I. Bergqvist, B. Lundberg, L. Nilsson, and N. Starfelt Phys. Letters 19, 670 (1966)	Pb		82

METHOD	REF. NO.	
Van de Graaff	66 Be 1	EGF

REACTION	RESULT	EXCITATION ENERGY	SOURCE TYPE	SOURCE RANGE	DETECTOR TYPE	DETECTOR RANGE	ANGLE
N,G	SPC	14	D	7	NAI-D	8-18	

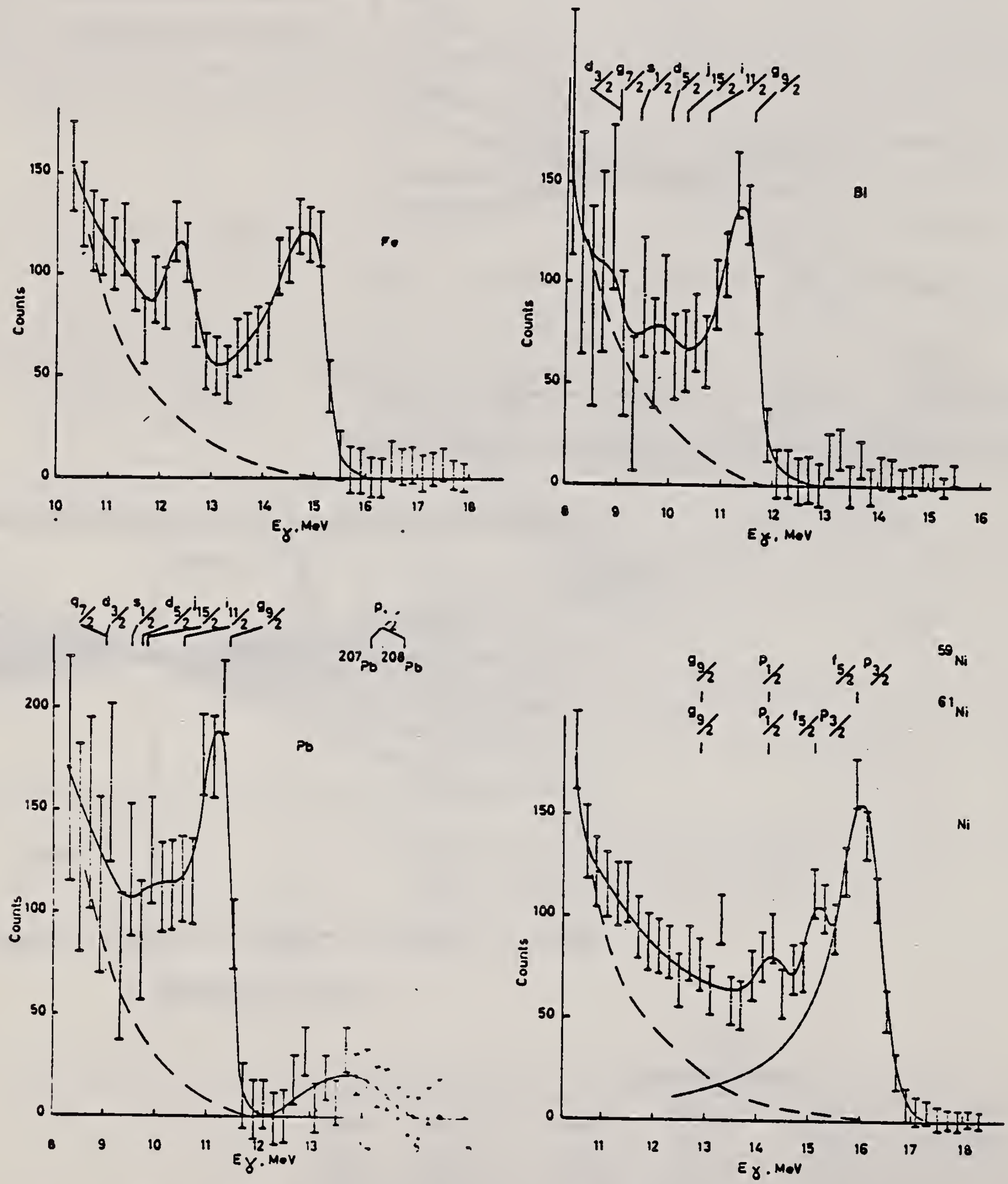

Fig. 1. Gamma-ray spectra emitted in the capture of 7.4 MeV neutrons. The dashed line is the spectrum calculated for the decay of a compound nucleus. The dot-dashed line is the response function of the gamma-ray spectrometer for 16.0 MeV γ rays. Single-particle states as determined from (d,p) reactions are shown.

REF.	ELEM. SYM.	A	Z
N. De Botton, J. Miller, C. Schuhl, G. Tamas and C. Tzara Nucl. Phys. 75, 396 (1966)	Pb		82

METHOD	REF. NO.	
Photon Monochromator	66 De 1	JDM

REACTION	RESULT	EXCITATION ENERGY	SOURCE TYPE	SOURCE RANGE	DETECTOR TYPE	DETECTOR RANGE	ANGLE
G,G	RLX	12 - 17	D	12 - 17	NAI-D		DST

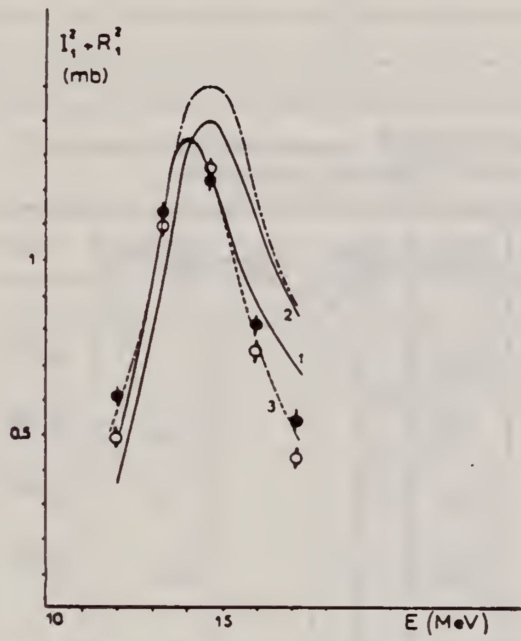

Fig. 1. Sections efficaces de diffusion dipolaire vers l'avant. Résultats déduits de raies de Lorentz: 1) maximum à 13.3 MeV, 2) maximum à 14 MeV, 3) résultat expérimental. – courbe en traits mixtes: déduite de l'absorption mesurée – cercles pleins et vides: points déduits des résultats expérimentaux de diffusion, relatifs au Pb et Bi respectivement.

Tableau 1
Donnés expérimentales

E_γ (MeV)	$d\sigma/d\Omega$ (μb/sr) Pb $\theta = 90°$	Pb 135°	Bi 90°	Bi 135°
12	305±20	348±25	246±15	252±15
13.33	570±20	690±30	550±20	692±30
14.67	602±20	910±25	635±20	925±30
16.00	407±20	648±30	369±20	540±30
17.17	270±15	412±20	215±15	412±15

Tableau 2
Section efficace et terme d'interférence à $\theta = 0$

E (MeV)	$X = I_1^2+R_1^2$ (mb) Pb	Bi	$Y = I_1 I_2 + R_1 R_2$ (mb) Pb	Bi
12.00	0.61±0.04	0.49±0.03	0.15 ±0.05	0.17±0.03
13.33	1.14±0.04	1.10±0.04	0.26 ±0.05	0.19±0.05
14.67	1.20±0.04	1.27±0.04	−0.008±0.04	0.04±0.05
16.00	0.81±0.04	0.74±0.04	−0.054±0.05	0.02±0.04
17.17	0.54±0.04	0.43±0.03	−0.010±0.035	−0.12±0.03

REF.	ELEM. SYM.	A	Z
H. M. Gerstenberg and E. G. Fuller NBS Tech. Note 416, June 1967	Pb		82

METHOD	REF. NO.	
	67 Ge 2	hmg

REACTION	RESULT	EXCITATION ENERGY	SOURCE TYPE	SOURCE RANGE	DETECTOR TYPE	DETECTOR RANGE	ANGLE
G,N	ABY	THR-27	C	22,27	BF3-I		4PI

Table 7. Comparison of neutron yields. Yields are given in units of (neutron cm^2/MeV nucleus)$\times 10^{-26}$. The estimated uncertainties in Y and Y_c are of the order of 6% and 10%, respectively.

Element	E_o	$Y(E_o)$	UCRL (Y_c)	Saclay (Y_c)	Va. (Y_c)	NBS(Old) (Y_c)	UCRL Exp (Y_c/Y)	Saclay Exp (Y_c/Y)	Va. Exp (Y_c/Y)	NBS(Old) Exp (Y_c/Y)	Ref.
Pb	27	103	86				0.83				26,30
	22	111	92	116			0.83	1.05			
Au	27	89	97				1.09				24,30,
	22	92	98	88		115	1.07	0.96		1.25	38
Ta	27	81	82	77			1.01	0.95			27,30,
	22	85	79	80		113	0.93	0.94		1.33	38
Ho	27	67	75				1.12				27,31,
	22	69	77	82		103	1.12	1.19		1.49	39
Ag	27	36									
	22	34.8									
Cu	27	14.4	13.2				0.92				28,30
	22	12.6	11.5	12.4			0.91	0.98			
Co	27	12.7	12.1				0.95				29,34
	22	10.6	9.9		13.5		0.94		1.27		
Ca	27	1.69		1.13	1.01			0.67	0.60		32,35
P	27	2.35			1.76				0.75		36
Al	27	1.92	1.62		1.38		0.84		0.72		25,37
O^{16}	27	0.54	0.42	0.48	0.42		0.78	0.89			16,32, 37
C	27	0.50	0.35	0.33	0.46		0.70	0.66			25,32, 33

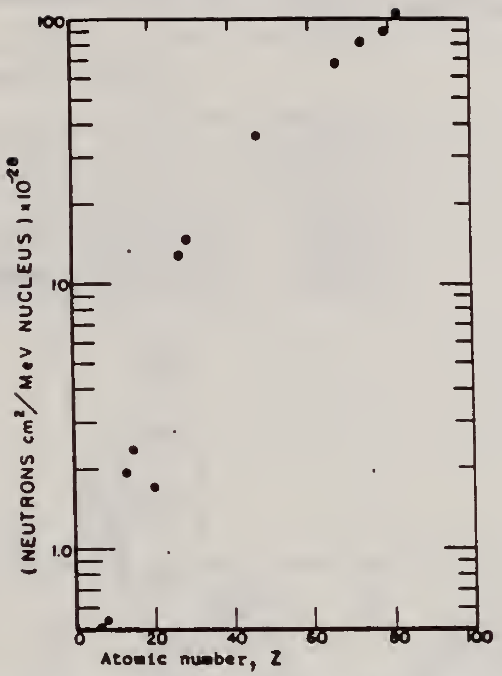

Fig. 31. Absolute neutron yield as a function of atomic number. The neutron yield from calcium ($Z = 20$) is particularly low in comparison with the other elements because its (γ,n) threshold is high compared to the mean energy of the giant resonance.

REF.	ELEM. SYM.	A	Z
S. M. Hussain and K. G. McNeill Can. J. Phys. 45, 2851 (1967)	Pb		82

METHOD	REF. NO.	
	67 Hu 2	EGF

REACTION	RESULT	EXCITATION ENERGY	SOURCE TYPE	SOURCE RANGE	DETECTOR TYPE	DETECTOR RANGE	ANGLE
G,N	ABY	THR-22	C	22	THR	4-	DST

YIELD AT E_0 = 22 MeV

$^{28}Si(n,p)$ ACTIVATION BY PHOTONEUTRONS

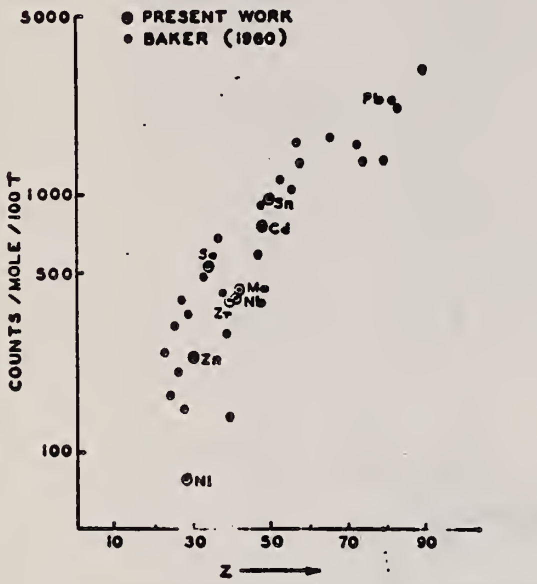

FIG. 3. The yields of fast photoneutrons from various elements as measured in the present work and by Baker. The present results have been normalized to Baker's measurements for lead.

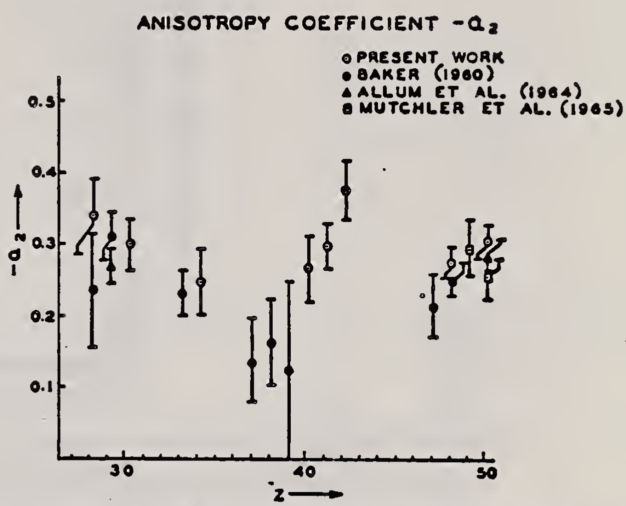

FIG. 2. The anisotropy coefficients a_1, in the formula $W(\theta) = a_0(1 + a_1P_1 + a_2P_2)$, obtained in the present work, and those obtained by other workers in the same part of the Periodic Table.

TABLE I

Element	a_0*	a_1	a_2
Nickel	77 (1.0±0.05)	0.14±0.04	−0.34±0.06
Zinc	236 (1.0±0.04)	0.06±0.03	−0.30±0.04
Selenium	525 (1.0±0.05)	0.10±0.04	−0.25±0.05
Zirconium	380 (1.0±0.05)	0.03±0.04	−0.27±0.05
Niobium	392 (1.0±0.03)	0.01±0.02	−0.30±0.03
Molybdenum	410 (1.0±0.03)	0.05±0.03	−0.41±0.04
Cadmium	755 (1.0±0.02)	0.05±0.01	−0.28±0.02
Tin	955 (1.0±0.02)	0.08±0.02	−0.30±0.02
Lead	2274 (1.0±0.02)	0.06±0.02	−0.48±0.02

*For comparison purposes the experimental value of a_0 for Pb has been normalized to coincide with that obtained by Baker and McNeill (1961) and is the yield per mole per 100 roentgen. All other values of a_0 have also been quoted with the same normalization.

REF.	ELEM. SYM.	A	Z
A. V. Mitrofanova, Yu. N. Ranyuk, and P. V. Sorokin J. Nucl. Phys. (USSR) 6, 703 (1967) Sov. J. Nucl. Phys. 6, 512 (1968)	Pb		82

METHOD	REF. NO.	
	67 Mi 1	HMG

REACTION	RESULT	EXCITATION ENERGY	SOURCE		DETECTOR		ANGLE
			TYPE	RANGE	TYPE	RANGE	
G,F	ABX	300-999		300-999	FRG-I		DST

999 = 1600 MEV

Angular distribution measured for Pb was found isotropic; for other elements it was assumed isotropic.

Nucleus	Fissionability D	Cross section σ_x, $\mu\beta$	Nucleus	Fissionability D	Cross section σ_x, $\mu\beta$
Bi	0.11±0.01	7.8±0.6	Os	0.0058±0.0005	0.37±0.04
Pb	0.050±0.004	3.4±0.3	Re	0.0056±0.0006	0.35±0.04
Tl	0.031±0.003	2.1±0.2	Ta	0.0045±0.0005	0.27±0.03
Au	0.019±0.002	1.25±0.10	Hf	0.0042±0.0004	0.25±0.03
Pt	0.012±0.002	0.80±0.08			

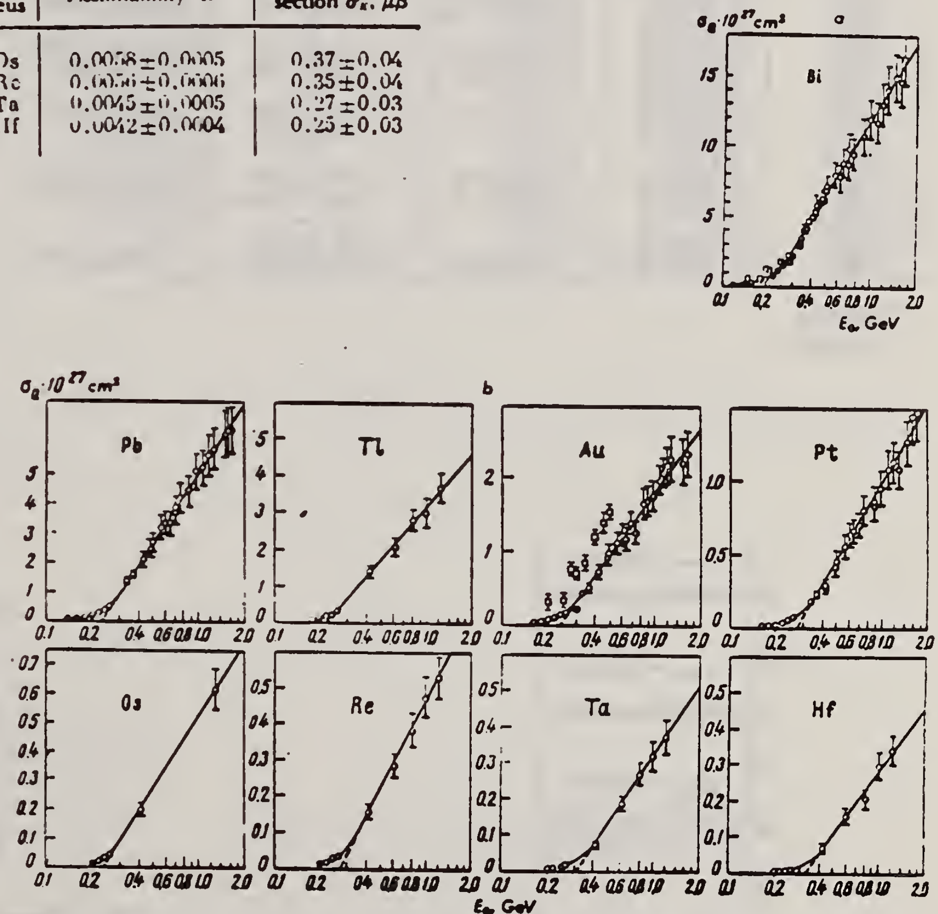

Fig. 1. Photofission fragment yields. O-present work; □-Jungerman and Steiner.[1] The curves were plotted through the experimental points.

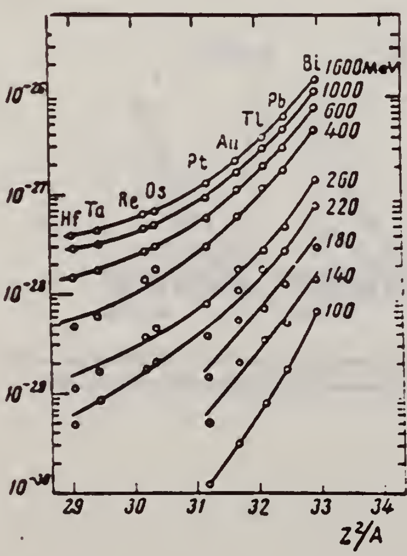

Fig. 2. Photofission fragment yields as a function of Z^2/A. The ordinates are values of σ_q in units of cm².

REF.	ELEM. SYM.	A	Z
Yu. N. Ranyuk and P. V. Sorokin J. Nucl. Phys. (USSR) 5, 37 (1967) Sov. J. Nucl. Phys. 5, 26 (1967)	Pb		82

METHOD	REF. NO.	
	67 Ra 2	HMG

REACTION	RESULT	EXCITATION ENERGY	SOURCE TYPE	SOURCE RANGE	DETECTOR TYPE	DETECTOR RANGE	ANGLE
G,F	ABX	THR-260	C	100-260	EMU-I		DST

Table II

$E_{\gamma max}$, MeV	Cross section per equivalent γ quantum, 10^{-27} cm² Bi	Pb	Au	Pt
100	0.07±0.005	0.017±0.002	0.003±0.0005	0.0012±0.0002
120	0.15±0.01	0.032±0.003	0.014±0.001	0.0035±0.0003
140	0.20±0.01	0.054±0.004	0.020±0.001	0.0053±0.0006
150 *	0.61±0.12	—	—	—
160	0.31±0.01	0.096±0.005	0.037±0.001	0.012±0.0005
180	0.46±0.02	0.13±0.01	0.055±0.001	0.015±0.001
180 *	0.68±0.09	—	—	—
200	0.62±0.02	0.20±0.01	0.082±0.002	0.031±0.001
200 *	1.3 ±0.24	—	0.31±0.09	—
200 **	0.7	—	—	—
220	0.83±0.03	0.28±0.01	0.108±0.003	0.039±0.001
240	1.22±0.03	0.36±0.01	0.146±0.003	0.063±0.001
240 **	1.5	—	—	—
250 *	1.78±0.22	—	0.33 ±0.07	—
260	1.50±0.04	0.50±0.02	0.180±0.004	0.085±0.002

*From [20].
**From [11].

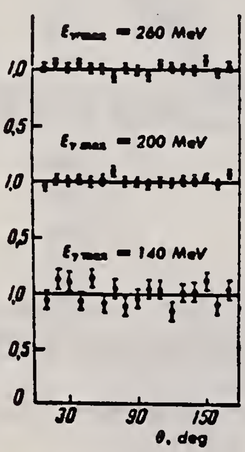

Fig. 2. Angular distributions of fragments (in relative units) from the fission of lead induced by γ rays.

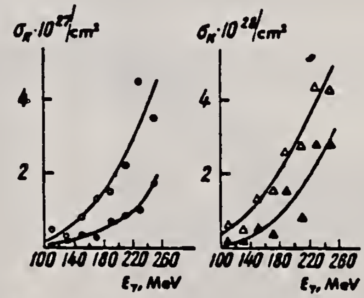

Fig. 3. Photofission cross sections. ○ – Bi, ● – Pb, △ – Au, ▲ – Pt. The curves were calculated from smoothed yield curves.

REF.	ELEM. SYM.	A	Z
J. W. Jury, J. S. Hewitt, and K. G. McNeill Can. J. Phys. 46, 1823 (1968)	Pb		82
METHOD	**REF. NO.** 68 Ju 1		EGF

REACTION	RESULT	EXCITATION ENERGY	SOURCE		DETECTOR		ANGLE
			TYPE	RANGE	TYPE	RANGE	
G,N	NOX	THR-22	C	22	THR	5-	DST

$$W(\theta) = a_o + a_1P_1 + a_2P_2$$

TABLE I

Target element	Z	Energy	a_0*	a_1/a_0	a_2/a_0
Vanadium	23	32	640 ± 50	0.11 ± 0.10	−0.09 ± 0.11
Chromium	24	22	365 ± 39	0.02 ± 0.08	0.00 ± 0.10
Manganese	25	22	450 ± 33	0.07 ± 0.05	−0.11 ± 0.06
Bromine	35	27	874 ± 54	0.05 ± 0.06	−0.15 ± 0.08
Molybdenum	42	22	610 ± 60	0.09 ± 0.05	−0.35 ± 0.06
Ruthenium	44	27	1100 ± 25	0.12 ± 0.02	−0.29 ± 0.03
Rhodium	45	27	1270 ± 47	0.06 ± 0.03	−0.14 ± 0.03
Palladium	46	27	1350 ± 29	0.26 ± 0.02	−0.12 ± 0.02
Antimony	51	27	2140 ± 62	0.04 ± 0.08	−0.25 ± 0.11
Lanthanum	57	27	1940 ± 70	0.12 ± 0.10	−0.52 ± 0.14
Praseodymium	59	30	1800 ± 58	0.20 ± 0.08	−0.40 ± 0.09
Platinum	78	27	2600 ± 52	0.17 ± 0.02	−0.15 ± 0.03
Lead	82	22	2274 ± 59	0.08 ± 0.08	−0.46 ± 0.09

*The yield per mole per 100 r was normalized to a yield of 2274 for the lead sample at the same energy.

REF.	ELEM. SYM.	A	Z
N. N. Kaushal, E. J. Winhold, P. F. Yergin, H. A. Medicus and R. H. Augustson Phys. Rev. 175, 1330 (1968)	Pb		82

METHOD	REF. NO.	
[Page 1 of 2]	68 Ka 1	HMG

REACTION	RESULT	EXCITATION ENERGY	SOURCE TYPE	SOURCE RANGE	DETECTOR TYPE	DETECTOR RANGE	ANGLE
G,N	ABX	50-85	C	55,85	TOF-D	10-85	67
							(67.5)

NEUT ENGY SPEC

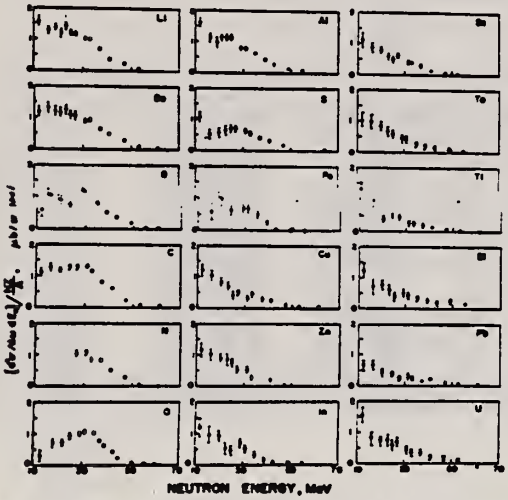

FIG. 6. Observed neutron spectra due to 55–85-MeV difference photon spectra. The effective cross sections have been divided by NZ/A.

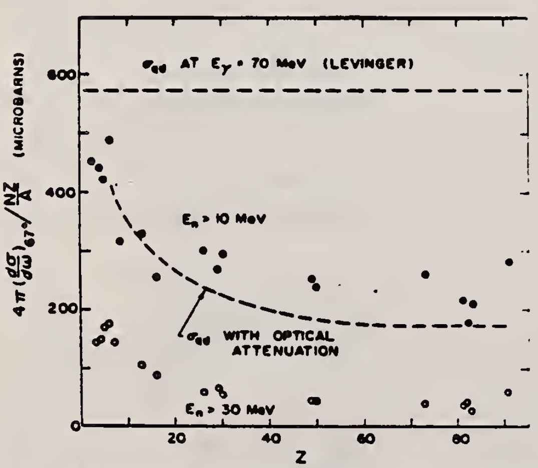

FIG. 7. Effective cross sections for production of fast neutrons with energies greater than 10 MeV (solid circles) and 30 MeV (open circles) by the 55–85-MeV photon difference spectrum. The dashed curves are modified quasideuteron model predictions as discussed in the text.

TABLE I. Comparison of present cross-section values in mb for production of high-energy photoneutrons by 55–85-MeV photons with measured cross sections $\sigma(\gamma,Tn)$, also in mb, for total photoneutron production. The present cross-section values are uncertain by 8 to 10% because of counting statistics and normalization errors; in addition all values depend on an absolute normalization in terms of the deuteron photodisintegration cross section, which is known to about 10% at these energies.

Target	$4\pi(d\sigma/d\omega)_{67°}$ ($E_n>10$ MeV) [Present experiment]	$\sigma(\gamma,Tn)$ Jones and Terwilliger[a]	Costa *et al.*[b]	Other results
Li	0.75		1.0	
Be	1.0	2.7	2.3	2.3[c]
B	1.0		1.4	
C	1.5	1.3	1.4	2.4[d]
O	1.3		1.6	
Al	2.8	5.5	4.6	8[d]
S	2.1		4.4	6.5[d]
Fe	4.2	16	12	
Cu	4.3	20	19	
Zn	4.4		15	
In	7.4			
Sn	7.0			
Ta	10.7	95		
Tl	10.7			
Pb	8.3	100		
Bi	13			
U	16	65		

[a] Average cross sections between 55 and 85 MeV, as read from Figs. 4 and 5 of Ref. 4.
[b] $\int_0^m \sigma dE - \int_0^m \sigma dE/50$, as taken from Fig. 4 of Ref. 5 and Table I of Ref. 6.
[c] S. Costa, L. Pasqualini, G. Piragino, and L. Rossio, Nuovo Cimento 42, 306 (1966).
[d] G. Bishop, S. Costa, S. Ferroni, R. Malvano, and G. Ricco, Nuovo Cimento 42, 148 (1966).

REF.	ELEM. SYM.	A	Z
N. N. Kaushal, E. J. Winhold, P. F. Yergin, H. A. Medicus and R. H. Augustson Phys. Rev. 175, 1330 (1968)	Pb		82
METHOD [Page 2 of 2]	REF. NO. 68 Ka 1		HMG

REACTION	RESULT	EXCITATION ENERGY	SOURCE TYPE	SOURCE RANGE	DETECTOR TYPE	DETECTOR RANGE	ANGLE

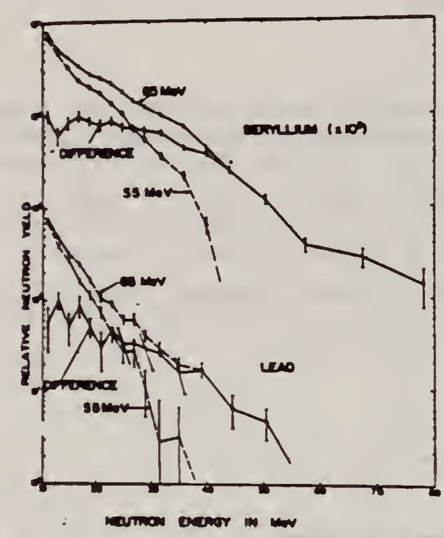

FIG. 5. Neutron energy spectra for beryllium and lead due to 55- and 85-MeV bremsstrahlung, together with the corresponding difference neutron spectra. Error bars indicate statistical errors only.

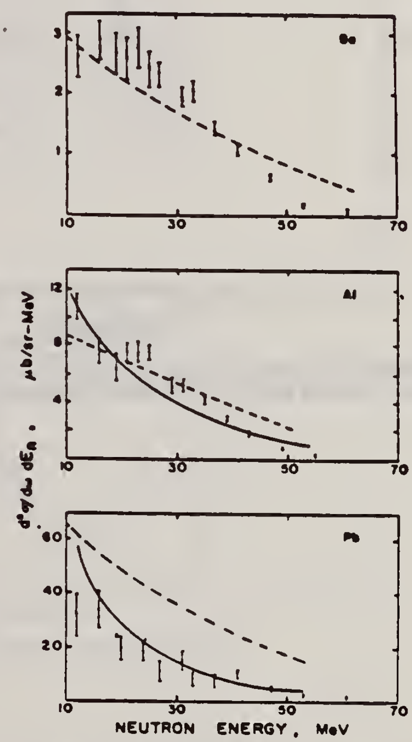

FIG. 8. Neutron energy spectra for beryllium, aluminum, and lead. The dashed curves are Dedrick's quasideuteron model calculations of the primary neutron spectra, arbitrarily multiplied by 1.15. For aluminum and lead these have been modified by estimates of the effects of secondary interactions on the outgoing neutrons, as discussed in the text, to produce the solid curves.

REF.	ELEM. SYM.	A	Z
K. G. McNeill, J. S. Hewitt, and J. W. Jury Can. J. Phys. 46, 1974 (1968)	Pb		82

METHOD	REF. NO.	
	68 Mc 1	egf

REACTION	RESULT	EXCITATION ENERGY	SOURCE TYPE	SOURCE RANGE	DETECTOR TYPE	DETECTOR RANGE	ANGLE
G,XN	NOX	THR-32	C	22-32	THR-I	5-	DST

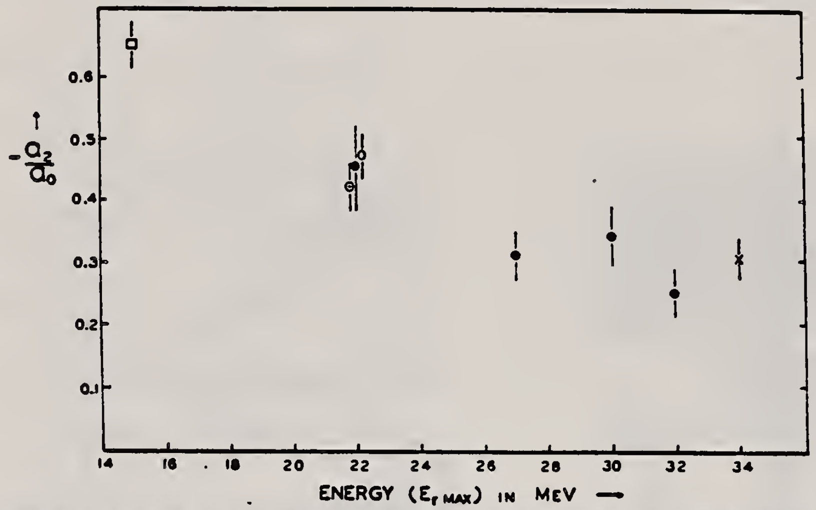

FIG. 1. The variation of anisotropy of fast photoneutrons from lead with maximum X-ray energy: ●, present work; ○, Hussain and McNeill (1967); ⊙, Baker and McNeill (1961); ×, Allum *et al.* (1964); □, Mutchler (1965).

REF.	ELEM. SYM.	A	Z
T. Tomimasu J. Phys. Soc. Japan 25, 655 (1968)	Pb		82
METHOD	REF. NO. 68 To 1		egf

REACTION	RESULT	EXCITATION ENERGY	SOURCE TYPE	SOURCE RANGE	DETECTOR TYPE	DETECTOR RANGE	ANGLE
G,XN	ABX	10-24	C	10-24	BF3-I		4PI

MONITOR CALIBRATIONS

Table II. Parameters of the photoneutron cross sections for natural Cu and Pb. *The contribution of the (γ, p) cross section for Cu was considered.

	K_m (MeV)	σ_m (mb)	Γ (MeV)	$\sigma_0 = \Sigma$ (MeV-mb)	Σ/Σ_0	σ_{-2} (mb/MeV)	$\frac{\sigma_{-2}}{0.00225\ A^{5/3}}$
Cu	17.2 ± 0.3	78 ± 8	8.0 ± 0.5	587 ± 90	0.62 ± 0.1	1.81 ± 0.24	0.75 ± 0.11 (0.95 ± 0.14*)
Pb	14.1 ± 0.3	660 ± 60	5.0 ± 0.2	3910 ± 590	1.32 ± 0.2	18.6 ± 2.4	1.13 ± 0.17

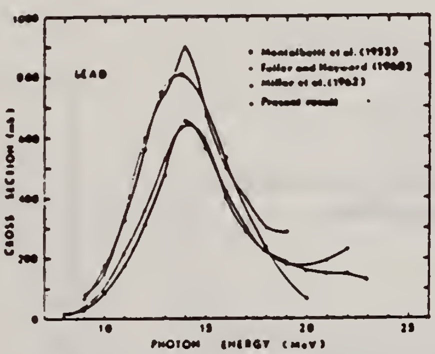

Fig. 13. Comparison of photoneutron cross sections for natural Pb.

REF.	ELEM. SYM.	A	Z
R. Garfagnini, G. Piragino & A. Zanini Atti Accad. Naz. Lincei, Rend. Cl. Sci. Fis. Mat. Natur. 47, 33 (1969)	Pb		82
METHOD	REF. NO.		
	69 Ga 3		egf

REACTION	RESULT	EXCITATION ENERGY	SOURCE		DETECTOR		ANGLE
			TYPE	RANGE	TYPE	RANGE	
G,XN	SPC	8-85	C	85	CCH-D		135

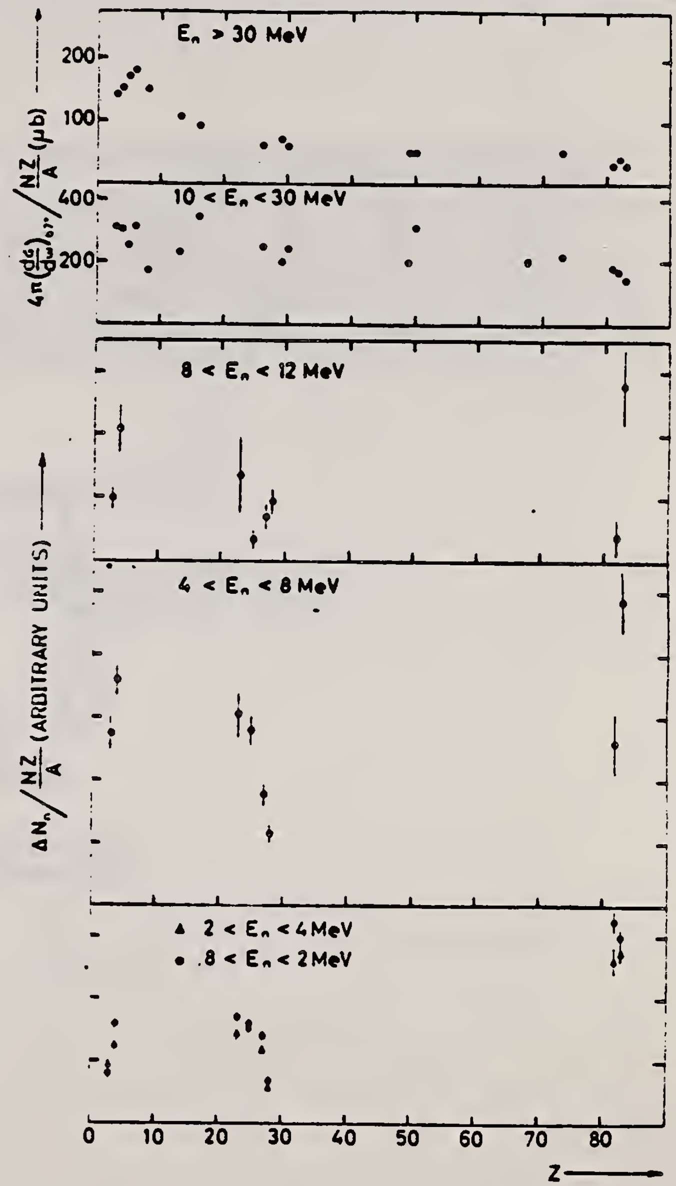

Fig. 2. – Number of photoneutrons emitted at 135°, normalized to the sum rule factor NZ/A, as a function of Z. In the upper part is reported the effective cross section divided by NZ/A for photoproduction of fast neutrons by 55 85 MeV bremsstrahlung photons as deduced by Kaushal *et al.* [1].

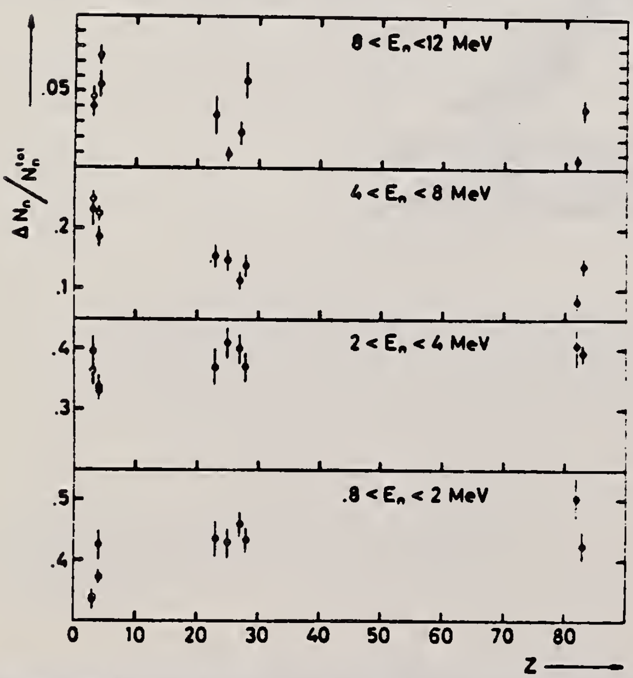

Fig. 1. – Percentage of the photoneutrons emitted at 135°, in the respective energy interval as a function of Z, by a γ-ray bremsstrahlung beam with $E_{\gamma max}$ = 85 MeV. The open circles represent the values obtained at 90° for ^{7}Li and ^{9}Be.

[1] N.N. Kaushal et al., Phys. Rev. 175, 1330 (1968).

REF.
H. Tsubota, N. Fujiwara, H. Ishimaru, E. Tanaka, T. Aizawa, M. Kanazawa and N. Mutsuro
J. Phys. Soc. Japan 26, 1 (1969)

ELEM. SYM.	A	Z
Pb		82

METHOD

REF. NO.	
69 Ts 1	egf

REACTION	RESULT	EXCITATION ENERGY	SOURCE TYPE	SOURCE RANGE	DETECTOR TYPE	DETECTOR RANGE	ANGLE
G,N	NOX	14-26	C	26	SCI-D	7-	DST
				(25.5)			

Paper gives summary of angular distribution measurements.

Table I. A summary of the results.
$W(\theta)=A+B\sin^2\theta+C\cos\theta$

Target	E_{th}(MeV)	A	B	C	B/A	C/A
Bi	7.4	0.65±0.02	0.35±0.11	0.16±0.05	0.55±0.20	0.24±0.10
	8.7	0.66±0.01	0.34±0.06	0.18±0.03	0.51±0.10	0.27±0.06
Pb	7.4	0.45±0.05	0.55±0.11	0.10±0.01	1.22±0.25	0.22±0.04
	8.7	0.75±0.03	0.26±0.03	0.17±0.03	0.22±0.03	0.22±0.03
Ta	7.4	0.69±0.02	0.32±0.03	0.03±0.01	0.46±0.05	0.05±0.02
	8.7	0.80±0.04	0.20±0.02	0.05±0.03	0.25±0.04	0.07±0.04

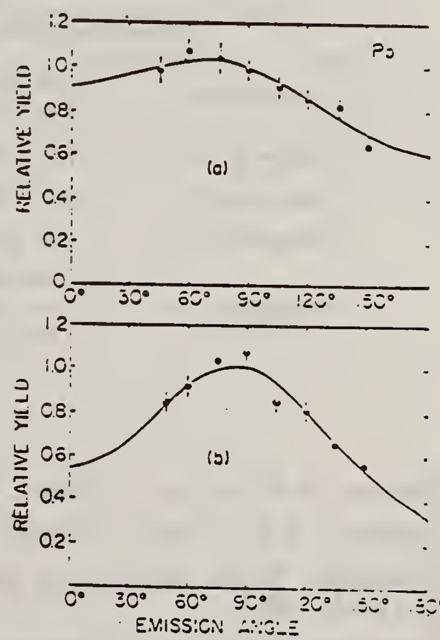

Fig. 5. The angular distributions of fast photo-neutrons from Pb irradiated with 25.5 MeV bremsstrahlung.
(a) The neutron detecting bias energy is set at 8.7 MeV
(b) The neutron detecting bias energy is set at 7.4 MeV.

REF.	ELEM. SYM.	A	Z
I. Kimura, S. A. Hayashi, K. Kobayashi, S. Yamamoto, and T. Shibata Ann. Repts Res. Reactor Inst. Kyoto Univ. <u>3</u>, 75 (1970)	Pb		82
METHOD	REF. NO. 70 Ki 2		egf

REACTION	RESULT	EXCITATION ENERGY	SOURCE TYPE	SOURCE RANGE	DETECTOR TYPE	DETECTOR RANGE	ANGLE
G,XN	SPC	7-18	C	15-18	TOF-D		DST

THICK TARGETS

Table 1. Neutron yield from lead, bismuth, iron, beryllium and uranium targets bombarded by electron beam

Worker	Target	Conversion factor (neutrons/electron)	Electron Energy (MeV)
Present authors	Pb 5×10×10(cm³)	9.5×10⁻⁴	~18
	Bi 5×10×10(cm³)	1.05×10⁻³	~18
	Fe 5×10×10(cm³)	9.3×10⁻⁵	~18
	Be 8.9cm dia.×25cm	2.3×10⁻⁴	~18
	Pb 5×10×10(cm³)	6.5×10⁻⁴	14
Okabe et al.[24]	Pb (22.6g/cm² thick)	1.5×10⁻⁴	13
Feld[25]	Pb (thick)	1.0×10⁻⁴	16
Barber et al.[26]	Pb (22.89g/cm² thick)	7.0×10⁻⁴	14
Coates et al.[6]	U 6cm dia. sphere	2.5×10⁻³	45

Table 2. Nuclear temperature for lead obtained from photoneutron spectrum measurement

Present authors	0.89 MeV (2 MeV to 3.5 MeV)
	1.49 MeV (4 MeV to 7 MeV)
Gayther et al.[9]	0.98 MeV (1 MeV to 4 MeV)
Marco et al.[27]	0.9 MeV (2 MeV to 4 MeV)
Glazunov et al.[14]	0.98 MeV (0.2 MeV to 1.3 MeV)
Verbinski et al.[15]	1.035 MeV (1 MeV to 3.5 MeV) for Pb-208
	1.41 MeV (>3.5 MeV) for Pb-208
	0.92 MeV (1 MeV to 3.5 MeV) for Pb-206

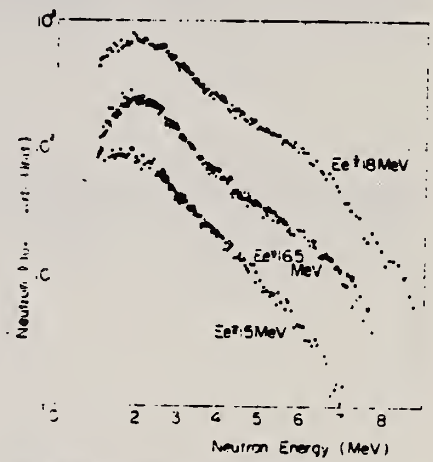

Fig. 5. Energy spectra of photoneutrons from a lead target bombarded by electron beams of three different energies.

[6] Coates, M.S. et al., J. Nucl. Energy, <u>22</u> (1968) 547.

[9] Gayther, D.B. et al., J. Nucl. Energy, <u>21</u> (1967) 733.

[14] Glazunov, Yü.Ya. et al., J. Exp. Theor. Phys. (USSR) <u>46</u> (1964) 1906.

[15] Verbinski, V.V. et al., ORNL-3714, <u>1</u> (1964) 20.

[24] Okabe, S. et al., Ann.Repts. Radiation Center of Osaka, Pref., Japan <u>3</u> (1962) 65.

[26] Barber, W.C. et al., Phys. Rev. <u>116</u> (1956) 1551.

[27] DeMarco et al., Nuovo Cimento, <u>44</u>, 1 (1966) 172.

(over)

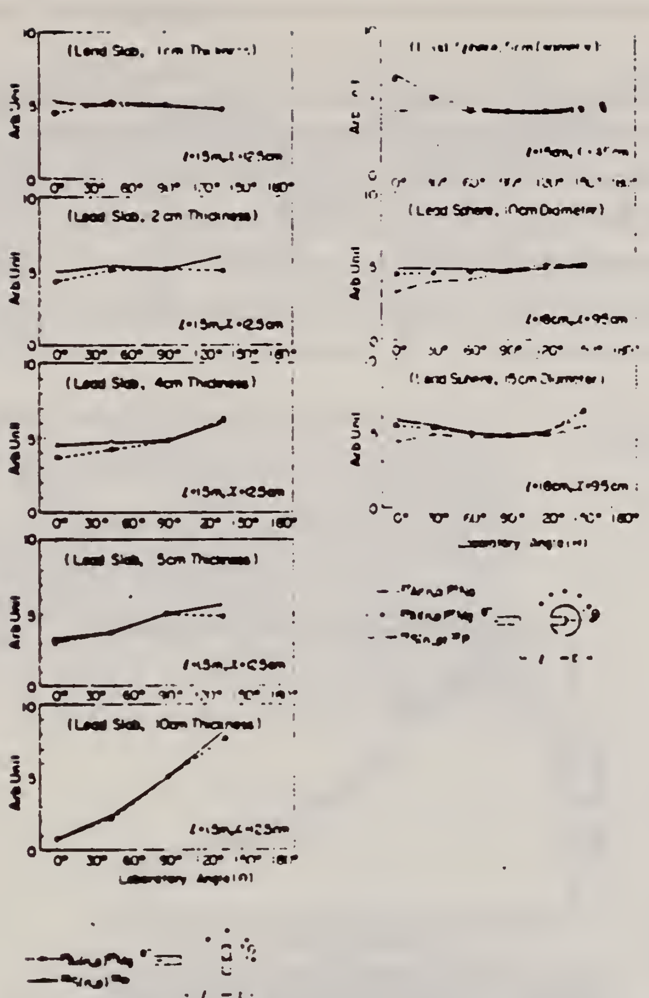

Fig. 4 Angular distribution of photoneutrons from lead targets bombarded by electrons of about 18 MeV, measured by the $^{27}Al(n,p)\,^{27}Mg$, $^{27}Al(n,\alpha)\,^{24}Na$ and $^{32}S(n,p)\,^{32}P$ reactions. The statistical error on each point is about 0.1 %, and it is involved in these circles. The uncertainties of angles on each point are $\Delta\theta = \pm 0.05°$ for 12.5 cm from the center of sources, $\Delta\theta = \pm 0.66°$ for 9.5 cm and $\Delta\theta = \pm 1.38°$ for 4.5 cm.

REF. K. G. McNeill, J. W. Jury, and J. S. Hewitt
Can. J. Phys. 48, 950 (1970)

ELEM. SYM.	A	Z
Pb		82

METHOD

REF. NO.	
70 Mc 1	egf

REACTION	RESULT	EXCITATION ENERGY	SOURCE		DETECTOR		ANGLE
			TYPE	RANGE	TYPE	RANGE	
G,XN	SPC	8-31	C	31	TOF-D	1-6	98

TABLE II

Correlation between peaks in the cross section and the neutron spectrum for the reaction $^{208}Pb(\gamma,n)^{207}Pb$*

Excitation energy from Saclay data, assuming ground state transitions ($E_{threshold}$ = 7.2 MeV) (MeV)	From neutron spectra (present work) (MeV)	From Saclay data via Fig. 2 (MeV)
2.0	1.9	2.0
	2.2	2.3
2.6	2.5	2.6
	2.7	
	2.9	
3.2	3.1	3.2
	3.5	3.4
	3.8	3.7
4.0		
	4.3	4.4

*The error on the experimentally determined neutron energy is in all cases between 70 and 100 kV.

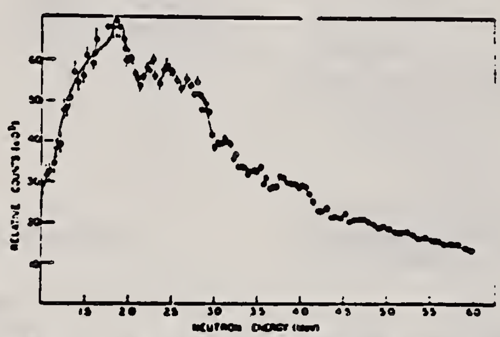

FIG. 2. The photoneutron spectrum obtained by the irradiation of lead by bremsstrahlung of maximum energy 31 MeV, the flight path direction being at 98° to the bremsstrahlung beam. The line is merely to guide the eye.

REF.

Yu. P. Antuf'ev, V. L. Agranovich, V. B. Ganenko, V. S. Kuz'menko, I. I. Miroshnichenko, and P. V. Sorokin
Yad. Fiz. 13, 473 (1971); Sov. J. Nucl. Phys. 13, 265 (1971)

ELEM. SYM.	A	Z
Pb		82

METHOD

REF. NO.	
71 An 1	hmg

REACTION	RESULT	EXCITATION ENERGY	SOURCE TYPE	SOURCE RANGE	DETECTOR TYPE	DETECTOR RANGE	ANGLE
G,P	SPC	37-999	C	700,999	TEL-D	25-400	DST
G,D	SPC	42-999	C	700,999	TEL-D	25-400	DST

999=1.2 GEV, REL D/P

Yield of protons 30-400 MeV, deuterons 30-200 MeV.

Table I. Values of the parameter τ, MeV

Target	E_0 = 700 MeV										E_0 = 1200 MeV					
	Protons					Deuterons					Protons			Deuterons		
	40°	60°	80°	100°	120°	40°	60°	80°	100°	120°	30°	60°	120°	30°	60°	120°
Li	46	42	34	30	27	28	24	22	21	20		45	28		27	24
Be	48	43	36	30	27	28	26	24	22	19		45	28		27	24
C	50	44	38	30	26	34	33	29	23	19	60	48	35	37	34	22
Si		43			28		27			22		46	35		28	25
Ca												45	29		27	24
Ta					28					21		45	34		27	24
Pb											51		29	36		22

The measured secondary-particle spectra for kinetic energies $T > 80$ MeV are well described by the expression

$$d^2\sigma / d\Omega dTQ = \text{const}\, T \exp(-T/\tau), \qquad (1)$$

which is identical to the formula for the evaporation process.[4] In Table I we have given the values of the parameter τ for the nuclei studied, at various angles. The accuracy in determination of τ is about 10%.

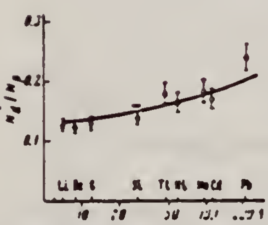

FIG. 4. The ratios N_d/N_p as a function of target-nucleus mass number A at an angle $\theta = 60°$ for E_0 = 1200 MeV. Solid curve—$A^{0.13}$.

V. Emma, S. Lo Nigro and C. Milone
Lettere al Nuovo Cimento 2, 117 (1971)

Pb		82
REF. NO. 71 Em 1		egf

METHOD

REACTION	RESULT	EXCITATION ENERGY	SOURCE TYPE	SOURCE RANGE	DETECTOR TYPE	DETECTOR RANGE	ANGLE
G,F	ABY	THR-999	C	300-999	FRAG-I		4PI

999 = 1000 MEV

TABLE I. – *Fission cross-sections per photon between* 300 *and* 1000 MeV.

	Our results		Previous results	
	σ_k (mb)	$\bar{\sigma}_k$ (mb)	σ_k (mb)	
Bi	7.6 ± 0.2	7.9 ± 1.3	7.8 ± 0.2 (3)	7.8 ± 0.8 (2)
Pb	3.3 ± 0.1	3.2 ± 1.5	3.4 ± 0.3 (3)	

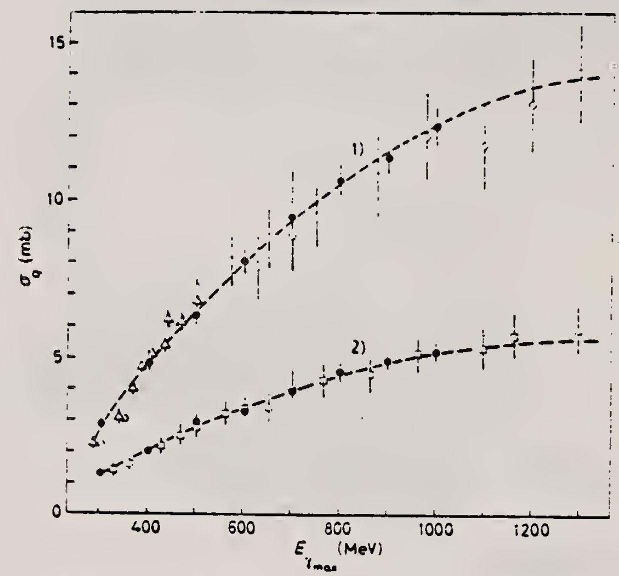

Fig. [illegible] – Our experimental data of the photofission cross-section per equivalent quantum for Bi and Pb compared with previous results. Experimental points: ● our data calculated as mean values of the results obtained with thin and thick targets; △ ref. (1); ○, □ ref. (2). The dashed lines are the best curves calculated by the least-squares method taking into account our results only. 1) Bi, 2) Pb.

(1) J. A. Jungerman and H. M. Steiner: *Phys. Rev.*, 106, 585 (1957).
(2) H. G. de Carvalho, G. Cortini, E. Del Giudice, G. Potenza and R. Rinzivillo: *Nuovo Cimento*, 32, 293 (1964).
(3) A. V. Mitrofanova, Yu. N. Ranyuk and P. V. Sorokin: *Sov. Journ. Nucl. Phys.*, 6, 512 (1968).

REF.	ELEM. SYM.	A	Z
I.A. Grishaev, A.N. Krinitsyn, N.I. Lapin, V.I. Nikiforov, G.D. Pugachev, and B.I. Shramenko Yad. Fiz. 14, 35 (1971) Sov. J. Nucl. Phys. 14, 20 (1972)	Pb		82
METHOD	REF. NO. 71 Gr 2		hmg

REACTION	RESULT	EXCITATION ENERGY	SOURCE TYPE	SOURCE RANGE	DETECTOR TYPE	DETECTOR RANGE	ANGLE
G,PI+	ABY	150-560		560	EMU-D		DST
G,PI-	ABY	150-560		560	EMU-D		DST

PI-/PI+ YIELD RATIO

Cross section for photoproduction of π^- and π^+ mesons for E_e = 560 MeV

Nucleus	10^{-30} cm²/sr·MeV·equiv-quant						
	θ = 60°			θ = 120°			
	Data of ref. 7, T = 33 MeV	Our data, T = 40 MeV		Our data			
				T = 40 MeV		T = 60 MeV	
	π^+	π^+	π^-	π^+	π^-	π^+	π^-
C	21.4±0.8	20.6±1.8	28.2±2	27.6±2.1	36.8±2.8	21.6±2.1	26.8±2.6
Al	42.4±1.0	36.5±3	47.5±4	57±4	76±5.4	40.2±3.5	52±4.7
Cu	78.8±1.6	71.6±5.8	98±8.6	109±7.5	152±10.8	91.5±8.6	93.5±10.7
Pb				208±18.5	309±27	170±19	290±26.5

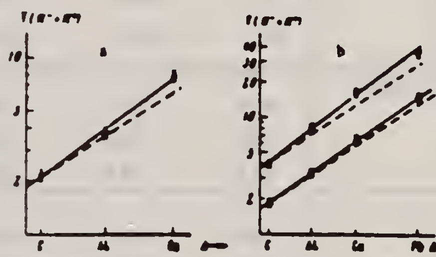

FIG. 1. Total yield of charged mesons as a function of atomic weight. The solid straight line is the experimental dependence, and the dashed straight line is the $A^{2/3}$ law. a – ϑ = 60°, T = 40 MeV; b – ϑ = 120°. Points: O – T = 40 MeV, Δ – T = 65 MeV.

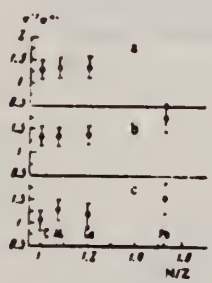

FIG. 3. π^-/π^+ yield ratio as a function of N/Z. a – ϑ = 60°, T = 40 MeV, b – ϑ = 120°, T = 40 MeV; c – ϑ = 120°, T = 65 MeV

REF.	ELEM. SYM.	A	Z
J. Maly Phys. Letters 35B, 148 (1971)	Pb		82

METHOD	REF. NO.	
	71 Ma 2	egf

REACTION	RESULT	EXCITATION ENERGY	SOURCE TYPE	SOURCE RANGE	DETECTOR TYPE	DETECTOR RANGE	ANGLE
E,F	SPC	THR-999	D	500,999	FRG-I		4PI

999 = 1.3 GEV

Table 1
Estimated energies and cross-sections of fission fragment formations produced by 1300 MeV electrons (detected on (B) foils)

Range in mylar (μm) (passing foil No.)	Estimated energy of fragment in MeV $A = 25$, $Z = 10$	$A = 50$, $Z = 20$	$A = 75$, $Z = 30$	$A = 100$, $Z = 40$	Cross section in μb U	Pb	W
(0.foil)					3×10^{5}	6×10^{3}	400
55 μm (4. foil)	79	185	294	391	1.7	2.2	4.1
67 μm (5. foil)	89	222	362	484	1.8	1.0	1.2
79 μm (6. foil)	105	260	422	576	3.6	1.2	1.8
E_{kin} from Q values (MeV)					Kinetic energy from fission of:		
	23.6	60.1	60.0	49.8	^{186}W		
	22.4	61.6	80.0	66.9	^{208}Pb		
	49.2	92.0	111.0	111.3	^{238}U		
B_{lab} (MeV)					B_{lab} for fusion with:		
	92.6	192	302	433	^{186}W		
	99.7	203.5	315	442	^{208}Pb		
	107	209	334	462	^{238}U		

[over]

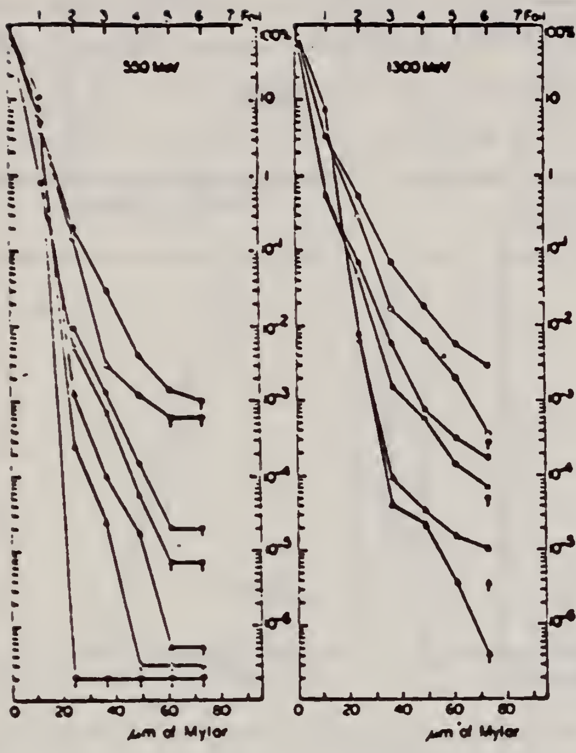

Fig. 1. Penetration of fission fragments through mylar foils from fission induced in U, Pb and W by electrons and bremsstrahlung. Explanation of symbols:
Cf spontaneous fission O; U fission front foils Δ and back foils ▲; Pb fission front foils ☐ and back foils ▣; W fission front foils ○ and back foils ● .
Symbols with arrows (e.g. ⊙) denote background level.

REF.	ELEM. SYM.	A	Z
T. Methasiri and S. A. E. Johansson Nucl. Phys. A167, 97 (1971)	Pb		82

METHOD	REF. NO.	
	71 Me 1	egf

REACTION	RESULT	EXCITATION ENERGY	SOURCE TYPE	SOURCE RANGE	DETECTOR TYPE	DETECTOR RANGE	ANGLE
G,F	ABY	THR-900	C	300-900	FRG-I		4PI

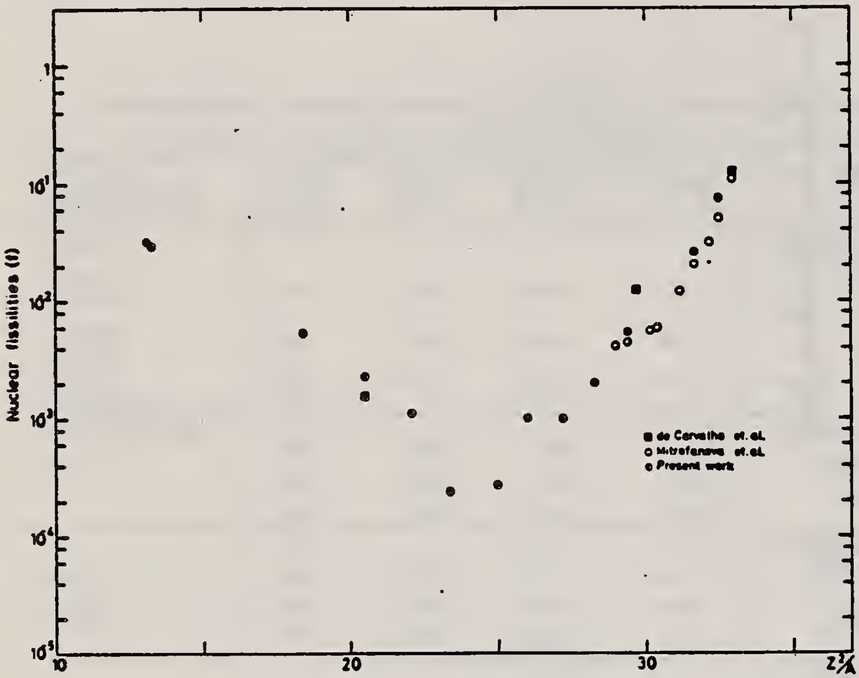

Fig. 2. Nuclear fissilities as a function of Z^2/A.

Table 1

The constant fission cross sections above the threshold

Element	σ_f (cm²)	Element	σ_f (cm²)
Pb	$(5.0\pm0.2)\times10^{-27}$	La	$(1.1\pm0.1)\times10^{-29}$
Au	$(1.7\pm0.1)\times10^{-27}$	Sn	$(4.3\pm1.1)\times10^{-29}$
Ta	$(3.3\pm0.2)\times10^{-28}$	Ag	$(8.4\pm2.0)\times10^{-29}$
Yb	$(1.2\pm0.2)\times10^{-28}$	Mo	$(1.7\pm0.4)\times10^{-28}$
Ho	$(5.5\pm0.3)\times10^{-29}$	Cu	$(6.6\pm1.2)\times10^{-28}$
Gd	$(5.3\pm0.8)\times10^{-29}$	Ni	$(5.8\pm0.1)\times10^{-28}$
Nd	$(1.3\pm0.2)\times10^{-29}$		

[over]

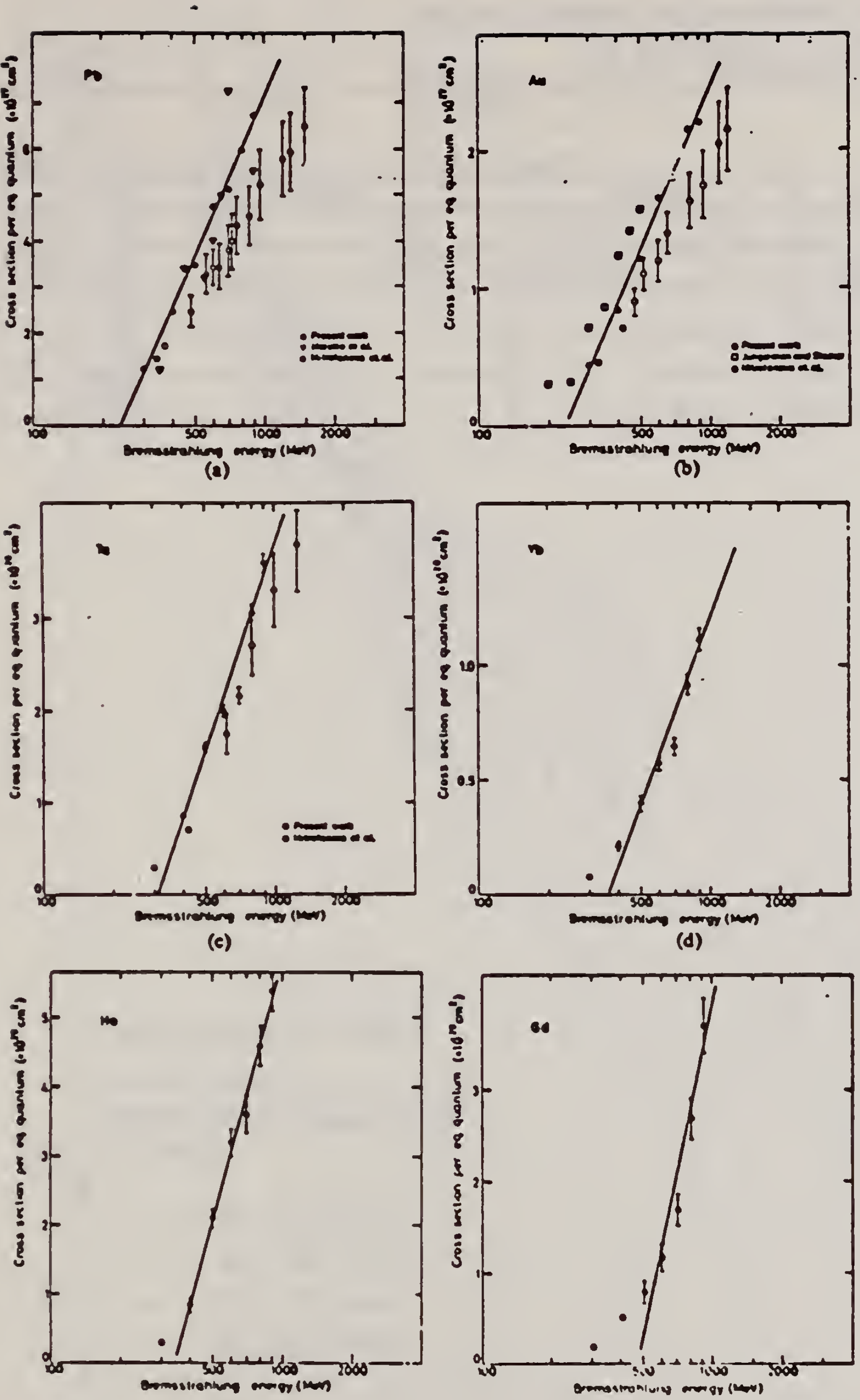

Fig. 1. Cross sections per equivalent quantum $\sigma_q(\bar{E})$ as a function of log $\bar{E}$.

REF.		ELEM. SYM.	A	Z
	H. J. Von Eyss, H. Schier, and B. Schoch Elba-71, Tagungsbericht Elektronen Beschleuniger Arbeits Gruppen (Sept. 1971) Justus Liebig-Universitat Giessen. p. 391	Pb		82
METHOD	Page 1 of 2.	REF. NO. 71 Vo 1		hmg

REACTION	RESULT	EXCITATION ENERGY	SOURCE		DETECTOR		ANGLE
			TYPE	RANGE	TYPE	RANGE	
E,N	ABX	THR-266	C	150-266	TOF-D		90

Over for figure.

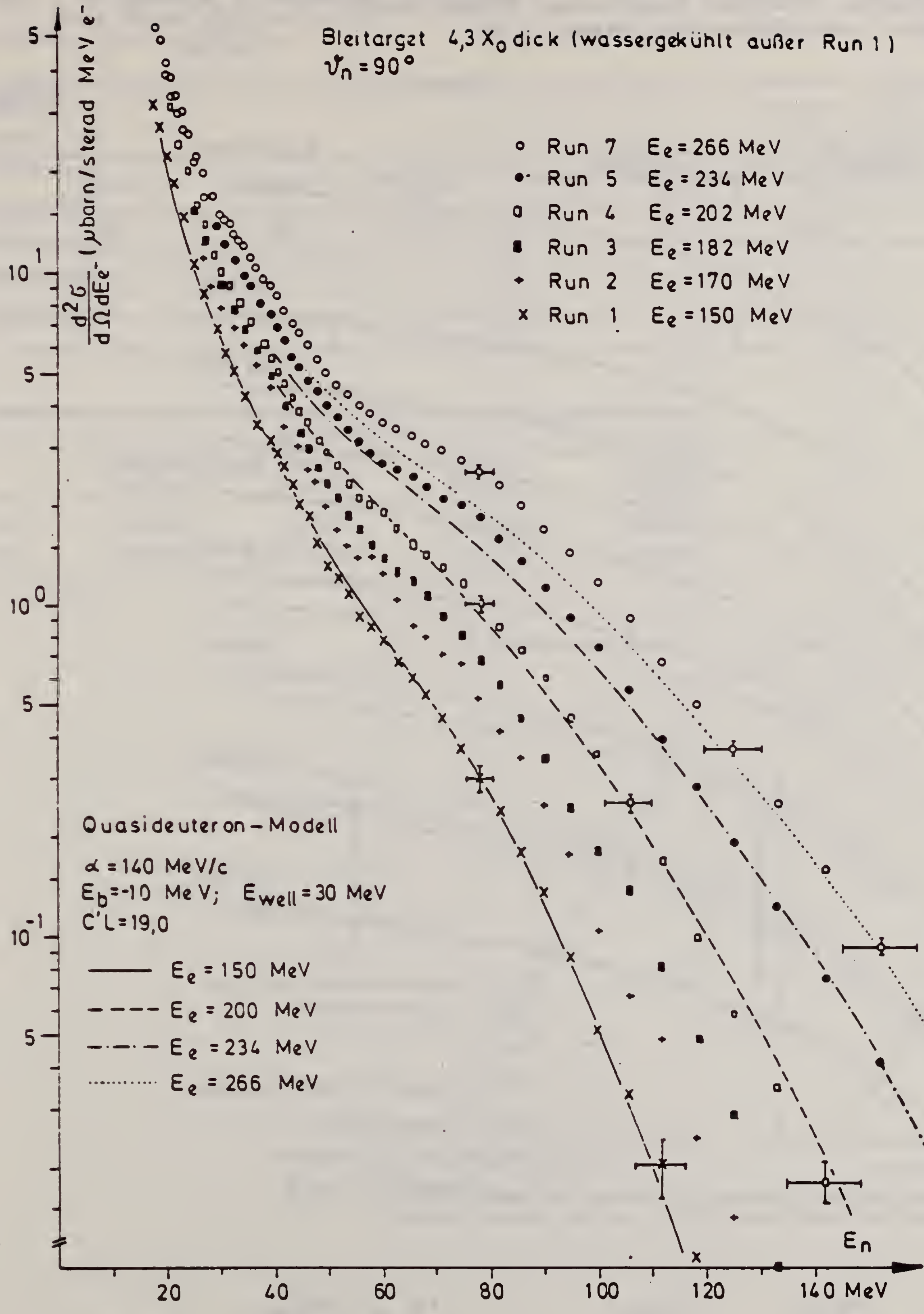

Figur 2: Differentieller Neutronenproduktions-Wirkungsquerschnitt der Runserie 1 als Funktion der Neutronenenergie für verschiedene Primärelektronenenergien

REF

H. J. Von Eyss, H. Schier, and B. Schoch
Elba-71, Tagungsbericht Elektronen Beschleuniger Arbeits Gruppen
(Sept. 1971) Justus Liebig-Universitat Giessen, p.391

ELEM. SYM.	A	Z
Pb		82
REF. NO.		
71 Vo 1		hmg

METHOD

ANGLE

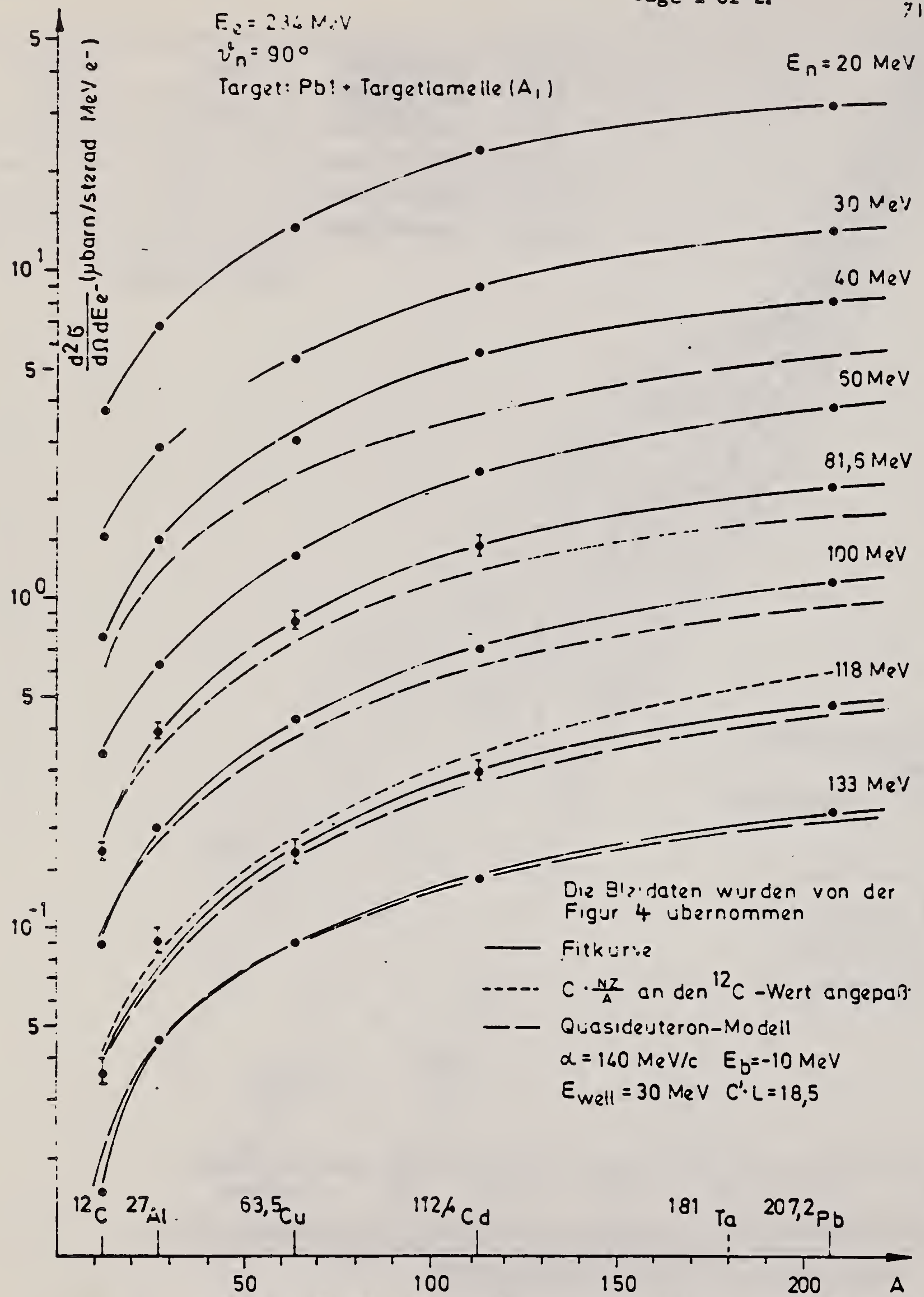

Figur 3: Differentieller Neutronenproduktions-Wirkungsquerschnitt als Funktion der Massenzahl A für einige Neutronenenergien

REF. G. Andersson, L. Blomqvist, B. Forkman, G. G. Jonsson, A. Jarund, I. Kroon, K. Lindgren and B. Schroder
Nucl. Phys. A197, 44 (1972)

ELEM. SYM.	A	Z
Pb		82

METHOD

REF. NO. 72 An 8 egf

REACTION	RESULT	EXCITATION ENERGY	SOURCE TYPE	SOURCE RANGE	DETECTOR TYPE	DETECTOR RANGE	ANGLE
G,F	ABX	1- 7	C	1- 7	ACT-I		4PI

ENERGIES GEV

TABLE 3
Experimental mean photofission cross sections $\bar{\sigma}_f$ (mb) from refs. [8,18,31]) compared to the results of the present work

	Present work 0.3–7.4 GeV	Ref. [18]) 0.3–0.9 GeV	Ref. [31]) 0.3–1.0 GeV	Ref. [8]) 0.3–1.6 GeV
Au	1.44±0.10	1.7±0.1	1.19±0.06	1.25±0.1
Pb	3.8 ±0.3	5.0±0.2	3.3 ±0.1	3.4 ±0.3

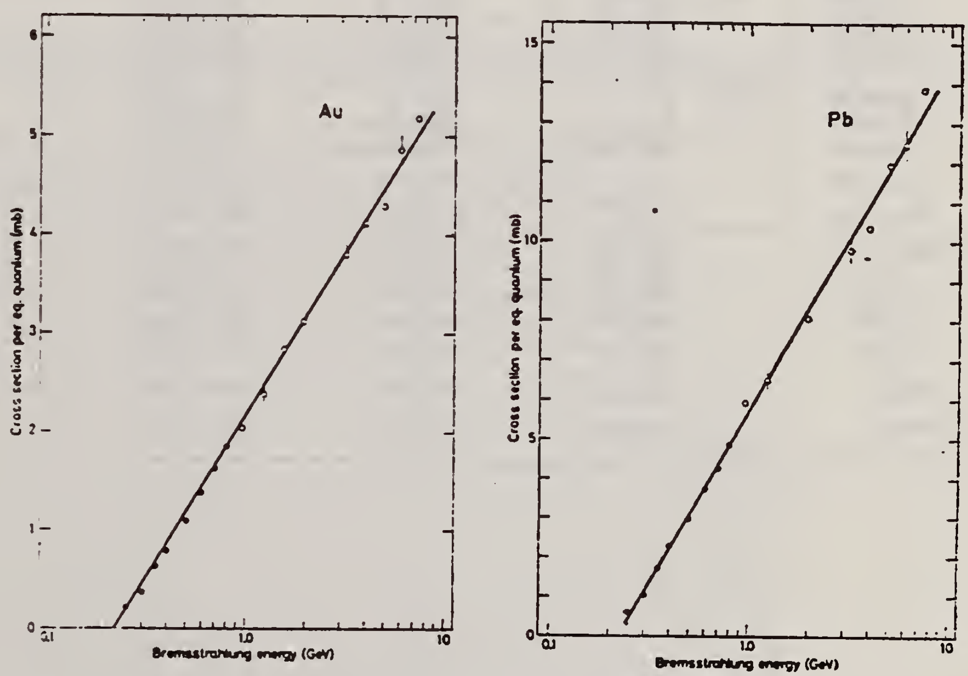

Fig. 17. The gold and lead photofission cross sections per equivalent quantum σ_q as a function of bremsstrahlung peak energy E_{max}. The filled points are taken from our earlier experiment [19]).

(over)

Table 6

Partial reaction cross sections relative to the total photoabsorption cross section, σ/σ_{tot} (in %)

Reaction	0.3 GeV	1.0 GeV	5.0 GeV
$^{12}C(\gamma, n)$	10 ± 5	6.8 ± 3.4	0 ± 5
$^{27}Al(\gamma, \pi^+)$	0.2 ± 0.1	0.1 ± 0.1	0.04 ± 0.02
$(\gamma, 2pn)$	1.7 ± 0.9	1.5 ± 0.8	1.7 ± 0.6
$^{127}I(\gamma, 3n)$	1.6 ± 0.8	0 ± 3	5.5 ± 2.8
$(\gamma, 6n)$	0.9 ± 0.5	1.2 ± 0.6	1.5 ± 0.8
$(\gamma, 7n)$	0.9 ± 0.5	0.5 ± 0.3	0.1 ± 0.1
$(\gamma, 8n)$	0.7 ± 0.4	0.6 ± 0.3	0.4 ± 0.2
$(\gamma, 9n)$	0.3 ± 0.2	0.2 ± 0.1	0.5 ± 0.3
$\Sigma(\gamma, xn)$	4.4 ± 2.2	2.6 ± 1.3	7.8 ± 3.9
$(\gamma, p5n)$	1.7 ± 0.9	1.7 ± 0.9	0.9 ± 0.5
$(\gamma, p7n)$	1.9 ± 1.0	2.1 ± 1.1	0.9 ± 0.5
$(\gamma, p9n)$	1.6 ± 0.8	1.6 ± 0.8	1.3 ± 0.7
$\Sigma(\gamma, pxn)$	5.2 ± 2.6	5.4 ± 2.7	3.1 ± 1.6
$(\gamma, 2p3n)$	0.6 ± 0.3	0.3 ± 0.2	0.3 ± 0.2
$(\gamma, 2p5n)$	0.5 ± 0.3	0.6 ± 0.3	0.8 ± 0.4
$(\gamma, 2p7n)$	1.3 ± 0.7	1.0 ± 0.5	0.4 ± 0.2
$(\gamma, 2p9n)$	1.1 ± 0.6	1.7 ± 0.9	2.4 ± 1.2
$(\gamma, 2p10n)$	2.7 ± 1.4	1.9 ± 1.0	5.0 ± 2.5
$\Sigma(\gamma, 2pxn)$	6.3 ± 3.2	5.6 ± 2.8	8.8 ± 4.4
$(\gamma, 4p12n)$	1.5 ± 0.8	2.4 ± 1.2	2.0 ± 1.0
$(\gamma, 4p14n)$	0.8 ± 0.4	1.9 ± 1.0	2.5 ± 1.3
$(\gamma, 4p15n)$	0.4 ± 0.2	0.6 ± 0.3	1.5 ± 0.8
$\Sigma(\gamma, 4pxn)$	2.7 ± 1.4	4.9 ± 2.5	6.0 ± 3.0
$(\gamma, 6p17n)$		0.5 ± 0.3	1.5 ± 0.8
$(\gamma, 6p18n)$	0.1 ± 0.1	0.2 ± 0.1	0.1 ± 0.1
$\Sigma(\gamma, 6pxn)$	0.1 ± 0.1	0.7 ± 0.4	1.6 ± 0.8
$(\gamma, 8p18n)$		0.8 ± 0.4	2.5 ± 1.3
$\Sigma(\gamma, ypxn)$	19 ± 10	20 ± 10	30 ± 15
$^{197}Au(\gamma, 3n)$	0.9 ± 0.5	2.2 ± 1.1	1.5 ± 0.8
$(\gamma, 7n)$	0.8 ± 0.4	1.3 ± 0.7	2.4 ± 1.2
$(\gamma, 9n)$	0.8 ± 0.4	0.6 ± 0.3	0.3 ± 0.2
$(\gamma, 11n)$	0.4 ± 0.2	0.9 ± 0.5	0.5 ± 0.3
$\Sigma(\gamma, xn)$	2.9 ± 1.5	5.1 ± 2.6	4.6 ± 2.3
$Au(\gamma, f)$	1.5 ± 0.4	2.7 ± 0.7	6.9 ± 2.0
$Pb(\gamma, f)$	3.1 ± 0.8	6.9 ± 1.7	17 ± 5

REF.	V.P. Kovalev, V.P. Kharits, V.V. Gordeev, V.I. Isaev (USSR) Atomnaya Energiya 32, 496 (1972)	ELEM. SYM.	A	Z
		Pb		82
METHOD		REF. NO.		
		72 Ko 8		hmg

REACTION	RESULT	EXCITATION ENERGY	SOURCE TYPE	SOURCE RANGE	DETECTOR TYPE	DETECTOR RANGE	ANGLE
G,N	NOX	6- 22	C	22	THR-I		DST

Мишень	Энергии электронов, Мэв	Детектор	Угол, град							В/А
			30	50	70	90	110	130	150	
Al	22,5	$P^{31}(n,p)$	1,05±0,08	1,03±0,08	0,97±0,08	1,0±0,08	0,98±0,08	1,02±0,08	1,04±0,08	Изотропное
	22,5	$Al^{27}(n,p)$	0,99±0,15	0,95±0,15	1,02±0,15	1,00±0,14	0,96±0,13	1,07±0,13	1,01±0,13	»
Ti	22,5	$P^{31}(n,p)$	1,04±0,07	0,96±0,07	1,03±0,07	1,00±0,07	0,98±0,07	1,05±0,07	1,03±0,07	»
	22,5	$Al^{27}(n,p)$	1,06±0,13	0,94±0,13	1,04±0,12	1,00±0,12	0,95±0,11	0,98±0,11	1,02±0,10	»
Cu	12,8	$P^{31}(n,p)$	0,97±0,10	1,04±0,10	1,02±0,10	1,00±0,10	1,01±0,10	0,99±0,10	0,96±0,10	»
	17,0	$P^{31}(n,p)$	1,03±0,07	0,97±0,07	1,00±0,07	1,00±0,07	1,06±0,07	0,95±0,07	0,88±0,07	»
	22,5	$P^{31}(n,p)$	0,87±0,05	0,94±0,05	0,97±0,05	1,00±0,05	0,99±0,05	0,93±0,05	0,91±0,05	0,18±0,04
	22,5	$Al^{27}(n,p)$	0,75±0,09	0,86±0,07	0,98±0,06	1,00±0,05	1,02±0,05	0,94±0,04	0,90±0,04	0,28±0,06
Mo	22,5	$P^{31}(n,p)$	0,99±0,05	0,93±0,05	0,98±0,05	1,00±0,05	0,99±0,05	0,92±0,05	0,84±0,05	0,21±0,04
	22,5	$Al^{27}(n,p)$	0,80±0,08	0,95±0,08	0,95±0,07	1,00±0,06	0,94±0,05	0,83±0,04	0,72±0,04	0,44±0,08
	22,5	$Al^{27}(n,\alpha)$	0,72±0,08	0,84±0,08	0,89±0,08	1,00±0,08	0,95±0,08	0,87±0,08	0,63±0,08	0,78±0,18
W	22,5	$P^{31}(n,p)$	0,85±0,04	0,99±0,04	0,98±0,04	1,00±0,04	0,98±0,04	0,92±0,04	0,087±0,04	0,25±0,04
	22,5	$Al^{27}(n,p)$	0,78±0,06	0,84±0,06	0,89±0,05	1,00±0,05	0,97±0,04	0,86±0,04	0,75±0,04	0,54±0,06
Pb	22,5	$P^{31}(n,p)$	0,79±0,04	0,85±0,04	0,96±0,04	1,00±0,04	0,93±0,04	0,88±0,04	0,84±0,04	0,36±0,05
	22,5	$Al^{27}(n,p)$	0,70±0,09	0,81±0,08	0,94±0,07	1,00±0,06	0,94±0,06	0,80±0,05	0,69±0,05	0,69±0,12

(over)

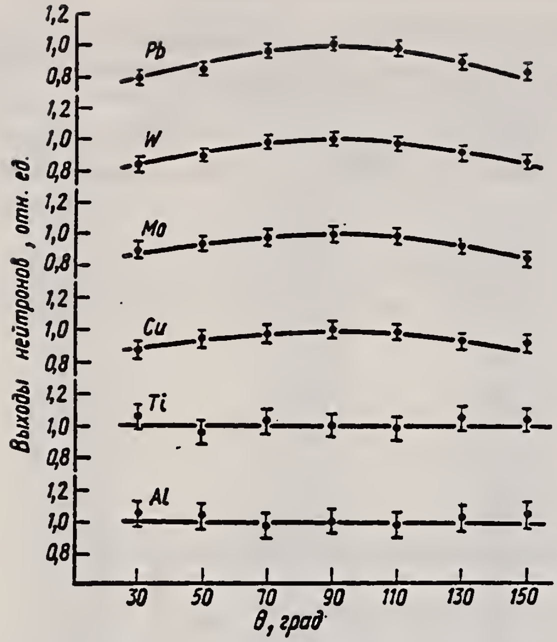

Угловые распределения быстрых фотонейтронов на Al, Ti, Cu, Mg, W, Pb, облучаемых электронами с энергией 22,5 *Мэв*. Детектор P^{31} (*n*, *p*) Si^{31}.

REF.	ELEM. SYM.	A	Z
I. Kroon and B. Forkman Nucl. Phys. A179, 141 (1972)	Pb		82
METHOD	REF. NO. 72 Kr 3		egf

REACTION	RESULT	EXCITATION ENERGY	SOURCE TYPE	SOURCE RANGE	DETECTOR TYPE	DETECTOR RANGE	ANGLE
G,F	ABY	THR-999	C	350-999	TRK-I		DST

999 = 1 GEV

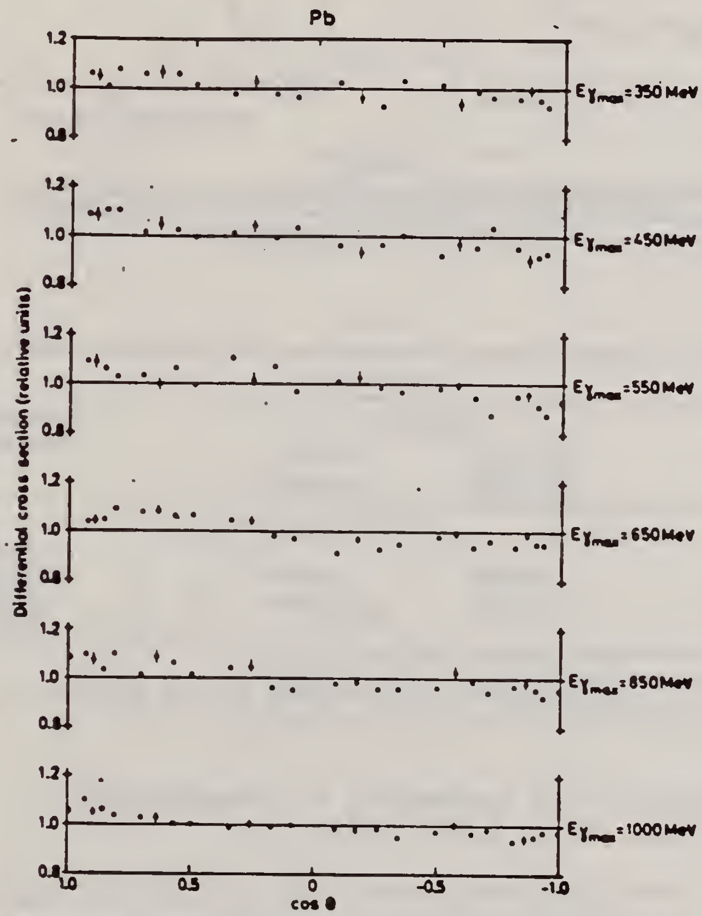

Fig. 2. The differential lead cross section per unit solid angle in relative units as a function of cos θ where θ is the angle between beam and fragment directions for bremsstrahlung energies indicated.

(over)

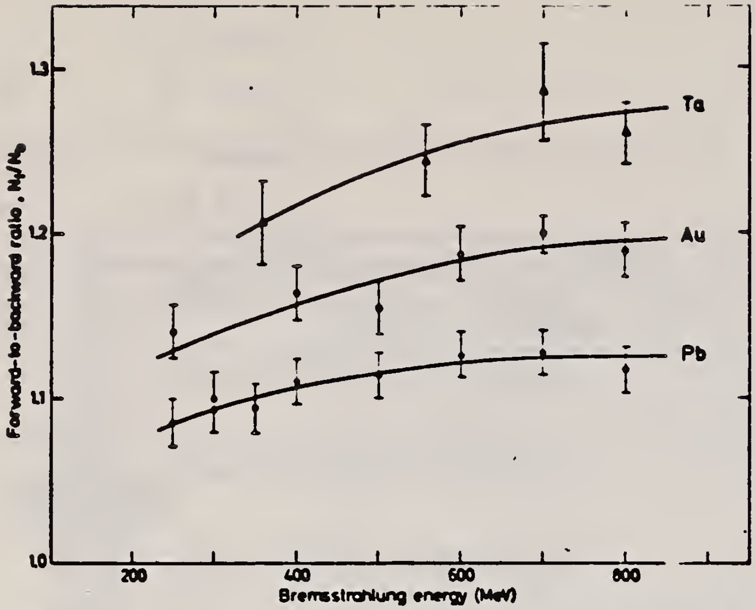

Fig. 4. The tantalum, gold and lead forward-to-backward ratios as a function of bremsstrahlung energy.

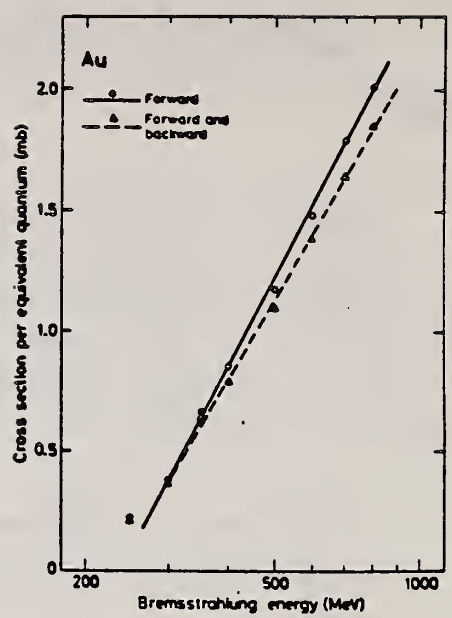

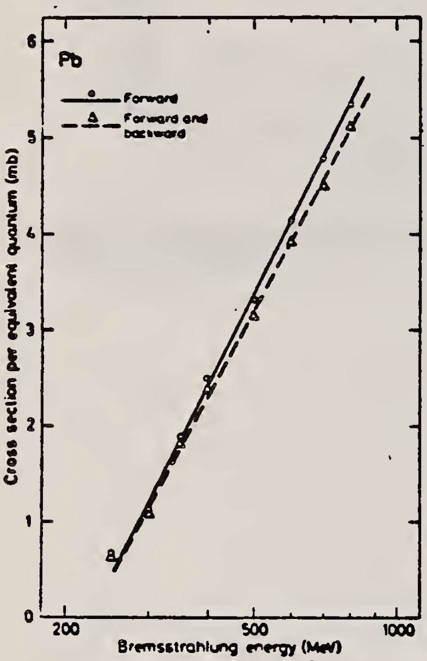

Figs. 5 and 6. The lead and gold photofission cross section per equivalent quantum as a function of bremsstrahlung energy calculated from the number of fission fragment tracks in the forward glass plate (full curve). The corrected cross sections are also shown (dashed curve).

TABLE 1

Ratios between the number of fragments in the forward and backward directions recorded in glass detectors, N_f/N_b

Element	Present work		Proton sandwich experiment [c])
	from angular distribution [a])	sandwich experiment [b])	
Ta		1.29 ± 0.04	
Re			1.42 ± 0.08
Au	1.19 ± 0.02	1.20 ± 0.01	1.45 ± 0.07
Pb	1.11 ± 0.02	1.13 ± 0.01	1.61 ± 0.15
^{238}U			1.26 ± 0.05

[a]) Ratios calculated from the angular distributions at 700 MeV.
[b]) Ratios obtained with the sandwich technique, 700 MeV for Au and Pb, 800 MeV for Ta.
[c]) From ref. [9]). Proton induced fission at proton energy 660 MeV.

9
V.A. Kon'shin, E.S. Matusevich, V.I. Regushevskii, Sov. J. Nucl. Phys. 2, 489 (1966).

REF.

R.F. Barrett, J.R. Birkelund, B.J. Thomas, K.S. Lam, and H.H. Thies
Nucl. Phys. A210, 355 (1973)

ELEM. SYM.	A	Z
Pb		82

METHOD

REF. NO.	
73 Ba 20	egf

REACTION	RESULT	EXCITATION ENERGY	SOURCE TYPE	SOURCE RANGE	DETECTOR TYPE	DETECTOR RANGE	ANGLE
G,N	NOX	THR- 27	C	10- 27	BF3-I		4PI

MEAN NEUT ENERGY

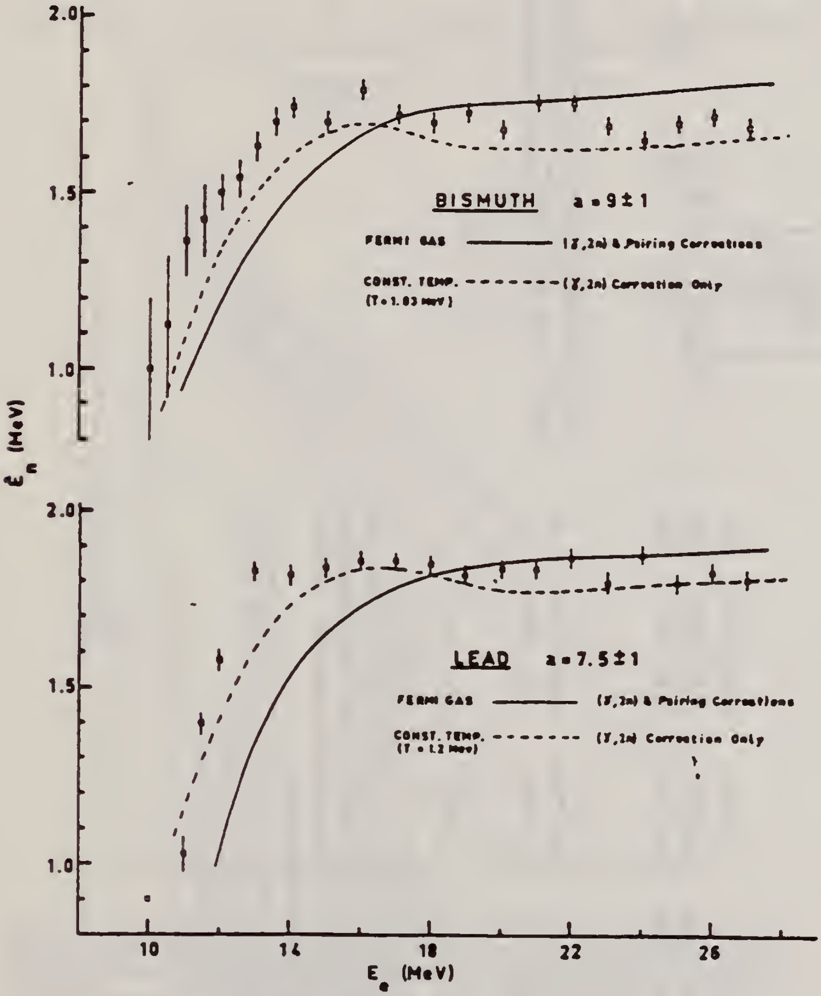

Fig. 11. Same as fig. 5, for lead and bismuth.

1
H. Baba and S. Baba, 'Japan Atomic Energy Research Institute report JAERI-1183 (1969).
2
H. Baba, Nucl. Phys. A159, 625 (1970).
15
T.D. Newton, Can. J. Phys. 34, 804 (1956).

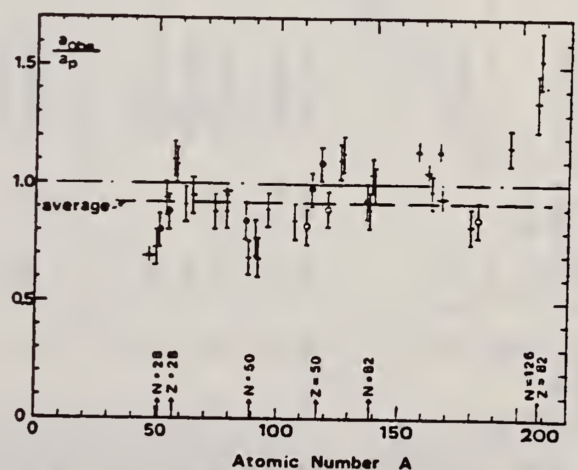

Fig. 15. Ratio a_{obs}/a_p versus atomic number A. Here a_{obs} is the level density parameter taken from the neutron resonance work of refs. [1,2]), and a_p is the level density parameter derived from the present (γ, n) work. Filled circles represent points where nuclei in the neutron resonance and in the (γ, n) experiment were the same. Open circles represent points where the respective nuclei were approximately matched. Triangles represent points which are based on measurement of neutron mean energies at two bremsstrahlung energies only.

(over)

Table 3 (continued)

Target	N (residual nucleus)[a]	Goodness of fit[b] no p.c.	Goodness of fit[b] with p.c.	$\hat{E}_e(24)$ (MeV)[c]	T (MeV)[d]	a_p (MeV^{-1})[e]	a_{obs} (MeV^{-1})[f]	a_{obs}/a_p
Ba	75 1%		F	1.16		16.5–^{136}Ba	15.39–^{136}Ba	0.93
	77 2%							
	78 7%							
	79 8%							
	80 11%							
	81 71%							
La	80 100%	F	F	1.25	0.72	15.5–^{138}La	13.76–^{139}La	0.89
Ce	81 89%	F	G	1.24	0.70	17.0–^{139}Ce	17.8 –^{141}Ce	1.04
	83 11%							
Pr	81 100%	G	G	1.17	0.65	17.0–^{140}Pr	17.05–^{142}Pr	1.00
Tb[g])	93 100%			1.15		19.3–^{158}Tb	21.85–^{160}Tb	1.14
Dy[g])	93 2%			1.06		20.9–$^{161.5}$Dy	21.9 –^{162}Dy	1.05
	94 19%							
	95 25%							
	96 25%							
	97 28%							
Ho	97 100%	P	G	1.06	0.56	21.4–^{164}Ho	20.66–^{166}Ho	0.97
Er[g])	95 2%			1.11		19.2–^{166}Er	21.9 –^{166}Er	1.14
	97 33%							
	98 23%							
	99 27%							
	101 15%							
Tm[g])	99 100%			1.03		24.0–^{168}Tm	22.58–^{170}Tm	0.94
Ta	107 100%		G	1.00	0.49	26.0–^{180}Ta	21.2 –^{181}Ta	0.82
W	107 26%	G	F	0.98	0.50	27.0–^{183}W	23.0 –^{183}W	0.85
	108 14%							
	109 31%							
	111 28%							
Au	117 100%		G	1.19		17.5–^{196}Au	20.24–^{198}Au	1.16
Pb ($Z = 82$)	123 24%		V.P.	1.87	1.20	7.5–^{206}Pb	10.1 –^{207}Pb	1.35
	124 23%							
	125 52%							
Bi	125 100%		F	1.65	1.03	9.0–^{208}Bi	13.8 –^{210}Bi	1.53

[a]) Neutron numbers and abundances of respective residual nuclei in (γ, n) experiments.
[b]) These give an assessment of the goodness of fit of a calculated $\hat{E}_n$ versus E_0 curve to the observed data, using the Fermi gas level density formula both without and with pairing corrections.
[c]) Bremsstrahlung photoneutron mean energies $\hat{E}_e$ for peak bremsstrahlung energy $E_0 = 24$ MeV.
[d]) Nuclear temperature from fit with constant-temperature formula.
[e]) Level density parameter a_p derived from the present (γ, n) experiment, using a Fermi gas formula plus pairing correction, and corresponding residual nucleus (the atomic weight shown is the weighted average of atomic weights of the respective isotopes present).
[f]) As column 7, but using data on n-resonance absorption from refs. [1,2]).
[g]) Measurements of $\hat{E}_e(E_0)$ for these nuclei were made only for $E_0 = 21$, 23 and 24 MeV.

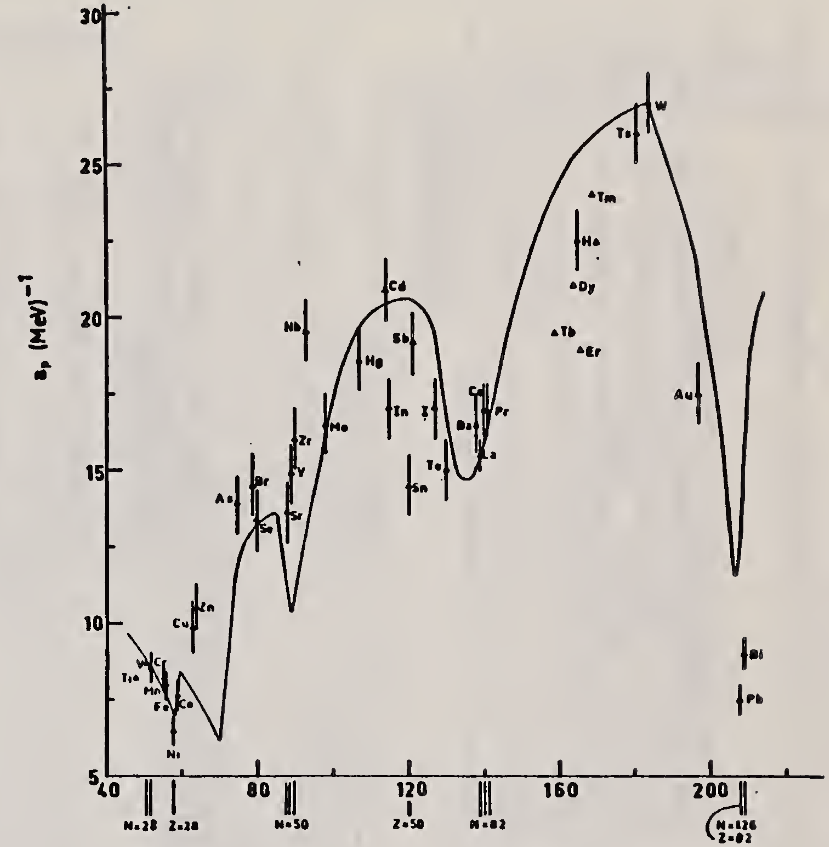

Fig. 12. Experimental values of the level density parameter a_p (Fermi gas formula plus pairing correction) versus atomic number A. The continuous curve is a least-squares fit to the data of a theoretical calculation from Newton [15]).

REF.	ELEM. SYM.	A	Z
H. J. von Eyss and G. Lührs Z. Physik 262, 393 (1973)	Pb		82
METHOD	REF. NO. 73 Ey 3		egf

REACTION	RESULT	EXCITATION ENERGY	SOURCE TYPE	SOURCE RANGE	DETECTOR TYPE	DETECTOR RANGE	ANGLE
E,XN	SPC	THR-270	C	150-270	TOF-D		90
G,XN	SPC	THR-234	C	234	TOF-D		90

NEUT E ABV 12 MEV

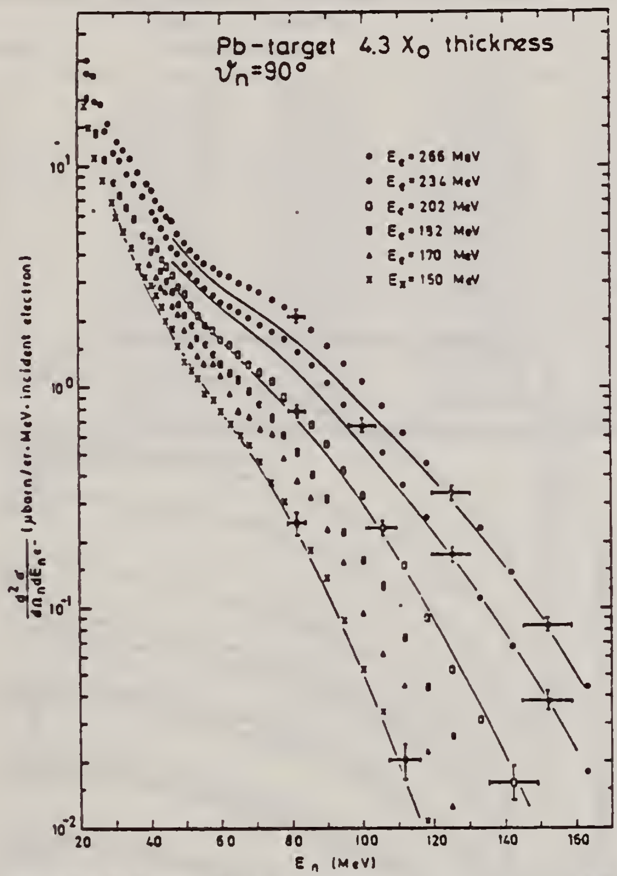

Fig. 7. Photoneutron spectra produced by electrons on a thick lead target (4.3 X_0 thickness) with primary energies of 150, 170, 182, 202, 234 and 266 MeV. These results are compared with the predictions of a quasi-deuteron model calculation (solid lines) with the parameters (defined in the text): $\alpha = 140$ MeV/c, $E_{well} = 30$ MeV, $E_b = -10$ MeV and $C'L = 19.0$

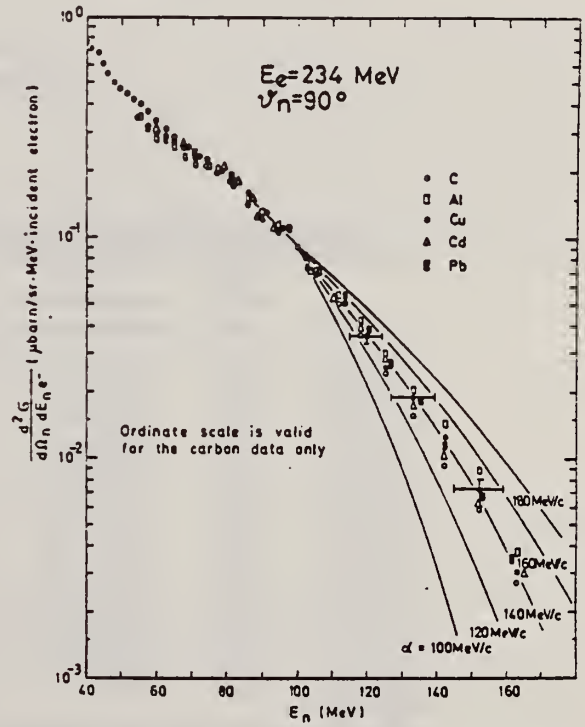

Fig. 8. Comparison of the shape of the high-energy part of the photoneutron spectra from C, Al, Cu, Cd and Pb. These measurements were performed with the same γ-shower spectrum, produced in a 0.3 cm thick lead sheet (see Fig. 2b). All spectra were fitted to the value for carbon at $E_n = 100$ MeV. The values predicted by a quasi-deuteron model (solid lines), which are also fitted at $E_n = 100$ MeV, were calculated with the parameters (defined in the text): $E_b = -10$ MeV, $E_{well} = 30$ MeV and $C'L = 19.0$ for different impulse parameters $\alpha = 100$, 120, 140, 160 and 180 MeV/c

(over)

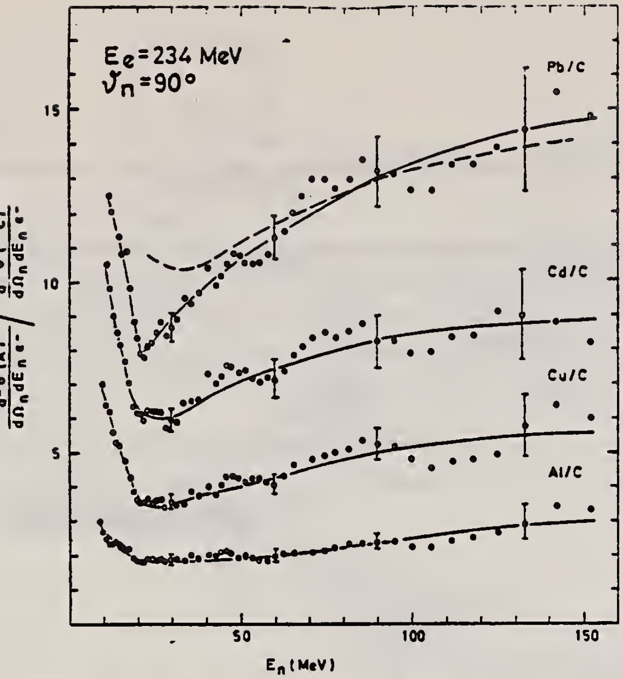

Fig. 10. Neutron yield from targets of mass number A relative to carbon, measured at $E_e=234$ MeV. The target arrangement is that of Fig. 2b. The solid lines are fit curves through the experimental values. The dashed curve shows the energy dependence of the ratio of the nuclear absorption factors $f_a(\mathrm{Pb})/f_a(\mathrm{C})$, taken from Fig. 6. The error bars correspond to the statistical error

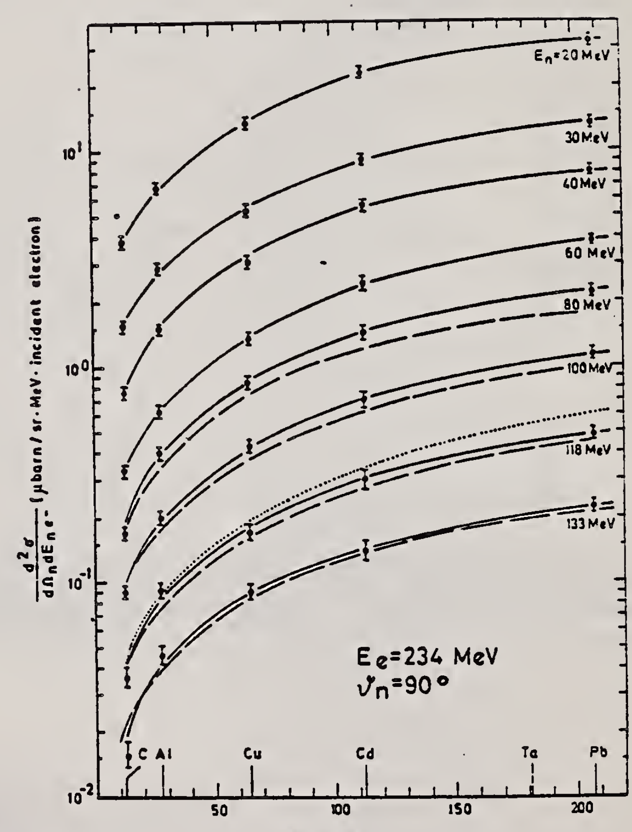

Fig. 9. Dependence of the production cross section on the mass number A with the neutron energy as parameter, measured at $E_e=234$ MeV. The γ-quanta were produced in a 0.3 cm thick lead sheet (see Fig. 2b) in front of the target of mass number A. The solid lines are fit curves through the measured values. The dashed lines are values calculated using a quasi-deuteron model with the parameters (defined in the text): $E_b=-10$ MeV, $E_{well}=30$ MeV, $\alpha=140$ MeV/c and $C'L=19.0$. The dotted curve represents the dependence NZ/A, fitted at $A=12$. The error bars correspond to the statistical error

REF.

E. Hayward, W.C. Barber, and J.J. McCarthy
Phys. Rev. C10, 2652 (1974)

ELEM. SYM.	A	Z
Pb		82

METHOD

REF. NO.	
74 Ha 4	hmg

REACTION	RESULT	EXCITATION ENERGY	SOURCE TYPE	SOURCE RANGE	DETECTOR TYPE	DETECTOR RANGE	ANGLE
$ G,G	ABX	15	D	15	NAI-D		90
		(15.1)		(15.1)			

POL PHOTONS

TABLE I. Results.

Target	$d\sigma^{\parallel}/d\Omega_r$ (Arbitrary units)	$d\sigma^{\perp}/d\Omega_r$ (Arbitrary units)	η_r	η	η(DCM)
Cd	0.042 ± 0.028	0.39 ± 0.05	0.11 ± 0.07	0.09 ± 0.07	0.19
In [a]	0.026 ± 0.020	0.54 ± 0.04	0.05 ± 0.04	0.03 ± 0.04	0.19
Sn	0.084 ± 0.036	0.65 ± 0.06	0.13 ± 0.06	0.11 ± 0.06	0.07
Sb [a]	0.14 ± 0.030	0.77 ± 0.05	0.18 ± 0.05	0.16 ± 0.05	
Nd [a]	0.14 ± 0.07	1.03 ± 0.10	0.14 ± 0.07	0.12 ± 0.07	
Ta	0.24 ± 0.10	1.47 ± 0.14	0.16 ± 0.07	0.14 ± 0.07	0.20
W	0.52 ± 0.10	1.66 ± 0.12	0.31 ± 0.07	0.29 ± 0.07	0.20
Pt	0.23 ± 0.08	1.94 ± 0.13	0.12 ± 0.04	0.10 ± 0.04	0.08
Au	0.39 ± 0.11	2.08 ± 0.15	0.19 ± 0.06	0.17 ± 0.06	0.07
Hg [a]	0.33 ± 0.09	2.16 ± 0.15	0.15 ± 0.04	0.13 ± 0.04	0.03
Pb [a]	0.19 ± 0.14	2.42 ± 0.19	0.08 ± 0.06	0.06 ± 0.06	0
Bi	0.10 ± 0.15	2.65 ± 0.26	0.04 ± 0.06	0.02 ± 0.06	0
Th [a]	0.31 ± 0.12	2.26 ± 0.19	0.14 ± 0.05	0.12 ± 0.05	0.07
U [a]	0.21 ± 0.11	2.38 ± 0.19	0.09 ± 0.05	0.07 ± 0.05	0.08

[a] Data not previously reported.

TABLE II. Comparison with Saclay data.

Target	$\lvert A_0\rvert^2$ This experiment (Arbitrary units)	$\lvert A_0\rvert^2$ Saclay (mb)	Ratio
Cd	0.337 ± 0.058	0.508	0.663 ± 0.114
In [a]	0.507 ± 0.046	0.591	0.859 ± 0.078
Sn	0.550 ± 0.072	0.822	0.669 ± 0.096
Sb [a]	0.590 ± 0.061	0.794	0.743 ± 0.077
Nd [a]	0.837 ± 0.100	1.170	0.715 ± 0.086
Ta	1.19 ± 0.18	1.88	0.633 ± 0.096
W	1.05 ± 0.17	2.05	0.512 ± 0.083
Pt	1.67 ± 0.16	2.70	0.619 ± 0.059
Au	1.62 ± 0.20	2.92	0.555 ± 0.068
Hg [a]	2.16 ± 0.20	3.29	0.540 ± 0.060
Pb [a]	2.20 ± 0.27	3.43	0.641 ± 0.078
Bi	2.53 ± 0.31	3.43	0.737 ± 0.090
Th [a]	1.89 ± 0.22	2.73	0.692 ± 0.080
U [a]	2.13 ± 0.22	2.83	0.754 ± 0.077
			0.656 ± 0.021

[a] Data not previously reported.

REF.	ELEM. SYM.	A	Z
H.E. Jackson, G.E. Thomas, and K.J. Wetzel Phys. Rev. C9, 1153 (1974)	Pb		82
METHOD	REF. NO. 74 Ja 2		hmg

REACTION	RESULT	EXCITATION ENERGY	SOURCE TYPE	SOURCE RANGE	DETECTOR TYPE	DETECTOR RANGE	ANGLE
G,G	ABX	10	D	10	SCD-D		DST
		(10,83)		(10.83)			

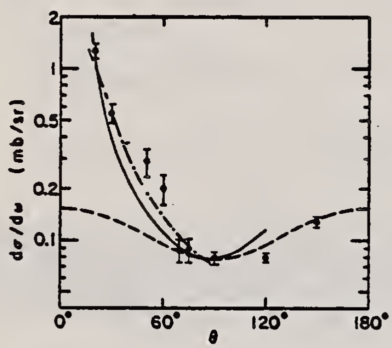

FIG. 6. Angular variation of the elastic scattering cross section in lead. The measured values are shown together with the errors of measurement. The solid curve represents the values calculated using the Delbrück amplitudes of the CERN group (Ref. 18), the broken curve, using those of the Trondheim group (Ref. 19), and the dashed curve is the variation expected for no Delbrück scattering. The two curves which include Delbrück scattering are extended only to the same large angle for which the corresponding Delbrück amplitudes have been computed.

TABLE III. Comparison of calculated and observed values of the 90° cross sections for elastic scattering and of the ratio at 90° of Raman to elastic scattering by various nuclei for 10.83-MeV photons. The parameters used in the calculations are given in Table II.

Target	$d\sigma_{clas}(90°)/d\Omega$ (mb/sr) Calc	Exp	$d\sigma^{(90°)}_{Raman}/d\sigma^{(90°)}_{clas}$ Calc	Exp
Tb	0.036	0.031 ± 0.003	0.80	0.51 ± 0.06
Ta	0.055	0.037 ± 0.003	0.28	0.18 ± 0.04
Pb	0.076	0.079 ± 0.005	0	
Bi		0.101 ± 0.006	0	~0
Th	0.128	0.129 ± 0.015	0.91	0.80 ± 0.08
U	0.157 [a]	0.182 ± 0.017	1.03	0.85 ± 0.08

[a] If the Livermore parameters (Ref. 33) for ^{235}U are used then this calculated value would be 0.210 mb/sr.

18
F. Ehlotzky and G.C. Sheppy, Nuovo Cimento 33, 1185 (1964).
19
K. Mork and P. Papatzacos, private communication.
33
C.D. Bowman, G.F. Auchampaugh, and S.C. Fultz, Phys. Rev. 133, B676 (1964).

REF. V. S. Evseev, T. N. Mamedov, O. V. Selyugin
Yad. Fiz. 21, 245 (1975)
Sov. J. Nucl. Phys. 21, 129 (1975)

ELEM. SYM.	A	Z
Pb		82

METHOD

REF. NO.	
75 Ev 1	hmg

REACTION	RESULT	EXCITATION ENERGY	SOURCE		DETECTOR		ANGLE
			TYPE	RANGE	TYPE	RANGE	
G,N	SPC	6- 31	C	31	SCI-D		140

Neutron energy spectra have been measured in the energy range $2 \leq E_n \leq 5$ MeV for photoexcitation of the nuclei Ta, Pb, Bi, and Th by bremsstrahlung with maximum energy 31 MeV. From the neutron spectra we have determined values of the nuclear temperature $\bar{T}$ after emission of the first neutron: 1.01 ± 0.04, 1.12 ± 0.04, 1.11 ± 0.04, and 1.25 ± 0.05 MeV respectively for Ta, Pb, Bi, and Th. Comparison of the values obtained for the nuclear level-density parameter with the predictions of the statistical theory of nuclear reactions shows that this theory does not describe the decay of collective nuclear states of the giant dipole resonance type.

REF. G. Bologna, V. Bellini, V. Emma, A.S. Figuera, S. Lo Nigro
C. Milone and G.S. Pappalardo
Il Nuovo Cimento 35A, 91 (1976)

ELEM. SYM.	A	Z
Pb		82

METHOD

REF. NO. 76 Bo 15 egf

REACTION	RESULT	EXCITATION ENERGY	SOURCE TYPE	SOURCE RANGE	DETECTOR TYPE	DETECTOR RANGE	ANGLE
G,F	RLX	220-500	D	220-500	TRK-I		4PI

COHERENT BREMS

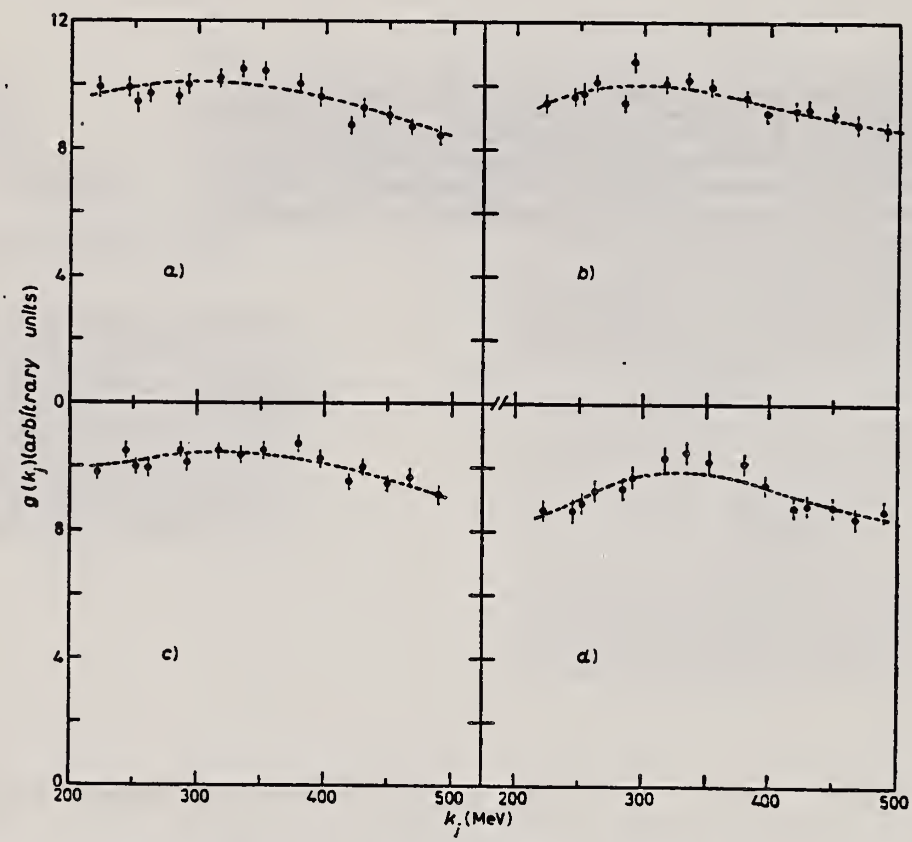

Fig. 6. – Photofission yields per equivalent quantum of Bi, Pb, Au and Pt as a function of the first peak energy k_j of photons. The dots are the experimental data; the dashed curves represent the yield functions estimated as described in sect. 5. *a*) Bi (γ, f), *b*) Pb (γ, f), *c*) Au (γ, f), *d*) Pt (γ, f).

over

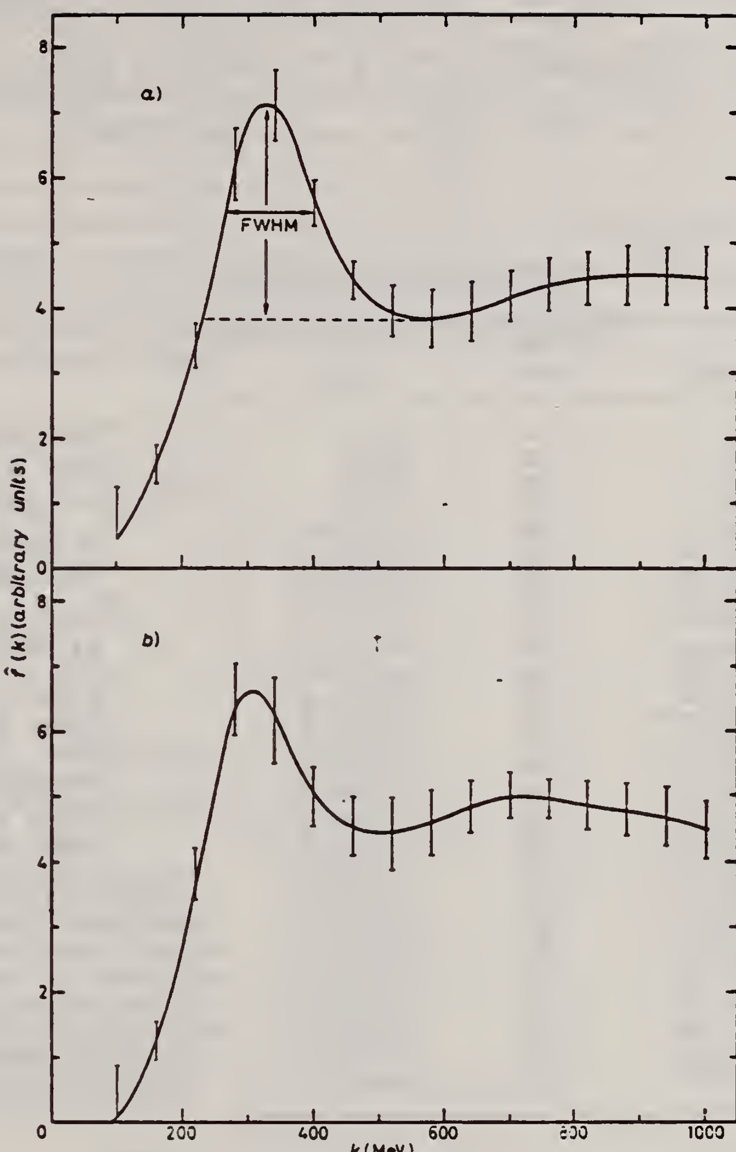

Fig. 7. – Photofission cross-section estimated by our unfolding method. For Bi the procedure used to deduce the FWHM of the first maximum is indicated. *a*) Bi (γ, f), *b*) Pb (γ, f).

REF.	ELEM. SYM.	A	Z
V. Emma, S. Lo Nigro, C. Milone Nucl. Phys. A257, 438 (1976)	Pb		82

METHOD	REF. NO.	
	76 Em 2	egf

REACTION	RESULT	EXCITATION ENERGY	SOURCE TYPE	SOURCE RANGE	DETECTOR TYPE	DETECTOR RANGE	ANGLE
G,F	ABY	THR-999	C	999	TRK-I		4PI

999 = 1 GEV

TABLE 1

Measured values of σ_q at $E = 1000$ MeV and deduced values of σ_k assumed constant from E_0 to 1000 MeV

Element	Z^2/A	σ_q (mb)	E_0 (MeV)	σ_k (mb)
Bi	32.96	12.3 ± 0.6	200	7.6 ± 0.6
Pb	32.45	5.4 ± 0.4	220	3.6 ± 0.3
Tl	32.10	4.1 ± 0.3	230	2.8 ± 0.3
Au	31.68	2.0 ± 0.15	240	1.4 ± 0.2
Pt	31.18	1.1 ± 0.08	255	$(8 \pm 0.7) \times 10^{-1}$
Re	30.21	$(3.7 \pm 0.3) \times 10^{-1}$	280	$(2.9 \pm 0.3) \times 10^{-1}$
W	29.78	$(3.5 \pm 0.3) \times 10^{-1}$	290	$(2.8 \pm 0.3) \times 10^{-1}$
Ta	29.45	$(3.3 \pm 0.3) \times 10^{-1}$	300	$(2.7 \pm 0.3) \times 10^{-1}$
Hf	29.04	$(1.7 \pm 0.2) \times 10^{-1}$	310	$(1.4 \pm 0.2) \times 10^{-1}$
Yb	28.31	$(1.3 \pm 0.1) \times 10^{-1}$	330	$(1.2 \pm 0.1) \times 10^{-1}$
Tm	28.18	$(7.5 \pm 0.8) \times 10^{-2}$	335	$(6.8 \pm 0.8) \times 10^{-2}$
Ho	27.21	$(3.6 \pm 0.4) \times 10^{-2}$	355	$(3.5 \pm 0.4) \times 10^{-2}$
Dy	26.80	$(2.6 \pm 0.3) \times 10^{-2}$	360	$(2.5 \pm 0.3) \times 10^{-2}$
Tb	26.58	$(2.5 \pm 0.3) \times 10^{-2}$	370	$(2.5 \pm 0.3) \times 10^{-2}$
Gd	26.04	$(1.6 \pm 0.2) \times 10^{-2}$	380	$(1.7 \pm 0.2) \times 10^{-2}$
Sm	25.56	$(1.3 \pm 0.2) \times 10^{-2}$	390	$(1.4 \pm 0.2) \times 10^{-2}$
Nd	24.96	$(9.2 \pm 0.9) \times 10^{-3}$	405	$(1 \pm 0.1) \times 10^{-2}$
Ce	24.00	$(8 \pm 0.9) \times 10^{-3}$	420	$(9 \pm 1) \times 10^{-3}$
La	23.39	$(8.4 \pm 0.9) \times 10^{-3}$	430	$(1 \pm 0.1) \times 10^{-3}$
Sb	21.36	$(1.2 \pm 0.2) \times 10^{-2}$	460	$(1.5 \pm 0.3) \times 10^{-2}$
Te	21.19	$(8.8 \pm 1) \times 10^{-3}$	465	$(1.2 \pm 0.2) \times 10^{-2}$
Sn	21.06	$(1.3 \pm 0.2) \times 10^{-2}$	465	$(1.7 \pm 0.3) \times 10^{-2}$
Cd	20.49	$(1.7 \pm 0.3) \times 10^{-2}$	470	$(2.2 \pm 0.4) \times 10^{-2}$
Ag	20.47	$(2 \pm 0.3) \times 10^{-2}$	470	$(2.6 \pm 0.4) \times 10^{-2}$
Zn	13.76	$(2 \pm 0.4) \times 10^{-1}$	515	$(3 \pm 0.6) \times 10^{-1}$
Cu	13.44	$(2.4 \pm 0.5) \times 10^{-1}$	515	$(3.6 \pm 0.8) \times 10^{-1}$
Ni	13.35	$(2.4 \pm 0.5) \times 10^{-1}$	510	$(3.6 \pm 0.8) \times 10^{-1}$
Fe	12.10	$(3 \pm 0.6) \times 10^{-1}$	510	$(4.4 \pm 0.9) \times 10^{-1}$

[4] A.V. Mitrofanova et al. Sov. J. Nucl. Phys. 6, 512 (1968).

[7] T. Methasiri et al., Nucl. Phys. A167, 97 (1971).

[12] J.R. Nix et al., Nucl. Phys. 81, 61 (1966).

[20] N.A. Perifilov et al., JETP (Sov. Phys.) 14, 623 (1962); Proc. Symp. on the physics & chemistry of fission, Salzburg 1965, vol. 2 (IAEA) Vienna, 1965, p.283.

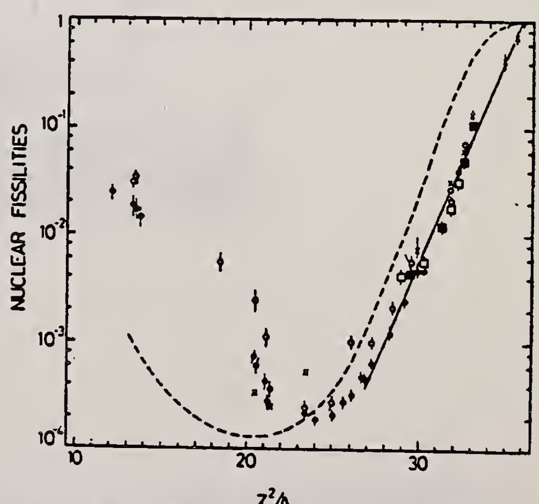

Fig. 2. Nuclear fissilities as a function of Z^2/A. Experimental points: solid circles represent our data; squares, the data from ref. [4]); open circles, the data from ref. [7]); and crosses, the data from (p,f) experiments[20]). The straight line is the best fit calculated from our data for $Z^2/A > 26$. The dashed curve is the curve VI calculated by Nix and Sassi[12]).

REF.		ELEM. SYM.	A	Z
S. Kahane, R. Moreh and O. Shahal Phys. Rev. C 18, 1217 (1978)		Pb		82
METHOD		REF. NO.		
		78 Ka 6		hg

REACTION	RESULT	EXCITATION ENERGY	SOURCE TYPE	SOURCE RANGE	DETECTOR TYPE	DETECTOR RANGE	ANGLE
G,G	ABX	6- 12	C	6- 12	SCD-D		DST
		(6.84-11.39)		(6.84-11.39)			

Monoenergetic photons at eight energies in the range 6.84–11.39 MeV were elastically scattered from targets of ^{181}Ta, Pb, and ^{238}U at θ = 1.21°–1.50°. The differential scattering cross section at such angles was measured relative to the Compton cross section. The photon beam was obtained from the Ni(n,γ) reaction using thermal neutrons. Strong evidence for the contribution of both Rayleigh and the real Delbruck amplitudes and for their destructive interference was obtained.

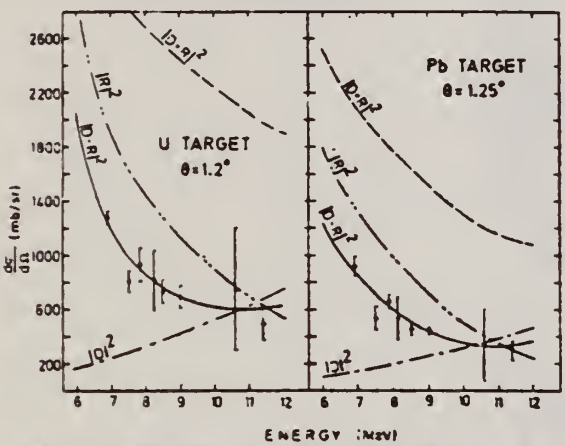

FIG. 3. Differential cross sections for elastic scattering of photons from U and Pb. The solid curves denoted $|D-R|^2$ represent theoretical values obtained by including the Rayleigh, Delbruck, nuclear resonance, and Thomson scattering amplitudes. The dashed curves denoted $|R|^2$ and $|D|^2$ represent almost pure contributions of Rayleigh and Delbruck scattering, respectively. $|D+R|^2$ represents the coherent sum of Delbruck and Rayleigh contributions taken to have the *same* phase. The NR and NT coherent contributions were also included in the dashed curves.

TABLE I. Differential cross section (mb/sr) of elastic photon scattering from U at θ = 1.21° ±0.26° and Pb at θ = 1.25° ± 0.26°. Columns 4 and 7 give the cross section after excluding the real D amplitudes.

	U (Z = 92)			Pb (Z = 82)		
E (keV)	Exp.	Theory	No real D	Exp.	Theory	No real D
6837	1274 ± 50	1265	2118	917 ± 68	885	1443
7819	932 ± 120	890	1675	657 ± 53	631	1138
8120	812 ± 220	834	1600	533 ± 160	570	1064
8533	732 ± 90	760	1494	452 ± 45	503	967
8999	691 ± 50	694	1392	443 ± 15	436	868
10596	747 ± 450	604	1169	340 ± 260	333	642
11388	489 ± 114	607	1108	294 ± 70	337	594

REF. K. Baba, I. Endo, M. Fujisaki, S. Kadota, Y. Sumi, H. Fujii, Y. Murata, S. Noguchi, A. Murakami
Nucl. Phys. A322, 349 (1979)

ELEM. SYM.	A	Z
PB		82

METHOD

REF. NO.	
79Ba8	hg

REACTION	RESULT	EXCITATION ENERGY	SOURCE TYPE	SOURCE RANGE	DETECTOR TYPE	DETECTOR RANGE	ANGLE
G,PI-	SPC	*668	C	700	MAG-D		44
G,PI+	SPC	*668	C	700	MAG-D		44

*AVG PHOTON ENERGY

Abstract: The photoproduction of charged pions in the sub GeV region has been studied for two nuclear targets, copper and lead, by using a magnetic spectrometer. The photon energies are determined in steps of 50 MeV by a subtraction method for the bremsstrahlung spectrum. The observed pion momentum spectra reveal characteristic features of quasi-free production (QFP) even for such heavy nuclei as copper and lead. The data are compared with results obtained by a PWIA calculation, which give a good fit to the data. The QFP cross sections per relevant nucleon at 44.2° and the average photon energy $\langle k \rangle = 668$ MeV are found to be approximately proportional to $A^{-1/3}$.

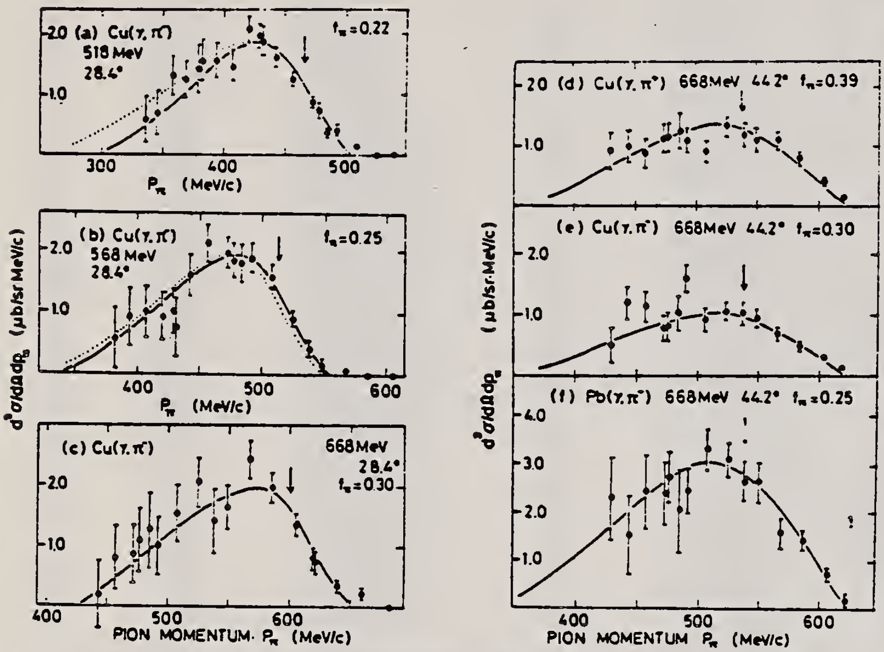

Fig. 1. Typical examples of the measured pion spectra. Errors are statistical only. The solid curves are $f_\pi \times$(PWIA calculation) with parameter values $p_F = 270$ MeV/c, $\varepsilon = 25$ MeV and f_π being shown in the figure. The dotted curves in (a) and (b) correspond to the cases in which $p_F = 300$ MeV/c while ε is unchanged, and $\varepsilon = 35$ MeV while p_F is unchanged, respectively. Arrows denote the values of the pion momentum, p_{free}, which is calculated from the assumption that the target nucleon is free and at rest.

OVER

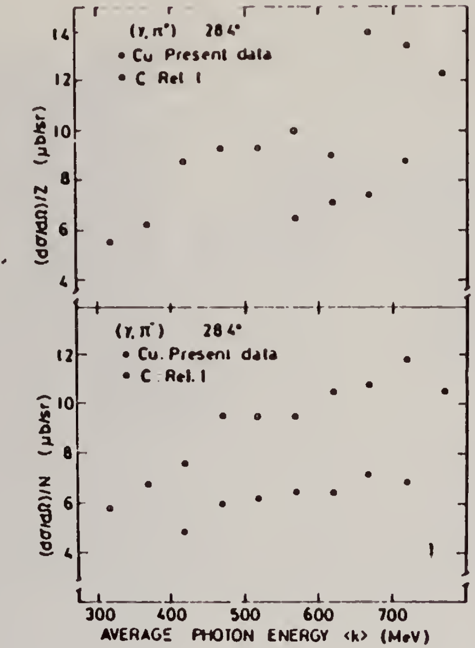

Fig. 3. The QFP cross section at $\theta_\pi = 28.4°$ for copper as a function of $\langle k \rangle$. Note that the plotted values are those divided by the proton (neutron) number Z (N) for π^+ (π^-), together with the same quantities for carbon taken from 1 for comparison. Errors of the order of 10% due to fitting uncertainty are not shown.

QFP = QUASI-FREE PRODUCTION

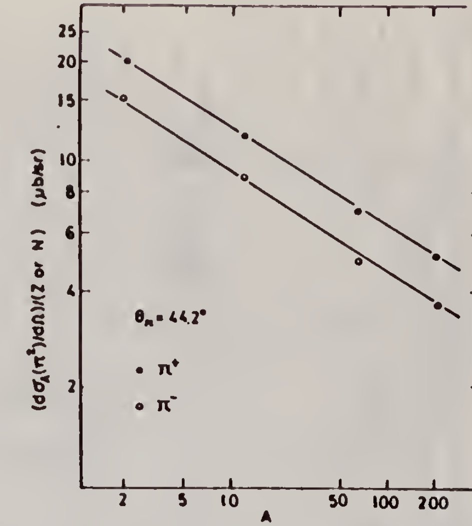

Fig. 4. The QFP cross section at $\theta_\pi = 44.2°$ and $\langle k \rangle = 668$ MeV as a function of the mass number A. The π^+ (π^-) cross section is divided by Z (N). Errors of the order of 10% due to fitting uncertainty are not shown. Data points at $A = 2$ are taken from ref. [3]). The solid lines are:

$$\frac{d\sigma_A(\pi^+)}{d\Omega}\frac{1}{Z} = 24.3A^{-0.3}, \quad \text{and} \quad \frac{d\sigma_A(\pi^-)}{d\Omega}\frac{1}{N} = 18.4A^{-0.3},$$

in units of μb/sr.

QFP = QUASI-FREE PRODUCTION

TABLE 2

Double differential cross section $d^2\sigma/d\Omega_\pi dp_\pi$ for the reactions $\gamma + A \to \pi^\pm + X$, where A is taken to be copper or lead, as a function of the average photon energy $\langle k \rangle$ and the pion momentum p_π

$\langle k \rangle$ [MeV]	p_π [MeV/c]	$d^2\sigma/d\Omega_\pi dp_\pi$ [μb/(sr · MeV/c)]	$\langle k \rangle$ [MeV]	p_π [MeV/c]	$d^2\sigma/d\Omega_\pi dp_\pi$ [μb/(sr · MeV/c)]
	π^- for copper at 28.4°			*π^- for copper at 28.4°*	
	431	0.07 ± 0.07		485	0.00 ± 0.02
	420	0.04 ± 0.04		472	0.05 ± 0.02
	407	0.33 ± 0.11		457	0.12 ± 0.04
	394	0.26 ± 0.11		443	0.39 ± 0.90
	382	0.69 ± 0.19		429	0.79 ± 0.13
	379	0.67 ± 0.17		431	0.47 ± 0.15
	369	0.77 ± 0.15		420	0.89 ± 0.13
	357	1.41 ± 0.23		407	1.33 ± 0.20
	346	1.83 ± 0.28		394	1.84 ± 0.23
418	336	1.71 ± 0.35	468	382	1.86 ± 0.31
	324	1.37 ± 0.38		379	2.09 ± 0.34
	316	1.91 ± 0.34		369	2.03 ± 0.25
	306	1.50 ± 0.39		357	1.37 ± 0.32
	296	1.73 ± 0.43		346	1.61 ± 0.38
	287	0.84 ± 0.43		336	1.26 ± 0.41
	281	2.02 ± 0.69		325	1.58 ± 0.55
	274	0.97 ± 0.51		317	1.07 ± 0.46
	266	0.87 ± 0.57		306	0.82 ± 0.49
	257	0.89 ± 0.59		297	0.72 ± 0.53
	250	-0.36 ± 0.60		288	2.27 ± 0.55

REF.	V.I. Noga, Yu.N. Ranyuk, Yu.N. Telegin Sov. Atom. Ener. 47, 735 (1979)	ELEM. SYM.	A	Z
		Pb		82
METHOD		REF. NO.		
		79 No 2		hg

REACTION	RESULT	EXCITATION ENERGY	SOURCE		DETECTOR		ANGLE
			TYPE	RANGE	TYPE	RANGE	
E,N	RLY	6-999	D	230-999	ACT-D		4PI

999=1.2 GEV

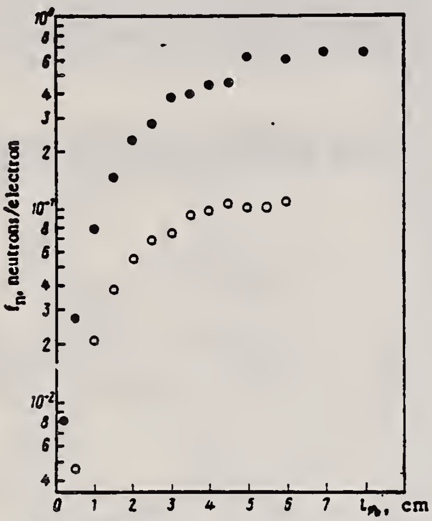

Fig. 1. Neutron yield f_n as a function of target thickness l_{Pb} at 230 (○) and 1200 MeV (●).

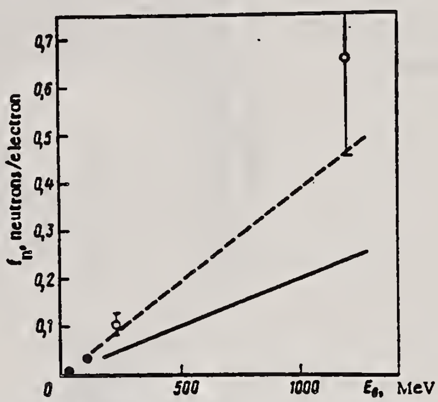

Fig. 2. Neutron yield f_n as a function of electron energy E_0 under saturation conditions: results of [3, 4] (●), our results (○); ---- calculated in [5], —— calculated in [6].

REF.	ELEM. SYM.	A	Z
S.A. Hayashi, S. Yamamoto, I. Kimura, K. Kobayashi, T. Mori, S. Kanazawa, H. Nishihara, S.A. Bokharee, R.W. Emmett, R.C. Block, M. Becker, D.R. Harris, B.K. Malaviya Ann. Rpt. Res. Reac. Inst., Kyoto Univ. 13, 23 (1980)	Pb		82

METHOD	REF. NO.	
	80 Ha 6	egf

REACTION	RESULT	EXCITATION ENERGY	SOURCE TYPE	SOURCE RANGE	DETECTOR TYPE	DETECTOR RANGE	ANGLE
G,XN	SPC	7-60	C	30,60	TOF-D		DST

ANG DST WITH ACT DET

Three kinds of photoneutron targets, the cylindrical lead target, and the spherical and spheroidal tantalum targets were designed as pulsed-neutron sources with an electron linear accelerator for the fast neutron spectrum study in assemblies of reactor materials. Angular distributions of photoneutrons and X-rays from these targets bombarded by about 30- and 60-MeV electrons were obtained by the activation method and the results show fairly isotropic photoneutron distributions except to the forward and extraordinarily sharp forward peak of X-rays. Among these three targets the spheroidal tantalum target is seen to be superior to others from the viewpoints of the isotropy of photoneutrons and of a lower forward peak of X-rays even at the higher bombarding energy. However, for the lower electron energy, about 30 MeV, both the lead target and the spherical tantalum target can be usable for the above purpose, although the maximum beam power of the former is restricted to about 120 watts.

Neutron spectra from these targets were measured in the energy range from 20 keV to 10 MeV by the LINAC TOF method. It was found that neutron spectra from tantalum targets are apparently softer than that from the lead target.

With the above characteristics obtained experimentally, these targets will be used for the neutron spectra measurements in assemblies of reactor materials.

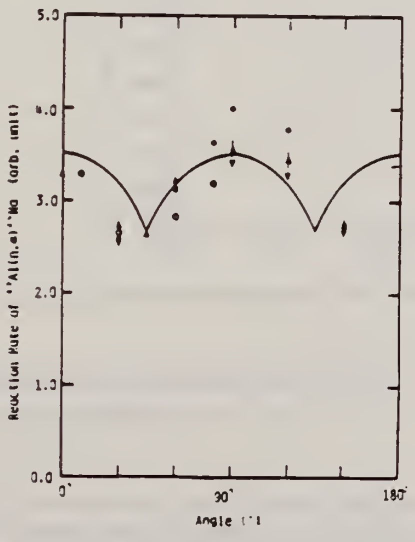

Fig. 4. Angular distribution of photoneutrons emanated from the cylindrical lead target bombarded by 32-MeV electrons. The ^{24}Na activity from the ^{27}Al(n, α)^{24}Na reaction was measured with a Ge(Li) detector.

▲ and ▼ show the measured reaction rate of the activation foils, which were placed on the vertical plane at the position of 20 cm from the effective center of the target. ○ and ● show the measured rate, on the horizontal plane. Solid curve shows the calculated one normalized at 45 degrees.

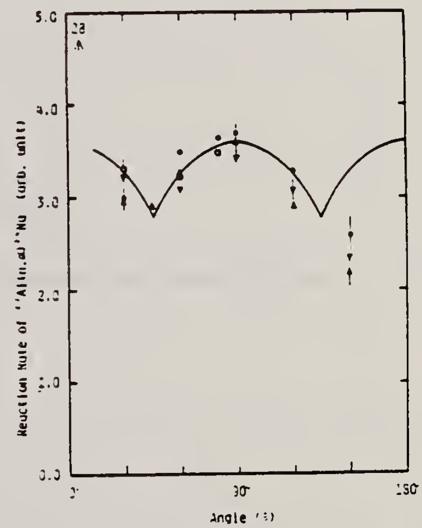

Fig. 5. Angular distribution of photoneutrons emanated from the cylindrical lead target bombarded by 62-MeV electrons. The ^{24}Na activities from Al foils are shown. The symbols are the same as in Fig. 4. A number shown by arrow is the value at zero degree.

(over)

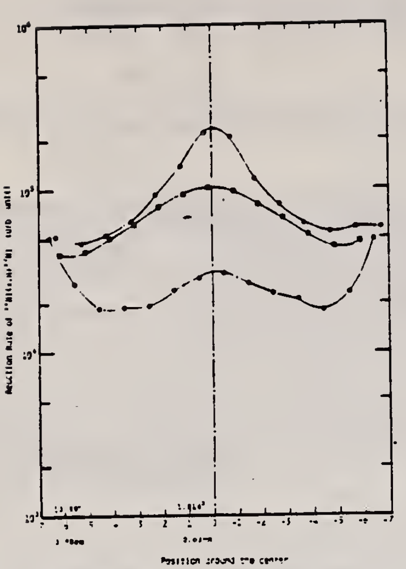

Fig. 12. Distributions of X-rays near the forward direction around the central axis of the electron beam from the spherical tantalum target bombarded by 36-MeV electrons and the spheroidal tantalum target by 64-MeV and 28-MeV electrons (*vid.* Fig. 1(b)). The ^{57}Ni activities from Ni foils by 36-MeV, 64-MeV and 28-MeV electrons are shown as the symbols □, ● and ○, respectively.

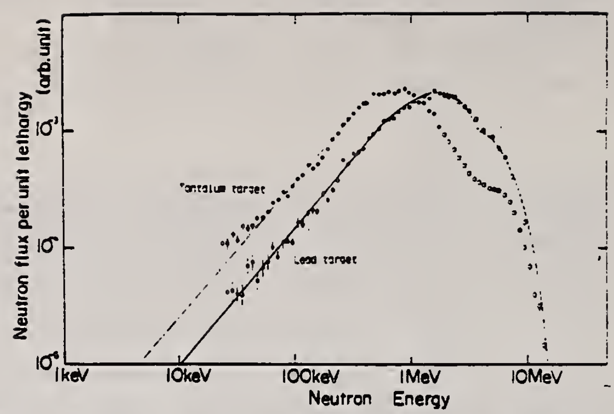

Fig. 14. Photoneutron spectra from the lead target and the spherical tantalum target bombarded by approximately 30-MeV electrons.

—·— curve is obtained by eye guide fitting of the measured tantalum target data and —— curve is for the lead data. ---- curve is obtained by fitting the data of the lead target with nuclear temperatures of evaporation spectra. $T_1 = 0.89$ MeV (≤ 3.8 MeV neutrons) and $T_2 = 1.70$ MeV (> 3.8 MeV neutrons). ●●●● shows data measured with the ^{6}Li glass scintillation or the ^{10}B-vaseline-plug NaI(Tl) detectors. ○○○○ shows data with the liquid scintillation detector.

REF. J. Arends, J. Eyink, A. Hegerath, K.G. Hilger, B. Mecking, G. Nöldeke, H. Rost
Phys. Lett. 98B, 423 (1981)

ELEM. SYM.	A	Z
Pb		82

METHOD

REF. NO.	
81 Ar 1	hg

REACTION	RESULT	EXCITATION ENERGY	SOURCE		DETECTOR		ANGLE
			TYPE	RANGE	TYPE	RANGE	
G,MU-T	ABX	215-386	D	215-386	TOF-D		4PI

DATA ALSO IN 81AR3

Double differential cross sections for the photo-emission of protons and charged pion production were investigated for a number of target nuclei (He, Be, C, O, Al, Ti, Cu, Sn, Pb) in the photon energy range k = (215–386) MeV. On the basis of these experimental results the total hadronic cross section was determined.

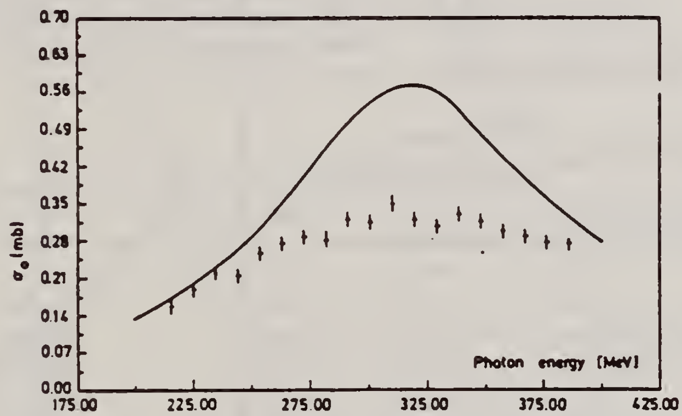

Fig. 7. Parameter σ_0 as a function of photon energy (data points) compared to the mean cross section for a free nucleon (solid line).

The total hadronic cross sections for all measured elements can be parametrized in the form

$$\sigma(k,A) = \sigma_0(k) \cdot A^x ,$$

A being the atomic number, with a constant exponent x = 1.1. The photon energy dependence of σ_0 is shown in fig. 7. Compared to the mean cross section for a free nucleon (the solid line in fig. 7) the excitation of the Δ-resonance is suppressed. Such a suppression is expected in the Δ-hole model [11].

REF. J. Arends, J. Eyink, A. Hegerath, K.G. Hilger, B. Mecking,
G. Nöldeke, H. Rost
Nucl. Phys. A358, 367c (1981)

ELEM. SYM.	A	Z
Pb		82

METHOD	REF. NO.	
	81 Ar 3	hg

REACTION	RESULT	EXCITATION ENERGY	SOURCE TYPE	SOURCE RANGE	DETECTOR TYPE	DETECTOR RANGE	ANGLE
G,MU-T	ABX	215-386	D	215-386	TOF-D		4PI

Abstract: Double differential cross sections for the photoemission of protons and charged pion photoproduction were investigated for a number of target nuclei (He, Be, C, O, Al, Ti, Cu, Sn, Pb) using the tagged bremsstrahlung beam at the Bonn 500 MeV-Synchrotron in the photon range k = (215-386)MeV. On the basis of these experimental results the total hadronic cross section was determined.

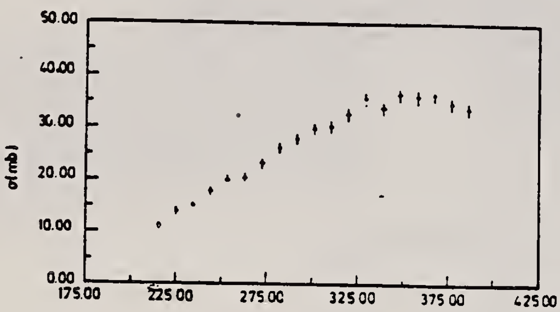

Fig. 2. Cross section for the process: γ + Pb → p + X.
The proton threshold is 58 MeV.

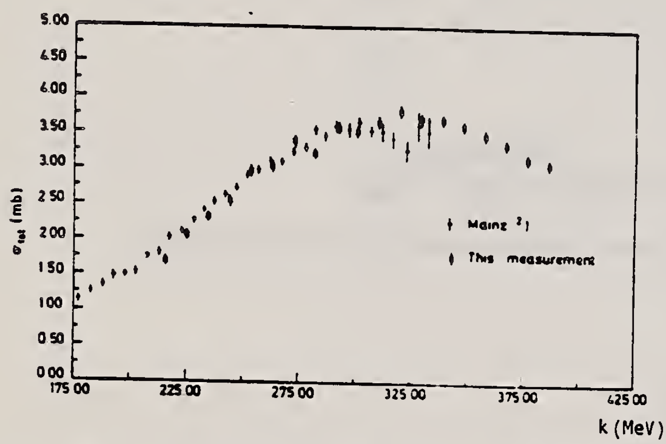

Fig. 3. Total hadronic cross section for Be. The data are compared to the cross section taken from ref.).

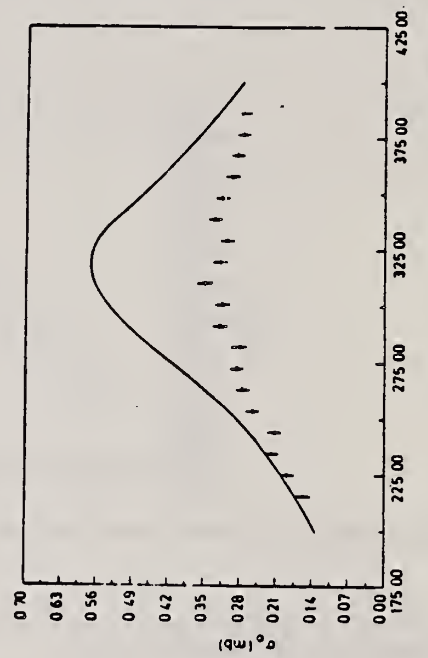

Fig. 4. Parameter σ_0 compared to the cross section for a free nucleon (full line).

The photon energy dependence of the total cross sections for heavier nuclei are similar to the Be results. The complete data set can be parametrized in the form

$$\sigma(k,A) = \sigma_0(k) \cdot A^x.$$

The exponent is constant x = 1.1. The photon energy dependence of σ_0 is shown in fig. 4. Compared to the mean cross section for a free nucleon, the excitation of the Δ-resonance is suppressed.

REF. A. Leprêtre H. Beil, R. Bergère, P. Carlos, J. Fagot, A. De Miniac, A. Veyssière
Nucl. Phys. A367, 237 (1981)

ELEM. SYM.	A	Z
Pb		82

METHOD

REF. NO.	
81 Le 1	egf

REACTION	RESULT	EXCITATION ENERGY	SOURCE TYPE	SOURCE RANGE	DETECTOR TYPE	DETECTOR RANGE	ANGLE
G,SN	ABX	25-140	D	25-140	MOD-I		4PI
G,XN	ABX	25-140	D	25-140	MOD-I		4PI

(G,SN) NO G,1N IN G,SN

$$\sigma^{(i)}(E_\gamma) = \sum_{i=i} \sigma(\gamma, in : E_\gamma) .$$

Abstract: The total photonuclear absorption cross section for Sn, Ce, Ta, Pb and U has been studied from 25 to 140 MeV using a continuously variable monochromatic photon beam obtained from the annihilation in flight of monoenergetic positrons. The basic experimental results are a set of data giving sums of inclusive multiple photoneutron production cross sections of the form $\sigma^{(i)}(E_\gamma) = \sum_{i=i}\sigma(\gamma, in : E_\gamma)$ for neutron multiplicities ranging from $i = 1$ to 12. From these data the total photonuclear absorption cross section $\sigma(\text{tot} : E_\gamma)$ has been deduced. It is concluded that Levinger's modified quasideuteron model describes the total cross sections reasonably well. When these data are combined with lower energy data and integrated to 140 MeV they indicate the need for an enhancement factor K for the Thomas-Reiche-Kuhn sum rule of 0.76 ± 0.10. No evidence was found that would indicate an A-dependence for the enhancement factor.

E | PHOTONUCLEAR REACTIONS Sn, Ce, Ta, Pb, U(γ, xn), E_γ = 25–140↓ MeV; measured $a(E_\gamma)$ summed for x = 1–12; deduced $\sigma(E_\gamma$, total), integrated σ, interaction models. Monochromatic photons.

TABLE 3

Integrated cross sections

	Sn	Ce	Ta	Pb	U	U
$\sigma_0 = 0.06NZ/A$ (MeV · b)	1.74	2.04	2.61	2.97	3.40	3.40
$E_{\gamma 0}$(MeV)	29.7	25	25	25	18	18.30
$M = \int_{B_{1n}}^{E_{\gamma 0}} \sigma_{GDR}(E_\gamma)\, dE_\gamma$ (MeV · b)	2.0±0.15 [a]	2.13±0.15 [b]	2.90±0.23 [b]	3.48±0.23 [c]	2.98±0.15 [d]	3.58 [e]
(σ_0 unit)	1.15±0.09	1.04±0.07	1.11±0.09	1.17±0.08	0.88±0.05	1.05
$N = \int_{E_{\gamma 0}}^{140\ \text{MeV}} \sigma^{(2)}(E_\gamma)\, dE_\gamma$ (Mev · b)	0.96±0.1	1.27±0.1	1.73±0.15	1.69±0.15	2.59±9.2	2.59±0.2
(σ_0 unit)	0.55±0.06	0.63±0.05	0.66±0.06	0.57±0.05	0.76±0.06	0.76±0.06
$M+N$ (MeV · b)	2.96±0.2	3.40±0.2	4.63±0.3	5.17±0.3	5.57±0.3	6.17±0.3
(σ_0 unit)	1.70±0.12	1.67±0.10	1.77±0.10	1.74±0.10	1.64±0.10	1.81±0.10
$(M+N)$ + evaluation of the $\int_{E_{\gamma 0}}^{140\ \text{MeV}} \lvert\sigma^{(1)} - \sigma^{(2)}\rvert\, dE_\gamma$ contribution $= (1+K)$ (σ_0 unit)	1.74±0.15	1.71±0.15	1.81±0.15	1.78±0.15	1.68±0.15	1.85±0.15
$\int^{m_\pi} \sigma_L(E_\gamma)\, dE_\gamma$ (σ_0 unit)	1.28 [a]	1.24 [b]	1.30 [b]	1.35 [c]	1.18 [d]	1.43 [e]

[a]) Ref. [26]). [b]) Ref. [27]). [c]) Ref. [5]). [d]) Ref. [28]). [e]) Ref. [29]).

The symbols M and N are defined in the text. The last row gives the integrated cross sections for the Lorentz line fit, $\sigma_L(E_\gamma)$ to the GDR data, published in the above references.

(OVER)

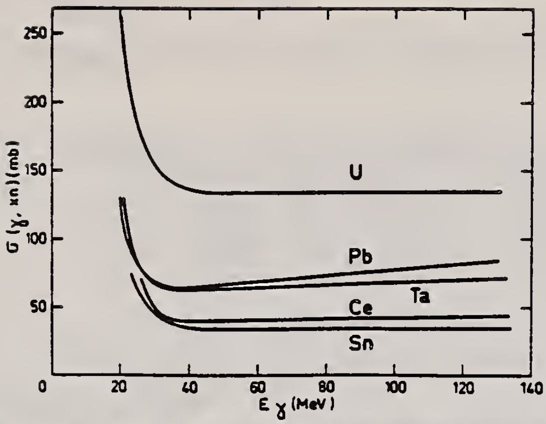

Fig. 11. The general behaviour of the "smoothed" average neutron yield cross sections $\sigma(\gamma, xn) = \sum_i i\sigma(\gamma, in: E_\gamma)$ for the Sn, Ce, Ta, Pb and U nuclei studied in the present paper (see text).

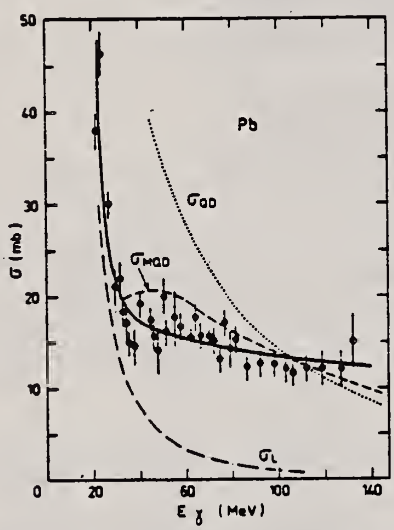

Fig. 15. Total photonuclear absorption cross sections $\sigma(\mathrm{tot}: E_\gamma) \approx \sigma^{(2)}(E_\gamma)$ from the present paper, represented by the experimental points and the corresponding full lines, are shown for Pb, Sn, Ce, Ta and U. These experimental results for photon energies E_γ between 20 and 140 MeV are compared with: (a) Lorentz line fits to the GDR data of the appropriate nucleus represented by the dot-dash $\sigma_L(E_\gamma)$ plots. (b) Quasideuteron cross sections, $\sigma_{QD}(E_\gamma) = (4.6NZ/A)\sigma_D(E_\gamma)$ for the appropriate nuclei, represented by the dotted $\sigma_{QD}(E_\gamma)$ plots. Here $\sigma_D(E_\gamma)$ is the photodisintegration cross section of deuterium. (c) Modified quasideuteron cross sections, $\sigma_{QDM}(E_\gamma) = (8NZ/A)\sigma_D(E_\gamma)\exp(-D/E_\gamma)$ with $D = 60$ MeV, represented by the dashed $\sigma_{MQD}(E_\gamma)$ plots. Pertinent GDR data for Pb, Sn, Ce, Ta and U were taken from refs. [5,26-28]).

REF.		ELEM. SYM.	A	Z
M. Schumacher, F. Smend, W. Mückenheim, P. Rullhusen, H.G. Börner Z. Phys. A300, 193 (1981)		Pb		82
METHOD		REF. NO.		
		81 Sc 6		egf

REACTION	RESULT	EXCITATION ENERGY	SOURCE TYPE	SOURCE RANGE	DETECTOR TYPE	DETECTOR RANGE	ANGLE
G,G	ABX	2-7		2-7	SCD-D		90

2.60-6.67 MEV

Elastic scattering by nuclei in the range of mass numbers between 64 and 238 has been studied with monochromatic photons in the energy range between 2 and 8 MeV. These photons were provided either by a Ti(n, γ) source installed in the tangential through channel of the Grenoble high flux reactor, or by ^{24}Na and ^{56}Co sources produced by deuteron bombardment of Al or Fe at the Göttingen cyclotron. The photoexcitation of 23 nuclear levels has been observed and the decay properties and groundstate widths of the majority of these levels have been determined. For the lead scattering target the coherent elastic differential cross section has been studied in detail. There is evidence that below the photo-neutron threshold the elastic scattering via virtual photoexcitation of the nucleus can be approximated by extrapolating the real part of the Giant Dipole Resonance amplitude along a Lorentzian curve. Coulomb corrections to Delbrück scattering seem to play a small role at 6.5 MeV.

Table 1. Differential cross sections for elastic scattering $(d\sigma/d\Omega)^{exp}$ of photons from ^{56}Co and ^{24}Na sources by different scattering targets, in units of μb/sr. Errors in the last digits are given in parentheses.

θ deg	Scattering targets	2.599[a] (MeV)	2.754[b] (MeV)	3.010[a] (MeV)	3.202[a] (MeV)	3.254[a] (MeV)	3.273[a] (MeV)	3.452[a] (MeV)
90	^{238}U	52.7(25)	57.5(25)[c]	56(16)	47(4)	456 (10)[c]	34(6)	49(14)
	^{209}Bi	33.1(30)	32 (2)	33(11)	32(4)	25.6(20)	29(6)	33(15)
	^{nat}Pb	31.5(23)	31.0(16)	35 (8)	27(3)	26.6(22)	25(4)	23 (8)
	^{nat}Tl	31.5(33)	-	27(12)	32(5)	24 (3)	22(7)	34(15)
	^{nat}Hg	30.0(27)	-	24(10)	28(5)	25.5(18)	26(8)	20 (8)
	^{nat}W	22.5(11)	-	17 (7)	19(3)	18.4(15)	18(5)	21 (6)
	^{181}Ta	20.0(15)	19.2 (6)	193(20)[c]	20(4)	17.3(21)	18(5)	21 (8)
	^{165}Ho	15.9(13)	-	17(10)	13(6)	15.6(20)	18(8)	-
	^{nat}Nd	11.4 (7)	14.2 (5)[d]	15 (7)	14(3)	24.2(12)[d]	13(3)	9 (6)
	^{nat}Ce	11.1 (9)	11.0 (5)	-	11(3)	9.5(13)	8(4)	-
	^{127}J	8.4(10)	8.6 (5)	-	9(2)	7 (1)	5(3)	-
	^{nat}Sb	8.0(11)	-	-	10(4)	6.8(19)	-	1,270(50)[c]
	^{nat}Sn	6.5 (7)	7.0 (5)	-	5(2)	7.6 (8)	6(3)	-
	^{nat}Cd	6.2 (5)	-	-	6(2)	6.6 (8)	7(3)	-
120	^{238}U	55.1(25)	64 (4)[c]	43(15)	55(5)	574 (10)[c]	48(5)	48(11)
	^{181}Ta	27.5(15)	25.0 (9)	227(20)[c]	22(5)	21 (2)	22(8)	-
	^{nat}Nd	17.9(30)	17.0 (9)[d]	-	-	29.8(47)[d]	-	-

[a] ^{56}Co source in Fe lattice [b] ^{24}Na source in Al lattice (part of data have been published elsewhere)
[c] Transitions to excited states observed in addition to the ground-state transition
[d] Photoexcitation of nuclear level identified from the size of the differential cross section

(OVER)

Table 2. Elastic differential cross sections $d\sigma/d\Omega(\Theta=90°)$ in μb/sr measured with the Ti(n,γ) source and compared with theoretical predictions. n: predicted number of levels in a $\Delta E=25$ eV interval at 6.5 MeV. Errors in the last digits are given in parentheses

Scattering target	6.418 MeV		6.555 MeV		6.759 MeV		7.168 MeV		n
	exp.	th.	exp.	th.	exp.	th.	exp.	th.	
^{238}U	23 (12)	10.3	-	-	-	-	-	-	45
^{209}Bi	-	-	219(39)[b,c]	8.0	12 (4)	7.4	1.5(3)·10[5 b,c]	5.7	0.1
^{nat}Pb	7.0(15)	8.6	-	-	6.5(11)	7.4	-	-	0.05
^{nat}Tl	2,586 (92)[a,c]	7.5	-	-	13 (3)[b]	6.0	-	-	0.4
^{nat}Hg	12 (3)	7.8	74(17)[b]	6.5	6.7(15)	6.4	-	-	3.4
^{nat}W	159 (10)[a,c]	6.6	306(33)[a,c]	6.3	20 (2)[a,c]	5.6	-	-	13
^{181}Ta	68 (4)[a,c]	6.3	-	-	10.1(12)[b,c]	5.3	-	-	28
^{165}Ho	15 (3)[b]	4.7	-	-	9.5(14)[b]	3.9	-	-	18
^{nat}Ce	4.1(21)	4.1	-	-	17 (1)[b,c]	3.6	-	-	0.04
^{nat}Sn	4.2(13)	3.0	-	-	2.5 (5)	2.7	-	-	1.9
^{nat}Mo	1,474 (44)[a,c]	2.5	407(39)[a,c]	2.5	8.5(15)[b,c]	2.3	817(258)[b,c]	2.0	0.5
^{nat}Zn	2.4 (8)	1.6	-	-	1.8 (5)	1.5	-	-	0.3

[a] Transitions to excited states observed
[b] Photoexcitation identified from size of differential cross section
[c] Photoexcitation reported in [11]

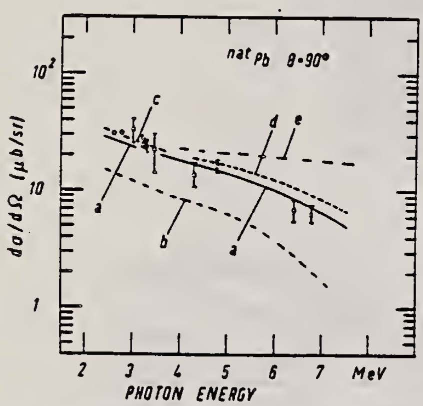

Fig. 8. Differential cross sections for elastic scattering of photons by Pb through $\Theta=90°$ versus energy. (a) calculated including R, T, lowest-order D, and N (Lorentzian shape) scattering. (b) same as (a) but not including lowest-order D scattering. (c) same as (a) but in addition including Coulomb corrections to the D amplitudes. (d) same as (a) but replacing the Lorentzian shape of the GDR by a Breit-Wigner shape. (e) same as (a) but omitting N scattering. (GDR-parameters: $E_1=13.42$ MeV, $\sigma_1=640$ mb, $\Gamma_1=4.05$ MeV.) The data for $E_\gamma=4.291$ and 4.767 have been transferred from $\Theta=120°$ to 90° in proportion to the theoretical predictions (a)

REF. G.W. Dodson, E.C. Booth, F.L. Milder, B.E. Parad, B.L. Roberts, D.R. Tieger, J. Comuzzi
Phys. Rev. C26, 2548 (1982)

ELEM. SYM.	A	Z
Pb		82

METHOD

REF. NO.	
82 Do 3	egf

REACTION	RESULT	EXCITATION ENERGY	SOURCE TYPE	SOURCE RANGE	DETECTOR TYPE	DETECTOR RANGE	ANGLE
G,PIØ	ABY	THR*20	C	140-155	CKV-I		1PI

*MEV ABOVE THR

Photoproduction of π^0 mesons off targets of ^{6}Li, ^{12}C, ^{28}Si, ^{40}Ca, natural Cd, and natural Pb was studied using a bremsstrahlung beam with endpoint energies of 140, 145, 150, and 155 MeV. Photoproduction from a liquid hydrogen target was employed as a normalization. The measured yields were found to be in disagreement with published theoretical cross sections for ^{6}Li$(\gamma,\pi^0)^6$Li and also in disagreement with a simple schematic model which assumed only coherent contributions from the M_{1+} multipole. The schematic model, however, did approximately predict the relative magnitudes of the yield curves for the energy range 14–20 MeV over threshold.

NUCLEAR REACTIONS ^{6}Li, ^{12}C, ^{28}Si, ^{40}Ca, Cd, Pb, (γ,π^0); $E_\gamma = 140-155$ MeV; measured σ; test of reaction model.

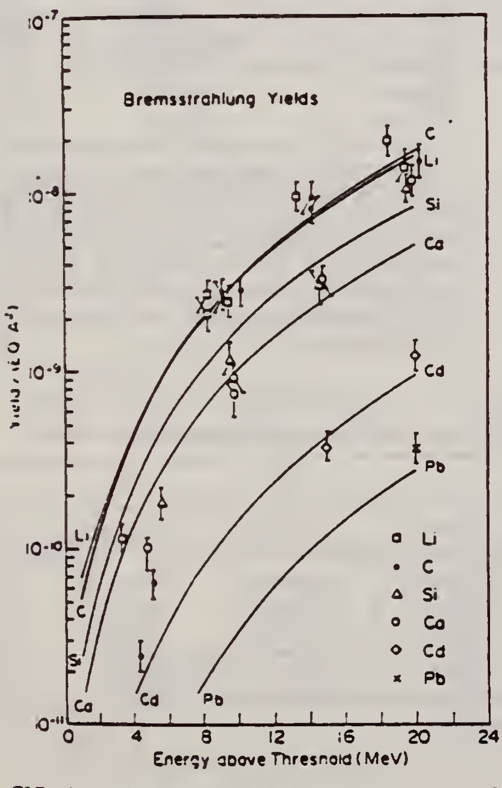

FIG. 6. The experimental and calculated yields for (γ,π^0) off a range of complex nuclei. The data were scaled so that the ^{12}C$(\gamma,\pi^0)^{12}$C experimental yield fit the calculated yield at 9.7 MeV over threshold (see text).

REF. A. Leprêtre, H. Beil, R. Bergère, P. Carlos, J. Fagot, A. Veyssière, I. Halpern
Nucl. Phys. A390, 221 (1982)

ELEM. SYM.	A	Z
Pb		82

METHOD

REF. NO.	
82 Le 3	egf

REACTION	RESULT	EXCITATION ENERGY	SOURCE TYPE	SOURCE RANGE	DETECTOR TYPE	DETECTOR RANGE	ANGLE
G,XN	NOX	30-140	D	30-140	MOD-I		4PI

See also A. Leprêtre et al. NP A390, 240 (1982)

MULT ANAL 81LE1

Abstract: From event-by-event records of observed photoneutron multiplicities for photons from 30 to 140 MeV on several heavy targets (Sn, Ce, Ta and Pb), it was possible to determine the mean number of photoneutrons, $\bar{\nu}$, for each photon energy and the widths W of the multiplicity distributions. The mean neutron numbers increase smoothly from about three to six over the photon energy span for all four targets. The widths go from about one to two neutrons in the same interval. When these measurements are combined with other photonuclear information, it is possible to extract the average numbers of fast neutrons and fast protons and the average number of evaporation neutrons emitted per photoabsorption.

E

PHOTONUCLEAR REACTIONS Sn, Ce, Ta, Pb(γ, xn), E = 25–140 MeV; measured photoneutron mean numbers, width distributions; deduced fast evaporation neutron, fast proton average numbers. Monochromatic photons.

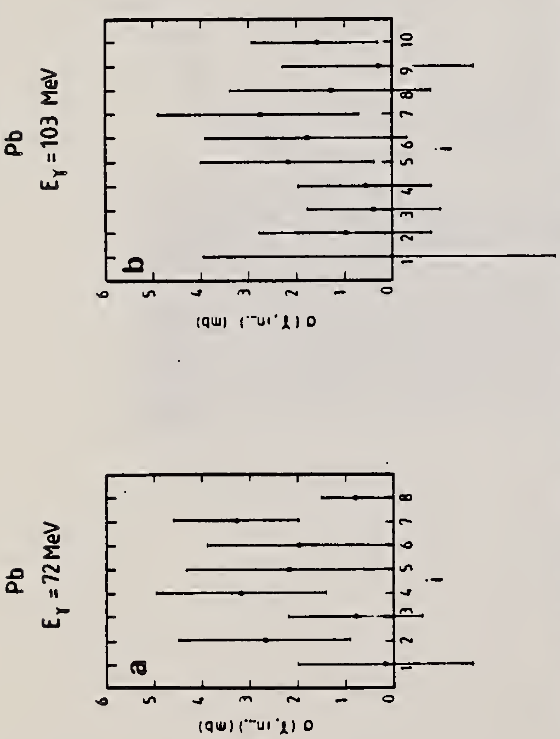

Fig. 1. (a) Partial photoneutron cross sections $\sigma(\gamma, in \cdots)$ for Pb at a fixed "monochromatic" photon energy of E_γ = 72 MeV, plotted against the measured photoneutron multiplicity i. Data points were obtained from ref. [1]. (b) Partial photoneutron cross sections $\sigma(\gamma, in \cdots)$ for Pb at a fixed "monochromatic" photon energy of E_γ = 103 MeV, plotted against the measured photoneutron multiplicity i. Data points were obtained from ref. [1].

Table 1

Nucleon emission features following absorption of a 70 MeV photon by a Pb nucleus

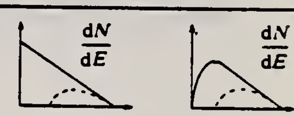

	case (a)	case (b)
α	0.31	0.35
β	1.46	1.37
$\bar{\nu}_f$	0.74 ± 0.16	0.66 ± 0.15
$\bar{\pi}_f$	0.23 ± 0.04	0.23 ± 0.04
$\bar{\nu}_s$	4.1 ± 0.3	4.1 ± 0.3
$\bar{E}_f$ (MeV)	27.3 ± 6	26.6 ± 6
$\bar{E}^*$ (MeV)	42.7 ± 5	43.4 ± 5

Experimental data are taken from ref. [1]) and fig. 2 of this paper. ν stands for neutrons and π for protons; f stands for fast particles and s for evaporated particles. $\bar{E}^*$ is the residual excitation energy after all fast particles have escaped – carrying with them energy $\bar{E}_f$. The coefficients α and β have to do with the ratio of fast neutrons to fast protons that are emitted. They are explained in the text. The uncertainties in this table are statistical only.

Table 2

Photonucleon emission features for four targets at 70 MeV

	Sn	Ce	Ta	Pb
$\bar{\nu}$	4.3 ± 0.2	4 ± 0.2	4.5 ± 0.2	4.8 ± 0.2
$\bar{\nu}_f$	0.50 ± 0.11	0.59 ± 0.13	0.71 ± 0.16	0.66 ± 0.15
$\bar{\pi}_f$	0.24 ± 0.05	0.26 ± 0.05	0.27 ± 0.05	0.23 ± 0.04
$\bar{\nu}_s$	3.8 ± 0.3	3.4 ± 0.3	3.8 ± 0.3	4.1 ± 0.3
$\bar{E}_f$ (MeV)	23.4 ± 5	26.3 ± 6	28.7 ± 6	26.6 ± 6
$\bar{E}^*$ (MeV)	46.6 ± 6	43.7 ± 5	41.3 ± 5	43.4 ± 5

(See caption under table 1.)

(OVER)

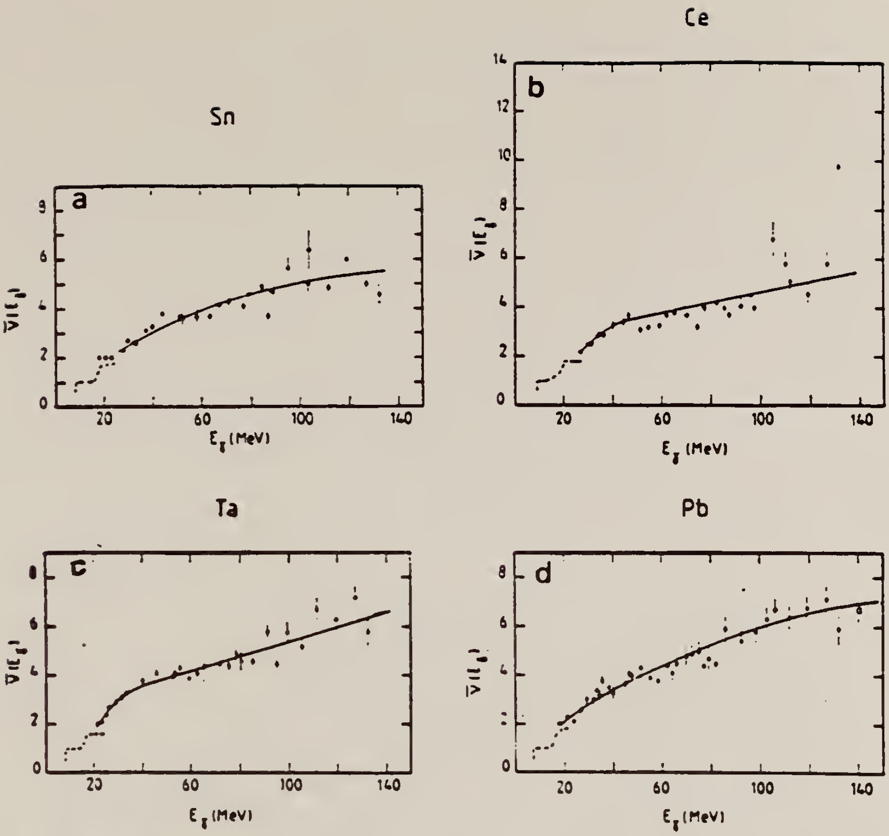

Fig. 2. Average experimental photoneutron multiplicities $\bar{\nu}(E_\gamma)$ plotted against photon energy E_γ for 25 MeV ≤ E_γ ≤ 140 MeV. Data points were evaluated using results from ref. [1]. The full line represents a smoothed average behaviour. The dashed line represents $\bar{\nu}(E_\gamma)$ values, measured in the giant dipole resonance (GDR) region, in previous Saclay experiments [7]. Fig. 2a: Sn; fig. 2b: Ce; fig. 2c: Ta; fig. 2d: Pb [where the ⌶ point refers to the SIN [19]) measurement with stopped π^-].

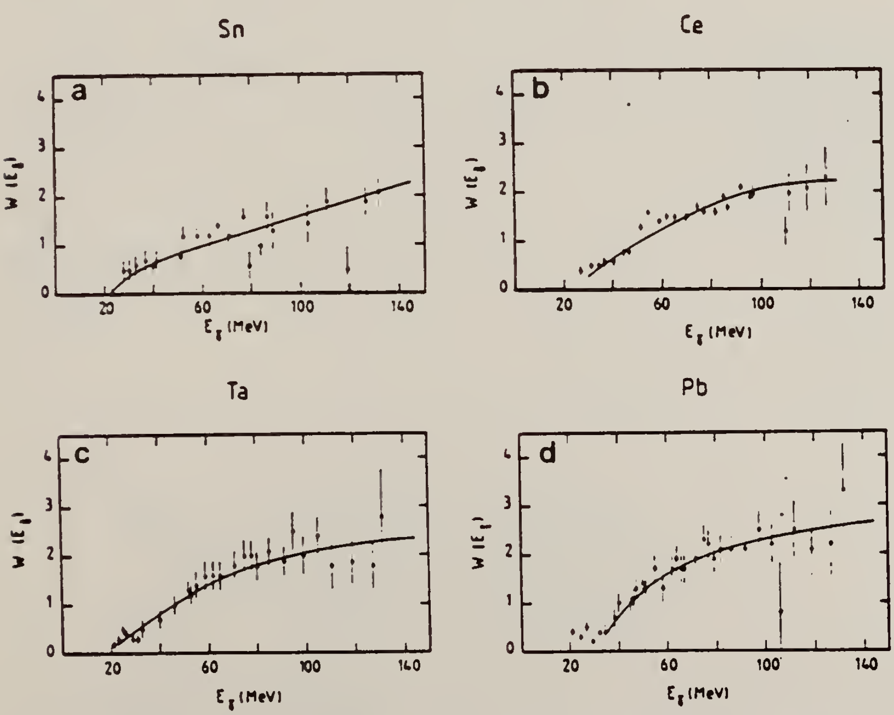

Fig. 3. Widths, $W(E_\gamma)$ of the experimental photoneutron multiplicity distributions as a function of the photon energy E_γ for 25 MeV ≤ E_γ ≤ 140 MeV. Data points were evaluated using results from ref. [1]. The full line represents a smoothed average behaviour. Fig. 3a: Sn; fig. 3b: Ce; fig. 3c: Ta; fig. 3d: Pb.

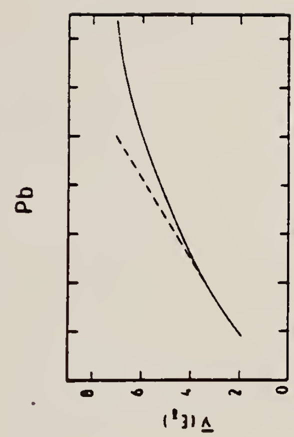

Fig. 4. Average experimental photoneutron multiplicities $\bar{\nu}(E_\gamma)$ for lead plotted against photon energy E_γ for 25 MeV ≤ E_γ ≤ 140 MeV. The full line represents the smoothed average behaviour of fig. 2d. The dashed line represents the prediction of the calculation of Chiang and Wu [12]).

Pb
A=204

Pb
A=204

Pb
A=204

REF.	D. Turck, H.-G. Clerc, H. Trager Phys. Lett. 63B, 283 (1976)	ELEM. SYM.	A	Z
		Pb	204	82

METHOD	REF. NO.	
	76 Tu 2	egf

REACTION	RESULT	EXCITATION ENERGY	SOURCE TYPE	SOURCE RANGE	DETECTOR TYPE	DETECTOR RANGE	ANGLE
E,F	ABX	24- 50	D	38- 50	TRK-I		4PI

FISSION BARRIER

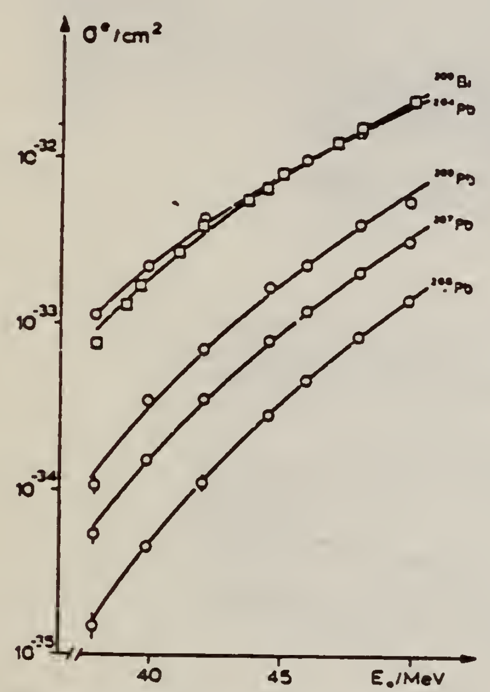

Fig. 1. Cross section σ^e for electron induced fission in $^{204,206,207,208}Pb$ and ^{209}Bi as a function of the incident electron energy E_0.

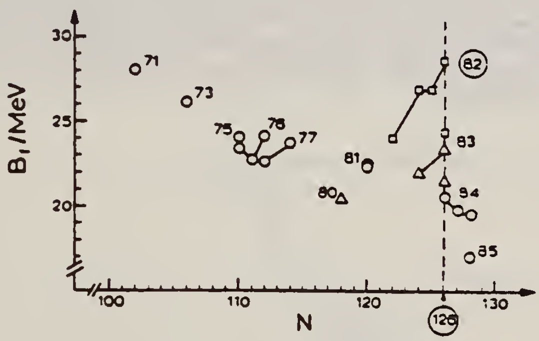

Fig. 2. Summary of fission barrier heights obtained from fits to experimental fission cross sections for nuclei with $Z \leq 85$. ○: α-induced fission [12]. For ^{201}Tl, the value of 22.5±1.5 of ref. [3] is also included; △: proton-induced fission [12]; □: electron induced fission (present work). Values for different isotopes of the same element are connected by straight lines. The nuclear charge numbers are indicated. The erors are ± 1.0 MeV for proton and α-induced fission [12] and ± 1.5 MeV for electron induced fission.

1 U. Mosel, Phys. Rev. C6 (1972) 971.
3 D.S. Burnett et al., Phys. Rev. B134 (1964) 952.
12 L.G. Moretto et al., Phys. Lett. B38 (1972) 952.

Table 2

Fission barriers B_f as determined from electron induced fission. In the last column theoretical fission barriers according to ref. [1] with surface independent pairing strength are listed.

isotope	B_f (MeV)	$B_f^{theor.}$ (MeV)
^{204}Pb	24.0±1.5	24.0
^{206}Pb	26.3±1.5	26.2
^{207}Pb	26.9±1.5	
^{208}Pb	28.6±1.5	28.1
^{209}Pb	24.3±1.5	

REF. K. Masumoto, T. Kato, N. Suzuki
Nucl. Inst. Meth. 157, 567 (1978)

ELEM. SYM.	A	Z
Pb	204	82

METHOD

REF. NO.	
78 Ma 10	hg

REACTION	RESULT	EXCITATION ENERGY	SOURCE		DETECTOR		ANGLE
			TYPE	RANGE	TYPE	RANGE	
G,N	ABY	8-68	C	30-68	ACT - I		4PI
G,3N	ABY	24-68	C	30-68	ACT - I		4PI
G,2N	ABY	15-68	C	30-68	ACT - I		4PI

Analysis is made of reactions interfering with photon activation analysis procedures.

TO PB-202M

The activation yield curves have been presented for a number of photonuclear reactions in the energy range from 30 to 68 MeV, in order to evaluate quantitatively the interferences due to competing reactions in multielement photon activation analysis. The general features of the yields as functions of both target mass number and excitation energy were elucidated from the data obtained, discussion being given on the results in terms of the reaction mechanism.

Simultaneous neutron activation due to appreciable neutron production from the converter and surrounding materials has also been studied, and, finally, the magnitudes of interferences in real multielement analysis were given in the form of their energy dependences.

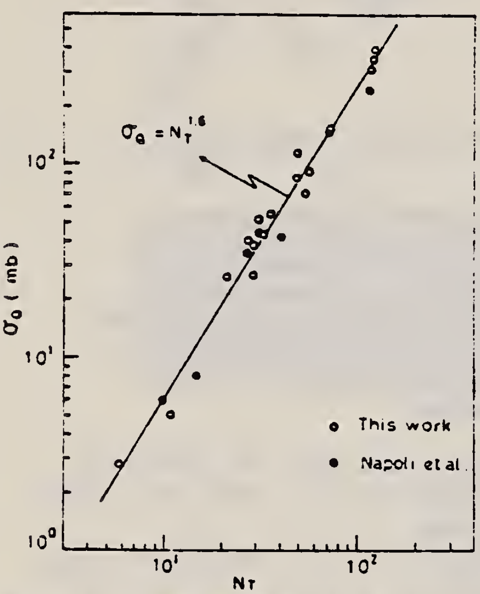

Fig. 2. Yield per equivalent quanta versus target neutron number.

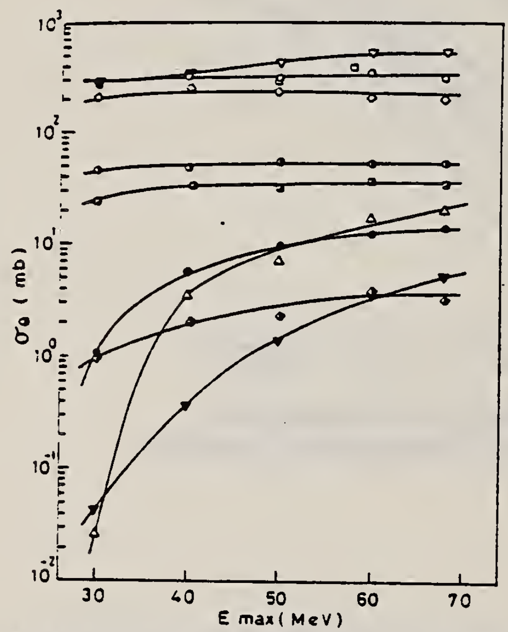

Fig. 8. Activation yield curves for the reactions on Pb, Tl and Hg.

□ $^{204}Hg(\gamma,n)^{203}Hg$.	◇ $^{198}Hg(\gamma,n)^{197g}Hg$.
◪ $^{198}Hg(\gamma,n)^{197m}Hg$.	◆ $^{199}Hg(\gamma,p)^{198}Au$.
▽ $^{204}Pb(\gamma,n)^{203}Pb$.	▼ $^{204}Pb(\gamma,2n)^{202m}Pb$.
△ $^{204}Pb(\gamma,3n)^{201}Pb$.	○ $^{203}Tl(\gamma,n)^{202}Tl$.
◑ $^{203}Tl(\gamma,2n)^{201}Tl$.	● $^{203}Tl(\gamma,3n)^{200}Tl$.

(over)

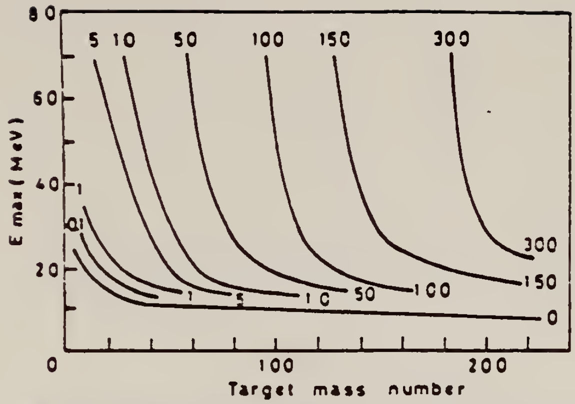

Fig. 9. Yields of the (γ, n) reactions as a function of bremsstrahlung maximum energy and target mass number. The numerical values in the figure are yields per equivalent quanta in mb.

Pb
A=206

Pb
A=206

Pb
A=206

REF.

K. N. Geller, J. Halpern, and E. G. Muirhead
Phys. Rev. 118, 1302-12 (1960)

ELEM. SYM.	A	Z
Pb	206	82

METHOD

Betatron; neutron threshold; ion chamber

REF. NO.	
60 Ge 3	NVB

REACTION	RESULT	EXCITATION ENERGY	SOURCE TYPE	SOURCE RANGE	DETECTOR TYPE	DETECTOR RANGE	ANGLE
G,N	NØX	THR	C THR		BF3-I		4 PI

THRESHØLD

TABLE I. Summary and comparison of neutron separation energies inferred from present threshold measurements with values predicted from mass data and reaction energies. All energies are expressed in the center-of-mass system in Mev.

Reaction	No. runs	Present results	Other results	Method	Reference
$Pb^{206}(\gamma,n)Pb^{205}$	1	8.09 ±0.07	8.10 ±0.05	LSA	s
			8.09 ±0.1	$Pb^{206}(d,t)Pb^{205}$	e

ᵃ P. M. Van Patter and W. Whaling, Revs. Modern Phys. 26, 402 (1954); 29, 756 (1957).
ᵉ J. R. Huizenga, Physica 21, 410 (1955).

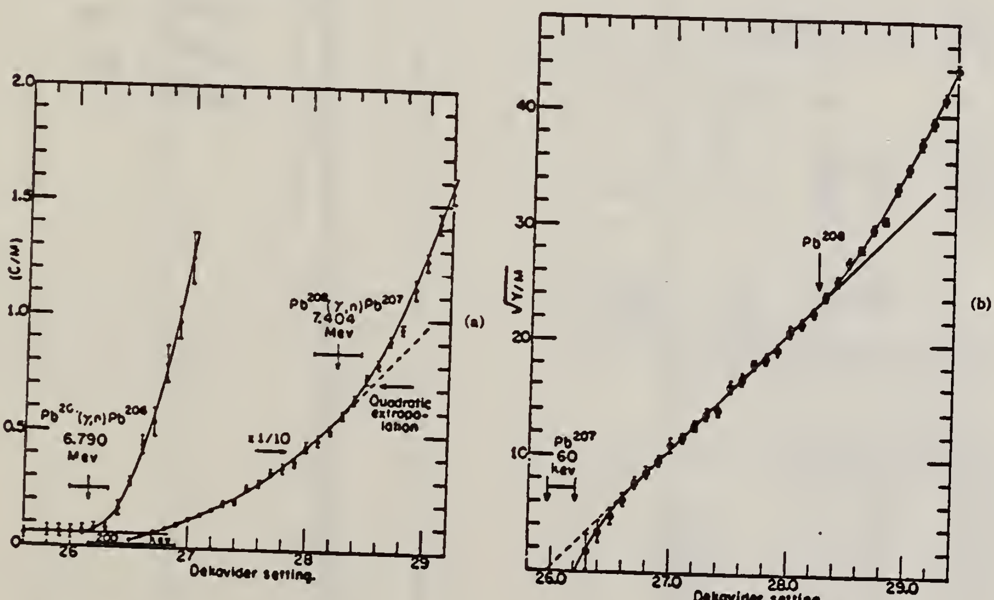

FIG. 2. (a) Neutron yield data for lead from 6.7 Mev to 7.7 Mev, and (b) square root plot of yield data. Linear extrapolation of $(Y/M)^{\frac{1}{2}}$ predicts an apparent threshold 60 kev lower than what is obtained from yield data in the immediate vicinity of threshold.

Ref. K. Reibel , A.K. Mann Phys. Rev. 118, 701 (1960)	Elem. Sym. Pb	A "206"	Z 82
Method: γ's from $F^{19}(p,\alpha\gamma)$ reaction; protons from VandeGraaff; NaI	Ref. No. 60 Re 1		JHH

Reaction	E or ΔE	E_o	Γ	$\int \sigma dE$	Jπ	Notes
(γ,γ)	$E_p = 2.05$					$\langle\bar{\sigma}\rangle = 10.5 \pm 0.8$ mb
					1	D (average level spacing based on J): 6.7 ± 4.5 kev
						$\bar{\Gamma}_{\gamma o}/\bar{\Gamma}_{\gamma} = 0.6 \pm 0.3$
						$\bar{\Gamma}_{\gamma} = 0.9 \pm 0.4$ eV
						$\bar{\Gamma}_{\gamma o} = 0.5 \pm 0.3$ eV
	$E_p = 2.40$					$\langle\bar{\sigma}\rangle = 9.9 \pm 1.5$ mb
	$E_{\gamma} = 6.9$					$\langle\bar{\sigma}\rangle = 9.7 \pm 1.5$ mb
	$E_{\gamma} = 7.1$					$\langle\bar{\sigma}\rangle = 11 \pm 1.6$ mb
						Samples contained: Pb^{206} - 88%, Pb^{207} - 9%, Pb^{208} - 3%

Ref. E.G. Fuller, E. Hayward Nuclear Phys. 33, 431 (1962)	Elem. Sym. Pb	A 206	Z 82
Method 50 MeV betatron; BF_3, NaI counters	Ref. No. 62 Fu 4		JHH

Reaction	E or ΔE	E_0	Γ	$\int \sigma dE$	Jπ	Notes
$Pb^{206,7,8}$						∫ corrected for multiple neutron production.
(γ,γ)	4.5-8.5					Self-absorption measurements made at 7 MeV.
(γ,xn)				$\int^{18.5} = 3.93$ MeV-b		

Table 1

Observed transmissions corrected for electronic absorption

Absorber	Thickness (g/cm²)	Targets: Pb (17.2 g/cm²)		"Pb206" (13.6 g/cm²)		[illegible]	
Pb	10.8					[illegible]	[illegible]
	14.4	0.663	0.032	[illegible]	[illegible]		
		0.694	0.017 *)				
"Pb206"	11.2	0.976	0.050	0.74	[illegible]	1.002	[illegible]
				0.599	0.031 *)		
Bi	12.2	1.018	0.050	1.045	[illegible]	[illegible]	[illegible]
						[illegible]	[illegible] *)
Pb	7.65	0.822	0.029			[illegible]	[illegible]
"Pb206"	7.83	0.790	0.028			[illegible]	[illegible]
"Pb207"	7.86	0.797	0.028			[illegible]	[illegible]
"Pb208"	7.47					[illegible]	[illegible]
Bi	7.49					[illegible]	[illegible]

*) Measured with both target and absorber at liquid nitrogen temperature

Table 3

Average level parameters at 6 MeV

	Lead	Radio-lead	Bismuth
[illegible] Γ^2	[illegible] 1.0	1 - 400	0 - [illegible]
σ_0^2 (b)	24—18	29—205	10—[illegible]
Γ (eV)	[illegible]	0.15 - 3.1	[illegible]
σ_0 (max) (b)	183	205	[illegible]
[illegible] Γ	0.13 - 0.21	0.14 - 1.0	0.2 - 1.0
σ (7 MeV) (mb)	21	20	21
$\int \sigma dE$ (MeV · mb)	42	40	48

SEE PAGE 2 FOR FIGURES.

Ref.	Elem. Sym.	A	Z
	Pb	206	82

Method		Ref. No.	
	PAGE 2	62 Fu 4	JHH

$\int \sigma dE$

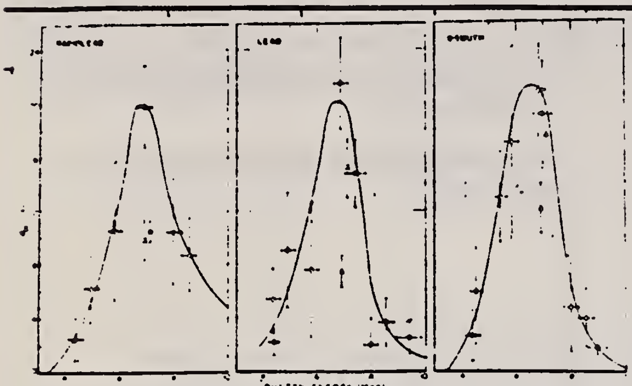

Fig. 1. The elastic scattering cross sections for lead, radiolead and bismuth. The indicated errors are based only on the number of counts. The [illegible] represent data obtained in an earlier experiment [illegible]. The points indicated by triangles at 6.9 and 7.1 MeV are the results of Reibel and Mann [5].

Ref 3: Fuller & Hayward - Phys. Rev. 101, 692 (1956)

Ref 5: Reibel & Mann - Phys. Rev. 118, 701 (1960)

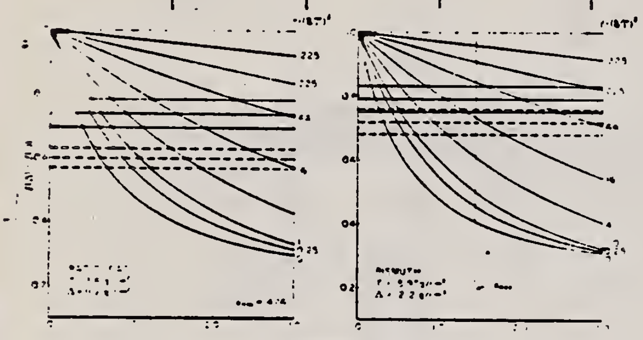

Fig. 5. Self-absorption attenuation curves for radio-lead and bismuth. The ratio $f(\Delta)/f(0)$ as defined in the text (eq. (4)) has been evaluated as a function of the peak absorption cross section σ^0_γ, for the target and absorber thicknesses used in the experiments. The horizontal lines represent the measured attenuations and their uncertainties for the experiments performed at room temperature (solid lines) and liquid nitrogen temperature (dashed lines). The quantity σ_{max} is the maximum possible value of the average peak absorption cross section at 6 MeV in units of 3 times the electronic absorption cross section. This maximum value assumes electric dipole scattering and represents an average over all possible spins for the excited states.

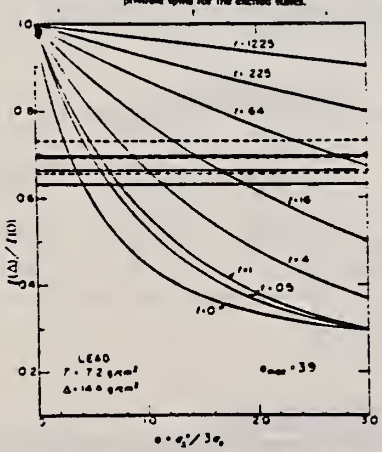

Fig. 6. Self-absorption attenuation curves for lead. See description for fig. 5.

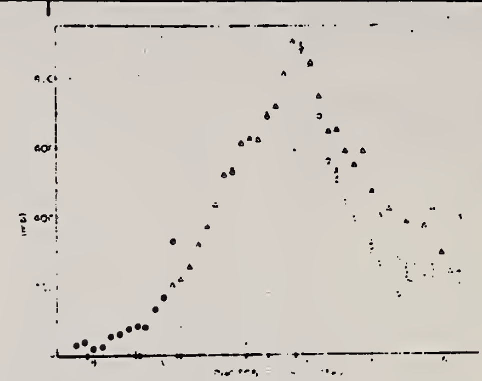

Fig. 7. The neutron production cross section for Pb [illegible]. The [illegible] represent the [illegible] correction for neutron multiplicity. Points were obtained from [illegible] MeV [illegible] neutron yield curve except near threshold [illegible]. The points represented by the open circles have been corrected for [illegible]. The arrows beneath the axis of abscissas indicate the energies of the important dipole transition calculated by Balashov, et al. [11]. The heights of the vertical lines are proportional to the calculated strengths of the transitions.

Ref 11: Balashov, Shevchenko & Yudin, to be published: Shevchenko, private communication.

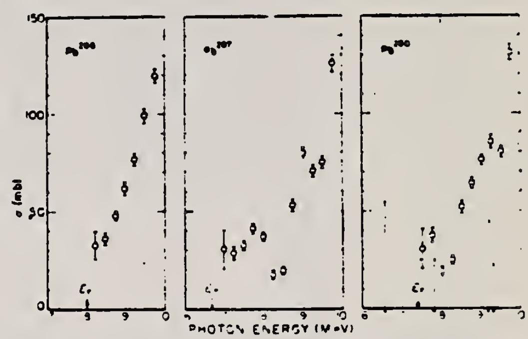

Fig. 8. The (γ, n) cross sections for the lead isotopes near threshold. The arrows indicate the positions of the (γ, n) thresholds. The arrows beneath the axis of abscissas indicate the energies of the important dipole transition calculated by Balashov et al. [11]. The heights of the vertical lines are proportional to the calculated strengths of the transitions.

Ref. P.Axel, K.Min, N.Stein, D.C.Sutton Phys.Rev.Letters 10, 299 (1963)	Elem. Sym. Pb	A 206	Z 82
Method: Bremsstrahlung monochromator	Ref. No. 63Axl		B G

Reaction	E or ΔE	E_o	Γ	∫σdE	Jπ	Notes
(γ,γ)		7.85	(350 KeV)			Quasi-elastic scattering - poor resolution of photon; detector did not separate high energy inelastic scattering from elastic scattering. Fig. 135° quasi-elastic cross section. Target Pb^{206} 88%, Pb^{207} 9%, Pb^{208} 3%. Cross section scales assume all scattering due to Pb^{206}. Triangles indicate Pb^{208} contributions from its three levels. Optical model considered.

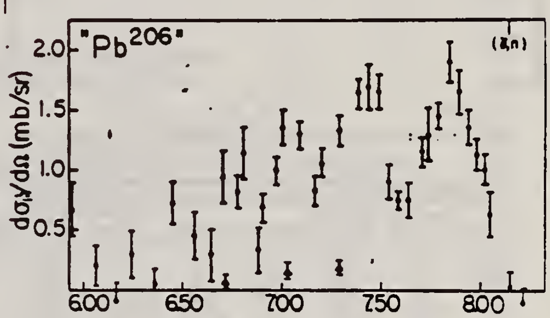

FIG. 1. 135° differential quasi-elastic photon scattering cross sections. The energy resolution values irregularly from about 75 keV to 200 keV because some measurements were combined. Relevant (γ,n) thresholds are shown along upper abscissa in 1(a)-1(c). (a) The target consisted of a natural mixture of Pb isotopes (Pb^{204}, 1%; Pb^{206}, 25%; Pb^{207}, 22%; Pb^{208}, 52%). The cross-section scale assumes that the observed scattering was due entirely to Pb^{208}. The solid lines show the limits of the cross section attributable to Pb^{206}. The data are consistent with three very narrow nuclear levels at 6.72 MeV, 7.03 MeV, and 7.29 MeV; the apparent cross sections are a function of the resolution. (b) The target was enriched Pb^{206} (Pb^{206}, 88%; Pb^{207}, 9%; Pb^{208}, 3%). The cross-section scale assumes all the scattering is due to Pb^{206}. The triangles indicate the energies of and the contributions attributable to the three levels in Pb^{208}.

REF.	ELEM. SYM.	A	Z
R.R. Harvey, J.T. Caldwell, R.L. Bramblett, S.C. Fultz Phys. Rev. 136, B126-31 (1964)	Pb	206	82

METHOD	REF. NO.	
Positron annihilation; ion chamber	64 Ha 2	NVB

REACTION		RESULT	EXCITATION ENERGY	SOURCE		DETECTOR		ANGLE
				TYPE	RANGE	TYPE	RANGE	
G,N	170	ABX	6-27	D	6-26	BF3-I		4PI
G,2N	171+	ABX	12-27	D	12-26	BF3-I		4PI

170+

Sample enriched to 99.77% Pb^{206}.

$(\gamma,2n)$ threshold 14.87 ± 0.15 MeV

TABLE I. Integrated cross sections in MeV-b, up to 28 MeV, for Pb isotopes and Bi.

Isotope	$\int_0^{28}\sigma(\gamma,n)dE$	$\int_0^{28}\sigma(\gamma,2n)dE$	$\int_0^{28}\sigma dE$	$\int_0^{28}\sigma dE+W$	$0.06NZ/A$
Pb^{206}	2.22	0.56	2.78±0.28	3.07±0.36	2.96
Pb^{207}	2.05	0.60	2.65±0.27	2.95±0.30	2.97
Pb^{208}	1.96	0.95	2.91±0.29	3.21±0.32	2.98
Bi^{209}	2.17	0.76	2.93±0.29	3.25±0.33	3.00

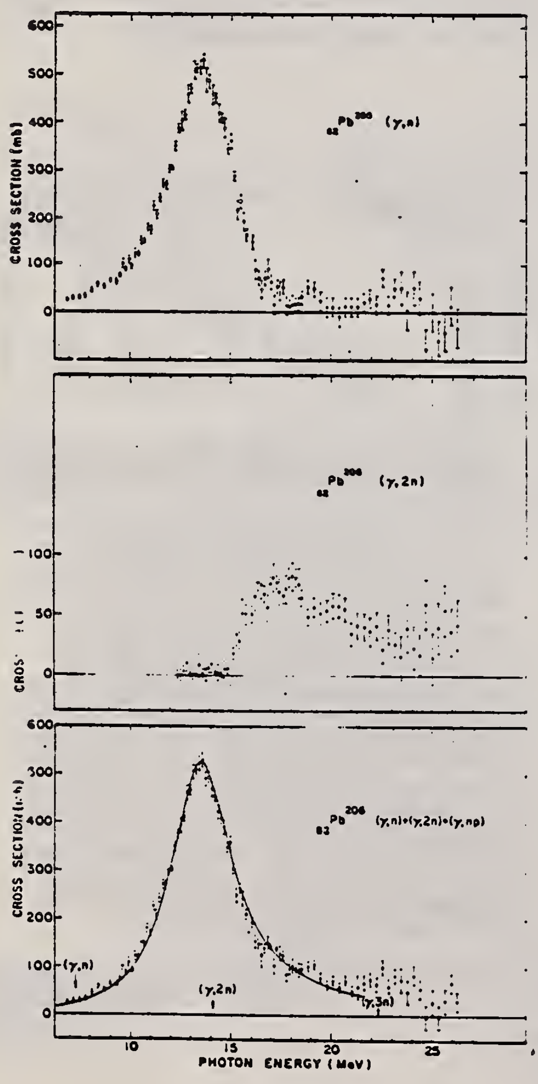

TABLE II. Lorentz line parameters and σ_{-2} values for Pb isotopes and Bi.

Isotope	Peak σ_0 (mb)	Width Γ (MeV)	E_0 (MeV)	σ_{-2} (mb/MeV)	$0.00225A^{5/3}$ (mb/MeV)
Pb^{206}	525	3.75	13.7	15.6±1.6	[illegible]
Pb^{207}	485	3.87	13.6	14.5±1.5	[illegible]
Pb^{208}	495	3.78	13.6	14.1±1.4	[illegible]
Bi^{209}	520	3.83	13.5	16.6±1.7	[illegible]

FIG. 1. Points shown in top figure are $\sigma[(\gamma,n)+(\gamma,np)]$ for Pb^{206} which was obtained from single-neutron counting data. Center figure shows data points for $\sigma(\gamma,2n)$, obtained from double-neutron counting data. Bottom figure shows data for $\sigma[(\gamma,n)+(\gamma,np)]+\sigma(\gamma,2n)$ for Pb^{206}, which represent the formation cross section for the compound nucleus. Solid curve is a plot of a Lorentz line having parameters given in Table II. The data are uncertain below 8 MeV owing to low beam intensities encountered

REF.	ELEM. SYM.	A	Z
G. Ben-David, B. Arad, J. Balderman, and Y. Schlesinger Phys. Rev. 146, B852 (1966)	Pb	206	82

METHOD	REF. NO.	
Nuclear Resonance Scattering using N,G reactions.	66 Be 3	JDM

REACTION	RESULT	EXCITATION ENERGY	SOURCE TYPE	SOURCE RANGE	DETECTOR TYPE	DETECTOR RANGE	ANGLE
G,G	RLX	5 - 10	D	5 - 10	NAI-D	5 - 10	135

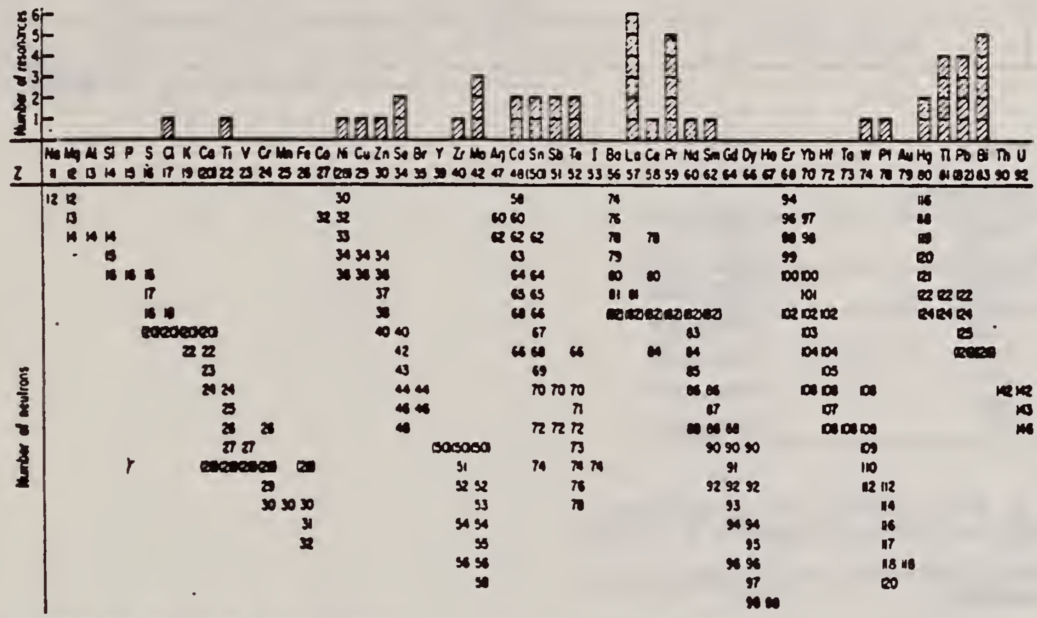

FIG. 3. Histogram of distribution of observed resonances among the different targets. The atomic number is given directly beneath the chemical symbol followed by the neutron numbers of the naturally occurring isotopes. Magic numbers are shown in brackets.

TABLE III. List of effective cross sections.

Scatterer	Energy (MeV)	Gamma source	δ (mb)	Scatterer	Energy (MeV)	Gamma source	δ (mb)
Sm^{148}	8.997	Ni	100	Sn	7.01	Cu	110
Pr^{141}	8.881	Cr	9	Nd	6.867	Co	30
La	8.532	Ni	6	Pr^{141}	6.867	Co	3
Te	8.532	Ni	3[e]	Te	6.7	Ni	...
Cu	8.499	Cr	24	La	6.54	Ag	12
Zr	8.496	Se	3050	Cd	6.474	Co	110
Zn	8.119	Ni	13	Mo	6.44	Hg	25[g]
Se	7.817	Ni	50	La	6.413	Ti	72
Se	7.76	K	90	Mo	6.413	Ti	10
Sb	7.67	V	...[b]	Tl	6.413	Ti	25
Cd	7.64	Fe	40[c]	W	~6.3	Ti	...[b]
Ni	7.64	Fe	7[c]	Sb	6.31	Hg	6[g]
Pr^{141}	7.64	Fe	12[c]	Ti	6.31	Hg	2[g]
Tl	7.64	Fe	370[c]	Sn	6.27	Ag	75
La	7.634	Cu	7	Pb^{208}	6.15	Gd	...[i]
Mo	7.634	Cu	11	Te	5.8	Ni	...[f]
Bi^{209}	7.634	Cu	4	La	6.12	Cl	35
Te	7.528	Ni	66[d]	Pr^{141}	6.12	Cl	110
Bi^{209}	7.416	Se	100	Pt	5.99	Hg	40[a,g]
Bi^{209}	7.300	As	80[e]	Tl	5.99	Hg	5[g]
Pb^{208}	7.285	Fe	4100	Pb^{208}	5.9	Sr	...[h]
Cl	7.285	Fe	34	Ce	5.646	Co	17
Pr^{141}	7.185	Se	80	Bi^{209}	5.646	Co	55
Tl	7.16	Cu	120	Pb^{208}	5.53	Ag	70
La	7.15	Mn	50	Hg	5.44	Hg	75[g]
Bi^{209}	7.149	Ti	2000	Hg	4.903	Co	385

[a] High-energy component of a complex spectrum.
[b] A broad scattered spectrum with no observable peak structure.
[c] There are actually two lines of energies 7.647 and 7.633 MeV having equal intensities in the iron capture gamma spectrum. The cross section has therefore been corrected, although there is no possibility at present of deciding which line is responsible for each resonance.
[d] Is probably an independent level in the complex spectrum of Ni γ rays on Te.
[e] Rough estimate.
[f] May be inelastic component from 7.528 level in Te.
[g] The relative line intensities in this case are due to Groshev and co-workers.
[h] No line is known for the source at this energy.
[i] Difficult to resolve among the many source lines present at this energy.

REF.	ELEM. SYM.	A	Z
J. F. Ziegler and G. A. Peterson Proc. Gatlinburg Conference 319 (1966)	Pb	206	82

METHOD	REF. NO.	
	66 Zi 2	hmg

REACTION	RESULT	EXCITATION ENERGY	SOURCE TYPE	SOURCE RANGE	DETECTOR TYPE	DETECTOR RANGE	ANGLE
E,E/	RLX		D	28-70	MAG-D		DST

B(EL)

TABLE 1

Values of B(E3↑)

Isotope	Energy level	B(E3↑) (e^2b^3)
^{209}Bi	2.58	0.527 ± .012
	2.58 2.73	0.773 ± .020
^{208}Pb	2.615	0.788 ± .028
^{207}Pb	2.62 2.66	0.740 ± .012
^{206}Pb	2.60	0.702 ± .032

2. Tuan, S. T., and Wright, L. E., Bull. Am. Phys. Soc. 11, 338 (1966); Reynolds, J. T., Ph. D. Thesis, Duke University; Onley, D. S., private communications.
3. Elton, L. R. B., "Nuclear Sizes," Oxford Univ. Press, London, 1961); Hofstadter, R., private communication.

REF.
R. R. Hurst and D. J. Donahue
Nucl. Phys. A91, 365 (1967)

ELEM. SYM.	A	Z
Pb	206	82

METHOD
Neutron capture gamma rays

REF. NO.	
67 Hu 1	EGF

REACTION	RESULT	EXCITATION ENERGY	SOURCE TYPE	SOURCE RANGE	DETECTOR TYPE	DETECTOR RANGE	ANGLE
G,N	ABX	9-11	D	9-11	BF3-1		4PI

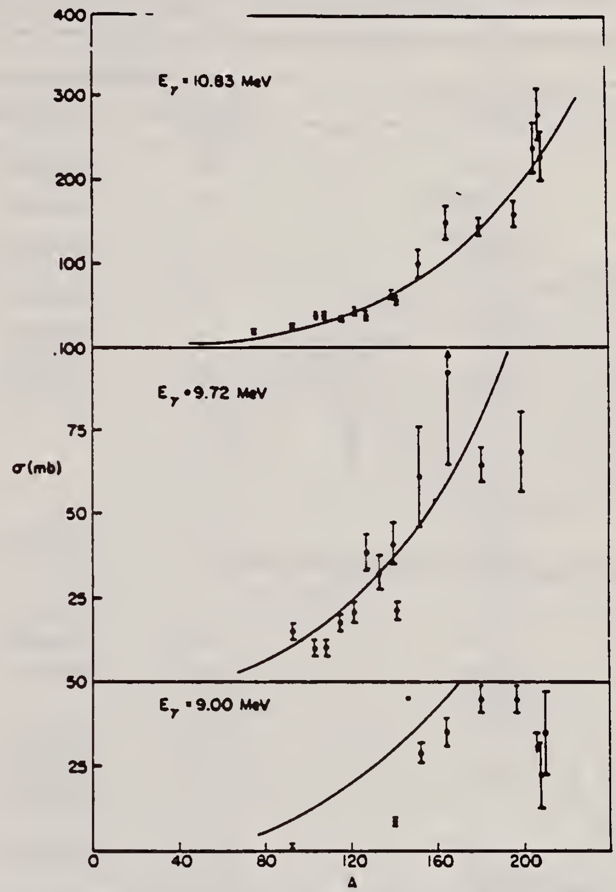

Fig. 1. Cross section (in mb) versus mass number of the target for gamma-ray energies of 9.00, 9.72 and 10.83 MeV. The solid lines are plots of eq. (1) in the text.

TABLE 1
Photoneutron cross sections (mb)

Target	7.72 MeV	9.00 MeV	9.72 MeV	10.83 MeV
^{59}Co				9.0 ± 0.8
^{75}As				20.4 ± 1.7
^{93}Nb		0.53 ± 0.10	14.6 ± 2.2	25.8 ± 2.1
^{103}Rh			10.6 ± 1.7	38.8 ± 3.1
^{107}Ag, ^{109}Ag			10.0 ± 1.5	37.6 ± 2.9
^{115}In			17.1 ± 2.6	33.3 ± 2.7
^{121}Sb, ^{123}Sb			20.7 ± 3.1	42.5 ± 3.6
^{127}I			38.7 ± 5.8	38.8 ± 3.1
^{133}Cs			31.7 ± 4.8	52.5 ± 3.8
^{139}La		8.61 ± 0.86	40.8 ± 6.5	63.0 ± 5.0
^{141}Pr			21.5 ± 3.2	58.3 ± 4.1
^{151}Eu, ^{153}Eu		28.9 ± 3.2	61.3 ± 14.7	102 ± 18
^{165}Ho		35.6 ± 4.3	92.2 ± 27.6	150 ± 20
^{181}Ta	4.14 ± 0.36	45.4 ± 3.7	65.0 ± 5.5	146 ± 12
^{197}Au		44.5 ± 3.6	68.4 ± 13.5	160 ± 15
^{206}Pb		< 34.3		238 ± 29
^{208}Pb		22.6 ± 11.3		280 ± 31
^{209}Bi		36.1 ± 12.0		226 ± 27

U.S. DEPARTMENT OF COMMERCE
NATIONAL BUREAU OF STANDARDS

REF.	ELEM. SYM.	A	Z
J. F. Ziegler and G. A. Peterson Phys. Rev. <u>165</u>, 1337 (1968)	Pb	206	82
METHOD	**REF. NO.** 68 Zi 1		HMG

REACTION	RESULT	EXCITATION ENERGY	SOURCE		DETECTOR		ANGLE
			TYPE	RANGE	TYPE	RANGE	
E,E/	FMF	2-5	D	28-73	MAG-D	28-73	100

SEP ISTOPS, B(EL)

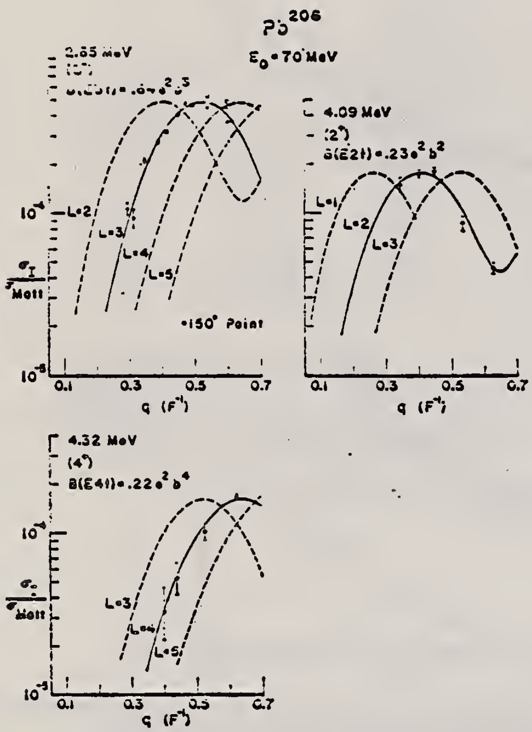

FIG. 13. Experimental relative cross sections versus momentum transferred to the nucleus Pb206 normalized to an initial electron energy of 70 MeV for excitations at 2.649, 4.09, and 4.32 MeV. The solid curve is the best fit of the GBROW calculation assuming the Tassie hydrodynamical model for the specified transition multipolarity and the dashed curves are arbitrarily normalized for other transition multipolarities.

OVER

TABLE II. Experimental values of reduced nuclear transition probabilities $B(EL)$ for the excitation of a nucleus from its ground state to an excited state as determined by the electron scattering methods of this experiment and by other methods. The units of $B(EL)$ are e^2b^L where e is the electron charge, b is 10^{-24} cm^2 (1 b), and L is the multipolarity of the transition. $B(EL)_{sp}$ is the single-particle estimate of Eq. (10).

			This experiment			
Nuclide	Level (MeV)	Transition character	$B(EL, 0 \rightarrow L)$ e^2b^L	$G = \frac{B(EL)}{B(EL)_{sp}}$	Ref.	Other experiments $B(EL, 0 \rightarrow L)$ e^2b^L
Pb^{206}	4.09	$E2$	0.25±0.02	6.2	a	(p,p')0.20
Pb^{207}	4.080[b] 4.125[b]	$E2$	0.26±0.02	7.0	c d	(α,α')0.33 (p,p')0.18
Pb^{208}	4.07	$E2$	0.30±0.02	8.1	c e	(α,α')0.33 (p,p')0.17
Pb^{206}	2.65	$E3$	0.64±0.04	35	a	(p,p')0.53
Pb^{207}	2.625[b] 2.664[b]	$E3$	0.67±0.04	37	c d	(α,α')0.56 (p,p')0.32
Pb^{208}	2.614	$E3$	0.72±0.04	39.5	c f g e h i j k	(α,α')0.57 (e,e')0.53 (p,p')0.67 (p,p')0.56 $(C^{12},C^{12\prime})$0.83 (p,p')0.84 (p,p')0.97 (n,n')0.71
Bi^{209}	2.6[l]	$E3$	0.67±0.05	37	c f m	(α,α')0.57 (e,e')0.55 (p,p')0.65
Pb^{206}	4.32	$E4$	0.22±0.02	25	a	(p,p')0.058
Pb^{207}	4.29	$E4$	0.21±0.03	24	c	(α,α')0.12
Pb^{208}	4.31	$E4$	0.23±0.02	26	c f e	(α,α')0.13 (e,e')0.24 (p,p')0.057
Pb^{208}	5.25	$E3$ $(E4)$	0.13±0.03 0.14±0.07	7.2 16		
Pb^{208}	5.6	$E3$	0.09±0.03	5	c	(α,α')0.16
Pb^{208}	6.2	$E2$ $(E0)$	0.07±0.02	2		
Pb^{208}	3.2	$E5$	0.06±0.02	14	c e	(α,α')0.03 (p,p')0.034

[a] G. Vallois, J. Saudinos, and O. [illegible], Phys. Letters 24, 512 (1967).
[b] Peaks were not resolved in this experiment [illegible] taken from J. C. Hafele and R. Woods, Phys. Letters 24, 579 (1966).
[c] [illegible] Alster, Phys. Rev. 141, 1138 [illegible] Letters 25B 459 (1967).
[d] G. Vallois, J. Saudinos, O. Beer, [illegible] P. Lopato, Phys. Letters 22, 659 (1966).
[e] J. Saudinos, G. Vallois, O. Beer, [illegible] P. Lopato, Phys. Letters 22, 492 (1966).
[f] H. Crannell, R. Helm, [illegible] and M. [illegible]man, Phys. Rev. 123, 923 (1961); and H. W. Kendall and J. Oeser, *ibid.* 130, 245 (1963).
[g] A. Scott and M. P. Fricke, Phys. Letters 20, 654 [illegible].
[h] A. Z. Hrynkiewicz, S. Kopta, S. [illegible] and T. Walczak, Nucl. Phys. 79, 495 (1966), references cited therein, and see text of this section.
[i] G. R. Satchler, R. H. Bassel, and [illegible], Phys. Letters 5, 256 (1963).
[j] T. Stovall and N. M. Hintz, Phys. Rev. 135, B330 (1964).
[k] P. H. Stelson *et al.*, Nucl. Phys. 68, 97 (1965).
[l] Approximate energy of seven [illegible]. J. C. Hafele and R. Woods, Phys. Letters 24, 579 (1966).
[m] S. Hinds, H. Marchant, J. H. [illegible], and O. Nathan, Phys. Letters 20, 674 (1966).

C. D. Bowman, B. L. Berman and H. E. Jackson Phys. Rev. 178, 1827 (1969)	ELEM. SYM.	A	Z
	Pb	206	82

METHOD	REF. NO.	
	69 Bo 1	hmg

REACTION	RESULT	EXCITATION ENERGY	SOURCE		DETECTOR		ANGLE
			TYPE	RANGE	TYPE	RANGE	
G,N	SPC	THR-10	C	8-10	TOF-D		135

G-Width

Tabular data given.

TABLE VI. Resonance parameters.

Isotope	Energy in (n, γ) This work	b	c	$g\Gamma_{\gamma 0}$[a] This work	d	$g\Gamma_\gamma$ c	b	Spectroscopic data b	d
	(keV)	(keV)	(keV)	(eV)	(eV)	(eV)	(eV)	l	J^π
Pb^{206}	3.00		3.02	0.08±0.03[e]		0.078±0.005			
	10.4		10.2	0.06±0.02		0.13±0.02			
	16.6	16.7	16.2	0.14±0.04		0.66±0.07	0.3±0.07	(>0)	(2^+)
	25.3			<0.2					
		29	29.5	<0.4		0.20±0.06	0.35±0.13	(>0)	(2^+)
		37	37.6	<0.4		0.7±0.1		(>0)	(2^+)
	40.9[f]	41.7	41.0	4.13	4.13	3.8±0.4	4.13±0.9	0	(1^-)
Pb^{207}	3.4		3.36	0.14±0.03		0.077±0.006			
			10.8	<0.05		0.06±0.01			
	11.4[g]		11.3	0.54±0.08		0.07±0.02			
	12.3	12.2		0.05±0.03				(>0)	
	14.6[g]		14.2	0.55±0.10		0.20±0.04			
	16.6[f]	16.5	16.5	0.63	0.63±0.03	0.70±0.08	0.8±0.12	(>0)	($\frac{1}{2}^-$)
	20.1		19.6	0.169±0.08		0.32±0.06			
		21	21.8	<0.05		0.28±0.1	0.18±0.07		
	25.1	25.1	24.9	0.4±0.15	0.28±0.03	1.1±0.2	0.77±0.12	(>0)	($\frac{1}{2}^-$)
Pb^{208} [h]	1.55			0.40±0.06					
	7.34			3.4±0.30					
	10.2			1.0±0.15					
	16.0			0.50±0.15					
	33.6								
	49.9								

[a] The statistical factor g is different depending on whether neutrons or photons excite the nucleus. To make easier a comparison of the results, the present values for Pb^{206} and Pb^{207} have been multiplied by the ratio $(2I'+1)/(2I''+1)$ where I' is the spin of the target for the photonuclear experiment and I'' is the target spio for the inverse experiment. The Pb^{208} values are unmodified.
[b] Reference 4.
[c] Reference 6.
[d] Reference 7.

[e] The uncertaioties io the values for $g\Gamma_{\gamma 0}$ for all isotopes do not include a ±15% uncertainty in oormalization.
[f] The preseot data were normalized at these resonances using the data from Ref. 7.
[g] These peaks are associated with transitions both to the ground state and the first excited state of Pb^{206}. The excited-state transitions are the strooger (see text).
[h] For Pb^{208}, the energies have not been transformed ioto the (η, γ) system.

REF. V. V. Verbinski and W. R. Burrus
Phys. Rev. 177, 1671 (1969)

ELEM. SYM.	A	Z
Pb	206	82

METHOD

REF. NO.	
69 Ve 1	hmg

REACTION	RESULT	EXCITATION ENERGY	SOURCE TYPE	SOURCE RANGE	DETECTOR TYPE	DETECTOR RANGE	ANGLE
G,XN	SPC	THR-33	C	33	TOF-D	0-14	DST

ENRICHED PB206

TABLE II. (γ,n) reactions induced by 33-MeV end-point thin-target bremsstrahlung.

Target	E_γ giant resonance peak (MeV)	θ	T[a] (MeV)	Thresholds (γ,n)	(γ,pn)	$(\gamma,2n)$
^{27}Al	~22	55°	3.07±0.1	13.1	19.4	24.4
		93°	3.07±0.1			
^{206}Pb	~13	90°	1.50±0.1	8.0	14.8	14.8
		141°	1.43±0.1			
^{208}Pb	~13	90°	1.52±0.1	7.4	14.8	14.1
		141°	1.52±0.1			
^{209}Bi	~13	90°	1.66±0.1	7.4	11.1	14.3
		141°	1.47±0.1			

[a] From plot of $\ln[\phi(E)/\sigma_c E^{5/11}]$ versus E.

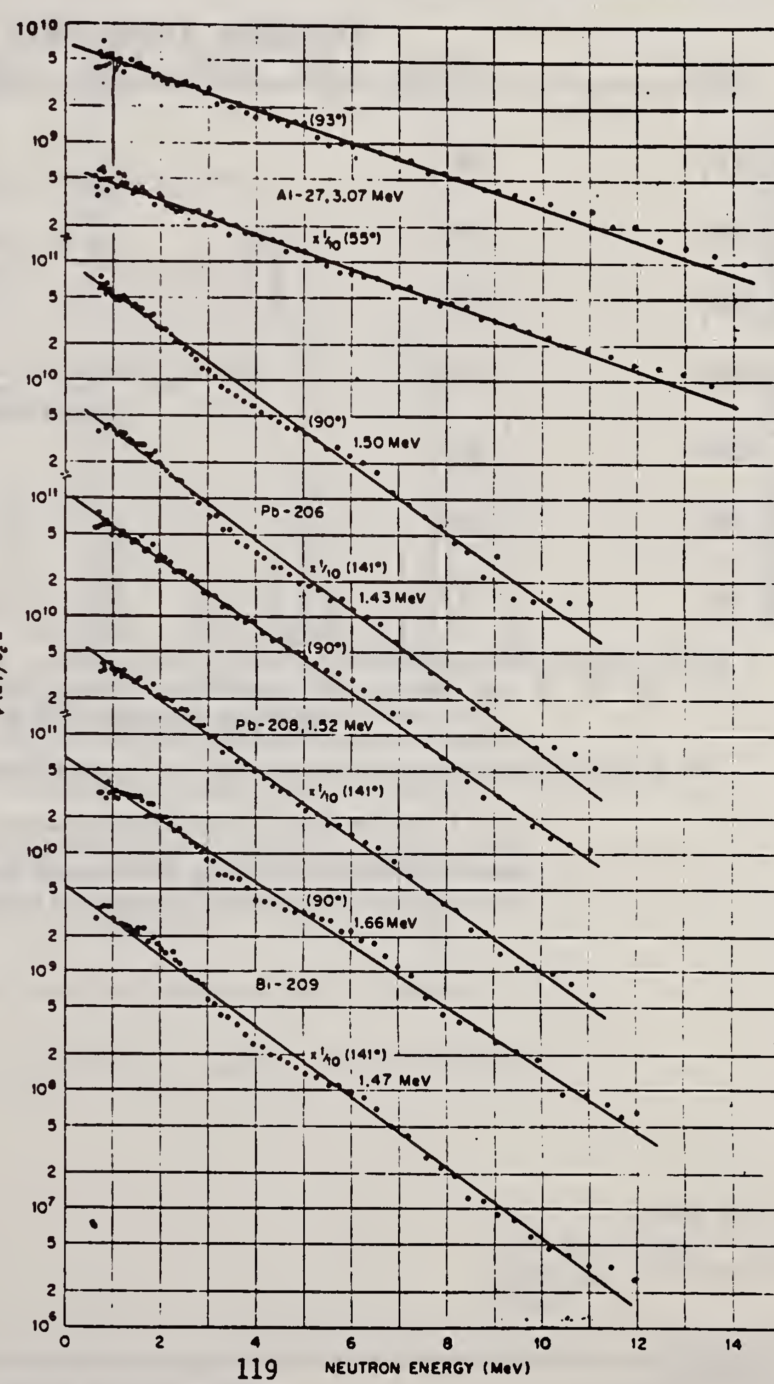

FIG. 7. Evaporation-analysis plots of neutron spectra from (γ,n) reactions. The logarithmic plots of $\phi(E)/(\sigma_c E^{5/11})$ show moderately good straight-line fits. Values of T, the magnitude of the reciprocal slope, are shown. In some cases, T is slightly higher at 90° than at 141°, indicating that a weak component of direct emissions is present. These are preferentially emitted at 90°, the direction of the electromagnetic field.

FORM NBS-418
(REV. 7-14-64)
USCOMM-DC 28010-P64

57

REF. R. J. Baglan, C. D. Bowman and B. L. Berman
Phys. Rev. C3, 672 (1971)

ELEM. SYM.	A	Z
Pb	206	82

METHOD

REF. NO.	
71 Ba 2	hmg

REACTION	RESULT	EXCITATION ENERGY	SOURCE TYPE	SOURCE RANGE	DETECTOR TYPE	DETECTOR RANGE	ANGLE
G,N	ABX	8-10	C	9,10	TOF-D		135
		(8.08-10)					

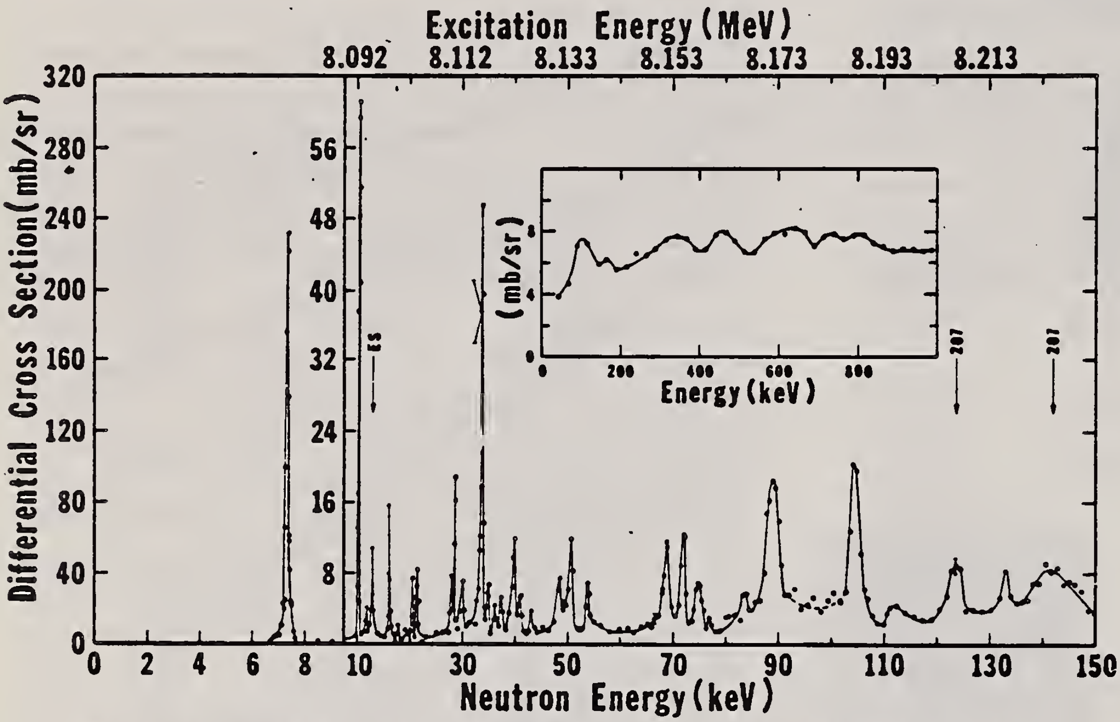

FIG. 8. The 135° differential threshold photoneutron cross section for ^{206}Pb (see caption to Fig. 4).

FIG. 4. The 135° differential threshold photoneutron cross section for ^{207}Pb at low energies versus the energy of the emitted neutron (lower scale) and the excitation energy (upper scale). The arrows indicate peaks which decay to excited states of the residual nucleus (ES), or peaks owing to contaminating isotopes in the photoneutron sample. The inset shows the ^{207}Pb(γ, n) cross section averaged with a square 40-keV wide smoothing function.

Also see:
R. J. Baglan et al.
Phys. Rev. C3, 2475
(1971)

[over]

TABLE IV (*Continued*)

Nucleus	E_L (keV)	E_{ex} (MeV)	$g_\gamma \Gamma_{\gamma 0} \Gamma_n / \Gamma$ (eV)	GS or ES	J^π	$\Gamma_{\gamma 0}$ (eV)	E_n (keV) (This work)	E_n (keV) from neutron-induced reactions (Ref. a)	(Ref. b)	(Ref. c)
^{208}Pb	2.9 [e]	7.379	0.16				3.0			
	8.9 [e]		0.62	ES						
	9.9 [e]	7.386	0.12	GS [e]			10.1			
	15.9 [e]	7.392	0.17	GS [e]	2^+ [a]	0.06	16.2	17		
	24.9 [d]	7.401	<0.40	GS [d]			25.3			
	30.2	7.406	0.30	GS	1^+ [f]	0.23	30.7	29		
	35.4		0.22	ES						
	37.5	7.413	1.8	GS	2^+ [a,f]	0.64	38.1	37		
	40.8 [e]	7.417	7.2	GS	1^- [a]	4.8	41.4	41		
	90.0	7.466	2.6	GS			91.3			
	98.6		1.9	ES						
	114	7.490	2.0		1^+ [f]	1.6	115			
	129	7.506	5.4	GS			131			129
	138		3.6	ES						
	156	7.533	0.98	GS			158			
	166	7.543	0.90	GS			168			
	182	7.559	16.0	GS	1^+ [f]	12.6	184			
	257	7.634	26.2	GS	1^- [f]	17.5	260			
	299		4.0	ES						
	318	7.696	11.0	GS	1^+ [f]	7.7	321			
	493	7.872	3.2				498			
	547	7.926	12.3	GS	$1^-(1^+)$ [f]	8.2	553			
	558	7.937	4.6				564			
	620	7.999	17.2	GS	1^+ [f]	14.6	627			
	659	8.039	8.6		1^+ [f]	6.3	666			
	860	8.241	10.0	GS	1^+ [f]	7.8	869			
^{206}Pb	1.5 [d]	8.085	0.4	GS [d]			1.6			
	7.3 [e]	8.090	3.4	GS [e]			7.5			
	10.3 [e]	8.093	1.1	GS [e]			10.5			
	12.9 [e]		0.12	ES						
	16.1 [e]	8.098	0.40	GS [e]			16.4			
	28.5	8.111	0.54				29.0			
	33.7 [e]	8.116	2.5	GS [e]			34.3			
	40.0	8.123	0.86				40.7			
	50.7 [e]	8.133	1.3	GS [e]			51.5			
	53.6	8.136	0.52				54.4			
	68.9	8.152	1.5				69.9			
	72.1	8.155	1.4				73.2			
	75.1	8.158	0.90				76.2			
	88.9	8.171	4.5				90.2			
	104	8.187	4.9				106			

[a] See Ref. 6.
[b] See Ref. 10; approximate energy values taken from cross-section figure.
[c] See Ref. 13.
[d] See Ref. 3; resonance not seen in the present work.
[e] Also seen in Ref. 3; resonance parameters from present work.
[f] From angular distribution measurement (see text).

[3] C.D. Bowman, B.L. Berman, and H.E. Jackson, Phys. Rev. 178, 1827 (1969).

[6] J.A. Biggerstaff, J.R. Bird, J.H. Gibbons, and W.M. Good, Phys. Rev. 154, 1136 (1967).

[10] J.A. Farrell, G.C. Kyker, Jr., E.G. Bilpuch, and H.W. Newson, Phys. Letters 17, 286 (1965).

[13] E.G. Bilpuch, K.K. Seth, C.D. Bowman, R.H. Tabony, R.C. Smith, and H.W. Newson, Ann. Phys. (N.Y.) 14. 387 (1961).

REF.	ELEM. SYM.	A	Z
F. R. Metzger Ann. Phys. 66, 697 (1971)	Pb	206	82

METHOD	REF. NO.	
	71 Me 2	egf

REACTION	RESULT	EXCITATION ENERGY	SOURCE		DETECTOR		ANGLE
			TYPE	RANGE	TYPE	RANGE	
G,G	LFT	2	D	2	SCD-D		DST

Γ_{γ} = 9.8 ± 1.8 MeV.

2=1.704 MEV

TABLE I

Angular Distribution of the 1.704 MeV Resonance Radiation[a]

Spin	$N_{ee}(98°)/N_{ee}(127°)$ Experiment	Theory
1	1.43 ± 0.18	1.50
2		4.01

[a] The observed ratios of the counting rates in the 98° and 127° geometries are compared with the ratios expected for spin 1 and spin 2. The 98° geometry was approximately twice as efficient as the 127° geometry.

REF.		ELEM. SYM.	A	Z
	Yu. I. Sorokin, V.A. Khrushchev, and B.A. Yur'ev Izv. Akad. Nauk SSSR. Ser. Fiz. 37, 156 (1973) Bull. Acad. Sci. USSR, Phys. Ser. 37, 137 (1973)	Pb	206	82
METHOD		REF. NO.		
		73 So 21		hmg

REACTION	RESULT	EXCITATION ENERGY	SOURCE		DETECTOR		ANGLE
			TYPE	RANGE	TYPE	RANGE	
G,XN	ABX	8- 27	C	8- 27	BF3-I		4PI

SEE ALSO 75SO12

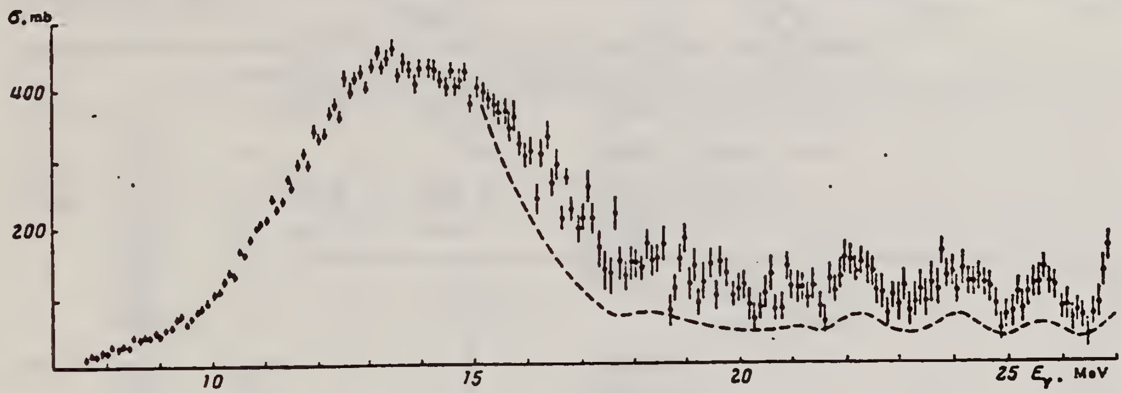

Fig. 1. Cross sections for ^{206}Pb: the (,Tn) cross section $\sigma(\gamma n) + 2\sigma(\gamma,2n) + \sigma(\gamma,np) + \ldots$ obtained with a processing step of 1 MeV (points), and the photo-absorption cross section $\sigma_\gamma = \sigma(\gamma n) + \sigma(\gamma,2n) + \sigma(\gamma,np) + \ldots$, obtained with al-allowance for multiplicity according to the statistical theory (dashed curve).

Integral Cross Sections, MeV·b

Reaction and E_γ range	^{206}Pb	^{208}Pb
$\sigma(\gamma,Tn)$ to 20 MeV	3,10	3,38
σ_γ to 20 MeV	2,80	2,81
$\sigma(\gamma,Tn)$ to 27 MeV	3,93	4,32
σ_γ to 27 MeV	3,21	3,28
$\sigma(\gamma,Tn)$ 20—27 MeV	0,83	0,94
σ_γ 20—27 MeV	0,41	0,47
$\sigma(E1) = 0.06\ \frac{NZ}{A}$	2,95	2,98
$\sigma(E2)$	0,5	0,5
$\sigma(T_>)$ [14]	0,013	0,013

REF.	C. P. Swann PICNS-73, Vol.I, p.317 Asilomar	ELEM. SYM.	A	Z
		Pb	206	82

METHOD	REF. NO.	
	73 Sw 13	hmg

REACTION	RESULT	EXCITATION ENERGY	SOURCE		DETECTOR		ANGLE
			TYPE	RANGE	TYPE	RANGE	
G,G	LFT	3- 5	C	5	SCD-D		DST

Table: Properties of States Observed in $^{206,207,208}Pb$ and ^{209}Bi

J-PI, 3 LEVELS

Nuclei	E_γ (keV)	J^π	Γ_0/Γ	$g\Gamma_0^2/\Gamma$ (eV)	Γ_0 (eV)	G(EL)	G(M1)
	3742	1	1		0.13(2)	0.001	0.12
^{206}Pb	4114	2^+	1		0.30(6)	5	
	4326	1	1		0.90(9)	0.004	0.56
	4602	1	1		0.23(3)	0.001	0.12
	3300	$1/2^+$ a)			0.039(6)		
	3928	$(3/2^-)$	1	0.68(7)			
	4104	$3/2^-$	1		0.55(6)	8	
^{207}Pb	4140	$5/2^-$	1		0.46(5)	6	
	4627	$1/2^+$ b)	1		0.64(7)	0.003	
	4872	1/2,3/2	1	3.6(5)		∿0.01	∿1.2
	4982	1/2,3/2	1	4.0(5)		∿0.01	∿1.2
^{208}Pb	4087	2^+	1		0.49(5)	7	
	4843	1	1		5.1(5)	0.02	2.3
	2826	$5/2^-$	(.63) c)		0.09(1)		
	3977	5/2--13/2		0.82(8)			
	4085	$5/2^-$--$13/2^-$		0.28(3)		∿5	
	4144	"		0.07(2)		∿1	
^{209}Bi	4156	"		0.21(4)		∿3	
	4176	"		0.21(4)		∿3	
	4206	"		0.25(3)		∿4	
	4747	7/2--11/2		2.9(5)		∿0.013	∿1.4
	4784	"		2.7(5)		∿0.012	∿1.3
	4822	"		1.4(3)		∿0.005	∿0.7

a) see ref. 3 b) see ref. 4 c) see ref. 5

3) S.M. Smith, P.G. Roos, C. Moazed and A.M. Bernstein, Nucl. Phys. A173, 32 (1971).
4) R.A. Mayer, B.L. Cohen and R.C. Diehl, Phys. Rev. C2, 1898 (1970).
5) R.A. Broglia, J.S. Lilley, R. Perazzo and W.R. Phillips, Phys. Rev. C1, 1508 (1970).

FORM NBS-418
(REV. 7-14-64)
USCOMM-NBS-DC

REF.	ELEM. SYM.	A	Z
C. P. Swann J. Franklin Institute 298, 321 (1974)	Pb	206	82

METHOD	REF. NO.	
	74 Sw 11	egf

REACTION	RESULT	EXCITATION ENERGY	SOURCE		DETECTOR		ANGLE
			TYPE	RANGE	TYPE	RANGE	
G,G	LFT	3- 5	C	4- 5	SCD-D		DST

6 LEVELS 3744-5038 KEV

TABLE II

Properties of states observed in ^{206,207,208}Pb and ^{209}Bi; G(EL) and G(M1) are the reduced transition probabilities in Weisskopf units

Nuclei	E_γ (keV)	J^π	Γ_0/Γ	$g\,\Gamma_0^2/\Gamma$ (eV)	Γ_0 (eV)	G(EL)	G(M1)
^{206}Pb	3744	1^-	1		0·13 (2)	0·001	
	4114	2^+	1		0·30 (6)	5	
	4330	1^+	1		0·90 (9)		0·56
	4606	1	1		0·23 (3)	0·001	0·12
	4974	1	1	0·8 (2)		0·003	0·32
	5038	1	1	2·3 (5)		0·007	0·90
^{207}Pb	3300	$1/2^{+}$*			0·039 (6)		
	3928	$3/2^-$	1		0·34 (4)		
	4104	$3/2^-$	1		0·55 (6)	8	
	4140	$5/2^-$	1		0·46 (5)	6	
	4627	$1/2^{+}$†	1		0·64 (7)	0·003	
	4872	$1/2^-, 3/2^-$	1	3·6 (5)			~1·2
	4982	$1/2^-, 3/2^-$	1	4·0 (5)			~1·2
^{208}Pb	4087	2^+	1		0·49 (5)	7	
	4843	1^+	1		5·1 (8)		2·3
^{209}Bi	2826	$5/2^-$	(0·63)‡		0·09 (1)		
	3977	5/2−13/2		0·82 (8)			
	4085	$5/2^- - 13/2^-$		0·28 (3)		~5	
	4144	$5/2^- - 13/2^-$		0·07 (2)		~1	
	4156	$5/2^- - 13/2^-$		0·21 (4)		~3	
	4176	$5/2^- - 13/2^-$		0·21 (4)		~3	
	4206	$5/2^- - 13/2^-$		0·25 (3)		~4	
	4747	$7/2^- - 11/2^-$		2·9 (5)			~1·4
	4785	$7/2^- - 11/2^-$		2·7 (5)			~1·3
	4822	$7/2^- - 11/2^-$		1·4 (3)			~0·7

* See Ref. (11). † See Ref. (12). ‡ See Ref. (7).

[7] C.P. Swann, Phys. Rev. Letts. 32, 1449 (1974).

[11] S.M. Smith et al., Nucl. Phys. A173, 32 (1971).

[12] R.A. Mayer et al., Phys. Rev. C2, 1898 (1970).

REF.	ELEM. SYM.	A	Z
Yu. I. Sorokin and B. A. Yur'ev Izv. Akad. Nauk SSSR. Ser. Fiz. <u>39</u>, 114 (1975) Bull. Acad. Sci. (USSR) Phys. Ser. <u>39</u>, 98 (1975)	Pb	206	82
METHOD	REF. NO. 75 So 12		hmg

REACTION	RESULT	EXCITATION ENERGY	SOURCE TYPE	SOURCE RANGE	DETECTOR TYPE	DETECTOR RANGE	ANGLE
G,XN	ABI	8- 27	C	8- 27	BF3-I		4PI

SEE 73SO21

Table 1

Element	A	σ_0, (γ, Tn) MeV · b, to 27 MeV		$\sigma_{0\gamma}$ MeV · b, to 20 MeV	$\sigma_{0\gamma}$ MeV · b, 20–27 MeV	σ_{-1}, mb	σ_{-2}, mb × × MeV^{-1}	E_m, MeV	K, MeV	(1.4−1) MeV^{-1}	Threshold (γ,2n), MeV	σ_0 (E1), MeV × × b
Sn	112	2,23	1,90	1,49	0,41	112	6,7	15,8	20.1	10.2	19,2	1,66
	114	2,26	1,86	1,39	0,47	108	6.5	15.7	21.5	10.2	18.1	1,68
	116	2,40	1,85	1,40	0,45	110	6,6	15,6	21.7	8.1	17,1	1,71
	117	2,52	1,86	1,39	0,47	110	6,7	15,4	21.6	7.3	16,5	1,72
	118	2,46	1,92	1,50	0,39	115	7.1	15.5	20.7	[illegible].6	16,3	1,71
	119	2,63	1,85	1,42	0,44	111	6,8	15,4	22,0	13,2	15,8	1,74
	120	2,69	2,07	1,69	0,38	127	7,9	15,3	19.1	3,6	15,6	1,75
	122	2,94	2,03	1,51	0,52	119	7,1	15,6	21,8	4,5	15,0	1,77
	124	2,90	1,93	1,44	0,49	114	6.9	15,5	23,2	5,4	14,4	1,79
W	182	3,68	2.78	2,32	0,46	184	12,5	–	24,2	5,2	14,9	2,63
	184	4,88	2,95	2,33	0,72	196	13,0	—	23.7	5,2	13,6	2,65
Au	197	4,05	3,15	2,81	0,34	226	15,5	13,3	20,9	17.1	11,8	2,84
Pb	206	3,93	3,21	2,80	0,41	225	16,1	13,5	23,1	6.6	14,8	2,96
	208	4,32	3,28	2,81	0,47	231	16.7	13,3	22,6	9.6	14,1	2,98
Bi	209	4,59	3.47	2,96	0,51	216	17,9	13,2	21,3	10,2	14,3	3,00

REF.	J. E. McFee, W. V. Prestwich, T. J. Kennett Phys. Rev. C13, 1864 (1976)	ELEM. SYM.	A	Z
		Pb	206	82
METHOD		REF. NO. 76 Mc 3		hmg

REACTION	RESULT	EXCITATION ENERGY	SOURCE TYPE	SOURCE RANGE	DETECTOR TYPE	DETECTOR RANGE	ANGLE
G,N	ABX	8- 9	D	8- 9	ION-D		90

8999,8533,8120 KEV

The photoneutron spectrum of natural lead has been observed for photoexcitation energies of 8999, 8533, and 8120 keV using a high-resolution ^{3}He ionization chamber. The photons were obtained from the (n,γ) reaction on a nickel target positioned in a nuclear reactor. The Q values for the three reactions ^{208}Pb$(\gamma,n)^{207}$Pb, ^{207}Pb$(\gamma,n)^{206}$Pb, and ^{206}Pb$(\gamma,n)^{205}$Pb have been determined and are, respectively, 7369 ± 5, 6743 ± 3, and 8087 ± 3 keV. Neutron groups corresponding to different final states following excitation by one of the three photon components have been observed and their partial cross sections are reported. The distribution and some systematics of the neutron reduced widths have been studied. The absolute cross sections of the reaction ^{208}Pb$(\gamma,n)^{207}$Pb at 8999 and 8533 keV photon energies have been found to be 6.8 ± 2.9 and 5.0 ± 2.1 mb, respectively.

TABLE V. Reduced widths contrasted with spectroscopic factors.

Residual nucleus	E_x (keV)	J^π	l_n[a] E1	l_n[a] E2	Neutron Reduced Widths E_γ=8999 keV	E_γ=8533 keV (±27%)	E_γ=8120 keV	Spectroscopic factors $C^2S/(2J+1)$ (p,d)	(d,t)
^{207}Pb								b	b
	0	$\frac{1}{2}^-$	0	1	163	128		0.72	0.71
	570	$\frac{5}{2}^-$	2	1	210	309		0.90 [c]	0.97 [c]
	898	$\frac{3}{2}^-$	0	1	191	327		1.27	1.33
								d	
^{206}Pb	0	0+	0	1	26	107	321	0.30	...
	803	2+	0	1	959	305		0.11	...
	1165	0+	0	1	294	118		0.19	...
	1460	2+	0	1	152	e		0.38	...
	1684	4+	2	1	474	e		0.02 [c]	...
	1704	1+	0	1	285	0		0.38	...
	1784	2+	0	1	178	e		0.07	...
^{205}Pb	263	$\frac{3}{2}^-$	0	1	190	e		1.02 [f]	1.56 [g]

[a] Minimum possible neutron angular momentum for a given photon multipolarity.
[b] Reference 18.
[c] Spectroscopic factor for $l_n=3$. All others are $l_n=1$.
[d] W. A. Lanford and G. M. Crawley, Phys. Rev. C 9, 646 (1974).
[e] May exist but cannot be resolved from neighboring components.
[f] K. Yagi, T. Ishimatsu, Y. Ishizaki, and Y. Saji, Nucl. Phys. A110, 41 (1968).
[g] R. Tickle and J. Bardwick, Phys. Rev. 178, 2006 (1969).

TABLE VI. Absolute photoneutron cross sections.

Target isotope	Photon energy (keV)	Cross section[a] (mb)	Lower bound[a] (mb)	Upper bound[a] (mb)
208	8999	6.8	...	...
	8533	5.0	...	...
207	8999	...	29.9	40.1
	8533	...	8.0	26.8
	8120	...	5.6	...
206	8999	...	2.3	14.0
	8533	...	0	15.1

[a] 10% relative error; 45% absolute error.

(over)

TABLE IV. Low-lying states in ^{207}Pb, ^{206}Pb, and ^{205}Pb.

Residual isotope	E_γ (keV)	E_x (keV)	J^π	Observed neutron energy (lab) (keV ± 5)	Relative[a] intensity (±10%)	$\sigma_{\gamma n'}$[b] (mb)
207	8999	0[c]	$\frac{1}{2}^-$	1615	100	3.1
		570	$\frac{5}{2}^-$	1054	42	1.3
		898	$\frac{3}{2}^-$	727	79	2.4
	8533	0	$\frac{1}{2}^-$	1159	66	2.1
		570	$\frac{5}{2}^-$	601	12	0.4
		898	$\frac{3}{2}^-$	263	81	2.5
206	8999	0[d]	0^+	2256[e]	19	0.6
		803	2^+	1446	556	17.2
		1165(±10)	0^+	1087	148	4.6
		1460	2^+	789	65	2.0
		1684	4^+	573	15	0.5
		1704(±1)	1^+	551	102	3.2
		1784(±2)	2^+	473	59	1.8
	8533	0	0^+	1780	69	2.1
		803	2^+	982	147	4.5
		1165(±10)	0^+	619	45	1.4
		1704(±1)	1^+	...	0	0.0
	8120	0	0^+	1370[e]	181	5.6
205	8999	263[f]	$\frac{3}{2}^-$	643	74	2.3
			Unresolved groups			
A 206	8999	1340	3^+	908	76	
205	8999	0	$\frac{5}{2}^-$			
205	8999	2	$\frac{1}{2}^-$			
B 206	8533	1340	3^+	446	65	
205	8533	0	$\frac{5}{2}^-$			
205	8533	2	$\frac{1}{2}^-$			
C 205	8999	576	$\frac{3}{2}^-$	330	44	
206	8533	1460	2^+			
D 205	8533	263	$\frac{3}{2}^-$	181	37	
207	8120	570	$\frac{5}{2}^-$			
206	7724	803	2^+			
207	7555	0	$\frac{1}{2}^-$			
E 206	8999	2150(±1)	2^+	110	61	
205	8999	803	$(\frac{1}{2}^-, \frac{3}{2}^-)$			
			Unassigned group			
...	...	...	...	597	5	

[a] Arbitrary normalization corrected for isotopic abundance and photon yield. Unresolved group intensities have no isotopic abundance or photon yield correction and are merely quoted relative to the group corresponding to population of the ^{207}Pb ground state following 8999-keV photoexcitation.

[b] Relative error 10%, absolute error 45%.

[c] Reference 18.

[d] Reference 19.

[e] Centroid accurate to only 15 keV.

[f] Reference 20.

[18] M. R. Schmorak et al., Nucl. Data B5, 207 (1971).

[19] K. K. Seth, Nucl. Data B7, 161 (1972).

[20] J. H. Hamilton et al., Phys. Rev. C6, 1265 (1972).

REF.	D. Turck, H.-G. Clerc, H. Trager Phys. Lett. 63B, 283 (1976)	ELEM. SYM.	A	Z
		Pb	206	82
METHOD		REF. NO.		
		76 Tu 2		egf

REACTION	RESULT	EXCITATION ENERGY	SOURCE TYPE	SOURCE RANGE	DETECTOR TYPE	DETECTOR RANGE	ANGLE
E,F	ABX	27- 50	D	38- 50	TRK-I		4PI

FISSION BARRIER

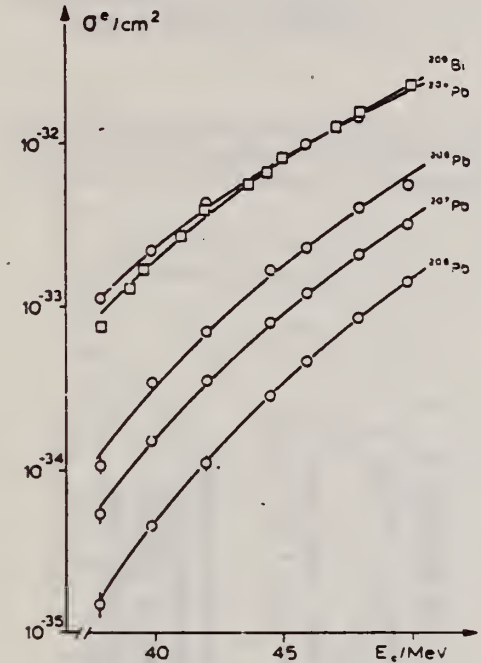

Fig. 1. Cross section σ^e for electron induced fission in ^{204,206,207,208}Pb and ^{209}Bi as a function of the incident electron energy E_0.

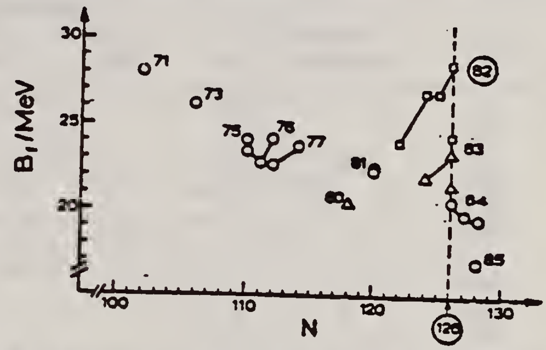

Fig. 2. Summary of fission barrier heights obtained from fits to experimental fission cross sections for nuclei with $Z < 85$. o: α-induced fission [12]. For ^{201}Tl, the value of 22.5±1.5 of ref. [3] is also included; △: proton-induced fission [12]; □: electron induced fission (present work). Values for different isotopes of the same element are connected by straight lines. The nuclear charge numbers are indicated. The erors are ± 1.0 MeV for proton and α-induced fission [12] and ± 1.5 MeV for electron induced fission.

1 U. Mosel, Phys. Rev. C6 (1972)971.
3 D.S. Burnett et al., Phys. Rev. B134 (1964)952.
12 L.G. Moretto et al., Phys. Lett. B38 (1972)471.

Table 2
Fission barriers B_f as determined from electron induced fission. In the last column theoretical fission barriers according to ref. [1] with surface independent pairing strength are listed.

isotope	B_f (MeV)	$B_f^{theor.}$ (MeV)
^{204}Pb	24.0±1.5	24.0
^{206}Pb	26.3±1.5	26.2
^{207}Pb	26.9±1.5	
^{208}Pb	28.6±1.5	28.1
^{209}Pb	24.3±1.5	

REF.	ELEM. SYM.	A	Z
D.F. Coope, L.E. Cannell, and M.K. Brussel Phys. Rev. C 15, 1977 (1977)	Pb	206	82

METHOD	REF. NO.	
	77 Co 3	hmg

REACTION	RESULT	EXCITATION ENERGY	SOURCE TYPE	SOURCE RANGE	DETECTOR TYPE	DETECTOR RANGE	ANGLE
G,G	LFT	4 - 7	C	6,10	SCD-D		125
		(4.974-6.84)		(6.6,9.7)			

Using bremsstrahlung produced with 6.6 and 9.7 MeV beams, nuclear resonance fluorescence measurements were made on targets of ^{206,207,208}Pb and ^{209}Bi. Ground state transition widths for previously unknown energy levels with widths ≳ 1 eV were obtained. An interpretation of several of these levels in terms of a particle-core weak coupling model is suggested.

10 LEVELS 5.0-6.8 MeV

TABLE IV. Observed levels and their strengths. *The value for Γ_0 assumes $g\Gamma_0/\Gamma = 3$ for ^{206}Pb and ^{208}Pb, and $g\Gamma_0/\Gamma = 1$ for ^{207}Pb and ^{209}Bi.* Values in parentheses have uncertainties in excess of 50%. Statistical uncertainties are given for well-defined peaks. Total uncertainties include uncertainties in flux calibration. Energy values are believed to be accurate to ±3 keV for the starred (★) ^{208}Pb levels and to ±5 keV for the other levels.

Energy (MeV)	Nucleus	Γ_0 (eV)	Uncertainty (%) Statistical	Total	Other measurements $g\Gamma_0^2/\Gamma$ (eV)	Γ_0 (eV)	References
6.54	(Pb) 206	7.4		40			
6.73		5.5		40			
5.902		4.4	15	40			
5.854		(3.0)					
5.798		(1.0)					
5.639		(0.5)					
5.615		(1.0)					
5.577		(0.5)					
5.039		1.6	15	40			
4.974		0.8		40			
6.753	(Pb) 207	(<10)					
5.716		(3)					
5.600		(8)					
5.490		(12)					
5.223		(8)					
5.209		(8)					
4.950		(7)			4.0 $\Gamma_0/\Gamma = 1$		12
4.875 }		(13)			3.6 $\Gamma_0/\Gamma = 1$		12
4.847 }							12
7.332★	(Pb) 208	38	10	35		35, 41	11, 10
7.083★		14	10	35		15, 17 ± 2	11, 5
7.063★		29	10	35		15, 31 ± 3	11, 5
6.721★		15	20	40		15, 14	11, 10
6.357		(0.5)					
6.305		(1.0)					
6.262		4.1		45			
5.513★		28	2	35		15	11
5.293★		8.6	5	35		5	11
4.842★		6.3	5	35	$J^\pi = 1^+$	5.1 ± 0.8	12
4.085★		0.51		40	$J^\pi = 2^+$	0.5 ± 0.1	12
5.549	(Bi) 209	6.6		40			
5.522 }							
5.509 }		17	5	35			
5.498 }							
5.422		8.3		45			
5.293		12	15	40			
4.845 }					1.4		12
4.803 }		(10)			2.7		12
4.771 }					2.9		12
4.501		(3)					
4.223		(3)					

[5] C.P. Swann, Nucl. Phys. A201, 534 (1973)

[10] P. Axel, K. Min, N. Stein, and D.C. Sutton, Phys. Rev. Lett. 10, 299 (1963)

[11] A.M. Khan and J.W. Knowles, Bull. Am. Phys. Soc. 12, 538 (1967); J.W. Knowles, A.M. Khan, and W.F. Mills (unpublished)

[12] C.P. Swann, Proceedings of the International Conference on Photonuclear Reactions and Applications, (U.S. Atomic Energy Commission Office of Information Services, Oak Ridge, Tennessee, 1975), p.317

REF. Y. Birenbaum, Z. Berant, A. Wolf, R. Moreh
Phys. Lett. 88B, 239 (1979)

ELEM. SYM.	A	Z
Pb	206	82

METHOD

REF. NO.	
79 Bi 13	hg

REACTION	RESULT	EXCITATION ENERGY	SOURCE TYPE	SOURCE RANGE	DETECTOR TYPE	DETECTOR RANGE	ANGLE
G,N	RLY	8-12	D	8-12	SCI-D		DST
		(8.5-11.4)		(8.5-11.4)			

$$W(\theta)=\sum_{0}^{3} ai\ Pi(\cos\theta)$$

Neutron angular distributions around $\theta = 90°$ from the $^{206}Pb(\gamma, n)$ reaction were measured using n-capture γ-rays, E_γ = 8.5–11.4 MeV, and a high-resolution ^3He spectrometer. Pronounced asymmetry around $\theta = 90°$ was observed indicating the existence of E1–E2 and possibly E1–M1 interference effects.

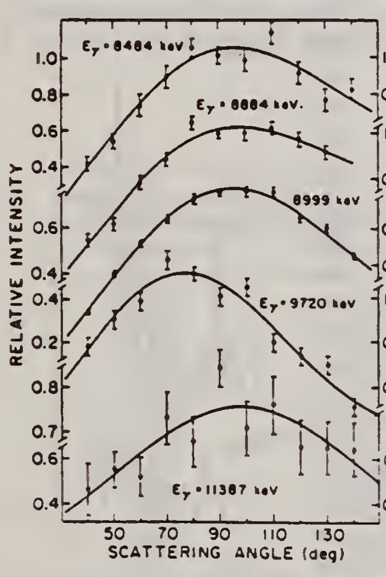

Fig. 2. Angular distribution of the neutron group leading to the ground +2.3 keV state in ^{205}Pb for various incident γ-energies.

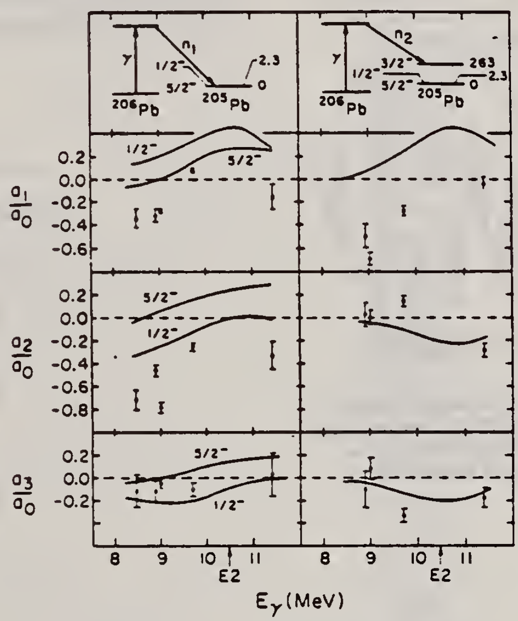

Fig. 3. Angular distribution coefficients a_i/a_0 for the transitions to the ground +2.3 keV states and to the 263 keV state in ^{205}Pb as a function of E_γ. The energy of the E2 ISGR is indicated. The solid curves are calculated [11] with the direct-semidirect model and are identified by the spin of the final state.

REF.	R.M. Laszewski and P. Axel Phys. Rev. C 19, 342 (1979)	ELEM. SYM.	A	Z
		Pb	206	82
METHOD		REF. NO.		
		79 La 1		hg

REACTION	RESULT	EXCITATION ENERGY	SOURCE TYPE	SOURCE RANGE	DETECTOR TYPE	DETECTOR RANGE	ANGLE
G,G	ABX	4- 8	D	5-8	NAI-D		135
		(4.5-8.1)					

Average elastic photon scattering cross sections were measured for ^{209}Bi, ^{208}Pb, ^{207}Pb, ^{206}Pb, Tl and Hg at excitation energies between 4.5 MeV and the neutron emission threshold, with an energy resolution in the range between 50 and 150 keV. This resolution was sufficient to determine the strengths of most of the strong levels in this energy region for ^{208}Pb; there are concentrations of strength in a few levels near 5.5 and 7 MeV with the sum of $B(E1)\uparrow$ values equal to about 0.84 and 0.65 e^2 fm^2, respectively; each of these two groups of levels corresponds to only about 0.63% of the electric dipole sum rule. In the neighboring isotopes, approximately the same amount of strength is distributed among many more energy levels; although this strength is spread in energy more than it is in ^{208}Pb, it remains relatively localized.

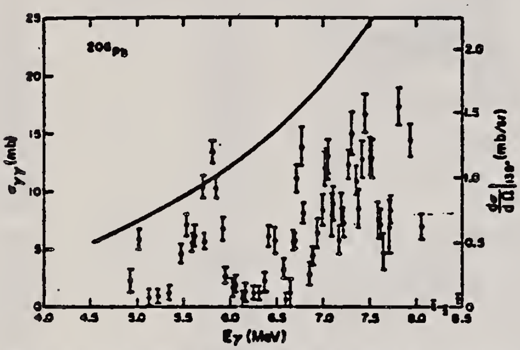

FIG. 4. ^{206}Pb (enriched to 88% 206 isotope): experimental average elastic photon scattering cross sections The solid curve is a low energy extrapolation of the Lorentz line which fits the giant dipole resonance.

TABLE VI. Transition strength comparison at 5.5 and 7 MeV.

Nucleus	5.0–6.0 MeV $\int\sigma_{\gamma\gamma}dE$ (MeV mb)	5.0–6.0 MeV %^{208}Pb strength	6.5–7.5 MeV $\int\sigma_{\gamma\gamma}dE$ (MeV mb)	6.5–7.5 MeV %^{208}Pb strength
Bi	10.4	68%	10.7	44%
^{208}Pb	15.2	100%	24.4	100%
^{207}Pb	12.6	83%	···	···
^{206}Pb	15.8	104%	20.2	83%
Tl	8.3	55%	7.8	32%
Hg	11.6	76%	···	···

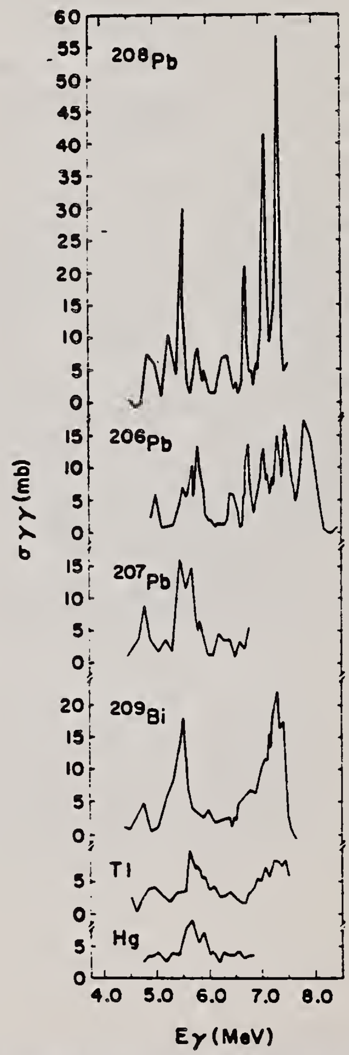

FIG. 12. Comparison of the measured cross sections of, respectively, from the top, ^{208}Pb, ^{206}Pb, ^{207}Pb, ^{209}Bi, Tl, and Hg.

ELEM. SYM.	A	Z
Pb	206	82

METHOD

REF. NO.	
80 Ch 3	hg

REACTION	RESULT	EXCITATION ENERGY	SOURCE TYPE	SOURCE RANGE	DETECTOR TYPE	DETECTOR RANGE	ANGLE
G,G	SPC	4-8	C	9	SCD-D		DST
				(8.5)			

Resonant photon scattering from ^{206,207,208}Pb and ^{209}Bi has been measured from 4 MeV to the neutron thresholds using enriched targets, Ge(Li) detectors and bremsstrahlung beams with end-point energies of 7.0, 7.5, 7.6, 8.0, 8.5, and 10.4 MeV. Energies and values of $g\Gamma_0{}^2/\Gamma$ were obtained for many levels not observed in previous photon experiments. Spins of levels in ^{206}Pb and ^{208}Pb were determined from the angular distributions, and ground-state branching ratios were obtained from self-absorption measurements for seven transitions in ^{208}Pb. The results are compared with earlier spectroscopic studies and with lower resolution average cross-section measurements. The spectra of ^{207}Pb and ^{209}Bi are discussed in terms of the excitations of the ^{208}Pb core.

NUCLEAR REACTIONS ^{206,207,208}Pb, ^{209}Bi(γ,γ); enriched targets; resonance fluorescence with 7.0, 7.5, 7.6, 8.0, 8.5, and 10.4 MeV bremsstrahlung. Measured E_γ, I_γ at 90° and 127°, and self-absorption; deduced $g\Gamma_0^2/\Gamma$, Γ_0/Γ, J.

TABLE X. ^{206}Pb angular distribution measurements. Listed uncertainties are statistical only.

Energy (MeV)	$W(90°)/W(127°)$	J
4.115	1.76±0.44	2
4.329	0.69±0.17	1
4.972	0.60±0.16	1
5.038	0.69±0.06	1
5.580	0.67±0.14	1
5.615	0.81±0.13	1
5.692	0.65±0.19	1
5.732	0.81±0.15	1
5.760	0.69±0.18	1
5.846	0.73±0.22	1
5.857	0.66±0.09	1
5.903	0.67±0.09	1
6.509	0.74±0.17	1
6.724	0.76±0.13	1
6.820	0.81±0.16	1
7.062	0.80±0.19	1
7.078	0.90±0.25	1
7.202	0.70±0.22	1
7.310	0.69±0.19	1
7.423	0.84±0.26	1
7.506	1.11±0.54	(1)
7.543	0.73±0.21	1
7.570	0.82±0.53	1
7.846	0.85±0.20	1
7.880	0.88±0.37	1
7.891	0.84±0.23	1
7.903	0.79±0.19	1
7.972	0.92±0.45	1
8.000	0.91±0.26	1

TABLE IX. Comparison of measured level widths for ^{206}Pb. Values of Γ_0^2/Γ were extracted from the present experiment assuming dipole transitions for levels whose spins were not measured; uncertainties include statistical and calibration errors. Parentheses indicate tentative assignments; levels in brackets are probably unresolved multiplets.

Energy[a] (MeV±keV)	J[a]	Γ_0^2/Γ[a] (eV)	Γ_0^2/Γ[b] (eV)	Γ_0^2/Γ[c] (eV)
4.115±2	2	0.58±0.15		0.30±0.06
4.329±4	1	0.48±0.11		0.90±0.09
4.604±4		0.58±0.16		0.23±0.03
4.972±2	1	0.95±0.22	0.8±0.3	0.8 ±0.2
5.038±2	1	2.6 ±0.4	1.6±0.6	2.3 ±0.5
5.470±4		0.7 ±0.2		
5.580±2	1	1.7 ±0.3	0.5[f]	
5.615±2	1	1.8 ±0.4	1.0[f]	
5.692±4	1	0.8 ±0.2	0.5[f]	
5.732±2[d]	1	1.3 ±0.3		
5.760±4	1	0.9 ±0.2		
5.798±4[d]		1.1 ±0.3	1.0[f]	
5.816±4		0.5 ±0.2		
5.846±2	1	1.1 ±0.2 }	3.0[f]	
5.857±2	1	2.0 ±0.4 }		
5.903±2	1	3.0 ±0.6	4.4±1.8	
6.509±2[e]	1	1.9 ±0.4		
6.724±4	1	3.4 ±0.6	5.5±2.2	
6.820±2	1	4.7 ±0.9	7.4±3.0	
7.062±4	1	2.5 ±0.6		
7.078±4[e]	1	0.9 ±0.3		
(7.127±2)		1.0 ±0.2		
(7.202±4)[e]	1	1.8 ±0.4		
{7.310}	1	3.7 ±0.9		
7.423±4	1	1.6 ±0.4		
7.464±4		0.9 ±0.4		
7.487±4[d]		1.7 ±0.4		
7.506±2	(1)	1.2 ±0.4		
7.543±2	1	2.3 ±0.6		
7.570±4	1	1.1 ±0.5		
{7.815}		0.8 ±0.2		
{7.846}	1	1.9 ±0.4		
7.880±2	1	1.1 ±0.3		
7.891±4	1	1.6 ±0.4		
7.903±4	1	2.2 ±0.5		
7.972±4	1	1.0 ±0.3		
{8.000}	1	1.6 ±0.4		
{8.040}		0.27±0.09		

[a] This work.
[b] Reference 10.
[c] Reference 36.
[d] May include contribution from an additional level.
[e] May be an inelastic transition; see text and Table XI
[f] Uncertainty reported "in excess of 50%."

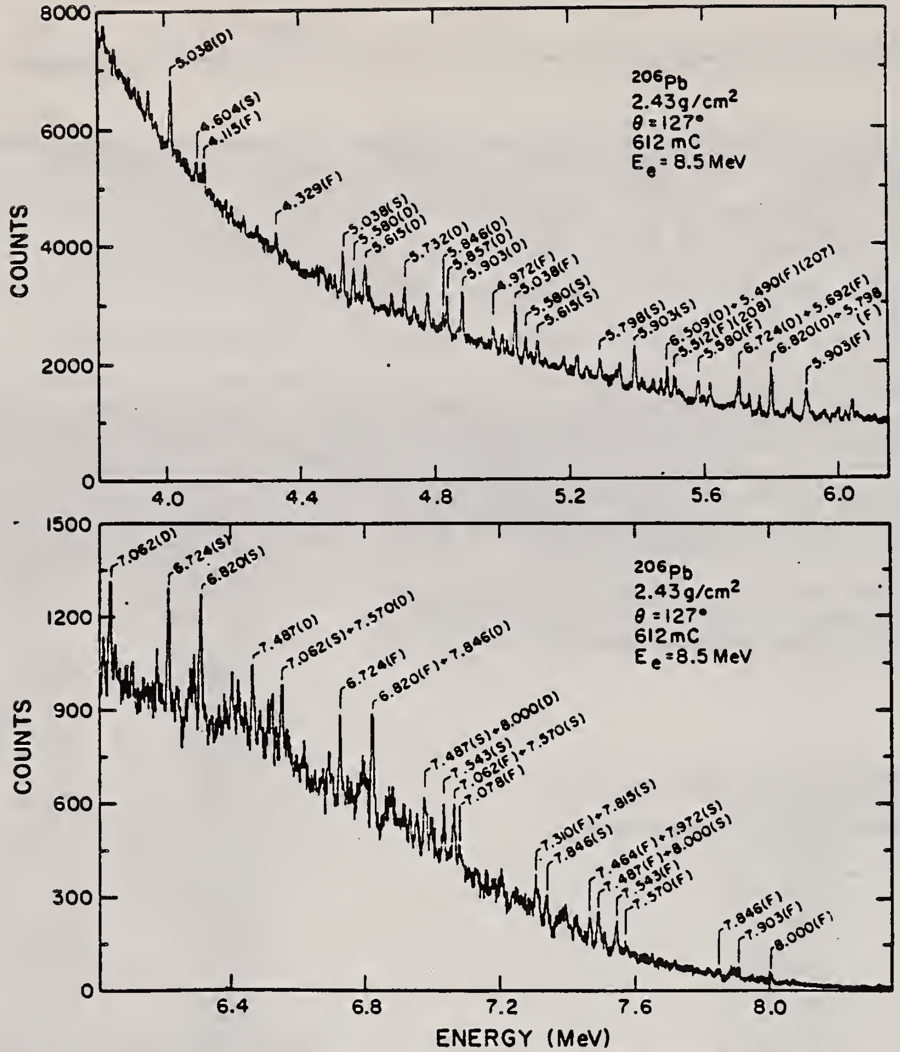

FIG. 12. Spectrum for 8.5 MeV bremsstrahlung scattered at 127° from an enriched (88%) ^{206}Pb target. One channel corresponds to 1.47 keV.

REF. T. Chapuran, R. Vodhanel, M.K. Brussel
Phys. Rev. C22, 1420 (1980)

ELEM. SYM.	A	Z
Pb	206	82

METHOD

REF. NO.	
80 Ch 3	hg

REACTION	RESULT	EXCITATION ENERGY	SOURCE		DETECTOR		ANGLE
			TYPE	RANGE	TYPE	RANGE	
G,G	SPC	4-8	C	9	SCD-D		DST
				(8.5)			

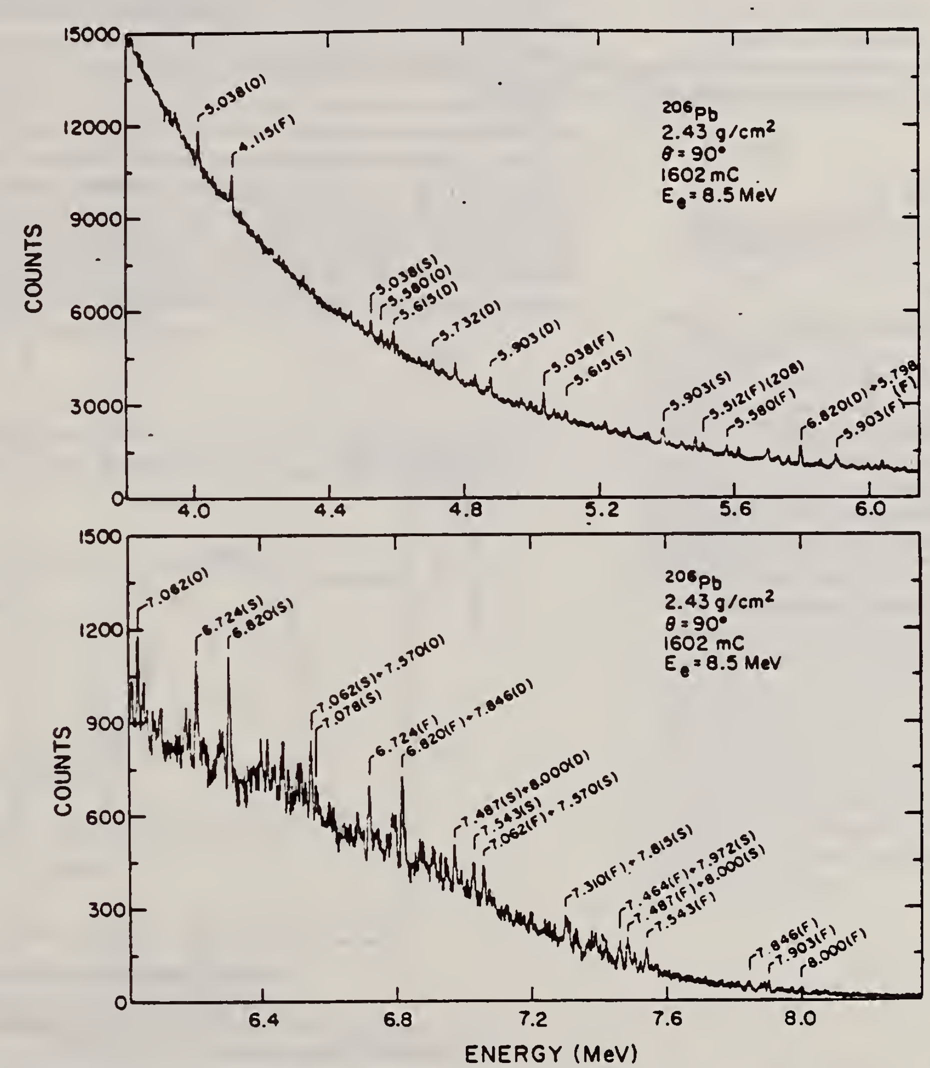

FIG. 13. Spectrum for 8.5 MeV bremsstrahlung scattered at 90° from an enriched (88%) ^{206}Pb target. One channel corresponds to 1.47 keV.

REF. C.N. Papanicolas, J. Heisenberg, J. Lichtenstadt, J.S. McCarthy
Phys. Lett. 99B, 96 (1981)

ELEM. SYM.	A	Z
Pb	206	82

METHOD

REF. NO.	
81 Pa 1	hg

REACTION	RESULT	EXCITATION ENERGY	SOURCE TYPE	SOURCE RANGE	DETECTOR TYPE	DETECTOR RANGE	ANGLE
E,E/	ABX	4-5	D	0*3	MAG-D		DST

*MOM,FM-1 2 E10 LEV

We report the identification of new high multipolarity transitions in ^{207}Pb and ^{206}Pb by the measurement of their form factor. A comparison to the corresponding excitations in ^{208}Pb is presented.

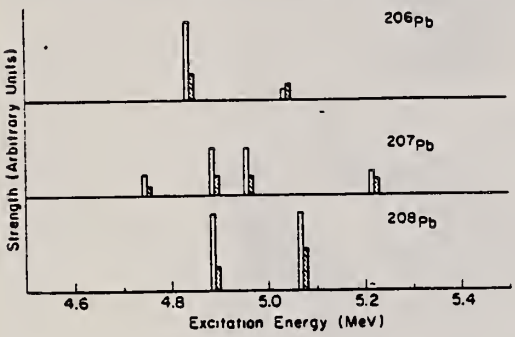

Fig. 1. Excitation energy and strength of the E10 transitions observed in ^{208}Pb, ^{207}Pb and ^{206}Pb. Their strength (corresponding to the first maximum of their form factor) is given in arbitrary units. The open bars represent the strength at 90° and they are enlarged by a factor of 10 as compared to the solid ones (strength at 160°)

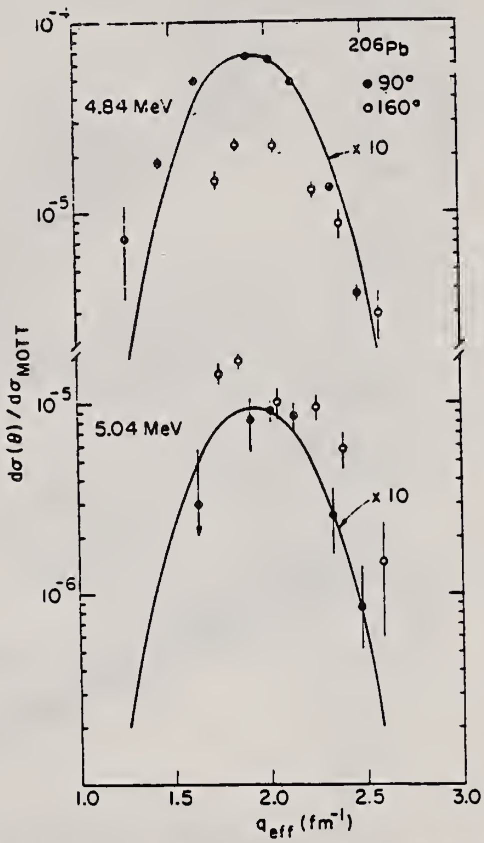

Fig. 3. $d\sigma/d\sigma_{Mott}$ at 90° and 160° for the two transitions in ^{206}Pb which we identify as being of E10 character.

REF. R.D. Starr, P. Axel, L.S. Cardman
Phys. Rev. C25, 780 (1982)

ELEM. SYM.	A	Z
Pb	206	82

METHOD

REF. NO.	
82 St 1	hg

REACTION	RESULT	EXCITATION ENERGY	SOURCE TYPE	SOURCE RANGE	DETECTOR TYPE	DETECTOR RANGE	ANGLE
G,G	ABX	9-12	D	9-12	NAI-D		DST
		(9.5-12)		(9.5-12)			

The elastic photon scattering cross sections of ^{208}Pb and ^{206}Pb were measured at 90° and 135° in the energy range from 9.5 to 12 MeV with a tagged photon beam whose energy spread was about 125 keV. The ^{206}Pb cross section rises monotonically with energy, and is consistent with a total photon interaction cross section which has a Lorentzian energy dependence with a peak cross section of 650 mb at 13.6 MeV and a width $\Gamma \simeq 3.8$ MeV. The ^{208}Pb scattering cross section is larger and has some rapid variations with energy; there is a narrow extra peak near 10.04 MeV and there are abrupt increases in the cross section just below 10.6 and 11.3 MeV. The relative scattering observed at the two angles indicates that all of the scattering, including the rapid variations with energy, is dominated by dipole interactions. This dipole assignment for the fine structure is important for the proper interpretation of inelastic electron scattering by ^{208}Pb. Some of the observed fine structure in inelastic electron scattering must be dipole; the fine structure previously reported as being due to electric quadrupole excitation should be considered as tentative until the correct dipole contributions are included.

[NUCLEAR REACTIONS ^{206,208}Pb($\gamma\gamma$), $E = 9.5-12$ MeV; measured $\sigma(E;\theta)$; resolution 125 keV; observed fine structure; inferred dipole excitation.]

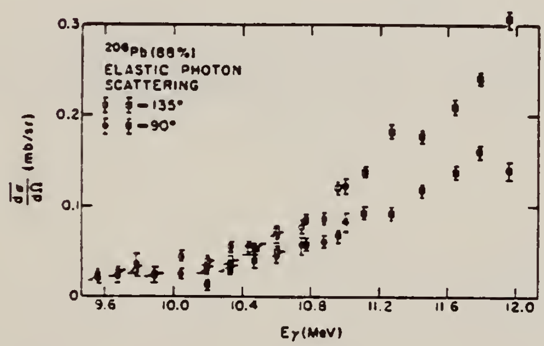

FIG. 3. Differential elastic scattering cross sections for the enriched ^{206}Pb target: See caption of Fig. 2 for an explanation of the symbols.

The open symbols give the values obtained at 135°, while the dark symbols correspond to 90°. In both cases, the circles give the data obtained in the lower energy range (run 1 in Table I), while the squares were obtained during the higher energy run. The errors are statistical.

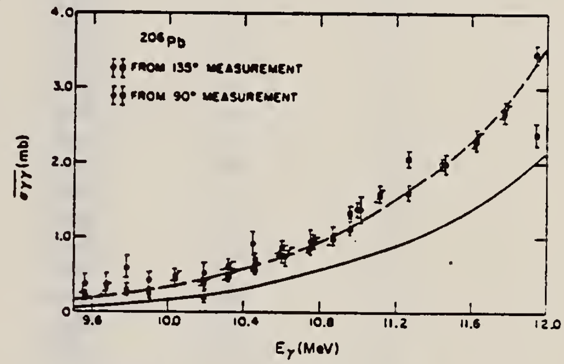

FIG. 6. The elastic photon scattering cross sections for the enriched ^{206}Pb target: The significance of the symbols are explained in the caption to Fig. 5. The lines represent the elastic scattering that would be expected for a giant dipole resonance with a maximum absorption cross section at 13.6 MeV. The solid line corresponds to a peak cross section of 514 mb and a resonance width of 3.85 MeV; the dashed line corresponds to a peak cross section of 650 mb and a resonance width of 3.7 MeV.

The values of the cross sections integrated over angle were inferred from the data at 135° (open symbols) and 90° (solid symbols) using Eq. (16). The circles correspond to the lower energy run (i.e., run 1 in Table I), while the squares correspond to run 2. The observed cross sections are well above the solid line expected if the photoabsorption were an extrapolation to low energy of the giant dipole resonance. The dashed line illustrates the scattering that would be expected if there were additional concentrations of photon absorption, as described in the text.

(over)

TABLE I. Elastic scattering cross sections.

Run No.	Counter	Energy (MeV)	^{208}Pb $\sigma_{\gamma\gamma}$[a] (mb)	^{208}Pb $\sigma_{\gamma\gamma}$[b] (mb)	^{206}Pb[c] $\sigma_{\gamma\gamma}$[a] (mb)	^{206}Pb[c] $\sigma_{\gamma\gamma}$[b] (mb)
2	1	11.95	5.46±0.23	5.46±0.30	3.44±0.12	2.38±0.15
2	2	11.78	5.05±0.20	4.72±0.25	2.71±0.10	2.68±0.13
2	3	11.64	4.03±0.20	4.12±0.28	2.33±0.10	2.30±0.13
2	4	11.45	4.43±0.17	4.16±0.28	1.98±0.08	1.98±0.12
2	5	11.27	4.98±0.19	5.01±0.23	2.04±0.09	1.59±0.10
2	6	11.12	3.45±0.16	3.05±0.25	1.54±0.07	1.57±0.10
1	1	11.00	2.22±0.22	1.71±0.20	1.37±0.09	1.37±0.17
2	7	10.96	2.35±0.15	2.23±0.20	1.33±0.08	1.12±0.10
1	2	10.87	2.32±0.25	1.91±0.18	0.98±0.07	1.02±0.13
2	8	10.77	2.23±0.12	2.16±0.18	0.96±0.06	0.96±0.08
1	3	10.75	1.92±0.23	1.78±0.18	0.86±0.08	0.96±0.15
1	4	10.60	1.98±0.21	2.11±0.18	0.75±0.07	0.75±0.12
2	9	10.60	2.30±0.12	2.21±0.18	0.82±0.06	0.85±0.08
2	10	10.46	1.50±0.12	1.64±0.18	0.58±0.06	0.70±0.08
1	5	10.45	1.12±0.19	1.27±0.17	0.61±0.06	0.92±0.12
1	6	10.32	0.52±0.16	0.87±0.12	0.63±0.06	0.59±0.10
2	11	10.32	0.86±0.11	0.96±0.18	0.47±0.06	0.49±0.08
1	7	10.19	0.73±0.19	0.99±0.13	0.38±0.06	0.52±0.12
2	12	10.19	1.17±0.12	0.75±0.20	0.41±0.06	0.20±0.08
1	8	10.04	1.91±0.07	2.03±0.17	0.49±0.06	0.44±0.10
1	9	9.90	0.87±0.20	1.12±0.13	0.23±0.04	0.42±0.10
1	10	9.78	0.56±0.16	0.64±0.13	0.31±0.06	0.59±0.17
1	11	9.67	−0.02±0.15	0.15±0.13	0.30±0.06	0.37±0.15
1	12	9.56	0.29±0.13	0.18±0.17	0.22±0.04	0.37±0.13

[a]Calculated from 135° differential cross section assuming dipole radiation.
[b]Calculated from 90° differential cross section assuming dipole radiation.
[c]Not corrected for 2.7% ^{208}Pb or 9.0% ^{207}Pb in enriched ^{206}Pb target.

PB
A=207

PB
A=207

PB -
A=207

REF.	ELEM. SYM.	A	Z
M.D. DeSouza Santos, J. Goldemberg, R.R. Pieroni, E. Silva, O.A. Borello, S.S. Villaca, J.L. Lopes Int. Conf. Peaceful Uses of Atomic Energy II [UN, NY] 169 (1955)	Pb	207.	82

METHOD	REF. NO.	
Betatron; proton yield; radioactivity; r-chamber	55 De 1	EGF

REACTION	RESULT	EXCITATION ENERGY	SOURCE		DETECTOR		ANGLE
			TYPE	RANGE	TYPE	RANGE	
G,P	ABX	11-21	C	11-21	ACT-I		4 PI

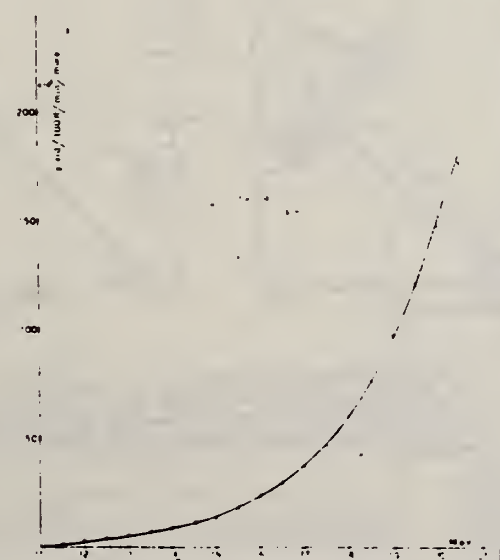

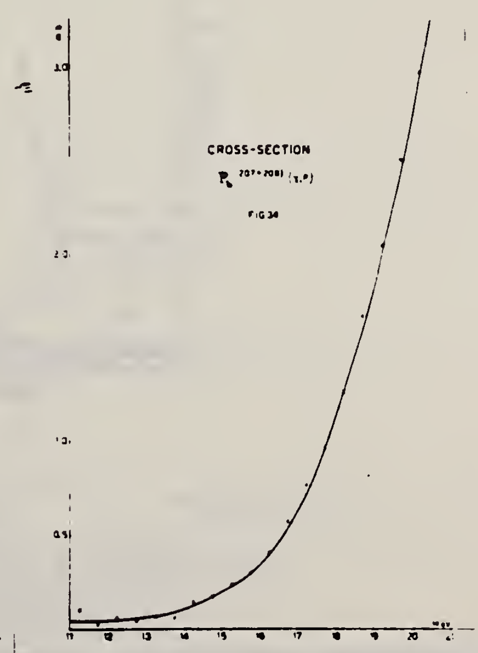

.. N. Geller, J. Halpern, and E. G. Muirhead
Phys. Rev. 118, 1302-12 (1960)

ELEM. SYM.	A	Z
Pb	207	82

METHOD

Betatron; neutron threshold; ion chamber

REF. NO.	
60 Ge 3	NVB

REACTION	RESULT	EXCITATION ENERGY	SOURCE TYPE	SOURCE RANGE	DETECTOR TYPE	DETECTOR RANGE	ANGLE
G,N	NØX	THR	C THR		BF3-I		4 PI

THRESHØLD

TABLE I. Summary and comparison of neutron separation energies inferred from present threshold measurements with values predicted from mass data and reaction energies. All energies are expressed in the center-of-mass system in Mev.

Reaction	No. runs	Present results	Other results	Method	Reference
$Pb^{207}(\gamma,n)Pb^{206}$	3	6.790±0.023	6.734±0.008	$Pb^{206}(n,\gamma)Pb^{207}$	e
			6.75 ±0.06	mass data	q
			6.736±0.020	$Pb^{206}(d,p)Pb^{207}$	t
			6.722±0.012	mass data	r

[e] P. M. Van Patter and W. Whaling, Revs. Modern Phys. 26, 402 (1954); 29, 756 (1957).
[q] W. H. Johnson, Jr., and V. B. Bhanot, Phys. Rev. 107, 6 (1957).
[r] J. L. Benson, R. A. Damerow, and R. R. Ries, Phys. Rev. 113, 1105 (1959).
[s] J. R. Huizenga, Physica 21, 410 (1955).
[t] M. T. McEllistrem et al., Phys. Rev. 111, 1636 (1958).

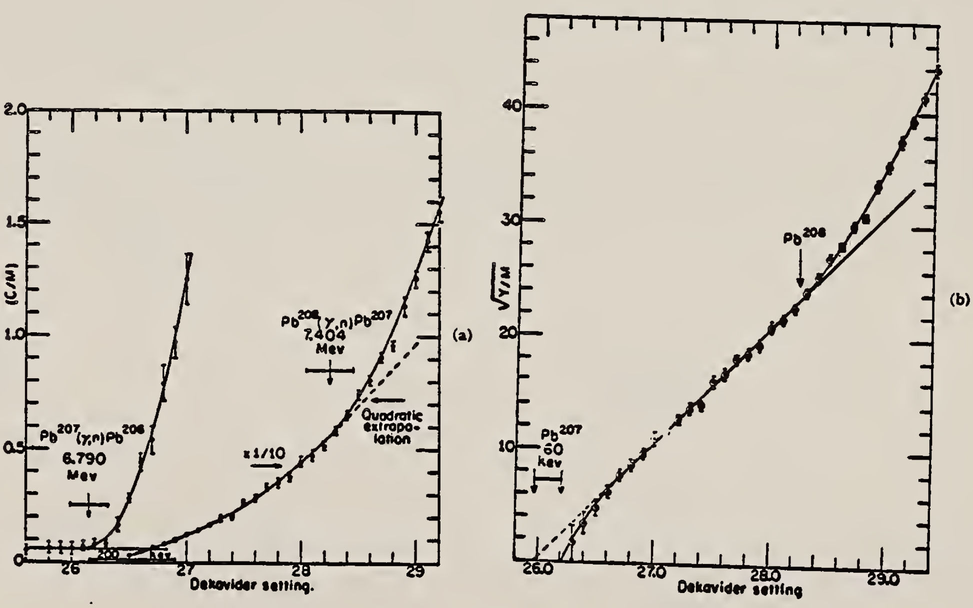

FIG. 2. (a) Neutron yield data for lead from 6.7 Mev to 7.7 Mev, and (b) square root plot of yield data. Linear extrapolation of $(Y/M)^{\frac{1}{2}}$ predicts an apparent threshold 60 kev lower than what is obtained from yield data in the immediate vicinity of threshold.

Ref. P.C. Stein, A.C. Odian, A. Wattenberg, R. Weinstein
Phys. Rev. 119, 348 (1960)

Elem. Sym.	A	Z
Pb	207	82

Method
320 MeV synchrotron; proton telescope; neutron counter

Ref. No.	
60 St 1	JHH

Reaction	E or ΔE	E_0	Γ	$\int \sigma dE$	Jπ	Notes
$Pb^{207}(\gamma,np)$	Bremss. 320					$(\sigma/\sigma_{H^2}) = 13.4 \pm 2.1$ $[\sigma_{H^2} = 63\ \mu b]$ Mean photon energy - 262 MeV Proton counter at 76°

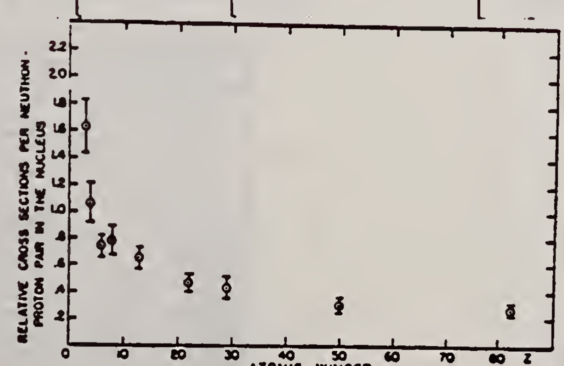

FIG. 2. Relative cross sections per neutron-proton pair in the nucleus versus atomic number. The cross section of the element of interest is divided by the cross section for deuterium and by the factor NZ/A.

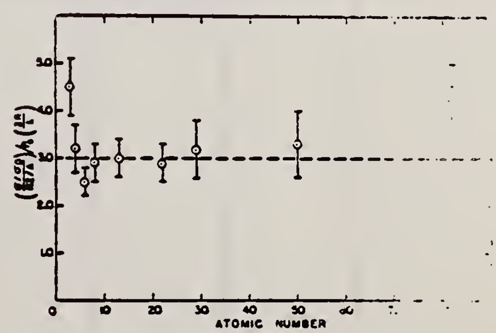

FIG. 3. The relative cross sections [illegible] corrected for the probability of escape [illegible] number. The probability of escape [illegible] $r_0 = 1.30 \times 10^{-13}$ cm and $\lambda =$ [illegible] escape factor is given in expression [illegible] of Fig. 2 divided by $P(2R/$[illegible]

Ref. E.G. Fuller, E. Hayward Nuclear Phys. 33, 431 (1962)	Elem. Sym.	A	Z
	Pb	207	82

Method	Ref. No.	
50 MeV betatron; BF_3, NaI counters	62 Fu 4	JHH

Reaction	E or ΔE	E_0	Γ	$\int \sigma dE$	Jπ	Notes
$Pb^{206,7,8}$						$\int$ corrected for multiple neutron production.
(γ,γ)	4.5-8.5					
(γ,xn)				$\int^{18.5} = 3.93$ MeV-b		Self-absorption measurements made at 7 MeV.

TABLE 1

Observed transmissions corrected for electronic absorption

Absorber	Thickness (g cm^{-2})	Targets: Pb (7.2 g cm^{-2})		"Pb[illegible]" (3.6 g cm^{-2})		Bi (5.97 g cm^{-2})	
Pb	10.8					0.895	0.031
	14.4	0.663	0.032	0.846	0.049		
		0.694	0.037 a)				
"Pb[illegible]"	11.2	0.976	0.050	0.74	0.043	1.002	0.048
				0.599	0.031 a)		
Bi	12.2	1.018	0.050	1.045	0.038	0.792	0.040
						0.719	0.038 a)
Pb	7.65	0.822	0.029			0.903	0.028
"Pb[illegible]"	7.83	0.790	0.028			0.910	0.028
"Pb[illegible]"	7.86	0.797	0.028			0.915	0.028
"Pb[illegible]"	7.47					0.965	0.029
Bi	7.49					0.790	0.025

a) Measured with both target and absorber at liquid nitrogen temperature.

TABLE 3

Average level parameters at 6 MeV

	Lead	Radio-lead	Bismuth
[illegible] (6 Γ)^2	[illegible] 1.0	1 - 400	0 – 64
σ_0^2 (b)	24—38	29—205	10—48
Γ (eV)	3.1	0.15 – 3.[illegible]	> 0.39
σ_0 (max) (b)	183	205	68
$\gamma \cdot \Gamma$	0.13 - 0.21	0.14 – 1.0	0.2 – 1.0
$\sigma_{\gamma n}$ (7 MeV) (mb)	21	20	21
$\int_4^{7.5} \sigma_{\gamma n} dE$ (MeV · mb)	42	40	48

SEE PAGE 2 FOR FIGURES.

Ref.	Elem. Sym.	A	Z
	Pb	207	82
Method	Ref. No.		
PAGE 2	62 Fu 4		JHH

$\int \sigma dE$

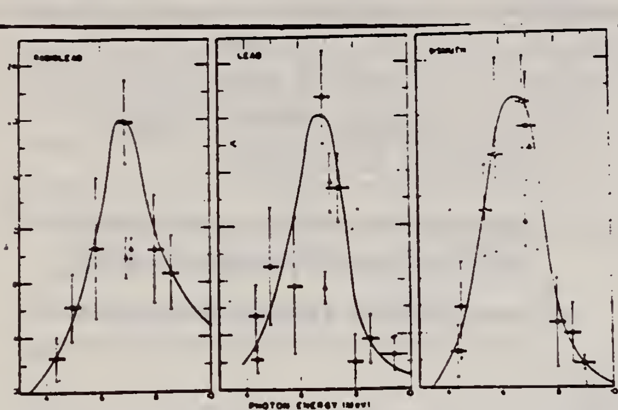

Fig. 1. The [illegible] cross sections for lead, radio-lead and bismuth. [illegible]

Ref 3: Fuller & Hayward - Phys. Rev. 101, 692 (1956)

Ref 5: Reibel & Mann - Phys. Rev. 118, 701 (1960)

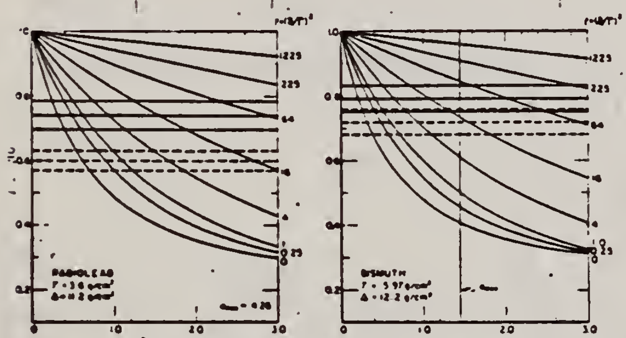

Fig. 5. Self-absorption attenuation curves for radio-lead and bismuth. The ratio as defined in the text (eq. (4)) has been evaluated as a function of the peak absorption cross section σ_0^c, for the target and absorber thicknesses used in the experiments. The horizontal lines represent the measured attenuations and their uncertainties for the experiments performed at room temperature (solid lines) and liquid nitrogen temperature (dashed lines). The quantity s_{max} is the maximum possible value of the average peak absorption cross section at 6 MeV in units of 3 times the electronic absorption cross section. This maximum value assumes electric dipole scattering and represents an average over all possible spins for the excited states.

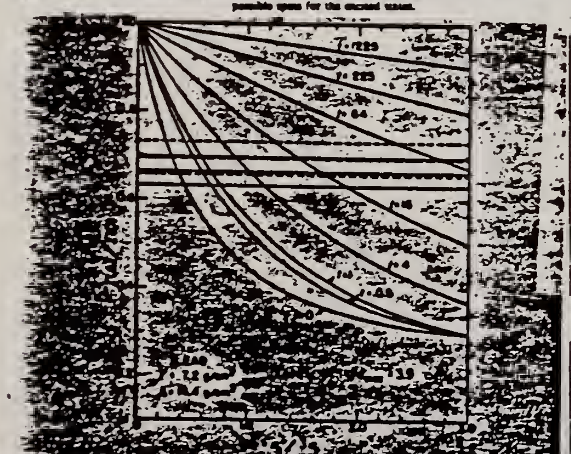

Fig. 6. Self-absorption attenuation curves for lead. See description for fig. 5.

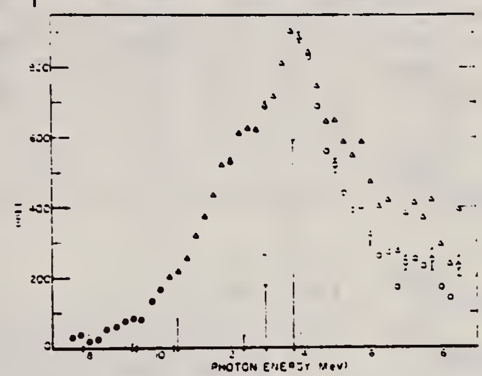

Fig. 7. The neutron production cross section for Pb[208]. The triangles represent the cross section before correction for neutron multiplicity. Points were obtained from a 1 MeV bin-width analysis of the neutron yield curve except near threshold (indicated by closed circles) where a half-MeV bin-width was used. The points represented by the open circles have been corrected for the neutron multiplicity. The arrows beneath the axis of abscissas indicate the energies of the important dipole transition calculated by Balashov, *et al.* [11]). The heights of the vertical lines are proportional to the calculated strengths of the transitions.

Ref 11: Balashov, Shevchenko & Yudin, to be published: Shevchenko, private communication.

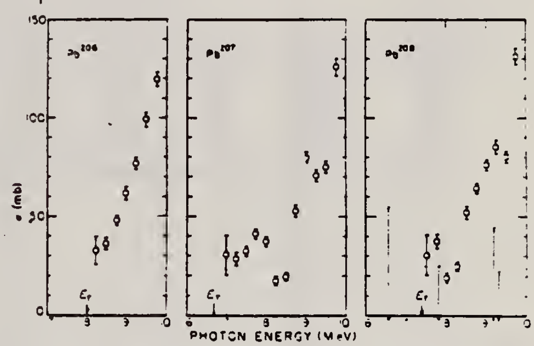

Fig. 8. The (γ, n) cross sections for the lead isotopes near threshold. The arrows indicate the position of the (γ, n) thresholds. The arrows beneath the axis of abscissas indicate the energies of the important dipole transition calculated by Balashov *et al.* [11]). The heights of the vertical lines are proportional to the calculated strengths of the transitions.

Ref. Yu. I. Sorokin, V.G. Shevchenko, B.A. Yur'ev Zhur.Eksptl. i Teoret.Fiz. 43, 1600 (1962); Soviet Phys.JETP 16, 1127 (1963)	Elem. Sym. Pb	A 207	Z 82
Method 35 MeV Betatron - counters (activity of Ti^{206} and Ti^{207} detected.	Ref. No. 62Sol		BG

Reaction	E or ΔE	E_0	Γ	∫σdE	Jπ	Notes
$Pb^{207}(\gamma,p)Ti^{206}$	15 - 33	26		$55\pm20)_0^{33}$		Cross section obtained from corrected yield curve.
$Pb^{208}(\gamma,p)Ti^{207}$						Assumptions made on contribution of $Pb^{208}(\gamma,pn)Ti^{206}$ reaction to σ_T - contribution greatly overestimated.
$Pb^{207}(\gamma,p)Ti^{206}$	15- 33	26.5		$60\pm20)_0^{33}$		
$Pb^{208}(\gamma,p)Ti^{207}$						
$Pb^{208}(\gamma,pn)Ti^{206}$						
$Pb^{208}(\gamma,d)Ti^{206}$						

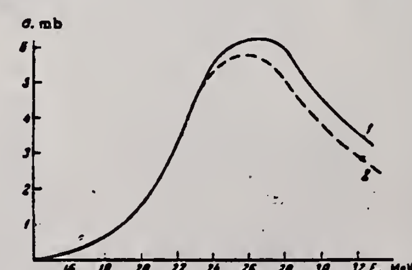

FIG. 2. Cross section of photonuclear reactions in lead: 1 – cross section calculated from the total yield curve, 2 – cross section for the (γ, p) reaction.

REF.

R.R. Harvey, J.T.Caldwell, R.L. Bramblett, S.C. Fultz
Phys. Rev. 136, B126-31 (1964)

ELEM. SYM.	A	Z
Pb	207	82

METHOD

Positron annihilation; ion chamber

REF. NO.	
64 Ha 2	NVB

REACTION		RESULT	EXCITATION ENERGY	SOURCE		DETECTOR		ANGLE
				TYPE	RANGE	TYPE	RANGE	
G,N	173	ABX	6-27	D	6-26	BF3-I		4PI
G,2N	174+	ABX	12-27	D	12-26	BF3-I		4PI

Sample eneriched to 92.8% Pb^{207} 173+

(γ,2n) threshold 14.44 ± 0.43 MeV

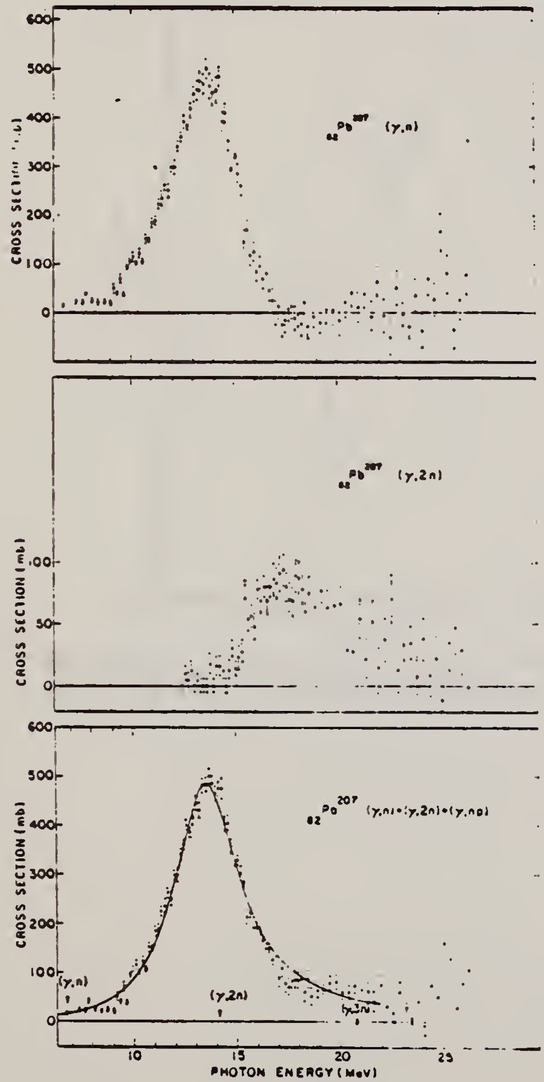

FIG. 2. Top figure shows data points for $\sigma[(\gamma,n)+(\gamma,np)]$ for Pb^{207}, obtained from single-neutron counting data. Center figure shows data for $\sigma(\gamma,2n)$ obtained from double-neutron counting data. Data points for the compound nucleus formation cross section of Pb^{207}, i.e., $\sigma[(\gamma,n)+(\gamma,np)]+\sigma(\gamma,2n)$ are shown in bottom figure. Solid curve is a plot of a Lorentz line having the parameters given in Table II. The data are uncertain below 8 MeV owing to low beam intensities encountered.

TABLE II. Lorentz line parameters and σ_{-2} values for Pb isotopes and Bi.

Isotope	Peak σ_0 (mb)	Width Γ (MeV)	E_0 (MeV)	σ_{-2} (mb/MeV)	$0.00225A^{5/3}$ (mb/MeV)
Pb^{206}	525	3.75	13.7	15.6±1.6	16.2
Pb^{207}	485	3.87	13.6	14.5±1.5	16.3
Pb^{208}	495	3.78	13.6	14.1±1.4	16.4
Bi^{209}	520	3.83	13.5	16.6±1.7	16.6

TABLE I. Integrated cross sections in MeV-b, up to 28 MeV, for Pb isotopes and Bi.

Isotope	$\int_0^{28}\sigma(\gamma,n)dE$	$\int_0^{28}\sigma(\gamma,2n)dE$	$\int_0^{28}\sigma dE$	$\int_0^{28}\sigma dE+W$	$0.06NZ/A$
Pb^{206}	2.22	0.56	2.78±0.28	3.07±0.36	2.96
Pb^{207}	2.05	0.60	2.65±0.27	2.95±0.30	2.97
Pb^{208}	1.96	0.95	2.91±0.29	3.21±0.32	2.98
Bi^{209}	2.17	0.76	2.93±0.29	3.25±0.33	3.00

FORM NBS-418
(REV. 7-14-64)
USCOMM-DC 26010-P64

REF.

A. De Marco, R. Garfagnini and G. Piragino
Nuovo Cimento 44B, 172 (1966)

ELEM. SYM.	A	Z
Pb	207	82

METHOD

REF. NO.	
66 De 2	JDM

REACTION	RESULT	EXCITATION ENERGY	SOURCE		DETECTOR		ANGLE
			TYPE	RANGE	TYPE	RANGE	
G,N	SPC	THR - 80	C	80	CCH-D	0 - 15	135

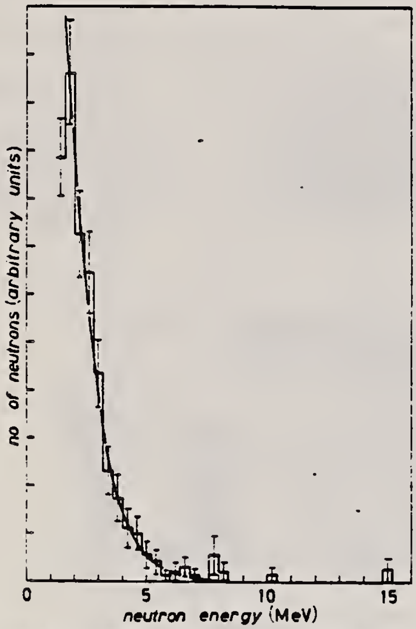

Fig. 3. – Energy distribution of photon-eutrons from Pb. The solid line has the same meaning as in Fig. 2.

REF.	J. F. Ziegler and G. A. Peterson Proc. Gatlinburg Conference 319 (1966)	ELEM. SYM.	A	Z
		Pb	207	82

METHOD	REF. NO.	
	66 Zi 2	hmg

REACTION	RESULT	EXCITATION ENERGY	SOURCE TYPE	SOURCE RANGE	DETECTOR TYPE	DETECTOR RANGE	ANGLE
E,E/	RLX		D	28-70	MAG-D		DST

B(EL)

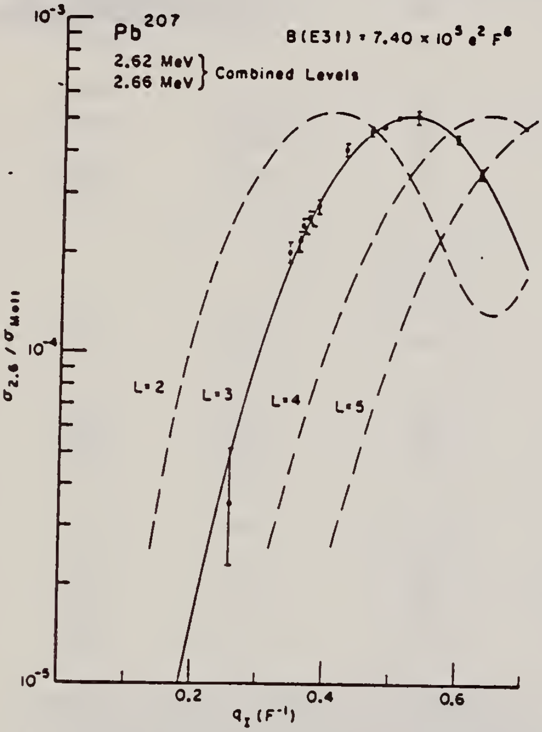

Fig. 1. Inelastic cross sections for the excitation of ^{207}Pb by 70 MeV electrons vs. elastic scattering momentum transfer in inverse Fermi.

TABLE 1

Values of B(E3↑)

Isotope	Energy level	B(E3↑) (e^2b^3)
^{209}Bi	2.58	0.527 ± .012
	2.58 } 2.73 }	0.773 ± .020
^{208}Pb	2.615	0.788 ± .028
^{207}Pb	2.62 } 2.66 }	0.740 ± .012
^{206}Pb	2.60	0.702 ± .032

2. Tuan, S. T., and Wright, L. E., Bull. Am. Phys. Soc. 11, 338 (1966); Reynolds, J. T., Ph. D. Thesis, Duke University; Onley, D. S., private communications.
3. Elton, L. R. B., "Nuclear Sizes," Oxford Univ. Press, London, 1961); Hofstadter, R., private communication.

REF.

J. F. Ziegler and G. A. Peterson
Phys. Rev. 165, 1337 (1968)

ELEM. SYM.	A	Z
Pb	207	82

METHOD

REF. NO.	
68 Zi 1	HMG

REACTION	RESULT	EXCITATION ENERGY	SOURCE		DETECTOR		ANGLE
			TYPE	RANGE	TYPE	RANGE	
E,E/	FMF	2-5	D	28-73	MAG-D	28-73	100

SEP ISTOPS, B(EL)

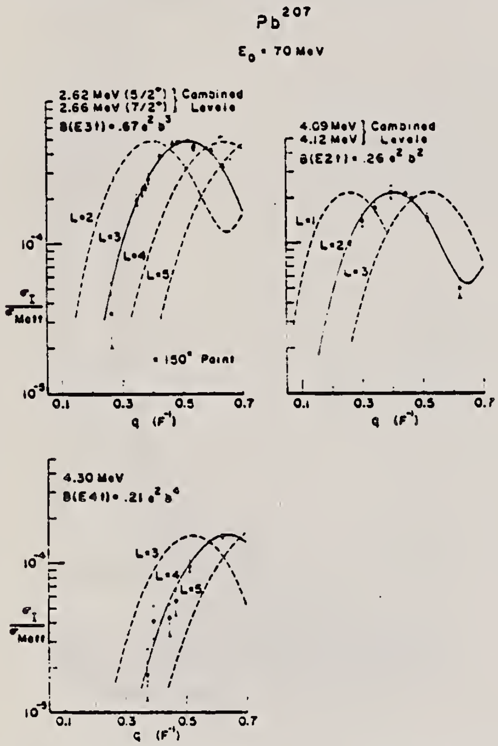

FIG. 14. Experimental relative cross sections versus momentum transferred to the nucleus Pb^{207} normalized to an initial electron energy of 70 MeV for excitations at about 2.6, 4.1, and 4.39 MeV. The solid curve is the best fit of the GBROW calculation assuming the Tassie hydrodynamical model for the specified transition multipolarity, and the dashed curves are arbitrarily normalized for other transition multipolarities.

OVER

TABLE II. Experimental values of reduced nuclear transition probabilities $B(EL)$ for the excitation of a nucleus from its ground state to an excited state as determined by the electron scattering methods of this experiment and by other methods. The units of $B(EL)$ are e^2b^L where e is the electron charge, b is 10^{-24} cm² (1 b), and L is the multipolarity of the transition. $B(EL)_{sp}$ is the single-particle estimate of Eq. (10).

Nuclide	Level (MeV)	Transition character	This experiment: $B(EL, 0\rightarrow L)$ e^2b^L	This experiment: $G=\frac{B(EL)}{B(EL)_{sp}}$	Ref.	Other experiments $B(EL, 0\rightarrow L)$ e^2b^L
Pb^{206}	4.09	$E2$	0.23±0.02	6.2	a	(p,p')0.20
Pb^{207}	4.070[b], 4.125[b]	$E2$	0.26±0.02	7.0	c d	(α,α')0.33 (p,p')0.18
Pb^{208}	4.07	$E2$	0.30±0.02	8.1	c e	(α,α')0.35 (p,p')0.17
Pb^{206}	2.65	$E3$	0.64±0.04	35	a	(p,p')0.33
Pb^{207}	2.625[b], 2.664[b]	$E3$	0.67±0.04	37	c d	(α,α')0.56 (p,p')0.32
Pb^{208}	2.614	$E3$	0.72±0.04	39.5	c f g e h i j k	(α,α')0.57 (e,e')0.53 (p,p')0.67 (p,p')0.36 $(C^{12},C^{12\prime})$0.83 (p,p')0.84 (p,p')0.97 (n,n')0.71
Bi^{209}	2.6[l]	$E3$	0.67±0.05	37	c f m	(α,α')0.57 (e,e')0.55 (p,p')0.65
Pb^{206}	4.32	$E4$	0.22±0.02	25	a	(p,p')0.038
Pb^{207}	4.29	$E4$	0.21±0.03	24	c	(α,α')0.12
Pb^{208}	4.31	$E4$	0.23±0.02	26	c f e	(α,α')0.13 (e,e')0.24 (p,p')0.057
Pb^{208}	5.25	$E3$ ($E4$)	0.13±0.03 0.14±0.07	7.2 16		
Pb^{208}	5.6	$E3$	0.09±0.03	5	c	(α,α')0.16
Pb^{208}	6.2	$E2$ ($E0$)	0.07±0.02	2		
Pb^{208}	3.2	$E5$	0.06±0.02	14	c e	(α,α')0.03 (p,p')0.034

[a] G. Vallois, J. Saudinos, and O. Beer, Phys. Letters 24, 512 (1967).
[b] Peaks were not resolved in this experiment. Energies taken from J. C. Hafele and R. Woods, Phys. Letters 24, 579 (1966).
[c] J. Alster, Phys. Rev. 141, 1138 (1966); Phys. Letters 25B 459 (1967).
[d] G. Vallois, J. Saudinos, O. Beer, M. Gendrot, and P. Lopato, Phys. Letters 22, 659 (1966).
[e] J. Saudinos, G. Vallois, O. Beer, M. Gendrot, and P. Lopato, Phys. Letters 22, 492 (1966).
[f] H. Crannell, R. Helm, H. Kendall, J. Oeser, and M. Yearian, Phys. Rev. 123, 923 (1961); and H. W. Kendall and J. Oeser, *ibid.* 130, 245 (1963).
[g] A. Scott and M. P. Fricke, Phys. Letters 20, 654 (1966).
[h] A. Z. Hrynkiewicz, S. Kopta, S. Szymczyk, and T. Walczak, Nucl. Phys. 79, 495 (1966), references cited therein, and see text of this section.
[i] G. R. Satchler, R. H. Bassel, and R. M. Drisko, Phys. Letters 5, 256 (1963).
[j] T. Stovall and N. M. Hintz, Phys. Rev. 135, B330 (1964).
[k] P. H. Stelson *et al.*, Nucl. Phys. 68, 97 (1965).
[l] Approximate energy of seven unresolved peaks, J. C. Hafele and R. Woods, Phys. Letters 24, 579 (1966).
[m] S. Hinds, H. Marchant, J. H. Bjerregaard, and O. Nathan, Phys. Letters 20, 674 (1966).

C. D. Bowman, B. L. Berman, and H. E. Jackson Phys. Rev. <u>178</u>, 1827 (1969)	ELEM. SYM.	A	Z
	Pb	207	82

METHOD	REF. NO.	
	69 Bo 1	hmg

REACTION	RESULT	EXCITATION ENERGY	SOURCE TYPE	SOURCE RANGE	DETECTOR TYPE	DETECTOR RANGE	ANGLE
G,N	SPC	THR-9	C	7-9	TOF-D		135

Tabular data given.

<u>G-WIDTH</u>

TABLE VI. Resonance parameters.

Isotope	Energy in (n, γ) This work	b	c	$g\Gamma_{\gamma 0}$[a] This work	d	$g\Gamma_{\gamma}$ c	b	Spectroscopic data b	d
	(keV)	(keV)	(keV)	(eV)	(eV)	(eV)	(eV)	l	J^{π}
Pb^{208}	3.00		3.02	0.08±0.03[e]		0.078±0.005			
	10.4		10.2	0.06±0.02		0.13±0.02			
	16.6	16.7	16.2	0.14±0.04		0.66±0.07	0.3±0.07	(>0)	(2^+)
	25.3			<0.2					
		29	29.5	<0.4		0.20±0.06	0.35±0.13	(>0)	(2^+)
		37	37.6	<0.4		0.7±0.1		(>0)	(2^+)
	40.9[f]	41.7	41.0	4.13	4.13	3.8±0.4	4.13±0.9	0	(1^-)
Pb^{207}	3.4		3.36	0.14±0.03		0.077±0.006			
			10.8	<0.05		0.06±0.01			
	11.4[g]		11.3	0.54±0.08		0.07±0.02			
	12.3	12.2		0.05±0.03				(>0)	
	14.6[g]		14.2	0.55±0.10		0.20±0.04			
	16.6[f]	16.5	16.5	0.63	0.63±0.03	0.70±0.08	0.8±0.12	(>0)	$(\frac{1}{2}^-)$
	20.1		19.6	0.169±0.08		0.32±0.06			
		21	21.8	<0.05		0.28±0.1	0.18±0.07		
	25.1	25.1	24.9	0.4±0.15	0.28±0.03	1.1±0.2	0.77±0.12	(>0)	$(\frac{1}{2}^-)$
Pb^{206} [h]	1.55			0.40±0.06					
	7.34			3.4±0.30					
	10.2			1.0±0.15					
	16.0			0.50±0.15					
	33.6								
	49.9								

[a] The statistical factor g is different depending on whether neutrons or photons excite the nucleus. To make easier a comparison of the results, the present values for Pb^{208} and Pb^{207} have been multiplied by the ratio $(2I'+1)/(2I''+1)$ where I' is the spin of the target for the photonuclear experiment and I'' is the target spin for the inverse experiment. The Pb^{206} values are unmodified.
[b] Reference 4.
[c] Reference 6.
[d] Reference 7.

[e] The uncertainties in the values for $g\Gamma_{\gamma 0}$ for all isotopes do not include a ±15% uncertainty in normalization.
[f] The present data were normalized at these resonances using the data from Ref. 7.
[g] These peaks are associated with transitions both to the ground state and the first excited state of Pb^{208}. The excited-state transitions are the stronger (see text).
[h] For Pb^{206}, the energies have not been transformed into the (n, γ) system.

REF.

C. D. Bowman, R. J. Baglan, and B. L. Berman
Phys. Rev. Letters 23, 796 (1969)

ELEM. SYM.	A	Z
Pb	207	82

METHOD

REF. NO.	
69 Bo 4	hmg

REACTION	RESULT	EXCITATION ENERGY	SOURCE		DETECTOR		ANGLE
			TYPE	RANGE	TYPE	RANGE	
G,N	ABX	THR-8	D	8	TOF-D		135

Erratum attached:
Phys. Rev. Letters 24, 193 (1970)

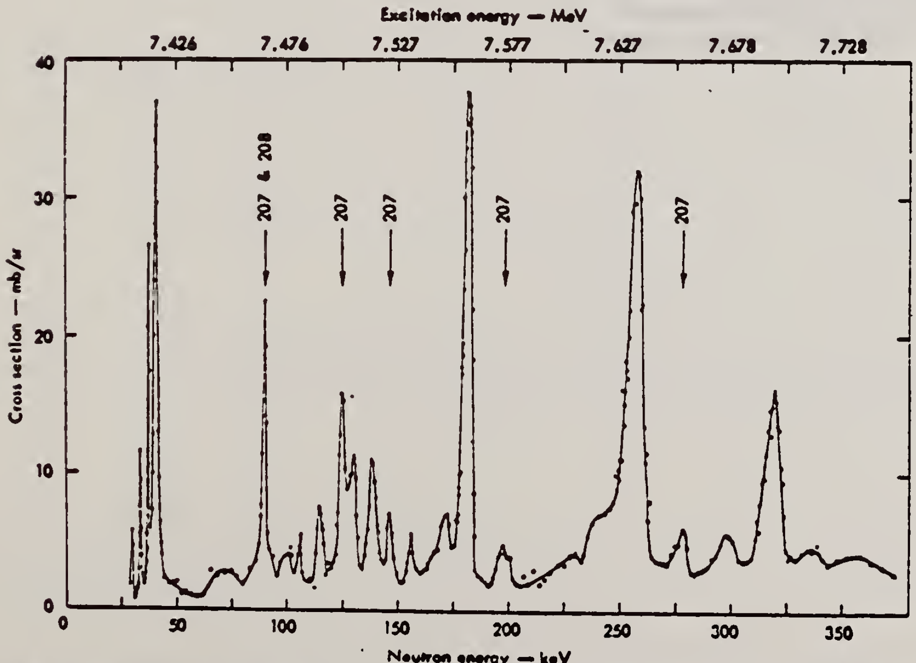

FIG. 1. Threshold photoneutron cross section in mb/sr for natural lead derived from the neutron spectrum emitted at 135° as a function of both laboratory neutron energy and incident photon energy. Levels not Pb^{208} are designated by vertical arrows.

[over]

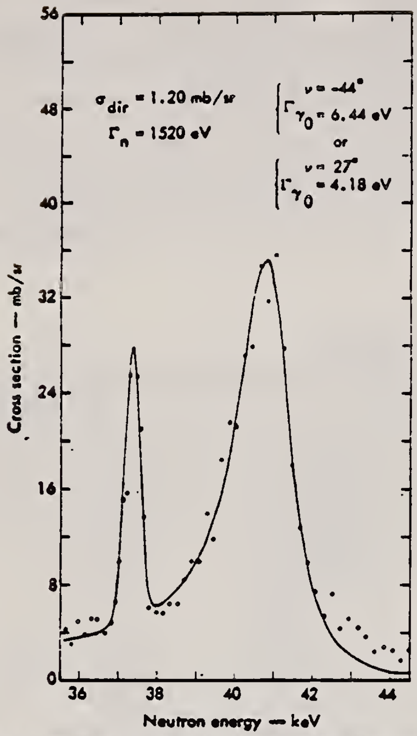

FIG. 2. The data of this figure are taken from Fig. 1. The solid curve is a shape fitted to the data using the resolution determined from the narrow peak at 37.3 keV. The spins for the 37.3- and 40.7-keV peaks are 2^+ and 1^-, respectively (Ref. 14), so there is no interference between them.

REF.

C. D. Bowman, R. J. Baglan, and B. L. Berman
Phys. Rev. Letters 24, 193 (1970)

ELEM. SYM.	A	Z
Pb	207	82

METHOD

REF. NO.	
70 Bo 1	hmg

REACTION	RESULT	EXCITATION ENERGY	SOURCE		DETECTOR		ANGLE
			TYPE	RANGE	TYPE	RANGE	
G,N	ABX	THR-8	D	8	TOF-D		135

ERRATUM FOR 69 BO 4
PRL 23, 796 (1969)

REF. R. J. Baglan, C. D. Bowman and B. L. Berman
Phys. Rev. C3, 672 (1971)

ELEM. SYM.	A	Z
Pb	207	82

METHOD

REF. NO. 71 Ba 2 hmg

REACTION	RESULT	EXCITATION ENERGY	SOURCE TYPE	SOURCE RANGE	DETECTOR TYPE	DETECTOR RANGE	ANGLE
G,N	ABX	6-10	C	7-10	TOF-D		135
		(6.73-9.8)					

415

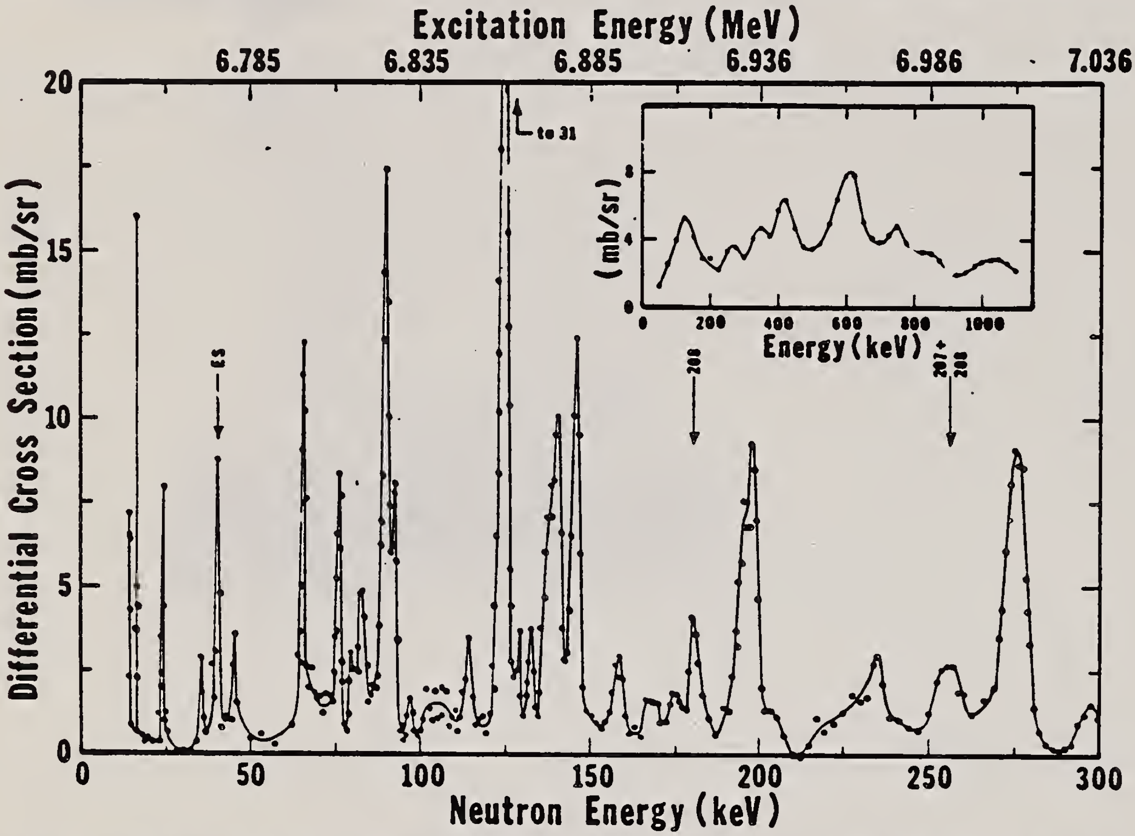

FIG. 4. The 135° differential threshold photoneutron cross section for ^{207}Pb at low energies versus the energy of the emitted neutron (lower scale) and the excitation energy (upper scale). The arrows indicate peaks which decay to excited states of the residual nucleus (ES), or peaks owing to contaminating isotopes in the photoneutron sample. The inset shows the ^{207}Pb(γ, n) cross section averaged with a square 40-keV wide smoothing function.

Also see:
R. J. Baglan et al.
Phys. Rev. C3,
2475 (1971)

[over]

TABLE IV. Resonance parameters for ^{207,208,206}Pb. For all resonances, the area under the peak in the 135° differential cross section is multiplied by 4π to yield approximate values for $g_\gamma\Gamma_{\gamma0}\Gamma_n/\Gamma \approx g_\gamma\Gamma_{\gamma0}$. For those resonances where J^π is known, the differential area is multiplied by the appropriate factor F from Table I to obtain $\Gamma_{\gamma0}$. E_L is the laboratory neutron energy for the (γ,n) reaction and E_n is the corresponding laboratory neutron energy for a neutron-induced reaction. Column 5 labels the peak as a ground-state (GS) or excited-state (ES) transition as determined in this work alone. Clearly, if a peak is seen in a neutron-induced reaction (columns 9–11), it must be GS. For excited-state transitions, $g_\gamma\Gamma_{\gamma0}\Gamma_n/\Gamma$ is computed as if the residual nucleus were left in its first excited state (second, for ^{206}Pb) with the use of the multiplicative factor from Table II.

Nucleus	E_L (keV)	E_{ex} (MeV)	$g_\gamma\Gamma_{\gamma0}\Gamma_n/\Gamma$ (eV)	GS or ES	J^π	$\Gamma_{\gamma0}$ (eV)	E_n (keV) (This work)	E_n (keV) from neutron-induced reactions (Ref. a)	(Ref. b)	(Ref. c)
^{207}Pb	3.3[d]	6.738	0.07	GS[d]			3.4			
	11.2[d]		0.054	ES[d]						
	12.1[d]	6.747	0.03	GS[d]			12.3			
	14.3[e]		0.34	ES[e]						
	16.2[e]	6.751	0.21	GS	$\frac{1}{2}^{-a}$	0.42	16.5	16.5		
	19.8[d]	6.755	0.08	GS[d]			20.1			
	24.9[e]	6.760	0.71	GS	$\frac{3}{2}^{-a}$	0.81	25.3	25		
	35.8	6.771	0.97		$\frac{3}{2}^{-a}$	1.1	36.4	35		
	40.7		5.0	ES						
	45.1	6.780	1.2		$\frac{3}{2}^{-a}$	1.3	45.8	46		
	65.7	6.801	1.6	GS	$\frac{1}{2}^{+a}$	3.2	66.6	66		
	76.1	6.811	1.1	GS			77.1			
	82.6	6.818	1.1				83.8			85
	90.0	6.825	3.1	GS			91.2			
	92.5	6.828	0.88				93.8			
	97.0	6.832	0.30				98.3			
	114	6.849	0.82	GS			115			
	125	6.860	6.6	GS			127			126
	133	6.868	0.86				135			
	140	6.876	4.0	GS			142			
	146	6.881	2.9	GS			148			
	159	6.895	1.1				161		161	
	168	6.904	0.78	GS			170			
	175	6.911	0.78	GS			177			
	196	6.932	1.9	GS			198		198	197
	198	6.934	2.8	GS			200			
	205	6.941	0.63		$\frac{1}{2}^{+b}$	1.3	208		207	
	217	6.953	0.57		$\frac{1}{2}^{+b}$	1.1	220		219	
	234	6.970	1.9	GS			237			
	242		3.1	ES						
	253	6.989	2.4	GS	$\frac{1}{2}^{+b}$	4.7	256		256	
	276	7.012	6.3	GS			279		278	
	301	7.038	2.8				305			
	342	7.079	4.7		$\frac{1}{2}^{+b}$	9.4	346		348	
	350	7.087	5.1		$\frac{1}{2}^{+b}$	10.3	354		355	
	356	7.093	4.2				360			
	374	7.111	0.88		$\frac{1}{2}^{+b}$	1.8	379		383	
	391	7.128	2.9		$\frac{1}{2}^{+b}$	5.8	396		396	
	407	7.144	4.0	GS			412			
	416	7.153	4.7	GS	$\frac{1}{2}^{+b}$	9.5	421		422	
	426	7.163	4.1	GS			431			
	454	7.191	2.5				459		460	
	466	7.204	4.2				472		473	
	488	7.225	0.94		$\frac{1}{2}^{+b}$	1.9	494		495	
	503	7.241	4.7				509		511	
	523	7.261	3.7				529			
	533		3.4	ES						
	543	7.281	1.5		$\frac{1}{2}^{+b}$	2.9	549		550	
	572	7.310	8.5	GS			578			

d) [3] C.D. Bowman, B.L. Berman, and H.E. Jackson, Phys. Rev. 178, 1827 (1969).

e) [6] J.A. Biggerstaff, J.R. Bird, J.H. Gibbons, and W.M. Good, Phys. Rev. 154, 1136 (1967).

a) [10] J.A. Farrell, G.C. Kyker, Jr., E.G. Bilpuch, and H.W. Newson, Phys. Letters 17, 286 (1965).

c) [13] E.G. Bilpuch, K.K. Seth, C.D. Bowman, R.H. Tabony, R.C. Smith, and H.W. Newson, Ann. Phys. (N.Y.) 14, 387 (1961).

REF. R. J. Baglan, C. D. Bowman and B. L. Berman
Phys. Rev. C3, 672 (1971)

ELEM. SYM.	A	Z
Pb	207	82

METHOD

REF. NO.	
71 Ba 2	hmg

REACTION	RESULT	EXCITATION ENERGY	SOURCE TYPE	SOURCE RANGE	DETECTOR TYPE	DETECTOR RANGE	ANGLE

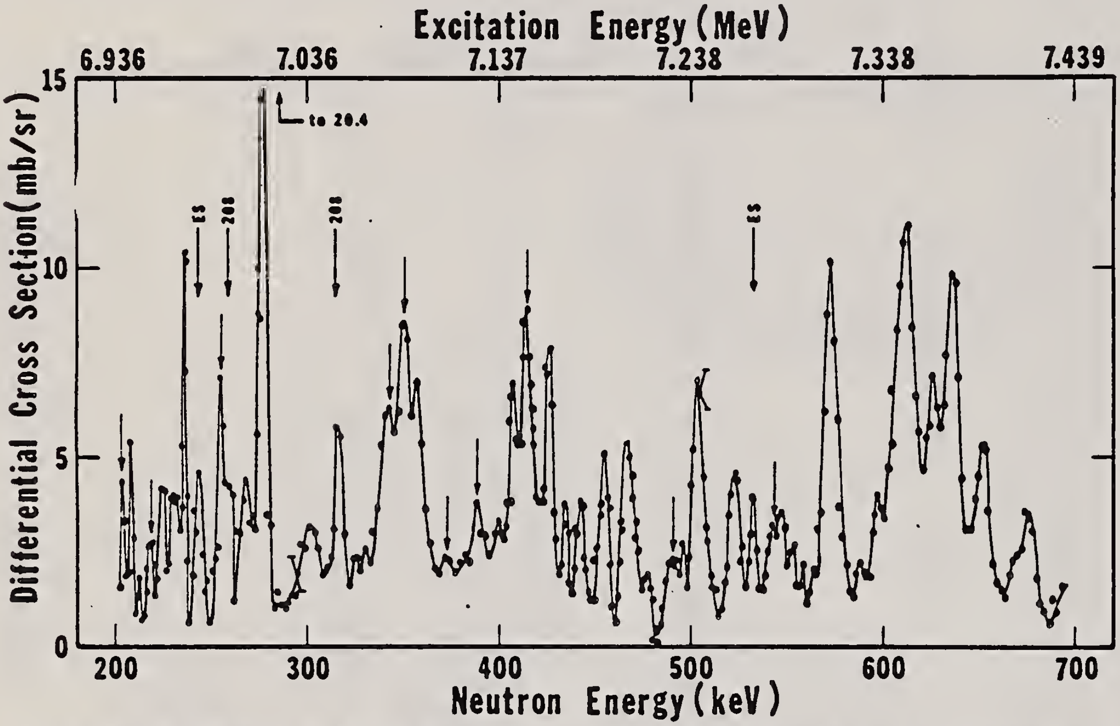

FIG. 5. The 135° differential threshold photoneutron cross section for ^{207}Pb, at high energies (see caption to Fig. 4). The 10 unlabeled arrows above the data indicate the positions of $J^{\pi} = \frac{1}{2}^{+}$ states obtained from the neutron total cross-section measurement on ^{206}Pb.

FIG. 4. The 135° differential threshold photoneutron cross section for ^{207}Pb at low energies versus the energy of the emitted neutron (lower scale) and the excitation energy (upper scale). The arrows indicate peaks which decay to excited states of the residual nucleus (ES), or peaks owing to contaminating isotopes in the photoneutron sample. The inset shows the ^{207}Pb(γ, n) cross section averaged with a square 40-keV wide smoothing function.

REF.	ELEM. SYM.	A	Z
K. Shoda, A. Suzuki, M. Sugawara, T. Saito, H. Miyase, S. Oikawa Phys. Rev. C3, 1999 (1971)	Pb	207	82

METHOD	REF. NO.	
	71 Sh 2	hmg

REACTION	RESULT	EXCITATION ENERGY	SOURCE		DETECTOR		ANGLE
			TYPE	RANGE	TYPE	RANGE	
E,P	ABX	12-14	D	19-21	MAG-D	7-16	125
							(123.5)

The radiative widths of the $E1$ transition through the ground isobaric analog states of ^{207}Tl and ^{209}Pb in ^{207}Pb and ^{209}Bi, respectively, were determined from the cross section of the $(e,e'p)$ reaction. The results are 98 and 140 eV, respectively, after the correction for the interference from the continuous part of the reaction. They correspond to an effective charge of 0.56 and 21, respectively. The $E1$ matrix elements were determined and used for the estimation of β matrix elements $|i\xi``\int\vec{r}"|$. The result is 0.055 in natural units ($\hbar = c = m_e = 1$) for the β-decay $^{207}\mathrm{Tl}(3s_{1/2}{}^{-1}) \rightarrow {}^{207}\mathrm{Pb}(3p_{1/2}{}^{-1})$. In the case of $^{209}\mathrm{Pb}(2g_{9/2}) \rightarrow {}^{209}\mathrm{Bi}(1h_{9/2})$, the result is 0.043, which is much larger than the theoretical estimate. For the $E1$ isobaric analog states of the first excited state of ^{209}Pb in ^{209}Bi, the radiative width and the effective charge were also determined to be 170 eV and 0.46, respectively.

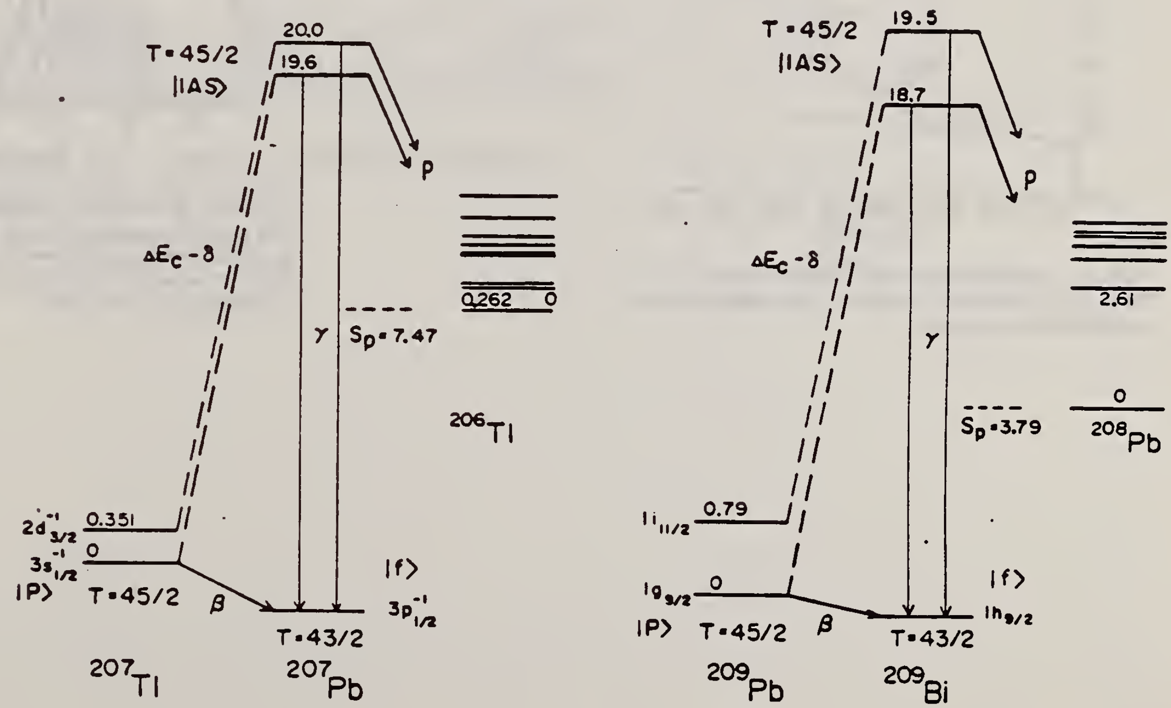

FIG. 1. The level diagram for the relations of $E1$ IAS and β decay. The energy levels are indicated in units of MeV. The single-particle configurations of the relevant states are indicated.

[over]

TABLE I. Radiative widths of $E1$ IAS in ^{207}Pb and ^{209}Bi. The errors include statistical uncertainties only.

Nucleus	Ground state	IAS	E_x (MeV)	Γ_γ^R (eV)	Γ_γ^{IAS} (eV)	$2(T+1)\Gamma_\gamma^{IAS}$ (keV)	$2(T+1)\frac{\Gamma_\gamma^{IAS}}{\Gamma_W}$	$2(T+1)\frac{\Gamma_\gamma^{IAS}}{\Gamma_{sp}}$
^{207}Pb	$\frac{1}{2}^-(3p_{1/2}^{-1})$	$\frac{1}{2}^+(3s_{1/2}^{-1})$	19.6	160 ± 50	98 ± 30	4.4 ± 1.3	0.25 ± 0.08	0.32 ± 0.09
^{209}Bi	$\frac{9}{2}^-(1h_{9/2})$	$\frac{9}{2}^+(2g_{9/2})$	18.7	180 ± 20	140 ± 20	6.3 ± 0.8	0.40 ± 0.05	430 ± 55
^{209}Bi	$\frac{9}{2}^-(1h_{9/2})$	$\frac{11}{2}^+(1i_{11/2})$	19.5	220 ± 30	170 ± 20	7.6 ± 1.0	0.43 ± 0.06	0.21 ± 0.03

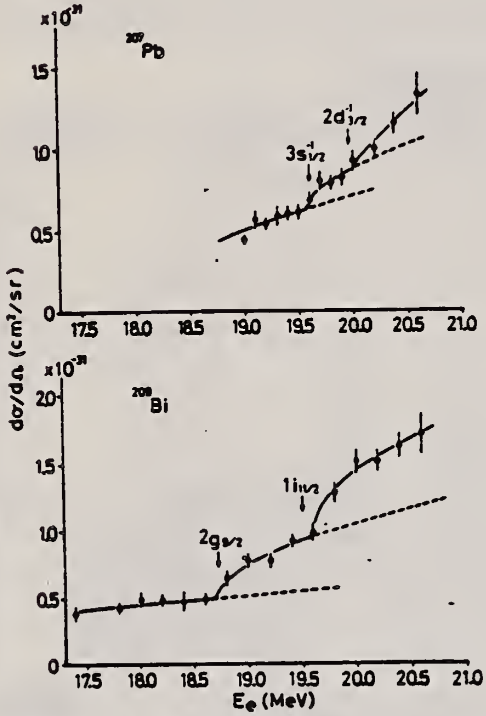

FIG. 3. Cross sections of the ^{207}Pb$(e,e'p)$ and ^{209}Bi$(e,e'p)$ reactions at $\theta = 125.3°$. The positions of the IAS are shown by arrows.

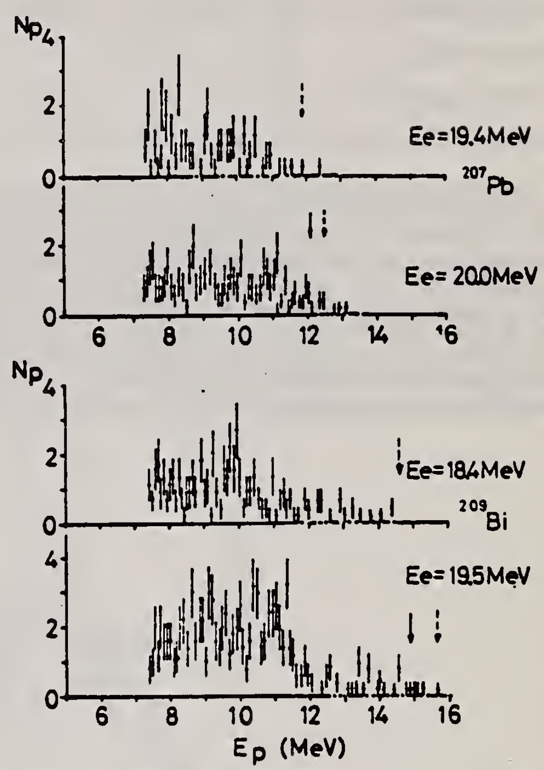

FIG. 2. Examples of the proton energy distributions. The positions expected for the maximum end-point energy of the protons are shown by the dashed vertical arrows. The solid vertical arrows indicate the position of p_0 through the ground IAS.

REF.	ELEM. SYM.	A	Z
K. Shoda, M. Sugawara, T. Saito, H. Miyase, A. Suzuki, S. Oikawa, and J. Uegaki PICNS-72, 321 Sendai	Pb	207	82
METHOD	REF. NO.		
	72 Sh 10		hvm

REACTION	RESULT	EXCITATION ENERGY	SOURCE TYPE	SOURCE RANGE	DETECTOR TYPE	DETECTOR RANGE	ANGLE
E,P	ABI	19	C	17- 21	MAG-D		UKN
		(19.5)					

I A STATES

Table 1. Examples of radiative width of IAR obtained from (e,e'p) experiment in lead region. The result from $^{208}Pb(p,\gamma_0)$ are also shown with parenthesis. (Ref. (5))

Nucleus	Ground State	IAS	E_x (MeV)	Γ_γ^A (eV)	$2(T+1)\frac{\Gamma_\gamma^A}{\Gamma_W}$	$2(T+1)\frac{\Gamma_\gamma^A}{\Gamma_{sp}}$
^{207}Pb	$3p^{-1}_{1/2}$	$3s^{-1}_{1/2}$	19.6	98±30	0.25±0.08	0.32±0.09
^{209}Bi	$1h_{9/2}$	$2g_{9/2}$	18.7	140±20 (<10)	0.40±0.05	430±55 ($\sim$0.33)
^{209}Bi	$1h_{9/2}$	$1i_{11/2}$	19.5	170±20 ($\sim$190)	0.43±0.06	0.21±0.03 (0.20)

5
K.A. Snover, J.F. Amann, W. Hering, P. Paul, Phys. Letters 37B, 29 (1971).

REF.	C. P. Swann Nucl. Phys. A201, 534 (1973)	ELEM. SYM.	A	Z
		Pb	207	82

METHOD	REF. NO.	
	73 Sw 4	egf

REACTION	RESULT	EXCITATION ENERGY	SOURCE TYPE	SOURCE RANGE	DETECTOR TYPE	DETECTOR RANGE	ANGLE
G,G	LFT	7	D	7	SCD-D		UKN

7 = 7.19,7.21

TABLE I

Summary of observed levels in ^{208}Pb, ^{207}Pb and ^{209}Bi and some of their properties

Nucleus	E_γ (keV)	Spin	Γ_0/Γ	$g\Gamma_0^2/\Gamma$ (eV)	Γ_0 (eV)			s.p. estimate (W.u.)	
					present	ref. [3]	ref. [2]	E1	M1
^{208}Pb	7071 ± 2	1	1		31 ± 3	15	30 ± 13	0.036	4.4
	7091 ± 2	1	1		17 ± 2	15		0.019	2.3
^{207}Pb	7186 ± 5	$\frac{1}{2}$, $\frac{3}{2}$		15 ± 4					
	7206 ± 5	$\frac{1}{2}$, $\frac{3}{2}$		25 ± 5					
^{209}Bi	7179 ± 5	$\frac{7}{2}$, $\frac{9}{2}$, $\frac{11}{2}$		24 ± 5					
	7202 ± 5	$\frac{7}{2}$, $\frac{9}{2}$, $\frac{11}{2}$		30 ± 5					

Weisskopf units given are based on our data.

REF.	C. P. Swann PICNS-73, Vol.I, p.317 Asilomar	ELEM. SYM.	A	Z
		Pb	207	82
METHOD		REF. NO.	73 Sw 13	hmg

REACTION	RESULT	EXCITATION ENERGY	SOURCE TYPE	SOURCE RANGE	DETECTOR TYPE	DETECTOR RANGE	ANGLE
G,G	LFT	3- 5	C	5	SCD-D		DST

J-PI, 7 LEVELS

Table: Properties of States Observed in $^{206,207,208}Pb$ and ^{209}Bi

Nuclei	E_γ (keV)	J^π	Γ_0/Γ	$g\Gamma_0^2/\Gamma$ (eV)	Γ_0 (eV)	G(EL)	G(M1)
^{206}Pb	3742	1	1		0.13(2)	0.001	0.12
	4114	2^+	1		0.30(6)	5	
	4326	1	1		0.90(9)	0.004	0.56
	4602	1	1		0.23(3)	0.001	0.12
^{207}Pb	3300	$1/2^+$ a)			0.039(6)		
	3928	$(3/2^-)$	1	0.68(7)			
	4104	$3/2^-$	1		0.55(6)	8	
	4140	$5/2^-$	1		0.46(5)	6	
	4627	$1/2^+$ b)	1		0.64(7)	0.003	
	4872	1/2,3/2	1	3.6(5)		~0.01	~1.2
	4982	1/2,3/2	1	4.0(5)		~0.01	~1.2
^{208}Pb	4087	2^+	1		0.49(5)	7	
	4843	1	1		5.1(5)	0.02	2.3
^{209}Bi	2826	$5/2^-$	(.63) c)		0.09(1)		
	3977	5/2--13/2		0.82(8)			
	4085	$5/2^-$--$13/2^-$		0.28(3)		~5	
	4144	"		0.07(2)		~1	
	4155	"		0.21(4)		~3	
	4176	"		0.21(4)		~3	
	4206	"		0.25(3)		~4	
	4747	7/2--11/2		2.9(5)		~0.013	~1.4
	4784	"		2.7(5)		~0.012	~1.3
	4822	"		1.4(3)		~0.005	~0.7

a) see ref. 3 b) see ref. 4 c) see ref. 5

3) S.M. Smith, P.G. Roos, C. Moazed and A.M. Bernstein, Nucl. Phys. A173, 32 (1971).
4) R.A. Mayer. B.L. Cohen and R.C. Diehl, Phys. Rev. C2, 1898 (1970).
5) R.A. Broglia, J.S. Lilley, R. Perazzo and W.R. Phillips, Phys. Rev. C1, 1500 (1970).

FORM NBS-418 (REV. 7-14-64) USCOMM-NBS-DC

REF.

L.R. Medsker and H.E. Jackson
Phys. Rev. C9, 709 (1974)

ELEM. SYM.	A	Z
Pb	207	82

METHOD

REF. NO.	
74 Me 3	hmg

REACTION	RESULT	EXCITATION ENERGY	SOURCE TYPE	SOURCE RANGE	DETECTOR TYPE	DETECTOR RANGE	ANGLE
G,N	SPC	6- 9	C	7, 9	TOF-D		DST

J-PI G-WIDTH

TABLE IV. Neutron resonance energies and parameters for states in ^{207}Pb with $J^\pi = \frac{3}{2}^\pm$. The $E_n(n,\gamma)$ in column 2 were calculated from the measured $E_n(\gamma,n)$.

^{207}Pb(γ,n) $E_n(\gamma,n)$ Obs. (keV)	^{206}Pb(n,γ) $E_n(n,\gamma)$ Calc. (keV)	E_n (±0.2%) (keV)	^{207}Pb(γ,n) R (90°/135°)	$g\frac{\Gamma_{\gamma_0}\Gamma_n}{\Gamma}$ (eV)
82.8	83.9		1.30 ± 0.35	0.11
175	177		1.37 ± 0.29	0.28
233	235		1.36 ± 0.09	1.4
260	263		1.31 ± 0.19	0.8
267	271		(2.03)	0.8
289	293	291.2	1.38 ± 0.18	0.7
305	309	305.6	1.43 ± 0.22	0.5
338	342		1.49 ± 0.11	0.8
355	359	358.8	1.39 ± 0.18	1.4
395	400	402.2	1.30 ± 0.24	1.0
448	453	455	1.53 ± 0.17	2.1
461	466	469	1.30 ± 0.13	3.2
467	472	474	1.48 ± 0.26	1.1
485	490	493	1.48 ± 0.26	1.1
540	546	549	1.36 ± 0.19	1.1
586	593		(2.21)	0.9
592	599		1.53 ± 0.11	2.6
603	610	612	1.65 ± 0.10	6.5
646	654		1.36 ± 0.07	5.9
657	664		1.68 ± 0.20	1.0
663	670		1.37 ± 0.29	0.9
670	677		1.54 ± 0.11	3.9
679	687		1.65 ± 0.36	0.8
711	719		1.39 ± 0.13	2.2
726	734		1.44 ± 0.14	0.5
741	749		1.40 ± 0.11	3.3
755	763		1.40 ± 0.09	4.0
790	798		1.55 ± 0.19	1.2
899	909		1.40 ± 0.20	1.1
912	922		1.45 ± 0.21	1.1
928	938		1.40 ± 0.19	1.4
965	976		1.30 ± 0.17	1.7
982	993		1.46 ± 0.17	1.8
1047	1059		1.50 ± 0.24	2.1
1107	1119		1.71 ± 0.23	2.0
1122	1134		1.58 ± 0.16	3.5
1194	1207		1.38 ± 0.16	3.2
1260	1274		1.65 ± 0.18	4.6
1293	1307		1.36 ± 0.24	1.9
1343	1358		1.30 ± 0.21	3.0
N = 40		Total		77.3

TABLE II. Energies and parameters for s-wave resonances in the ^{206}Pb(n,γ) and ^{207}Pb(γ,n) reactions. The $E_n(n,\gamma)$ in column 4 were calculated from the measured $E_n(\gamma,n)$.

E_n [a] (±0.2%) (keV)	^{206}Pb(n,γ) E_n [b] (keV)	Γ_n^0 (eV)	$E_n(n,\gamma)$ Calc. (keV)	^{207}Pb(γ,n) $E_n(\gamma,n)$ Obs. (keV)	R (90°/135°)	$\frac{\Gamma_{\gamma_0}\Gamma_n}{\Gamma}$ (eV)
	66.0	0.97	68	85.	0.91 ± 0.10	1.8
	206.0	2.64	204	202	0.94 ± 0.11	0.5
	218.5	1.82	219.1	216.4	0.95 ± 0.13	0.4
	255.5	2.97	255	252	0.83 ± 0.13	0.17
(346)	348.0	13.60	345	341	1.04 ± 0.16	1.6
352.8	353.5	6.73	351	347	1.06 ± 0.18	5.6
378.5	381.3	4.70	···	···	···	···
395.2	394.8	7.64	···	···	···	···
(418)	420.0	7.72	420	415	1.06 ± 0.14	2.5
493.0	493.3	12.53	(495)	(490)		(0.4)
549.0	548.7	7.29	(548)	(541)		(0.7)
(617)	618.5	5.09				
(658)	661.5	0.92	···	···	···	···
	681.2	1.21	···	···	···	···
	725.0	2.35	728	718	1.10 ± 0.17	5.9
			N = 10	Total		19.6

[a] Reference 9.
[b] Reference 5.

TABLE VI. Integrated strengths of excitations to states with spin and parity J^π. N is the number of states observed. The first three entries are for $E_n \leq 717$ keV.

J^π	Multipolarity	N	$\sum g\frac{\Gamma_{\gamma_0}\Gamma_n}{\Gamma}$ (eV)
$\frac{1}{2}^+$	$E1$	10	9.8
$\frac{1}{2}^-, \frac{3}{2}^-$	$M1, M1+E2$	45	89.5
$\frac{3}{2}^\pm$	$E1, M1$	40	77.3
$E_n > 717$ keV $\frac{1}{2}^\pm, \frac{3}{2}^\pm$	$E1, M1, M1+E2$	8	35.1
$E_n > 717$ keV $\frac{3}{2}^-$	$M1+E2$	4	17.2

(over)

TABLE III. Energies and resonance parameters for states below 718 keV with $J^{\pi}=\frac{1}{2}^{-}$ and $\frac{3}{2}^{-}$. The $E_n(n,\gamma)$ in column 2 were calculated from the measured $E_n(\gamma,n)$.

^{207}Pb(γ,n) $E_n(\gamma,n)$ Obs. (keV)	^{206}Pb(n,γ) $E_n(n,\gamma)$ Calc. (keV)	E_n [a] (±0.2%) (keV)	^{207}Pb(γ,n) R(90°/135°)	$g\frac{\Gamma_{\gamma_0}\Gamma_n}{\Gamma}$ (eV)
16.2	16.5		0.87±0.12	0.22
24.8	25.2		1.09±0.30	0.15
92	92		0.84±0.14	0.8
114	115		1.18±0.27	0.33
123	125		1.14±0.07	5.4
139	141		1.23±0.10	2.1
145	147		0.91±0.08	2.5
168	170		1.31±0.25	0.31
172	174		0.89±0.16	0.3
197	199		0.99±0.06	4.0
215	218		0.89±0.09	0.3
226	229		1.12±0.10	0.4
240	243		0.98±0.08	0.7
256	259		1.20±0.15	0.4
263	266	267.1	1.28±0.20	0.5
274	277	277.6	1.09±0.10	4.0
278	281		1.28±0.30	0.7
297	301		1.23±0.11	1.5
311	315	315.7	1.22±0.14	0.6
333	337		1.22±0.12	0.9
344	348	350.0	1.05±0.24	1.0
351	355		1.09±0.10	1.5
367	371		1.09±0.21	0.8
383	387		1.11±0.16	1.4
403	408	(408)	1.00±0.12	1.5
409	413		0.91±0.28	0.8
412	417	418	1.17±0.10	2.8
422	426	429	1.25±0.08	5.8
429	434	436	1.13±0.12	2.1
437	442	440	1.14±0.18	1.5
451	456		1.12±0.14	1.2
516	522		0.97±0.11	2.1
526	532	528	0.97±0.12	1.7
544	550		0.86±0.19	0.5
560	566		1.04±0.13	1.3
567	573	576	0.96±0.05	7.7
575	581		1.15±0.17	1.3
600	807		0.93±0.09	2.1
616	623	619	1.20±0.09	2.5
622	629	631	1.25±0.07	5.9
630	637		1.10±0.05	10.7
642	649		1.13±0.14	1.4
686	693		1.28±0.15	0.8
698	706		0.97±0.10	2.8
704	712		1.28±0.12	2.2
$N=45$		Total		89.5

[a] Reference 9.

TABLE V. Neutron resonance energies and parameters for states in ^{207}Pb with $J^{\pi}=\frac{1}{2}^{\pm}$ and $\frac{3}{2}^{-}$ and with $E_n>717$ keV. The $E_n(n,\gamma)$ were calculated from the measured $E_n(\gamma,n)$.

$E_n(\gamma,n)$ Obs. (keV)	$E_n(n,\gamma)$ Calc. (keV)	R(90°/135°)	$g\frac{\Gamma_{\gamma_0}\Gamma_n}{\Gamma}$ (eV)
764	772	1.05±0.05	6.8
778	787	1.13±0.07	4.2
801	810	1.19±0.09	2.8
845	854	1.14±0.12	8.0
869	879	1.21±0.06	3.0
881	891	1.04±0.10	4.5
940	951	1.09±0.10	2.7
1015	1027	0.88±0.09	2.8
1030	1041	0.95±0.09	3.8
1089	1080	1.26±0.08	7.2
1095	1107	0.75±0.07	3.9
1165	1177	1.16±0.13	2.6
$N=12$	Total		52.3

TABLE VII. Integrated strengths $\sum\Gamma_{\gamma_0}$ and reduced widths $\bar{k}$ for $M1$ transitions in ^{208}Pb and ^{207}Pb.

Isotope	$\sum\Gamma_{\gamma_0}(M1)$ Experiment	Calculated	$\bar{k}_{M1}$ Experiment	Estimate [a]
^{208}Pb	>51 eV [b]	100 eV	>0.12	0.02
^{207}Pb	>125 eV	200 eV	>0.25	0.02

[a] See Ref. 15.
[b] See Ref. 2.

2
C,D. Bowman, R.J. Baglan, B.L. Berman, and T.W. Phillips, Phys. Rev. Lett. 25, 1302 (1970).
5
J.A. Farrell, G.C. Kyker, Jr., E.G. Bilpuch, and H.W. Newson, Phys. Lett. 17, 286 (1965).
9
B.J. Allen, R.L. Macklin, C.Y. Fu, and R.R. Winters, Phys. Rev. C7, 2598 (1973).
15
L.M. Bollinger, in International Symposium on Nuclear Structure, Dubna, 1968 (International Atomic Energy Agency, Vienna, Austria, 1969), p.317.

REF.	C. P. Swann J. Franklin Institute 298, 321 (1974)	ELEM. SYM.	A	Z
		Pb	207	82

METHOD	REF. NO.	
	74 Sw 11	egf

REACTION	RESULT	EXCITATION ENERGY	SOURCE		DETECTOR		ANGLE
			TYPE	RANGE	TYPE	RANGE	
G,G	LFT	3- 5	C	4- 5	SCD-D		DST

7 LEVELS 3300-4982 KEV

TABLE II

Properties of states observed in ^{206,207,208}Pb and ^{209}Bi; G(EL) and G(M1) are the reduced transition probabilities in Weisskopf units

Nuclei	E_γ (keV)	J^π	Γ_0/Γ	$g\Gamma_0^2/\Gamma$ (eV)	Γ_0 (eV)	G(EL)	G(M1)
^{206}Pb	3744	1^-	1		0·13 (2)	0·001	
	4114	2^+	1		0·30 (6)	5	
	4330	1^+	1		0·90 (9)		0·56
	4606	1	1		0·23 (3)	0·001	0·12
	4974	1	1	0·8 (2)		0·003	0·32
	5038	1	1	2·3 (5)		0·007	0·90
^{207}Pb	3300	$1/2^{+*}$			0·039 (6)		
	3928	$3/2^-$	1		0·34 (4)		
	4104	$3/2^-$	1		0·55 (6)	8	
	4140	$5/2^-$	1		0·46 (5)	6	
	4627	$1/2^{+}$†	1		0·64 (7)	0·003	
	4872	$1/2^-, 3/2^-$	1	3·6 (5)			~1·2
	4982	$1/2^-, 3/2^-$	1	4·0 (5)			~1·2
^{208}Pb	4087	2^+	1		0·49 (5)	7	
	4843	1^+	1		5·1 (8)		2·3
^{209}Bi	2826	$5/2^-$	(0·63)‡		0·09 (1)		
	3977	5/2–13/2		0·82 (8)			
	4085	$5/2^-$–$13/2^-$		0·28 (3)		~5	
	4144	$5/2^-$–$13/2^-$		0·07 (2)		~1	
	4156	$5/2^-$–$13/2^-$		0·21 (4)		~3	
	4176	$5/2^-$–$13/2^-$		0·21 (4)		~3	
	4206	$5/2^-$–$13/2^-$		0·25 (3)		~4	
	4747	$7/2^-$–$11/2^-$		2·9 (5)			~1·4
	4785	$7/2^-$–$11/2^-$		2·7 (5)			~1·3
	4822	$7/2^-$–$11/2^-$		1·4 (3)			~0·7

* See Ref. (11). † See Ref. (12). ‡ See Ref. (7).

[7] C.P. Swann, Phys. Rev. Letts. 32, 1449 (1974).

[11] S.M. Smith et al., Nucl. Phys. A173, 32 (1971).

[12] R.A. Mayer et al., Phys. Rev. C2, 1898 (1970).

REF.	J. E. McFee, W. V. Prestwich, T. J. Kennett Phys. Rev. C13, 1864 (1976)	ELEM. SYM.	A	Z
		Pb	207	82
METHOD		REF. NO.	76 Mc 3	hmg

REACTION	RESULT	EXCITATION ENERGY	SOURCE TYPE	SOURCE RANGE	DETECTOR TYPE	DETECTOR RANGE	ANGLE
G,N	ABX	8- 9	D	8- 9	ION-D		90

8999,8533,8120 KEV

The photoneutron spectrum of natural lead has been observed for photoexcitation energies of 8999, 8533, and 8120 keV using a high-resolution ^{3}He ionization chamber. The photons were obtained from the (n,γ) reaction on a nickel target positioned in a nuclear reactor. The Q values for the three reactions ^{208}Pb$(\gamma,n)^{207}$Pb, ^{207}Pb$(\gamma,n)^{206}$Pb, and ^{206}Pb$(\gamma,n)^{205}$Pb have been determined and are, respectively, 7369 ± 5, 6743 ± 3, and 8087 ± 3 keV. Neutron groups corresponding to different final states following excitation by one of the three photon components have been observed and their partial cross sections are reported. The distribution and some systematics of the neutron reduced widths have been studied. The absolute cross sections of the reaction ^{208}Pb$(\gamma,n)^{207}$Pb at 8999 and 8533 keV photon energies have been found to be 6.8 ± 2.9 and 5.0 ± 2.1 mb, respectively.

TABLE V. Reduced widths contrasted with spectroscopic factors.

Residual nucleus	E_x (keV)	J^π	l_n[a] $E1$	l_n[a] $E2$	Neutron Reduced Widths $E_\gamma=8999$ keV	$E_\gamma=8533$ keV (±27%)	$E_\gamma=8120$ keV	Spectroscopic factors $C^2S/(2J+1)$ (p,d)	(d,t)
^{207}Pb								b	b
	0	$\frac{1}{2}^-$	0	1	163	128		0.72	0.71
	570	$\frac{5}{2}^-$	2	1	210	309		0.90[c]	0.97[c]
	898	$\frac{3}{2}^-$	0	1	191	327		1.27	1.33
								d	
^{206}Pb	0	0^+	0	1	26	107	321	0.30	···
	803	2^+	0	1	959	308		0.11	···
	1165	0^+	0	1	294	118		0.19	···
	1460	2^+	0	1	152	e		0.38	···
	1634	4^+	2	1	474	e		0.02[c]	···
	1704	1^+	0	1	285	0		0.38	···
	1784	2^+	0	1	178	e		0.07	···
^{205}Pb	263	$\frac{3}{2}^-$	0	1	190	e		1.02[f]	1.56[g]

[a] Minimum possible neutron angular momentum for a given photon multipolarity.
[b] Reference 18.
[c] Spectroscopic factor for $l_n=3$. All others are $l_n=1$.
[d] W. A. Lanford and G. M. Crawley, Phys. Rev. C 9, 646 (1974).
[e] May exist but cannot be resolved from neighboring components.
[f] K. Yagi, T. Ishimatsu, Y. Ishizaki, and Y. Saji, Nucl. Phys. A110, 41 (1968).
[g] R. Tickle and J. Bardwick, Phys. Rev. 178, 2006 (1969).

TABLE VI. Absolute photoneutron cross sections.

Target isotope	Photon energy (keV)	Cross section[a] (mb)	Lower bound[a] (mb)	Upper bound[a] (mb)
208	8999	6.8	···	···
	8533	5.0	···	···
207	8999	···	29.9	40.1
	8533	···	8.0	26.8
	8120	···	5.6	···
206	8999	···	2.3	14.0
	8533	···	0	15.1

[a] 10% relative error; 45% absolute error.

(over)

TABLE IV. Low-lying states in ^{207}Pb, ^{206}Pb, and ^{205}Pb.

Residual isotope	E_γ (keV)	E_x (keV)	J^π	Observed neutron energy (lab) (keV ± 5)	Relative[a] intensity (± 10%)	$\sigma_{\gamma n}$[b] (mb)
207	8999	0[c]	$\frac{1}{2}^-$	1515	100	3.1
		570	$\frac{5}{2}^-$	1054	42	1.3
		898	$\frac{3}{2}^-$	727	79	2.4
	8533	0	$\frac{1}{2}^-$	1159	66	2.1
		570	$\frac{5}{2}^-$	601	12	0.4
		898	$\frac{3}{2}^-$	263	81	2.5
206	8999	0[d]	0^+	2256[e]	19	0.6
		803	2^+	1446	556	17.2
		1165(±10)	0^+	1087	148	4.6
		1460	2^+	789	65	2.0
		1684	4^+	573	15	0.5
		1704(±1)	1^+	551	102	3.2
		1784(±2)	2^+	473	59	1.8
	8533	0	0^+	1780	69	2.1
		803	2^+	982	147	4.5
		1165(±10)	0^+	619	45	1.4
		1704(±1)	1^+	...	0	0.0
	8120	0	0^+	1370[e]	181	5.6
205	8999	263[f]	$\frac{3}{2}^-$	643	74	2.3
			Unresolved groups			
A 206	8999	1340	3^+	908	76	
205	8999	0	$\frac{5}{2}^-$			
205	8999	2	$\frac{1}{2}^-$			
B 206	8533	1340	3^+	446	65	
205	8533	0	$\frac{5}{2}^-$			
205	8533	2	$\frac{1}{2}^-$			
C 205	8999	576	$\frac{3}{2}^-$	330	44	
206	8533	1460	2^+			
D 205	8533	263	$\frac{3}{2}^-$	181	37	
207	8120	570	$\frac{5}{2}^-$			
206	7724	803	2^+			
207	7555	0	$\frac{1}{2}^-$			
E 206	8999	2150(±1)	2^+	110	61	
205	8999	803	$(\frac{1}{2}^-, \frac{3}{2}^-)$			
			Unassigned group			
...	...	...	...	597	5	

[a] Arbitrary normalization corrected for isotopic abundance and photon yield. Unresolved group intensities have no isotopic abundance or photon yield correction and are merely quoted relative to the group corresponding to population of the ^{207}Pb ground state following 8999-keV photoexcitation.

[b] Relative error 10%, absolute error 45%.

[c] Reference 18.

[d] Reference 19.

[e] Centroid accurate to only 15 keV.

[f] Reference 20.

[18] M.R. Schmorak et al., Nucl. Data B5, 207 (1971).

[19] K. K. Seth, Nucl. Data B7, 161 (1972).

[20] J. H. Hamilton et al., Phys. Rev. C6, 1265 (1972).

REF.	ELEM. SYM.	A	Z
D. Turck, H.-G. Clerc, H. Trager Phys. Lett. 63B, 283 (1976)	Pb	207	82

METHOD	REF. NO.	
	76 Tu 2	egf

REACTION	RESULT	EXCITATION ENERGY	SOURCE TYPE	SOURCE RANGE	DETECTOR TYPE	DETECTOR RANGE	ANGLE
E,F	ABX	27- 50	D	38- 50	TRK-I		4PI

FISSION BARRIER

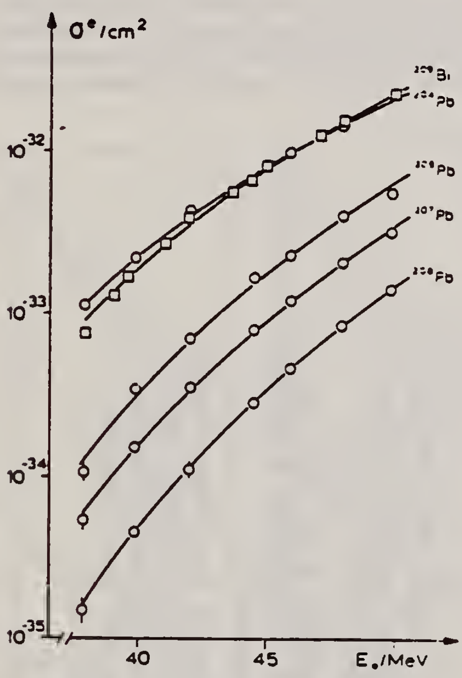

Fig. 1. Cross section σ^e for electron induced fission in ^{204,206,207,208}Pb and ^{209}Bi as a function of the incident electron energy E_0.

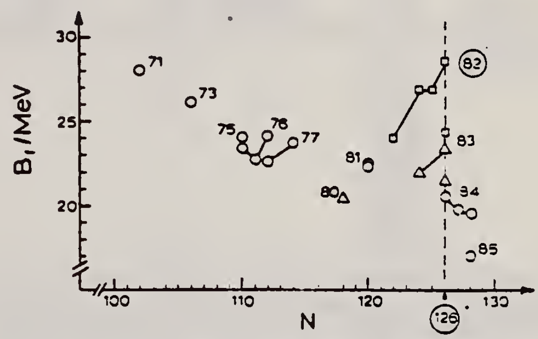

Fig. 2. Summary of fission barrier heights obtained from fits to experimental fission cross sections for nuclei with $Z < 85$. o: α-induced fission [12]. For ^{201}Tl, the value of 22.5±1.5 of ref. [3] is also included; △: proton-induced fission [12]; □: electron induced fission (present work). Values for different isotopes of the same element are connected by straight lines. The nuclear charge numbers are indicated. The erors are ± 1.0 MeV for proton and α-induced fission [12] and ± 1.5 MeV for electron induced fission.

1 U. Mosel, Phys. Rev. C6 (1972) 971.
3 D.S. Burnett et al., Phys. Rev. B134 (1964) 952.
12 L.G. Moretto et al., Phys. Lett. B38 (1972) 471.

Table 2
Fission barriers B_f as determined from electron induced fission. In the last column theoretical fission barriers according to ref. [1] with surface independent pairing strength are listed.

isotope	B_f (MeV)	$B_f^{theor.}$ (MeV)
^{204}Pb	24.0±1.5	24.0
^{206}Pb	26.8±1.5	26.2
^{207}Pb	26.9±1.5	
^{208}Pb	28.6±1.5	28.1
^{209}Pb	24.3±1.5	

REF.	ELEM. SYM.	A	Z
D.F. Coope, L.E. Cannell, and M.K. Brussel Phys. Rev. C 15, 1977 (1977)	Pb	207	82

METHOD	REF. NO.
	77 Co 3

REACTION	RESULT	EXCITATION ENERGY	SOURCE TYPE	SOURCE RANGE	DETECTOR TYPE	DETECTOR RANGE	ANGLE
G,G	LFT	4 - 7	C	6,10	SCD-D		125
		(4.847-6.753)		(6.6,9.7)			

Using bremsstrahlung produced with 6.6 and 9.7 MeV beams, nuclear resonance fluorescence measurements were made on targets of ^{206,207,208}Pb and ^{209}Bi. Ground state transition widths for previously unknown energy levels with widths ≥ 1 eV were obtained. An interpretation of several of these levels in terms of a particle-core weak coupling model is suggested.

9 LEVELS 4.8-6.7 MeV

TABLE IV. Observed levels and their strengths. *The value for Γ_0 assumes $g\Gamma_0/\Gamma = 3$ for ^{206}Pb and ^{208}Pb, and $g\Gamma_0/\Gamma = 1$ for ^{207}Pb and ^{209}Bi.* Values in parentheses have uncertainties in excess of 50%. Statistical uncertainties are given for well-defined peaks. Total uncertainties include uncertainties in flux calibration. Energy values are believed to be accurate to ±3 keV for the starred (★) ^{208}Pb levels and to ±5 keV for the other levels.

Energy (MeV)	Nucleus	Γ_0 (eV)	Uncertainty (%) Statistical	Total	Other measurements $g\Gamma_0^2/\Gamma$ (eV)	Γ_0 (eV)	References
6.54	(Pb) 206	7.4		40			
6.73		5.5		40			
5.902		4.4	15	40			
5.854		(3.0)					
5.795		(1.0)					
5.639		(0.5)					
5.615		(1.0)					
5.577		(0.5)					
5.039		1.6	15	40			
4.974		0.8		40			
6.753	(Pb) 207	(<10)					
5.716		(3)					
5.600		(8)					
5.490		(12)					
5.223		(8)					
5.209		(8)					
4.980		(7)			4.0 $\Gamma_0/\Gamma = 1$		12
4.875 }		(13)			3.6 $\Gamma_0/\Gamma = 1$		12
4.847 }							12
7.332★	(Pb) 208	38	10	35		35,41	11,10
7.083★		14	10	35		15,17±2	11,5
7.063★		29	10	35		15,31±3	11,5
6.721★		15	20	40		15,14	11,10
6.357		(0.5)					
6.305		(1.0)					
6.262		4.1		45			
5.513★		28	2	35		15	11
5.293★		8.6	5	35		5	11
4.842★		6.3	5	35	$J^\pi = 1^+$	5.1±0.8	12
4.085★		0.51		40	$J^\pi = 2^+$	0.5±0.1	12
5.549	(Bi) 209	6.6		40			
5.522 }							
5.509 }		17	5	35			
5.498 }							
5.422		8.3		45			
5.293		12	15	40			
4.845 }		•			1.4		12
4.803 }		(10)			2.7		12
4.771 }					2.9		12
4.501		(3)					
4.228		(3)					

5 C.P. Swann, Nucl. Phys. A201, 534 (1973)

10 P. Axel, K. Min, N. Stein, and D.C. Sutton, Phys. Rev. Lett. 10, 299 (1963)

11 A.M. Khan and J.W. Knowles, Bull. Am. Phys. Soc. 12, 538 (1967); J.W. Knowles, A.M. Khan, and W.F. Mills (unpublished)

12 C.P. Swann, Proceedings of the International Conference on Photonuclear Reactions and Applications, (U.S. Atomic Energy Commission Office of Information Services, Oak Ridge, Tennessee, 1975), p.317

REF. C.N. Papanicolas, J. Heisenberg, J. Lichtenstadt, A.N. Courtemanche and J.S. McCarthy
Phys. Rev. Lett. 41, 537 (1978)

ELEM. SYM.	A	Z
Pb	207	82

METHOD

REF. NO. 78 Pa 1 rs

REACTION	RESULT	EXCITATION ENERGY	SOURCE TYPE	SOURCE RANGE	DETECTOR TYPE	DETECTOR RANGE	ANGLE
E,E/	FMF	1- 4	D	50-320	MAG-D		90

High-resolution inelastic electron-scattering cross sections from ^{207}Pb have been measured in the range of momentum transfer 0.37 fm$^{-1}\leq q \leq$2.30 fm^{-1}. Form factors have been extracted for low-lying neutron hole states and some one-particle, two-hole states. Models for the induced charge of the neutron are compared with the data.

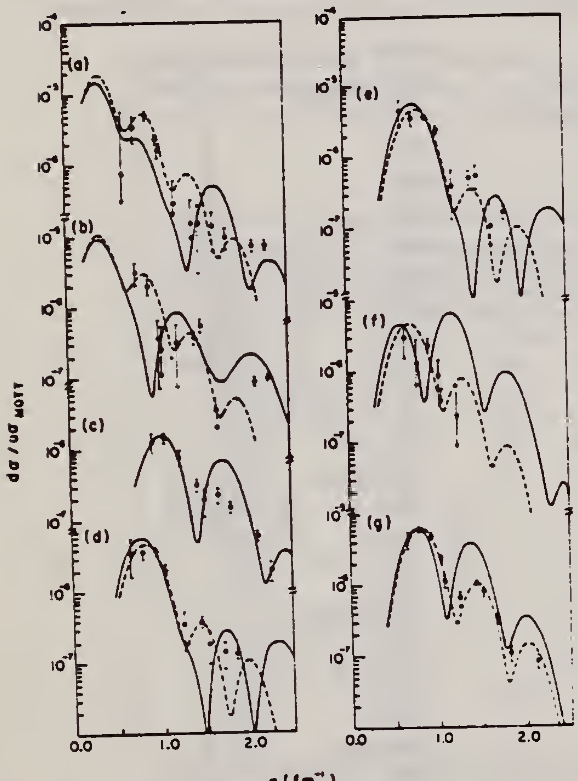

FIG. 3. Fits to the extracted form factors. The solid curves represent effective charge calculations while the dashed curves were obtained assuming that $\rho_{tr}{}^{L}(r)$ of the transition in question is identical to the closest collective state in ^{208}Pb but different in strength (as discussed in text). (a) 0.571 MeV, $3p_{1/2}{}^{-1}\to 2f_{5/2}{}^{-1}$; (b) 0.899 MeV, $3p_{1/2}{}^{-1}\to 3p_{3/2}{}^{-1}$; (c) 1.634 MeV, $3p_{1/2}{}^{-1}\to 1i_{13/2}{}^{-1}$; (d) 2.340 MeV, $3p_{1/2}{}^{-1}\to 2f_{7/2}{}^{-1}$; (e) 2.728 MeV, $3p_{1/2}\to 2g_{9/2}$; (f) 3.413 MeV, $3p_{1/2}{}^{-1}\to 1h_{9/2}{}^{-1}$; (g) 3.509 MeV, $3p_{1/2}\to 1i_{11/2}$. There is no dashed curve for (c) since no strong 7$^-$ state in ^{208}Pb was observed.

TABLE I. The extracted effective charges for the levels of ^{207}Pb under consideration are tabulated in the third column. The excitation energies of the collective ^{208}Pb states whose transition charge was scaled down to fit the ^{207}Pb data and the corresponding scaling factors are listed in the last two columns.

Excitation energy (MeV)	Single-particle description	e_{t}..	Excitation in ^{208}Pb (MeV)	Scaling factor ^{207}Pb
0.571	$3p_{1/2}{}^{-1}\to 2f_{5/2}{}^{-1}$	1.02^{a}	4.086	8.09×10^{-2}
0.899	$3p_{1/2}{}^{-1}\to 3p_{3/2}{}^{-1}$	0.70^{a}	4.086	4.58×10^{-2}
1.634	$3p_{1/2}{}^{-1}\to 1i_{13/2}$	1.19		
2.340	$3p_{1/2}{}^{-1}\to 2f_{7/2}{}^{-1}$	1.39	4.324	5.13×10^{-2}
2.728	$3p_{1/2}\to 2g_{9/2}$	1.21	3.198	1.18×10^{-1}
3.413	$3p_{1/2}{}^{-1}\to 1h_{9/2}{}^{-1}$	1.83	4.324	2.27×10^{-2}
3.509	$3p_{1/2}\to 1i_{11/2}$	1.81	3.709	2.60×10^{-1}

[a] Taken from Ref. 4.

[4] O. Hausser, F.C. Khanna, and D. Ward, Nucl. Phys. A194, 113 (1972).

REF. R.M. Laszewski and P. Axel
Phys. Rev. C 19, 342 (1979)

ELEM. SYM.	A	Z
Pb	207	82

METHOD

REF. NO.	
79 La 1	hg

REACTION	RESULT	EXCITATION ENERGY	SOURCE TYPE	SOURCE RANGE	DETECTOR TYPE	DETECTOR RANGE	ANGLE
G,G	ABX	4- 7	D	4-7	NAI-D		135
		(4.5-6.7)		4.5-6.8			

Average elastic photon scattering cross sections were measured for ^{209}Bi, ^{208}Pb, ^{207}Pb, ^{206}Pb, Tl and Hg at excitation energies between 4.5 MeV and the neutron emission threshold, with an energy resolution in the range between 50 and 150 keV. This resolution was sufficient to determine the strengths of most of the strong levels in this energy region for ^{208}Pb; there are concentrations of strength in a few levels near 5.5 and 7 MeV with the sum of $B(E1)\uparrow$ values equal to about 0.84 and 0.65 e^2 fm^2, respectively; each of these two groups of levels corresponds to only about 0.63% of the electric dipole sum rule. In the neighboring isotopes, approximately the same amount of strength is distributed among many more energy levels; although this strength is spread in energy more than it is in ^{208}Pb, it remains relatively localized.

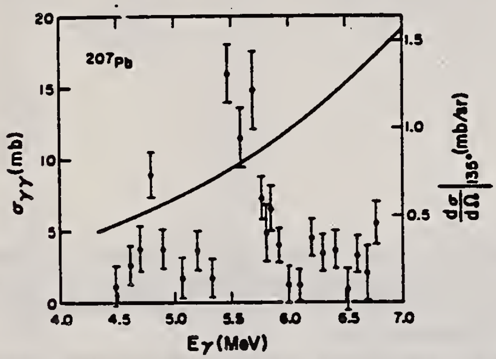

FIG. 5. ^{207}Pb (enriched to 85% 207 isotope): See caption of Fig. 4.

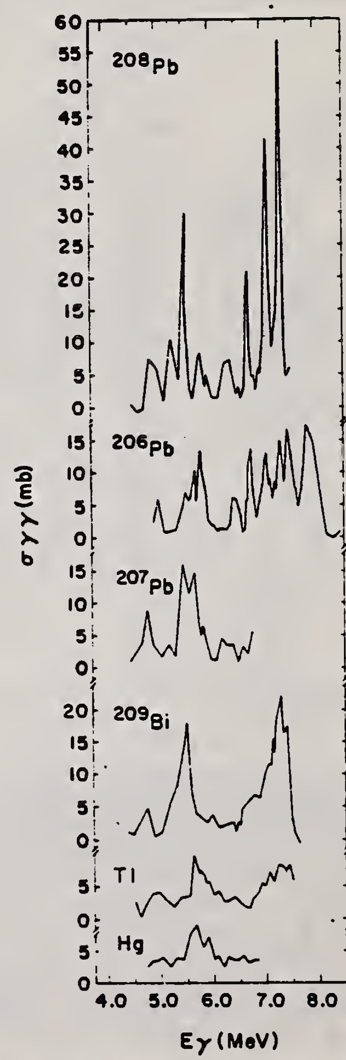

FIG. 12. Comparison of the measured cross sections of, respectively, from the top, ^{208}Pb, ^{206}Pb, ^{207}Pb, ^{209}Bi, Tl, and Hg.

TABLE VI. Transition strength comparison at 5.5 and 7 MeV.

Nucleus	5.0–6.0 MeV $\int\sigma_{\gamma\gamma}dE$(MeV mb)	5.0–6.0 MeV %^{208}Pb strength	6.5–7.5 MeV $\int\sigma_{\gamma\gamma}dE$(MeV mb)	6.5–7.5 MeV %^{208}Pb strength
Bi	10.4	68%	10.7	44%
^{208}Pb	15.2	100%	24.4	100%
^{207}Pb	12.6	83%	...	...
^{206}Pb	15.8	104%	20.2	83%
Tl	8.3	55%	7.8	32%
Hg	11.6	76%	...	...

REF. T. Chapuran, R. Vodhanel, M.K. Brussel
Phys. Rev. C22, 1420 (1980)

ELEM. SYM.	A	Z
Pb	207	82

METHOD

REF. NO.	
80 Ch 3	hg

REACTION	RESULT	EXCITATION ENERGY	SOURCE TYPE	SOURCE RANGE	DETECTOR TYPE	DETECTOR RANGE	ANGLE
G,G	SPC	4-8	C	7,8 (7,7.65)	SCD-D		127

Resonant photon scattering from ^{206,207,208}Pb and ^{209}Bi has been measured from 4 MeV to the neutron thresholds using enriched targets, Ge(Li) detectors and bremsstrahlung beams with end-point energies of 7.0, 7.5, 7.6, 8.0, 8.5, and 10.4 MeV. Energies and values of $g\Gamma_0{}^2/\Gamma$ were obtained for many levels not observed in previous photon experiments. Spins of levels in ^{206}Pb and ^{208}Pb were determined from the angular distributions, and ground-state branching ratios were obtained from self-absorption measurements for seven transitions in ^{208}Pb. The results are compared with earlier spectroscopic studies and with lower resolution average cross-section measurements. The spectra of ^{207}Pb and ^{209}Bi are discussed in terms of the excitations of the ^{208}Pb core.

[NUCLEAR REACTIONS ^{206,207,208}Pb, ^{209}Bi(γ,γ); enriched targets; resonance fluorescence with 7.0, 7.5, 7.6, 8.0, 8.5, and 10.4 MeV bremsstrahlung. Measured E_γ, I_γ at 90° and 127°, and self-absorption; deduced $g\Gamma_0^2/\Gamma$, Γ_0/Γ, J.]

TABLE VII. Comparison of measured level widths for ^{207}Pb. Values of $g\Gamma_0^2/\Gamma$ were extracted from the present experiment assuming dipole angular distributions. Uncertainties include statistical and calibration errors.

Energy[a] (MeV ± keV)	$g\Gamma_0^2/\Gamma$[a] (eV)	$g\Gamma_0^2/\Gamma$[b] (eV)	$g\Gamma_0^2/\Gamma$[c] (eV)
4.871 ± 2	7.1 ± 1.1	13[e,f]	3.6 ± 0.5
4.981 ± 2	6.1 ± 1.2	7[f]	4.0 ± 0.5
5.489 ± 2	11.4 ± 1.9	12[f]	
5.596 ± 2	9.0 ± 1.4	8[f]	
5.611 ± 2[d]	5.5 ± 0.9		
5.690 ± 2	3.0 ± 0.6		
5.714 ± 2	6.2 ± 1.2	3[f]	
5.734 ± 2	5.1 ± 1.1		
5.794 ± 4	2.4 ± 1.0		
6.179 ± 2[d]	3.3 ± 0.7		
6.542 ± 4	2.3 ± 0.6		
6.735 ± 4	2.7 ± 0.7		
6.749 ± 4	7.2 ± 1.4	<10[f]	
6.818 ± 4	5.1 ± 0.9		
7.306 ± 4	3.0 ± 0.8		

[a] This work.
[b] Reference 10.
[c] Reference 36.
[d] Possible inelastic transitions; see text for discussion.
[e] Contains contribution from an additional level; see text for discussion.
[f] Uncertainties "in excess of 50%."

(OVER)

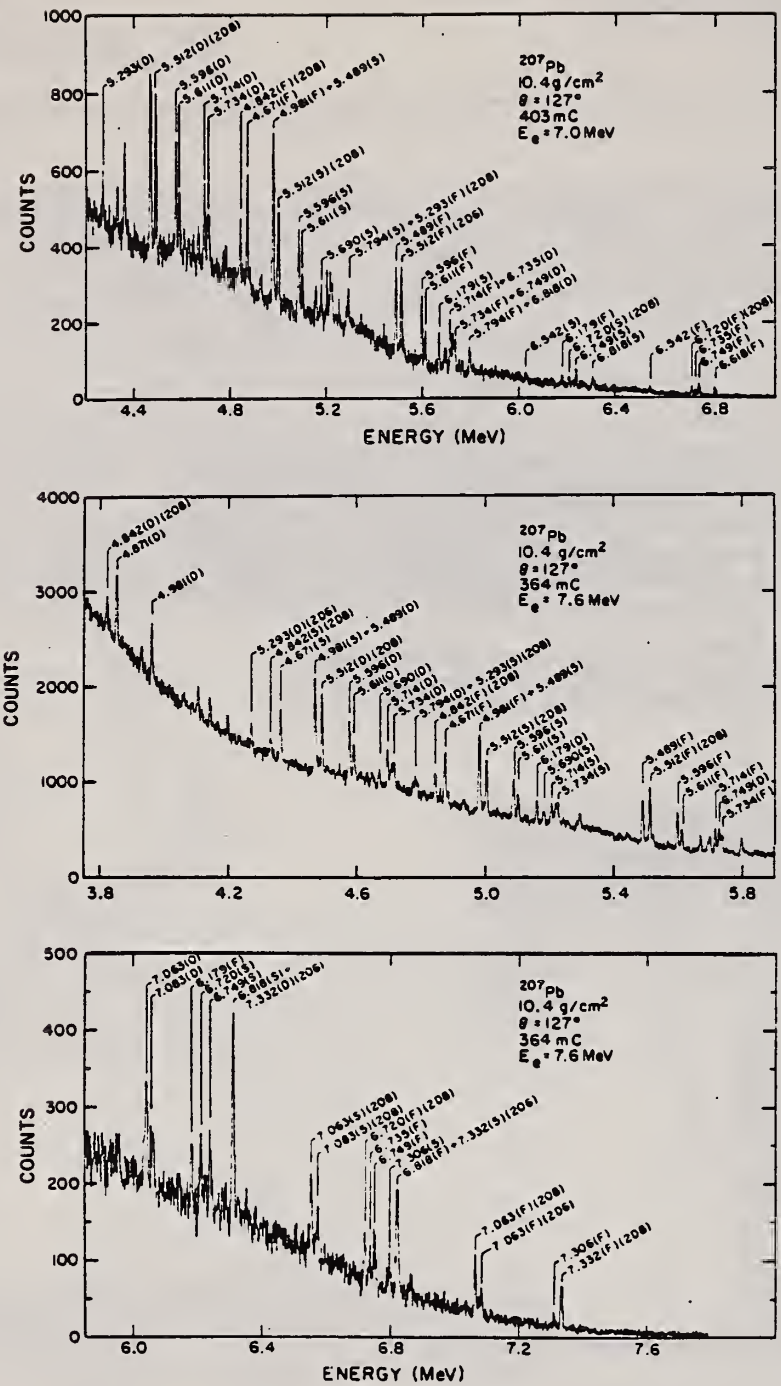

FIG. 9. Spectra for 7.0 MeV (upper figure) and 7.6 MeV (two lower figures) bremsstrahlung scattered at 127° from a cylindrical target of enriched (84.8%) ^{207}Pb. One channel corresponds to 1.36 keV in the 7.0 MeV spectrum and 1.48 keV in the 7.6 MeV data.

REF. C.N. Papanicolas, J. Lichtenstadt, C.P. Sargent, J. Heisenberg, J.S. McCarthy
Phys. Rev. Lett. 45, 106 (1980)

ELEM. SYM.	A	Z
Pb	207	82

METHOD

REF. NO.	
80 Pa 1	hg

REACTION	RESULT	EXCITATION ENERGY	SOURCE TYPE	SOURCE RANGE	DETECTOR TYPE	DETECTOR RANGE	ANGLE
E,E/	ABX	0-4	D	0*3	MAG-D		DST

*Q .5-3 FM-1,6 LEVELS

Transverse form factors have been extracted for the low-lying neutron hole (particle) states of ^{207}Pb from inelastic-electron-scattering data. A systematic, multipolarity- and momentum-transfer-independent quenching of ~55% in the transverse amplitude is observed when compared with single-particle predictions for both electric and magnetic transitions. The magnitude of the observed effect is not readily explained by our present theoretical understanding of this nucleus.

PACS numbers: 25.30.Cq, 21.10.Ky, 21.10.Pc, 27.80.+w

TABLE I. The quenching factors for the scattering amplitude for the single-particle (-hole) transitions of ^{207}Pb under investigation are tabulated in the last column. The excitation energy, spin-parity assignment, single-particle description, and allowed modes of excitation of the corresponding states are also given.

Excitation energy (MeV)	I^π assignment	Single-particle description	Multi-polarity	Quenching of transverse amplitude
0.571	5/2⁻	$3p_{1/2}^{-1} - 2f_{5/2}^{-1}$	$E2$	0.60
			$M3$	0.70
0.899	3/2⁻	$3p_{1/2}^{-1} - 3p_{3/2}^{-1}$	$E2$	0.60
			$M1$	0.70
1.634	13/2⁺	$3p_{1/2}^{-1} - 1i_{13/2}^{-1}$	$E7$	0.45
			$M6$	0.50
2.340	7/2⁻	$3p_{1/2}^{-1} - 2f_{7/2}^{-1}$	$E4$	0.50
			$M3$	0.60
2.728	9/2⁺	$3p_{1/2} - 2g_{9/2}$	$E5$	0.50
			$M4$	0.50
3.509	11/2⁺	$3p_{1/2} - 1i_{11/2}$	$E5$	0.60
			$M6$	0.50

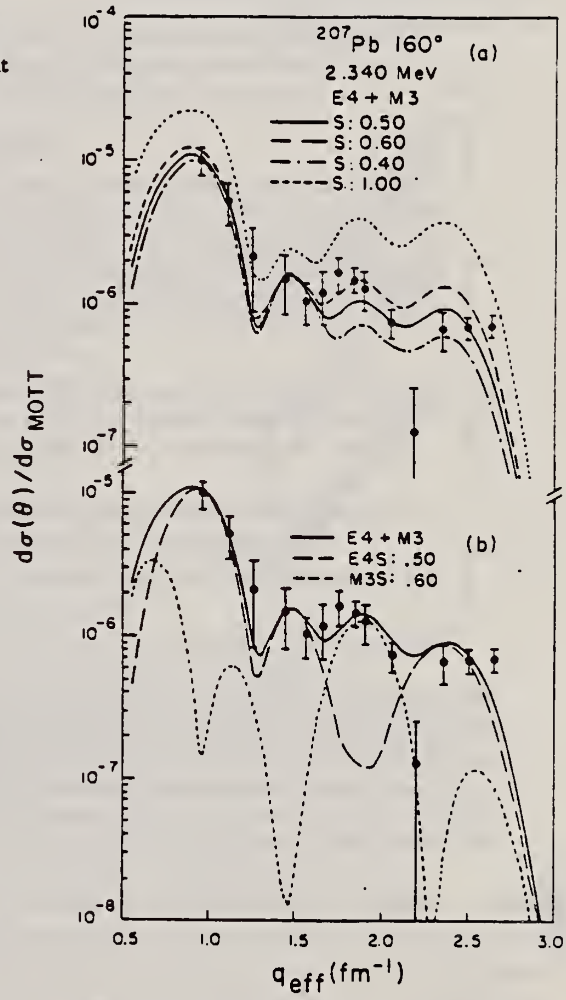

FIG. 1. (a) $d\sigma/d\sigma_{Mott}$ for the 2.340 MeV state in ^{207}Pb measured at 160°. The curves shown correspond to single-particle predictions with Hartree-Fock wave functions whereby the resulting amplitude has been scaled by the factor indicated. Core-polarization contribution has been fixed by our 90° measurements (Ref. 4). (b) A different scaling of the magnetic and the transverse electric contributions is possible in this case and results in a better fit.

REF. R.O. Avakyan, A.É. Avetisyan, N.Z. Akopov, S.S. Danagulyan, I.Kh. Kosakov, A.A. Oganesyan, Zh.V. Petrosyan, S.P Taroyan, G.M. Élbakyan
Sov. J. Nucl. Phys. 33, 192 (1981)
Yad. Fiz. 33, 362 (1981)

ELEM. SYM.	A	Z
Pb	207	82

METHOD

REF. NO.	
81 Av 10	hg

REACTION	RESULT	EXCITATION ENERGY	SOURCE TYPE	SOURCE RANGE	DETECTOR TYPE	DETECTOR RANGE	ANGLE
$ G,XP	RLX	0*2	D	0*2	TEL-D		100

We report the results of a study of the reaction $\gamma A \to pX$ at an angle $\theta_{\gamma p} = 100°$ lab in a beam of quasimonochromatic polarized photons. The measurements were made for three values of photon energy (E_γ = 0.69, 1.40, and 1.95 GeV) in the nuclei ^{12}C, ^{64}Cu, and ^{207}Pb. The range of kinetic energies of the protons was ≃100–230 MeV. It is shown that the slope parameter B for the invariant cross section $f = C\exp(-Bp^2)$ is a weak function of A and does not depend on E_γ, but the parameter $C_\gamma = C/A\bar{\sigma}$, increases with increase of E_γ, the slope of the lines $C_\gamma(E_\gamma)$ being greater for larger A.

COH-BRMS .69*1.95 GEV

PACS numbers: 25.20. + y, 13.60.Rj

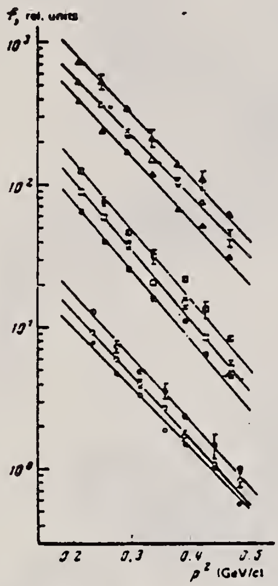

FIG. 2. Invariant cross sections f for photoproduction of cumulative protons as a function of their momentum squared for three target nuclei (^{12}C—lower family of points, ^{64}C—middle family of points, ^{207}Pb—upper family of points). The solid, hollow, and combined points correspond respectively to the values E_γ = 0.69, 1.40 and 1.95 GeV. The curves are described in the text.

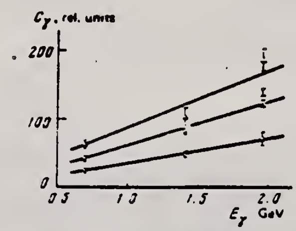

FIG. 3. The dependence of the parameter C_γ on E_γ. Points: ○—^{12}C, □—^{64}Cu, △—^{207}Pb.

TABLE II.

E_γ, GeV	Parameter	Nucleus ^{12}C	^{64}Cu	^{207}Pb
0.69	B	9.50±0.61	11.01±0.22	10.19±0.36
	C	$71.9^{+14.9}_{-11.7}$	663^{+61}_{-55}	3252^{+372}_{-302}
1.40	B	10.45±0.31	11.21±0.22	9.63±0.45
	C	$105.4^{-9.9}_{-9.0}$	973^{+61}_{-56}	3858^{+505}_{-447}
1.95	B	10.36±0.49	11.14±0.37	10.07±0.31
	C	$136.0^{+20.6}_{-18.0}$	1317^{+130}_{-116}	6201^{+542}_{-490}

Note. The parameter B is given in units of $(\text{GeV}/c)^{-2}$, while C is given in relative units.

TABLE I. Invariant cross section f (in relative units)

Nucleus	E_γ, GeV	T_p, MeV 116	135	153	173	190	210	230
^{12}C	0.69	7.83±0.13	4.80±0.10	3.40±0.08	1.88±0.05	1.55±0.05	1.05±0.04	0.58±0.03
	1.40	9.18±0.34	6.04±0.30	4.04±0.25	[illegible]	1.68±0.10	1.07±0.12	0.85±0.09
	1.95	13.12±1.00	7.21±0.71	4.91±0.53	3.62±0.46	2.31±0.35	[illegible]	1.00±0.22
		T_p, MeV 106	126	145	164	193	203	221
^{64}Cu	0.69	64.75±0.59	39.66±0.66	28.10±0.55	15.97±0.43	11.54±0.33	6.49±0.25	4.59±0.20
	1.40	59.54±2.52	58.45±2.14	37.70±1.78	21.15±1.41	14.58±1.05	8.57±0.80	5.21±0.61
	1.95	125.0±6.65	77.[illegible]±5.23	46.82±4.11	31.61±3.50	21.82±2.44	13.42±1.87	8.37±1.42
		T_p, MeV 105	123	143	163	182	201	222
^{207}Pb	0.69	392.7±9.3	242.1±5.4	172.5±4.6	119.2±3.7	66.8±2.6	51.4±2.2	31.2±1.2
	1.40	520.3±23.2	365.8±17.8	229.2±13.2	147.2±9.9	106.2±8.7	76.8±7.0	42.8±5.3
	1.95	734.0±68.0	525.0±50.6	338.6±36.7	213.4±29.3	137.4±21.1	108.5±16.9	62.4±12.5

REF.		ELEM. SYM.	A	Z
R.O. Avakyan, A.É. Avetisyan, N.Z. Akopov, S.S. Danagulyan, I.Kh. Kosakov, A.A. Oganesyan, Zh.V. Petrosyan, S.P. Taroyan, G.M. Élbakyan Sov. J. Nucl. Phys. 33, 448 (1981) Yad. Fiz. 33, 858 (1981)		Pb	207	82
METHOD		REF. NO.	81 Av 13	hg

REACTION	RESULT	EXCITATION ENERGY	SOURCE TYPE	SOURCE RANGE	DETECTOR TYPE	DETECTOR RANGE	ANGLE
$ G,XP	ASM	0*2	C	0*2	UKN		100

COH-BRMS .69*1.95 GEV

At the present time it is rather well established that the experimental values of the invariant cross section $f=(E/p^2)(d^2\sigma/d\Omega dp)$ of the reaction

$$aA \to bX \qquad (1)$$

in the cumulative region[1,2] are described by an exponential dependence of the form $f=C\exp(-Bp^2)$. Most of the experiments in which reaction (1) induced by various particles (π, p, γ, ...), has been studied were designed to study the energy, angular, and A dependence of the parameters B and C.[3-9] As a result of the investigations it is has been established that the parameter B does not depend on the mass number A of the target nucleus, on the type of incident particle, or on its energy, beginning with $E_a \simeq 1$ GeV, while the parameter $C_p = C/\sigma_{tot}$ (σ_{tot} is the total cross section for the aA interaction) does not depend on the type of particle a. In addition to the established properties of the quantitles B and C it would be interesting to check the dependence of the parameters B and C on the direction of polarization of the initial particle. For this purpose it is necessary to measure the asymmetry Σ of the cross section for reaction (1) as a function of the direction of the initial-particle polarization vector.

In the present work we report the results of a study of the photoproduction of cumulative protons at an angle $\theta_{\gamma p}=100°$ in the laboratory system in the nuclei ^{12}C, ^{64}Cu, and ^{207}Pb for three photon energy values (E_γ = 0.69, 1.40, and 1.95 GeV). The possibility of measurement at a definite photon energy was based on the use of the method of subtraction of the coherent peak[10,11] in the spectrum of quasimonochromatic polarized photons emitted by electrons in passing through a diamond crystal.[12] The existence of a significant degree of polarization of the photons in the coherent peak has enabled us to measure the value of the cross-section asymmetry Σ of the reaction $\gamma A \to pX$. The asymmetry was calculated from the relation

$$\Sigma = \frac{1}{\bar{P}_\gamma}\frac{y^\perp - y^\parallel}{y^\perp + y^\parallel - 2y^\circ},$$

where $y^\perp$, $y^\parallel$ are the reaction yields in the case of perpendicular and parallel orientation of the photon polarization vector with respect to the reaction plane in the coherent bremsstrahlung spectrum; y° is the reaction yield for an ordinary bremsstrahlung spectrum; $\bar{P}_\gamma$ is the average value of photon polarization in the subtracted coherent peak.

Measurements of Σ were made in the nuclei ^{12}C, ^{64}Cu, and ^{207}Pb for protons with kinetic energy respectively T_p = 173, 164, and 163 MeV. The energy bin was ΔT = ±60 MeV.

The experimental apparatus and measurement technique have been described in detail elsewhere.[13]

Numerical values of Σ with their standard deviations $\sigma(\Sigma)$ are given in the table.

The values of $\sigma(\Sigma)$ contain both the statistical error and the error in determination of the quantity $\bar{P}_\gamma$.[13]

From the figure, where we have shown Σ as a function of E_γ for the three nuclei it can be seen that the absolute values of the asymmetry in the region investigated are insignificant and depend weakly on E_γ. We note that Σ for carbon is close to zero for all E_γ, and the maximum value 0.29 ± 0.16 is achieved in the case of lead for E_γ = 1.95 GeV. The data show that within experimental error the asymmetry is almost indepen-

TABLE I.

E_γ, GeV	Nucleus ^{12}C Σ	^{12}C $\sigma(\Sigma)$	^{64}Cu Σ	^{64}Cu $\sigma(\Sigma)$	^{207}Pb Σ	^{207}Pb $\sigma(\Sigma)$
0.69	−0.0761	±0.0233	[illegible]	[illegible]	−0.1192	±0.0323
1.40	0.0402	±0.0386	[illegible]	[illegible]	[illegible]	[illegible]
1.95	0.0380	±0.0936	[illegible]	[illegible]	[illegible]	±0.1633

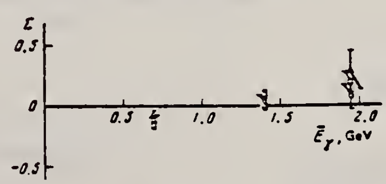

FIG. 1. Asymmetry Σ of the cross section for photoproduction of cummulative protons as a function of the photon energy E_γ for target nuclei ^{12}C (○), ^{64}Cu (□), and ^{207}Pb (△).

REF. Y. Birenbaum, Z. Berant, S. Kahane, A. Wolf, R. Moreh
Nucl. Phys. A369, 483 (1981)

ELEM. SYM.	A	Z
Pb	207	82
REF. NO. 81 Bi 6		hg

METHOD

REACTION	RESULT	EXCITATION ENERGY	SOURCE TYPE	SOURCE RANGE	DETECTOR TYPE	DETECTOR RANGE	ANGLE
G,N	RLY	6-11	D	7 - 12	SCI-D		DST
		(6.7-11)		(7 - 11.4)			

$$I(E_\gamma,G) = \frac{a_1P_1 + a_3P_3}{1 + a_2P_2}$$

Abstract: Angular distributions of photoneutrons from the $^{207,208}Pb(\gamma, n_0)$ reactions were measured at 11 angles around $\theta = 90°$. The γ-source, $E_\gamma = 7$-11.4 MeV, contained discrete lines ($\Delta E \lesssim 30$ eV) obtained from n-capture and was used in conjunction with a high-resolution ^{3}He spectrometer. Strong evidence for an E2 contribution and for E2-E1 and possibly E1-M1 interference was obtained in both ^{207}Pb and ^{208}Pb. The results are compared with calculations using a direct-semidirect model which involved an E1 and isoscalar E2 giant resonances. The results indicate that this model could explain only certain features of the data while most of the other features remain unexplained.

E

NUCLEAR REACTIONS $^{208,207}Pb(\gamma, n)$, $E = 7.0$-11.4 MeV; measured $\sigma(\theta)$ for $\theta = 40°$-140°. Deduced E2-E1 and M1-E1 interference effects.

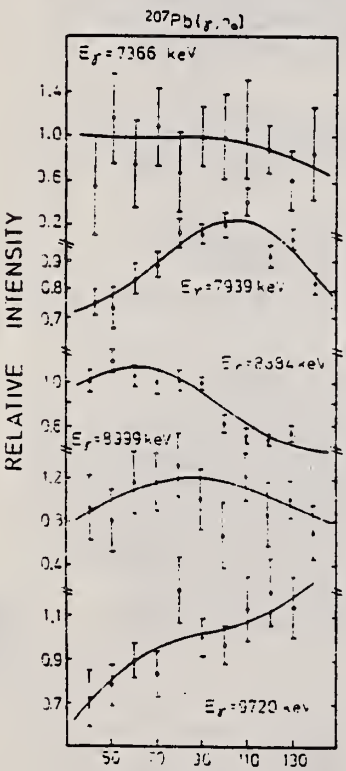

Fig. 5. Angular distributions of neutrons from the $^{207}Pb(\gamma, n)$ reaction leading to the ground state in ^{206}Pb for various incident photon energies.

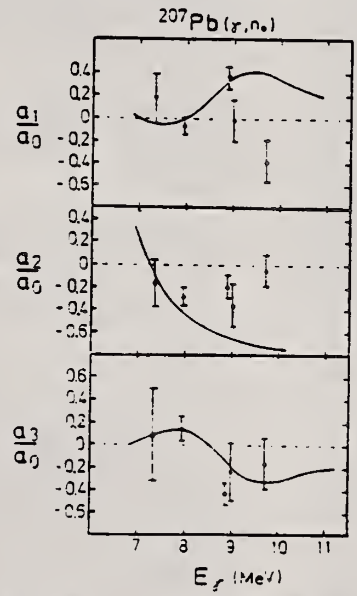

Fig. 8. Angular distribution coefficients a_i/a_0 for the (γ, n) transitions to the ^{206}Pb ground state. The solid curves are calculated using the DSD model.

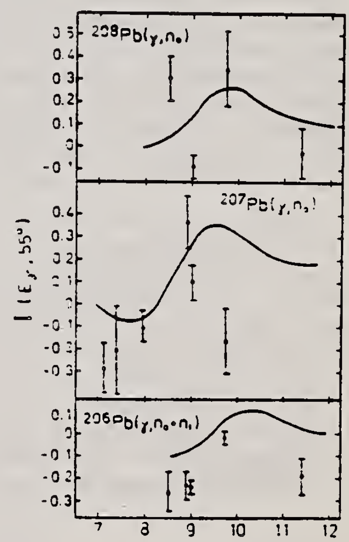

Fig. 9. Measured interference factor $I(E_\gamma, \theta)$ for the three reactions $^{206,207,208}Pb(\gamma, n_0)$. The data for the ^{206}Pb target were taken from ref. [ ]. The solid curves are calculated using the DSD model

REF. C.N. Papanicolas, J. Heisenberg, J. Lichtenstadt, J.S. McCarthy
Phys. Lett. 99B, 96 (1981)

ELEM. SYM.	A	Z
Pb	207	82

METHOD

REF. NO.	
81 Pa 1	hg

REACTION	RESULT	EXCITATION ENERGY	SOURCE		DETECTOR		ANGLE
			TYPE	RANGE	TYPE	RANGE	
E,E/	ABX	4-6	D	0*3	MAG-D		DST

*MOM,FM-1 4 E10 LEV

We report the identification of new high multipolarity transitions in ^{207}Pb and ^{206}Pb by the measurement of their form factor. A comparison to the corresponding excitations in ^{208}Pb is presented.

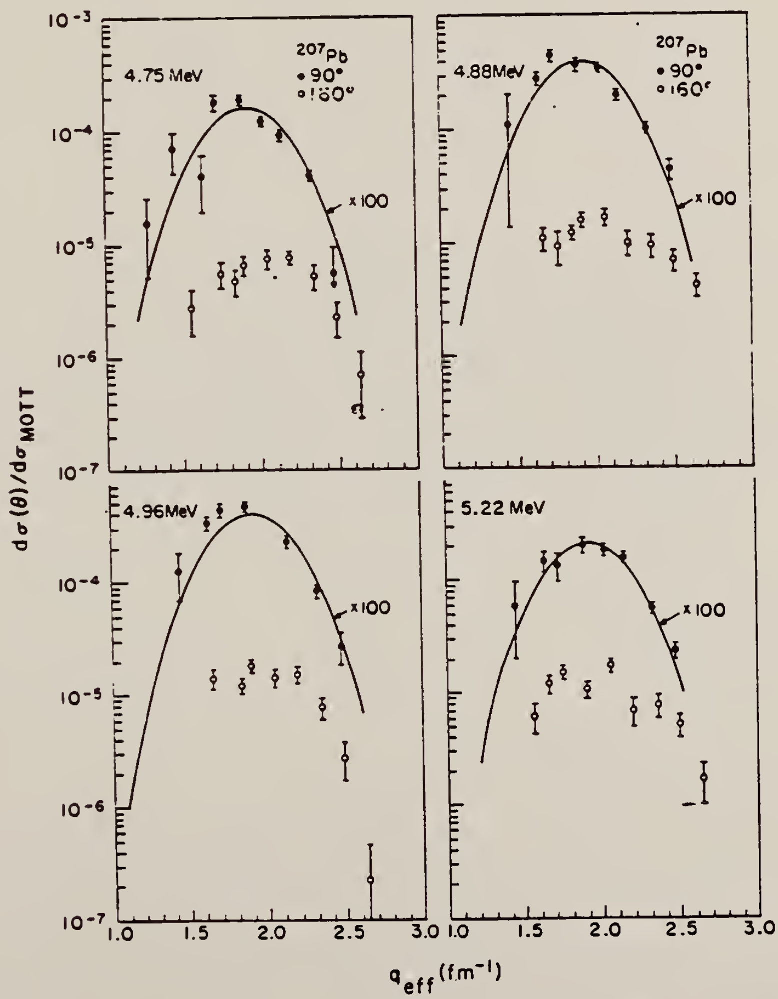

Fig. 2. $d\sigma/d\sigma_{Mott}$ at 90° and 160° for the four transitions of ^{207}Pb which we identify as being of E10 character. The solid line through the 90° data is the shape resulting from $\pi(h_{9/2}, h_{11/2}^{-1})$ configuration scaled appropriately (see discussion in text).

(OVER)

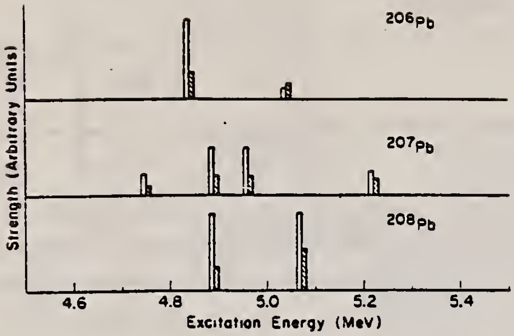

Fig. 1. Excitation energy and strength of the E10 transitions observed in ^{208}Pb, ^{207}Pb and ^{206}Pb. Their strength (corresponding to the first maximum of their form factor) is given in arbitrary units. The open bars represent the strength at 90° and they are enlarged by a factor of 10 as compared to the solid ones (strength at 160°)

PB
A=208

PB
A=208

PB
A=208

REF.	ELEM. SYM.	A	Z
M.D. DeSouza Santos, J. Goldemberg, R.R. Pieroni, E. Silva, O.A. Borello, S.S. Villaca, J.L. Lopes Int. Conf. Peaceful Uses of Atomic Energy II [UN, NY] 169 (1955)	Pb	208	82

METHOD	REF. NO.	
Betatron; proton yield; radioactivity; r-chamber	55 De 1	EGF

REACTION	RESULT	EXCITATION ENERGY	SOURCE		DETECTOR		ANGLE
			TYPE	RANGE	TYPE	RANGE	
G,P	ABX	11-21	C	11-21	ACT-I		4 PI

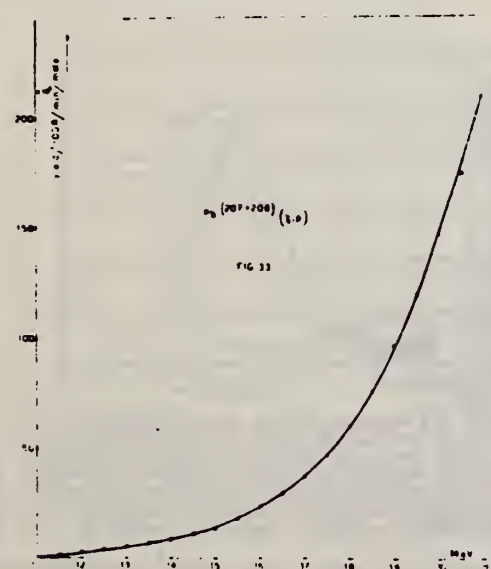

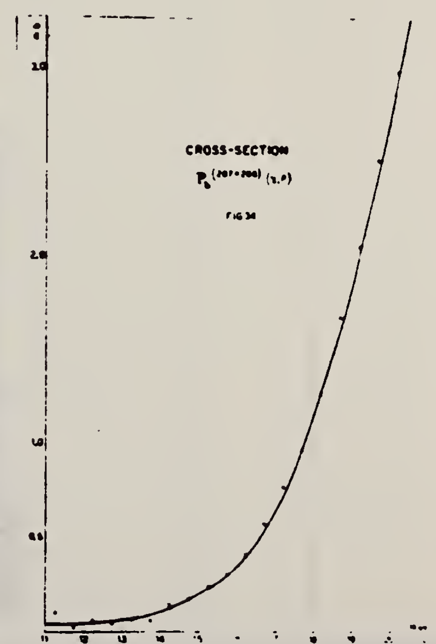

Ref. M.E. Toms, W.E. Stephens
Phys. Rev. 98, 626 (1955)

Elem. Sym.	A	Z
Pb	208	82

Method Betatron; protron spectrum, yield, angular distribution; nuclear emulsions

Ref. No.	
55 To 1 15	NVB

Reaction	E or ΔE	E_0	Γ	$\int \sigma dE$	Jπ	Notes
$Pb^{208}(\gamma,xp)$	Bremss. 23					Lead enriched in 208.

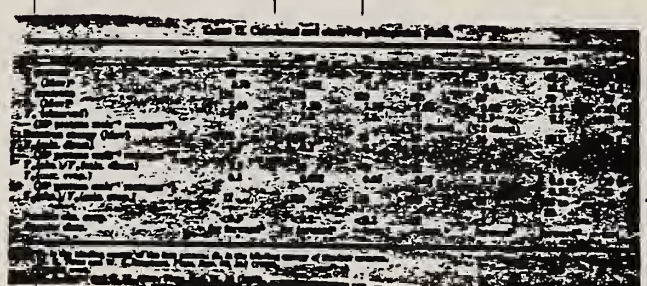

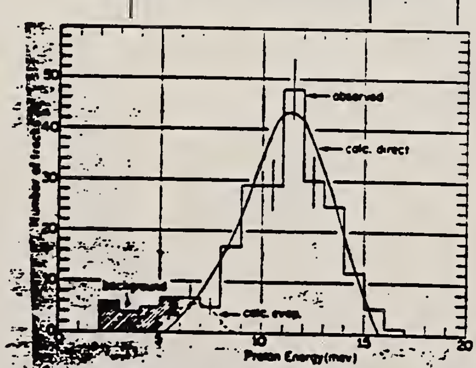

FIG. 2. The histogram gives the energy distribution of the photoprotons from lead 208 exposed to 23-Mev bremsstrahlung. The smooth curve is the distribution calculated for the direct process and normalized to the observed protons. The dashed curve is the calculated distribution for the evaporation process fitted to indicate the maximum possible evaporation yield. The shaded groups are background.

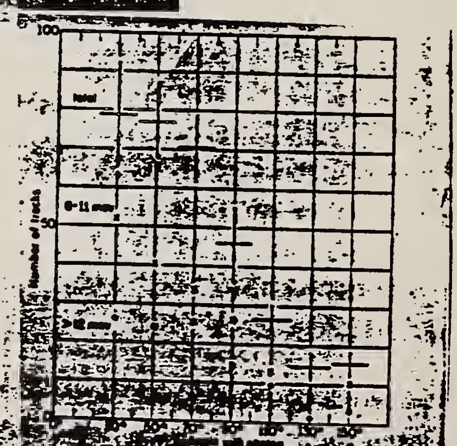

FIG. 4. The numbers of lead-208 photoprotons per unit solid angle in arbitrary units is plotted as a function of their angle from the photon direction. In addition, the crosses show the angular distribution of photoprotons of 8 to 11 Mev energy, the circles photoprotons over 12 Mev.

Ref. J.D. Prentice, K.G. McNeill
Phil. Mag 1, 373 (1956)

Elem. Sym.	A	Z
Pb	208	82

Method
22 MeV synchrotron; NaI; neutron yield; Cu^{63} reaction

Ref. No.	
56 Pr 1	EGF

Reaction	E or ΔE	E_o	Γ	$\int \sigma dE$	Jπ	Notes
$Pb^{208}(\gamma,n)$	Bremss. 22					$\frac{\text{Yield }(Pb^{208})}{\text{Yield (natural lead)}} = 1.15 \pm 0.24$

Ref. U. Farinelli, F. Ferrero, R. Malvano, S. Menardi, E. Silva Phys. Rev. 112, 1994 (1958)	Elem. Sym. Pb	A 208	Z 82
Method Betatron; activity measured.	Ref. No. 58 Fa 1		EH

Reaction	E or ΔE	E_o	Γ	$\int \sigma dE$	Jπ	Notes
$Pb^{208}(\gamma,n)Pb^{207m}$	10 - 20	14	< 2			Figure 4: Reference 9: Toms and Stephens, Phys Rev. 108, 77 (1957); our reference 57 To 1.

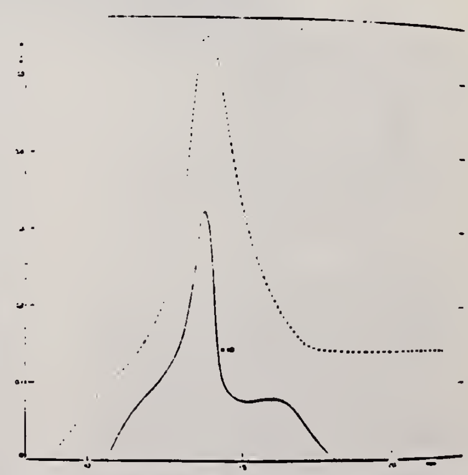

FIG. 4. Cross section of the $Pb^{208}(\gamma,n\gamma')Pb^{207m}$ photoreaction (solid line), and that of the photoneutron reaction in lead (dashed line—from reference No. 9

Ref. W.C. Barber, F. Berthold, G. Fricke, F.E. Gudden
Phys. Rev. 120, 2081 (1960)

Elem. Sym.	A	Z
Pb	208	82

Method Stanford Mark II Linac; magnetic spectrometer; plastic scintillator counter telescope

Ref. No. 60 Ba 4 — JHH

Reaction	E or ΔE	E_o	Γ	∫σdE	Jπ	Notes
$(e^-, e^-{}')$	42.5	4.14±0.20				Both E_o measurement at $\theta = 160°$.
		15 (giant reson.)		6500^{+6000}_{-3000} Mev-mb		

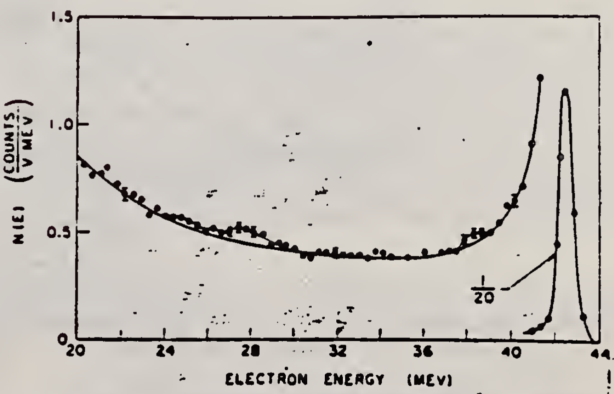

Fig. 10. Energy distribution of electrons, which were initially 42.5 Mev, after 160° scattering from a Pb target.

K. M. Geller, J. Halpern, and E. G. Muirhead
Phys. Rev. 118, 1302-12 (1960)

ELEM. SYM.	A	Z
Pb	208	82

Betatron; neutron threshold; ion chamber

REF. NO.	
60 Ge 3	NVB

REACTION	RESULT	EXCITATION ENERGY	SOURCE		DETECTOR		ANGLE
			TYPE	RANGE	TYPE	RANGE	
G,N	NØX	THR	C	THR	BF3-I		4 PI

THRESHØLD

TABLE I. Summary and comparison of neutron separation energies inferred from present threshold measurements with values predicted from mass data and reaction energies. All energies are expressed in the center-of-mass system in Mev.

Reaction	No. runs	Present results	Other results	Method	Reference
$Pb^{208}(\gamma,n)Pb^{207}$	3	7.404±0.028	7.36 ±0.05	$Pb^{208}(d,t)Pb^{207}$	e
			7.380±0.008	$Pb^{207}(n,\gamma)Pb^{208}$	e
			7.38 ±0.06	mass data	q
			7.357±0.012	mass data	r

[e] P. M. Van Patter and W. Whaling, Revs. Modern Phys. 26, 402 (1954); 29, 756 (1957).
[q] W. H. Johnson, Jr., and V. B. Bhanot, Phys. Rev. 107, 6 (1957).
[r] J. L. Benson, R. A. Damerow, and R. R. Ries, Phys. Rev. 113, 1105 (1959).

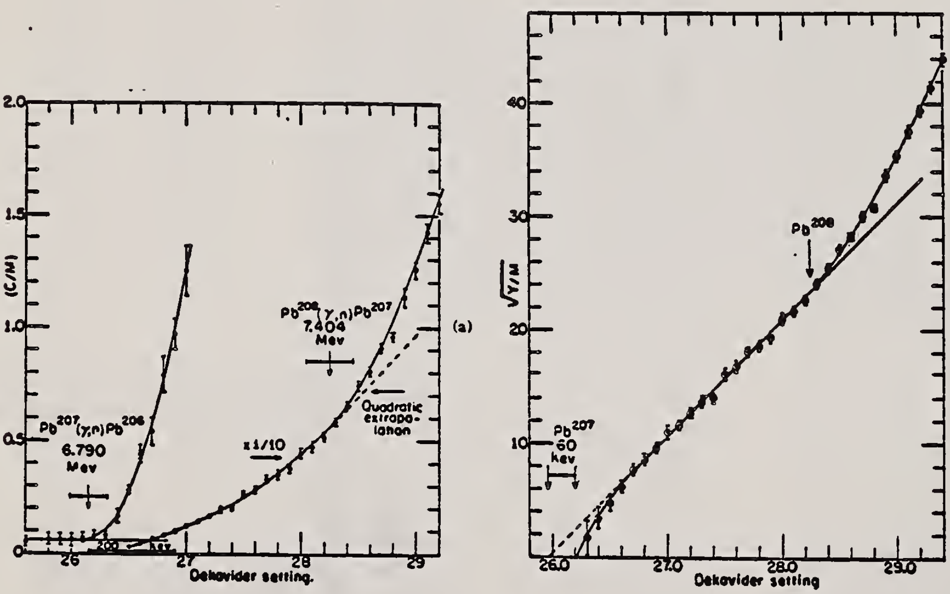

FIG. 2. (a) Neutron yield data for lead from 6.7 Mev to 7.7 Mev, and (b) square root plot of yield data. Linear extrapolation of $(Y/M)^{\frac{1}{2}}$ predicts an apparent threshold 60 kev lower than what is obtained from yield data in the immediate vicinity of threshold.

Ref. H. Crannell, R. Helm, H. Kendall, J. Oeser, M. Yearian
Phys. Rev. 123, 923 (1961)

Elem. Sym.	A	Z
Pb	208	82

Method: Linac; Čerenkov counter telescope

Ref. No.	
61 Cr 1	JHH

Reaction	E or ΔE	E_o	Γ	$\int \sigma dE$	Jπ	Notes
$(e^-,e^{-\prime})$	183					Measured γ transition rate Γ_m =
		2.60			3^-	$\Gamma_m = (3.80\pm1.4)10^{10}\ sec^{-1}$; (E3) $G = \Gamma_m/\Gamma_{sp} = 3.08\pm11.4$
		4.3			4^+	$\Gamma_m = (2.23\pm0.7)10^{8}\ sec^{-1}$; (E4) $G = \Gamma_m/\Gamma_{sp} = 36.6\pm12$
						Fits R_o = 1.20 fermi
						[Γ_{sp} = single-particle estimate of the γ transition rate.]

Fig. 16. Energy-level diagram for Pb[208] showing the known excited states below 5.5 Mev. (See caption for Fig. 13.)

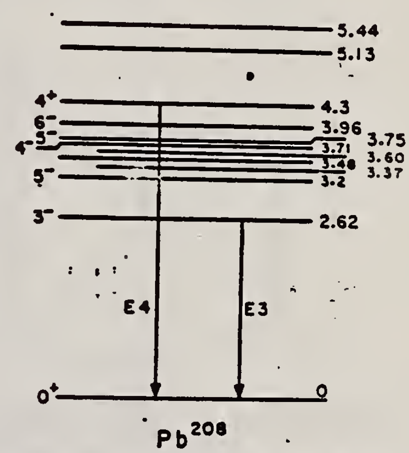

Fig. 13. In this and the following four figures are shown portions of the energy-level structures of the nuclei investigated in the present experiment. The information is, for the most part, taken from reference 15. The γ-ray transitions shown are those whose decay rates were determined directly in the present experiment or inferred from a knowledge of the γ-ray branching ratios in de-excitation of the nucleus. The spin and parity of each level are shown at the left, where known, and the energy of the excited states in Mev on the right. The best assignments of the transition multipolarities are indicated. This figure shows the energy-level structure of Ni[58].

Table IV. [illegible]

Multipole	Nuclide	E (Mev)	$B(E\lambda)/B(\lambda)_{sp}$	B_λ (Mev)	$(B_\lambda)_{hm}$	$B_\lambda/(B_\lambda)_{hm}$	C_λ (Mev)	(f/Mev)
[illegible]	[illegible]	[illegible]	14.3 ±1.9	60.5± 9	4.16	16.7 ±2.2	145± 19	0.745 ±0.097
	[illegible]	[illegible]	6.45±1.6	100 ± 30	4.16	23.6 ±9.2	1070±390	0.407 ±0.15
	[illegible]	[illegible]	17.1 ±2.1	66.2± 7.8	[illegible]	14.65±2.0	116± 14	0.790 ±[illegible]
[illegible]	[illegible]	[illegible]	13.2 ±1.8	100 ± 14	[illegible]	22.2 ±3.2	[illegible]	[illegible]
	[illegible]	[illegible]	15.9 ±2.3	[illegible]	[illegible]	19.3 ±3.1	1430±230	0.404 ±0.074
	[illegible]	[illegible]	7.8 ±1.8	144 ± 34	[illegible]	31.2 ±7.6	3700±873	[illegible]
	[illegible]	[illegible]	[illegible]	[illegible]	[illegible]	11.7 ±[illegible]	[illegible]± 700	[illegible] ±0.18
[illegible]	[illegible]	[illegible]	2.2 ±0.46	[illegible]	[illegible]	[illegible]	[illegible]	[illegible]
	[illegible]	[illegible]	2.5 ±0.57	[illegible]	[illegible]	1730 ±400	[illegible]	0.15 ±0.035
	[illegible]	[illegible]	[illegible]	[illegible]	[illegible]	[illegible]	[illegible]	0.106 ±0.03
	[illegible]	[illegible]	4.95±0.74	[illegible]	[illegible]	[illegible]	[illegible]	0.125 ±0.019
	[illegible]	[illegible]	[illegible]	[illegible]	[illegible]	[illegible]	[illegible]	[illegible] ±0.11

Ref 37: Crut, Sweetman, Wall - Nuclear Phys. 17, 655 (1960).

Ref 15: Data on the decay schemes are taken principally from Nuclear Data Sheets National Academy of Sciences, National Research Council (U.S. Government Printing Office, Washington, D.C., 1959)

Ref. E.G. Fuller, E. Hayward Nuclear Phys. 33, 431 (1962)	Elem. Sym. Pb	A 208	Z 82
Method 50 MeV betatron; BF_3, NaI counters	Ref. No. 62 Fu 4		JHH

Reaction	E or ΔE	E_0	Γ	$\int \sigma dE$	Jπ	Notes
$Pb^{206,7,8}$						∫ corrected for multiple neutron production.
(γ,γ)	4.5-8.5					
(γ,xn)	(571)			$\int^{18.5} = 3.93$ MeV-b		Self-absorption measurements made at 7 MeV.

571

TABLE 1

Observed transmissions corrected for electronic absorption

Absorber	Thickness (g cm⁻²)	Targets: Pb (7.2 g cm⁻²)		"Pb[illegible]" (3.6 g cm⁻²)		Bi (5.97 g cm⁻²)	
Pb	10.8					[illegible]	[illegible]
	14.4	0.663	0.032	0.846	0.049		
		0.694	0.037 a)				
"Pb[illegible]"	11.2	0.976	0.050	0.74	0.043	1.002	0.048
				0.599	0.031 a)		
Bi	12.2	1.018	0.050	1.045	0.038	0.792	0.040
						0.719	0.038 a)
Pb	7.65	0.822	0.029			0.903	0.028
"Pb[illegible]"	7.83	0.790	0.028			0.910	0.028
"Pb[illegible]"	7.86	0.797	0.028			0.915	0.028
"Pb[illegible]"	7.47					0.965	0.029
Bi	7.49					0.790	0.025

a) Measured with both target and absorber at liquid nitrogen temperature

TABLE 3

Average level parameters at 6 MeV

	Lead	Radio-lead	Bismuth
[illegible] (6 Γ)²	· 10	1 – 400	0 – 64
σ_0^2 (b)	24—38	29—205	10—48
Γ (eV)	· 3.1	0.15 – 3.1	~ 0.39
σ_γ (max) (b)	183	205	68
γ/Γ	0.13 – 0.21	0.14 – 1.0	0.2 – 1.0
$\sigma_{\gamma\gamma}$ (7 MeV) (mb)	21	20	21
$\int \sigma dE$ (MeV · mb)	42	40	48

SEE PAGE 2 FOR FIGURES.

Method		Elem. Sym.	A	Z
		Pb	208	82
	PAGE 2	Ref. No. 62 Fu 4		JHH

$\int \sigma dE$

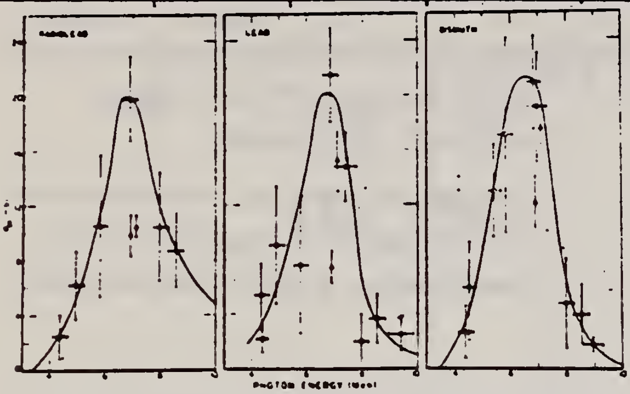

Fig. 1. [illegible]

Ref 3: Fuller & Hayward - Phys. Rev. 101, 692 (1956)

Ref 5: Reibel & Mann - Phys. Rev. 118, 701 (1960)

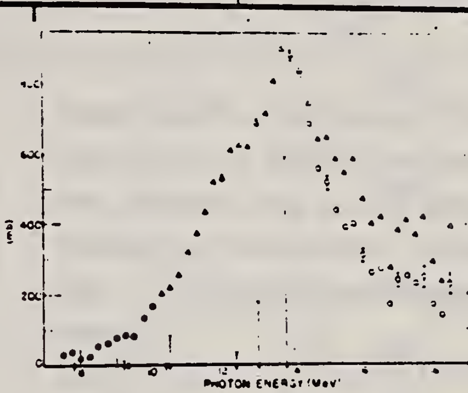

Fig. 7. The neutron production cross section for Pb208. The triangles represent the cross section before correction for neutron multiplicity. Points were obtained from a 1 MeV bin-width analysis of the neutron yield curve except near threshold (indicated by closed circles) where a half-MeV bin-width was used. The points represented by the open circles have been corrected for the neutron multiplicity. The arrows beneath the axis of abscissas indicate the energies of the important dipole transition calculated by Balashov, et al. [11] The heights of the vertical lines are proportional to the calculated strengths of the transitions.

Ref 11: Balashov, Shevchenko & Yudin, to be published: Shevchenko, private communication.

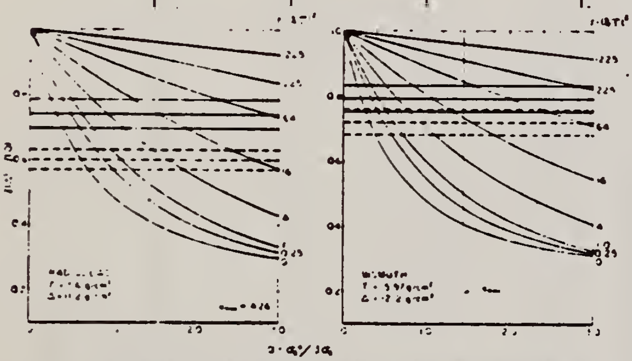

Fig. 5. Self-absorption attenuation curves for radio-lead and bismuth. The ratio I(∆)/I(0) as defined in the text (eq. (4)) has been evaluated as a function of the peak absorption cross section σ_0^*, for the target and absorber thicknesses used in the experiments. The horizontal lines represent the measured attenuations and their uncertainties for the experiments performed at room temperature (solid lines) and liquid nitrogen temperature (dashed lines). The quantity σ_{max} is the maximum possible value of the average peak absorption cross section at 8 MeV in units of 3 times the electronic absorption cross section. This maximum value assumes elastic dipole scattering and represents an average over all possible spins for the excited states.

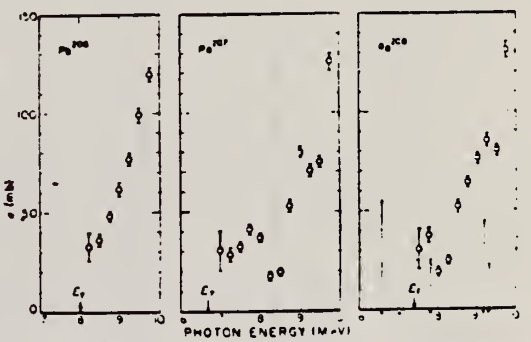

Fig. 8. The (γ, n) cross sections for the lead isotopes near threshold. The arrows indicate the positions of the (γ, n) thresholds. The arrows beneath the axis of abscissas indicate the energies of the important dipole transition calculated by Balashov et al. [11] The heights of the vertical lines are proportional to the calculated strengths of the transitions.

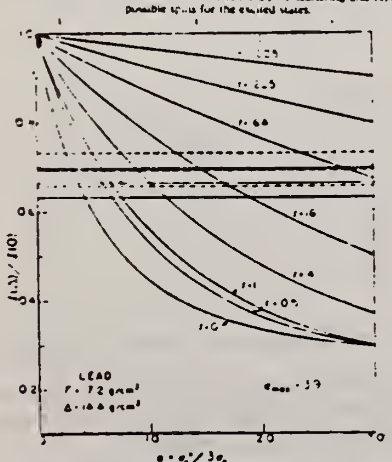

Fig. 6. Self-absorption attenuation curves for lead. See description for fig. 5.

Ref. Yu.I.Sorokin, V.G.Shevchenko, B.A.Yur'ev Zhur.Eksptl. i Teoret.Fiz. 43, 1600 (1962); Soviet Phys.JETP 16, 1127 (1963)	Elem. Sym. Pb	A 208	Z 82
Method 35 MeV Betatron - counters (activity of Ti^{206} and Ti^{207} detected.	Ref. No. 62Sol		BG

Reaction	E or ΔE	E_0	Γ	$\int \sigma dE$	Jπ	Notes
$Pb^{207}(\gamma,p)Ti^{206}$	15 - 33	26		$55\pm20)_0^{33}$		Cross section obtained from corrected yield curve.
$Pb^{208}(\gamma,p)Ti^{207}$						Assumptions made on contribution of $Pb^{208}(\gamma,pn)Ti^{206}$ reaction to σ_T - contribution greatly overestimated.
$Pb^{207}(\gamma,p)Ti^{206}$	15- 33	26.5		$60\pm20)_0^{33}$		
$Pb^{208}(\gamma,p)Ti^{207}$						
$Pb^{208}(\gamma,pn)Ti^{206}$	-					
$Pb^{208}(\gamma,d)Ti^{206}$						

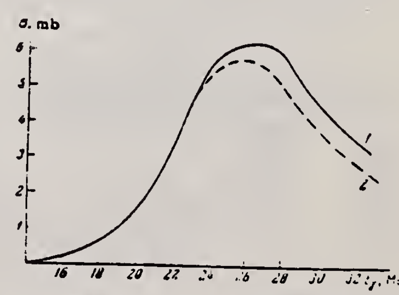

FIG. 2. Cross section of photonuclear reactions in lead: 1 — cross section calculated from the total yield curve, 2 — cross section for the (γ, p) reaction.

Ref.	Elem. Sym.	A	Z
P.Axel, K.Min, N.Stein, D.C.Sutton Phys.Rev.Letters 10, 299 (1963)	Pb	208	82

Method	Ref. No.	
Bremsstrahlung monochromator	63Axl	BG

Reaction	E or ΔE	E_o	Γ	$\int \sigma dE$	Jπ	Notes
		ground state rad.widths				
(γ,γ)		6.72	15 eV			Quasi-elastic scattering - poor resolution of photon; detector did not separate high energy inelastic scattering from elastic scattering. Fig. 135° quasi-elastic cross section.
		7.03	30			Optical model considered.
		7.29	40			

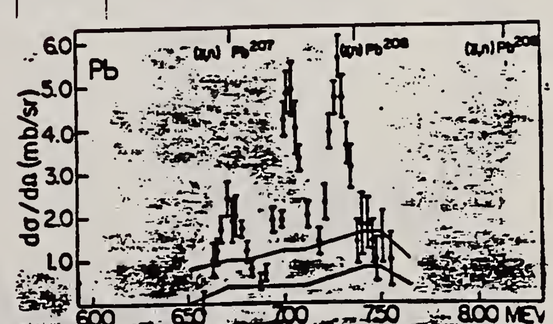

Ref.	W. Bertozzi, C.P. Sargent, W. Turchinetz Phys. Letters 6, 108 (1963)	Elem. Sym. Pb	A 208	Z 82
Method	Neutron Time of Flight	Ref. No. 63 Be 4		EF

Reaction	E or ΔE	E_0	Γ	$\int \sigma dE$	Jπ	Notes
(γ,n)	9.3 10.3 Bremss.					

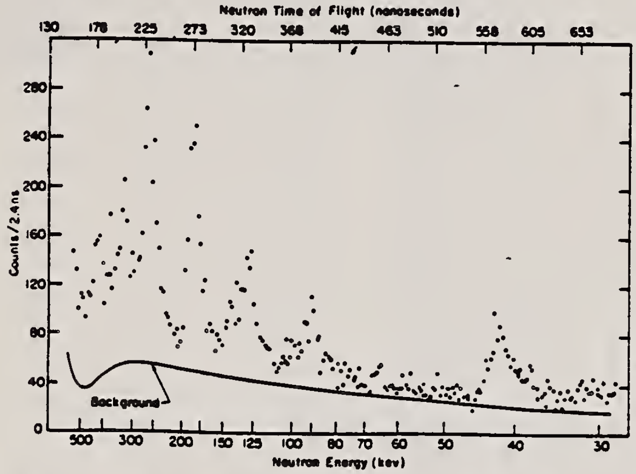

Fig. 1. Time of flight spectrum for Pb(γ, n) using a target of "natural lead", an electron energy of 8.15 MeV and the Ag(n, γ) detector at 1.58 m from the (γ, n) target.

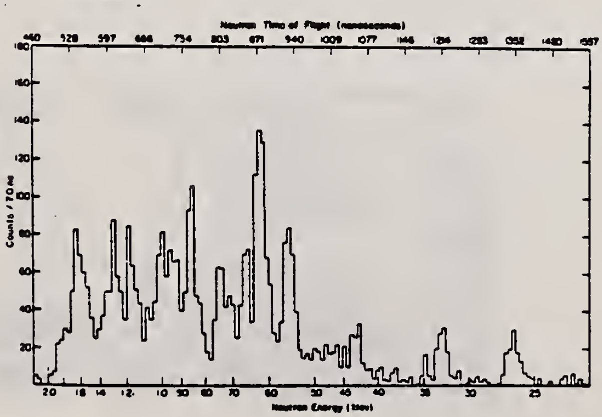

Fig. 2. Time of flight spectrum for Pb^{208}(γ, n) using a recoil detector at 9.31 m from the (γ, n) target, and an electron energy of 9.3 MeV.

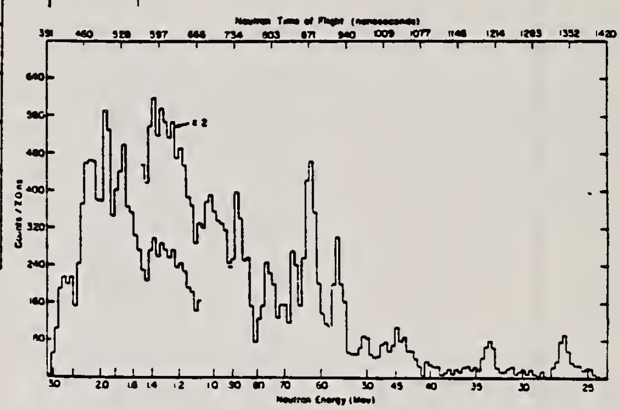

Fig. 3. Time of flight spectrum for Pb^{208}(γ, n) using a recoil detector at 9.31 m from the (γ, n) target and an electron energy of 10.3 MeV.

Table 1

Some representative level parameters in Pb^{208}. E_n = neutron energy; E_γ = corresponding level energy calculated from E_n assuming a neutron separation energy for Pb^{208} of 7.368 MeV [14]; $\int \sigma dE$ = integrated cross section for the level in question; Γ_0 - ground state radiative width obtained from $\int \sigma dE_\gamma$ assuming dipole radiation and $\Gamma_n \gg \Gamma_0$; Γ_t = upper limit on the total level width.

E_n (MeV)	E_γ (MeV)	$\int \sigma dE_\gamma$ (MeV-mb)	Γ_0 (eV)	Γ_t (keV)
0.264	7.632	3.7	19	< 9
0.324	7.692	2.9	15	< 10
0.437	7.806	2.4	13	< 40
0.557	7.925	2.3	13	< 70
0.624	7.992	3.9	22	< 80
0.666	8.034	1.4	8	< 70
0.853	8.221	2.7	16	< 100

REF.	ELEM. SYM.	A	Z
H.H. Fleischmann, F.W. Stanek Z. Physik 175, 172 (1963)	Pb	208	82

METHOD	REF. NO.	
$Fe^{56}(n,\gamma)$ source; photon scattering	63 Fℓ 2	NVB

REACTION	RESULT	EXCITATION ENERGY	SOURCE		DETECTOR		ANGLE
			TYPE	RANGE	TYPE	RANGE	
G,G	LFT	3-8	D	7	SCI-D		4PI
				(7.28)			

Γ_{γ_0} = 0.80±0.08 eV, assuming dipole transition.

Branching ratio:

γ/γ_0 = 1.4 with uncertainity of a factor of 1.5.

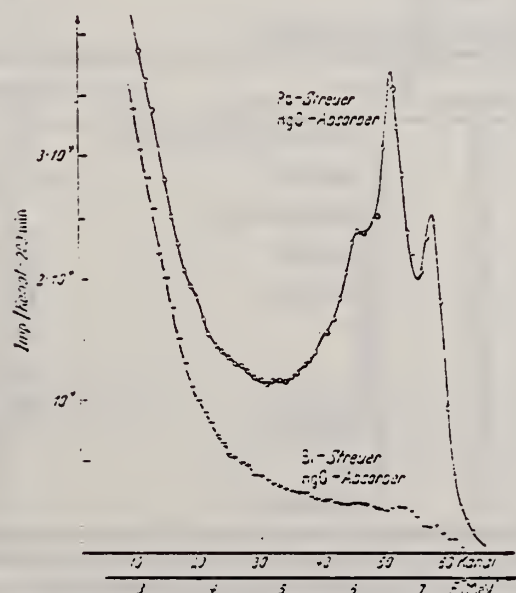

Fig. 1. Streuspektren von Pb- bzw. Bi-Streukörpern bei einem Absorber aus 12,6 g/cm² H_2O

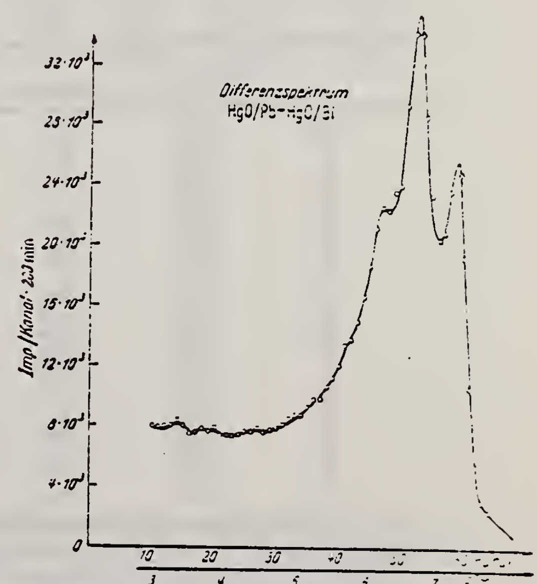

Fig. 2. Spektrum der eigentlichen Resonanzstreuung (Differenz der Spektren von Fig. 1)

REF.	ELEM. SYM.	A	Z
B. Arad (Huebschmann), G. Ben-David (Davis), I. Pelah, Y. Schlesinger Phys. Rev. 133, B684-700 (1964)	Pb	208	82

METHOD	REF. NO.	
Reactor, (n,γ) reactions source	64 Ar 1	NVB

REACTION	RESULT	EXCITATION ENERGY	SOURCE TYPE	SOURCE RANGE	DETECTOR TYPE	DETECTOR RANGE	ANGLE
G,G	ABX	7 - 8	D	7 - 8	NAI-D		135
		(See Table II)					

WIDTH

7.285 MeV resonance:
Self-absorption experiment gives level width $\Gamma_o = 0.8 \pm 0.03$ eV.

TABLE II. Capture gamma-ray sources and their properties.[a]

Source	Chemical composition	Mass kg	Principal γ rays (in MeV)
Al	Metal	1.640	7.73
Cl	polyvinyl Chloride	0.380	8.55, 7.78, 7.41, 6.96, 6.64, 6.12, 5.72
Co	CoO	0.230	7.49, 7.20, 6.98, 6.87, 6.68, 6.48, 5.97, 5.67
Cr	Metallic powder	0.480	9.72, 8.88, 8.49, 7.93, 7.09, 6.65, 5.60
Cu	Metal	1.860	7.91, 7.63, 7.29, 7.14, 7.00, 6.63
Fe	Metallic powder	0.440	9.30, 7.64, 7.28, 6.03
Hg	$Hg_2(NO_3)_2 \cdot 2H_2O$	0.310	6.44, 6.31, 5.99, 5.67, 5.44
Mn	MnO_2	0.240	7.26, 7.15, 7.04, 6.96, 6.79, 6.10, 5.76
Ni	Metal	0.900	9.00, 8.50, 8.10, 7.83, 7.58, 6.84, 6.64
Ti	TiO_2	0.210	6.75, 6.56, 6.42
V	V_2O_5	0.120	7.30, 7.16, 6.86, 6.51, 6.46, 5.87, 5.73
Y	Y_2O_3	0.200	6.07, 5.63

[a] more detailed information, additional lines, intensities, etc., see Ref. 6.

TABLE III. Effective cross sections.

γ source	Energy (MeV)	Scatterer Element	Protons	Neutrons	$\langle\sigma_{\gamma\gamma}\rangle$ (mb)	Notes
Hg	5.44	Hg	80	116, 118, 119, 120, 121, 122, 124	128	
Cl	6.12	Pr^{141}	59	*82*	103	a
V	6.508	Sn	*50*	62, 64–70, 72	14	
Co	6.690	Pr^{141}	59	*82*	2.7	a
Co	6.867	Nd	60	82, 83, 84, 85, 86, 88	22	
Al	6.98	Pb^{208}	*82*	*126*	2900	b
Cl	6.98	Pb	*82*	124, 125, *126*	346	a
Ti	6.996	Bi^{209}	83	*126*	1560	b
Cu	7.01	Sn	*50*	62, 64–70, 72	1000	b
Ti	7.149	Pb^{208}	*82*	*126*	1000	b
Co	7.201	Pb^{208}	*82*	*126*	25	
Mn	7.261	Pb^{208}	*82*	*126*	25	a
Fe	7.285	Pb^{208}	*82*	*126*	4100	a
V	7.305	Pb^{208}	*82*	*126*	12.5	
Hg	7.32	Pb	*82*	124, 125, *126*	5500	c
Fe	7.639	Ni	*28*	30, 32, 34, 36	10.5	d
Fe	7.639	Pr^{141}	59	*82*	10	d
Cr	8.499	Cu	29	34, 36	24.4	
Cr	8.881	Pr^{141}	59	*82*	9.3	
Ni	8.997	Sm	62	*82*, 85–88, 90, 92	2.8	

[a] A large error could be introduced in the cross-section values because of large differences in line intensities quoted by Bartholomew and Higgs and by Groshev *et al.* (Ref. 6).
[b] Because of the low counting rate, thick scatterers were used, which will introduce a systematic error in estimating $\langle\sigma_{\gamma\gamma}\rangle$ for resonances having a high nuclear cross section.
[c] The cross section was evaluated assuming the gamma intensity to be 0.02 photons per 100 captured neutrons (see text).
[d] Reference 6 gives the 7.639 line of iron capture gamma rays as a single line. However, a recent paper by Fiebiger, Kand, and Segel [Phys. Rev. 125, 2031 (1962)] reports two different lines of equal intensities having energies of 7.647 and 7.633 MeV. The present experiment cannot resolve an energy difference of 14 keV, therefore, there is no possibility of deciding which line is responsible for the scattering.

REF.	ELEM. SYM.	A	Z
R.R. Harvey, J.T. Caldwell, R.L. Bramblett, S.C. Fultz Phys. Rev. 136, B126-31 (1964)	Pb	208	82

METHOD	REF. NO.	
Positron annihilation; ion chamber	64 Ha 2	NVB

REACTION		RESULT	EXCITATION ENERGY	SOURCE		DETECTOR		ANGLE
				TYPE	RANGE	TYPE	RANGE	
G,N	176	ABX	6-27	D	6-26	BF3-I		4PI
G,2N	177+	ABX	12-27	D	12-26	BF3-I		4PI

Sample enriched to 99.75% Pb^{208}

176+

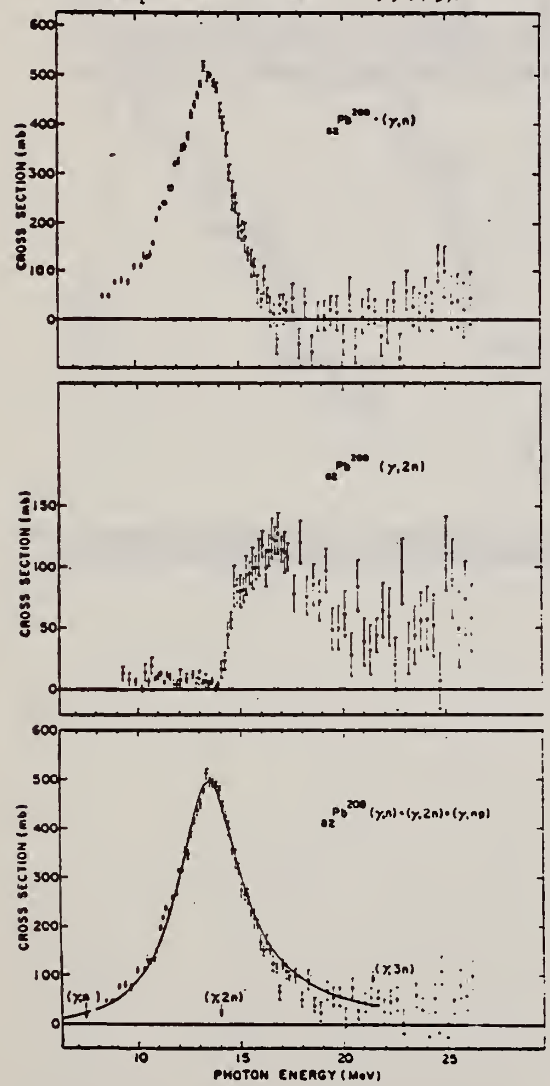

FIG. 3. Top figure shows data points for $\sigma[(\gamma,n)+(\gamma,np)]$ for Pb^{208}, obtained from single-neutron counting data. Center figure shows data for $\sigma(\gamma,2n)$ obtained from double-neutron counting data. Data points for the compound nucleus formation cross section of Pb^{208}, i.e., $\sigma[(\gamma,n)+(\gamma,np)]+\sigma(\gamma,2n)$ are shown in the bottom figure. Solid curve is a plot of a Lorentz line having the parameters given in Table II. The data are uncertain below 8 MeV owing to low beam intensities encountered.

TABLE II. Lorentz line parameters and σ_{-2} values for Pb isotopes and Bi.

Isotope	Peak σ_0 (mb)	Width Γ (MeV)	E_0 (MeV)	σ_{-2} (mb/MeV)	$0.00225A^{5/3}$ (mb/MeV)
Pb^{206}	525	3.75	13.7	15.6±1.6	16.2
Pb^{207}	485	3.87	13.6	14.5±1.5	16.3
Pb^{208}	495	3.78	13.6	14.1±1.4	16.4
Bi^{209}	520	3.83	13.5	16.6±1.7	16.6

TABLE I. Integrated cross sections in MeV-b, up to 28 MeV, for Pb isotopes and Bi.

Isotope	$\int_0^{28}\sigma(\gamma,n)dE$	$\int_0^{28}\sigma(\gamma,2n)dE$	$\int_0^{25}\sigma dE$	$\int_0^{28}\sigma dE+W$	$0.06NZ/A$
Pb^{206}	2.22	0.56	2.78±0.28	3.07±0.36	2.96
Pb^{207}	2.05	0.60	2.65±0.27	2.95±0.30	2.97
Pb^{208}	1.96	0.95	2.91±0.29	3.21±0.32	2.98
Bi^{209}	2.17	0.76	2.93±0.29	3.25±0.33	3.00

FORM NBS-418
(REV. 7-14-64)
USCOMM-DC 28010-P64

REF.	ELEM. SYM.	A	Z
J.A. McIntyre and J.D. Randall Phys. Letters 17, 137 (1965)	Pb	208	82

METHOD	REF. NO.	
Reactor, capture gamma rays Compton scattered	65 Mc 1	EGF

REACTION	RESULT	EXCITATION ENERGY	SOURCE		DETECTOR		ANGLE
			TYPE	RANGE	TYPE	RANGE	
G,G	LFT	7.28	D	7.28	D	NAI	DST

$\Gamma = 0.7 \pm 0.2$ eV

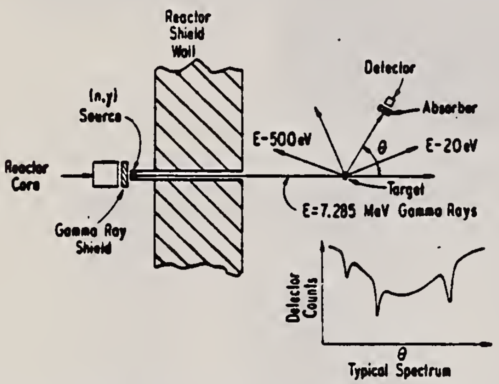

Fig. 1. Schematic diagram of the apparatus. An imaginary "typical" spectrum is shown at the lower right.

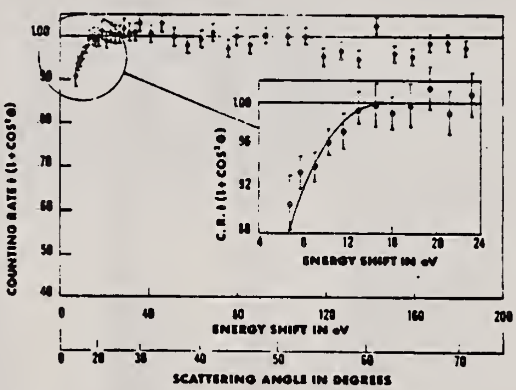

Fig. 2. Angular distribution of the elastically scattered gamma rays. The counting rate has been divided by $1 + \cos^2 \theta$. The two abscissa scales give the scattering angle and the corresponding shift in gamma ray energy with respect to the beam energy. The insert at the right shows the small angle data in detail.

REF.	ELEM. SYM.	A	Z
G. Ben-David, B. Arad, J. Balderman, and Y. Schlesinger Phys. Rev. 146, B852 (1966)	Pb	208	82

METHOD	REF. NO.	
Nuclear Resonance Scattering using N,G reactions.	66 Be 3	JDM

REACTION	RESULT	EXCITATION ENERGY	SOURCE TYPE	SOURCE RANGE	DETECTOR TYPE	DETECTOR RANGE	ANGLE
G,G	RLX	5 - 10	D	5 - 10	NAI-D	5 - 10	135

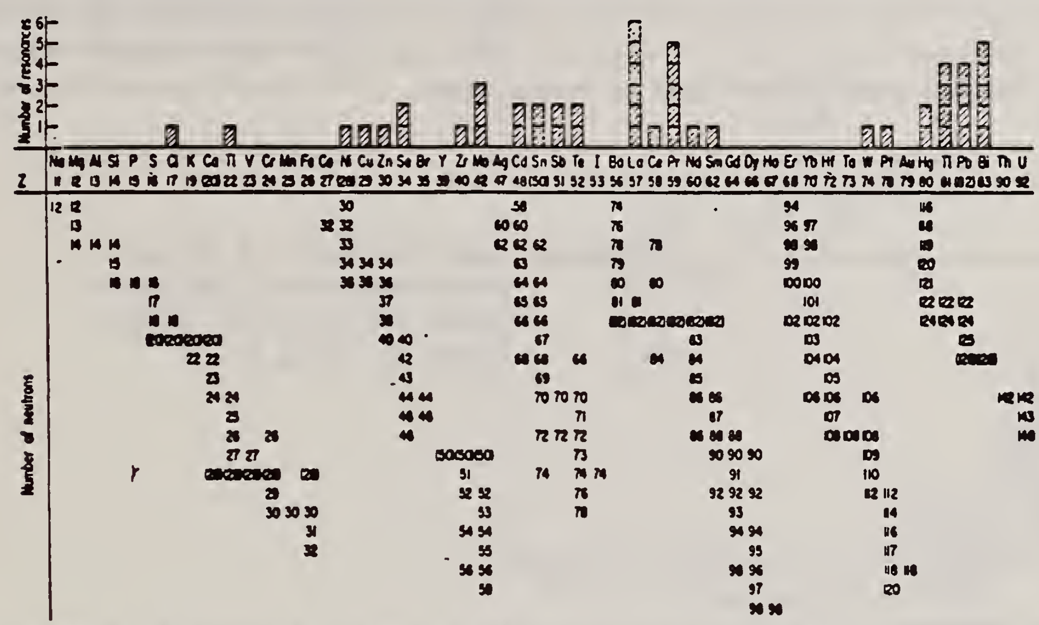

FIG. 3. Histogram of distribution of observed resonances among the different targets. The atomic number is given directly beneath the chemical symbol followed by the neutron numbers of the naturally occurring isotopes. Magic numbers are shown in brackets.

TABLE III. List of effective cross sections.

Scatterer	Energy (MeV)	Gamma source	σ (mb)	Scatterer	Energy (MeV)	Gamma source	σ (mb)
Sm^{144}	8.997	Ni	100	Sn	7.01	Cu	110
Pr^{141}	8.881	Cr	9	Nd	6.867	Co	30
La	8.532	Ni	6	Pr^{141}	6.867	Co	3
Te	8.532	Ni	3^{a}	Te	6.7	Ni	...
Cu	8.499	Cr	24	La	6.54	Ag	12
Zr	8.496	Se	3050	Cd	6.474	Co	110
Zn	8.119	Ni	13	Mo	6.44	Hg	25^{g}
Se	7.817	Ni	50	La	6.413	Ti	72
Se	7.76	K	90	Mo	6.413	Ti	10
Sb	7.67	V	$...^{b}$	Ti	6.413	Ti	25
Cd	7.64	Fe	40^{c}	W	~6.3	Ti	$...^{b}$
Ni	7.64	Fe	7^{c}	Sb	6.31	Hg	6^{a}
Pr^{141}	7.64	Fe	12^{c}	Ti	6.31	Hg	2^{a}
Ti	7.64	Fe	370^{c}	Sn	6.27	Ag	75
La	7.634	Cu	7	Pb^{208}	6.15	Gd	$...^{i}$
Mo	7.634	Cu	11	Te	5.8	Ni	$...^{f}$
Bi^{209}	7.634	Cu	4	La	6.12	Cl	35
Te	7.528	Ni	66^{d}	Pr^{141}	6.12	Cl	110
Bi^{209}	7.416	Se	100	Pt	5.99	Hg	$40^{a,g}$
Bi^{209}	7.300	As	80^{a}	Ti	5.99	Hg	5^{g}
Pb^{208}	7.285	Fe	4100	Pb^{208}	5.9	Sr	$...^{h}$
Cl	7.285	Fe	34	Ce	5.646	Co	17
Pr^{141}	7.185	Se	80	Bi^{209}	5.646	Co	55
Ti	7.16	Cu	120	Pb^{208}	5.53	Ag	70
La	7.15	Mn	50	Hg	5.44	Hg	75^{g}
Bi^{209}	7.149	Ti	2000	Hg	4.903	Co	385

[a] High-energy component of a complex spectrum.
[b] A broad scattered spectrum with no observable peak structure.
[c] There are actually two lines of energies 7.647 and 7.633 MeV having equal intensities in the iron capture gamma spectrum. The cross section has therefore been corrected, although there is no possibility at present of deciding which line is responsible for each resonance.
[d] Is probably an independent level in the complex spectrum of Ni γ rays on Te.
[e] Rough estimate.
[f] May be inelastic component from 7.528 level in Te.
[g] The relative line intensities in this case are due to Groshev and co-workers.
[h] No line is known for the source at this energy.
[i] Difficult to resolve among the many source lines present at this energy.

REF.	ELEM. SYM.	A	Z
E. J. Dowdy and J. A. McIntyre Phys. Rev. 145, B982 (1966)	Pb	208	82
METHOD γ rays from $^{14}N(n,\gamma)^{15}N$ reaction; resonance fluorescence	REF. NO. 66 Do 1		JDM

REACTION	RESULT	EXCITATION ENERGY	SOURCE TYPE	SOURCE RANGE	DETECTOR TYPE	DETECTOR RANGE	ANGLE
G,G	LFT	8	D		NAI		DST

Γ_o = 1.30 ± 0.25 eV assuming level decays only to ground state.

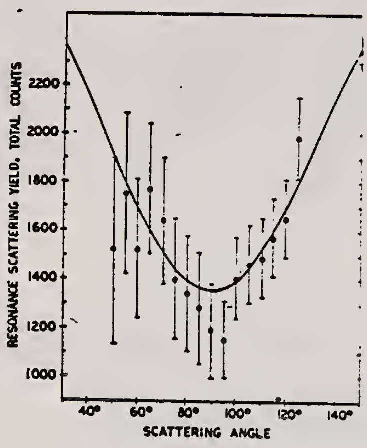

FIG. 6. Angular distribution of the resonance-scattered 7.297-MeV gamma rays. The curve drawn is the distribution 1360 $(1+\cos^2\theta)$.

Erratum: Line observed is 7.277 MeV
corrected width /1.4±0.25 eV.
Phys. Rev. 157, 1166 (1967)
[Ref. No. 67 Do 1]

REF.	ELEM. SYM.	A	Z
G.A. Peterson and J.F. Ziegler Phys. Letters 21, 543 (1966)	Pb	208	82

METHOD	REF. NO.	
	66 Pe 1	JDM

REACTION	RESULT	EXCITATION ENERGY	SOURCE TYPE	SOURCE RANGE	DETECTOR TYPE	DETECTOR RANGE	ANGLE
E,E/	FMF	0-6	D	70	MAG-D		130

Q is 0.21 - 0.65 fm^{-1}.

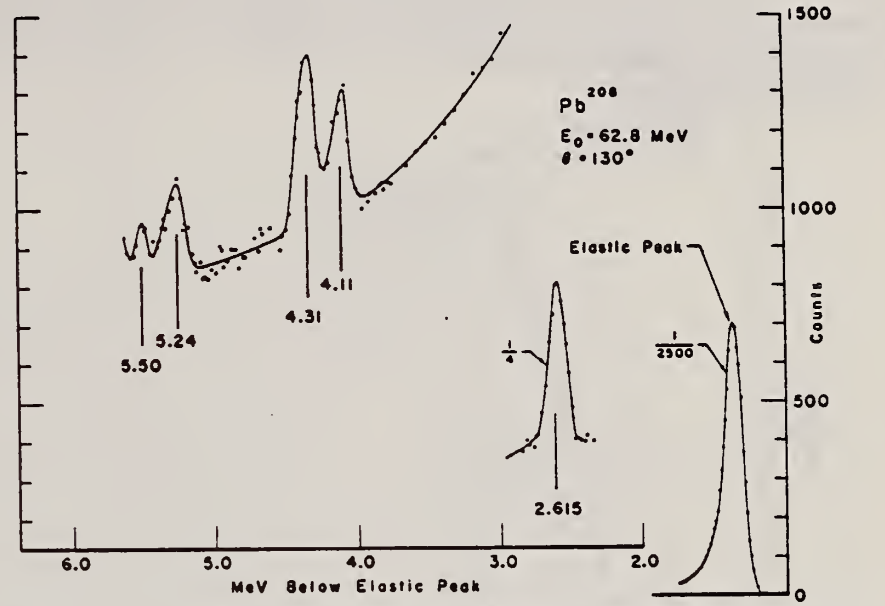

Fig. 1. Energy distribution of 62.8 MeV electrons scattered elastically and inelastically at 130° from a ^{208}Pb target.

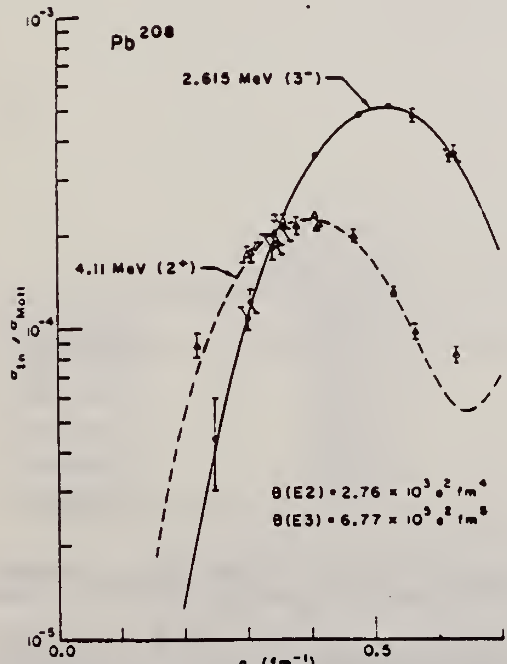

Fig. 2. Inelastic cross section for the excitation of ^{208}Pb in units of the point Mott cross section versus elastic scattering momentum transfer in units of inverse fm.

U.S. DEPARTMENT OF COMMERCE
NATIONAL BUREAU OF STANDARDS

REF.	ELEM. SYM.	A	Z
J. F. Ziegler and G. A. Peterson Proc. Gatlinburg Conference 319 (1966)	Pb	208	82

METHOD	REF. NO.	
	66 Zi 2	hmg

REACTION	RESULT	EXCITATION ENERGY	SOURCE TYPE	SOURCE RANGE	DETECTOR TYPE	DETECTOR RANGE	ANGLE
E,E/	RLX		D	28-70	MAG-D		DST

B(EL)

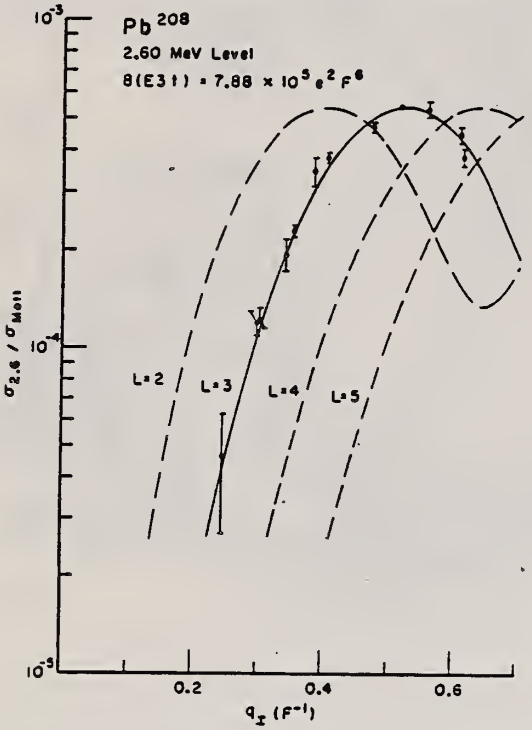

Fig. 2. Inelastic cross sections for the excitation of ^{208}Pb by 70 MeV electrons vs. elastic scattering momentum transfer in inverse Fermi.

TABLE 1

Values of B(E3↑)

Isotope	Energy level	B(E3↑) (e^2b^3)
^{209}Bi	2.58	0.527 ± .012
	2.58 } 2.73 }	0.773 ± .020
^{208}Pb	2.615	0.788 ± .028
^{207}Pb	2.62 } 2.66 }	0.740 ± .012
^{208}Pb	2.60	0.702 ± .032

. Tuan, S. T., and Wright, L. E., Bull. Am. Phys. Soc. 11, 338 (1966); Reynolds, J. T., Ph. D. Thesis, Duke University; Onley, D. S., private communications.

. Elton, L. R. B., "Nuclear Sizes," Oxford Univ. Press, London, 1961); Hofstadter, R., private communication.

REF.	ELEM. SYM.	A	Z
E. J. Dowdy and J. A. McIntyre Phys. Rev. 157, 1166 (1967)	Pb	208	82

METHOD	REF. NO.	
	67 Do 1	hmg

REACTION	RESULT	EXCITATION ENERGY	SOURCE		DETECTOR		ANGLE
			TYPE	RANGE	TYPE	RANGE	
G,G	LFT	7	D	7	NAI-D		DST

ERRATUM FOR 66 DO 1
Phys. Rev. 145, 982
(1969)

REF.	ELEM. SYM.	A	Z
M. Giannini, P. Oliva, D. Prosperi and G. Toumbev Nucl. Phys. A101, 145 (1967)	Pb	208	82

METHOD	REF. NO.	
	67 Gi 1	egf

REACTION	RESULT	EXCITATION ENERGY	SOURCE TYPE	SOURCE RANGE	DETECTOR TYPE	DETECTOR RANGE	ANGLE
G,G	LFT	7	D	6-8	NAI-D	4-8	DST

Note: Varied Doppler Width

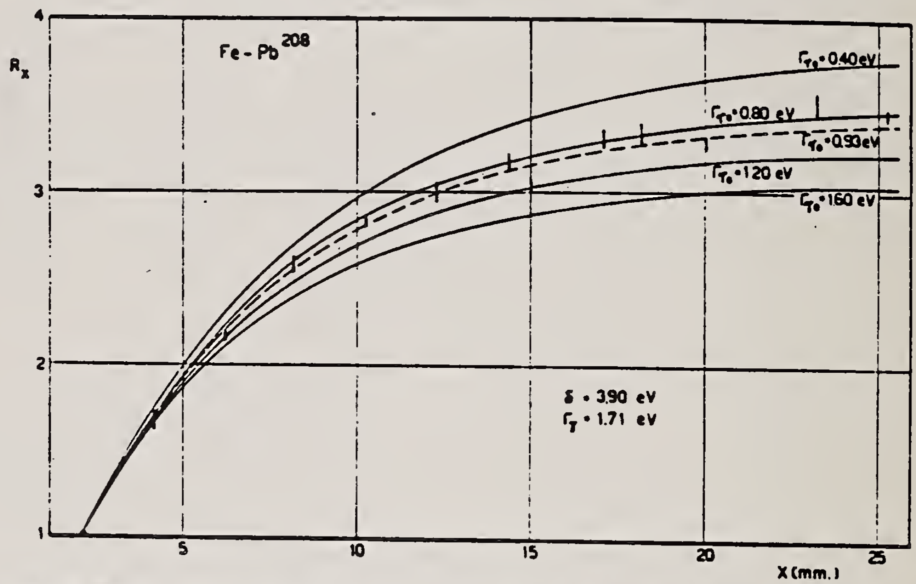

Fig. 8. Relative yield of 7.285 MeV γ-rays scattered from Pb versus the scatterer thickness x for different values of $\Gamma_{\gamma 0}$. Eq. (12) defines R_x.

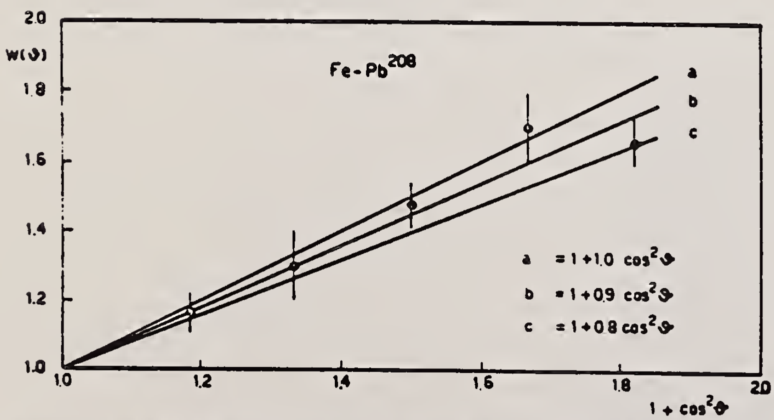

Fig. 2. Relative yield of 7.285 MeV γ-rays scattered from Pb versus $1+\cos^2\theta$, where θ is the angle between the incident beam and the scattered γ-rays.

[over]

TABLE 5

Fe-^{208}Pb resonance

	Our results		Ben David *et al.* [3])
	method (i) [a])	method (ii)	
$\langle\sigma_{\gamma\gamma}\rangle$ (b)	5.2 $\pm$1.5	5.2 $\pm$1.5	4.1
$\bar{\sigma}_{ra}$ (b)	16.2 $\pm$1.0	17.2 $\pm$1.7	
Γ_γ (eV)	1.4 $\pm$0.5	1.7 $\pm$0.6	$\approx$ 0.80 [b])
$\Gamma_{\gamma0}$ (eV)	0.84$\pm$0.05	0.93$\pm$0.09	0.80$\pm$0.03
δ (eV)	3.9 $\pm$0.3	4.0 $\pm$0.3	8.0 $\pm$1.0 [c])

[a]) These values are obtained by applying method (i) to the experimental data reported in our previously published work [4]).

[b]) With the assumption $\Gamma_{\gamma0}/\Gamma_\gamma \approx 1$.

[c]) Using a rotor technique, the authors [3]) obtain $\delta = 6.5\pm1.0$ eV.

REF. R. R. Hurst and D. J. Donahue
Nucl. Phys. A91, 365 (1967)

ELEM. SYM.	A	Z
Pb	208	82

METHOD

Neutron capture gamma rays

REF. NO.	
67 Hu 1	EGF

REACTION	RESULT	EXCITATION ENERGY	SOURCE TYPE	SOURCE RANGE	DETECTOR TYPE	DETECTOR RANGE	ANGLE
G,N	ABX	9-11	D	9-11	BF3-1		4PI

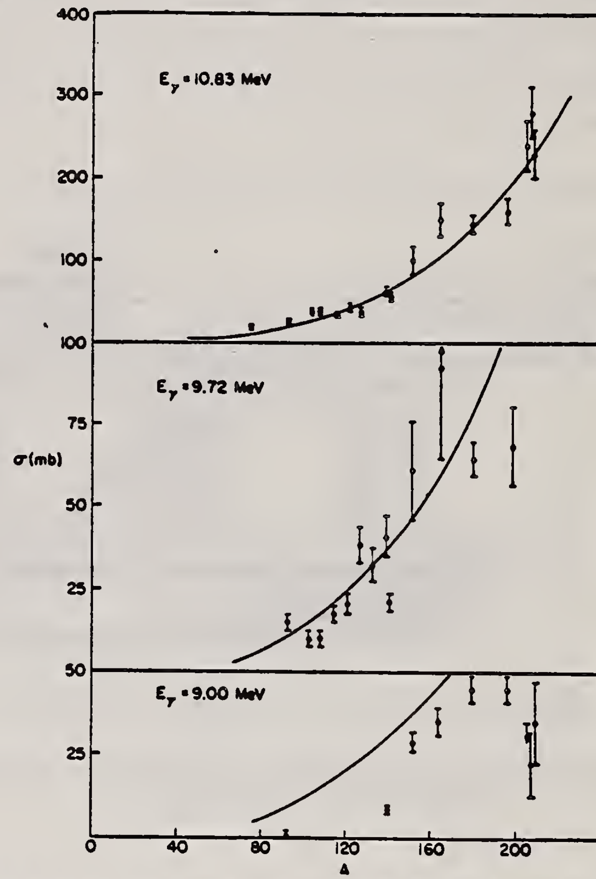

Fig. 1. Cross section (in mb) versus mass number of the target for gamma-ray energies of 9.00, 9.72 and 10.83 MeV. The solid lines are plots of eq. (1) in the text.

TABLE 1
Photoneutron cross sections (mb)

Target	7.72 MeV	9.00 MeV	9.72 MeV	10.83 MeV
^{59}Co				9.0± 0.8
^{75}As				20.4± 1.7
^{93}Nb		0.53± 0.10	14.6± 2.2	25.8± 2.1
^{103}Rh			10.6± 1.7	38.8± 3.1
^{107}Ag, ^{109}Ag			10.0± 1.5	37.6± 2.9
^{115}In			17.1± 2.6	33.3± 2.7
^{121}Sb, ^{123}Sb			20.7± 3.1	42.5± 3.6
^{127}I			38.7± 5.8	38.8± 3.1
^{133}Cs			31.7± 4.8	52.5± 3.8
^{139}La		8.61± 0.86	40.8± 6.5	63.0± 5.0
^{141}Pr			21.5± 3.2	58.3± 4.1
^{151}Eu, ^{153}Eu		28.9 ± 3.2	61.3±14.7	102 ±18
^{165}Ho		35.6 ± 4.3	92.2±27.6	150 ±20
^{181}Ta	4.14±0.36	45.4 ± 3.7	65.0± 5.5	146 ±12
^{197}Au		44.5 ± 3.6	68.4±13.5	160 ±15
^{206}Pb		<34.3		238 ±29
^{208}Pb		22.6 ±11.3		280 ±31
^{209}Bi		36.1 ±12.0		226 ±27

REF.

S. V. Starobdubtsev, R. B. Begzhanov, A. A. Islamov
Dokl. Akad. Nauk SSSR 174, 332 (1967)
Soviet Phys. Dokl. 12, 472 (1967)

ELEM. SYM.	A	Z
Pb	208	82

METHOD

REF. NO.	
67 St 1	egf

REACTION	RESULT	EXCITATION ENERGY	SOURCE TYPE	SOURCE RANGE	DETECTOR TYPE	DETECTOR RANGE	ANGLE
G,G	LFT	7	D	7	NAI-D	4-7	135

Self-absorption measurement

7=7.28 MEV

TABLE 1

Nucleus	Transition energy, MeV	$I_i^\pi \to I_f^\pi$	Γ_γ, eV	Nucleus	Transition energy, MeV	$I_i^\pi \to I_f^\pi$	Γ_γ, eV
$_{28}Ni^{58}_{30}$	7.64	$1^- \to 0^+$	1.0 ±0.10	$_{48}Cd^{114}_{66}$	7.64	$1^- \to 0^+$	0.20±0.05
	6.47	$1^- \to 2^+$	0.33±0.11		7.08	$1^- \to 2^+$	0.05±0.01
	5.60	$1^- \to 2^+$	1.26±0.38		6.50	$1^- \to 0^+$	0.13±0.03
	5.34	$1^- \to 0^+$	0.60±0.18		5.80	$1^- \to 2^+$	0.18±0.04
	5.0	$1^- \to 2^+$	0.36±0.14	$_{82}Pb^{208}_{126}$	7.28	$1^- \to 0^+$	0.78 ±0.03
	4.70	$1^- \to 2^+$	2.15±0.64				

REF. B. I. Goryachev, V. S. Ishkhanov, I. M. Kapitonov, and V. G. Shevchenko
ZhETF Pis'ma 7, 210 (1968)
JETP Letters 7, 161 (1968)

ELEM. SYM.	A	Z
Pb	208	82

METHOD

REF. NO.	
68 Go 3	hmg

REACTION	RESULT	EXCITATION ENERGY	SOURCE TYPE	SOURCE RANGE	DETECTOR TYPE	DETECTOR RANGE	ANGLE
G,XN	ABX	THR-22	C	THR-22	BF3-I		4PI

σ_{int} (18.5 MeV) = 4.0 MeV-barn.

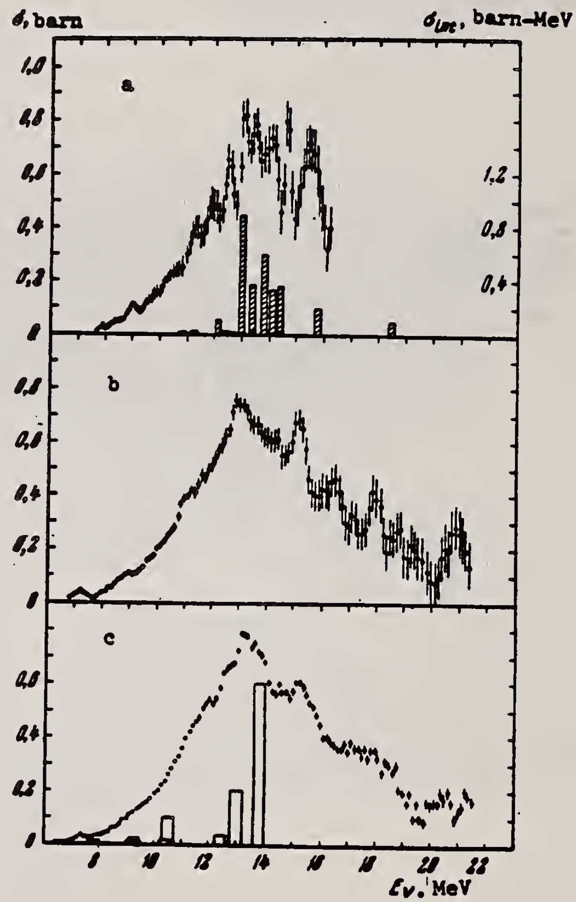

Effective neutron-production cross section in the interaction between γ-quanta and the Pb^{208} nucleus: a - analysis with energy steps ΔE = 0.2 MeV. Vertical columns - theoretical calculations by Bunatyan [3] (the calculated absolute values are marked on the right, the experimental ones on the left); b - analysis in energy steps ΔE = 0.5 MeV; c - analysis in energy steps ΔE = 1.0 MeV. Vertical columns - theoretical calculation of Balashov, Shevchenko, and Yudin [2].

REF.	ELEM. SYM.	A	Z
C. J. Kapadia, V. E. Michalk and J. A. McIntyre Nucl. Instr. and Meth. 59, 197 (1968)	Pb	208	82

METHOD	REF. NO.	
	68 Ka 3	egf

REACTION	RESULT	EXCITATION ENERGY	SOURCE		DETECTOR		ANGLE
			TYPE	RANGE	TYPE	RANGE	
G,MU-T	LFT	7	D	7	NAI-D	7	
		(7.277)		(7.277)			

Used resonance scattering by Pb to vary energy of 7.277 MeV photons from ^{57}Fe neutron capture. Did self-absorption in scattered beam.

7=7.277 MEV

TABLE 1

Values of Γ_0 and δ, for the 7.277 MeV level in ^{208}Pb as obtained to date.

Case no.	Γ_0 (eV)	δ (eV)	Reference no.
1	0.80 ± 0.08	4.8 ± 0.4	a)
2	$0.1 \leqq \Gamma \leqq 4$	≦ 26 eV	b)
3	0.8 ± 0.03	8.0 ± 1	c)
4		6.5 ± 1	d)
5	0.86 ± 0.06	5.0 ± 0.5	e)
6	0.7 ± 0.2		f)
7	0.68 ± 0.09	8.00 ± 0.14	g)
8	0.56 ± 0.08 ($\Gamma_0 = \Gamma$)	7.50 ± 0.60	h)

a) H. H. Fleischmann and F. W. Stanek, Z. Phys. **175** (1963) 172.
b) C. S. Young and D. J. Donahue, Phys. Rev. **132** (1963) 1724.
c) B. Arad, G. Ben-David, I. Pelah and Y. Schlesinger, Phys. Rev. Rev. **133** (1964) B684.
d) B. Arad, G. Ben-David and Y. Schlesinger, Phys. Rev. 136 (1964) B370.
e) M. Giannini, P. Oliva, D. Prosperi and S. Sciuti, Nucl. Physics **65** (1965) 344.
f) J. A. McIntyre and J. D. Randall, Phys. Letters **17** (1965) 137.
g) S. Ramchandran, private communication.
h) This work.

REF.	ELEM. SYM.	A	Z
R. Moreh and M. Friedman Phys. Letters 26B, 579 (1968)	Pb	208	82

METHOD	REF. NO.	
	68 Mo 1	EGF

REACTION	RESULT	EXCITATION ENERGY	SOURCE TYPE	SOURCE RANGE	DETECTOR TYPE	DETECTOR RANGE	ANGLE
G,G	NOX	7	D	7	NAI-D	5-8	90

Compton polarimeter.

Table 1

Properties of levels populated by resonance scattering of iron capture γ rays; J_0 and J denote the spins of the ground and resonance levels, respectively.

Scattering isotope	J_0	Resonance level (MeV)	Resonance spin	$N(90,90)/N(90,0)$ exp.	calc.	Transition character
^{208}Pb	0^+	7.279	1	1.18 ± 0.03	1.18	E1
^{112}Cd	0^+	7.632	1	0.87 ± 0.04	0.855	M1
^{141}Pr	$\frac{5}{2}^+$	7.632	$\frac{7}{2}$	1.03 ± 0.02	1.03	E1
^{62}Ni	0^+	7.646	1	0.88 ± 0.04	0.855	M1
^{203}Tl	$\frac{1}{2}^+$	7.646	$\frac{1}{2}$	1.00 ± 0.01	1.00	-

REF. J. F. Ziegler and G. A. Peterson
Phys. Rev. 165, 1337 (1968)

ELEM. SYM.	A	Z
Pb	208	82

METHOD

REF. NO.	
68 Zi 1	HMG

REACTION	RESULT	EXCITATION ENERGY	SOURCE TYPE	SOURCE RANGE	DETECTOR TYPE	DETECTOR RANGE	ANGLE
E,E/	FMF	2-7	D	28-73	MAG-D	28-73	100

SEP ISTOPS, B(EL)

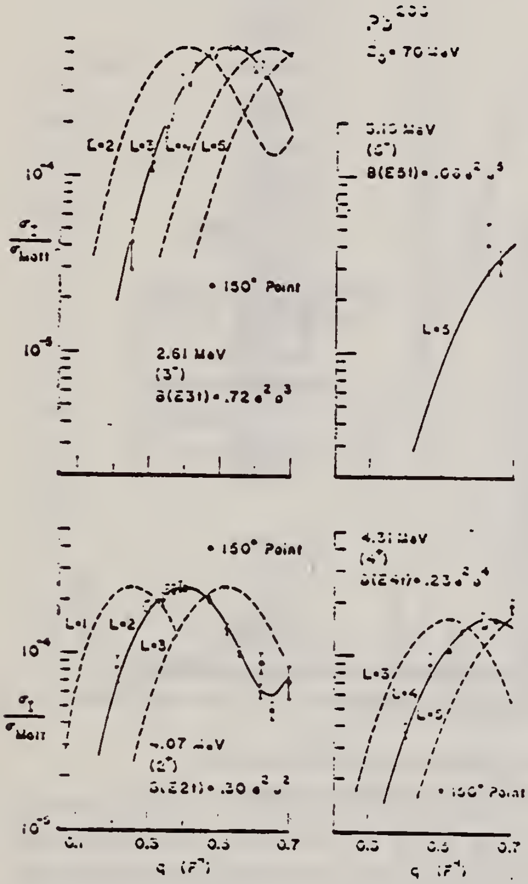

FIG. 11. Experimental relative cross sections versus momentum transferred to the nucleus Pb[illegible] normalized [illegible] electron energy of 70 MeV for excitations at 2.61, 3.1[illegible], and 4.31 MeV. The solid curve is the best fit of the G[illegible] calculation assuming the Tassie hydrodynamical model for the [illegible] transition multipolarity, and the dashed curves are arbitrarily normalized for other transition multipolarities.

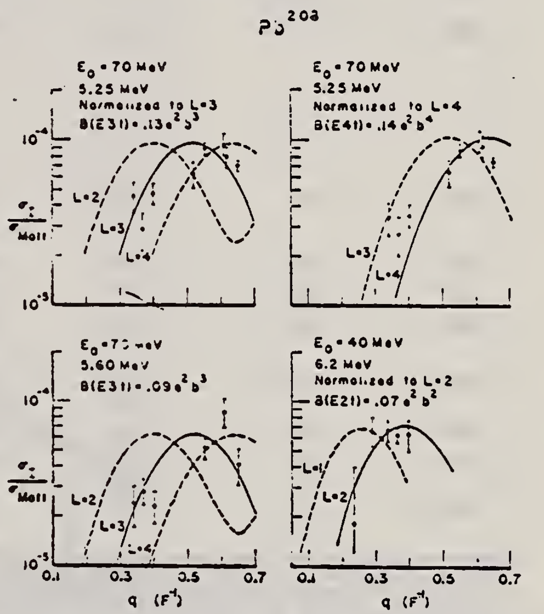

FIG. 12. Experimental relative cross sections versus momentum transferred to the nucleus Pb^{208} normalized to an initial electron energy of 70 MeV for excitations at 5.25 and 5.60 MeV, and to an initial energy of 40 MeV for the 5.2-MeV excitation. The solid curve is the best fit of the GBROW calculation assuming the Tassie hydrodynamical model for the specified transition multipolarity, and the dotted curves are arbitrarily normalized for other transition multipolarities.

OVER

TABLE II. Experimental values of reduced nuclear transition probabilities $B(EL)$ for the excitation of a nucleus from its ground state to an excited state as determined by the electron scattering methods of this experiment and by other methods. The units of $B(EL)$ are e^2b^L where e is the electron charge, b is 10^{-24} cm² (1 b), and L is the multipolarity of the transition. $B(EL)_{sp}$ is the single-particle estimate of Eq. (10).

		This experiment				
Nuclide	Level (MeV)	Transition character	$B(EL, 0\rightarrow L)$ e^2b^L	$G=\frac{B(EL)}{B(EL)_{sp}}$	Ref.	Other experiments $B(EL, 0\rightarrow L)$ e^2b^L
Pb^{206}	4.09	$E2$	0.23±0.02	6.2	a	(p,p')0.20
Pb^{207}	4.080[b] 4.125[b]	$E2$	0.26±0.02	7.0	c d	(α,α')0.33 (p,p')0.18
Pb^{208}	4.07	$E2$	0.30±0.02	8.1	c e	(α,α')0.33 (p,p')0.17
Pb^{206}	2.65	$E3$	0.64±0.04	35	a	(p,p')0.33
Pb^{207}	2.625[b] 2.664[b]	$E3$	0.67±0.04	37	c d	(α,α')0.56 (p,p')0.32
Pb^{208}	2.614	$E3$	0.72±0.04	39.5	c f g e h i j k	(α,α')0.57 (e,e')0.53 (p,p')0.67 (p,p')0.36 $(C^{12},C^{12}\gamma)$0.83 (p,p')0.84 (p,p')0.97 (n,n')0.71
Bi^{209}	2.6[l]	$E3$	0.67±0.05	37	c f m	(α,α')0.57 (e,e')0.55 (p,p')0.65
Pb^{206}	4.32	$E4$	0.22±0.02	25	a	(p,p')0.058
Pb^{207}	4.29	$E4$	0.21±0.03	24	c	(α,α')0.12
Pb^{208}	4.31	$E4$	0.23±0.02	26	c f e	(α,α')0.13 (e,e')0.24 (p,p')0.057
Pb^{208}	5.25	$E3$ $(E4)$	0.13±0.03 0.14±0.07	7.2 16		
Pb^{208}	5.6	$E3$	0.09±0.03	5	c	(α,α')0.16
Pb^{206}	6.2	$E2$ $(E0)$	0.07±0.02	2		
Pb^{208}	3.2	$E5$	0.06±0.02	14	c e	(α,α')0.03 (p,p')0.034

[a] G. Vallois, J. Sandinos, and O. Beer, Phys. Letters 24, 512 (1967).
[b] Peaks were not resolved in this experiment. Energies taken from J. C. Hafele and R. Woods, Phys. Letters 24, 579 (1966).
[c] J. Alster, Phys. Rev. 141, 1138 (1966); Phys. Letters 25B 459 (1967).
[d] G. Vallois, J. Sandinos, O. Beer, M. Gendrot, and P. Lopato, Phys. Letters 22, 659 (1966).
[e] J. Sandinos, G. Vallois, O. Beer, M. Gendrot, and P. Lopato, Phys. Letters 22, 492 (1966).
[f] H. Crannell, R. Helm, H. Kendall, J. Oeser, and M. Yearian, Phys. Rev. 123, 923 (1961); and H. W. Kendall and J. Oeser, *ibid.* 130, 245 (1963).
[g] A. Scott and M. P. Fricke, Phys. Letters 20, 654 (1966).
[h] A. Z. Hrynkiewicz, S. Kopta, S. Szymczyk, and T. Walczak, Nucl. Phys. 79, 495 (1966), references cited therein, and see text of this section.
[i] G. R. Satchler, R. H. Bassel, and R. M. Drisko, Phys. Letters 5, 256 (1963).
[j] T. Stovall and N. M. Hintz, Phys. Rev. 135, B330 (1964).
[k] P. H. Stelson *et al.*, Nucl. Phys. 68, 97 (1965).
[l] Approximate energy of seven unresolved peaks, J. C. Hafele and R. Woods, Phys. Letters 24, 579 (1966).
[m] S. Hinds, H. Marchant, J. H. Bjerregaard, and O. Nathan, Phys. Letters 20, 674 (1966).

REF. H. Beil, R. Bergere, P. Carlos and A. Veyssiere
C.R. Acad. Sci. Paris 269, 216 (1969)

ELEM. SYM.	A	Z
Pb	208	82

METHOD

REF. NO.	
69 Be 9	egf

REACTION	RESULT	EXCITATION ENERGY	SOURCE TYPE	SOURCE RANGE	DETECTOR TYPE	DETECTOR RANGE	ANGLE
G,XN	ABX	7-19	D	7-19	MOD-I		4PI

23+

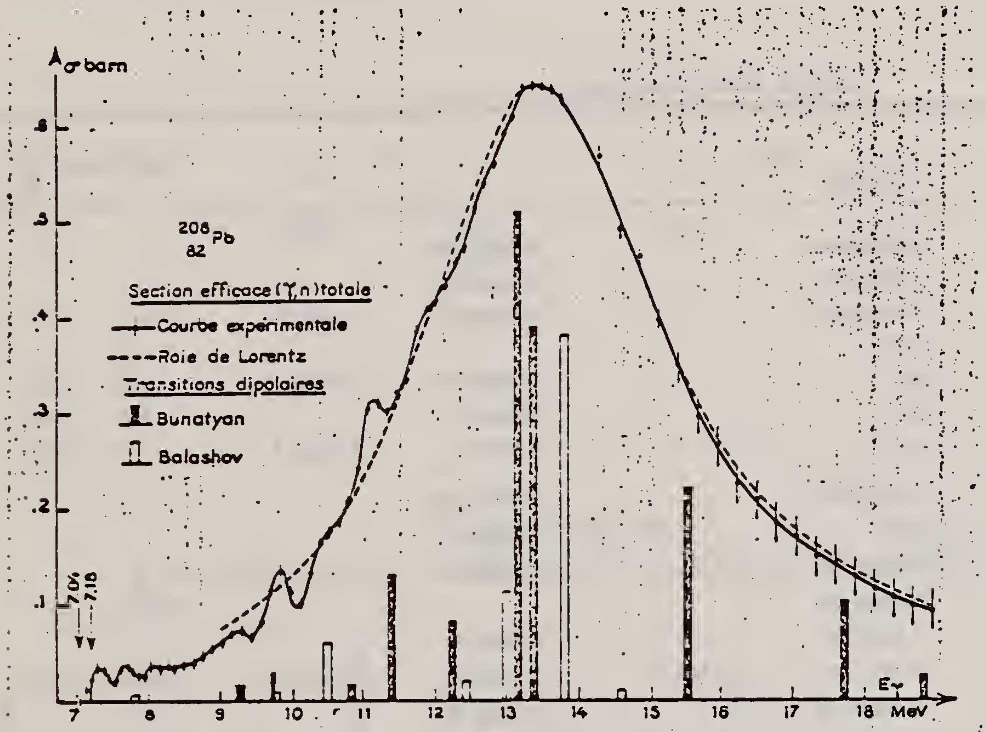

$E_\gamma = 10$ MeV [12]. Les sections efficaces $\sigma(\gamma, n)$, $\sigma(\gamma, 2n)$, $\sigma(\gamma, 3n)$ et $\sigma(\gamma, 4n)$ qui constituent au moins de 99 % de la section efficace $\sigma_T(\gamma, \text{total})$ ont été mesurées séparément avec un scintillateur liquide, chargé au Gd, détectant les photoneutrons avec une grande efficacité d'environ 60 % [13]. La cible de plomb contenait 91 % de ^{208}Pb.

REF.	ELEM. SYM.	A	Z
C. D. Bowman, B. L. Berman, and H. E. Jackson Phys. Rev. 178, 1827 (1969)	Pb	208	82

METHOD	REF. NO.	
	69 Bo 1	hmg

REACTION	RESULT	EXCITATION ENERGY	SOURCE TYPE	SOURCE RANGE	DETECTOR TYPE	DETECTOR RANGE	ANGLE
G,N	SPC	THR-10	C	7-10	TOF-D		135

Tablular data given. G-WIDTH

TABLE VI. Resonance parameters.

Isotope	Energy in (n,γ) This work	b	c	$g\Gamma_{\gamma 0}$[a] This work	d	$g\Gamma_\gamma$ c	b	Spectroscopic data b	d
	(keV)	(keV)	(keV)	(eV)	(eV)	(eV)	(eV)	l	J^π
Pb^{208}	3.00		3.02	0.08±0.03[e]		0.078±0.005			
	10.4		10.2	0.06±0.02		0.13±0.02			
	16.6	16.7	16.2	0.14±0.04		0.66±0.07	0.3±0.07	(>0)	(2^+)
	25.3			<0.2					
		29	29.5	<0.4		0.20±0.06	0.35±0.13	(>0)	(2^+)
		37	37.6	<0.4		0.7±0.1		(>0)	(2^+)
	40.9[g]	41.7	41.0	4.13	4.13	3.8±0.4	4.13±0.9	0	(1^-)
Pb^{207}	3.4		3.36	0.14±0.03		0.077±0.006			
			10.8	<0.05		0.06±0.01			
	11.4[g]		11.3	0.54±0.08		0.07±0.02			
	12.3	12.2		0.05±0.03				(>0)	
	14.6[g]		14.2	0.55±0.10		0.20±0.04			
	16.6[f]	16.5	16.5	0.63	0.63±0.03	0.70±0.08	0.8±0.12	(>0)	$(\frac{1}{2}^-)$
	20.1		19.6	0.169±0.08		0.32±0.06			
		21	21.8	<0.05		0.28±0.1	0.18±0.07		
	25.1	25.1	24.9	0.4±0.15	0.28±0.03	1.1±0.2	0.77±0.12	(>0)	$(\frac{1}{2}^-)$
Pb^{206} [h]	1.55			0.40±0.06					
	7.34			3.4±0.30					
	10.2			1.0±0.15					
	16.0			0.50±0.15					
	33.6								
	49.9								

[a] The statistical factor g is different depending on whether neutrons or photons excite the nucleus. To make easier a comparison of the results, the present values for Pb^{208} and Pb^{207} have been multiplied by the ratio $(2I'+1)/(2I''+1)$ where I' is the spin of the target for the photonuclear experiment and I'' is the target spin for the inverse experiment. The Pb^{208} values are unmodified.
[b] Reference 4.
[c] Reference 6.
[d] Reference 7.

[e] The uncertainties in the values for $g\Gamma_{\gamma 0}$ for all isotopes do not include a ±15% uncertainty in normalization.
[f] The present data were normalized at these resonances using the data from Ref. 7.
[g] These peaks are associated with transitions both to the ground state and the first excited state of Pb^{208}. The excited-state transitions are the stronger (see text).
[h] For Pb^{206}, the energies have not been transformed into the (n,γ) system.

REF.	ELEM. SYM.	A	Z
C. D. Bowman, R. J. Baglan and B. L. Berman Phys. Rev. Letters <u>23</u>, 796 (1969)	Pb	208	82
METHOD	REF. NO. 69 Bo 4		hmg

REACTION	RESULT	EXCITATION ENERGY	SOURCE TYPE	SOURCE RANGE	DETECTOR TYPE	DETECTOR RANGE	ANGLE
G,N	ABX	THR-8	D	8	TOF-D		135

Erratum attached:
Phys. Rev. Letters <u>24</u>, 193 (1970)

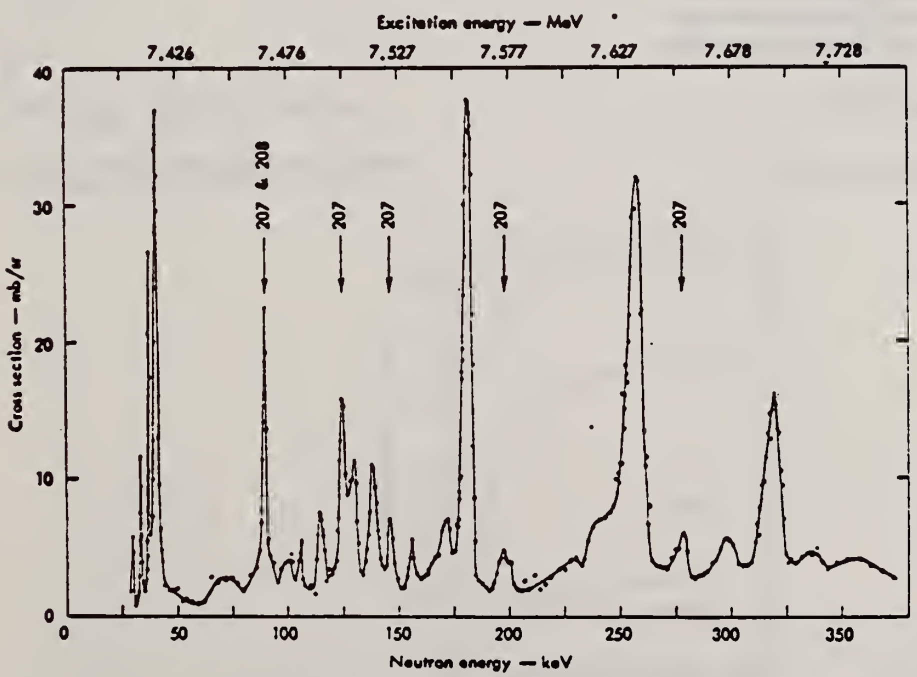

FIG. 1. Threshold photoneutron cross section in mb/sr for natural lead derived from the neutron spectrum emitted at 135° as a function of both laboratory neutron energy and incident photon energy. Levels not Pb^{208} are designated by vertical arrows.

over

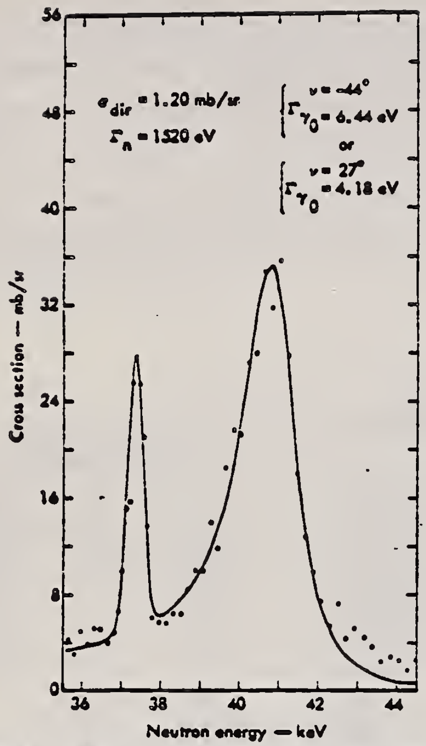

FIG. 2. The data of this figure are taken from Fig. 1. The solid curve is a shape fitted to the data using the resolution determined from the narrow peak at 37.3 keV. The spins for the 37.3- and 40.7-keV peaks are 2^+ and 1^-, respectively (Ref. 14), so there is no interference between them.

L. G. Moretto, R. C. Gatti, S. G. Thompson, J. T. Routti, J. H. Heisenberg, L. M. Middleman, M. R. Yearian, R. Hofstadter
Phys. Rev. 179, 1176 (1969)

ELEM. SYM.	A	Z
Pb	208	82

METHOD

REF. NO. 69 Mo 1 — hmg

REACTION	RESULT	EXCITATION ENERGY	SOURCE TYPE	SOURCE RANGE	DETECTOR TYPE	DETECTOR RANGE	ANGLE
E,F	ABX	THR-999	D	60-999	TRK-I		DST
G,F	ABX	THR-999	C	60-999	TRK-I		DST

Tabular data given; angular distribution isotopes — 999=1 GEV

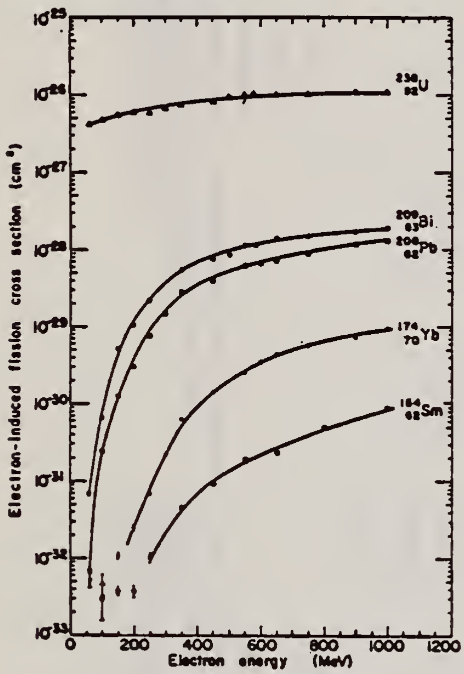

Fig. 2. Electron-induced fission cross-section data. Different symbols for the same isotope refer to different targets.

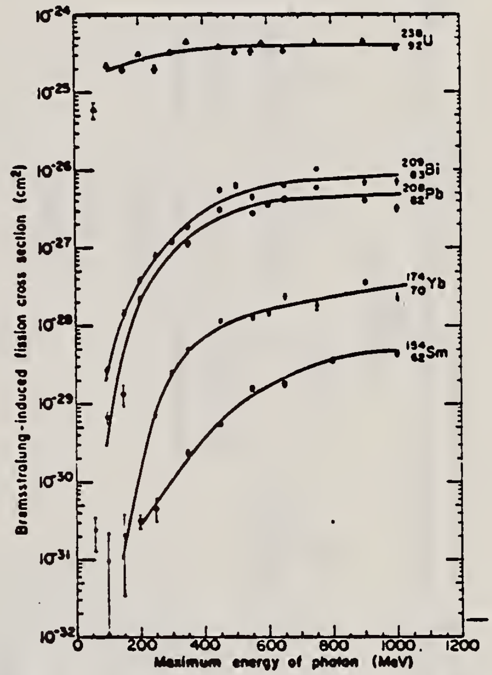

Fig. 4. Bremsstrahlung-induced fission cross section per equivalent quantum.

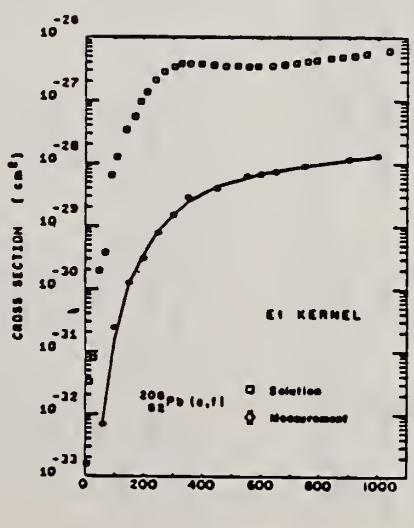

Fig. 8. Photofission cross section as a function of energy for $^{208}_{82}$Pb (open squares) as obtained by unfolding the electron-induced fission cross-section data (diamonds) with the $E1$ kernel. The solid line is the fit to the electron-induced fission cross sections which is obtained by folding back the photofission cross section into the $E1$ kernel.

REF.	ELEM. SYM.	A	Z
S. Ramchandran and J. A. McIntyre Phys. Rev. 179, 1153 (1969)	Pb	208	82
METHOD	REF. NO. 69 Ra 1		hmg

REACTION	RESULT	EXCITATION ENERGY	SOURCE		DETECTOR		ANGLE
			TYPE	RANGE	TYPE	RANGE	
G,G	LFT	8	D	8	NAI		DST

$W(\Theta) \sim [1 + a\, P_2(\cos\Theta)]$

8 = 7.277 MEV

[over]

Table II. Experiment compared to theory assuming a pure dipole transition.

			$\alpha \pm \Delta\alpha$ (Experimental)							
^{90}Zr	Cd	Sn	Hg	^{205}Tl	^{208}Pb	^{209}Bi (7.416 MeV)	^{209}Bi (7.149 MeV)	$A_2^2(J_0, J_1, L=1)$ (Theoretical)	J_0	J_1
0.489±0.027	0.488±0.034	0.490±0.095	0.48±0.11		0.485±0.026			0.500	0	1
	0.488±0.034	0.490±0.095	0.48±0.11	0.0017±0.0110				0.000	1/2	1/2
	0.488±0.034	0.490±0.095	0.48±0.11	0.0017±0.0110				0.250	1/2	3/2
			0.48±0.11					0.000	3/2	1/2
			0.48±0.11					0.160	3/2	3/2
			0.48±0.11					0.140	3/2	5/2
						0.195±0.033	0.184±0.074	0.024	9/2	7/2
						0.195±0.033	0.184±0.074	0.194	9/2	9/2
						0.195±0.033	0.184±0.074	0.083	9/2	11/2

Table V. Summary of energy-level parameters.

Element	^{90}Zr	Cd	Sn	Hg	^{205}Tl	^{208}Pb	^{209}Bi	^{209}Bi
Level energy (MeV)	8.496[a]	6.485[b]	6.988[c]	4.906[b]	7.647[d]	7.277[e]	7.416[e]	7.149[e]
γ ray source	Se	Co	Cu	Co	Fe	Fe	Se	Ti
$J_0 \to J_1$	0→1	0→1	0→1	0→1	1/2→1/2	0→1	9/2→7/2	9/2→7/2
		(1/2→3/2)	(1/2→3/2)	3/2→5/2	(1/2→3/2)		9/2→9/2	9/2→9/2
				(1/2→3/2)			9/2→11/2	9/2→11/2
				(3/2→3/2)				
Γ_0/Γ	0.8±0.2				0.85±0.17[f]	$0.95_{-0.11}^{+0.05}$	0.6±0.2	
Γ_0 (eV)	1.68±0.02				1.0[f]	0.68±0.03	0.14±0.09	
ε (eV)	5.60±0.15				11.5±0.2[f]	8.00±0.14	3.4±1.6	

[a] L. V. Groshev, V. N. Lutsenko, A. M. Demidov, and V. I. Pelekov, *Atlas of Gamma Spectra from Radiative Capture of Thermal Neutrons* (Pergamon Press, Inc., New York, 1959).
[b] E. B. Shera and D. W. Hafemeister, Phys. Rev. 150, 894 (1966).
[c] H. H. Bolotin (private communication from L. M. Bollinger).
[d] R. Moreh and G. Ben-Yaacov, Nuclear Research Center—Negev Report, NRCN-180, 1967, (unpublished).
[e] L. V. Groshev, A. M. Demidov, G. A. Kotelnikov, and V. N. Lutsenko, Nucl. Phys. 58, 465 (1964); G. T. Ewan and A. J. Tavendale, Nucl. Instr. Methods 26, 183 (1964).
[f] See Ref. 24a.

REF.	ELEM. SYM.	A	Z
V. V. Verbinski and W. R. Burrus Phys. Rev. 177, 1671 (1969)	Pb	208	82
METHOD	REF. NO. 69 Ve 1		hmg

REACTION	RESULT	EXCITATION ENERGY	SOURCE TYPE	SOURCE RANGE	DETECTOR TYPE	DETECTOR RANGE	ANGLE
G,XN	SPC	THR-33	C	33	TOF-D	0-14	DST

ENRICHED PB208

TABLE II. (γ,n) reactions induced by 33-MeV end-point thin-target bremsstrahlung.

Target	E_γ giant resonance peak (MeV)	θ	T[a] (MeV)	Thresholds (γ,n)	Thresholds (γ,pn)	Thresholds $(\gamma,2n)$
^{27}Al	~22	55°	3.07±0.1	13.1	19.4	24.4
		93°	3.07±0.1			
^{206}Pb	~13	90°	1.50±0.1	8.0	14.8	14.8
		141°	1.43±0.1			
^{208}Pb	~13	90°	1.52±0.1	7.4	14.8	14.1
		141°	1.52±0.1			
^{209}Bi	~13	90°	1.66±0.1	7.4	11.1	14.3
		141°	1.47±0.1			

[a] From plot of $\ln[\phi(E)/\sigma_c E^{5/11}]$ versus E.

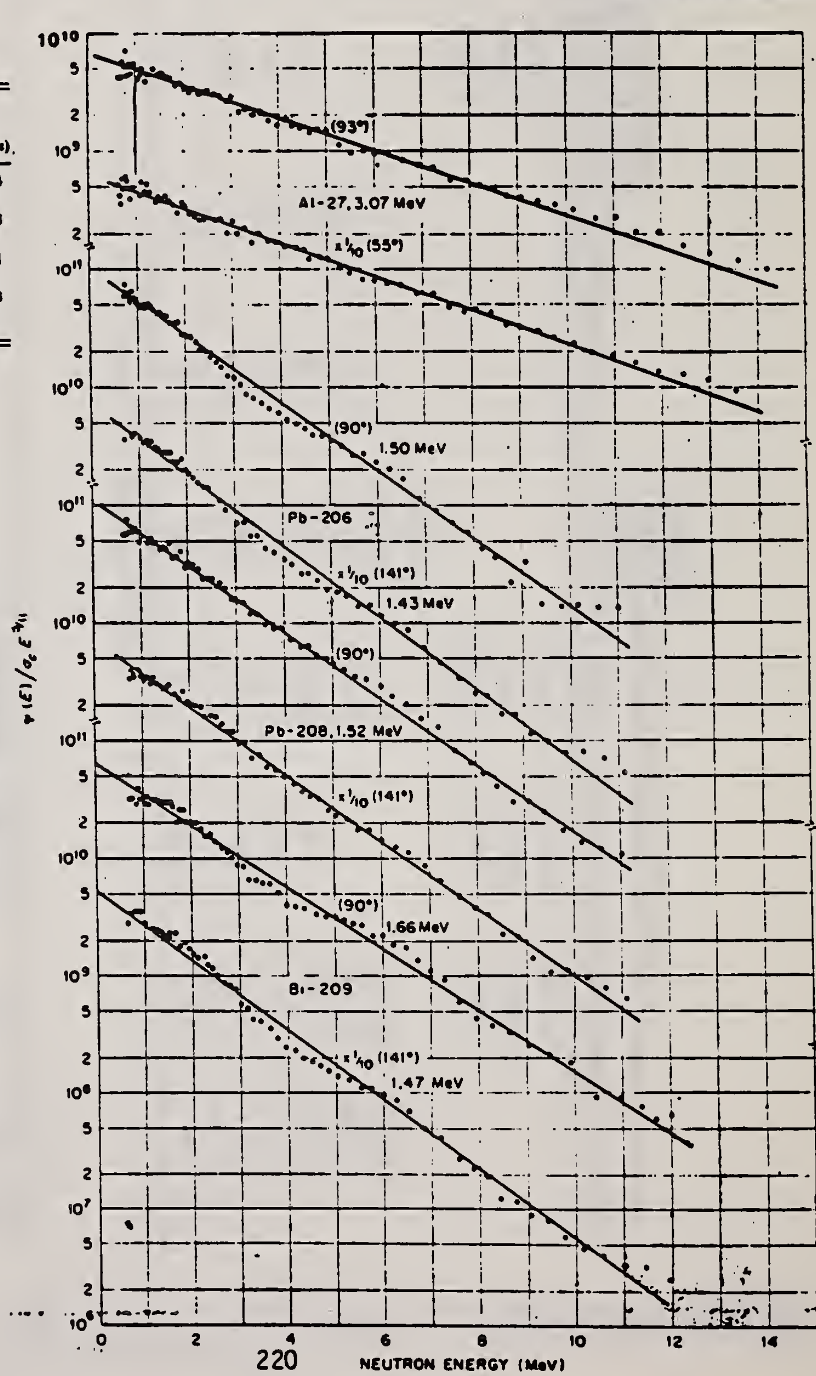

FIG. 7. Evaporation-analysis plots of neutron spectra from (γ,n) reactions. The logarithmic plots of $\phi(E)/(\sigma_c E^{5/11})$ show moderately good straight-line fits. Values of T, the magnitude of the reciprocal slope, are shown. In some cases, T is slightly higher at 90° than at 141°, indicating that a weak component of direct emissions is present. These are preferentially emitted at 90°, the direction of the electromagnetic field.

REF.

C. D. Bowman, R. J. Baglan, and B. L. Berman
Phys. Rev. Letters 24, 193 (1970)

ELEM. SYM.	A	Z
Pb	208	82

METHOD

REF. NO.	
70 Bo 1	hmg

REACTION	RESULT	EXCITATION ENERGY	SOURCE		DETECTOR		ANGLE
			TYPE	RANGE	TYPE	RANGE	
G,N	ABX	THR-8	D	8	TOF-D		135

ERRATUM FOR 69 BO 4
PRL 23, 796 (1969)

REF.	ELEM. SYM.	A	Z
C.D. Bowman, R.J. Baglan, B.L. Berman, T.W. Phillips Phys. Rev. Letters 25, 1302 (1970)	Pb	208	82

METHOD	REF. NO.	
	70 Bo 2	hmg

REACTION	RESULT	EXCITATION ENERGY	SOURCE TYPE	SOURCE RANGE	DETECTOR TYPE	DETECTOR RANGE	ANGLE
G,N	ABX	7 - 9	C	- 10	TOF-D	0-1	DST
		(7.38 - 8.43)		(- 9.8)			

SEVEN 1+ LEVELS

From threshold photoneutron cross-section and angular-distribution measurements on ^{208}Pb, seven 1^+ states have been detected, which have a total *M*1 strength of 51 eV. This *M*1 strength, centered at an excitation energy of 7.9 MeV and spread over a range of 700 keV, constitutes at least half and perhaps all of the total *M*1 strength obtained from shell-model calculations.

Table I. ^{208}Pb resonance parameters.

E_ℓ (keV)	$\frac{4\pi A}{2\pi^2 \lambda^2}$ (eV)[a,b]	$\frac{d\sigma}{d\Omega}\Big\vert_{90^\circ} / \frac{d\sigma}{d\Omega}\Big\vert_{135^\circ}$ Multiplicity	Recoil	J^π Ang. Dist.	π σ_t^c	J^π Final	$\Gamma_{\gamma 0}$ (eV)
30.2	0.30	1.41 ± 0.20		1^+		1^+	0.23
37.5	1.8	0.64 ± 0.09		2^+		2^+	0.64
40.8	7.2	1		1^-		1^-	4.8
90.0	2.6						
124	2.0	1.54 ± 0.22		1^+	+	1^+	1.6
129	5.4				+	$1^+,2^+$	(3.6,1.9)
182	16.0	1.61 ± 0.23	1.45 ± 0.20	1^+	+	1^+	12.6
257	26.2	1.10 ± 0.15	1	$1^-,1^+$	-	1^-	17.5
323	11.0	1.10 ± 0.15	1.13 ± 0.16	$1^-,1^+$	+	1^+	7.7
547	12.3	1.14 ± 0.16	0.94 ± 0.13	$1^-,1^+$		$1^-(1^+)$	8.2
620	17.2	1.80 ± 0.25	1.81 ± 0.25	1^+		1^+	14.6
660	8.6	1.15 ± 0.16	1.37 ± 0.20	1^+		1^+	6.3
860	10.0	1.51 ± 0.21	1.46 ± 0.20	1^+		1^+	7.8

[a] Errors in measurement of area are less than 10%. The integrations were carried out on the 135° data of Fig. 1.

[b] No states with values larger than 3 eV were observed between 860 and 1200 keV.

[c] Ref. 8. [E.G. Bilpuch, private communication.]

[over]

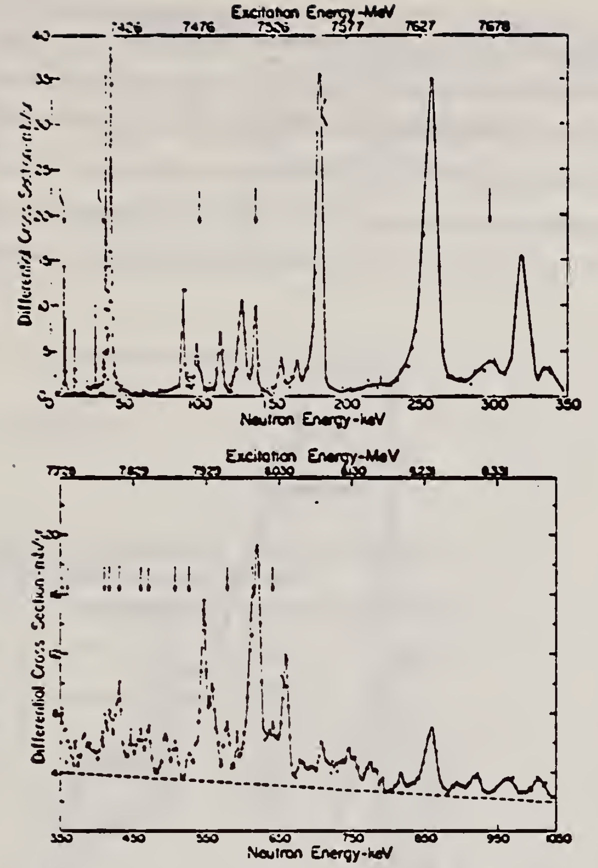

FIG. 1. The 135° differential photoneutron cross section for ^{208}Pb as a function of both the energy of the detected neutron and the corresponding excitation energy of the nucleus. The data of the two plots were taken with different detectors, possessing different resolution and background characteristics. The arrows in the upper plot denote resonances associated with transitions to states other than the ground state of ^{207}Pb. The data of the lower plot were taken with a natural lead sample — hence, the presence of contamination from resonances in ^{207}Pb (arrows). The dashed line in the lower plot represents background in that measurement. The error flags in both plots indicate statistical uncertainties only.

REF.	J. H. Heisenberg and I. Sick Phys. Letters 32B, 249 (1970)	ELEM. SYM.	A	Z
		Pb	208	82

METHOD	REF. NO.	
	70 He 2	egf

REACTION	RESULT	EXCITATION ENERGY	SOURCE		DETECTOR		ANGLE
			TYPE	RANGE	TYPE	RANGE	
E,E/		3	D	248,502	MAG-D		DST
		(2.6)					

q 0.5 fm^{-1} to 2.8 fm^{-1}

3 = 2.6 MEV

Analyzed for transition charge density

$$\rho_{tr}(r) = r^{L-1} \frac{d}{dr}\rho(r, c_{tr}, z_{tr})$$

$$\rho_1 = [1 + \exp((r^2 - c^2)/z^2)]^{-1}$$

$$\rho_2 = [1 + \exp((r-c)/z)]^{-1}$$

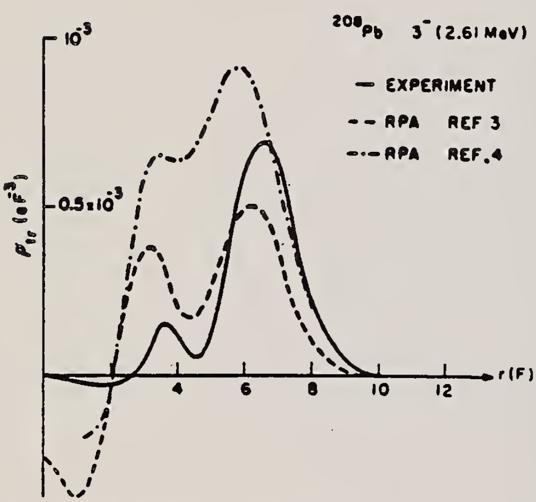

Fig. 3. Transition charge density —— best fit --- RPA calculation of ref. [3] ----- RPA calculation of ref. [4].

[3])V. Gillet, A.M. Green and E.A. Sanderson, Phys. Letters 11, 44 (1964); Nucl.Phys. 88 (1966)321.
[4])J. Blomquist, Phys. Letters 28, 22 (1968).

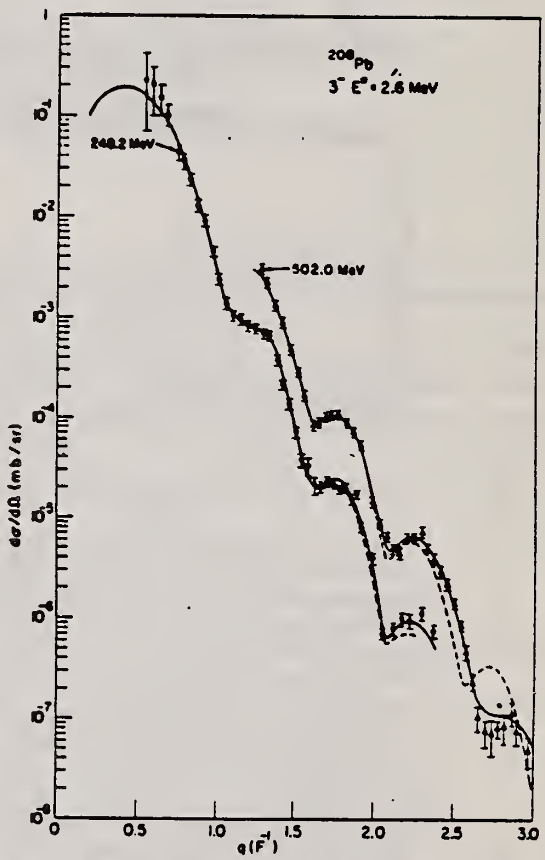

Fig. 2. Inelastic cross sections and calculated curves: —— best fit ----- modified Tassie model.

Table 1

Shape	c_{tr}	z_{tr}
1	6.414 fm	0.562 fm
2	6.250 fm	2.930 fm

REF.	B.S. Ishkhanov, I.M. Kapitonov, E.V. Lazutin, I.M. Piskarev, and O.P. Shevchenko Yad. Fiz. 12, 682 (1970) Sov. J. Nucl. Phys. 12, 370 (1971)	ELEM. SYM.	A	Z
		Pb	208	82
METHOD		REF. NO.		
		70 Is 3		hmg

REACTION	RESULT	EXCITATION ENERGY	SOURCE TYPE	SOURCE RANGE	DETECTOR TYPE	DETECTOR RANGE	ANGLE
G,XN 264	ABX	7-18	C	7-18	BF3-I		4PI
		(7.4 - 17.4)		(7.1-17.4)			
							264

Table I. Locations and integrated cross sections of individual resonances

Experiment, present work			Theory					
E_m, MeV	σ_m^{int}, MeV-mb	σ_m^{int}, %	E_m, MeV (ref. 8)	σ_m^{int}, % [8]	E_m, MeV (ref. 9)	σ_m^{int}, % [9]	E_m, MeV (ref. 9)	σ_m^{int}, % [9]
7.65	19.50	0.56						
			7.80	0.81				
8.06	12.63	0.38						
8.38	16.56	0.47						
8.78	18.61	0.53						
9.03	33.40	0,96						
					9.10	0.69		
			9.20	1.19	9.20	3.45		
			9.30	0.62				
9.40	34.20	0.98						
9.81	71.1	2.04			9.50	1.38		
					10.00	3.10		
							10.10	0.34
					10.20	2.76		
10.29	72.2	2,07						
			10.40	0,61				
			10.50	10,50				
10.62	63.8	1.83			10.60	5.17		
10.93	76.6	2.20			11.00	7.59	11.00	0.34
11.24	145.0	4.15						
					11.60	36.54		
11.76	247.5	7.10						
					12.10	4.14		
12.30	265	7.61						
			12.40	3.86			12.40	0.34
					12.50	12.40		
							12.60	0.68
12.84	331	9.50						
			13.00	18.95				
13.25	344	9.87						
							13.20	12.75
					13.40	0.69		
13.78	214	6.14	13.80	63.02			13.80	10.72
14.08	316	9.06			14.10	14.50	14.10	19.80
							14.30	0.68
							14.50	44.62
14.66	245	7.03						
15.13	210	6,02			15.20	5.52		
15.73	88	2.52						
							16.10	7.38
16.40	114	3.26						
					16.80	2.07		
17.13	98	2.81						
17.95	150	4.30					18.80	2.35
18.76	78	2.24						
19.52	88	2.52						
20.81	135	3.87						

Table II. Integrated parameters of cross sections for photoneutron reactions for Pb^{208}

Type of reaction	E_m, MeV	Γ_m, MeV	σ_m, mb	$\sigma_{int} = \int_0^s \sigma dE$, MeV-mb	s	Source of data
(γ, Tn)	13.34	4.5	900	3260	17.2	Present work
(γ, Tn)	13.5	4.5	800	4000	18.5	[10]
(γ, Tn)	13.5	4.5	900	3930	18.5	[8]
(γ, n)	13.5	3.0	495	1960	28	[6]
(γ, 2n)	16.5	>5.0	117	950	28	[6]

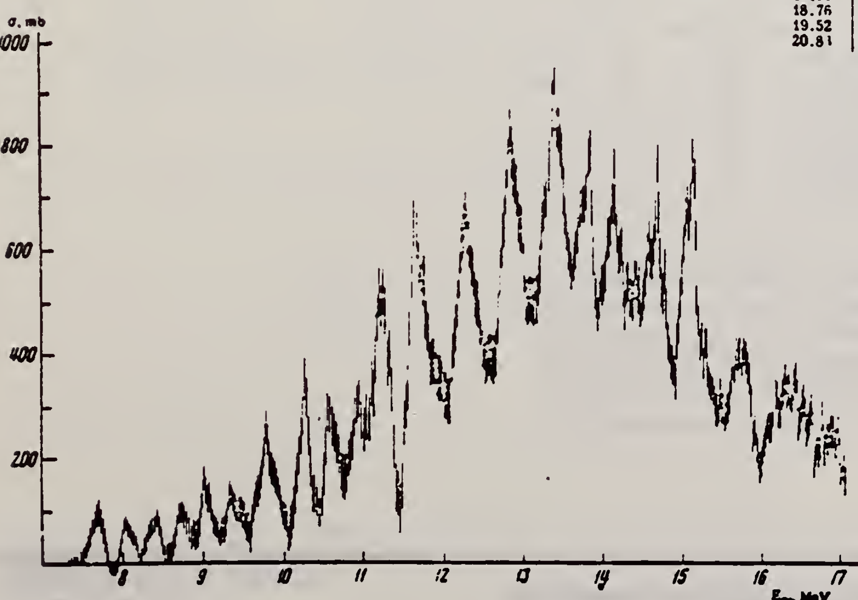

FIG. 1. Structure of the cross section for the reaction $Pb^{208}(\gamma, Tn)$.

$\sigma(\gamma, Tn) = \sigma(\gamma, n) + 2\sigma(\gamma, 2n)$

REF.	ELEM. SYM.	A	Z
R. Moreh, S. Shlomo, and A. Wolf Phys. Rev. C2, 1144 (1970)	Pb	208	82

METHOD	REF. NO.	
	70 Mo 2	hmg

REACTION	RESULT	EXCITATION ENERGY	SOURCE TYPE	SOURCE RANGE	DETECTOR TYPE	DETECTOR RANGE	ANGLE
G,G	ABX	7	D	7	SCD-D		DST
		(7.279)		(7.279)			

7=7.279, LFT

TABLE III. Summary of the results of spins, parities, and total widths of resonance levels excited by γ rays obtained from neutron capture in iron. Parities in parantheses are uncertain.

Isotope	Energy (MeV)	$\delta=\|E_\gamma-E_e\|$ (eV)	$J^\pi{}_0$	$J^\pi{}_r$	Transition	Γ_0/Γ_γ (±8%)	Γ_γ (10^{-3} eV)
^{50}Cr	8.888	18 ±1	0^+	1	...	0.90	750 ± 200
^{62}Ni	7.646	14 ±1	0^+	1^-	$E1$	0.64	480 ± 50
^{74}Ge	6.018	4.5 ± 0.5	0^+	1^-	$E1$	0.19	120 ± 15
^{75}As	7.646	7.4 ± 0.3	$3/2^-$	$1/2^{(+)}$	...	0.11	360 ± 100
^{109}Ag	7.632	9 ±1	$1/2^-$	3/2	...	0.7	2 ± 1
^{112}Cd	7.632	4.8 ± 0.4	0^+	1^-	$E1$	0.55	86 ± 15
^{139}La	6.018	8.2 ± 0.6	$7/2^+$	$7/2^-$	$E1$	0.50	51^{+14}_{-6}
^{141}Pr	7.632	$11.4^{+0.3}_{-0.9}$	$5/2^+$	$5/2^+$	$M1$	0.46	72^{+24}_{-6}
^{205}Tl	7.646	9.3 ± 0.3	$1/2^+$	$1/2^{(-)}$	...	0.58	980 ± 90
^{208}Pb	7.279	7.1 ± 0.3	0^+	1^+	$M1$	1.00	780 ± 60

TABLE IV. Effective elastic scattering cross section $\langle\sigma_r\rangle=\sigma_0^m(\Gamma_0/\Gamma_\gamma)\Psi(x_0,t_0)$, where δ, J, Γ_0, Γ_γ were taken from Table III. The temperature of the scatterer was 300°K, while that of the iron γ source was 640°K.

Target	Resonance energy (MeV)	$\langle\sigma_r\rangle$ (mb)
^{50}Cr	8.888	905
^{62}Ni	7.646	569
^{74}Ge	6.018	61
^{75}As	7.646	4.4
^{109}Ag	7.632	3.5
^{112}Cd	7.632	198
^{139}La	6.018	39
^{141}Pr	7.632	20
^{205}Tl	7.646	574
^{208}Pb	7.279	5560

REF. A. Veyssiere, H. Beil, R. Bergere, P. Carlos, A. Lepretre
Nucl. Phys. A159, 561 (1970)

ELEM. SYM.	A	Z
Pb	208	82

METHOD

REF. NO.	
70 Ve 1	egf

REACTION	RESULT	EXCITATION ENERGY	SOURCE TYPE	SOURCE RANGE	DETECTOR TYPE	DETECTOR RANGE	ANGLE
G,N	ABX	7-31	D	7-36	BF3-I		4PI
G,2N	ABX	14-31	D	7-36	BF3-I		4PI
G,3N	ABX	23-31	D	7-36	BF3-I		4PI
G,4N	ABX	30-36	D	7-36	BF3-I		4PI

330+

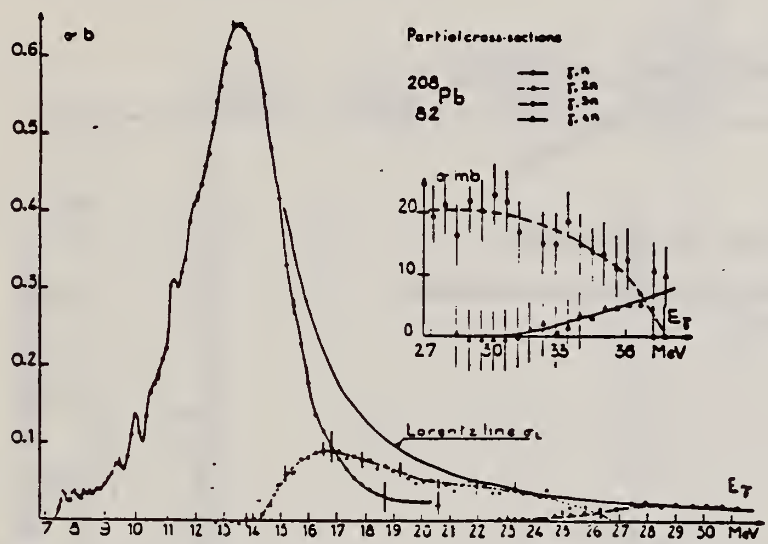

Fig. 1. Partial photoneutron cross sections $\sigma_{\gamma,n}$, $\sigma_{\gamma,2n}$, $\sigma_{\gamma,3n}$ and $\sigma_{\gamma,4n}$ of ^{208}Pb. We also show the descending part of the unique Lorentz line giving the best fit to the experimental $\sigma_{\gamma,T}(E)$ curve.

TABLE 5

Integrated cross sections and sum rule values of ^{208}Pb and ^{197}Au. The notation used is defined in the text

	Refs.	E_M (MeV)	σ_0 (MeV · b)	σ_0' (MeV · b)	$\frac{\sigma_0 A}{0.06\, NZ}$	$\frac{\sigma_0' A}{0.06\, NZ}$	σ_{-1} (mb)	σ_{-2} (mb · MeV^{-1})
	[1])	22	4.10 ± 0.06	5.10	1.37	1.71	280	20.5
^{208}Pb	[8])	28	2.91 ± 0.29	2.94	0.98	0.99		14.1 ± 1.4
	[23])	23	3.91 ± 0.59	5.18	1.31	1.74		18.6 ± 2.4
	present work	25	3.48 ± 0.23	4.00	1.17	1.34	251 ± 20	19.1 ± 2
	[1])	22	3.00 ± 0.05	3.99	1.06	1.40	200	14
^{197}Au	[9])	25	2.97 ± 0.3	3.53	1.05	1.24		15.3 ± 1.5
	present work	25	3.48 ± 0.2	4.07	1.23	1.42	238 ± 20	17.2 ± 2

[1] J.Miller, C.Schuhl and C.Tzara, Nucl.Phys.32 (1962)236.
[8] R.R.Harvey, J.T. Caldwell, R.L. Bramblett and S.C. Fultz, Phys.Rev. 136 (1964)B126.
[9] S.C.Fultz, R.L. Bramblett, J.T. Caldwell and N.A. Kerr, Phys.Rev. 127, (1962) 1273.
[23] T.Tomimasu, J. Phys. Soc.Jap.25 (1968)655.

[over]

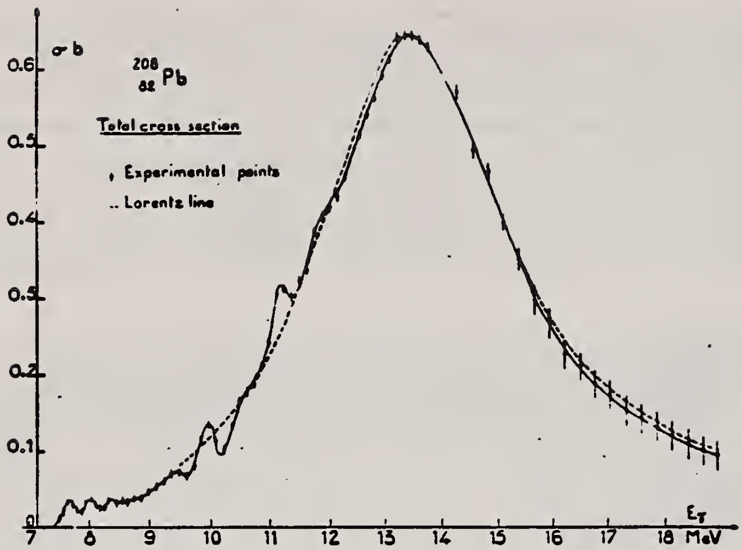

Fig. 3. Total photonuclear cross section $\sigma_{\gamma,T}(E)$ of ^{208}Pb and best Lorentz line fit corresponding to parameters given in table 3.

REF. R. J. Baglan, C. D. Bowman and B. L. Berman
Phys. Rev. C3, 672 (1971)

ELEM. SYM.	A	Z
Pb	208	82

METHOD

REF. NO.	
71 Ba 2	hmg

REACTION	RESULT	EXCITATION ENERGY	SOURCE TYPE	SOURCE RANGE	DETECTOR TYPE	DETECTOR RANGE	ANGLE
G,N	ABX	7 - 10	C	7-10	TOF-D		135
		(7.37-9.8)					

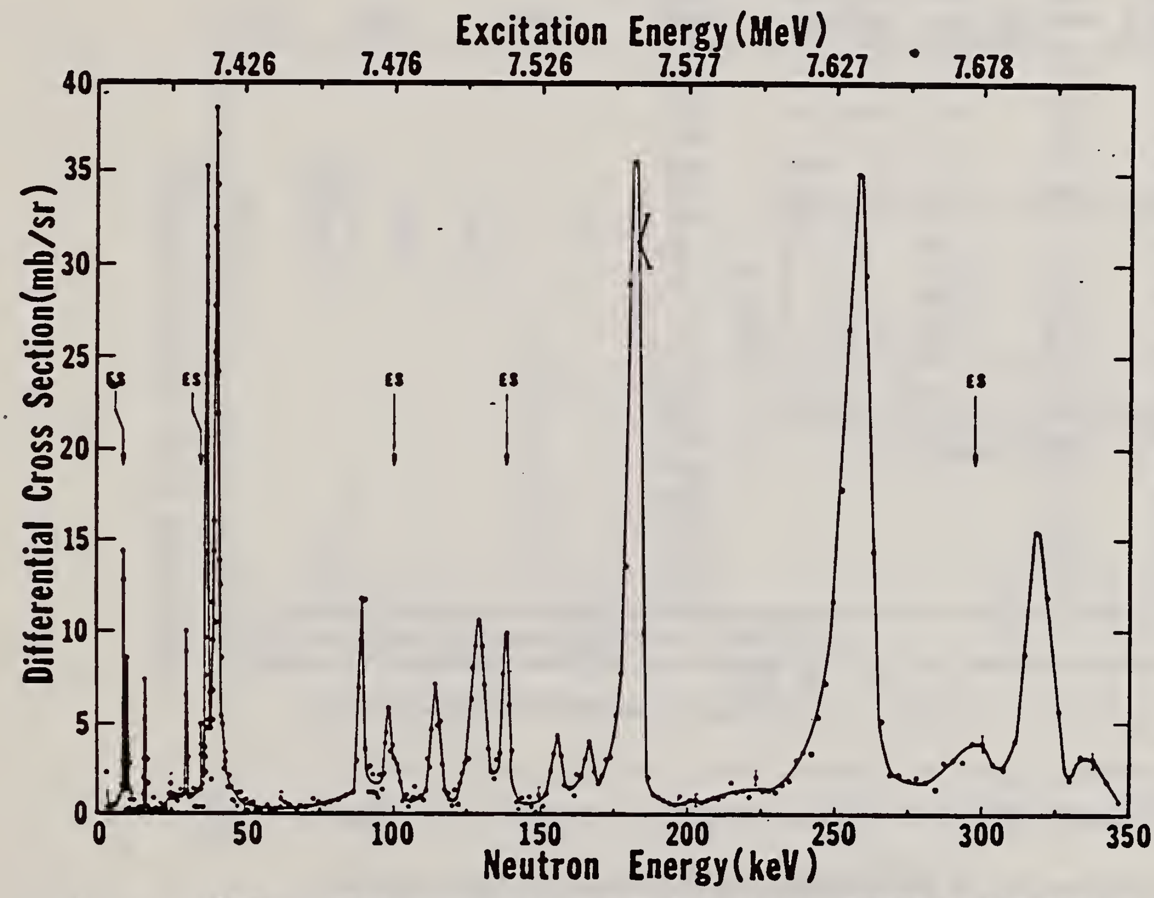

FIG. 6. The 135° differential threshold photoneutron cross section for ^{208}Pb, at low energies (see caption to Fig. 4). The 41-keV peak is asymmetric. (See text.)

FIG. 4. The 135° differential threshold photoneutron cross section for ^{207}Pb at low energies versus the energy of the emitted neutron (lower scale) and the excitation energy (upper scale). The arrows indicate peaks which decay to excited states of the residual nucleus (ES), or peaks owing to contaminating isotopes in the photoneutron sample. The inset shows the ^{207}Pb(γ,n) cross section averaged with a square 40-keV wide smoothing function.

Also see:
R. J. Baglan et al.
Phys. Rev. C3, 2475 (1971)

[over]

TABLE IV *(Continued)*

Nucleus	E_L (keV)	E_{ex} (MeV)	$g_\gamma\Gamma_{\gamma 0}\Gamma_n/\Gamma$ (eV)	GS or ES	J^π	$\Gamma_{\gamma 0}$ (eV)	E_n (keV) (This work)	E_n (keV) from neutron-induced reactions (Ref. a)	(Ref. b)	(Ref. c)
^{208}Pb	2.9 [e]	7.379	0.16				3.0			
	8.9 [e]		0.62	ES						
	9.9 [e]	7.386	0.12	GS [e]			10.1			
	15.9 [e]	7.392	0.17	GS [e]	2^+ [a]	0.06	16.2	17		
	24.9 [d]	7.401	<0.40	GS [d]			25.3			
	30.2	7.406	0.30	GS	1^+ [f]	0.23	30.7	29		
	35.4		0.22	ES						
	37.5	7.413	1.8	GS	2^+ [a,f]	0.64	38.1	37		
	40.8 [e]	7.417	7.2	GS	1^- [a]	4.8	41.4	41		
	90.0	7.466	2.6	GS			91.3			
	98.6		1.9	ES						
	114	7.490	2.0		1^+ [f]	1.6	115			
	129	7.506	5.4	GS			131			129
	138		3.6	ES						
	156	7.533	0.98	GS			158			
	166	7.543	0.90	GS			168			
	182	7.559	16.0	GS	1^+ [f]	12.6	184			
	257	7.634	26.2	GS	1^- [f]	17.5	260			
	299		4.0	ES						
	318	7.696	11.0	GS	1^+ [f]	7.7	321			
	493	7.872	3.2				498			
	547	7.926	12.3	GS	$1^-(1^+)$ [f]	8.2	553			
	558	7.937	4.6				564			
	620	7.999	17.2	GS	1^+ [f]	14.6	627			
	659	8.039	8.6		1^+ [f]	6.3	666			
	860	8.241	10.0	GS	1^+ [f]	7.8	869			
^{206}Pb	1.5 [d]	8.085	0.4	GS [d]			1.6			
	7.3 [e]	8.090	3.4	GS [e]			7.5			
	10.3 [e]	8.093	1.1	GS [e]			10.5			
	12.9 [e]		0.12	ES						
	16.1 [e]	8.098	0.40	GS [e]			16.4			
	28.5	8.111	0.54				29.0			
	33.7 [e]	8.116	2.5	GS [e]			34.3			
	40.0	8.123	0.86				40.7			
	50.7 [e]	8.133	1.3	GS [e]			51.5			
	53.6	8.136	0.52				54.4			
	68.9	8.152	1.5				69.9			
	72.1	8.155	1.4				73.2			
	75.1	8.158	0.90				76.2			
	88.9	8.171	4.5				90.2			
	104	8.187	4.9				106			

[a] See Ref. 6.
[b] See Ref. 10; approximate energy values taken from cross-section figure.
[c] See Ref. 13.
[d] See Ref. 3; resonance not seen in the present work.
[e] Also seen in Ref. 3; resonance parameters from present work.
[f] From angular distribution measurement (see text).

[3] C.D. Bowman, B.L. Berman, and H.E. Jackson, Phys. Rev. 178, 1827 (1969).

[6] J.A. Biggerstaff, J.R. Bird, J.H. Gibbons, and W.M. Good, Phys. Rev. 154, 1136 (1967).

[10] J.A. Farrell, G.C. Kyker, Jr., E.G. Bilpuch, and H.W. Newson, Phys. Letters 17, 286 (1965).

[13] E.G. Bilpuch, K.K. Seth, C.D. Bowman, R.H. Tabony, R.C. Smith, and H.W. Newson, Ann. Phys. (N.Y.) 14, 387 (1961).

REF. R. J. Baglan, C. D. Bowman and B. L. Berman
Phys. Rev. C3, 672 (1971)

ELEM. SYM.	A	Z
Pb	208	82

METHOD

[Page 2 of 2]

REF. NO.	
71 Ba 2	hmg

REACTION	RESULT	EXCITATION ENERGY	SOURCE TYPE	SOURCE RANGE	DETECTOR TYPE	DETECTOR RANGE	ANGLE

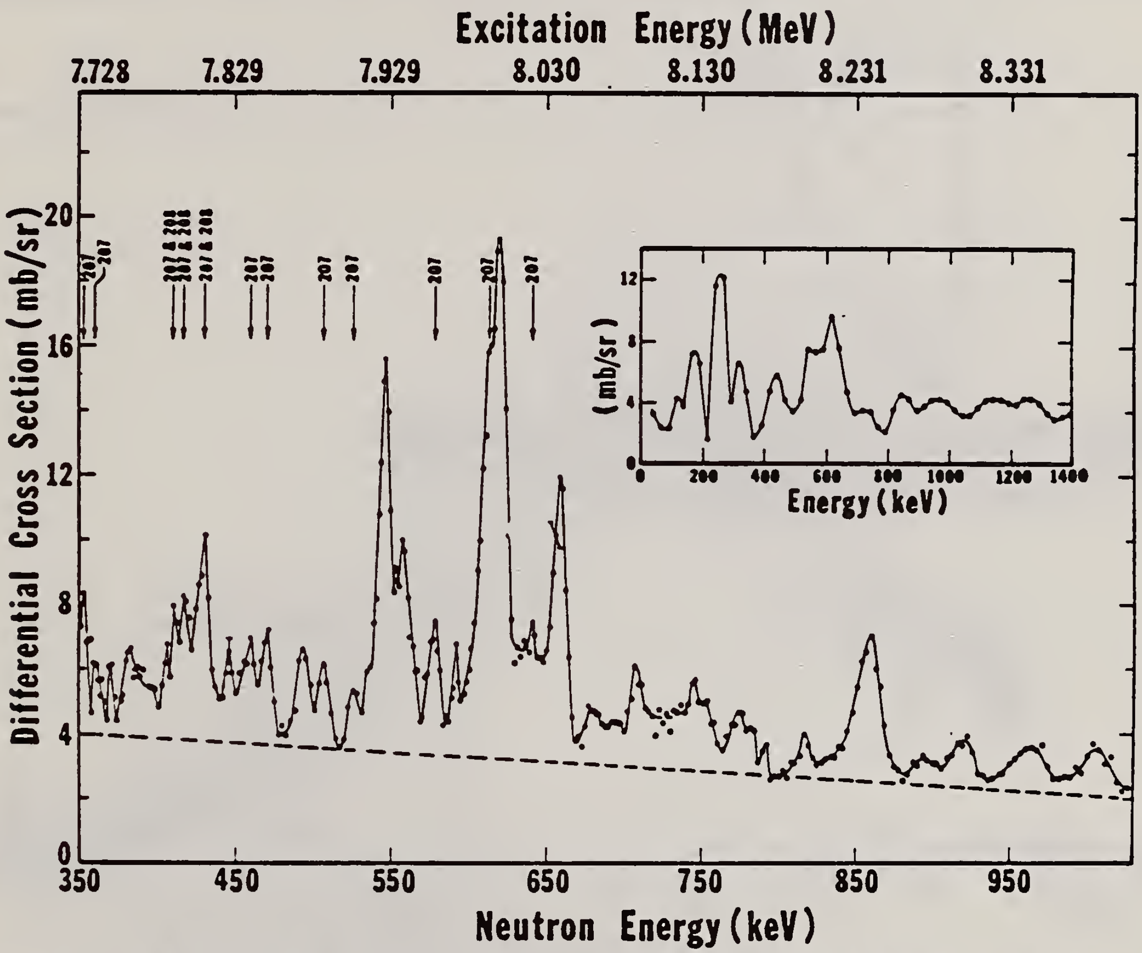

FIG. 7. The 135° differential threshold photoneutron cross section for ^{208}Pb, at high energies (see caption to Fig. 4). The dashed line indicates our best estimate of the background level.

REF. H. Dahmen, F. Dreyer, J. Staude and H. H. Thies
Nucl. Phys. A164, 140 (1971)

ELEM. SYM.	A	Z
Pb	208	82

METHOD

REF. NO.	
71 Da 1	egf

REACTION	RESULT	EXCITATION ENERGY	SOURCE TYPE	SOURCE RANGE	DETECTOR TYPE	DETECTOR RANGE	ANGLE
G,P	ABX	15-33	C	12-33	ACT-I		4PI

INC G,PN

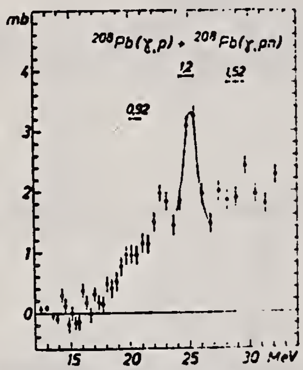

Fig. 2. The evaluated cross section of the reactions ^{208}Pb(γ, p)^{207}Tl + ^{208}Pb(γ, pn)^{206}Tl. The unfolding technique of Penfold and Leiss without smoothing was applied, bin width 2ΔE. The set of experimental yield points was divided in two "interlacing sets". The vertical error bars show the statistical errors, the horizontal ones the increasing bin width.

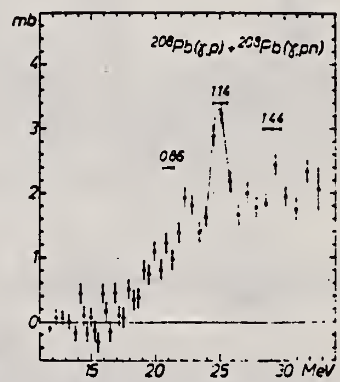

Fig. 3. The same cross section as in fig. 2, evaluated by application of the least-structure method of Cook [7]) to the whole set of yield points. The vertical error bars show the statistical errors, the horizontal ones the energy resolution defined by Cook [7]).

[7]B.C. Cook, Nucl. Instr. 24 (1963) 256.

REF.	B.I. Goryachev, B.S. Ishkhanov, and V.G. Shevchenko Proceedings of the Second Symposium on the Problems of Nuclear Physics, Novosibirsk, USSR, June 1970 (Kolybasov, V.M., Ed., Izdatel'stvo Nauka, Moscow 1971), pp. 362-78	ELEM. SYM. Pb	A 208	Z 82
METHOD		REF. NO. 71 Go 3		egf

REACTION	RESULT	EXCITATION ENERGY	SOURCE TYPE	SOURCE RANGE	DETECTOR TYPE	DETECTOR RANGE	ANGLE
G,XN	ABX	7- 17	C	7- 17	MOD-I		4PI

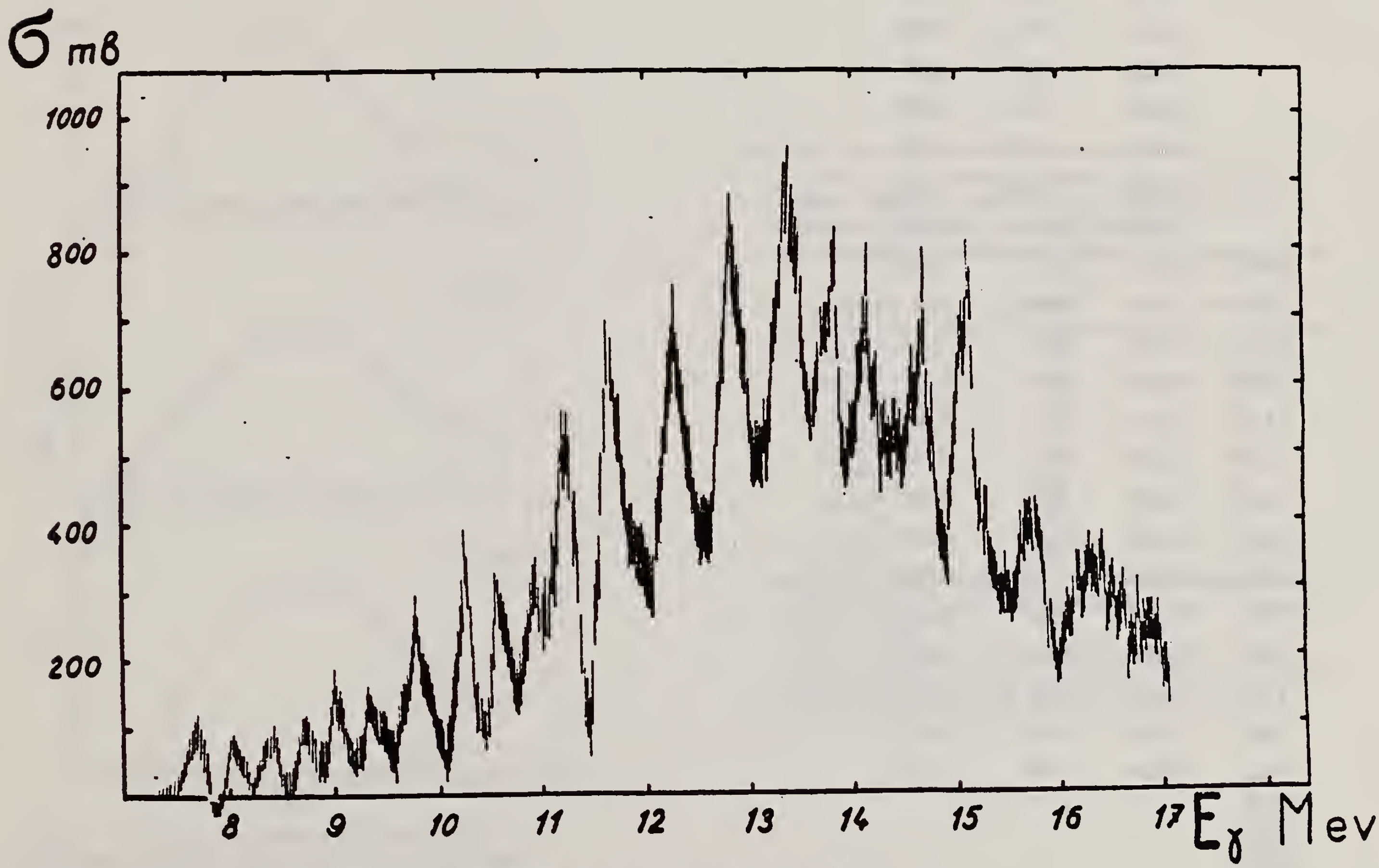

Фиг. 5. Сечение реакции $Pb^{208}(\gamma,n)$.

(over)

Таблица 2

Zr^{90}	Pb^{208}		
E_m(Мэв)	E_m(Мэв)	σ_m^{int}(Мэв·мбн)	σ_m^{int} (%)
	7,65	19,5	0,56
	8,06	12,63	0,36
	8,38	16,56	0,47
	8,78	18,61	0,53
	9,03	33,4	0,96
	9,40	34,2	0,98
	9,81	71,1	2,04
	10,29	72,2	2,07
	10,62	63,8	1,83
	10,93	76,6	2,20
	11,24	145,0	4,15
	11,76	247	7,10
12,4	12,3	265	7,61
12,6	12,84	331	9,5
13,1	13,25	344	9,37
13,7	13,78	214	6,14
14,2	14,08	316	9,06
14,6	14,66	245	7,03
14,9	15,13	210	6,02
15,3	15,73	88	2,52
15,8	16,40	114	3,26
16,5	17,13	98	2,81
16,9	17,95	150	4,30
17,3	18,76	78	2,24
18,6	19,52	88	2,52
19,3	20,83	135	3,87
21,3			
22,0			
22,8			
23,5			
24,2			
(25,5)			
27,8			

REF.	ELEM. SYM.	A	Z
E. J. Moniz, I. Sick, R. R. Whitney, J. R. Ficenec, R. G. Kephart and W. P. Trower Phys. Rev. Letters 26, 445 (1971)	Pb	208	82

METHOD	REF. NO.	
	71 Mo 3	hmg

REACTION	RESULT	EXCITATION ENERGY	SOURCE TYPE	SOURCE RANGE	DETECTOR TYPE	DETECTOR RANGE	ANGLE
E,E/	ABX	0-240	D	500	MAG-D		60

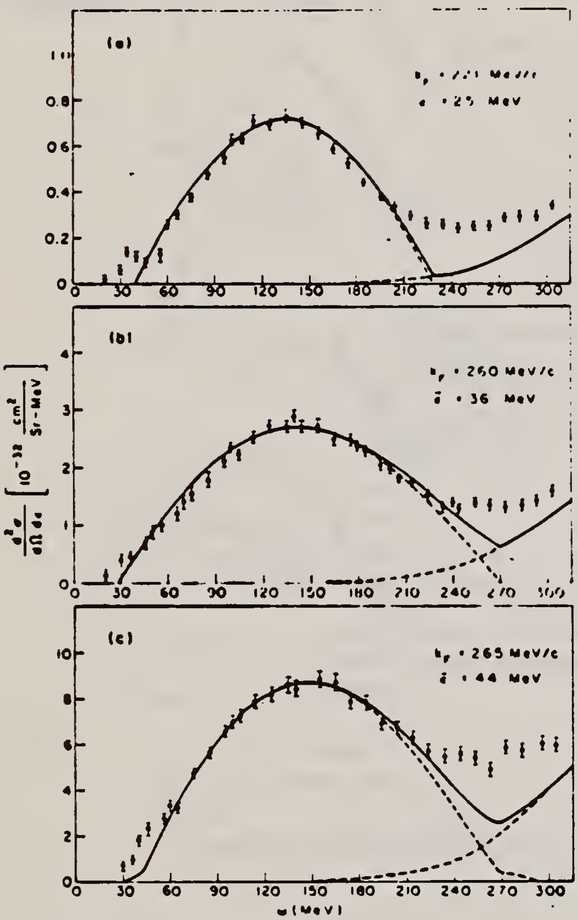

Fig. 1. Cross sections $d^2\sigma/d\Omega d\epsilon$ versus electron energy loss $\omega = \epsilon_1 - \epsilon_2$ for inelastic scattering of 500-MeV electrons at 60° from (a) carbon, (b) nickel, and (c) lead. Solid lines are the results of the Fermi-gas calculation with the nuclear parameters indicated on the figure.

Table I. Nuclear Fermi momentum k_F and average nucleon interaction energy $\bar{\epsilon}$ determined by least-squares fit of theory to quasielastic peak.

Nucleus	k_F (MeV/c)[a]	$\bar{\epsilon}$ (MeV)[b]
${}_3Li^6$	169	17
${}_6C^{12}$	221	25
${}_{12}Mg^{24}$	235	32
${}_{20}Ca^{40}$	251	28
${}_{28}Ni^{58.7}$	260	36
${}_{39}Y^{89}$	254	39
${}_{50}Sn^{118.7}$	260	42
${}_{73}Ta^{181}$	265	42
${}_{82}Pb^{208}$	265	44

[a]The fitting uncertainty in these numbers is approximately ±5 MeV/c.

[b]The fitting uncertainty in these numbers is approximately ±3 MeV. Simple estimates for $\bar{\epsilon}$ give numbers in reasonable agreement with those in the table.

REF.	ELEM. SYM.	A	Z
M. Nagao and Y. Torizuka Phys. Letters 37B, 383 (1971)	Pb	208	82

METHOD	REF. NO.	
	71 Na 2	egf

REACTION	RESULT	EXCITATION ENERGY	SOURCE TYPE	SOURCE RANGE	DETECTOR TYPE	DETECTOR RANGE	ANGLE
E,E/	LFT	2--4	D	183,248	MAG-D		DST

6 LEVELS

Table 1
Parameters for the Tassie transition charge and $B(EL)$ values

E_x (MeV)	J^π	c_{tr} (fm)	z_{tr} (fm)	$B(EL)$(W.u.) present (e,e')	(e,e') [8]	(p,p') [10]	(α,α') [11]	RPA [4]
2.61	3^-	5.8 ± 0.5	3.2 ± 0.2	43 ± 5	39.5 ± 2.0	32	41.1	13
3.20	5^-	5.58 ± 0.05	2.98 ± 0.03	11.1 ± 1.4	14 ± 5	17	14.1	3.59
3.70	5^-	6.55 ± 0.09	2.74 ± 0.15	8 ± 2		3.9		3.57
4.07	2^+	6.9	2.2	8.1*	8.1 ± 0.5	6.6	8	0.66
4.30	4^+	5.8	2.8	15	26 ± 2	11.4	14.8	0.88
4.40	6^+					11.7		

* The same value has been adopted of ref. [8]. (J. F. Ziegler and G. A. Peterson, Phys. Rev. 165 (1968) 1337.)

(over)

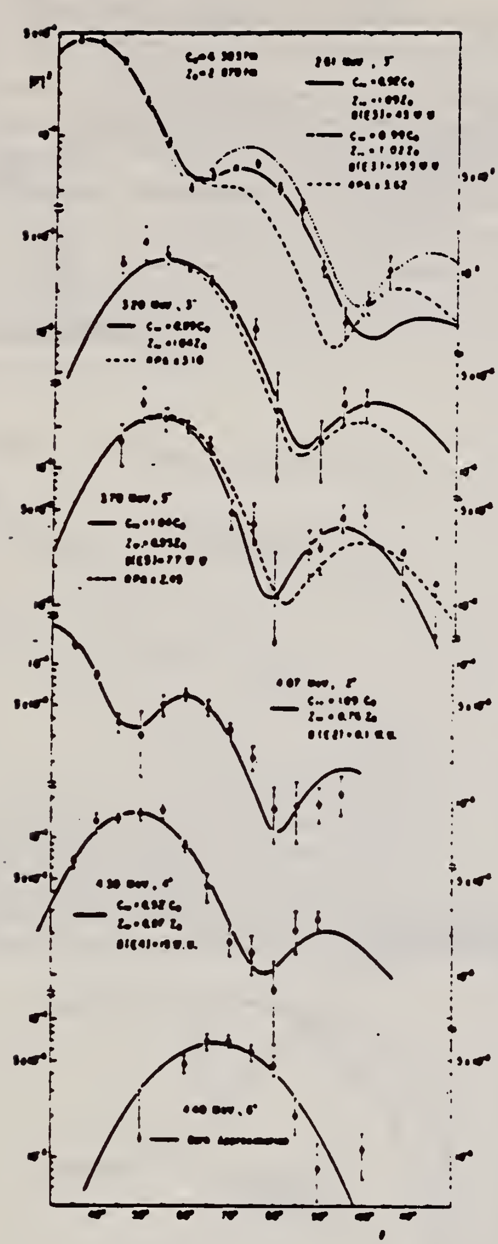

Fig. 1. The (e,e') form factors for excited states in ^{208}Pb. The dotted curve represents the Stanford data and the solid curves relate to the Tassie model where c_{tr} and z_{tr} are indicated for c_0 = 6.303 fm and z_0 = 2.878 fm. The dashed curve are the RPA form factors.

REF.	F. R. Buskirk, H. D. Graf, R. Pitthan, H. Theissen, O. Titze and Th. Walcher PICNS-72, p.199 Sendai	ELEM. SYM.	A	Z
		Pb	208	82
METHOD		REF. NO.		
		72 Bu 14		hvm

REACTION	RESULT	EXCITATION ENERGY	SOURCE TYPE	SOURCE RANGE	DETECTOR TYPE	DETECTOR RANGE	ANGLE
E,E/	FMF	7- 22	D	50, 65	MAG-D		DST

LEVELS 7.3-14.1

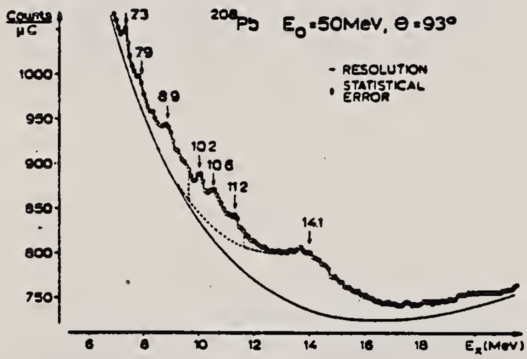

Figure 1 The spectrum of ^{208}Pb (e, e') for 50 MeV and 93°. Note the suppressed zero of the ordinate scale. Statistical errors are the size of the circles. The full line is the radiation tail plus background which was subtracted. The dashed curve is the extrapolation of the assumed E1 contribution. The area between the vertical dashed lines has been used to evaluate the E2 cross section.

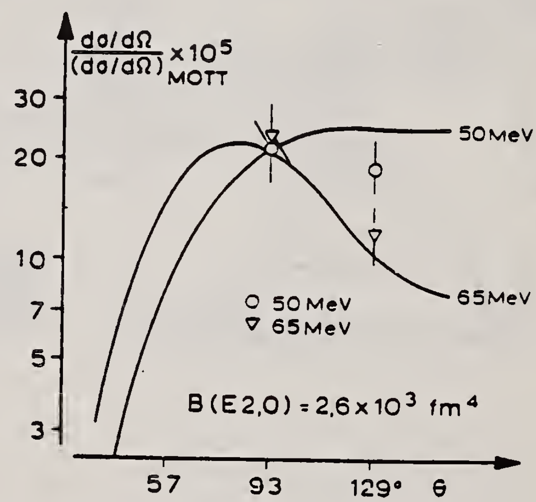

Figure 2 Ratio of inelastic cross section (sum of the cross sections of the 10.2, 10.6, and 11.2 MeV transitions as shown in Fig. 1) to Mott cross section as a function of scattering angle. The curves are DWBA calculations with $B(E2, 0) = 2.6 \times 10^3$ fm^4.

REF. F. R. Buskirk, H. D. Graf, R. Pitthan, H. Theissen, O. Titze, Th. Walcher
Phys. Lett. 42B, 194 (1972)

ELEM. SYM.	A	Z
Pb	208	82

METHOD

REF. NO.	
72 Bu 19	egf

REACTION	RESULT	EXCITATION ENERGY	SOURCE		DETECTOR		ANGLE
			TYPE	RANGE	TYPE	RANGE	
E,E/	ABX	9- 17	D	50, 65	MAG-D		DST

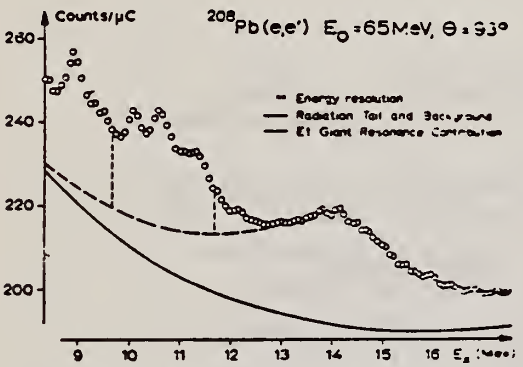

Fig. 1. The spectrum (circles) for 65 MeV and 93°. Note the suppressed zero of the ordinate scale. Statistical errors are the size of the circles. The full line is the radiation tail plus background which was subtracted. The dashed curve is the E1 contribution assumed. The area between the vertical dashed lines has been used to evaluate the E2 cross section.

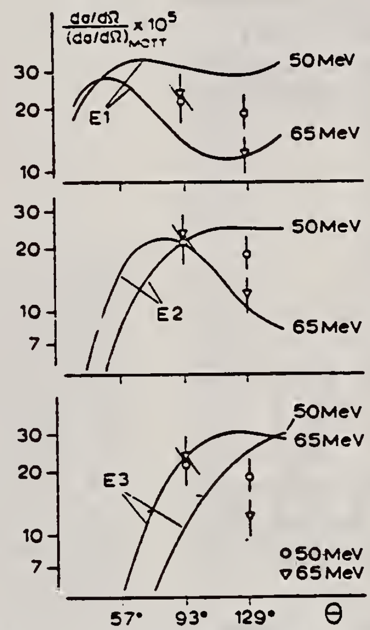

Fig. 2. Ratio of inelastic cross section (the sum of the cross sections of the 10.2, 10.6 and 11.2 MeV transitions, as shown in fig. 1) to Mott cross section as a function of scattering angle. The errors are discussed in the text. The curves are DWBA calculations with $B(E1,0) = 13\ fm^2$, $B(E2,0) = 2.6 \times 10^3\ fm^4$ and $B(E3,0) = 3.7 \times 10^5\ fm^6$ for the upper, middle and lower diagram, respectively.

Low-energy inelastic electron scattering experiments have been performed for ^{208}Pb with excitation energy ranging from 5 to 22 MeV. Resonances are observed at 7.3, 7.9, 8.9, 10.2, 10.6, 11.2 and 14.1 MeV. For the triplet at 10.2, 10.6 and 11.2 MeV, evidence is presented for an E2 assignment, with a reduced transition probability $B(E2,0) = (2.6 \pm 0.9) \times 10^3\ fm^4$.

REF.	ELEM. SYM.	A	Z
J. Friedrich Nucl. Phys. A191, 118 (1972)	Pb	208	82

METHOD	REF. NO.	
Page 1 of 2.	72 Fr 5	egf

REACTION	RESULT	EXCITATION ENERGY	SOURCE		DETECTOR		ANGLE
			TYPE	RANGE	TYPE	RANGE	
E,E/	ABX	2-4	D	124,167	MAG-D		DST

3 LEVELS TAB DATA

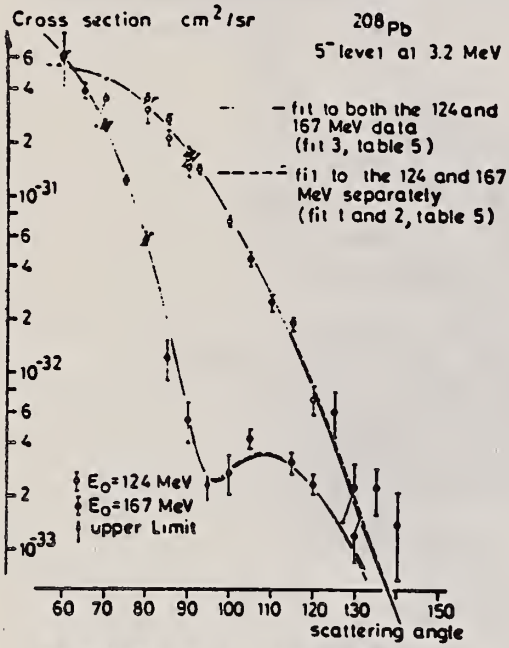

Fig. 6. Same as fig. 4; 5⁻ level at 3.2 MeV.

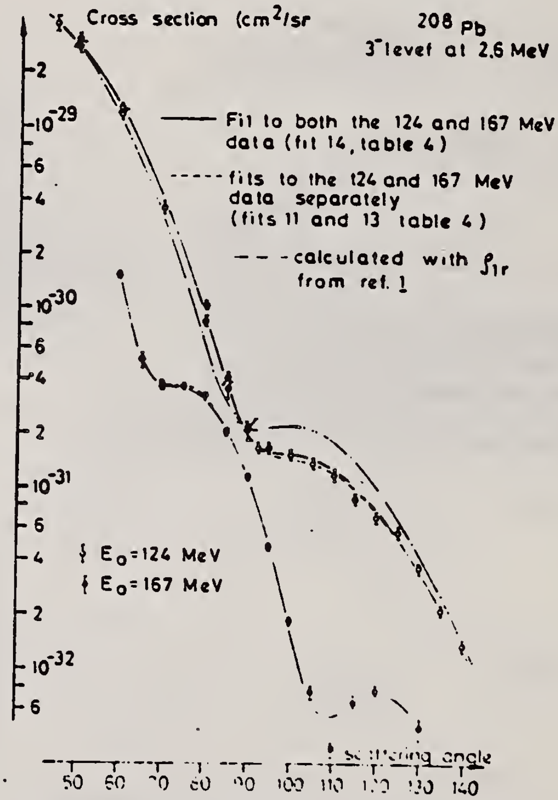

Fig. 4. Cross sections for the inelastic scattering of electrons with initial energies of 124 and 167 MeV from ^{208}Pb, 3⁻ level at 2.6 MeV.

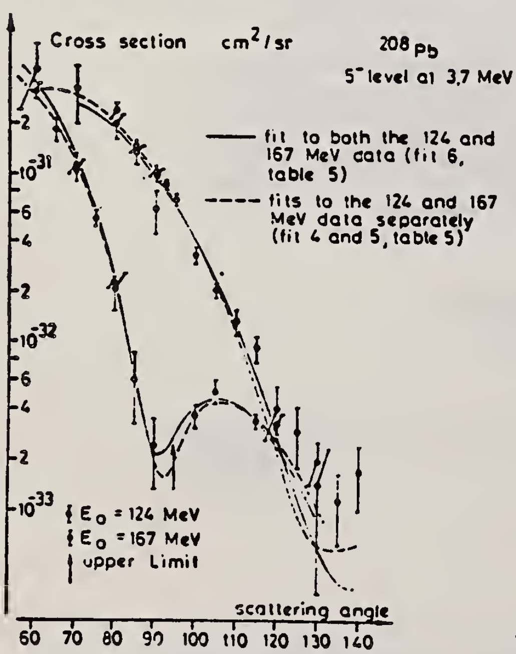

Fig. 7. Same as fig. 4; 5⁻ level at 3.7 MeV.

U.S. DEPARTMENT OF COMMERCE
NATIONAL BUREAU OF STANDARDS

Table I

Cross sections for the inelastic scattering from ^{208}Pb, 3^- level at 2.6 MeV

1	2	3	4	5	6
Energy (MeV)	Angle (degree)	$R = A_{inel}/A_{el}$		Cross section (cm²/sr)	
		MAIN	FRMAIN	1	2
124	45		4.34(3) ± 7.5 %	3.69(29) ± 3.5(30)	3.47(29)
	50		9.03(3) ± 6.9 %	3.03(29) ± 2.6(30)	2.80(29)
	50		8.10(3) ± 4.2 %	2.74(29) ± 1.7(30)	2.51(29)
	60		1.50(2) ± 2.3 %	1.27(29) ± 7.1(31)	1.21(29)
	60		1.39(2) ± 5.3 %	1.17(29) ± 8.4(31)	1.12(29)
	70		1.25(2) ± 6.8 %	3.59(30) ± 3.1(31)	3.62(30)
	80		1.08(2) ± 2.3 %	1.04(30) ± 6.0(32)	9.28(31)
	80		9.73(3) ± 6.0 %	8.52(31) ± 6.4(32)	8.34(31)
	85		9.00(3) ± 6.1 %	4.13(31) ± 3.1(32)	3.77(31)
	85		8.35(3) ± 9.0 %	3.54(31) ± 3.6(32)	3.50(31)
	90		1.09(2) ± 5.5 %	2.20(31) ± 1.6(32)	2.11(31)
	90		1.05(2) ± 10.5 %	2.14(31) ± 3.0(32)	2.03(31)
	90		1.13(2) ± 7.6 %	2.24(31) ± 2.0(32)	2.19(31)
	92.5		1.21(2) ± 5.6 %	1.67(31) ± 1.3(32)	1.59(31)
	95		1.78(2) ± 4.5 %	1.68(31) ± 1.1(32)	1.59(31)
	100		3.12(2) ± 4.5 %	1.53(31) ± 1.0(32)	1.44(31)
	105		4.58(2) ± 3.3 %	1.38(31) ± 1.0(32)	1.36(31)
	110		5.31(2) ± 5.6 %	1.19(31) ± 9.0(33)	1.21(31)
	115		4.87(2) ± 4.6 %	8.86(32) ± 5.9(33)	8.94(32)
	120		4.80(2) ± 5.0 %	6.96(32) ± 4.9(33)	6.95(32)
	125		4.85(2) ± 3.6 %	5.77(32) ± 4.5(33)	5.24(32)
	130		4.20(2) ± 4.1 %	3.60(32) ± 2.2(33)	3.20(32)
	135		3.98(2) ± 3.7 %	2.16(32) ± 1.5(33)	2.03(32)
	140		3.79(2) ± 5.2 %	1.39(32) ± 1.0(33)	1.23(32)
167	60	1.15(2) ± 6.1 %	1.16(2) ± 4.0 %	1.52(30) ± 7.0(32)	1.53(30)
	65	1.12(2) ± 8.9 %	1.16(2) ± 8.7 %	5.14(31) ± 4.6(32)	5.47(31)
	70	2.45(2) ± 8.2 %	2.59(2) ± 4.1 %	3.65(31) ± 1.7(32)	4.06(31)
	70	2.53(2) ± 8.7 %	2.53(2) ± 4.4 %	3.80(31) ± 1.8(32)	3.96(31)
	75	5.47(2) ± 3.8 %	5.63(2) ± 2.8 %	3.67(31) ± 1.7(32)	3.79(31)
	80	6.53(2) ± 3.8 %	6.80(2) ± 1.9 %	3.24(31) ± 1.1(32)	3.11(31)
	80	6.49(2) ± 3.6 %	6.66(2) ± 3.3 %	3.20(31) ± 1.8(32)	3.04(31)
	85	5.79(2) ± 3.5 %	5.57(2) ± 3.5 %	2.05(31) ± 1.2(32)	1.95(31)
	90	4.73(2) ± 4.2 %	4.80(2) ± 2.6 %	1.15(31) ± 5.0(33)	1.14(31)
	95	3.70(2) ± 6.8 %	3.64(2) ± 6.0 %	4.73(32) ± 2.8(33)	4.94(32)
	100	2.60(2) ± 11.5 %	2.72(2) ± 5.2 %	1.85(32) ± 1.0(33)	1.79(32)
	105	2.10(2) ± 14.0 %	2.67(2) ± 7.8 %	7.53(33) ± 6.1(34)	7.27(33)
	110	3.35(2) ± 24.0 %	3.46(2) ± 10.0 %	3.63(33) ± 3.7(34)	3.46(33)
	115	1.01(1) ± 14.0 %	1.19(1) ± 7.6 %	6.49(33) ± 5.1(34)	5.79(33)
	120	1.72(1) ± 10.0 %	2.01(1) ± 5.6 %	[illegible](33) ± 5.2(34)	7.03(33)
	130	1.50(1) ± 13.0 %	1.63(1) ± 11.0 %	4.76(33) ± 6.5(34)	4.32(33)

The ratio R of the areas A under the elastic and inelastic peak is determined by two different methods (programs MAIN and FRMAIN respectively). The inelastic cross sections (column 5) are determined with R according to FRMAIN and with the elastic cross sections which have been measured relative to ^{12}C [ref. [6]]. The cross sections in column 6 have been determined with the same R but with elastic cross sections which are calculated with a given charge distribution [14]. The numbers in brackets are the powers of 10.

[6] J. Friedrich and F. Lenz, Nucl. Phys. A183 (1972) 523

[14] J. Heisenberg, R. Hofstadter, J. S. McCarthy, I. Sick, B. C. Clark, R. Herman and D. G. Ravenhall, Phys. Rev. Lett. 23 (1969) 1402

REF.

J. Friedrich
Nucl. Phys. A191, 118 (1972)

ELEM. SYM.	A	Z
Pb	208	82

METHOD

REF. NO.	
72 Fr 5	egf

REACTION	RESULT	EXCITATION ENERGY	SOURCE TYPE	SOURCE RANGE	DETECTOR TYPE	DETECTOR RANGE	ANGLE

TABLE 2

Same as table 1 but for the 5^- level at 3.2 MeV

1	2	3	4	5	6
Energy (MeV)	Angle (degree)	$R = A_{inel}/A_{el}$			Cross section (cm^2/sr)
		MAIN		FRMAIN	
		a	b		
124	60			7.8 (4) ± 30 %	6.4 (31) ± 1.9(31)
	70			1.2 (3) ± 30 %	3.6 (31) ± 1.1(31)
	80			3.61(3) ± 6.5 %	3.48(31) ± 2.7(32)
	80			3.45(3) ± 17 %	3.03(31) ± 5.3(32)
	85			5.84(3) ± 4.3 %	2.68(31) ± 1.7(32)
	85			5.01(3) ± 9.5 %	2.12(31) ± 2.2(32)
	90			8.66(3) ± 4.1 %	1.82(31) ± 8.0(33)
	90			7.90(3) ± 7.8 %	1.61(31) ± 1.4(32)
	90			7.20(3) ± 12 %	1.43(31) ± 1.8(32)
	92.5			1.01(2) ± 4.7 %	1.44(31) ± 7.0(33)
	95			1.32(2) ± 4.4 %	1.29(31) ± 6.0(33)
	100			1.44(2) ± 4.0 %	7.30(32) ± 3.2(33)
	105			1.46(2) ± 8.0 %	4.39(32) ± 4.0(33)
	110			1.10(2) ± 10 %	2.48(32) ± 2.8(33)
	115			1.04(2) ± 7.8 %	1.89(32) ± 1.7(33)
	120			4.83(3) ± 18 %	7.0 (33) ± 1.3(33)
	125			5.1 (3) ± 30 %	6.1 (33) ± 1.8(33)
	130			2.6 (3) ± 37 %	2.2 (33) ± 8.2(34)
	135			4.1 (3) ± 29 %	2.2 (33) ± 6.5(34)
	140			3.8 (3) ± 52 %	1.4 (33) ± 7.2(34)
167	60	3.83 ± 0.59(3)	3.75 ± 0.67(3)	4.51(3) ± 8.9 %	5.91(31) ± 5.3(32)
	65	7.3 ± 0.9 (3)	6.9 ± 1.0 (3)	8.76(3) ± 9.5 %	3.88(31) ± 3.7(32)
	70	1.42 ± 0.17(2)	1.39 ± 0.18(2)	1.76(2) ± 5.6 %	2.48(31) ± 1.5(32)
	70	1.30 ± 0.20(2)	1.3 ± 0.2 (2)	1.60(2) ± 6.1 %	2.40(31) ± 1.5(32)
	75	1.56 ± 0.16(2)	1.56 ± 0.16(2)	1.87(2) ± 4.5 %	1.22(31) ± 6.0(33)
	80	6.88 ± 2.4 (3)	7.9 ± 1.5 (3)	1.17(2) ± 7.6 %	5.58(32) ± 4.4(33)
	80	8.9 ± 2.3 (3)	9.3 ± 1.4 (3)	1.17(2) ± 8.9 %	5.63(32) ± 5.1(33)
	85	1.3 ± 1.9 (3)	1.82 ± 1.2 (3)	3.3 (3) ± 26 %	1.21(32) ± 3.1(33)
	90	0.1 ± 15.6 (4)	0.5 ± 1.0 (3)	2.3 (3) ± 25 %	5.4 (33) ± 1.4(33)
	95	0.9 ± 20.6 (4)	0.2 ± 17.8 (4)	[illegible] 2(3)	< 2.6 (33)
	100	0.9 ± 2.6 (3)	0.1 ± 2.6 (3)	4.0 (3) ± 26 %	2.7 (33) ± 7.1(34)
	105	5.2 ± 4.2 (3)	2.4 ± 4.7 (3)	1.5 (3) ± 13 %	4.8 (33) ± 5.5(34)
	115	2.1 ± 1.5 (2)	2.3 ± 1.5 (2)	[illegible](2) ± 14 %	3.06(33) ± 4.3(34)
	120	2.0 ± 1.6 (2)	2.4 ± 1.6 (2)	6.25(2) ± 12 %	2.36(33) ± 2.8(34)
	130	1.5 ± 2.3 (2)	1.9 ± 2.5 (2)	4.1 (2) ± 28 %	1.20(33) ± 3.4(34)

The ratio *R* has been determined twice with MAIN taking into account different levels in the analysis. The cross sections (column 6) again have been determined with *R* as given in column 5 and with the elastic cross sections which have been measured relative to ^{12}C.

(over)

Table 3

Same as table 2 but for the 5^- level at 3.7 MeV

1	2	3	4	5	6
Energy (MeV)	Angle (degree)	$R = A_{inel}/A_{el}$			Cross section (cm^2/sr)
		MAIN		FRMAIN	
		a	b		
124	60			5 (4)±43 %	4.4 (31)±1.9(31)
	70			1.1 (3)±36 %	3.3 (31)±1.2(31)
	80			2.46(3)±10 %	2.37(31)±2.6(32)
	80			2.25(3)±16 %	1.97(31)±3.3(32)
	85			3.20(3)± 6.9 %	1.47(31)±1.2(32)
	85			3.19(3)±12 %	1.35(31)±1.7(32)
	90			5.13(3)± 5.2 %	1.08(31)±6.0(33)
	90			4.90(3)± 7.9 %	1.00(31)±9.0(33)
	90			3.20(3)±28 %	6.34(32)±1.8(32)
	92.5			6.37(3)± 4.3 %	9.11(32)±4.2(33)
	95			7.66(3)± 5.3 %	7.48(32)±5.6(33)
	100			6.96(3)± 9.3 %	3.53(32)±3.4(33)
	105			7.14(3)± 7.7 %	2.15(32)±1.9(33)
	110			6.25(3)±16 %	1.41(32)±2.4(33)
	115			5.4 (3)±17 %	9.8 (33)±1.7(33)
	120			3.0 (3)±35 %	4.4 (33)±1.5(33)
	125			2.7 (3)±42 %	3.2 (33)±1.3(33)
	130			1.7 (3)±74 %	1.5 (33)±1 (33)
	135			2.3 (3)±45 %	1.3 (33)±6 (34)
	140			5.1 (3)±41 %	1.9 (33)±8 (34)
167	60	1.42± 0.52(3)	1.13± 1.40(3)	2.38(3)± 9.6 %	3.12(31)±3.1(32)
	65	2.64± 0.86(3)	1.86± 2.03(3)	4.19(3)±17 %	1.86(31)±3.2(32)
	70	3.21± 1.60(3)	2.34± 3.30(3)	7.60(3)±14 %	1.07(31)±1.5(32)
	70	3.7 ± 1.8 (3)	1.4 ± 4.7 (3)	7.74(3)±15 %	1.16(31)±1.7(32)
	75	4.2 ± 2.1 (3)	3.8 ± 3.8 (3)	8.56(3)± 9.9 %	5.57(32)±5.6(33)
	80	2.0 ± 2.4 (3)	0.4 ± 3.0 (3)	4.90(3)± 9.0 %	2.34(32)±2.1(33)
	80	0.3 ± 2.1 (3)	1.0 ± 3.0 (3)	4.50(3)±25 %	2.16(32)±5.4(33)
	85	0.2 ± 1.8 (3)	0.3 ± 2.8 (3)	1.7 (3)±46 %	6.4 (33)±2.9(33)
	90	0.6 ±15.0 (4)	0.6 ±23.5 (4)	1.1 (3)±45 %	2.6 (33)±1.2(33)
	95	0.7 ±21.6 (4)	1.8 ±48.1 (4)	< 2(3)	< 2.6 (33)
	100	0.3 ± 2.7 (3)	0.2 ±63.3 (4)	5.88(3)±14 %	4.00(33)±6.0(34)
	105	7.6 ± 4.5 (3)	3.7 ±16.7 (3)	1.98(2)±11 %	5.58(33)±6.1(34)
	115	3.8 ± 1.6 (2)	3.7 ± 4.7 (2)	6.76(2)±10 %	3.68(33)±3.7(34)
	120	4.9 ± 1.8 (2)	5.3 ± 6.3 (2)	9.40(2)±12 %	3.55(33)±4.6(34)
	130	2.2 ± 2.4 (2)	1.9 ±10.8 (2)	7.40(2)±27 %	2.16(33)±6.3(34)

REF.	ELEM. SYM.	A	Z
K. Shoda, M. Sugawara, T. Saito, H. Miyase, A. Suzuki, S. Oikawa, and J. Uegaki PICNS-72, 321 Sendai	Pb	208	82
METHOD	REF. NO. 72 Sh 10		hvm

REACTION	RESULT	EXCITATION ENERGY	SOURCE TYPE	SOURCE RANGE	DETECTOR TYPE	DETECTOR RANGE	ANGLE
E,P	SPC	24- 27	C	24- 27	MAG-D		UKN

I A STATES

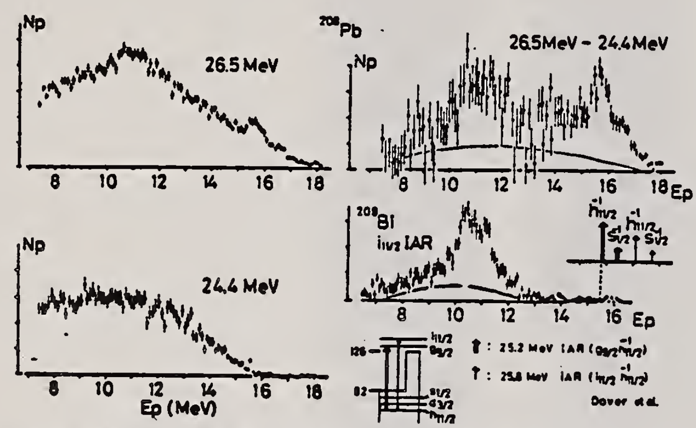

Fig. 9 Energy distribution of protons from ^{208}Pb(e,e'p) reaction. Top of the right hand side is a difference spectrum. Proton hole states and the core analogue state are indicated by arrows and ^{209}Bi result respectively.

REF.	ELEM. SYM.	A	Z
R. E. Toohey and H. E. Jackson Phys. Rev. C6, 1440 (1972)	Pb	208	82

METHOD	REF. NO.	
	72 To 1	hmg

REACTION	RESULT	EXCITATION ENERGY	SOURCE TYPE	SOURCE RANGE	DETECTOR TYPE	DETECTOR RANGE	ANGLE
G,N	LFT	7 - 9	C	9	TOF-D		DST
		(7.4 - 8.4)		(8.4)			

G-WIDTH, J-PI

TABLE I. $^{208}Pb(\gamma, n)^{207}Pb$ resonance parameters. Underlined resonances are discussed in the text.

	Argonne National Laboratory[a]			Lawrence Radiation Laboratory[b]			Oak Ridge National Laboratory[c]	
E_n (keV)	R (90°/135°)	J^π	$\Gamma_{\gamma 0}$ (eV)	R (90°/135°)	J^π	$\Gamma_{\gamma 0}$ (eV)	J^π	$\Gamma_{\gamma 0}$ (eV)
996	1.55±0.29	1	5.8					
951	1.34±0.36	1	3.5					
945	2.04±0.52	1	2.9					
907	1.25±0.20	1	6.5					
846	1.38±0.12	1	10.1	1.48±0.20	1^+	6.8		
737	0.99±0.12	1	3.5					
699	1.17±0.12	1	4.4					
<u>651</u>	1.11±0.08	1	11.8	1.37±0.20	1^+	5.5	2^+	7.3
<u>613</u>	1.23±0.08	1	19.7	1.81±0.25	1^+	12.8	1	7.2
<u>602</u>	1.25±0.09	1	8.0				1	8.5
551	0.80±0.08		3.3					
538	0.99±0.07	1	12.4	0.94±0.13	1^-, 1^+	7.2	1	11.1
491	1.01±0.16	1	2.0					
484	0.86±0.15		1.6				1	8.5
457	1.02±0.16	1	2.2					
445	0.68±0.13	2^+, 1^+	1.5					
422[d]	ES							
334	0.60±0.17	2^+, 1^+	0.7				1	2.3
<u>315</u>	0.94±0.07	1	10.2	1.13±0.16	1^+	6.7	1	8.5
297	0.90±0.25		0.9				1	0.7
<u>254</u>	1.00±0.07	1^-	18.4	1.00	1^-	15.3		28.3
<u>181</u>	1.67±0.16	1^+	9.9	1.45±0.20	1^+	11.0		13.6

[a] Present work.
[b] Reference 1.
[c] Reference 5.
[d] Decay to first excited state of ^{207}Pb.

[1] C. D. Bowman, R.J. Baglan, B.L. Berman & T.W. Phillips, Phys. Rev. Letters 25, 18, 1302 (1970).

[5] B.J. Allen and R.L. Macklin, Phys. Rev. Letters 25, 1675 (1971); in Proceedings of the Third Neutron Cross-Section and Technology Conference, Knoxville, Tenn. March 1970 (University of Tennessee, Knoxville, 1971), p.764.

(over)

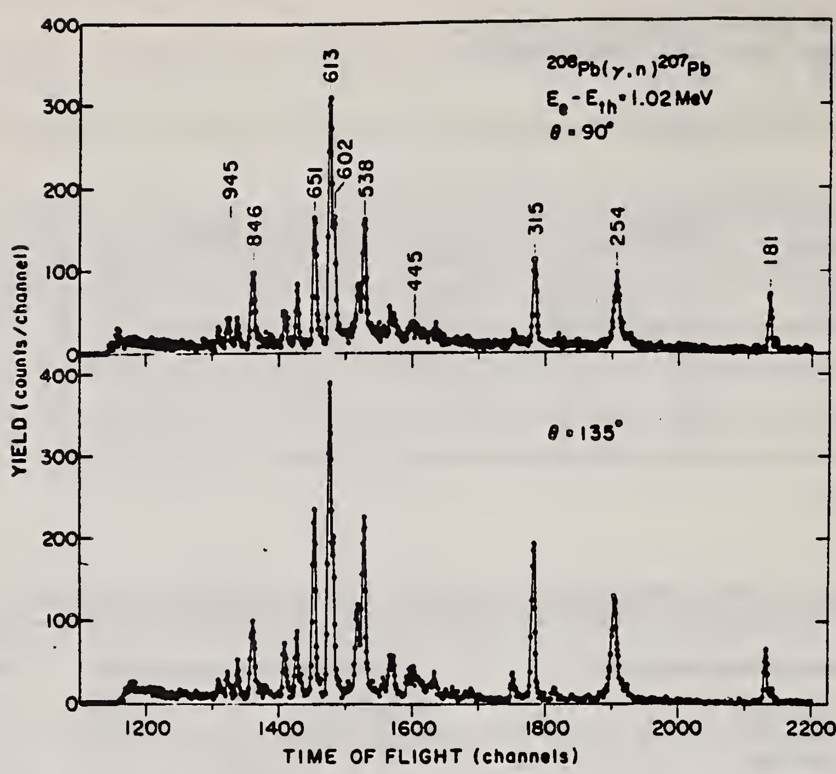

FIG. 1. Threshold photoneutron spectrum measured at 90 and 135°. The neutron yield from the $^{208}Pb(\gamma, n)$ reaction is plotted as a function of the neutron time of flight, and the peaks are labeled with the neutron energy E_n in keV.

REF. Y. Torizuka, Y. Kojima, T. Saito, K. Itoh, A. Nakada,
S. Mitsunobu, M. Nagao, K. Hosoyama, S. Fukuda
PICNS-72, p.171 Sendai

ELEM. SYM.	A	Z
Pb	208	82

METHOD

REF. NO.	
72 To 6	hvm

REACTION	RESULT	EXCITATION ENERGY	SOURCE TYPE	SOURCE RANGE	DETECTOR TYPE	DETECTOR RANGE	ANGLE
E,E/	SPC	0- 26	D	183	MAG-D		35

However, it should be noticed that this resonance has a fine structure.

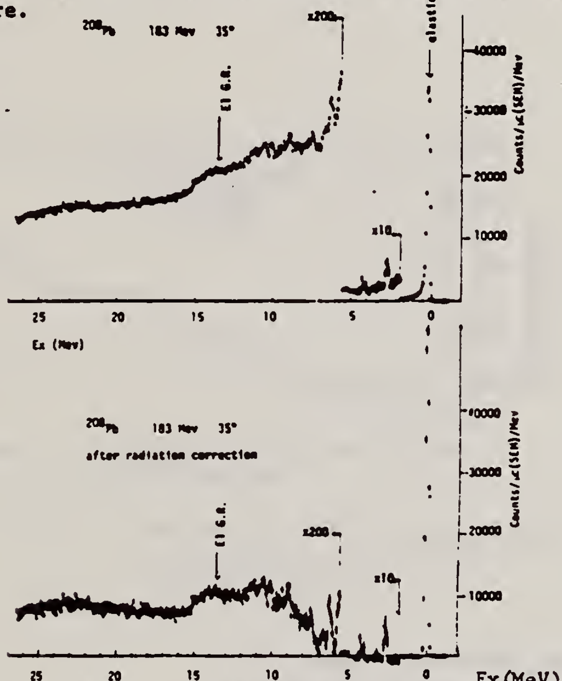

Fig. 2. The spectra of ^{208}Pb at 183 MeV and 35°. The E1 giant resonance is indicated at 13.5 MeV.

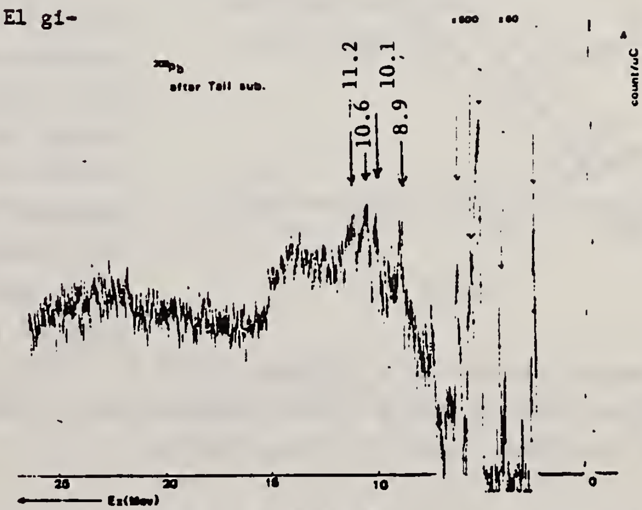

Fig. 3. The same spectrum as for Fig. 2. The structure is seen at 8.9, 10.1, 10.6, and 11.2 MeV. A broad bumps around 23 MeV indicates another resonance.

REF.	F.R. Buskirk, H.D. Graf, R. Pitthan, H. Theissen, O. Titze, and Th. Walcher PICNS-73, Vol.I, p.703 Asilomar	ELEM. SYM. Pb	A 208	Z 82
METHOD		REF. NO. 73 Bu 14		hmg

REACTION	RESULT	EXCITATION ENERGY	SOURCE		DETECTOR		ANGLE
			TYPE	RANGE	TYPE	RANGE	
E,E/	SPC	2- 20	C	50, 65	MAG-D		DST

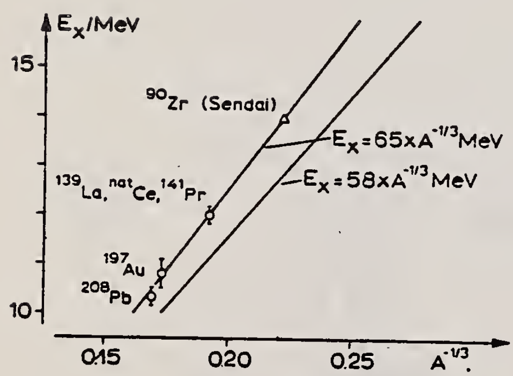

Fig. 2

The E2 resonance which is clearly visible at 10.8 ± 0.2 MeV exhausts more than 50 % of the sum rule. Fig. 2 shows the excitation energy of this resonance as a function of $A^{-1/3}$ for the nuclei measured at Darmstadt and the Sendai result for ^{90}Zr [5]. Bohr and Mottelson [9] predicted a collective E2 resonance whose isoscalar part should depend on A through $E_x=58\ A^{-1/3}$MeV. The data of Fig. 2 are consistent with $E_x=65\ A^{-1/3}$MeV suggesting to identify the observed resonances with this type of E2 excitation.

REF.	ELEM. SYM.	A	Z
Lawrence Fagg PICNS-73, Vol.I, p.663 Asilomar	Pb	208	82

METHOD	REF. NO.	
	73 Fa 5	hmg

REACTION	RESULT	EXCITATION ENERGY	SOURCE TYPE	SOURCE RANGE	DETECTOR TYPE	DETECTOR RANGE	ANGLE
E,E/	ABX	0- 15	D	50	MAG-D		180
				(50.4)			

PEAKS 7.3, 7.9, 9.3

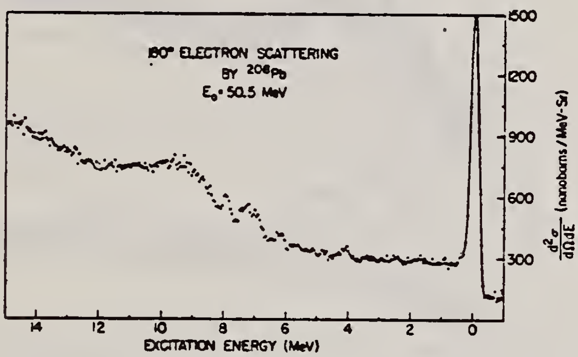

Fig. 16. Preliminary 180° electron scattering spectrum from ^{208}Pb

REF.	B. S. Ishkhanov and V.G. Shevchenko PICNS-73, Vol.I, p.511 Asilomar	ELEM. SYM.	A	Z
		Pb	208	82
METHOD		REF. NO.		
		73 Is 3		hmg

REACTION	RESULT	EXCITATION ENERGY	SOURCE		DETECTOR		ANGLE
			TYPE	RANGE	TYPE	RANGE	
G,N	RLX	7- 14	C	7- 14	BF3-I		4PI

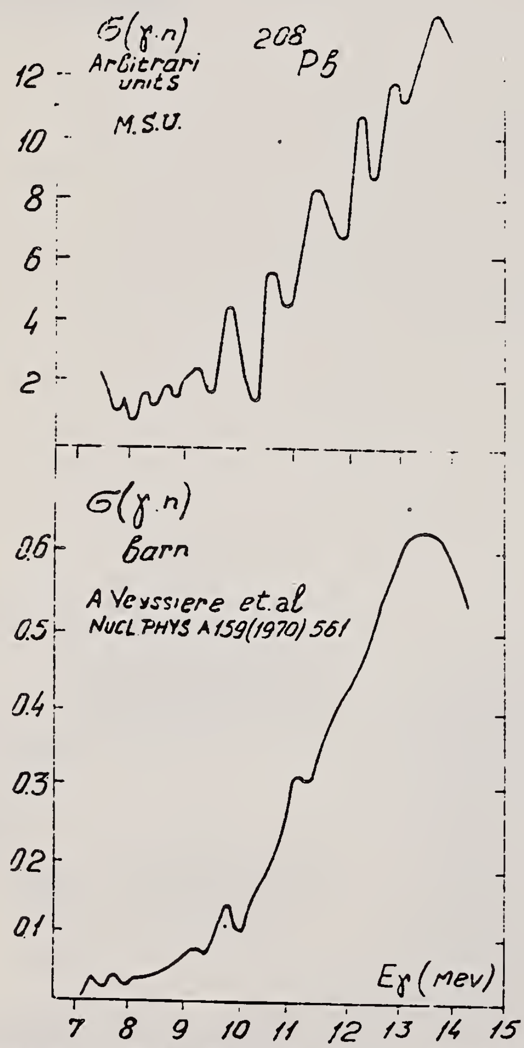

Fig.5. Comparison of our cross section of reaction ^{208}Pb (γ ,n) (upper figure) with the photoneutron cross section given in paper [12]. (lower figure).

REF. M. Nagao and Y. Torizuka
Phys. Rev. Letters 30, 1068 (1973)

ELEM. SYM.	A	Z
Pb	208	82

METHOD

REF. NO.	
73 Na 1	hmg

REACTION	RESULT	EXCITATION ENERGY	SOURCE TYPE	SOURCE RANGE	DETECTOR TYPE	DETECTOR RANGE	ANGLE
E,E/	FMF	6- 30	D	124-250	MAG-D		DST

8 RESONANCES DETECTED

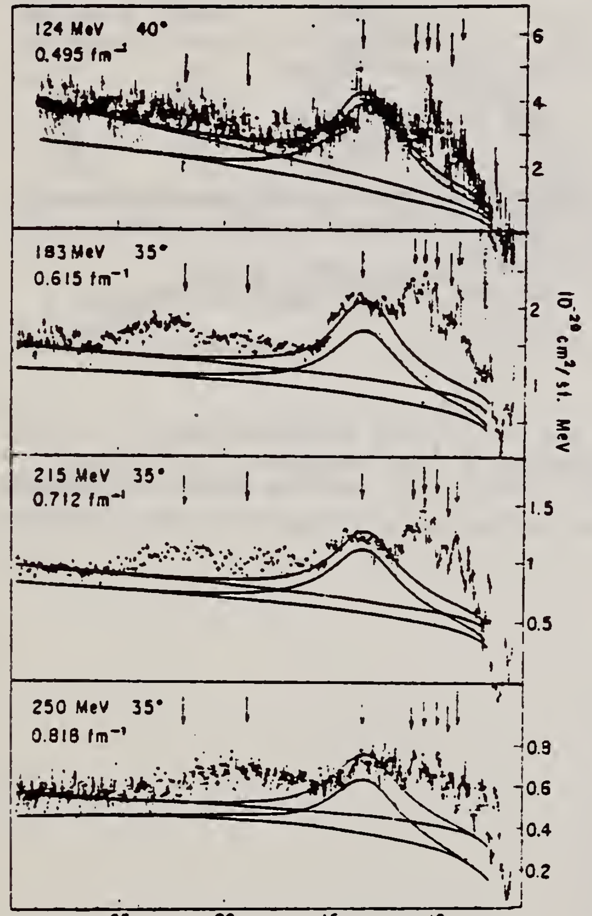

FIG. 1. Inelastic electron scattering spectra in ^{208}Pb at various momentum transfers. Arrows indicate positions of peaks at excitation energies 8.9, 9.4, 10.0, 10.6, 11.2, 13.4, 19, and 22 MeV.

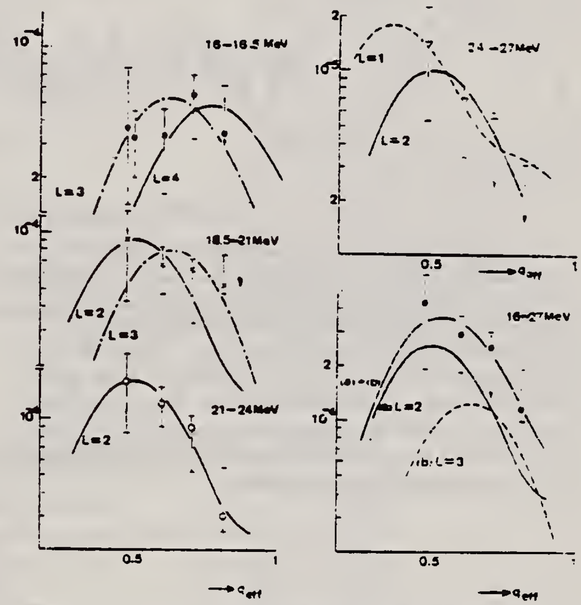

FIG. 3. Form factors integrated over the range of energies indicated in the upper corner. The form factor in the range 16–27 MeV was decomposed to the $E2$ and $E3$ components.

(over)

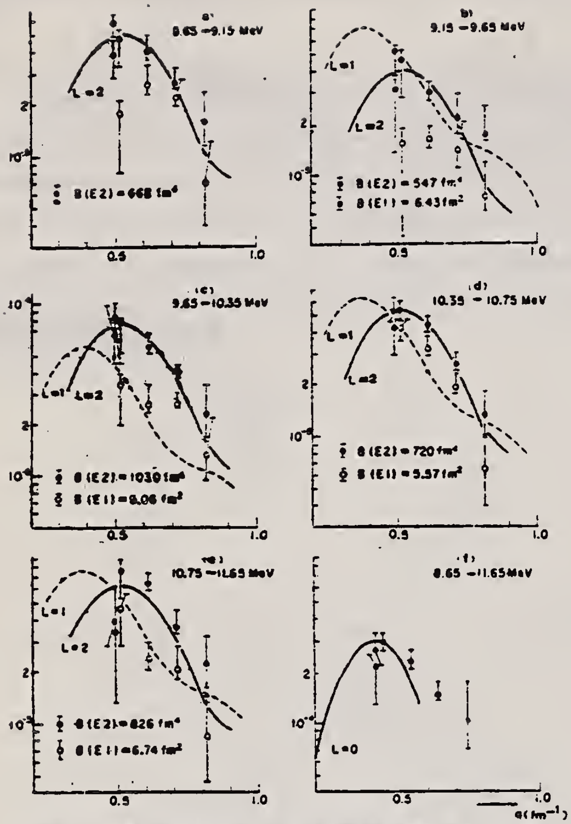

FIG. 2. Form factors for peaks at 8.9, 9.4, 10.0, 10.6, and 11.2 MeV integrated in the range of excitation energies indicated in the upper corner of each graph. Open circles, form factors extracted only from the peak parts which are seen manifestly. (a)–(e) Form factors plotted against q_{eff}. The $B(EL)$ values shown in the lower corner were obtained by comparing these form factors with the theoretical curves of $L=1$ and 2. (f) Sum of the form factors compared with the monopole form factor described in the text.

TABLE I. Values of $B(EL)$ and $|M(0)|^2$, and the percentage of the energy-weighted sum rule.

E_x	L	$B(EL)$[a] (fm^{2L})	Type of EWSR	Percentage of sum rule
8.6–11.6	2	$(3.8 \pm 0.4) \times 10^3$	$T=0$	47
	0	$\sim 8 \times 10^3$ [b]	$T=0$	100
$\simeq 19$[c]	3	$(1.3^{+0.5}_{-1.8}) \times 10^5$	$T=0$	44
$\simeq 22$[c]	2	$(3.4^{+1}_{-2}) \times 10^3$	$T=1$	60
	0	$\sim 7.2 \times 10^3$ [b]	$T=1$	126

[a] Errors from the model dependence of analysis are not included.

[b] $|M(0)|^2 = |\langle \sum_i \frac{1}{2}(1+\tau_3) r_i^2 \rangle|^2$ in fm^4.

[c] Derived from a broad bump at 16–27 MeV [see Fig. 3(c)].

REF.	Yu. I. Sorokin, V.A. Khrushchev, and B.A. Yur'ev Izv. Akad. Nauk SSSR. Ser. Fiz. 37, 156 (1973) Bull. Acad. Sci. USSR, Phys. Ser. 37, 137 (1973)	ELEM. SYM.	A	Z
		Pb	208	82
METHOD		REF. NO.		
		73 So 21		hmg

REACTION	RESULT	EXCITATION ENERGY	SOURCE		DETECTOR		ANGLE
			TYPE	RANGE	TYPE	RANGE	
G,XN	ABX	7- 27	C	7- 27	BF3-I		4PI

SEE ALSO 75SO12

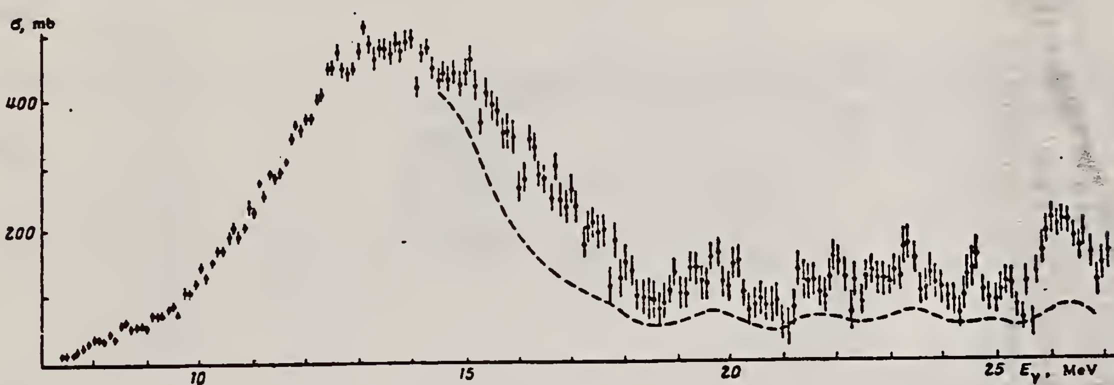

Fig. ℜ. Cross sections for ^{206}Pb: the (,Tn) cross section $\sigma(\gamma n) + 2\sigma(\gamma,2n) + \sigma(\gamma,np) + \ldots$ obtained with a processing step of 1 MeV (points), and the photoabsorption cross section $\sigma_\gamma = \sigma(\gamma n) + \sigma(\gamma,2n) + \sigma(\gamma,np) + \ldots$, obtained with al- allowance for multiplicity according to the statistical theory (dashed curve).

Integral Cross Sections, MeV·b

Reaction and E_γ range	[illegible]Pb	[illegible]Pb
$\sigma(\gamma,Tn)$ to 20 MeV	3.10	3,38
σ_γ to 20 MeV	2.80	2,81
$\sigma(\gamma,Tn)$ to 27 MeV	3.93	4,32
σ_γ to 27 MeV	3,21	3,28
$\sigma(\gamma,Tn)$ 20—27 MeV	0,83	0,94
σ_γ 20—27 MeV	0,41	0,47
$\sigma(E1)=0.06\,\frac{NZ}{A}$	2,95	2,98
$\sigma(E2)$	0,5	0,5
$\sigma(T_>)$ [14]	0,013	0,013

REF.	C. P. Swann Nucl. Phys. A201, 534 (1973)	ELEM. SYM.	A	Z
		Pb	208	82

METHOD	REF. NO.	
	73 Sw 4	egf

REACTION	RESULT	EXCITATION ENERGY	SOURCE TYPE	SOURCE RANGE	DETECTOR TYPE	DETECTOR RANGE	ANGLE
G,G	LFT	31	D	7	SCD-D		UKN

7 = 7.07, 7.09

TABLE 1

Summary of observed levels in ^{208}Pb, ^{207}Pb and ^{209}Bi and some of their properties

Nucleus	E_γ (keV)	Spin	Γ_0/Γ	$g\Gamma_0^2/\Gamma$ (eV)	Γ_0 (eV) present	Γ_0 (eV) ref. [3]	Γ_0 (eV) ref. [2]	s.p. estimate (W.u.) E1	s.p. estimate (W.u.) M1
^{208}Pb	7071±2	1	1		31±3	15	30±13	0.036	4.4
	7091±2	1	1		17±2	15		0.019	2.3
^{207}Pb	7186±5	$\frac{1}{2}, \frac{3}{2}$		15±4					
	7206±5	$\frac{1}{2}, \frac{3}{2}$		25±5					
^{209}Bi	7179±5	$\frac{7}{2}, \frac{9}{2}, \frac{11}{2}$		24±5					
	7202±5	$\frac{7}{2}, \frac{9}{2}, \frac{11}{2}$		30±5					

Weisskopf units given are based on our data.

REF. C. P. Swann
PICNS-73, Vol.I, p.317 Asilomar

ELEM. SYM.	A	Z
Pb	208	82

METHOD	REF. NO.	
	73 Sw 13	hmg

REACTION	RESULT	EXCITATION ENERGY	SOURCE TYPE	SOURCE RANGE	DETECTOR TYPE	DETECTOR RANGE	ANGLE
G,G	LFT	4- 5	C	5	SCD-D		DST

J-PI, 2 LEVELS

Table: Properties of States Observed in ^{206,207,208}Pb and ^{209}Bi

Nuclei	E_γ (keV)	J^π	Γ_0/Γ	$g\Gamma_0^2/\Gamma$ (eV)	Γ_0 (eV)	G(EL)	G(M1)
^{206}Pb	3742	1	1		0.13(2)	0.001	0.12
	4114	2^+	1		0.30(6)	5	
	4326	1	1		0.90(9)	0.004	0.56
	4602	1	1		0.23(3)	0.001	0.12
^{207}Pb	3300	$1/2^+$ a)			0.039(6)		
	3928	$(3/2^-)$	1	0.68(7)			
	4104	$3/2^-$	1		0.55(6)	8	
	4140	$5/2^-$	1		0.46(5)	6	
	4627	$1/2^+$ b)	1		0.64(7)	0.003	
	4872	1/2,3/2	1	3.6(5)		∿0.01	∿1.2
	4982	1/2,3/2	1	4.0(5)		∿0.01	∿1.2
^{208}Pb	4087	2^+	1		0.49(5)	7	
	4843	1	1		5.1(5)	0.02	2.3
^{209}Bi	2826	$5/2^-$	(.63) c)		0.09(1)		
	3977	5/2--13/2		0.82(8)			
	4085	$5/2^-$--$13/2^-$		0.28(3)		∿5	
	4144	"		0.07(2)		∿1	
	4156	"		0.21(4)		∿3	
	4176	"		0.21(4)		∿3	
	4206	"		0.25(3)		∿4	
	4747	7/2--11/2		2.9(5)		∿0.013	∿1.4
	4784	"		2.7(5)		∿0.012	∿1.3
	4822	"		1.4(3)		∿0.005	∿0.7

a) see ref. 3 b) see ref. 4 c) see ref. 5

3) S.M. Smith, P.G. Roos, C. Moazed and A.M. Bernstein, Nucl. Phys. A173, 32 (1971).

4) R.A. Mayer, B.L. Cohen and R.C. Diehl, Phys. Rev. C2, 1893 (1970).

5) R.A. Broglia, J.S. Lilley, R. Perazzo and W.R. Phillips, Phys. Rev. C1, 1508 (1970).

REF.	Y. Torizuka, Y. Kojima, T. Saito, K. Itoh, A. Nakada, S. Mitsunobu, M. Nagao, K. Hosoyama, S. Fukuda, H. Miura PICNS-73, Vol.I, p.675 Asilomar	ELEM. SYM.	A	Z
		Pb	208	82
METHOD		REF. NO. 73 To 1		hmg

REACTION	RESULT	EXCITATION ENERGY	SOURCE TYPE	SOURCE RANGE	DETECTOR TYPE	DETECTOR RANGE	ANGLE
E,E/	FMF	6- 32	D	124-250	MAG-D		DST

LEVELS 8.9-14.1

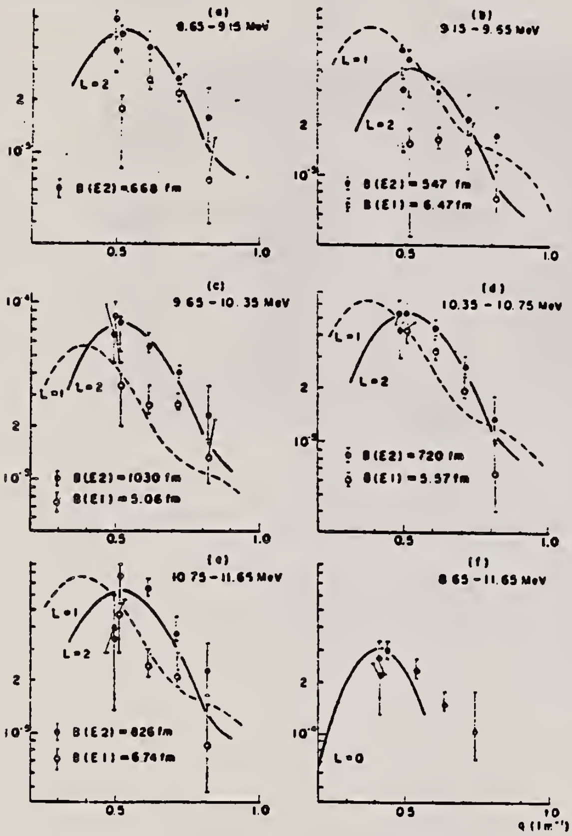

Fig. 10. The form factors for the peaks at 8.9, 9.4, 10.0, 10.6, and 11.2 MeV integrated over the range of energies indicated in the upper corner of each graph. The open circles are the form factors extracted only from the sharp peak parts. The B(EL) values shown in the lower corner were obtained by comparing these form factors with the theoretical curves of L=1 and 2.

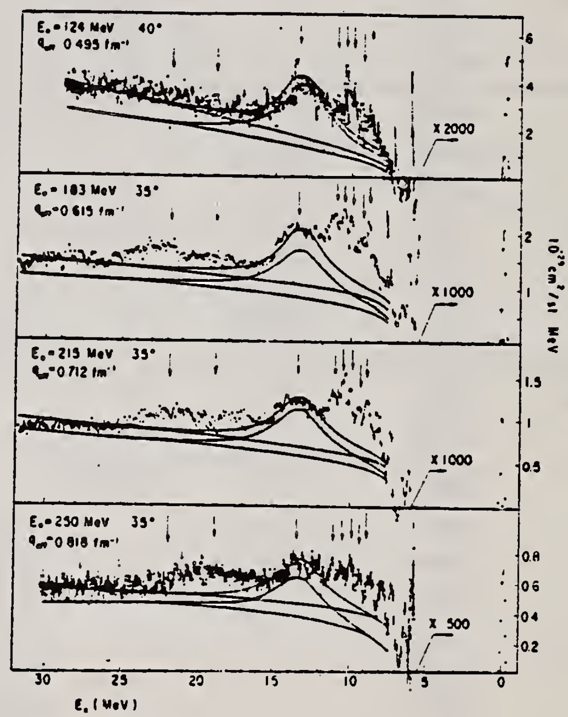

Fig. 9. Inelastic electron scattering spectra in the giant resonance region of ^{208}Pb. The arrows indicate peaks at 8.9, 9.4, 10.0, 10.6, 11.2, 13.4, ∿19, and ∿22 MeV.

(over)

Table IV. The B(EL) or $|M(0)|^2$ values and the occupation rates to the energy weighted sum rule (EWSR).

E_x	L	B(EL) in fm^{2L}*	Type of EWSR	Occupation rate in %
8.9	2	670±70	T=0	7.8
9.4	2	550±90	T=0	6.3
10.0	2	1030^{+50}_{-80}	T=0	13
10.6	2	720^{+20}_{-80}	T=0	8.4
11.2	2	830±130	T=0	11
8.6∿11.6	2	$(3.8±0.4)\times10^3$	T=0	47
	0	$\sim8\times10^3$**	T=0	100
≃19***	3	$(1.8^{+0.6}_{-1.6})\times10^5$	T=0	44
≃22***	2	$(3.4^{+1}_{-2})\times10^3$	T=1	60
	0	7.2×10^3**	T=1	126

* Errors from the model dependence of analysis are not included.

** $|M(0)|^2=|<\sum_i \frac{1+\tau_3}{2} r_i^2>|^2$ in fm^4

*** Derived from a broad bump of 16∿27 MeV.

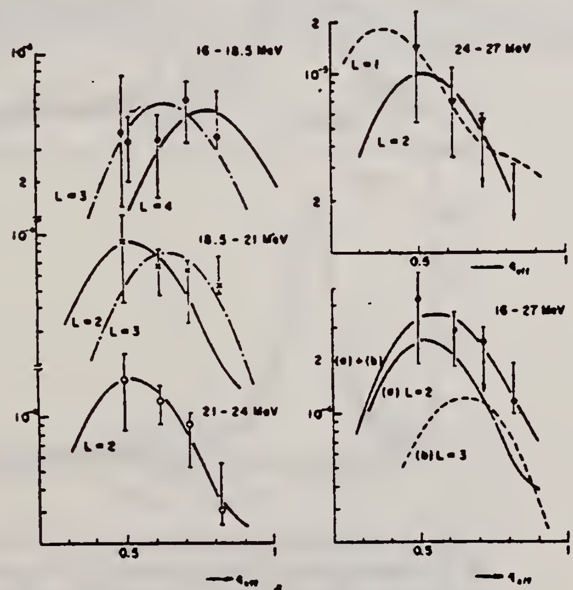

Fig. 11. The form factors integrated over the range of energies indicated in the upper corner of each graph. The form factor in the range 16-27 MeV was decomposed to the E2 and E3 components.

REF.

H. E. Jackson
Phys. Rev. C9, 1148 (1974)

EL. SYM.	A	Z
Pb	208	82

METHOD

REF. NO.	
74 Ja 1	hmg

REACTION	RESULT	EXCITATION ENERGY	SOURCE TYPE	SOURCE RANGE	DETECTOR TYPE	DETECTOR RANGE	ANGLE
G,N	ABX	7- 9	C	7- 9	TOF-D		DST

A series of experimental estimates of the nonresonant radiative neutron reaction cross section in ^{208}Pb have been reported recently. To date, the results from (γ,n) studies have been inconsistent with measurements of neutron-induced reactions. In an effort to resolve this discrepancy, the shape of the 41-keV resonance in the reaction $^{208}Pb(\gamma,n)^{207}Pb$ has been studied in detail by simultaneous measurements of the photoneutron spectra at 90 and 135°. A small asymmetry in the resonance shape implies the presence of a background cross section of $1.3^{+2.7}_{-0.7}$ mb. This value can be explained in terms of contributions from neighboring resonances plus a small direct-reaction component; there is no evidence for anomalous processes. The result is consistent with the most recent data from study of the reaction $^{207}Pb(n,\gamma_0)$.

[NUCLEAR REACTIONS $^{208}Pb(\gamma,n)$, bremsstrahlung end points 7.9, 8.4, and 9.0 MeV; studied shape 41-keV resonance, deduced background $\sigma(\gamma,n) = 1.3^{+2.7}_{-0.7}$ mb.]

TABLE II. Comparison of calculated and observed background cross sections for $^{208}Pb(\gamma,n)^{207}Pb$. The values corresponding to a $\sqrt{E_n}$ extrapolation of the thermal (γ,n) cross section are given in the fourth column. The results of a calculation discussed in Sec. IV are given in the last column.

E_n (keV)	Experimental σ_{bg} (n,γ) (mb)	Experimental σ_{bg} (γ,n) (mb)	Calculated σ_{bg} Extrap.[a] (mb)	Calculated σ_{bg} (γ,n) (mb)
0.025×10^{-3}	709 ± 10[b]	0.0012	0.0012	0.0012
1.95	3.2 ± 1.2[c]	0.45 ± 0.16	0.34	0.41
25	0.5[d]	0.9 ± 0.2	1.2	1.01
41	···	$1.3^{+2.7}_{-0.7}$[e]	1.5	1.15

[a] Cross sections extrapolated from the thermal capture cross section $\sigma_{th}(\gamma,n)$ by use of the relation

$$\sigma(\gamma,n) = \sigma_{th}(\gamma,n)[E_n/(0.025\times10^{-3})]^{1/2},$$

where E_n and the thermal energy are in keV.
[b] Reference 3.
[c] R. C. Greenwood and C. W. Reich, Phys. Rev. C 4, 2249 (1971).
[d] Reference 7.
[e] This work.

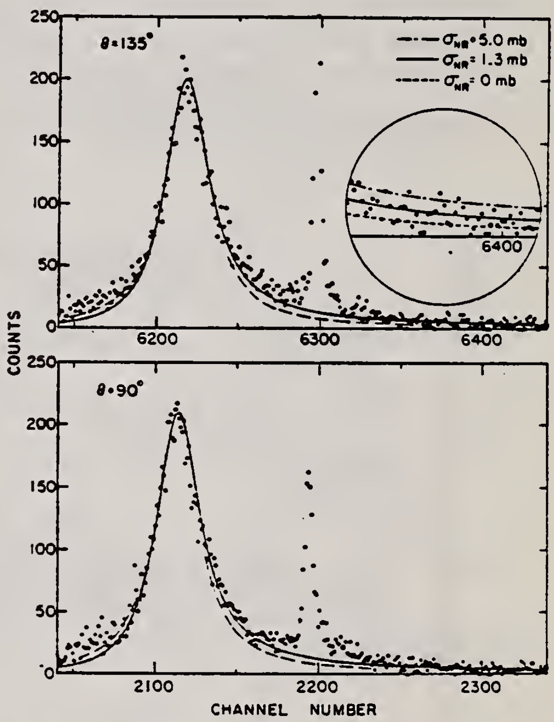

FIG. 1. Photoneutron time-of-flight spectra for ^{208}Pb in the region of the 40.5-keV resonance. The data were accumulated simultaneously on flight paths at 90 and 135° to the photon beam. The solid curve (the result of a least-squares fit) corresponds to an isotropic nonresonant cross section of 1.3 mb and a total resonance width of 1400 mb. The dotted curve is the shape expected for a vanishing nonresonant cross section. Both curves include the effects of resolution broadening. The region near the narrow resonance at 37 keV (at channel numbers 6300 and 2190 in the 135 and 90° data, respectively) was excluded from the analysis. The inset shows an enlarged view of the low-energy wing of the resonance as observed at 135°, and contains data obtained by averaging adjacent channels of the time-of-flight spectrum.

3
E.T. Jurney and H.T. Motz, Argonne National Laboratory Report No. ANL-6797, 1963 (unpublished) p.236.
7
O.A. Wasson and R.E. Chrien, in Proceedings of the International Conference on Photonuclear Reactions and Applications, Asilomar 1973, edited by B.L. Berman (Lawrence Livermore Laboratory, Livermore, California, 1973), Vol.1, p.311.

REF. R. Moreh, O. Šhahal, and I. Jacob
Nucl. Phys. A228, 77 (1974)

ELEM. SYM.	A	Z
Pb	208	82

METHOD

REF. NO. 74 Mo 7 egf

REACTION	RESULT	EXCITATION ENERGY	SOURCE TYPE	SOURCE RANGE	DETECTOR TYPE	DETECTOR RANGE	ANGLE
G,G	NOX	7	D	7	NAI-D		135

7=7.279 FUNC TEMP

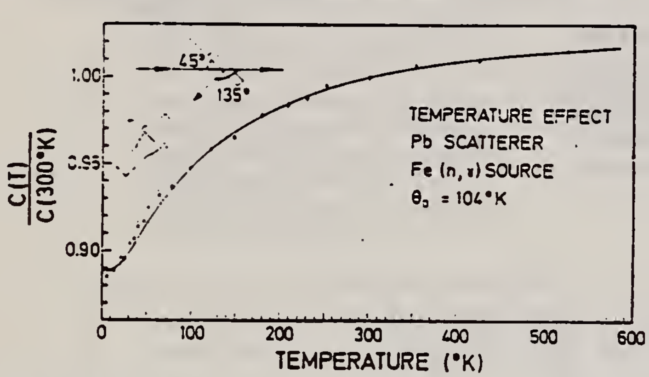

Fig. 5. Relative scattering yield from a Pb scatterer as a function of temperature. The scatterer thickness is 0.88 cm and the geometry is indicated in the figure. The scattering yield is normalised to $T = 300°K$. The solid line is the theoretical curve obtained using eq. (1) with $\theta_0 = 104°K$, $\delta = 7.3$ eV, $\Gamma = 0.78$ eV, $\Gamma_0/\Gamma = 1$, and corrected to account for the effect of the edges of the target.

REF. R. Pitthan, F.R. Buskirk, E.B. Dally, J.N. Dyer, and X.K. Maruyama
Phys. Rev. Lett. 33, 849 (1974)

(See Erratum: Phys. Rev. Lett. 34, 848 (1975))

ELEM. SYM.	A	Z
Pb	208	82

METHOD

REF. NO. 74 Pi 2 hmg

REACTION	RESULT	EXCITATION ENERGY	SOURCE TYPE	SOURCE RANGE	DETECTOR TYPE	DETECTOR RANGE	ANGLE
E,E/	FMF	3- 40	D	90	MAG-D		DST

B(EL)

Inelastic electron scattering with 90-MeV electrons shows previously observed giant resonances at excitation energies of $63A^{-1/3}$ ($E2$), $81A^{-1/3}$ ($E1$), $105A^{-1/3}$ ($E3$), and $130A^{-1/3}$ MeV ($E2$). Distorted-wave-Born-approximation analysis of additional structure at $53A^{-1/3}$ and $195A^{-1/3}$ MeV suggests a monopole assignment. Transverse contributions to the $E1$ matrix element are compatible with an electric spin-flip. Differing widths of the respective resonances in the two nuclei are explained through dynamic deformation of Au. The reduced electric transition strengths $B(EL)$ are given.

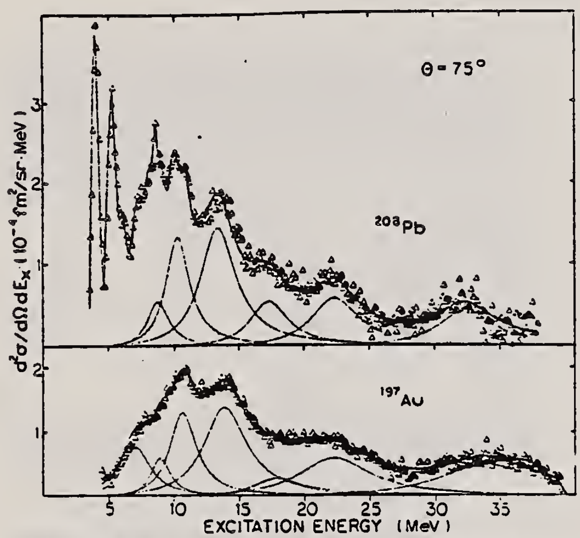

FIG. 2. Same as Fig. 1, after subtraction of the fitted background.

FIG. 1. Spectrum of 90-MeV electrons, scattered inelastically from Pb and Au. The fitted background which consists of the radiation tail and the machine background is shown. The counting rate is corrected for the constant momentum dispersion of the spectrometer. Thus the error increases with the excitation energy.

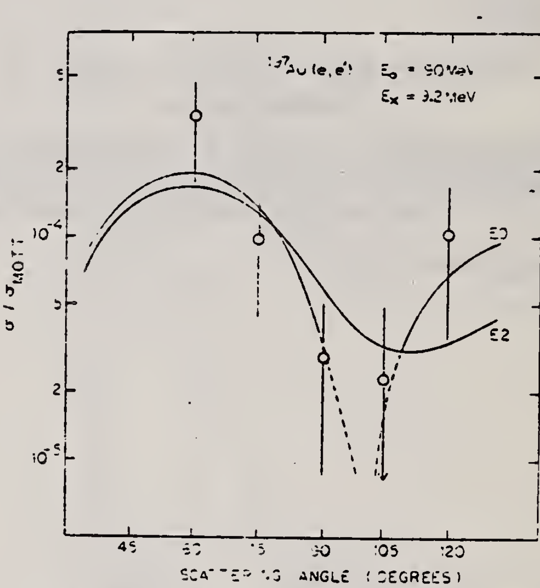

FIG. 3. Ratio of the inelastic cross section of the resonance at 9.2 MeV to the Mott cross section as a function of scattering angle. The curves show the results of DWBA calculations assuming an $E2$ or an $E0$ assignment. At 105° we did not see a resonance. The open circle corresponds to a resonance with a height of 1 standard deviation in the count rate and is, therefore, regarded as an upper limit. The error at 105° represents 1 additional standard deviation.

(over)

TABLE I. Comparison of results for Au and Pb as extracted from the 75° measurements. Columns 2 and 3 show multipolarity and isospin assignments assumed.

			^{197}Au						^{208}Pb					
E_x [$A^{-1/3}$ MeV]	EL	ΔT	E_x [MeV]	B(EL) [fm^{2L}] a)	Γ_{nat} [MeV]	EWSR b) [%]	SPU c)	Others B(EL)	E_x [MeV]	B(EL) [fm^{2L}] a)	Γ_{nat} [MeV]	EWSR b) [%]	SPU c)	Others B(EL)
53	E0	0	9.2	$(3.6\pm1.8)10^3$	2.2±0.5	35	--	--	8.0	$(5\pm3)10^3$	1.8±0.5	50	--	--
63	E2	0	10.8	$(5.2\pm1.2)10^3$	2.9±0.2	77	15.3	$(8.4\pm1.6)10^3$ h)	10.5	$(5.7\pm2.5)10^3$	2.8±0.3	95	21.5	$(2.6\pm0.9)10^3$ f)j) $(2.6\pm0.3)10^3$ g)j)
81	E1	1	14.0	100±20 d) 50±10 e)	4.5±0.2	200 100	15.0 7.5	82±11 d)h) 73± 5 i)	13.6	103±20 53±10	3.9±0.1	205 105	16 8	64±3 d/f) 71± 5 i)
105	E3	0 1	18.0	$(1.7\pm.3)10^5$	5.2±0.7	45 31	12.0	--	17.5	$(3.2\pm1.5)10^5$	4.2±0.7	90 60	17	$(1.3^{+2.6}_{-1.5})10^5$ g)
133	E2	1	23.0	$(4.6\pm1.5)10^3$	7±1	95	13.5	$(9.5\pm1.4)10^3$ h)	22.5	$(4.2\pm1.4)10^3$	5±1	85	14	$(3.4^{+1}_{-2})10^3$ g)
195	E0	1	33.5	$(10^{+3}_{-7})10^3$	10.5±2	250	--	--	33.0	$(5.5^{+2}_{-3})10^3$	6±1	150	--	--

[a] For the monopole $|M_{if}|^2$ (fm^4).
[b] Energy-weighted sum rule Ref. 19.
[c] Single particle units Ref. 20.
[d] Surface oscillation $\rho_{tr}(r) \sim d\rho_0(r)/dr$.
[e] Volume oscillation $\rho_{tr}(r) \sim \rho_0(r)$.
[f] Ref. 9.
[g] Ref. 8.
[h] Ref. 15.
[i] Ref. 14.
[j] Extracted from a 2-MeV-wide range only.

8
M. Nagao and Y. Torizuka, Phys. Rev. Lett. 30, 1068 (1973).
9
F.R. buskirk, H.D. Graf, R. Pitthan, H. Theissen, O. Titze, and Th. Walcher, Phys. Lett. 42B, 194 (1972).
14
M. Danos and W. Greiner, Phys. Rev. 134, B284 (1964).
15
A. Veyssiere, H. Beil, R. Bergere, P. Carlos, and A. Lepretre, Nucl. Phys. A159, 561 (1970).
19
N.I. Kassis, Technical Report, Institut fur Kernphysik der Universitat Mainz, 1969, unpublished.
20
R.A. Ferrell, Phys. Rev. 107, 1631 (1957); J. Weneser and E.K. Warburton, in The Role of Isospin in Electromagnetic Transitions, ed. D.H. Wilkinson (North-Holland, Amsterdam, 1969).

REF.		ELEM. SYM.	A	Z
W. Scholz, H. Bakhru , R. Colle, and Angela Li-Scholz Phys. Rev. C9, 1568 (1974)		Pb	208	82
METHOD		REF. NO. 74 Sc 2		hmg

REACTION	RESULT	EXCITATION ENERGY	SOURCE TYPE	SOURCE RANGE	DETECTOR TYPE	DETECTOR RANGE	ANGLE
G,G	LFT	7	D	7	SCD-D		DST
		(7.084)		(7.084)			

LEVEL 7.084 MEV

The Doppler-broadened 7.12-MeV transition from the $^{19}F(p,\alpha\gamma)^{16}O$ reaction has been used to fluoresce resonantly a level at 7.084 ± 0.002 MeV in ^{208}Pb. A spin value of $J = 1$ has been assigned by measuring the intensity of the scattered radiation at average scattering angles of 90 and 130°. From a study of the intensity growth of the scattered radiation with increasing scatterer thickness (production experiment), the following level parameters were extracted: integrated scattering cross section $\int \sigma_s dE = 2.07 \pm 0.18$ MeV mb, maximum absorption cross section $\sigma_A^{max} = 85^{+36}_{-31}$ b, total level width $\Gamma = 26^{+35}_{-12}$ eV, and partial width for the ground-state transition $\Gamma_0 = 16^{+6}_{-4}$ eV.

[NUCLEAR REACTIONS $^{208}Pb(\gamma,\gamma')$, $E \approx 7$ MeV; measured $\sigma(E_\gamma;\theta)$. ^{208}Pb deduced level Γ, Γ_0, σ_A^{max}, J. Natural Pb targets, resonance-fluorescence production experiment.]

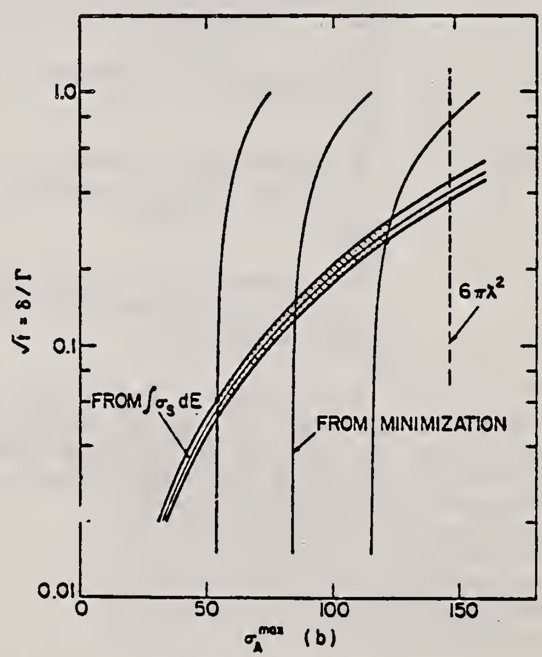

FIG. 3. Maximum absorption cross section vs $\sqrt{t}$ $=\delta/\Gamma$. The shaded region contains the values of σ_A^{max} and $\sqrt{t}$ that are compatible with the results of the production experiment. For details see text.

REF.	C.P. Swann Phys. Rev. Lett. 32, 1449 (1974)	ELEM. SYM.	A	Z
		Pb	208	82

METHOD	REF. NO.	
	74 Sw 7	hmg

REACTION	RESULT	EXCITATION ENERGY	SOURCE TYPE	SOURCE RANGE	DETECTOR TYPE	DETECTOR RANGE	ANGLE
$ G,G	LFT	5	C	5	SCD-D		DST
		(4.843)		(4.95)			

4843 KEV,POL,PHOTON

From measurements of resonance-fluorescence cross section, angular distribution, and polarization, the 4843-keV level of ^{208}Pb has been shown to have a 1^+ character and a width of 5.1 ± 0.8 eV with all of the decays to the ground state. As the probable lower member of the giant *M*1 excitation, this state is at a significantly lower energy and has a decay strength which is an order of magnitude larger than the predictions of simple shell-model calculations.

TABLE I. Comparison of the experimental and theoretical results for the "giant" *M*1 excitation in ^{208}Pb.

Experimental E_γ (MeV)	Experimental $B(M1, 1^+ \to 0^+)$ $[(e\hbar/2Mc)^2]$	Theoretical[a] E_γ (MeV)	Theoretical[a] $B(M1, 1^+ \to 0^+)$ $[(e\hbar/2Mc)^2]$
7.41 to 8.24[b] (7 levels)	(11.6)	7.52	16.0
7.28[c]	0.2	...	...
4.84[d]	3.8	5.45	0.4

[a]See Ref. 9. [b]See Ref. 7. [c]See Ref. 8. [d]Present study.

7) C.D. Bowman, R.J. Baglan, B.L. Berman, and T.W. Phillips, Phys. Rev. Lett. 25, 1302 (1970).
8) A. Wolf, R. Moreh, A. Nof, O. Shahal, and J. Tenenbaum, Phys. Rev. C6, 2276 (1972).
9) J.D. Vergados, Phys. Lett. 36B, 12 (1971).

REF.			ELEM. SYM.	A	Z
C. P. Swann J. Franklin Institute <u>298</u>, 321 (1974)			Pb	208	82
METHOD			REF. NO. 74 Sw 11		egf

REACTION	RESULT	EXCITATION ENERGY	SOURCE TYPE	SOURCE RANGE	DETECTOR TYPE	DETECTOR RANGE	ANGLE
G,G	LFT	3- 5	C	4- 5	SCD-D		DST

<u>2 LEVELS 4087,4843 KEV</u>

TABLE II

Properties of states observed in ^{206,207,208}Pb and ^{209}Bi; G(EL) and G(M1) are the reduced transition probabilities in Weisskopf units

Nuclei	E_γ (keV)	J^π	Γ_0/Γ	$g\Gamma_0^2/\Gamma$ (eV)	Γ_0 (eV)	G(EL)	G(M1)
^{206}Pb	3744	1^-	1		0·13 (2)	0·001	
	4114	2^+	1		0·30 (6)	5	
	4330	1^+	1		0·90 (9)		0·56
	4606	1	1		0·23 (3)	0·001	0·12
	4974	1	1	0·8 (2)		0·003	0·32
	5038	1	1	2·3 (5)		0·007	0·90
^{207}Pb	3300	$1/2^{+}$*			0·039 (6)		
	3928	$3/2^-$	1		0·34 (4)		
	4104	$3/2^-$	1		0·55 (6)	8	
	4140	$5/2^-$	1		0·46 (5)	6	
	4627	$1/2^{+}$†	1		0·64 (7)	0·003	
	4872	$1/2^-, 3/2^-$	1	3·6 (5)			~1·2
	4982	$1/2^-, 3/2^-$	1	4·0 (5)			~1·2
^{208}Pb	4087	2^+	1		0·49 (5)	7	
	4843	1^+	1		5·1 (8)		2·3
^{209}Bi	2826	$5/2^-$	(0·63)‡		0·09 (1)		
	3977	$5/2$–$13/2$		0·82 (8)			
	4085	$5/2^-$–$13/2^-$		0·28 (3)		~5	
	4144	$5/2^-$–$13/2^-$		0·07 (2)		~1	
	4156	$5/2^-$–$13/2^-$		0·21 (4)		~3	
	4176	$5/2^-$–$13/2^-$		0·21 (4)		~3	
	4206	$5/2^-$–$13/2^-$		0·25 (3)		~4	
	4747	$7/2^-$–$11/2^-$		2·9 (5)			~1·4
	4785	$7/2^-$–$11/2^-$		2·7 (5)			~1·3
	4822	$7/2^-$–$11/2^-$		1·4 (3)			~0·7

* See Ref. (11). † See Ref. (12). ‡ See Ref. (7).

[7] C.P. Swann, Phys. Rev. Letts. <u>32</u>, 1449 (1974).
[11] S.M. Smith et al., Nucl. Phys. <u>A173</u>, 32 (1971).
[12] R.A. Mayer et al., Phys. Rev. <u>C2</u>, 1898 (1970).

REF.		ELEM. SYM.	A	Z
	R.R. Whitney, I. Sick, J.R. Ficenec, R.D. Kephart, and W.P. Trower Phys. Rev. C9, 2230 (1974)	Pb	208	82
METHOD		REF. NO.		
		74 Wh 3		hmg

REACTION	RESULT	EXCITATION ENERGY	SOURCE		DETECTOR		ANGLE
			TYPE	RANGE	TYPE	RANGE	
E,E/	ABX	0-300	D	500	MAG-D		60

QUASIELASTIC SCAT

See further analysis of this data in reference 79Zi1

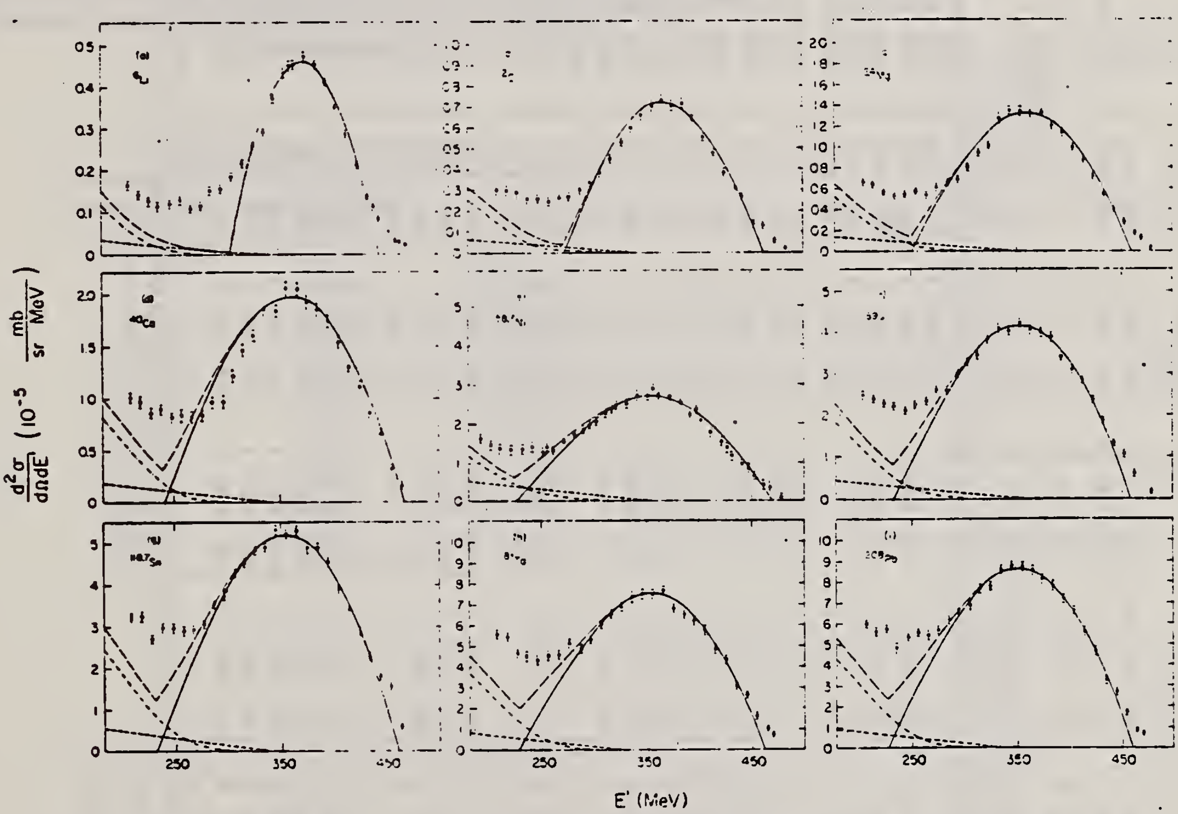

FIG. 1. The measured quasielastic peaks; the errors on the data points do not include an over-all 3% normalization uncertainty. The solid curve is a fit by the Fermi-gas model which yielded k_F (in MeV/c) and $\bar{\epsilon}$ (in MeV) as follows: (a) ^{6}Li (169, 17); (b) ^{12}C (221, 25); (c) ^{24}Mg (235, 32); (d) ^{40}Ca (249, 33); (e) $^{58.7}$Ni (260, 36); (f) ^{89}Y (254, 39); (g) $^{118.7}$Sm (260, 42); (h) ^{181}Ta (265, 42); (i) ^{208}Pb (265, 44). The fitting uncertainty in k_F is ±5 MeV/c and in $\bar{\epsilon}$ it is ±3 MeV. The small-amplitude dashed curve is the s-wave π-production contribution, the dot-dashed curve is the isobar excitation, and the large-amplitude dashed curve is the total result.

(OVER)

TABLE I. Proton-normalized and radiative-corrected cross sections $d^2\sigma/d\Omega dE' = (N \pm \Delta N) \times 10^{-n}$ in mb/sr MeV, for $E = 500$ MeV and $\theta = 60°$.

E'	^{6}Li			^{12}C			^{24}Mg			^{40}Ca			$^{58.7}$Ni			^{89}Y			$^{118.7}$Sn			$^{180.95}$Ta			^{208}Pb		
(MeV)	N	ΔN	n	N	ΔN	n	N	ΔN	n	N	ΔN	n	N	ΔN	n	N	ΔN	n	N	ΔN	n	N	ΔN	n	N	ΔN	n
480.0	···			1.79	0.19	7	3.83	0.42	7	···			1.22	0.17	6	1.71	0.19	6	···			···			···		
474.0	···			1.02	0.13	7	···			···			···			···			···			···			···		
470.0	1.72	0.18	7	5.75	0.52	7	1.55	0.15	6	···			3.90	0.29	6	5.85	0.41	6	···			7.09	0.67	6	7.00	0.68	6
464.0	2.49	0.29	7	1.38	0.11	6	1.91	0.17	6	2.72	0.15	6	4.48	0.33	6	5.68	0.37	6	8.32	0.71	6	1.16	0.08	5	9.82	0.79	6
460.0	2.96	0.30	7	1.20	0.09	6	2.58	0.19	6	···			···			···			···			1.54	0.10	5	1.81	0.10	5
454.1	5.02	0.47	7	9.21	0.71	7	2.96	0.20	6	4.20	0.17	6	7.00	0.41	6	1.07	0.05	5	1.85	0.09	5	1.70	0.11	5	2.31	0.11	5
450.0	···			···			···			···			8.92	0.47	6	1.03	0.05	5	1.83	0.09	5	···			···		
444.3	8.68	0.58	7	1.26	0.07	6	4.31	0.35	6	6.67	0.27	6	1.02	0.05	5	1.33	0.05	5	···			2.77	0.14	5	2.74	0.12	5
440.0	1.11	0.06	6	2.59	0.13	6	5.23	0.26	6	···			···			···			···			3.43	0.16	5	3.24	0.13	5
434.2	1.32	0.06	6	2.99	0.14	6	5.50	0.26	6	8.74	0.35	6	1.19	0.05	5	1.90	0.07	5	2.27	0.09	5	3.14	0.15	5	3.34	0.14	5
430.0	···			···			···			···			1.40	0.07	5	2.11	0.08	5	2.77	0.11	5	···			···		
424.3	2.12	0.08	6	3.75	0.15	6	7.31	0.29	6	1.12	0.04	5	1.54	0.08	5	2.31	0.09	5	2.88	0.12	5	4.43	0.18	5	4.74	0.19	5
414.4	2.88	0.12	6	4.75	0.19	6	8.78	0.35	6	1.32	0.05	5	1.78	0.10	5	2.88	0.11	5	3.40	0.14	5	4.98	0.20	5	5.64	0.23	5
404.5	3.51	0.11	6	5.46	0.22	6	1.02	0.04	5	1.56	0.06	5	2.09	0.08	5	3.09	0.12	5	3.90	0.16	5	5.89	0.24	5	6.57	0.26	5
400.0	···			6.25	0.25	6	1.09	0.04	5	···			2.35	0.09	5	3.34	0.13	5	4.29	0.17	5	6.56	0.27	5	7.00	0.28	5
394.7	[illegible]	0.17	[illegible]	[illegible]	[illegible]	6	1.15	0.05	5	1.75	0.07	5	2.22	0.09	5	3.41	0.14	5	4.56	0.18	5	6.29	0.25	5	7.25	0.29	5
385.7	[illegible]	0.18	[illegible]	[illegible]	[illegible]	[illegible]	1.21	0.05	5	1.86	0.07	5	2.51	0.10	5	3.91	0.16	5	4.88	0.19	5	6.36	0.26	5	7.88	0.32	5
374.9	[illegible]	0.19	[illegible]	[illegible]	[illegible]	6	1.33	0.05	5	1.91	0.08	5	2.72	0.11	5	4.02	0.16	5	4.88	0.19	5	6.87	0.28	5	8.19	0.33	5
365.0	[illegible]	[illegible]	[illegible]	[illegible]	[illegible]	6	1.32	0.05	5	2.08	0.08	5	2.69	0.10	5	4.04	0.16	5	5.34	0.21	5	7.77	0.31	5	8.61	0.34	5
360.0	1.50	[illegible]	6	[illegible]	0.28	6	1.32	0.05	5	···			2.88	0.11	5	4.11	0.16	5	5.69	0.23	5	7.92	0.33	5	8.42	0.34	5
355.2	4.15	0.17	[illegible]	6.97	0.25	6	1.36	0.05	5	2.08	0.08	5	2.69	0.11	5	4.23	0.17	5	5.22	0.21	5	7.51	0.30	5	···		
345.3	3.68	[illegible]	6	6.51	0.26	6	1.35	0.05	5	1.85	0.07	5	2.72	0.11	5	4.02	0.16	5	5.37	0.21	5	7.59	0.30	5	8.83	0.35	5
335.4	2.90	0.12	6	5.91	0.21	6	1.29	0.05	5	1.87	0.08	5	2.48	0.10	5	4.08	0.16	5	4.92	0.19	5	7.44	0.29	5	8.69	0.35	5
325.5	2.59	0.10	6	5.23	0.21	6	[illegible]	0.04	5	1.61	0.07	5	2.48	0.11	5	3.78	0.15	5	4.83	0.19	5	6.93	0.28	5	7.81	0.31	5
320.0	···			···			···			···			2.35	0.09	5	3.34	0.14	5	4.53	0.18	5	···			···		
315.7	2.16	0.10	6	4.43	0.18	6	9.41	0.38	6	1.47	0.06	5	2.26	0.09	5	3.43	0.14	5	4.34	0.17	5	6.61	0.26	5	7.76	0.31	5
305.8	1.84	0.09	6	3.79	0.15	6	8.61	0.32	6	1.23	0.05	5	2.03	0.08	5	3.27	0.13	5	4.32	0.17	5	6.11	0.24	5	6.92	0.28	5
300.0	···			···			···			···			1.97	0.08	5	3.11	0.12	5	4.03	0.16	5	···			···		
295.9	1.55	0.09	6	3.38	0.14	6	6.77	0.29	6	9.97	0.40	6	1.80	0.07	5	3.02	0.12	5	3.74	0.15	5	5.38	0.22	5	6.73	0.27	5
285.9	1.50	0.09	6	2.96	0.14	6	6.64	0.31	6	9.73	0.39	6	1.72	0.07	5	2.60	0.13	5	3.55	0.15	5	4.92	0.23	5	6.30	0.29	5
276.2	1.14	0.08	6	2.64	0.13	6	6.03	0.32	6	8.35	0.41	6	1.50	0.07	5	2.64	0.13	5	3.10	0.15	5	5.22	0.24	5	5.73	0.30	5
266.3	1.08	0.03	6	2.61	0.11	6	5.32	0.33	6	8.57	0.43	6	1.31	0.08	5	2.37	0.14	5	2.72	0.16	5	4.62	0.26	5	5.51	0.31	5
260.0	···			···			···			···			1.39	0.08	5	1.95	0.13	5	2.94	0.18	5	···			···		
256.4	1.26	0.09	6	2.43	0.15	6	5.71	0.35	6	8.33	0.45	6	1.27	0.08	5	2.27	0.14	5	2.87	0.18	5	4.57	0.28	5	5.63	0.33	5
246.6	1.20	0.09	6	2.55	0.16	6	5.47	0.36	6	8.55	0.48	6	1.39	0.09	5	2.14	0.14	5	2.95	0.19	5	4.33	0.28	5	5.40	0.35	5
236.7	1.15	0.10	6	2.54	0.16	6	5.18	0.38	6	8.71	0.51	6	1.34	0.09	5	2.24	0.15	5	3.02	0.20	5	4.35	0.30	5	4.90	0.34	5
226.8	1.27	0.11	6	2.88	0.19	6	5.62	0.42	6	8.72	0.51	6	1.29	0.10	5	2.29	0.16	5	2.73	0.20	5	4.57	0.30	5	5.88	0.37	5
216.9	1.43	0.14	6	2.91	0.21	6	6.35	0.49	6	9.81	0.56	6	1.34	0.10	5	2.38	0.17	5	3.26	0.22	5	5.42	0.36	5	5.76	0.38	5
207.0	1.66	0.16	6	2.94	0.21	6	6.59	0.52	6	1.02	0.06	5	1.43	0.11	5	2.51	0.18	5	3.24	0.22	5	5.58	0.37	5	6.11	0.40	5
197.2	1.78	0.17	6	3.42	0.24	6	7.01	0.59	6	···			1.59	0.12	5	2.77	0.20	5	3.43	0.24	5	5.67	0.38	5	5.99	0.41	5

REF.	I. C. Haacke and K. G. McNeill Can. J. Phys. 53, 1422 (1975)	ELEM. SYM.	A	Z
		Pb	208	82

METHOD	REF. NO.	
	75 Ha 4	hmg

REACTION	RESULT	EXCITATION ENERGY	SOURCE TYPE	SOURCE RANGE	DETECTOR TYPE	DETECTOR RANGE	ANGLE
G,N	LFT	7- 9	C	10	TOF-D		DST

Threshold photoneutron time-of-flight spectra from the ^{208}Pb(γ,n)^{207}Pb reaction have been measured at five angles to the incident photons. Angular distributions obtained for 14 resonances within 850 keV of the ^{208}Pb(γ,n) threshold have led to assignments of $M1$ strength totalling 67.5 ± 12 eV. The total $M1$ strength available from spin-flip transitions from the $i_{13/2}$ neutron shell and the $h_{11/2}$ proton shell has been calculated to be 100 eV (Weiss). Thus, the data confirm the existence of an $M1$ giant resonance just above threshold in ^{208}Pb.

TABLE 2. $\Gamma_{\gamma 0}$ values for ^{208}Pb resonances

Neutron energy (keV)	Excitation energy (MeV)	$\Gamma_{\gamma 0}$ (eV)
30.2	7.41	0.40 ± 0.15
37.7	7.41	1.01 ± 0.27
41.0	7.42	4.20 ± 0.72
90.0	7.47	0.9 ± 0.4
115.0	7.49	0.9 ± 0.3
128.0	7.50	1.50 ± 0.33
181.0	7.56	11.8 ± 1.5
256.0	7.63	17.7 ± 1.9
296.0	7.67	1.03 ± 0.25
316.0	7.69	7.03 ± 1.1
540.0	7.92	9.2 ± 2.0
610.0	7.99	21.2 ± 3.5
649.0	8.03	6.7 ± 1.3
844.0	8.22	7.3 ± 1.7

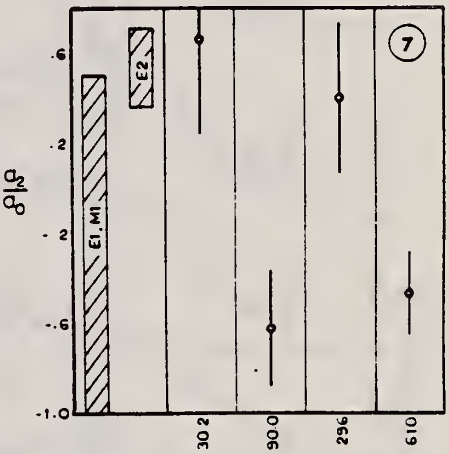

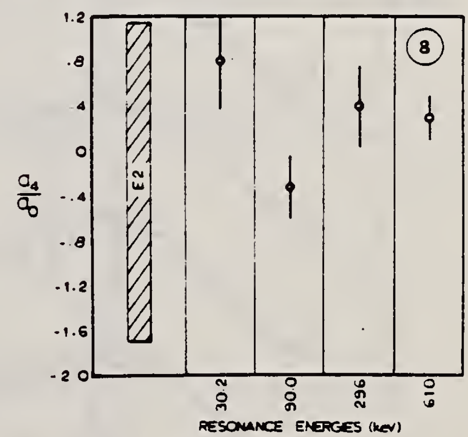

FIG. 7. a_2/a_0 ratios obtained from 3 parameter fit to data from ^{208}Pb resonances.
FIG. 8. a_4/a_0 ratios obtained from 3 parameter fit to data from ^{208}Pb resonances.

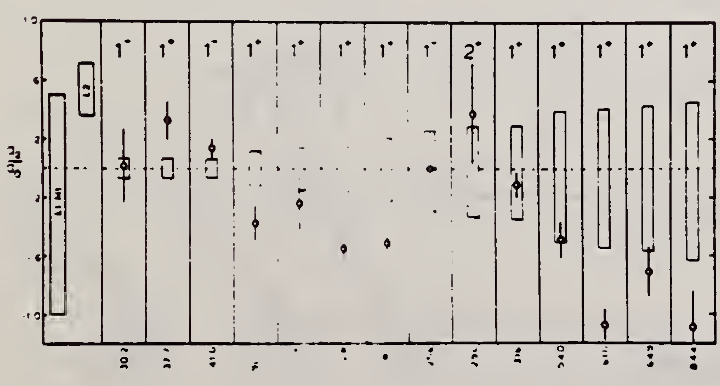

FIG. 6. Experimental a_2/a_0 ratios for ^{208}Pb resonances. Overall theoretically possible ranges of a_2/a_0 values for $E1$, $M1$, and $E2$ excitations are shown at the left of the figure. The rectangles shown with the individual data points indicate restricted ranges of possible a_2/a_0 values for $E1$ transitions, based on optical model calculations of d to s wave neutron decay ratios.

REF. R. G. Johnson, J. D. Irish, and K. G. McNeill
Can. J. Phys. 53, 1434 (1975)

ELEM. SYM.	A	Z
Pb	208	82

METHOD

REF. NO.	
75 Jo 2	hmg

REACTION	RESULT	EXCITATION ENERGY	SOURCE TYPE	SOURCE RANGE	DETECTOR TYPE	DETECTOR RANGE	ANGLE
G,N	ABX	8- 13	C	11- 16	TOF-D		98

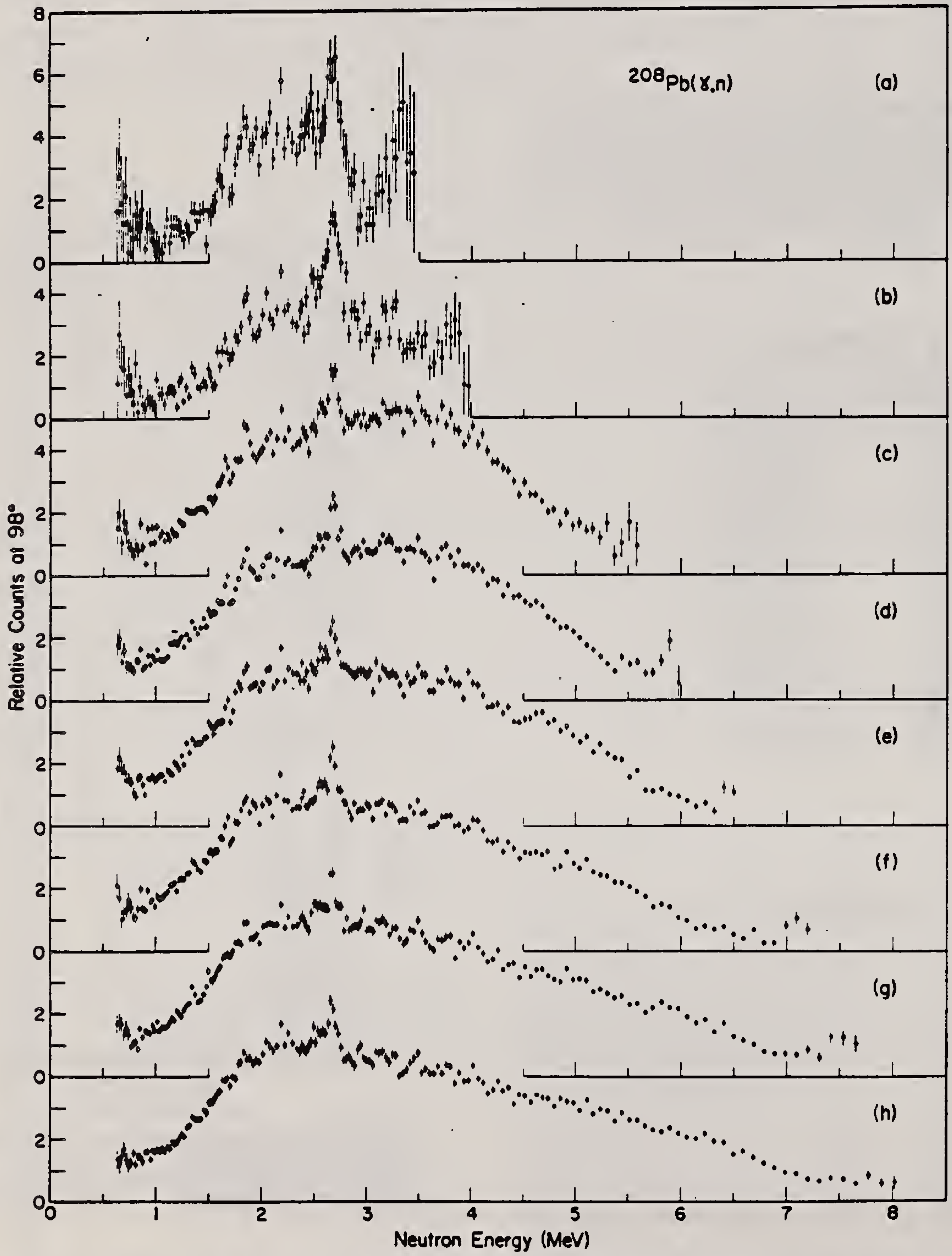

FIG. 2. Neutron energy spectra for the $^{208}Pb(\gamma,n)^{207}Pb$ reaction at bremsstrahlung endpoint energies of (*a*) 11.0, (*b*) 11.5, (*c*) 13.0, (*d*) 13.5, (*e*) 14.0, (*f*) 14.5, (*g*) 15.0, and (*h*) 15.5 MeV. The spectra are plotted as a function of center of mass neutron energies and have been corrected for the neutron efficiency and the bremsstrahlung shapes (assuming all transitions are to the ground state of ^{207}Pb).

(over)

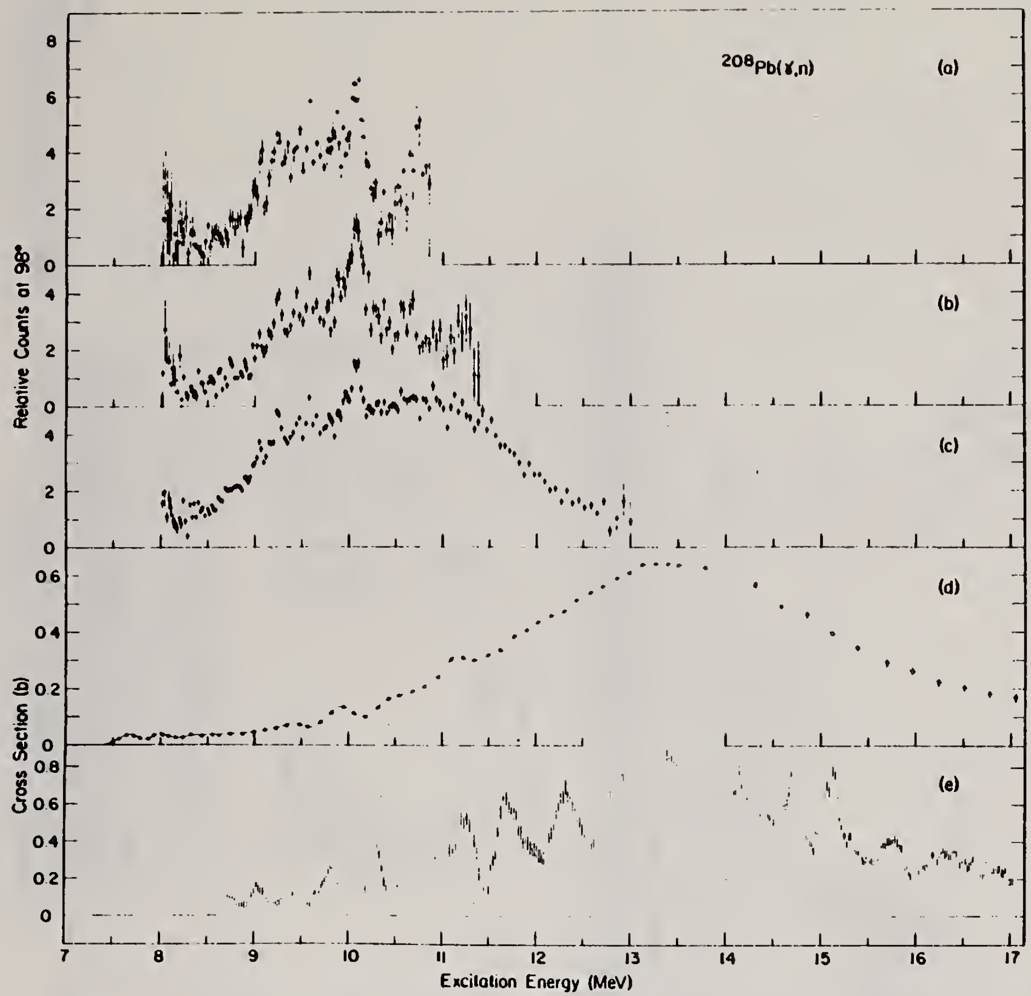

FIG. 3. Comparison of the present spectra for the $^{208}Pb(\gamma,n)^{207}Pb$ reaction (at bremsstrahlung endpoint energies of (*a*) 11.0 MeV, (*b*) 11.5 MeV, and (*c*) 13.0 MeV) with the cross section measurements of (*d*) Veyssiere *et al.* (1970) and (*e*) Ishkhanov *et al.* (1971*a*).

TABLE 2. Comparison of structure in the neutron energy spectra and the cross section for the $^{208}Pb(\gamma,n)^{207}Pb$ reaction

Energy of structure in the neutron spectra (MeV)		Energy of neutron transitions from resonances in the cross section (MeV)	
Present work	McNeill *et al.* (1970)	Veyssiere *et al.* (1970) (Beil *et al.* 1969*a,b*)	Ishkhanov *et al.* (1971*a*)
1.67	—	—	1.65 (9.03 gs)[a]
		1.6 (9.9 2nd)	1.54 (9.81 2nd)
		—	1.52 (11.24 4th)
1.85	1.9	2.0 (9.9 1st)	1.86 (9.81 1st)
2.06	—	2.0 (9.4 gs)	2.02 (9.40 gs)
		2.0 (9.9 1st)	1.86 (9.81 1st)
		2.1 (10.4 2nd)	2.02 (10.29 2nd)
		2.1 (11.8 4th)	2.04 (11.76 4th)
2.19	2.2	[2.2 (11.2 3rd)][b]	[2.23 (11.24 3rd)]
(2.54)[c]	2.5	2.5 (9.9 gs)	2.43 (9.81 gs)
		2.5 (10.4 1st)	2.34 (10.29 1st)
		—	2.35 (10.62 2nd)
2.68	2.7	2.5 (9.9 gs)	2.43 (9.81 gs)
		—	2.67 (10.62 1st)
		—	2.66 (10.93 2nd)
3.15	3.1	3.0 (10.4 gs)	2.91 (10.29 gs)
		—	2.98 (10.93 1st)
		2.9 (11.2 2nd)	2.97 (11.24 2nd)
		—	3.12 (12.84 4th)
3.27	—	—	3.24 (10.62 gs)
		3.3 (11.2 1st)	3.29 (11.24 1st)
3.50	3.5	—	3.55 (10.93 gs)
		3.5 (11.8 2nd)	3.49 (11.76 2nd)
		—	3.53 (13.25 4th)
3.77	3.8	3.8 (11.2 gs)	3.86 (11.24 gs)
		3.9 (11.8 1st)	3.81 (11.76 1st)
4.03	—	—	4.03 (12.30 gs)
		—	4.06 (13.78 4th)
(4.25)	4.3	4.4 (11.8 gs)	4.38 (11.76 gs)
			4.35 (12.30 1st)
			4.36 (14.08 4th)

[a] Information in parentheses indicates the excitation energy (in ^{208}Pb) and level (in ^{207}Pb) which define the neutron transition.
[b] Although this transition is to the third excited state of ^{207}Pb, it provides the only reasonable correspondence to this neutron group.
[c] Parentheses in this column indicate marginal evidence of structure.

REF.	R. A. Lindgren, W. L. Bendel, L. W. Fagg, and E. C. Jones, Jr. Phys. Rev. Lett. 35, 1423 (1975) (See Erratum Phys. Rev. Lett. 36, 116 (1976)	ELEM. SYM.	A	Z
		Pb	208	82
METHOD		REF. NO.	75 Li 1	hmg

REACTION	RESULT	EXCITATION ENERGY	SOURCE TYPE	SOURCE RANGE	DETECTOR TYPE	DETECTOR RANGE	ANGLE
E,E/	ABX	2- 9	D	37- 61	MAG-D		180

Transitions to states in ^{208}Pb at 7.40 and 7.91 MeV excitation are suggested to be components of a giant magnetic quadrupole resonance in ^{208}Pb.

LEVELS AT 7.91, 6.93

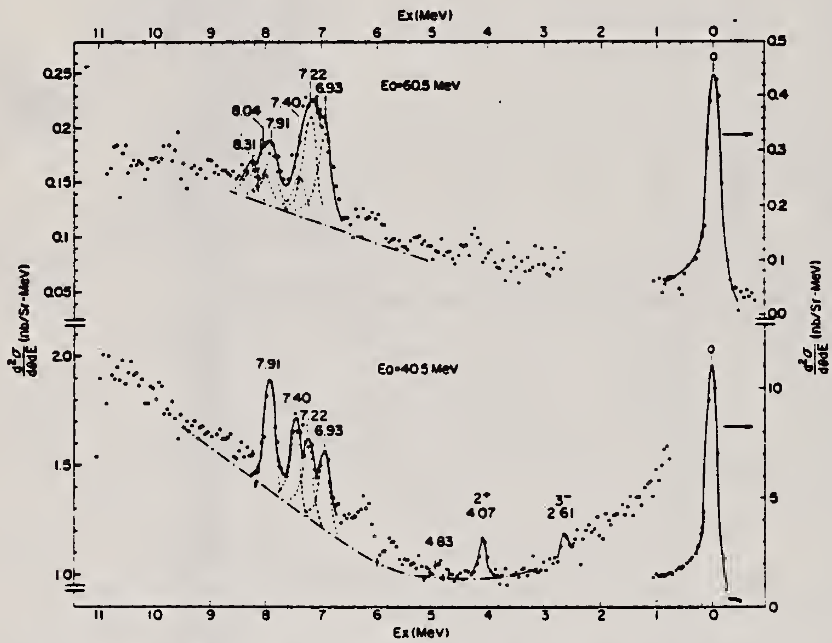

FIG. 1. Spectra of electrons scattered at 180° by ^{208}Pb at 60.5- and 40.5-MeV incident electron energy. The 7.91-MeV state is so weak at 60.5 MeV that peaks at 8.04 and 8.31 MeV together with the 7.91-MeV peak must be fit in order to reproduce the spectrum in that region. It is assumed that the individual peaks have the same width as the elastic peak.

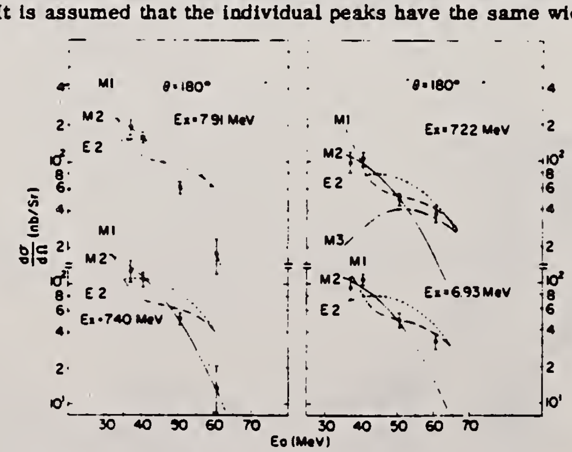

FIG. 2. A comparison of measured cross sections, as functions of E_0, with DWBA predictions based on transition densities calculated with one-particle, one-hole wave functions in an oscillator basis. The oscillator constant is 2.33 fm.

(over)

FORM NBS-418
(REV. 7-14-64)
USCOMM-NBS-DC

U.S. DEPARTMENT OF COMMERCE
NATIONAL BUREAU OF STANDARDS

ERRATUM

EVIDENCE FOR GIANT $M2$ STATES IN ^{208}Pb. R. A. Lindgren, W. L. Bendel, L. W. Fagg, and E. C. Jones, Jr. [Phys. Rev. Lett. 35, 1423 (1975)].

In Fig. 1 the units of $d^2\sigma/d\theta dE$ should be μb/sr MeV (not nb/sr MeV) on both vertical scales.

REF.		ELEM. SYM.	A	Z
	A. Schwierczinski, R. Frey, A. Richter, E. Spamer, H. Theissen, O. Titze, Th. Walcher, S. Krewald, R. Rosenfelder Phys. Rev. Lett. 35, 1244 (1975)	Pb	208	82
METHOD		REF. NO. 75 Sc 8		hmg

REACTION	RESULT	EXCITATION ENERGY	SOURCE TYPE	SOURCE RANGE	DETECTOR TYPE	DETECTOR RANGE	ANGLE
E,E/	ABX	6- 11	D	50	MAG-D		129

Reanalysis of part of previously published data found in 72Bul9. (Ref. 5)
F. R. Buskirk et al. Phys. Lett. 42B, 194 (1972).

BROAD PEAK AT 8.9 MEV

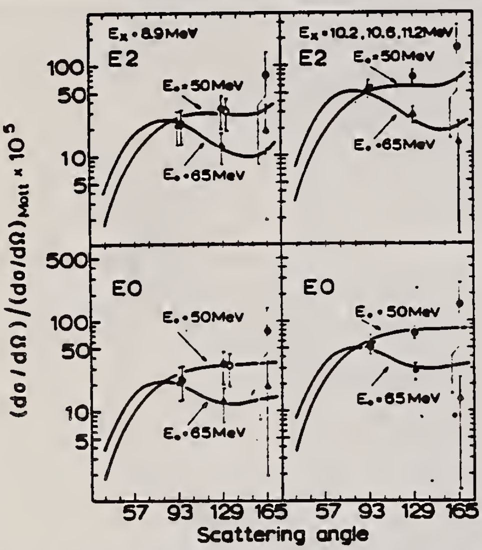

FIG. 2. Ratio of inelastic to Mott cross section as a function of scattering angle. The sum of the cross sections for the states at 10.2, 10.6, and 11.2 MeV excitation energy is given on the right-hand side; the cross section for the 8.9-MeV resonance is shown on the left-hand side. The full points show the results of the low-resolution data; the open circle is the result of the high-resolution measurement. The error bars include the uncertainties in the radiation tail and background subtraction. The full curves result from DWBA calculations described in the main text.

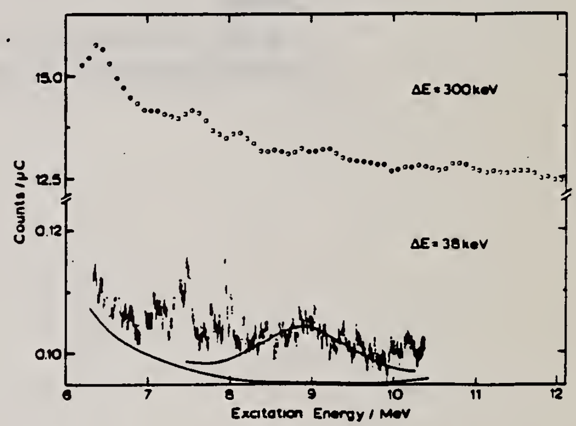

FIG. 1. Spectra of inelastically scattered electrons from ^{208}Pb. Moderate-resolution data (Ref. 5) are shown in the upper half, and high-resolution data in the lower half. The raw data are given. The solid lines indicate the background used in the analysis and the assumed line shape, respectively.

TABLE I. Results deduced from combined low- and high-resolution (e,e') data from Fig. 2. The uncertainties in the transition strengths are comparable for the low- and high-resolution data.

J^π	E_x (MeV)	$B(EL)$ (fm^{2L})	Γ (MeV)	B_{exp}/B_{EWSR}
2^+	8.9	3100 ± 1200	1.3 ± 0.2	0.35
2^+	10.8	6000 ± 1500[a]	2.7 ± 0.2	0.80
1^-	14.1	59 ± 5	4.05 ± 0.3[b]	1.12[c]

[a]Sum of triplet of states at 10.2, 10.6, and 11.2 MeV.
[b]Taken from the (γ,n) data of Ref. 2.
[c]Obtained from the Thomas-Reiche-Kuhn sum rule.

High-resolution inelastic electron scattering [full width at half-maximum (FWHM) ≃ 38 keV] with 50-MeV electrons on ^{208}Pb yields a width $\Gamma = 1.3 \pm 0.2$ MeV for the 8.9-MeV resonance. This result together with the results from a reanalysis of older data with moderate energy resolution (FWHM ≃ 300 keV) shows that the previous identification of the 8.9-MeV resonance as a monopole excitation is not conclusive. The excitation of this state may as well be $E2$. The giant quadrupole resonance at 10.8 MeV seen in former measurements has been reanalyzed.

[2]A. Veyssiere et al., Nucl. Phys. A159, 561 (1970).
[5]F.R. Buskirk et al., Phys. Lett. 42B, 194 (1972).

REF. K. Shoda, M. Sugawara, T. Saito, H. Miyase
Nucl. Phys. A246, 357 (1975)

ELEM. SYM.	A	Z
Pb	208	82

METHOD

REF. NO. 75 Sh 5 egf

REACTION	RESULT	EXCITATION ENERGY	SOURCE TYPE	SOURCE RANGE	DETECTOR TYPE	DETECTOR RANGE	ANGLE
E,P	NOX	8- 40	D	25,40	MAG-D		DST

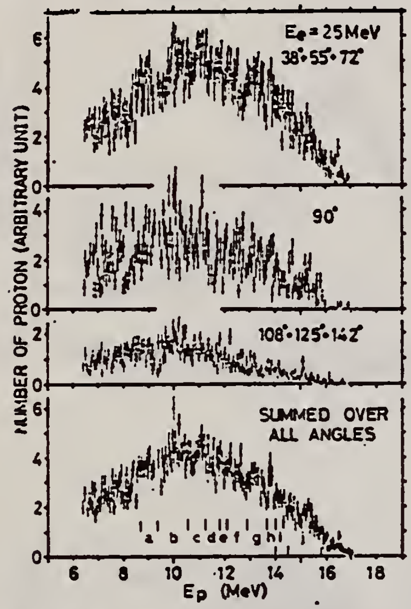

Fig. 1. Energy distributions of photoprotons with the (e, e'p) reaction by the 25.0 MeV electron beam. The emitting directions are indicated in the figure. The letters in the lowest figure show proton regions used to obtain angular distributions.

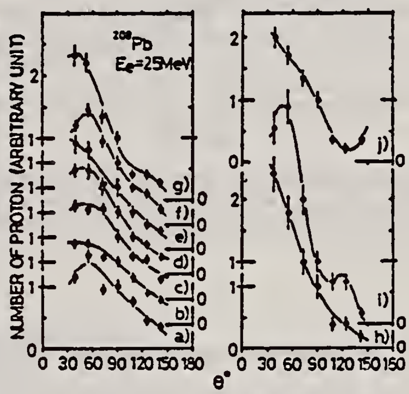

Fig. 3. Angular distributions of photoprotons. The letters show proton regions indicated in fig. 1 by the same notations. Solid lines are obtained by the least square fit with eq. (2). All data are normalized at $\theta = 90°$ to unity.

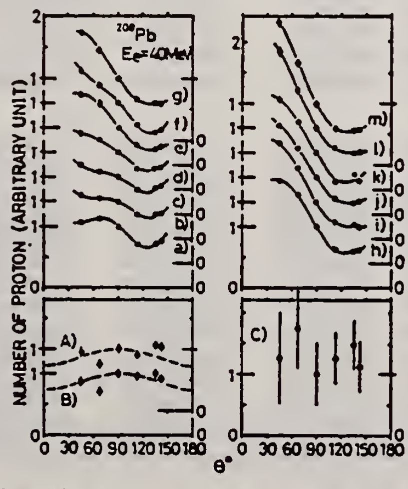

Fig. 4. Angular distributions of photoprotons. The letters show the proton regions indicated in fig. 2 by the same notation. The data (A), (B) and (C) correspond to IAR groups. Solid lines are obtained by the least square fit with eq. (2). Broken lines are the angular distributions obtained from the proton inelastic scattering data on ^{208}Pb [ref. [7]]. All data are normalized to unity at $\theta = 90°$.

[7] P. Richard et al., Phys. Rev. 183, 1007 (1969)

(over)

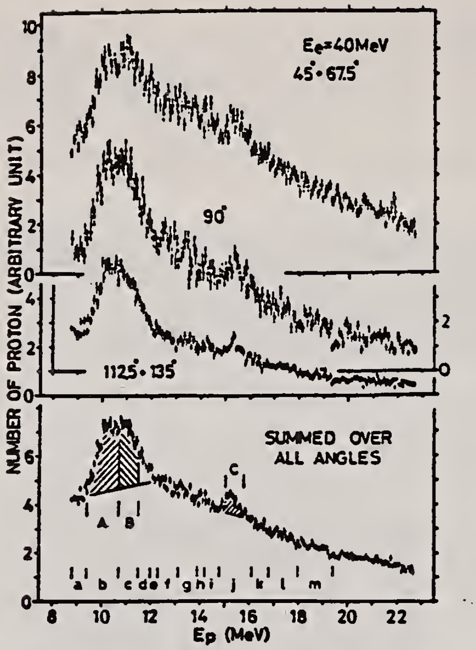

Fig. 2. Energy distributions of photoprotons measured with a mixed beam of bremsstrahlung and electrons of 40.0 MeV. The letters show the proton regions used to obtain angular distributions. The hatched area shows separated IAR proton groups for which angular distributions are measured.

TABLE 2

The parameters of angular distributions obtained by the least square fit with eq. (2) using the present data

Notation	Energy region of proton (MeV)	a_0	a_1	a_2	a_3	a_4
E_e = 25.0 MeV						
(a)	8.7– 9.4	0.83±0.16	0.59±0.32	−0.5±0.6	−0.2±0.5	−0.4±0.6
(b)	9.4–10.6	0.89±0.03	0.59±0.09	−0.2±0.2	−0.0±0.2	−0.0±0.2
(c)	10.6–11.3	0.99±0.10	0.69±0.20	−0.2±0.4	−0.2±0.3	−0.1±0.4
(d)	11.3–11.8	1.00±0.04	0.88±0.09	−0.1±0.2	−0.3±0.2	−0.2±0.2
(e)	11.8–12.1	0.95±0.15	0.93±0.30	0.0±0.5	0.0±0.5	−0.1±0.6
(f)	12.1–12.9	0.94±0.09	0.90±0.17	−0.4±0.3	−0.3±0.3	−0.6±0.3
(g)	12.9–13.7	1.11±0.19	1.35±0.37	0.2±0.7	−0.2±0.6	−0.5±0.7
(h)	13.7–14.0	1.24±0.19	1.65±0.40	0.6±0.7	0.1±0.6	−0.1±0.6
(i)	14.0–14.5	1.28±0.40	2.13±0.86	−0.8±1.4	−0.2±1.2	−2.1±1.2
(j)	14.5–15.8	1.07±0.06	1.06±0.11	0.5±0.2	−0.4±0.2	0.4±0.3
E_e = 40.0 MeV						
(a)	8.8– 9.4	0.95±0.01	0.19±0.02	0.05±0.04	−0.31±0.03	0.19±0.05
(b)	9.4–10.7	0.99±0.04	0.21±0.04	0.15±0.14	−0.08±0.10	0.22±0.18
(c)	10.7–11.5	1.02±0.02	0.26±0.03	0.22±0.08	−0.10±0.06	0.22±0.09
(d)	11.5–12.0	1.03±0.03	0.36±0.04	0.15±0.11	−0.19±0.07	0.09±0.14
(e)	12.0–12.3	1.06±0.05	0.57±0.07	0.10±0.19	−0.27±0.13	−0.02±0.23
(f)	12.3–13.1	1.05±0.02	0.66±0.02	0.29±0.06	−0.16±0.05	0.24±0.08
(g)	13.1–13.9	1.09±0.04	0.74±0.04	0.15±0.13	−0.30±0.08	−0.08±0.16
(h)	13.9–14.2	1.11±0.01	0.74±0.02	0.17±0.05	−0.37±0.03	−0.08±0.06
(i)	14.2–14.8	1.16±0.03	0.89±0.04	0.23±0.12	−0.23±0.07	−0.14±0.14
(j)	14.8–16.1	1.15±0.01	0.84±0.01	0.30±0.02	−0.20±0.01	0.01±0.02
(k)	16.1–16.8	1.14±0.12	0.83±0.17	0.31±0.50	−0.30±0.35	−0.01±0.59
(l)	16.8–18.0	1.26±0.01	1.11±0.01	0.48±0.03	−0.11±0.02	−0.07±0.04
(m)	18.0–19.4	1.29±0.02	1.22±0.02	0.58±0.07	−0.14±0.04	−0.02±0.08

REF. K. Shoda, S. Oikawa, T. Saito, H. Miyase, A. Suzuki
Nucl. Phys. A246, 365 (1975)

ELEM. SYM.	A	Z
Pb	208	82

METHOD

REF. NO. 75 Sh 6 egf

REACTION	RESULT	EXCITATION ENERGY	SOURCE TYPE	SOURCE RANGE	DETECTOR TYPE	DETECTOR RANGE	ANGLE
E,P	ABX	20- 29	D	19- 29	MAG-D		DST

Plane-wave Born approximation virtual-photon spectrum used to obtain photo cross section.

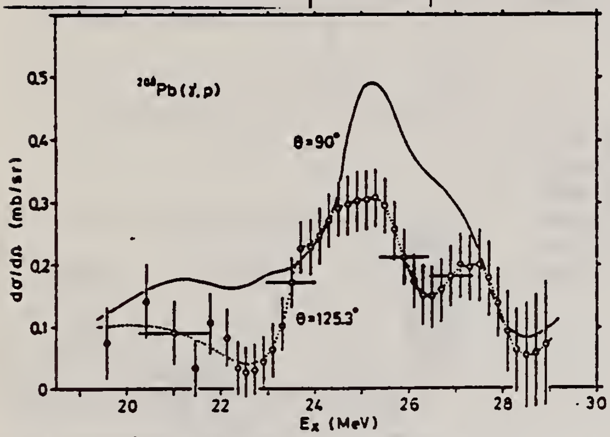

Fig. 4. Photoproton cross sections of ^{208}Pb analyzed from the (e, e′p) cross sections of fig. 3. The solid line is the $\theta = 90°$ result and the dotted line the $\theta = 125.3°$ result.

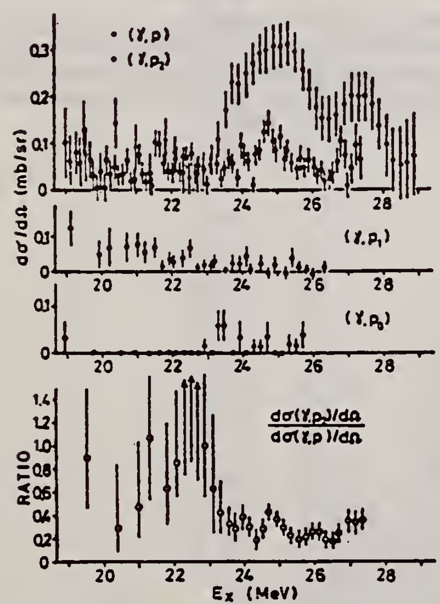

Fig. 7. The differential cross sections of (γ, p_0), (γ, p_1), (γ, p_2) and (γ, p) at $\theta = 125.3°$. The ratio between the (γ, p_2) and (γ, p) cross sections is also shown.

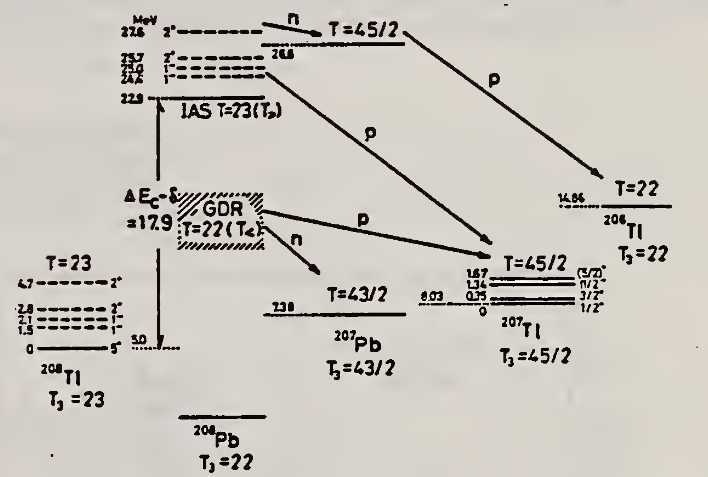

Fig 1. Level diagram and allowed transitions relating to the electromagnetic excitation of ^{208}Pb.

(over)

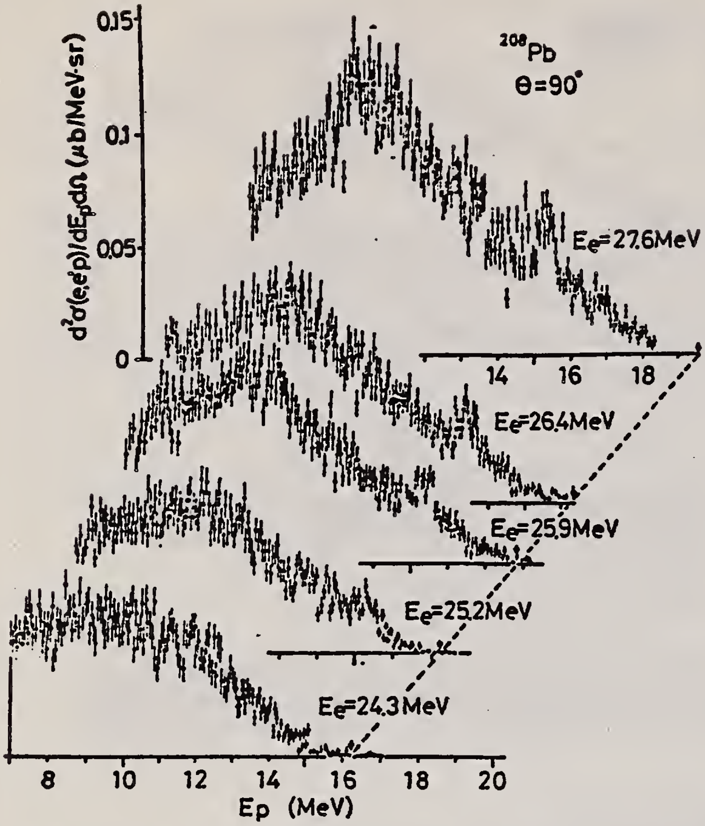

Fig. 2. Energy distributions of protons emitted at $\theta = 90°$ from ^{208}Pb bombarded with a mixed beam of electrons and bremsstrahlung. The ordinate is indicated for the cross sections of the (e, e′p) reaction. Broken lines show the maximum proton energies.

5 C.B. Dover et al., Phys. Lett. 32B (1970) 253

12 Yu. I. Sorokin et al., JETP (Sov. Phys.) 16 (1963) 1127

13 H. Dahmen et al., Nucl. Phys. A164 (1971) 140

18 A. Veyssiere et al., Nucl. Phys. A159 (1970) 561

20 V. Gillet et al., Nucl. Phys. 88 (1966) 321

21 T.T.S. Kuo et al., Phys. Lett. 31B (1970) 93

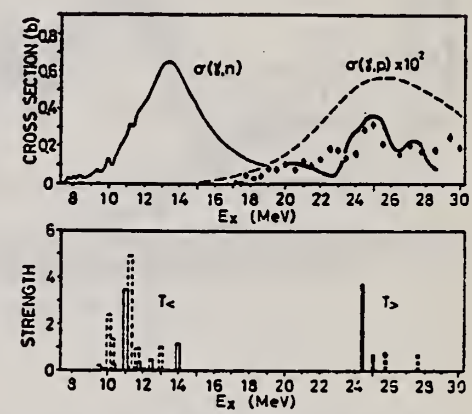

Fig. 8. Comparison of the cross sections of the photoreactions of ^{208}Pb. The (γ, n) cross sections are from ref. [18]). The (γ, p) results are as follows: the broken curve: ref. [12]); closed dots: ref. [13]); solid curve: present data. The lower figure gives the theoretical estimates: open solid line: ref. [20]) in sec^{-1}; open dashed line: ref. [21]) in W.u.; thick line: 1^- IAR, ref. [5]), Γ_γ in 100 eV steps; thick dashed line: 2^+ IAR, ref. [5]), Γ_γ in 100 eV steps.

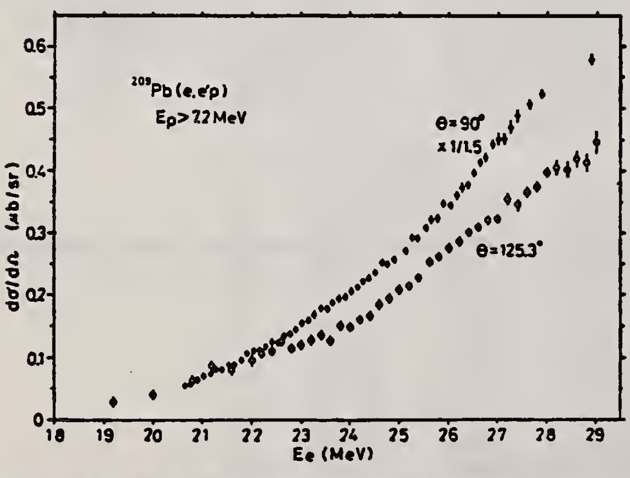

Fig. 3. The differential cross sections of the (e, e′p) reaction. The data at $\theta = 125.3°$ are obtained with an electron beam and those at $\theta = 90°$ are obtained with a mixed beam of electrons and bremsstrahlung. The effect of the bremsstrahlung is converted to the equivalent electron.

REF.	ELEM. SYM.	A	Z
N. K. Sherman, H. M. Ferdinande, K. H. Lokan, C. K. Ross Phys. Rev. Lett. 35, 1215 (1975)	Pb	208	82
METHOD	REF. NO. 75 Sh 9		hmg

REACTION	RESULT	EXCITATION ENERGY	SOURCE TYPE	SOURCE RANGE	DETECTOR TYPE	DETECTOR RANGE	ANGLE
G,N	ABX	7- 13	C	8- 13	TOF-D		90
				(8.8-12.5)			

We have observed more than fifty peaks between 400 keV and 4 MeV in photoneutron spectra of ^{208}Pb. Transitions occur to the ground state and first two excited states of ^{207}Pb from discrete absorption features, some of which are less than 100 keV wide even above 11 MeV. Three states, the most prominent of which is at 9.034 MeV, under lie a controversial electron-scattering resonance, supporting an $E2$ rather than $E0$ interpretation.

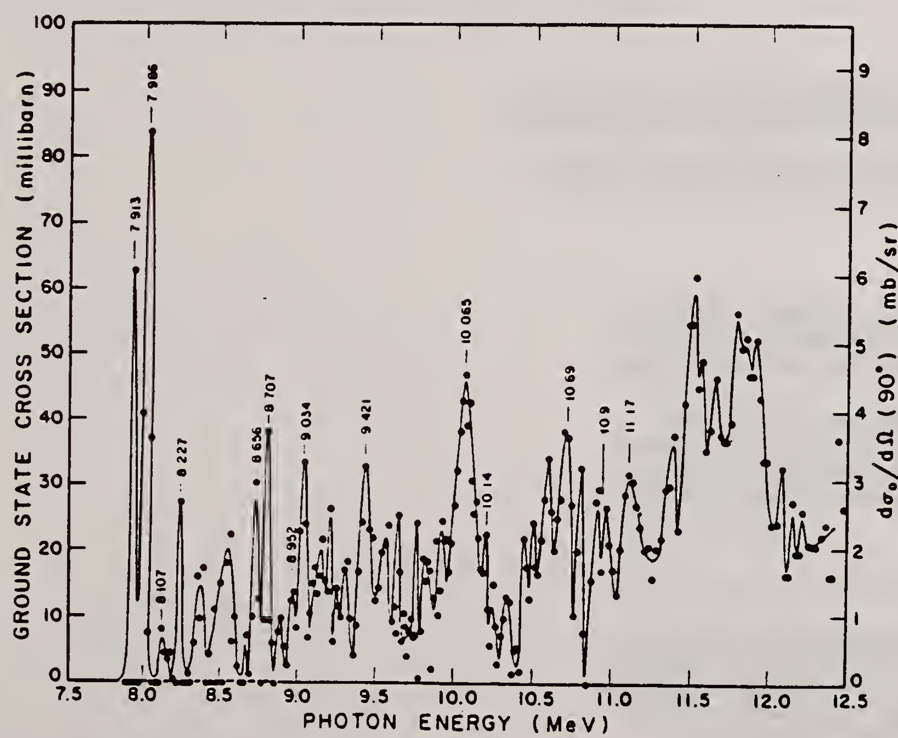

FIG. 2. Ground-state cross section from the upper 520-keV portions of the photoneutron spectra. Peaks are labeled with the photon energy in MeV. The total cross section is approximate (± 10%) since the angular distribution has not been measured. Total cross section obtained by assuming $\omega(\theta) = 2-P_2(\cos\theta)$.

(over)

TABLE I. Observed neutron peaks classified under energies T_0, corresponding to photon energies k in the ground-state cross section σ_0; and energies T_1 and T_2 corresponding to excited-state transitions with cross sections σ_1 and σ_2. Spins J and integrated total cross sections $\int\sigma_T$ of the ^{208}Pb states give radiative widths $\Gamma_{\gamma 0}$. Underlined peaks: ground- or excited-state nature evident in spectra (Fig. 1).

k (MeV)	T_0 (keV)	T_1 (keV)	T_2 (keV)	σ_1/σ_0	σ_2/σ_0	$\int\sigma_T$ [b] (MeV-mb)	J [c]	$\Gamma_{\gamma 0}$ (eV)
8.535	1163					1.1±0.3	1	7±2
8.707	1332					1.2±0.4	1	8±2
8.875	1500	$\underline{908}$	589	1.0±0.2	.01±.01	1.0±0.3	1	7±2
8.952	$\underline{1576}$	1013	703	0.6±0.1	0.5±0.3	1.2±0.2	1	8±2
9.034	$\underline{1658}^{a}$	1085	$\underline{765}$	0.7±0.2	0.2±0.1	3.0±0.4	2	13±2
9.421	$\underline{2043}^{a}$	1484	$\underline{1148}$	0.4±0.1	0.6±0.1	5.5±0.4	2	26±2
9.58	2210		$\underline{1282}$					
9.640	2261	1694	1356	0.4±0.1	0.5±0.1	1.8±0.1	1	14±1
9.701	2322	1746	1424	6.4±4.4	1.3±0.1	3.5±1.8	1	29±14
9.783	2410	$\underline{1833}^{a}$	$\underline{1536}$	4.8±3.2	0.7±0.1	4.6±2.3	1	38±19
9.863	2483	1918	1590	2.1±0.5	0.6±0.1	1.5±0.3	1	13±2
9.925	2545^{a}	1974						
10.065	$\underline{2684}^{a}$	2116	1781	0.3±0.1	0.2±0.1	12.1±1.6	2	64±23
10.14	2738	$\underline{2170}^{a}$	$\underline{1855}$	2.0±0.4	1.9±0.7	2.5±0.5	1	22±4
10.53	$\underline{3148}^{a}$							
10.69	$\underline{3309}$							
10.91	$\underline{3528}^{a}$							
11.17	3782^{a}							

[a] Peaks at about these energies have been previously observed (Ref. 4).
[b] $\int\sigma_T = \int\sigma_0(1 + \sigma_1/\sigma_0 + \sigma_2/\sigma_0)$.
[c] $E1$ or $M1$ transition assumed except where $E2$ strength is reported (Refs. 1, 2, 5, 6).

TABLE II. Measured widths Γ, radiative widths $\Gamma_{\gamma 0}$ in units of single-particle widths Γ_W, reduced matrix elements $B(E2\uparrow)$ for ^{208}Pb states believed to be 2^+, and fractions f of the energy-weighted sum rule found at photon energies k, if $J^\pi = 2^+$.

k (MeV)	Γ (keV)	$\Gamma_{\gamma 0}$ (Γ_W)	$B(E2\uparrow)$ (e^2-fm^4)	f
9.034	45 ± 9	3.6	1340 ± 210	0.15
9.421	104 ± 12	5.9	2150 ± 160	0.25
10.06	132 ± 22	10.5	3850 ± 1420	0.48

[1] R. Pitthan, F. R. Buskirk, E. B. Dally, J. N. Dyer, and X. K. Maruyama, Phys. Rev. Lett. 33, 849 (1974).
[2] M. Nagao and Y. Torizuka, Phys. Rev. Lett. 30, 1068 (1973).
[3] W. Bertozzi, C. P. Sargent, and W. Turchinetz, Phys. Lett. 6, 108 (1963); C. D. Bowman, R. J. Baglan, and B. L. Berman, Phys. Rev. Lett. 23, 796 (1969); R. E. Toohey and H. E. Jackson, Phys. Rev. C 6, 1440 (1972).
[4] R. G. Johnson, J. D. Irish, and K. G. McNeill, Can. J. Phys. 53, 1434 (1975).
[5] Reactor photon experiments (linewidth ~6 eV) indicate $E1$-$E2$ interference at 8.999 MeV, where the tails of these two peaks overlap: W. V. Prestwich and J. McFee, private communication. They observe a $\sigma_0:\sigma_1:\sigma_2$ ratio of 1.0:0.42:0.79 and $[I(42°) - I(138°)]/[I(42°) + I(138°)] = -0.41$.
[6] M. B. Lewis and F. E. Bertrand, Nucl. Phys. A196, 337 (1972); N. Marty, M. Morlet, A. Willis, V. Comparat, and R. Frascaria, Nucl. Phys. A238, 93 (1975).

REF.	ELEM. SYM.	A	Z
Yu. I. Sorokin and B. A. Yur'ev Izv. Akad. Nauk SSSR. Ser. Fiz. 39, 114 (1975) Bull. Acad. Sci. (USSR) Phys. Ser. 39, 98 (1975)	Pb	208	82
METHOD	REF. NO. 75 So 12		hmg

REACTION	RESULT	EXCITATION ENERGY	SOURCE TYPE	SOURCE RANGE	DETECTOR TYPE	DETECTOR RANGE	ANGLE
G,XN	ABI	7- 27	C	7- 27	BF3-I		4PI

SEE 73 SO21

Table 1

Element	A	σ_0, (γ, Tn) MeV · b to 27 MeV		$\sigma_{0\gamma}$, MeV · b to 20 MeV	$\sigma_{0\gamma}$, MeV · b 20–27 MeV	σ_{-1}, mb	σ_{-2}, mb × MeV^{-1}	E_m, MeV	K, MeV	α(A−1), MeV^{-1}	Threshold (γ,2n), MeV	σ_0 (E1), MeV × b
Sn	112	2,23	1,90	1,49	0,41	112	6,7	15,8	20.1	10.2	19,2	1,66
	114	2,26	1,66	1,39	0,47	108	6,5	15,7	21.5	10.2	18,1	1,68
	116	2,40	1,85	1,40	0,45	110	6,6	15,6	21,7	8,1	17,1	1,71
	117	2,52	1,86	1,39	0,47	110	6,7	15,4	21,6	7,3	16,5	1,72
	118	2,46	1,92	1,53	0,39	115	7,1	15,5	20.7	5,6	16,3	1,71
	119	2,63	1,86	1,42	0,44	111	6,8	15,4	22,0	13,2	15,8	1,74
	120	2,69	2,07	1,69	0,38	127	7,9	15,3	19,1	3,6	15,6	1,75
	122	2,94	2,03	1,51	0,52	119	7,1	15,6	21,8	4,5	15,0	1,77
	124	2,90	1,93	1,44	0,49	114	6,9	15,5	23,2	5,4	14,4	1,79
W	182	3,68	2,78	2,32	0,46	184	12,5	--	24,2	5,2	14,9	2,63
	184	4,68	2,95	2,33	0,72	196	13,0	—	23,7	5,2	13,6	2,65
Au	197	4,06	3,15	2,81	0,34	226	15,5	13,3	20,9	17,1	14,8	2,94
Pb	206	3,93	3,21	2,80	0,41	225	16,1	13,5	23,1	6,5	14,8	2,96
	208	4,32	3,28	2,81	0,47	231	16,7	13,3	22,6	9,6	14,1	2,98
Bi	209	4,59	3,47	2,96	0,51	216	17,9	13,2	21,3	10,2	14,3	3,09

REF.	T. E. Drake, H. L. Pai, I. Nascimento Nucl. Phys. A259, 317 (1976)	ELEM. SYM.	A	Z
		Pb	208	82

METHOD	REF. NO.	
	76 Dr 1	egf

REACTION	RESULT	EXCITATION ENERGY	SOURCE TYPE	SOURCE RANGE	DETECTOR TYPE	DETECTOR RANGE	ANGLE
E,F	ABX	25- 45	D	25- 45	TRK-I		DST

Abstract: The fission yields from the electrofission of ^{208}Pb and ^{209}Bi confirm the theoretically predicted large difference in the fission barrier energies of these nuclei. In addition the level density parameters at the fission saddle point were measured for ^{208}Pb and ^{209}Bi.

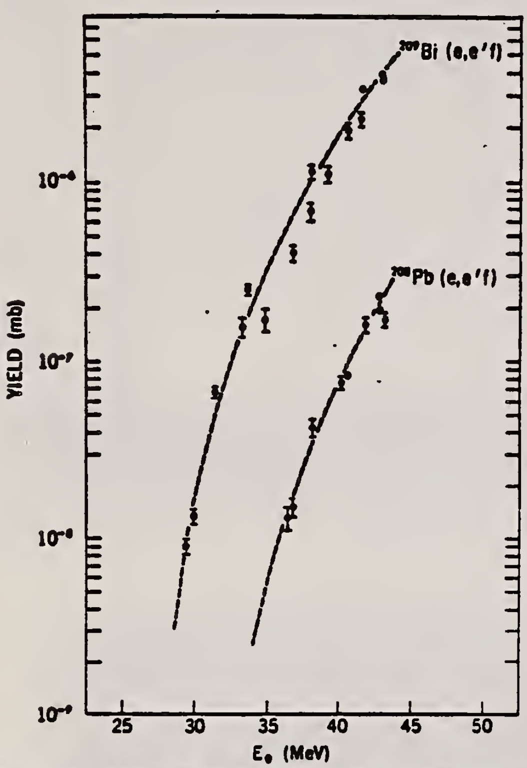

Fig. 3. The yield curves are shown for ^{209}Bi and ^{208}Pb. The data points are shown with the error bars and the theoretical fit as a dashed curve.

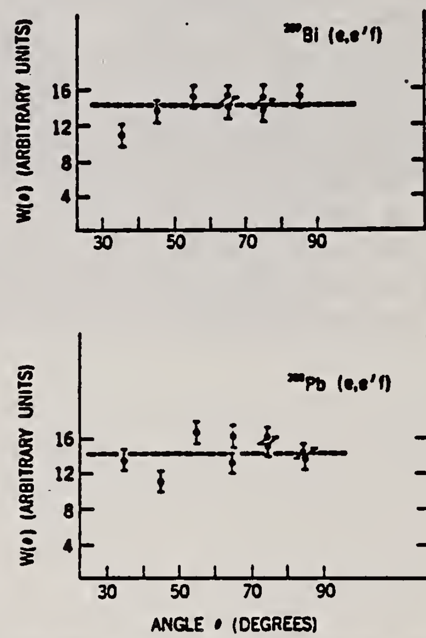

Fig. 2. The angular distribution of fission fragments from ^{209}Bi (top) and ^{208}Pb with respect to the direction of the incident electron beam of energy 43.1 and 42.8 MeV respectively.

TABLE I

The measured level density parameters and the fission barrier energies for ^{208}Pb and ^{209}Bi

	^{208}Pb	^{209}Bi
a_n (MeV^{-1})	8.1±1	10.2±1
a_f (MeV^{-1})	10.8±1	13.0±1
B_f (MeV)	27.6±0.5 [a])	23.4±0.5
Δ_n (MeV)	0.6	

[a]) This value of the fission barrier B_f includes the pairing energy Δ_f.

REF.	ELEM. SYM.	A	Z
J. Friedrich, N. Voegler, H. Euteneuer Phys. Lett. 64B, 269 (1976)	Pb	208	82

METHOD	REF. NO.	
	76 Fr 6	egf

REACTION	RESULT	EXCITATION ENERGY	SOURCE TYPE	SOURCE RANGE	DETECTOR TYPE	DETECTOR RANGE	ANGLE
E,E/	FMF	2- 7	D	120-290	MAG-D		DST

17 LEVELS

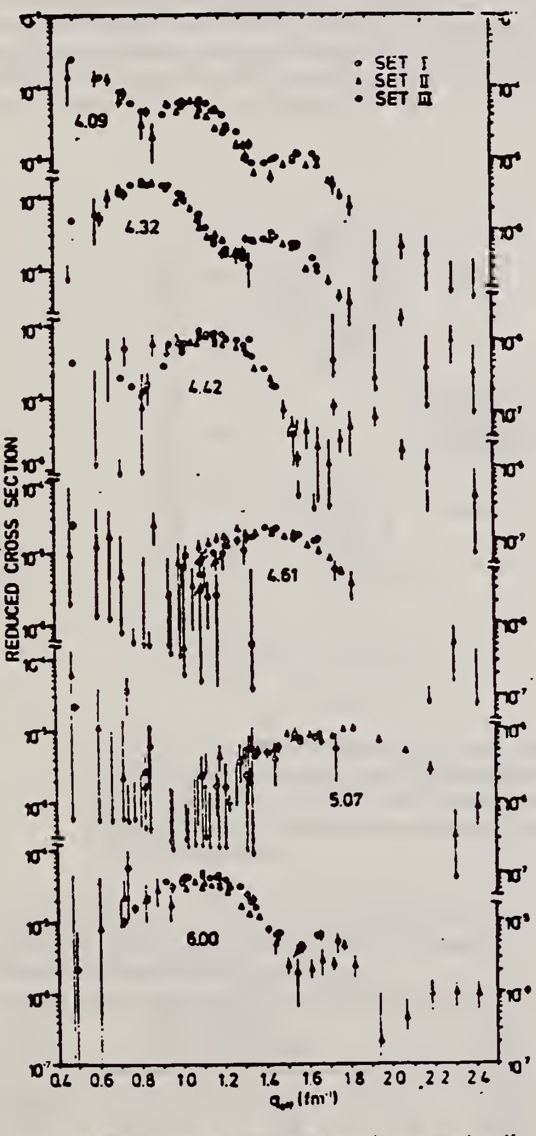

Fig. 3. Reduced cross section (= measured cross section divided by the Mott cross section, often called form factor) for the levels at the indicated energies. Sets I and III are explained in the text.

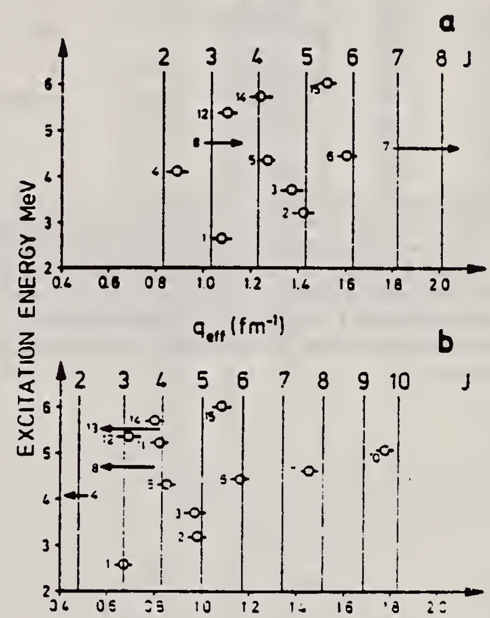

Fig. 2. Position of the first minimum (a) and maximum (b) of the measured form factors. The vertical bars indicate the corresponding positions for a transition charge with multipolarity J peaked at the surface of the nucleus. The numbers of the levels refer to the table.

(over)

Table 1
Energy, form factor maximum and multipolarity of the levels investigated in this experiment. – no. of level according to fig. 2.

No. of level	Energy (MeV)	Form factor maximum	Multipolarity from ee′	
			This experiment	Ref. [4]
1	2.615 [a]	5.2 ± 0.5 (−4)	3 [a]	3
2	3.198 [a]	3.7 ± 0.4 (−5)	5 [a]	5
3	3.709 [a]	2.0 ± 0.2 (−5)	5 [a]	–
4	4.086 [a]	–	2 [a]	2
5	4.324 [a]	1.45 ± 0.15 (−4)	4 [a]	4
6	4.424 [a]	6.9 ± 0.9 (−5)	6 [a]	–
7	4.61	1.8 ± 0.2 (−5)	8	–
8	4.70	2.5 (−5)	3	–
9	4.83	b	c	–
10	5.07	9 ± 1 (−6)	10	–
11	5.23	5.6 ± 0.6 (−5)	4 [e]	3(4)
12	5.35	6 ± 1 (−5)	3	–
13	5.53	3.2 ± 0.6 (−5)	3 [e]	3
14	5.69	4.5 ± 0.5 (−5)	4	5.6 MeV
15	6.00 [a]	4.5 ± 0.5 (−5)	6	–
16	6.17	d		2
17	6.25	d		

[a]: Spin and energy taken from [11], used here for calibration; [b]: more than one maximum; [c]: no clean structure in the form factor as a function of q, but there are clearly seen contributions from high-spin states ($J = 8-10$); [d]: no clean structure in the form factor as a function of q; [e]: several multipoles, the lowest one is given here. The numbers in brackets are the powers to ten.

REF.		ELEM. SYM.	A	Z
	R.J. Holt and H.E. Jackson Phys. Rev. Lett. 36, 244 (1976)	Pb	208	82
METHOD		REF. NO. 76 Ho 1		hmg

REACTION	RESULT	EXCITATION ENERGY	SOURCE TYPE	SOURCE RANGE	DETECTOR TYPE	DETECTOR RANGE	ANGLE
$ G,N	LFT	7- 9	C	7- 9	TOF-D		DST
		(7.9-8.4)					

POL N, THRESH MEAS

The photoneutron polarization from states near threshold was measured, for the first time, for the reaction $^{208}Pb(\gamma,n_0)^{207}Pb$ throughout the neutron energy range 500 to 1000 keV. Spin and parity assignments were made for these states. The giant *M1* resonance in ^{208}Pb was found to be less fragmented than previously thought. The data suggest that there is some "missing" *M1* strength in ^{208}Pb.

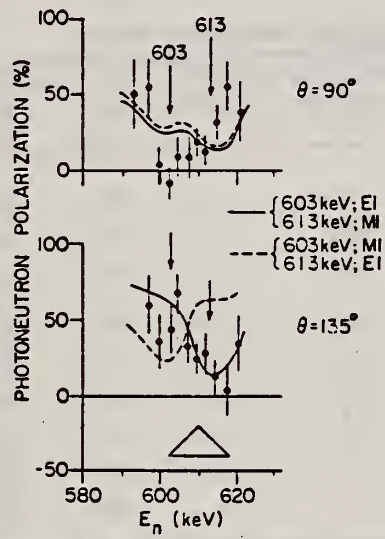

FIG. 2. The curves represent the calculated polarization using the isolated-level approximation [Eq. (1)] in the region of the 603–613-keV resonances. The triangle represents the energy resolution of the time-of-flight spectrometer.

TABLE I. Summary of results from the threshold photoneutron polarization experiment.

E_r (keV)	Polarization $\theta = 90°$	Polarization $\theta = 135°$	J^π	Γ_{γ_0} [a] (eV)
996	No	Yes	1^-	5.8
951	No	Yes	1^-	3.5
907	No	Yes	1^-	6.5
846	No	Yes	1^-	10.1
737	No	Yes	1^-	3.5
651	No	Yes	1^-	11.8
613	Yes	Yes	1^+	19.7
603	No	Yes	1^-	8.0
538	No	Yes	1^-	12.8

[a] Values of Γ_{γ_0} were taken from Ref.4.

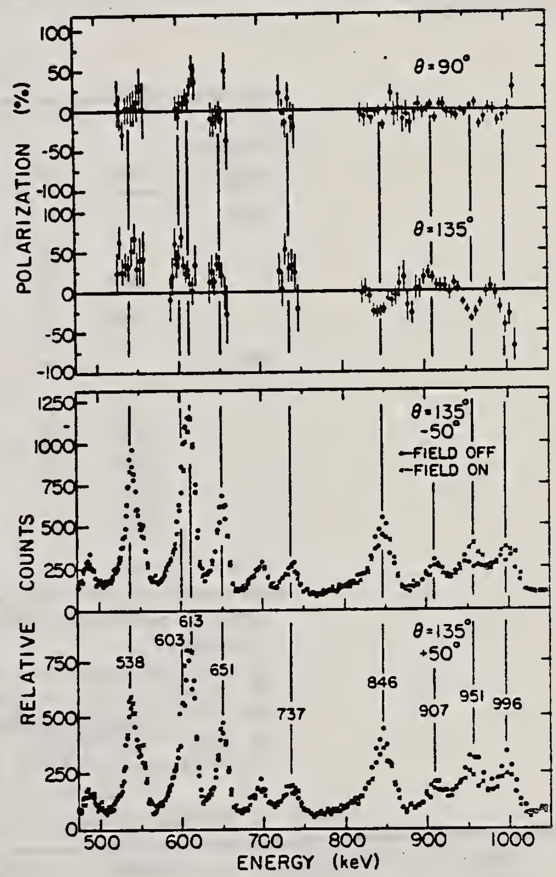

FIG. 1. Upper half: The measured photoneutron polarization in the energy range 500 to 1000 keV at angles of 90° and 135°. The error limits are primarily statistical in nature. Only the 613-keV resonance emits polarized neutrons at *both* 90° and 135°. Lower half: The raw time-of-flight spectra observed at 135° for neutron scattering angles of ± 50° with and without the solenoidal field.

U.S. DEPARTMENT OF COMMERCE
NATIONAL BUREAU OF STANDARDS

REF.	J. E. McFee, W. V. Prestwich, T. J. Kennett Phys. Rev. C13, 1864 (1976)	ELEM. SYM.	A	Z
		Pb	208	82
METHOD		REF. NO.		
		76 Mc 3		hmg

REACTION	RESULT	EXCITATION ENERGY	SOURCE		DETECTOR		ANGLE
			TYPE	RANGE	TYPE	RANGE	
G,N	ABX	8- 9	D	8- 9	ION-D		90

8999,8533,8120 KEV

The photoneutron spectrum of natural lead has been observed for photoexcitation energies of 8999, 8533, and 8120 keV using a high-resolution ^{3}He ionization chamber. The photons were obtained from the (n,γ) reaction on a nickel target positioned in a nuclear reactor. The Q values for the three reactions $^{208}Pb(\gamma,n)^{207}Pb$, $^{207}Pb(\gamma,n)^{206}Pb$, and $^{206}Pb(\gamma,n)^{205}Pb$ have been determined and are, respectively, 7369 ± 5, 6743 ± 3, and 8087 ± 3 keV. Neutron groups corresponding to different final states following excitation by one of the three photon components have been observed and their partial cross sections are reported. The distribution and some systematics of the neutron reduced widths have been studied. The absolute cross sections of the reaction $^{208}Pb(\gamma,n)^{207}Pb$ at 8999 and 8533 keV photon energies have been found to be 6.8 ± 2.9 and 5.0 ± 2.1 mb, respectively.

TABLE V. Reduced widths contrasted with spectroscopic factors.

Residual nucleus	E_x (keV)	J^π	l_n [a] $E1$	$E2$	Neutron Reduced Widths $E_\gamma = 8999$ keV	$E_\gamma = 8533$ keV ($\pm 27\%$)	$E_\gamma = 8120$ keV	Spectroscopic factors $C^2S/(2J+1)$ (p,d)	(d,t)
^{207}Pb								b	b
	0	$\frac{1}{2}^-$	0	1	163	123		0.72	0.71
	570	$\frac{5}{2}^-$	2	1	210	309		0.90 [c]	0.97 [c]
	898	$\frac{3}{2}^-$	0	1	191	327		1.27	1.33
								d	
^{206}Pb	0	0^+	0	1	26	107	321	0.30	...
	803	2^+	0	1	959	308		0.11	...
	1165	0^+	0	1	294	118		0.19	...
	1460	2^+	0	1	152	e		0.38	...
	1684	4^+	2	1	474	e		0.02 [c]	...
	1704	1^+	0	1	285	0		0.38	...
	1784	2^+	0	1	178	e		0.07	...
^{205}Pb	263	$\frac{1}{2}^-$	0	1	190	e		1.02 [f]	1.56 [g]

[a] Minimum possible neutron angular momentum for a given photon multipolarity.
[b] Reference 18.
[c] Spectroscopic factor for $l_n = 3$. All others are $l_n = 1$.
[d] W. A. Lanford and G. M. Crawley, Phys. Rev. C 9, 646 (1974).
[e] May exist but cannot be resolved from neighboring components.
[f] K. Yagi, T. Ishimatsu, Y. Ishizaki, and Y. Saji, Nucl. Phys. A110, 41 (1968).
[g] R. Tickle and J. Bardwick, Phys. Rev. 178, 2006 (1969).

TABLE VI. Absolute photoneutron cross sections.

Target isotope	Photon energy (keV)	Cross section [a] (mb)	Lower bound [a] (mb)	Upper bound [a] (mb)
208	8999	6.8	...	...
	8533	5.0	...	...
207	8999	...	20.9	40.1
	8533	...	3.0	26.8
	8120	...	5.6	...
206	8999	...	2.3	14.0
	8533	...	0	15.1

[a] 10% relative error; 45% absolute error.

(over)

TABLE IV. Low-lying states in ^{207}Pb, ^{206}Pb, and ^{205}Pb.

Residual isotope	E_γ (keV)	E_x (keV)	J^π	Observed neutron energy (lab) (keV ± 5)	Relative[a] intensity (± 10%)	$\sigma_{\gamma n}$[b] (mb)
207	8999	0[c]	$\frac{1}{2}^-$	1615	100	3.1
		570	$\frac{5}{2}^-$	1054	42	1.3
		898	$\frac{3}{2}^-$	727	79	2.4
	8533	0	$\frac{1}{2}^-$	1159	66	2.1
		570	$\frac{5}{2}^-$	601	12	0.4
		898	$\frac{3}{2}^-$	263	81	2.5
206	8999	0[d]	0^+	2256[e]	19	0.6
		803	2^+	1446	556	17.2
		1165(±10)	0^+	1057	148	4.6
		1460	2^+	789	65	2.0
		1684	4^-	573	15	0.5
		1704(±1)	1^+	551	102	3.2
		1784(±2)	2^+	473	59	1.8
	8533	0	0^+	1780	69	2.1
		803	2^+	982	147	4.5
		1165(±10)	0^+	619	45	1.4
		1704(±1)	1^+	...	0	0.0
	8120	0	0^+	1370[e]	181	5.6
205	8999	263[f]	$\frac{3}{2}^-$	643	74	2.3
			Unresolved groups			
A 206	8999	1340	3^+	903	76	
205	8999	0	$\frac{5}{2}^-$			
205	8999	2	$\frac{1}{2}^-$			
B 206	8533	1340	3^+	446	65	
205	8533	0	$\frac{5}{2}^-$			
205	8533	2	$\frac{1}{2}^-$			
C 205	8999	576	$\frac{3}{2}^-$	330	44	
206	8533	1460	2^+			
D 205	8533	263	$\frac{3}{2}^-$	181	37	
207	8120	570	$\frac{5}{2}^-$			
206	7724	803	2^+			
207	7555	0	$\frac{1}{2}^-$			
E 206	8999	2150(±1)	2^+	110	61	
205	8999	803	$(\frac{1}{2}^-, \frac{3}{2}^-)$			
			Unassigned group			
...	...	...	...	557	5	

[a] Arbitrary normalization corrected for isotopic abundance and photon yield. Unresolved group intensities have no isotopic abundance or photon yield correction and are merely quoted relative to the group corresponding to population of the ^{207}Pb ground state following 8999-keV photoexcitation.

[b] Relative error 10%, absolute error 45%.

[c] Reference 18.

[d] Reference 19.

[e] Centroid accurate to only 15 keV.

[f] Reference 20.

[18] M. R. Schmorak et al., Nucl. Data B5, 207 (1971).

[19] K. K. Seth, Nucl. Data B7, 161 (1972).

[20] J. H. Hamilton et al., Phys. Rev. C6, 1265 (1972).

REF.		ELEM. SYM.	A	Z
P. B. Smith Phys. Rev. C13, 2071 (1976)		Pb	208	82
METHOD		REF. NO.	76 Sm 4	hmg

REACTION	RESULT	EXCITATION ENERGY	SOURCE TYPE	SOURCE RANGE	DETECTOR TYPE	DETECTOR RANGE	ANGLE
G,G	LFT	7	D	7	NAI-D		90
		(7.685)		(7.685)			

RESONANCE ABSORPTION

$$\Gamma_{\gamma 0} = 14^{+6}_{-4} \text{ eV}$$

$$\Gamma = 1.1^{+0.5}_{-0.3} \text{ keV}$$

A neutron unbound state lying at $E_x = 7685$ keV in ^{208}Pb, purportedly belonging to the giant $M1$ resonance in this element, has been studied in resonance absorption with γ rays from the $E_p = 1354$-keV resonance in the $^{34}S(p,\gamma)^{35}Cl$ reaction. The absorber was 3-cm natural lead. The tungsten collimator subtended a (geometrical) half angle of 0.77° at the target. The absorption dip was fitted with a five-parameter Lorentz curve. The level parameters found are $E_n = 316.0 \pm 0.8$ keV, $\Gamma_t = 1.1^{+0.5}_{-0.3}$ keV, and $\Gamma_{\gamma 0} = 14^{+6}_{-4}$ eV.

REF.		ELEM. SYM.	A	Z
R.J. Sparks, H. Lancman, C. Van der Leun Nucl. Phys. A259, 13 (1976)		Pb	208	82
METHOD		REF. NO.		
		76 Sp 1		egf

REACTION	RESULT	EXCITATION ENERGY	SOURCE		DETECTOR		ANGLE
			TYPE	RANGE	TYPE	RANGE	
G,G	LFT	7	D	7	SCD-D		90

7 = 7.064 MEV

Abstract: The level at 7064.3±0.5 keV in ^{208}Pb has been excited in a resonant absorption experiment by Doppler shifted γ-radiation from the $^{34}S(p, \gamma)^{35}Cl$ reaction at E_p = 1974 keV. Analysis of the absorption integral gives Γ = 18±3 eV for the level width, assuming a 100 % ground state branch. The suitability of this technique for measuring lifetimes of nuclear bound states in the attosecond range is discussed.

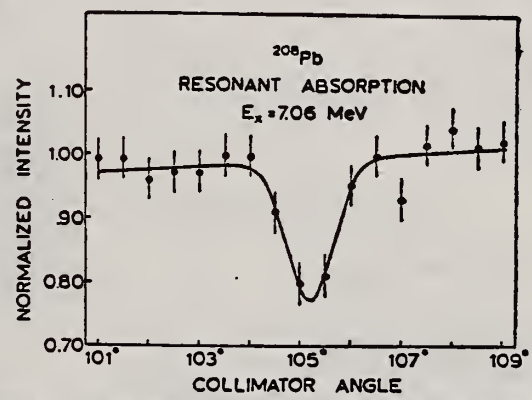

Fig. 3. Transmission of the 7.06 MeV γ-rays through the lead absorber and the slit. The solid curve is the result of fitting a Gaussian function plus a linear background to the experimental data. The dip minimum occurs at 105.20°±0.08° and the absorption integral is A_α = 0.26°±0.05°. The value of the normalized χ^2 for the fit is 0.68.

REF. D. Turck, H.-G. Clerc, H. Trager
Phys. Lett. 63B, 283 (1976)

ELEM. SYM.	A	Z
Pb	208	82

METHOD

REF. NO. 76 Tu 2 | egf

REACTION	RESULT	EXCITATION ENERGY	SOURCE TYPE	SOURCE RANGE	DETECTOR TYPE	DETECTOR RANGE	ANGLE
E,F	ABX	29- 50	D	38- 50	TRK-I		4PI

FISSION BARRIER

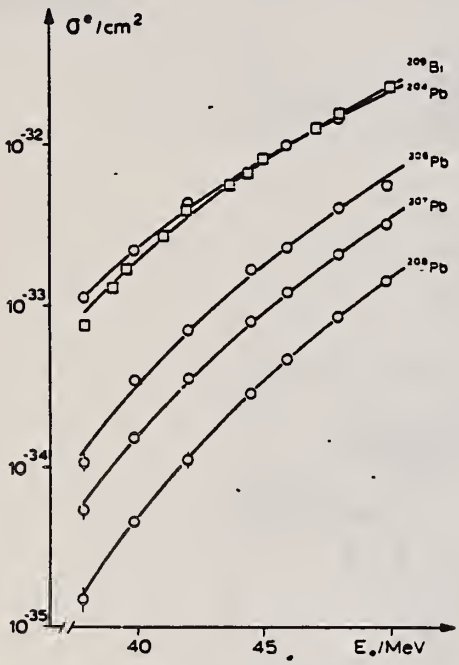

Fig. 1. Cross section σ^e for electron induced fission in ^{204,206,207,208}Pb and ^{209}Bi as a function of the incident electron energy E_0.

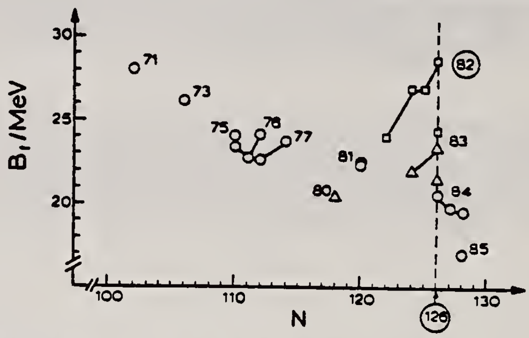

Fig. 2. Summary of fission barrier heights obtained from fits to experimental fission cross sections for nuclei with $Z \leq 85$. o: α-induced fission [12]. For ^{201}Tl, the value of 22.5±1.5 of ref. [3] is also included; Δ: proton-induced fission [12]; □: electron induced fission (present work). Values for different isotopes of the same element are connected by straight lines. The nuclear charge numbers are indicated. The erors are ±1.0 MeV for proton and α-induced fission [12] and ±1.5 MeV for electron induced fission.

[1] U. Mosel, Phys. Rev. C6 (1972) 971.
[3] D.S. Burnett et al., Phys. Rev. B134 (1964) 952.
[12] L.G. Moretto et al., Phys. Lett. B38 (1972) 471.

Table 2
Fission barriers B_f as determined from electron induced fission. In the last column theoretical fission barriers according to ref. [1] with surface independent pairing strength are listed.

isotope	B_f (MeV)	$B_f^{theor.}$ (MeV)
^{204}Pb	24.0±1.5	24.0
^{206}Pb	26.8±1.5	26.2
^{207}Pb	26.9±1.5	
^{208}Pb	28.6±1.5	28.1
^{209}Pb	24.3±1.5	

REF.	ELEM. SYM.	A	Z
K.V. Alanakyan, M.Dzh. Amaryan, R.A. Demirchyan, K.Sh. Egiyan, M.S. Ogandzhanyan, & Yu.G. Sharabyan Yad. Fiz. 25, 545 (March 1977) Sov. J. Nucl. Phys. 25, 292 (March 1977)	208	Pb	82

METHOD	REF. NO.	
	77 Al 9	hmg

REACTION	RESULT	EXCITATION ENERGY	SOURCE TYPE	SOURCE RANGE	DETECTOR TYPE	DETECTOR RANGE	ANGLE
G,P	ABX	72-999	C	2 *5	TEL-D	---	DST
				(4-5)			

COMMENTS: $f \sim \exp(-Bp^2)$

$$B = \frac{E}{p^4(d^2\sigma/d\Omega dpQ)}$$

*E,GEV, 999=4.5 GEV

The A^n-dependence and momentum spectra of photoprotons in the nuclei ^{12}C, ^{27}Al, ^{63}Cu, ^{118}Sn, and ^{208}Pb have been studied experimentally for maximum bremsstrahlung energies of 2.0, 3.0, and 4.5 GeV. The A-dependence shows that the proton photoproduction mechanism for $E_\gamma > 400$ MeV is identical for the entire kinetic-energy region 65–280 MeV and the angle region 45–150° for the secondary protons studied. The dependence of the exponent n on the transverse momentum $p_\perp$ is in good agreement with the same dependence for protons produced in nuclei by primary protons. In the momentum spectra of the invariant cross section $f = (E/p^2)(d^2\sigma/d\Omega dpQ) \sim \exp(-Bp^2)$ it is observed that the parameter B does not depend on the incident-photon energy and on the target nucleus, but depends on the proton-detection angle.

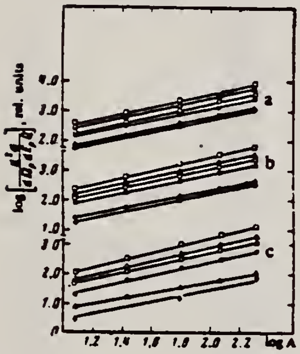

FIG. 1. Differential cross section for proton photoproduction as a function of atomic number A of the nucleus at $E_0 = 2$ GeV. The lines a correspond to $\vartheta_p = 60°$, b to 90: and c to 150°. Points: □—E_p = 64, Δ—80, ○—101, ■—137, ▲—209, and ●—280 MeV.

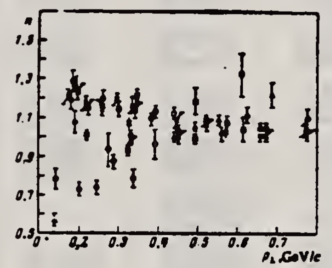

FIG. 3. The same as Fig. 2. Experimental points: ▲—E_0 = 0.13, ○—0.25, ▲—0.4, □—1.2, □—2.0, ×—3.0, and ●—4.5 GeV.

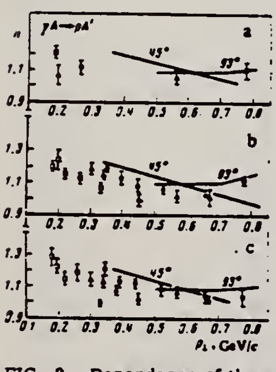

FIG. 2. Dependence of the exponent n in the A^n dependence of the cross section for the reaction $\gamma A \to pA'$ as a function of proton transverse momentum: a—E_0 = 2.0 GeV, b—E_0 = 3.0 GeV, c—E_0 = 4.5 GeV. The points for a and b: Δ—ϑ_p = 60°, ○—90°, □—150°; for c: Δ—ϑ_p = 46°, ○—86°, □—136°. The curves show the dependence of n on $p_\perp$ for the reaction $A(p,p')A'$ taken from Ref. 9.

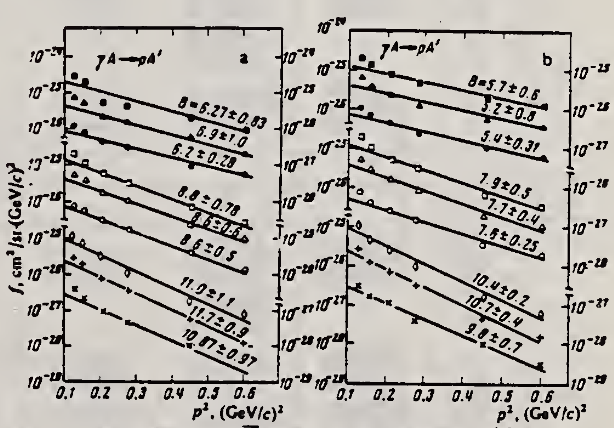

FIG. 4. Invariant cross section f as a function of p^2. a—for E_0 = 2.0 GeV, b—for E_0 = 3.0 GeV. Experimental points: ●, ▲, ■—for ϑ_p = 60° for the respective nuclei ^{12}C, ^{63}Cu, and ^{208}Pb; ○, Δ, □—the same for ϑ_p = 90°; ×, +, ◇—the same for ϑ_p = 150°.

TABLE II. Values of the parameter B in $(GeV/c)^{-2}$ in the relation $E_p/p_p^2 (d^2\sigma/d\Omega_p dp_p Q) = f \sim \exp(-Bp^2)$.

Target	E_0 = 2.0 GeV			3.0 GeV			4.5 GeV		
	ϑ_p = 60°	90°	150°	60°	90°	130°	46°	86°	136°
^{12}C	4.874±0.512	7.278±0.482	9.461±0.803	6.288±0.805	8.623±0.497	10.873±0.977	6.047±0.173	8.066±0.49	11.262±0.481
^{64}Cu	5.300±0.627	7.337±0.627	10.473±0.609	6.972±0.939	8.559±0.622	11.697±0.944	–	–	–
^{208}Pb	5.204±0.753	7.605±0.721	10.088±0.96	6.870±1.514	8.858±0.783	10.983±1.188	–	–	–

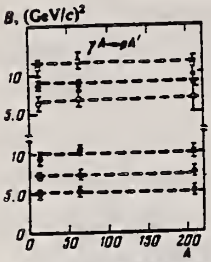

FIG. 6. Dependence of the parameter B from the relation $f \sim \exp(-Bp^2)$ on the atomic number of the target nucleus. The solid points refer to E_0 = 2.0 GeV, and the hollow points to E_0 = 3.0 GeV; the points ● and ○ are for ϑ_p = 60°, ▲ and △ are for 90°, and ■ and □ are for 150°.

TABLE I. Differential cross section $d^2\sigma/d\Omega dTQ$ of the reaction $\gamma A \to pA'$ in μb/MeV-sr.

A	E_γ, GeV	ϑ_p, deg	E_p, MeV					
			64	80	101	137	209	279
^{12}C	2	60	3.720±0.056	2.630±0.052	1.907±0.057	1.425±0.038	0.725±0.220	0.429±0.018
		90	2.274±0.045	1.587±0.047	1.130±0.039	0.763±0.022	0.256±0.008	0.117±0.007
		150	1.152±0.032	0.690±0.014	0.505±0.026	0.218±0.007	0.071±0.005	0.021±0.002
	3	60	4.240±0.100	3.424±0.063	1.960±0.043	1.629±0.046	0.653±0.024	0.452±0.019
		90	2.440±0.056	2.031±0.040	1.145±0.029	0.807±0.028	0.243±0.009	0.088±0.006
		150	1.360±0.042	0.877±0.029	0.438±0.016	0.300±0.010	0.057±0.003	–
^{27}Al	2	60	8.460±0.127	8.014±0.120	4.083±0.109	3.253±0.097	1.513±0.046	–
		90	5.920±0.107	3.750±0.086	2.502±0.084	1.718±0.052	0.603±0.018	–
		150	3.127±0.078	1.797±0.035	1.189±0.060	0.644±0.019	0.164±0.011	–
	3	60	9.960±0.239	7.492±0.131	4.160±0.092	3.527±0.100	1.568±0.058	0.925±0.037
		90	6.090±0.130	4.845±0.107	2.688±0.076	1.995±0.065	0.596±0.021	0.239±0.013
		150	3.730±0.103	2.943±0.081	1.234±0.042	0.747±0.025	0.136±0.006	–
	4,5	46	–	9.510±0.250	–	–	–	1.320±0.720
		86	–	6.200±0.095	–	–	–	0.248±0.020
		136	–	3.380±0.050	–	–	–	–
^{64}Cu	2	60	23.500±0.329	15.170±0.299	10.931±0.269	8.163±0.240	3.939±0.110	2.115±0.064
		90	16.721±0.268	9.757±0.231	6.856±0.082	4.411±0.134	1.424±0.042	0.743±0.037
		150	10.592±0.212	5.217±0.103	3.362±0.165	1.697±0.050	0.342±0.021	0.115±0.011
	3	60	26.180±0.590	20.580±0.340	10.200±0.191	8.594±0.246	3.869±0.140	1.661±0.064
		90	17.800±0.320	13.601±0.260	7.516±0.190	5.245±0.172	1.403±0.048	0.676±0.032
		150	11.600±0.271	7.834±0.205	3.388±0.107	2.287±0.075	0.368±0.017	0.097±0.008
	4,5	46	–	27.000±0.750	–	–	–	3.550±0.180
		86	–	17.401±0.250	–	–	–	0.785±0.060
		136	–	9.750±0.150	–	–	–	–
^{118}Sn	2	60	45.601±0.538	30.050±0.593	19.970±0.587	13.102±0.380	7.137±0.210	–
		90	32.550±0.553	18.890±0.466	13.840±0.428	8.297±0.320	2.588±0.078	–
		150	19.571±0.391	10.289±0.203	6.548±0.321	3.032±0.090	0.585±0.041	–
A	E_γ, GeV	ϑ_p, deg	64	80	101	137	209	279
^{118}Sn	3	60	55.070±1.270	39.920±0.680	17.800±0.430	16.550±0.490	7.026±0.036	3.873±0.140
		90	36.600±0.720	26.260±0.550	14.370±0.400	9.544±0.328	2.664±0.099	1.187±0.055
		150	22.500±0.560	14.590±0.350	6.251±0.210	4.103±0.150	0.664±0.033	–
	4,5	46	–	53.900±1.400	–	–	–	5.640±0.320
		86	–	32.200±0.51	–	–	–	1.420±0.114
		136	–	18.250±0.290	–	–	–	0.230±0.038
^{208}Pb	2	60	80.000±1.280	56.850±1.120	35.200±1.030	23.930±0.720	13.440±0.400	7.745±0.310
		90	60.990±0.970	34.080±0.800	23.690±0.720	14.220±0.480	4.522±0.135	2.453±0.120
		150	36.890±0.730	18.980±0.370	10.638±0.520	5.794±0.168	1.102±0.077	0.531±0.035
	3	60	100.740±2.130	76.030±1.200	28.[illegible]±0.670	28.000±0.820	12.810±0.450	7.092±0.250
		90	71.350±1.270	48.320±0.900	24.760±0.650	16.420±0.520	4.580±0.170	2.244±0.120
		150	42.090±0.970	27.240±0.680	12.150±0.[illegible]	7.294±0.250	1.220±0.034	0.589±0.039
	4,5	46	–	85.000±0.350	–	–	–	11.600±0.540
		86	–	58.780±0.920	–	–	–	3.050±0.214
		136	–	29.600±0.430	–	–	–	0.465±0.084
				80	119	166	231	291
^{12}C	4,5	46		5.210±0.280	3.670±0.088	2.530±0.064	1.190±0.046	0.785±0.042
		86		2.440±0.080	1.350±0.052	0.843±0.037	0.363±0.019	0.105±0.007
		136		1.330±0.029	0.427±0.020	0.196±0.015	0.045±0.005	0.018±0.002

D.F. Coope, L.E. Cannell, and M.K. Brussel
Phys. Rev. C 15, 1977 (1977)

ELEM. SYM.	A	Z
Pb	208	82

METHOD	REF. NO.	
	77 Co 3	hmg

REACTION	RESULT	EXCITATION ENERGY	SOURCE TYPE	SOURCE RANGE	DETECTOR TYPE	DETECTOR RANGE	ANGLE
G,G	LFT	4 - 7	C	6,10	SCD-D		125
		(4.085-7.332)		(6.6,9.7)			

Using bremsstrahlung produced with 6.6 and 9.7 MeV beams, nuclear resonance fluorescence measurements were made on targets of ^{206,207,208}Pb and ^{209}Bi. Ground state transition widths for previously unknown energy levels with widths ≳ 1 eV were obtained. An interpretation of several of these levels in terms of a particle-core weak coupling model is suggested.

11 LEVELS 4.1-7.3 MeV

TABLE IV. Observed levels and their strengths. *The value for* Γ_0 *assumes* $g\Gamma_0/\Gamma = 3$ *for* ^{206}*Pb and* ^{208}*Pb, and* $g\Gamma_0/\Gamma = 1$ *for* ^{207}*Pb and* ^{209}*Bi.* Values in parentheses have uncertainties in excess of 50%. Statistical uncertainties are given for well-defined peaks. Total uncertainties include uncertainties in flux calibration. Energy values are believed to be accurate to ±3 keV for the starred (★) ^{206}Pb levels and to ±5 keV for the other levels.

Energy (MeV)	Nucleus	Γ_0 (eV)	Uncertainty (%) Statistical	Total	Other measurements $g\Gamma_0^2/\Gamma$ (eV)	Γ_0 (eV)	References
6.54	(Pb) 206	7.4		40			
6.73		5.5		40			
5.902		4.4	15	40			
5.534		(3.0)					
5.796		(1.0)					
5.639		(0.5)					
5.615		(1.0)					
5.577		(0.5)					
5.039		1.6	15	40			
4.974		0.8		40			
6.753	(Pb) 207	(<10)					
5.716		(3)					
5.600		(8)					
5.490		(12)					
5.223		(5)					
5.209		(3)					
4.950		(7)			4.0 $\Gamma_0/\Gamma = 1$		12
4.875 }		(13)			3.6 $\Gamma_0/\Gamma = 1$		12
4.847 }							12
7.332★	(Pb) 208	38	10	35		35,41	11,10
7.033★		14	10	35		15,17 ± 2	11,5
7.063★		29	10	35		15,31 ± 3	11,5
6.721★		15	20	40		15,14	11,10
6.337		(0.5)					
6.305		(1.0)					
6.262		4.1		45			
5.515★		28	2	35		15	11
5.293★		8.6	5	35		5	11
4.842★		6.3	5	35	$J^\pi = 1^+$	5.1 ± 0.8	12
4.085★		0.51		40	$J^\pi = 2^+$	0.5 ± 0.1	12
5.549	(Bi) 209	6.6		40			
5.522 }							
5.509 }		17	5	35			
5.498 }							
5.422		8.3		45			
5.293		12	15	40			
4.845 }					1.4		12
4.803 }		(10)			2.7		12
4.771 }					2.9		12
4.501		(3)					
4.228		(3)					

[5] C.P. Swann, Nucl. Phys. A201, 534 (1973)
[10] P. Axel, K. Min, N. Stein, and D.C. Sutton, Phys. Rev. Lett. 10, 299 (1963)
[11] A.M. Khan and J.W. Knowles, Bull. Am. Phys. Soc. 12, 538 (1967); J.W. Knowles, A.M. Khan, and W.F. Mills (unpublished)
[12] C.P. Swann, Proceedings of the International Conference on Photonuclear Reactions and Applications, (U.S. Atomic Energy Commission Office of Information Services, 1975), p.317

REF.	R.J. Holt, R.M. Laszewski, H.E. Jackson Phys. Rev. C15, 827 (1977)	ELEM. SYM.	A	Z
		Pb	208	82

METHOD	REF. NO.	
	77 Ho 1	hmg

REACTION	RESULT	EXCITATION ENERGY	SOURCE TYPE	SOURCE RANGE	DETECTOR TYPE	DETECTOR RANGE	ANGLE
$ G,N	SPC	7- 8	C	UKN	TOF-D		DST
		(7.57-7.72)					

POL NEUTRONS

The photoneutron polarization from resonances near the threshold region was observed for the $^{208}Pb(\gamma,\vec{n}_0)^{207}Pb$ reaction. Resonances located at photoneutron energies of 180 and 315 keV, previously believed to be a large part of the giant $M1$ resonance, are shown to be $E1$ excitations.

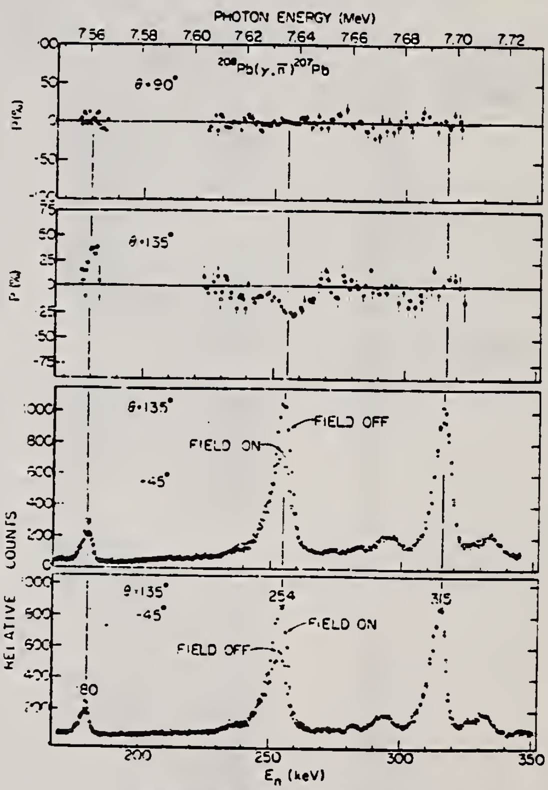

FIG. 1. Upper graphs represent the observations of the photoneutron polarization at 90° and 135° for the 180-, 254-, and 315-keV resonances. Lower graphs indicate the photoneutron spectra from ^{208}Pb after scattering from a Mg analyzer at angles of ± 45° and with and without the field of the neutron spin-precession solenoid.

REF.					ELEM. SYM.	A	Z
R. M. Laszewski, R. J. Holt, and H. E. Jackson Phys. Rev. Lett. 38, 813 (1977)					Pb	208	82
METHOD					REF. NO.		
					77 La 2		hmg

REACTION	RESULT	EXCITATION ENERGY	SOURCE		DETECTOR		ANGLE
			TYPE	RANGE	TYPE	RANGE	
$ G,NO	LFT	8- 10	D	9- 11	TOF-D		90
		(8.2-9.5)		(9.0-10.2)			

POL NEUTRONS, J-PI

Very-high-energy-resolution photoneutron time-of-flight measurements in combination with high-resolution measurements of photoneutron polarizations from the reaction $^{208}Pb(\gamma,n_0 t)^{207}Pb$ have enabled us to identify seven probable 1^+ resonances at excitations between 8.2 and 9.5 MeV. These resonances have a total strength $B(M1)\uparrow = (8.5 \pm 0.5)\mu_0^2$. This strength plus that previously reported at 7 and at 8 MeV can account for the $M1$ sum rule in ^{208}Pb.

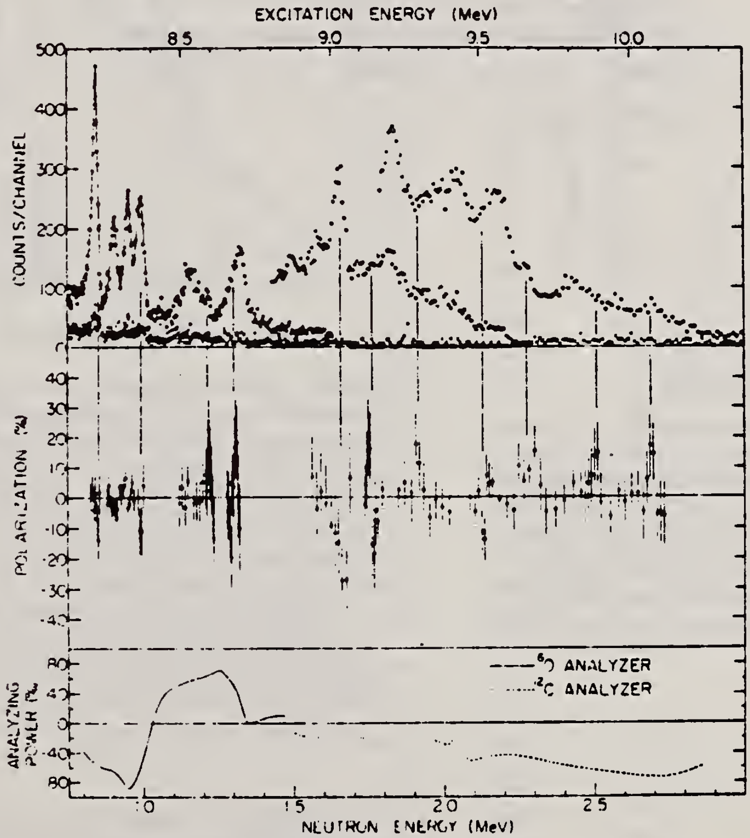

FIG. 1. The 90° photoneutron polarization time-of-flight spectra for endpoint energies of 9.0, 9.6, and 10.2 MeV are shown at the top. The measured background is indicated with ×'s. Below this is the measured polarization. The error bars are statistical. The analyzing powers of ^{16}O and ^{12}C are given at the bottom.

over

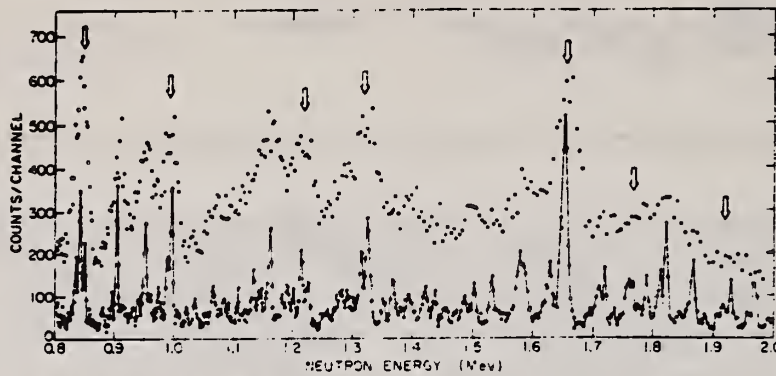

FIG. 3. Comparison of the 90°, 9.6-MeV endpoint very-high-resolution time-of-flight spectrum with the corresponding polarization spectrum. Arrows indicate the locations of significant nonzero polarizations.

TABLE I. Listed are (a) the energies at which nonzero polarization is observed (Fig. 1); (b) the energies of corresponding resonances in the very-high-resolution data (Fig. 2), the deduced spin and parity assignments J^{π}, and the ground-state radiation widths $\Gamma_{\gamma 0}$. Note that a lower limit was obtained for the *M*1 strength by assuming that, in each group, the resonance with the smallest width is the 1^+ resonance.

E_n(MeV)[a]	E_n(MeV)[b]	E_γ(MeV)[b]	J^{π}	$\Gamma_{\gamma 0}$(eV)
	.840	8.213		2.6 ± 0.5
0.85	.846	8.220	$1^-,1^+$	10.2 ± 0.3
	.855	8.228		2.6 ± 0.5
	.993	8.367		2.1 ± 0.1
0.99			$1^-,1^+$	
	.999	8.373		6.2 ± 0.1
	1.219	8.594		3.7 ± 0.1
1.22			$1^-,1^+$	
	1.22[illegible]	8.604		3.3 ± 0.1
	1.318	8.694		3.1 ± 0.2
1.32			$1^-,1^+$	
	1.328	8.703		9.2 ± 0.3
	1.631	9.008		4.4 ± 0.2
1.65			$1^-,1^+$	
	1.658	9.035		22.2 ± 0.4
	1.764	9.136		1.6 ± 1.0
1.77			$1^-,1^+$	
	1.770	9.142		4.1 ± 0.9
	1.921	9.2[illegible]		2.6 ± 0.5
1.92			$1^-,1^+$	
	1.[illegible]	9.312		6.3 ± 1.3
	2.132	9.[illegible]12		[illegible]
2.14			$1^-,(1^+,2^+)$	
	2.157	9.531		4.9 ± 1.0
	2.258	9.638		1.5 ± 0.3
2.26			$1^-,(1^+,2^+)$	
	2.274	9.654		7.9 ± 1.6
2.29			$1^-,(1^+,2^+)$	
	2.295	9.675		1.1 ± 0.2
2.52	2.524	[illegible]	$1^-,(1^+,2^+)$	6.5 ± [illegible]
2.69			$1^-,(1^+,2^+)$	

REF. R. Pitthan and F.R. Buskirk
Phys. Rev. C 16, 983 (1977)

ELEM. SYM.	A	Z
Pb	208	82

METHOD	REF. NO.	
	77 Pi 2	hmg

REACTION	RESULT	EXCITATION ENERGY	SOURCE TYPE	SOURCE RANGE	DETECTOR TYPE	DETECTOR RANGE	ANGLE
E,E/	SPC	8- 12	D	50,65	MAG-D		DST

NUCLEAR REACTIONS ^{208}Pb(e,e'), E_0 = 50 and 65 MeV, θ = 93° and 129°; measured $d^2\sigma/d\Omega dE_x$, deduced multipolarity, isospin, sum-rule exhaustion, reduced transition probabilities $B(E\lambda)$; discussion monopole giant resonance (breathing mode).

Reanalysis of 75Bu19

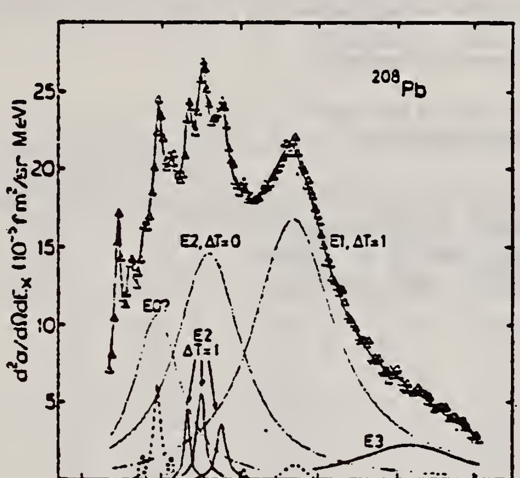

FIG. 1. Reanalysis of a spectrum of 64.6-MeV electrons (Ref. 1), scattered inelastically at 93° from ^{208}Pb with an overall resolution of 190 keV in the giant resonance region. The statistical error is smaller than the size of the experimental points. The triplet around 10.6 MeV is but a small fraction of the cross section. In addition to the states mentioned in the text one has to take into account lines at 7.4, 7.9, 8.4, and 9.4 MeV. More structure is visible at 12 and 14 MeV. The excitation energies of the freely fitted resonances, (8.9 ± 0.2) MeV ($E0$), (13.6 ± 0.2) MeV ($E1$), and (18.5 ± 0.9) MeV ($E3$) denote the maxima of the strength functions, not of the cross sections. It should especially be noted that the strength found for the $E1$ resonance, $B(E1)$ = 60 fm^2 is in essential agreement with the (γ,n) values of 55 and 75 fm^2 from Refs. 3 and 4, respectively.

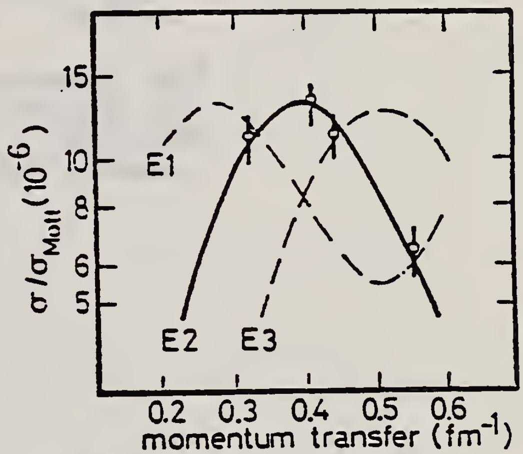

FIG. 2. Ratio of the inelastic cross section to the Mott cross section for the narrow line at 10.07 MeV. The curves show DWBA calculations for a primary energy of 64.6 MeV and an excitation energy of 10.07 MeV. The method of Ziegler and Peterson [Phys. Rev. 165, 1337 (1968)] was used to display points from measurements with different primary energies in the same drawing. Only measurements with scattering angle smaller than 130° were used to avoid transverse contributions.

[1] F.R. Buskirk, H.D. Graf, R. Pitthan, H. Theissen, O. Titze, and Th. Walcher, Phys. Lett. 42B, 194 (1972)

[3] B.L. Berman and S.C. Fultz, Rev. Mod. Phys. 47, 713 (1975); B.L. Berman, Atlas of Photoneutron Cross Sections (Bicentennial Edition, 1976) UCRL Report No. UCRL-73482 (unpublished).

[4] A. Veyssiere, H. Bell, R. Bergere, P. Carlos, and A. Lepretre, Nucl. Phys. A159, 561 (1970)

(over)

TABLE I. Excitation energies, B values, sum-rule fractions, and total widths of the $E2$ or $E0$ states in question. The rms ground-state radius of Friar and Negele [Nucl. Phys. A212, 92 (1973)] was used to calculate the $E2$ and $E0$ sum rules. The widths but not the strengths of the lines depend on the line shape used; a Breit-Wigner form was found to give the best fit. Multiplying the $E2$ sum rule by 1.34 gives the equivalent monopole sum rule for each state; the 8.9-MeV monopole state interpreted as $E2$, thus, corresponds to 0.33 EWSR ($E2$, $\Delta T = 0$). Isoscalar and isovector sums differ by the factor (N/Z).

E_x (MeV)	Γ (MeV)	$\lambda^{\pi}, \Delta T$	R[a]	$B(E\lambda)$ (fm^4)
10.07 ± 0.03	0.20 ± 0.05	2^+,1	0.013	150 ± 30
10.60 ± 0.04	0.32 ± 0.06	2^+,1	0.025	280 ± 40
11.37 ± 0.05	0.37 ± 0.05	2^+,1	0.019	200 ± 40
8.9 ± 0.2	2.0 ± 0.2	0^+,0	0.47	5300 ± 500
10.8[b]	2.6[b]	2^+,0	0.56	6200 ± 600

[a] $R = B(E\lambda, \Delta T) E_x / \text{EWSR}(E\lambda, \Delta T)$.

[b] The values from Youngblood *et al.* (Ref. 9) were used in order to achieve a fit compatible with the (α, α') experiments.

[9] D.H. Youngblood, J.M. Ross, C.M. Rosza, J.D. Bronson, A.D. Bacher, and D.R. Brown, Phys. Rev. C 13, 994 (1976); and private communication.

REF.	S. Raman, M. Mizumoto, and R.L. Macklin Phys. Rev. Lett. 39, 598 (1977)	ELEM. SYM.	A	Z
		Pb	208	82
METHOD		REF. NO.		
		77 Ra 4		hmg

REACTION	RESULT	EXCITATION ENERGY	SOURCE TYPE	SOURCE RANGE	DETECTOR TYPE	DETECTOR RANGE	ANGLE
N,G	LFT	7- 9	D	16*856	TOF-D		UKN
		(7.4-8.4)					

Eighteen $M1$ transitions to the ^{208}Pb ground state have been identified and their radiative widths measured in a study of the reaction $^{207}Pb(n,\gamma)$ combined with the results from recent neutron transmission and elastic scattering measurements. In the excitation region between 7.37 and 8.23 MeV, ~ 50% of the expected total $M1$ strength in ^{208}Pb has been located.

*ENERG IN KILOVOLTS

TABLE I. Comparison of present results for selected $J=1$ resonances with those of other measurements.

E_n (keV)	J^π	Ref. 14 Γ_n[a] (eV)	Present results Γ_γ[b] (eV)	Present results Γ_{γ_0}[b] (eV)	Ref. 6 Γ_{γ_0} (eV)	Ref. 7 Γ_{γ_0} (eV)	Ref. 8 Γ_{γ_0} (eV)
30.49	$1^{(-)}$	13	0.62 *2*	0.64 *2*	0.25	0.50	
37.73	1^+	31	0.83 *6*	0.76 *8*	0.71	1.26	
41.17[c]	1^-	1220	5.3 *3*	(5.3)	(5.3)	(5.3)	(5.3)
90.18	1^+	272	2.05 *4*	2.01 *4*		1.14	
101.81	1^-	69	0.35 *9*	0.32 *9*			
115.20	1^+	923	1.83 *11*	1.55 *9*	1.77	1.14	
127.88	1^+	613	2.95 *6*	2.59 *5*		1.89	
130.23	1^+	87	1.01 *2*	0.95 *3*			
155.72	1^+	115	0.71 *2*	0.66 *3*			
181.49	1^-	92	18.0 *6*	17.9 *10*	17.4[d]	18.6[d]	15.3[d]
256.11	1^-	3107	21.7 *4*	21.3 *4*	19.3	22.3	20.7
297.90	1^+	315	0.77 *5*	0.71 *5*		2.1	1.1
316.87	1^-	951	10.8 *2*	10.3 *2*	8.5	8.8	12.9
335.45	1^+	255	1.48 *4*	1.19 *5*			0.9
541.9	1^-	1547	8.2 *2*	7.6 *2*	9.1	11.6	15.6

[a]Neutron widths mainly from transmission data (Ref. 14). If $\Gamma_n \gg \Gamma_\gamma$, the Γ_γ values are insensitive to the exact value of Γ_n.

[b]In our notation, 0.62 *2* ≡ 0.62 ± 0.02, etc. The statistical fitting uncertainties shown do not include uncertainties due to angular distribution effects which are estimated to be < 10%. The uncertainty due to systematic effects is < 5% and, in the case of Γ_{γ_0}, < 7% including normalization at 41 keV.

[c]This resonance has essentially isotropic γ-ray angular distribution.

[d]Recalculated with $\Gamma_n = 92$ eV.

[6]C.D. Bowman, R.J. Baglan, B.L. Berman, and T.W. Phillips, Phys. Rev. Lett. 25, 1302 (1970

[7]L.C. Haacke and K.G. McNeill, Can. J. Phys. 53, 1422 (1975)

[8]R.E. Toohey and H.E. Jackson, Phys. Rev. C 6, 1440 (1972)

[14]D.J. Horen, J.A. Harvey, and N.W. Hill, Oak Ridge National Laboratory Report No. ORNL-5137, 1976 (unpublished), p.8, and private communication, and Phys. Rev. Lett. 38, 1344 (1977)

REF.	M. Sasao and Y. Torizuka Phys. Rev. C15, 217 (1977)	ELEM. SYM.	A	Z
		Pb	208	82

METHOD		REF. NO.	
	Page 1 of 2.	77 Sa 2	hmg

REACTION	RESULT	EXCITATION ENERGY	SOURCE TYPE	SOURCE RANGE	DETECTOR TYPE	DETECTOR RANGE	ANGLE
E,E/	FMF	2- 26	D	106-250	MAG-D		DST

ALSO QUASI-ELAS SCAT

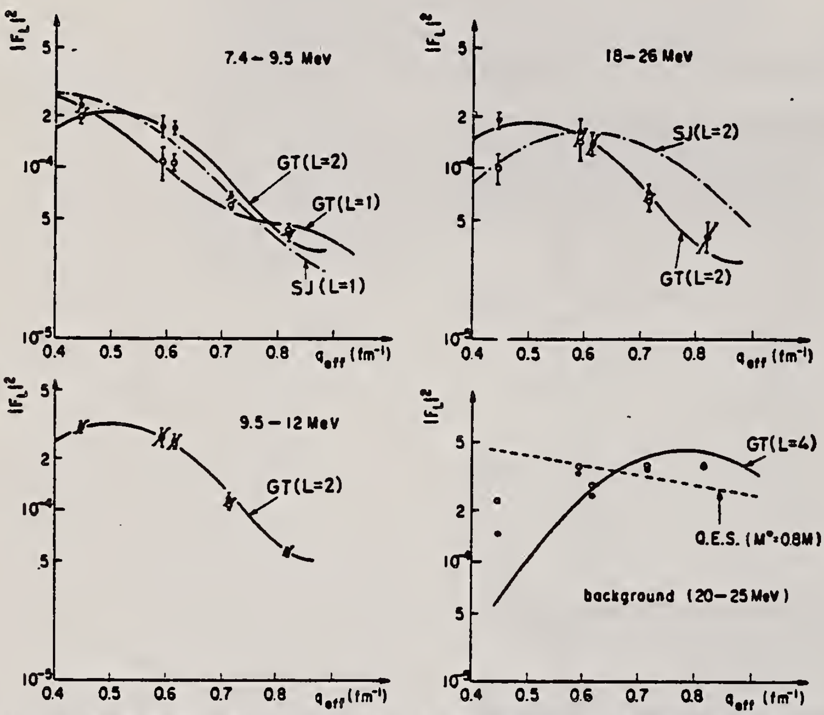

FIG. 7. The cross sections in specific energy ranges for the giant multipole resonances estimated phenomenologically as shown in Fig. 6 are compared with various models. The cross section of the background (right side lower part) is compared with the Fermi-gas model and $L=4$ GT form factor.

TABLE III. Percentages of the EWSR in ^{208}Pb below 26 MeV. Contributions from bound states (16% for $T=0$ $E2$ and 20% for $T=0$ $E3$) are included.

Multipole	Mode	ω (MeV)	GT expansion (%)	SJ expansion (%)
$E0$	$T=0$	12.5–15	97^{+27}_{-14}	10^{+20}_{-3}
$E1$	$T=1$	7.4–26	156^{+23}_{-35}	145^{+13}_{-30}
$E2$	$T=0$	7.4–12.5	92^{+14}_{-8}	52^{+12}_{-5}
$E2$	$T=1$	15–26	95^{+40}_{-13}	41^{+12}_{-6}
$E3$	$T=0$	7.4–26	165^{+15}_{-71}	94^{+11}_{-47}

[38] S. Krewald et al., Phys. Lett. 52B, 295 (1974).

[39] G. Bertsch et al., Phys. Rev. 18C, 125 (1975).

[40] K.E. Liu and G.E. Brown (unpublished).

[62] E. Lipparini et al., Phys. Rev. Lett. 36, 660 (1976).

[65] J.F. Ziegler et al., Phys. Rev. 165, 1337 (1968).

(over)

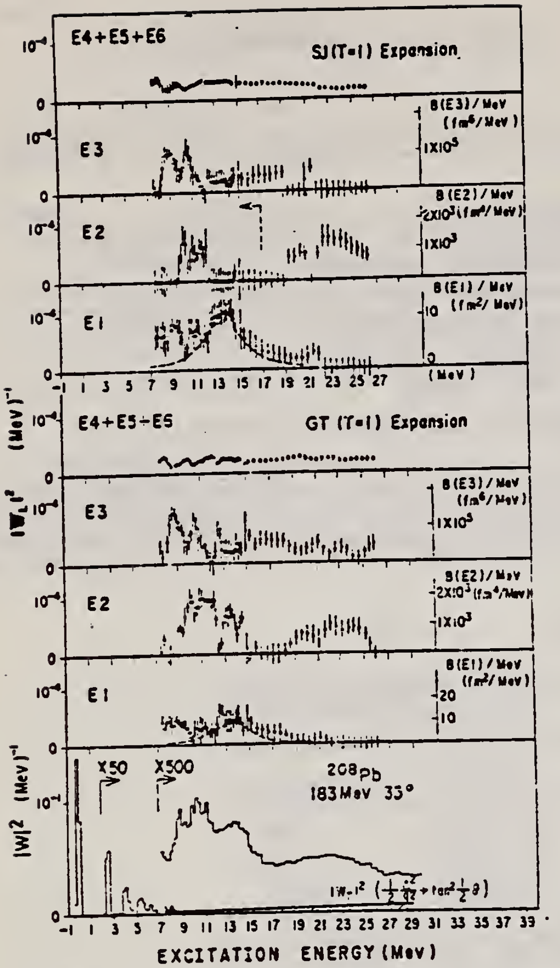

FIG. 8. The spectrum at 183 MeV, 35° was decomposed into spectra for $E1$, $E2$, $E3$, and the sum of $E4$, $E5$, and $E6$ using the q dependence of the Tassie model for the isoscalar mode and the GT model for isovector (lower part) and the SJ model for isovector (upper part). $B(EL)$/MeV at the right-hand side cannot be applied for the $E2$ component of the SJ-model expansion above 17 MeV. Errors are those from fitting. The lowest portion of the figure is the experimental spectrum after radiative unfolding.

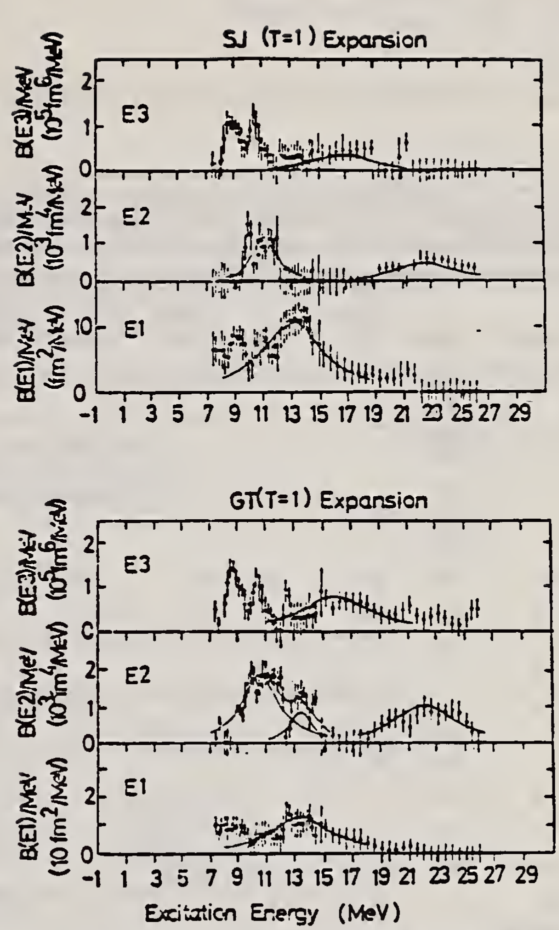

FIG. 9. The Breit-Wigner line shape fit to the $E1$, $E2(E0)$, and $E3$ strength distributions obtained by multipole expansion.

TABLE VI. The RPA calculations for the low-lying collective states in ^{208}Pb are compared with the experimental data of Refs. 62 and 65. $B(EL)$ is in Weisskopf units.

	Experiment		RPA values: Ring and Speth[a]		Bertsch and Tsai[b]		Liu and Brown[c]	
J^π	ω (MeV)	(W.u.) $B(EL)$	ω (MeV)	$B(EL)$ (W.u.)	ω (MeV)	$B(EL)$ (W.u.)	ω (MeV)	$B(EL)$ (W.u.)
3^-	2.61	36 ± 3	2.64	31	2.7	29	2.8	38
5^-	3.19	11.1 ± 1.4	3.39	7	3.3	6	3.4	14
5^-	3.71	8 ± 2	3.82	8				
2^+	4.07	8.1	4.49	8.5	5.4	7	5.6	7
4^+	4.32	15	4.69	9	5.4	7	6.4	16
6^+	4.42	11.7	4.77	11				

[a] From Ref. 38.
[b] Reference 39.
[c] Reference 40.

REF.	ELEM. SYM.	A	Z
M. Sasao and Y. Torizuka Phys. Rev. C15, 217 (1977)	Pb	208	82

METHOD	REF. NO.	
	77 Sa 2	hmg

RANGE	ANGLE

TABLE V. Excitation energies and percentages of the corresponding EWSR in ^{208}Pb. The errors of the present data include statistical and fitting uncertainties (Table II) and also differences between models (see the text).

Experiment	Ref. No.	2^+ ($T=0$) ω (MeV)	2^+ ($T=0$) EWSR (%)	0^+ ($T=0$) ω (MeV)	0^+ ($T=0$) EWSR (%)	1^- ($T=1$) ω (MeV)	1^- ($T=1$) EWSR (%)	2^+ ($T=1$) ω (MeV)	2^+ ($T=1$) EWSR (%)	3^- ($T=0$) ω (MeV)	3^- ($T=0$) EWSR (%)
(e,e')	3	8.9 9.4 10.0 10.6	~47					22	~60	19	~44
(e,e')	73	10.2 10.6 11.2	~25			14.1					
(e,e')	67	10.5	95	8.9	50	13.6	105,205	22.5	85	17.5	90
(e,e')	74	8.9 10.8	35 80			14.1					
(p,γ)	75							23.7			
(γ,n)	76	9.034 9.421 10.06	15 25 48								
(p,p')	5	11.2									
(α,α')	68	10.8									
(d,d')	12	10.8	32±5	13.5	60–100						
(e,e')	This work[a]	11	30–82	13.6	1–124	13.6	115–179	22.5	33–135	16	47–180

[a] Excitation energies obtained by the GT expansion.

TABLE II. $B(EL)$ values in fm^{2L} and ratios to energy weighted sum rules, obtained by multipole expansion using the Tassie- and GT-model q dependences or the Tassie and SJ q dependences (right).

E_x (MeV)	Expansion with GT model $E1$	$E2$	$E3$ (×10^5)	Expansion with SJ model for $T=1$ $E1$	$E2$	$E3$ (×10^5)
7.4–9.5	$19.0^{+2.5}_{-4.0}$	810^{+230}_{-180}	$1.70^{+0.24}_{-0.17}$	$15.0^{+2.1}_{-2.2}$	<160	$1.17^{+0.23}_{-0.49}$
	22% ($T=1$)	9% ($T=0$)	16% ($T=0$)	17% ($T=1$)		11% ($T=0$)
9.5–12	$14.2^{+4.4}_{-6.0}$	4410^{+660}_{-470}	$1.26^{+0.14}_{-0.49}$	$15.2^{+2.7}_{-3.8}$	2620^{+330}_{-460}	$1.25^{+0.23}_{-0.63}$
	21% ($T=1$)	59% ($T=0$)	15% ($T=0$)	22% ($T=1$)	35% ($T=0$)	15% ($T=0$)
12–15	$29.3^{+4.7}_{-5.9}$	3140^{+870}_{-440}	$1.10^{+0.26}_{-0.76}$	$29.5^{+3.3}_{-3.2}$	360^{+660}_{-330}	$0.70^{+0.25}_{-0.70}$
	54% ($T=1$)	53% ($T=0$)	16% ($T=0$)	52% ($T=1$)	6% ($T=0$)	10% ($T=0$)
15–18	$18.3^{+4.5}_{-4.7}$	130^{+580}_{-130}	$1.89^{+0.34}_{-0.46}$	$12.3^{+3.0}_{-3.0}$	<350	$1.1^{+0.73}_{-0.67}$
	41% ($T=1$)	2% ($T=1$)	34% ($T=0$)	28% ($T=1$)		20% ($T=0$)
18–26	$6.6^{+5.0}_{-6.6}$	5260^{+2000}_{-850}	$2.59^{+0.42}_{-1.88}$	$8.8^{+3.0}_{-3.8}$	2310^{+560}_{-330}	$0.74^{+0.45}_{-0.74}$
	20% ($T=1$)	94% ($T=1$)	63% ($T=0$)	26% ($T=1$)	41% ($T=1$)	18% ($T=0$)

TABLE IV. Strengths, center energies, and widths obtained by the Breit-Wigner line shape fit to multipole components in Fig. 9.

ω (MeV)	Mode	Γ (MeV)	$B(EL)$ or $\lvert\langle r^3\rangle\rvert^2$
GT expansion			
13.6	$E1(T=1)$	5.0	90 fm^2
10.8	$E2(T=0)$	3.2	9000 fm^4
13.6	$E2(T=0)$	1.8	2400 fm^4
	or $E0(T=0)$	1.8	4700 fm^4
22.5	$E2(T=1)$	5.0	8100 fm^4
16.0	$E3(T=0)$	6.0	5.2×10^5 fm^6
SJ expansion			
13.1	$E1(T=1)$	5.0	80 fm^2
11.0	$E2(T=0)$	2.0	3800 fm^4
22.5	$E2(T=1)$	5.0	2700 fm^4
16.6	$E3(T=0)$	5.4	2.3×10^5 fm^6

U.S. DEPARTMENT OF COMMERCE
NATIONAL BUREAU OF STANDARDS

REF. C. P. Swann
Phys. Rev. C 16, 2426 (1977)

ELEM. SYM.	A	Z
Pb	208	82

METHOD

REF. NO.	
77 Sw 7	hmg

REACTION	RESULT	EXCITATION ENERGY	SOURCE TYPE	SOURCE RANGE	DETECTOR TYPE	DETECTOR RANGE	ANGLE
$ G,G	LFT	4	C	5	SCD-D		126
		(4.843)		(4.95)			

The linear polarization of the resonantly produced 4843 keV radiation from ^{208}Pb has been remeasured, and the results are inconsistent with either a pure E1 or M1 transition. A comparison of self-absorption and scattering results suggests two levels with widths of about 2.5 eV. It is proposed that one has as 1^- and the other a 1^+ character.

POL SCAT 4.843 PHOT

TABLE I. Polarization results for the full energy and two escape peaks (D.E.) of the 4843 and 4087 keV scattered radiation.

E_γ (keV)	Present	$(N_\perp - N_{\parallel})/(N_\perp N_{\parallel})$ (%) Ref. 1	Average	J^π
4843	+(0.97 ± 1.75)	−(5.41 ± 2.86)		$1^{+,-}$
4087	−(5.95 ± 1.68)	−(5.43 ± 3.74)	−(5.86 ± 1.53)	2^+
4843 D.E.	+(0.23 ± 0.79)	+(0.5 ± 1.40)	+(0.30 ± 0.69)	
4087 D.E.	+(0.67 ± 1.00)	+(0.76 ± 2.62)	+(0.68 ± 0.93)	

TABLE II. Comparison of self-absorption and scattering results for the 4843 keV line of ^{208}Pb.

Self-absorption Γ_0 (eV)	Scattering Γ_0^2/Γ (eV)
$2.38^{+0.52}_{-0.27}$ [a]	4.9 ± 0.5 [a]
	5.1 ± 0.8 [b]
	5.7 ± 1.9 [c]
	6.3 ± 2.2 [d]

[a] Present study.
[b] See Ref. 1.
[c] See Ref. 4.
[d] See Ref. 5.

1 C.P. Swann, Phys. Rev. Lett. 32, 1449 (1974)
4 J.W. Knowles, A.M. Khan, and W.F. Mills (unpublished)
5 D.F. Coope, L.E. Cannell, and M.L. Brussel, Phys. Rev. C 15, 1977 (1977)

REF.	T.R. Yeh and H. Lancman Phys. Rev. C 16, 1268 (1977)	ELEM. SYM.	A	Z
		Pb	208	82

METHOD	REF. NO.	
	77 Ye 1	hmg

REACTION	RESULT	EXCITATION ENERGY	SOURCE		DETECTOR		ANGLE
			TYPE	RANGE	TYPE	RANGE	
G,G	LFT	8,8	D	2	SCD-D		85
		(7.06,7.08)		(2.5)			

level 7.06,7.08 MeV

The widths of the 7.06 and 7.08 MeV states in ^{208}Pb were determined in a resonance fluorescence experiment to be $\Gamma_0 = 29 \pm 3$ and 16 ± 3 eV, respectively. The $^{19}F(p,\alpha\gamma)^{16}O$ reaction was used to produce the incident γ rays.

TABLE I. Level widths obtained in this work and in previous experiments.

E_x (MeV)	J	Γ_0 (eV) This work	Ref. 7	Ref. 8	Ref. 9	Ref. 10	Ref. 11	Ref. 12
7.064	1	29 ± 3	18 ± 3	31 ± 3	29 ± 10		15	32 ± 2.0 [a]
7.084	1	16 ± 3		17 ± 2	14 ± 5	16^{+6}_{-4}	15	

[a] The two states were not resolved.

[7] R.J. Sparks, H. Lancman, and C. van der Leun, Nucl. Phys. A259, 13 (1976)

[8] C.P. Swann, Nucl. Phys. A210, 534 (1974)

[9] D.F. Coope, L.E. Cannel, and M.K. Brussel, Phys. Rev. C 15, 1977 (1977)

[10] W. Scholz, H. Bakhru, R. Colle, and A. Li-Schulz, Phys. Rev. C 9, 1568 (1974)

[11] A.M. Khan and J.W. Knowles, Bull. Am. Phys. Soc. 19, 538 (1967)

[12] R. Laszewski and P. Axel (unpublished)

REF.		ELEM. SYM.	A	Z
	E.A. Arakelyan, G.L. Bayatyan, G.S. Vartanyan, N.K. Grigoryan, S.G. Knyazyan, A.T. Margaryan, S.S. Stepanyan, P.K. Kir'yanov, V.A. Maisheev & A.M. Frolov Phys. Lett. 79B, 143 (November 1978)	Pb	208	82
METHOD		REF. NO.		
		78 Ar 9		hmg

REACTION	RESULT	EXCITATION ENERGY	SOURCE TYPE	SOURCE RANGE	DETECTOR TYPE	DETECTOR RANGE	ANGLE
G,MU-T	ABX	THR-30		12*30	NAI-D	---	4PI

*Energy in GeV

The total cross section of hadron photoproduction on C, Cu and Pb nuclei is measured for six energy values in the range 12–30 GeV. The obtained cross-section values for C and Cu nuclei have a weak energy dependence at high energies (above 20 GeV). The cross section for the Pb nucleus is somewhat higher in comparison with that expected, and energy dependence is not observed. The A-dependence of the effective number of hadrons agrees with VDM predictions.

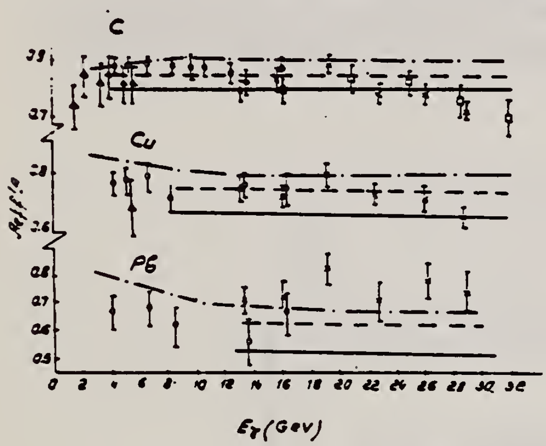

Fig. 3. Energy dependence of A_{eff}/A for C, Cu, Pb nuclei. For comparison the data of DESY and SLAC–UCSB, and also the theoretical curves, corresponding to VDM and to the case when the photon is ~20% of the time in a "pure" state, without shadowing. ^, DESY; c, SLAC–UCSB; ×, Serpukhov; ⊐, Serpukhov [4]; —— VDM; – – – 0.8 VDM + 0.2 pointlike interaction; –·– general VDM.

Table 1
Hadron photoproduction cross sections (in μb) for C, Cu, Pb nuclei for different energies of γ-quanta. Only statistical errors are given.

γ-quanta energy (GeV)	^{12}C	^{64}Cu	^{207}Pb
12.6–15.0	1084 ± 48	5600 ± 240	17140 ± 1170
15.0–17.7	1100 ± 43	5200 ± 310	17480 ± 1140
17.7–21.0	11‑5 ± 34	5740 ± 340	19680 ± 1720
21.0–24.6	1058 ± 53	5220 ± 460	16400 ± 1720
24.6–27.9	1047 ± 55	4870 ± 350	17920 ± 1920
27.9–30.0	930 ± 66	4730 ± 510	16840 ± 2810

Table 2
Value of A_{eff} for nuclei C, Cu, Pb for different energies of γ-quanta. Only statistical errors are given.

γ-quanta energy (GeV)	^{12}C	^{64}Cu	^{207}Pb
12.6–15.0	0.79 ± 0.04	0.77 ± 0.04	0.73 ± 0.05
15.0–17.7	0.81 ± 0.04	0.72 ± 0.05	0.75 ± 0.06
17.7–21.0	0.87 ± 0.4	0.80 ± 0.05	0.85 ± 0.7
21.0–24.6	0.80 ± 0.05	0.74 ± 0.07	0.72 ± 0.08
24.6–27.9	0.79 ± 0.05	0.69 ± 0.05	0.79 ± 0.09
27.9–30.0	0.71 ± 0.05	0.68 ± 0.07	0.75 ± 0.13

$$\frac{A_{eff}}{A} = \frac{\sigma_t(\gamma, A)}{Z\sigma_t(\gamma, p) + (A - Z)\sigma_t(\gamma, n)},$$

where

$$\sigma_t(\gamma, p) = (98.7 \pm 3.6) + (65 \pm 10)E^{-1/2}\mu b,$$

$$\sigma_t(\gamma, n) = \sigma_t(\gamma, p) - (18.3 \pm 6.1)E^{-1/2}\mu b.$$

REF. R. Frey, A. Richter, A. Schwierczinski, E. Spamer, O. Titze, and W. Knupfer
Phys. Lett. 74B, 45 (1978)

ELEM. SYM.	A	Z
Pb	208	82

METHOD

REF. NO.	
78 Fr 5	rs

REACTION	RESULT	EXCITATION ENERGY	SOURCE		DETECTOR		ANGLE
			TYPE	RANGE	TYPE	RANGE	
E,E/	ABX	6- 8	D	50,64	MAG-D		DST

High-resolution inelastic electron scattering (FWHM ≈ 33 keV) with 50 MeV and 63.5 MeV electrons on ^{208}Pb has been used to study magnetic excitations between E_x = 6 MeV and 8 MeV. Angular distributions were analyzed in terms of the DWBA with RPA wave functions. Eight $J^\pi = 2^-$ states carrying a total strength $\Sigma B(M2)\uparrow = 8500 \mu_K^2$ fm^2 have been found. The strong fragmentation is in qualitative agreement with theoretical predictions.

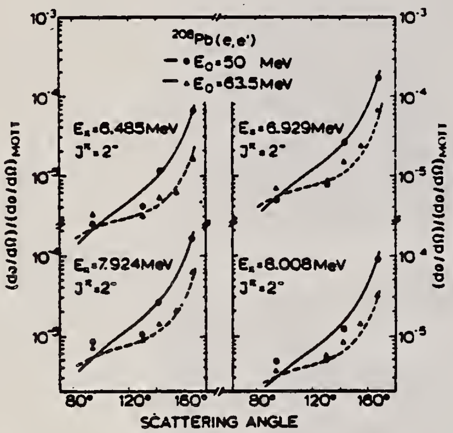

Fig. 2. Angular distributions for four states with $J^\pi = 2^-$.

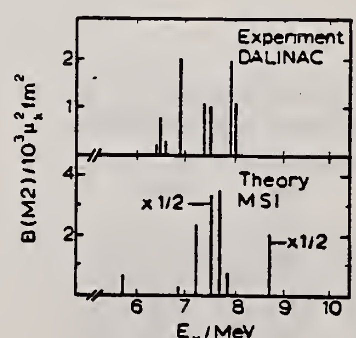

Fig. 3. Comparison between experimentally determined and theoretically predicted M2 strengths.

REF. W. Knupfer, Phys. Lett. 77B, 367 (1978)

ELEM. SYM.	A	Z
Pb	208	82

METHOD

REF. NO.	
78 Kn 7	rs

REACTION	RESULT	EXCITATION ENERGY	SOURCE TYPE	SOURCE RANGE	DETECTOR TYPE	DETECTOR RANGE	ANGLE
E,E/	RLY	7-9	D	24-64	MAG-D		DST

M2 LEVELS

The location of the M2 giant resonance in ^{28}Si, ^{90}Zr and ^{208}Pb, predicted within the framework of the MSI-RPA particle-hole model, has been confirmed by high-resolution inelastic electron scattering ($E_x \approx 44A^{-1/3}$ MeV). The fragmented M2 strength distribution can only be described assuming a mass-dependent quenching of the intrinsic g_s factor. This has the consequence that the long sought M1 strength is much reduced in heavy nuclei, an effect which is supported experimentally.

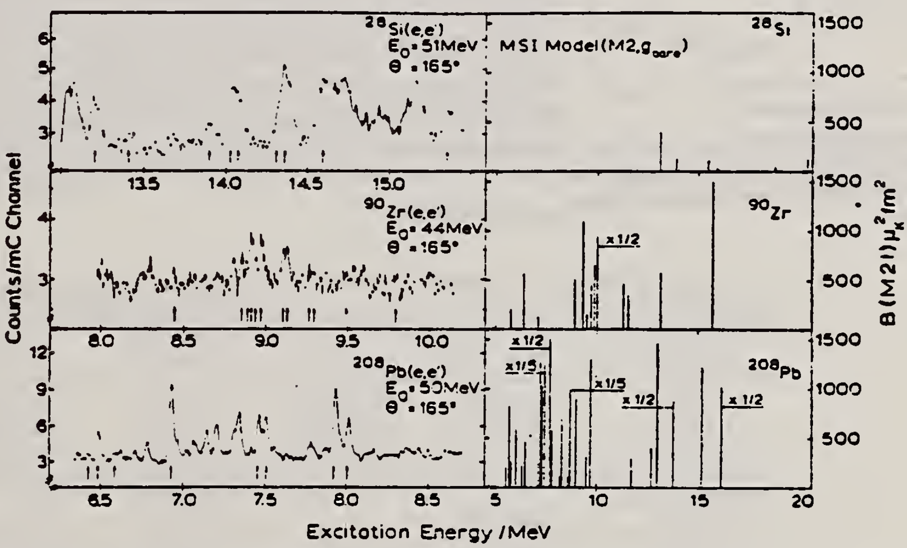

Fig. 1. The left part shows selected (e, e') spectra on ^{28}Si, ^{90}Zr and ^{208}Pb at various energies but all at θ = 165°. The 2$^-$ states are marked by arrows. The right part displays the model prediction for the M2 strength.

(over)

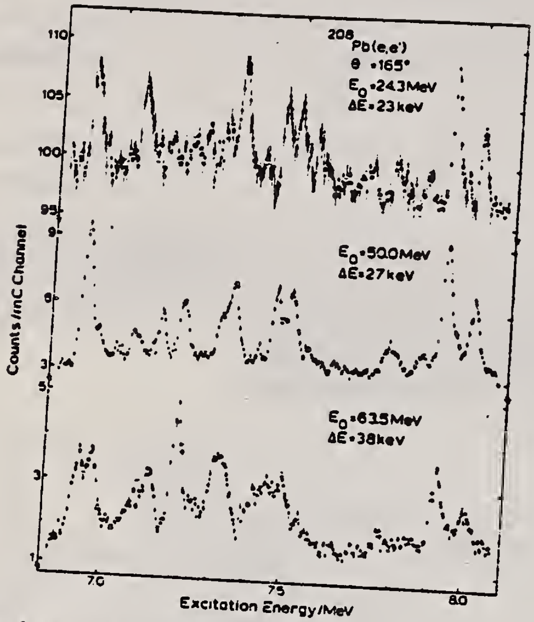

Fig. 3. Electron scattering spectra on ^{208}Pb at $\theta = 165°$ and at different bombarding energies demonstrating the energy dependence of transverse excitations. The spectra at $E_0 = 50$ and 63.5 MeV are from ref. [6].

REF. J.W. Knowles, A.M. Khan, W.F. Mills
Can. J. Phys. 56, 1021 (1978)

ELEM. SYM.	A	Z
Pb	208	82

METHOD

REF. NO.	
78 Kn 14	hg

REACTION	RESULT	EXCITATION ENERGY	SOURCE TYPE	SOURCE RANGE	DETECTOR TYPE	DETECTOR RANGE	ANGLE
G,G	RLX	5-9	D	4-9	SCD-D		DST
		(5.2-8.3)		(4.7-8.3)			

The scattering of gamma radiation from different isotopic mixtures of lead has been measured between 4.7 and 8.3 MeV with a variable energy beam with 175 keV resolution obtained by Compton scattering (n,γ) radiation of nickel from a curved aluminum plate. The elastically scattered radiation was detected with a 12.5 cm diameter, 12.5 cm long NaI(Tl) and with 27 or 49 cm^3 Ge(Li) detectors located at scattering angles of 135° and 90°, respectively. Relative scattering measurements from targets of natural lead, radio-lead, and lead enriched in ^{208}Pb show that the most prominent peaks of natural lead are in ^{208}Pb at 7332.6 ± 1.3, 7087.7 ± 4.6, 7064.4 ± 3.5, 6721.0 ± 1.8, 5507.6 ± 1.8, 5292.6 ± 3.3, 4836.5 ± 4.6 keV. Measurements of resonant scattering and resonant self-absorption of the more intense scattered radiations provide information on level widths.

La diffusion des rayons gamma par différents mélanges d'isotopes de plomb a été mesurée, entre 4.7 et 8.3 MeV, en utilisant un faisceau d'énergie variable ayant une résolution de 175 keV, fourni par diffusion Compton (n,γ) d'un rayonnement du nickel sur une plaque d'aluminium courbée. Le rayonnement diffusé élastiquement était observé au moyen d'un compteur NaI(Tl) de 12.5 cm de diamètre et 12.5 cm de longueur, et de détecteurs Ge(Li) de 27 ou 49 cm^3 placés à des angles de diffusion de 135° et 90° respectivement. Les mesures relatives de diffusion par des cibles de plomb naturel, de radio-plomb et de plomb enrichi en ^{208}Pb montrent que les pics les plus importants du plomb naturel proviennent de ^{208}Pb et sont situés à 7332.6 ± 1.3, 7087.7 ± 4.6, 7064.4 ± 3.5, 6721.0 ± 1.8, 5507.6 ± 1.8, 5292.6 ± 3.3, 4836.5 ± 4.6 keV. Des mesures de diffusion résonnantes et d'absorption résonnante des rayonnements diffusés les plus intenses fournissent des indications sur la largeur des niveaux.

Can. J. Phys., 56, 1021 (1978) [Traduit par le journal]

TABLE 3. Resonance scattering and self-absorption in ^{208}Pb, ^{207}Pb, and ^{206}Pb with a NaI(Tl) detector

Isotope	E_i (MeV)	S_N[a] (eV)	$S_N^{(1)}$ [NaI][b] (eV)	P_N[a]	$P_N^{(1)}$ [NaI][b]	$S_N^{(1)}$ [NaI] (90°)[c] (eV)
^{208}Pb	7.34	122.0±2.1	98.8±2.7	0.27±0.02	0.22±0.03	72.1±2.0
	7.07	116.1±5.4	101.3±6.1	0.29±0.05	0.19±0.05	73.9±4.4
	5.51	70.0±3.6	39.1±4.2	0.22±0.04	0.18±0.07	28.5±6.0
Isotope	**E_i (MeV)**	**S_E (eV)**	**$S_N^{(2)}$ [NaI] (eV)**		**$P_N^{(2)}$ [NaI]**	**$S_N^{(2)}$ [NaI] (90°) (eV)**
^{207}Pb	5.62	22.1±2.3	42.0±7.1		0.36±0.17	38.6±12
Isotope	**E_i (MeV)**	**S_R (eV)**	**$S_R^{(3)}$ [NaI] (eV)**	**P_R**	**$P_R^{(3)}$ [NaI]**	
^{206}Pb	7.96	120.4±5.9	122.2±6.4	0.37±0.04	0.36±0.05	
	7.55	89.4±8.2	88.4±8.6	0.41±0.09	0.40±0.10	

[a]For these measurements only the standard errors based on the statistical count are given.
[b]For these results, obtained from analysis of the measurements the limits of uncertainty include the statistical errors and uncertainties caused by the isotopic spectral separation outlined in Sect. 3. They also include, below 7.34 MeV, the uncertainties caused by lack of knowledge of $P_N^{(2)}$ of ^{207}Pb. To obtain absolute limits of uncertainty the ± 5% systematic uncertainty in the determination of Ω and β_s/β_0 must be included.
[c]Integrated scattering factors at 90° are obtained from the corresponding factors at 135°, column 4, by multiplying by the appropriate f_i factors for dipole radiation given in Table 1.

OVER

Table 4. Resonance total widths Γ_t of ^{208}Pb

		Present measurements		Other measurements				
		Quadrupole $G_t = 5$	Dipole $G_t = 3$	Dipole $G_t = 3$				
E (keV)	$S_{Ni}^{(1)}$ [Ge(Li)][a] (eV)	Γ_t^{a} (eV)	Γ_t^{a} (eV)	$\Gamma_t^{b,c}$ (eV)	$\Gamma_t^{b,d}$ (eV)	$\Gamma_t^{b,e}$ (eV)	Γ_t^{f} (eV)	$\Gamma_t^{b,g}$ (eV)
7332.6±1.3	72.1±2.0	—	42±1			38		
7087.7±4.6	29.9±6.6	9±2	15±3	16	26^{+35}_{-12}	14		16±3
7064.4±3.5	45.4±5.9	13±2	24±3	31		29	18±3	29±3
6721.0±1.8	26.3±6.6	7±2	13±3			15		
5525.3±3.4	23.8±7.3	5±2 (5±2)[h]	10±3 (8±2)[h]					
5507.6±1.8	43.1±8.3	10±2	18±3			28		
5292.6±3.3	17.9±4.7	4±1	7±2			8.6		
4836.5±4.6	16.4±5.5	2±1	6±2	5.1		6.3		

[a] For these measurements the limits of uncertainty include statistical errors and the uncertainty of the reference scattering factor $S_{Ni}^{(1)} = 72.1 \pm 2.0$ (above). To obtain absolute limits of uncertainty see footnote, Table 3.
[b] Scattering data.
[c] References 5 and 12.
[d] Reference 6.
[e] Reference 13.
[f] Transmission data, ref. 7.
[g] Reference 8.
[h] Effective resonance width for the 5525.3 ± 3.4 keV γ-ray assuming dipole or quadrupole transitions to the ground state of ^{207}Pb.

REF.	ELEM. SYM.	A	Z
A. Lepretre, H. Beil, R. Bergere, P. Carlos, J. Fagot, A. Veyssiere, J. Ahrens, P. Axel, and U. Kneissl Phys. Lett. 79B, 43 (1978)	Pb	208	82
METHOD	REF. NO. 78 Le 5		rs

REACTION	RESULT	EXCITATION ENERGY	SOURCE TYPE	SOURCE RANGE	DETECTOR TYPE	DETECTOR RANGE	ANGLE
G,XN	ABX	25-106	D	25-106	MOD-I		4PI

The $\sigma(\gamma,xn)$ cross sections of Pb have been measured above the giant dipole resonance region up to 106 MeV with a quasi-monochromatic photon beam obtained by the annihilation in flight of monochromatic positrons. The total cross section decreases linearly with energy from 20 mb at 35 MeV to 12 mb at 106 MeV. The integrated cross section up to 140 MeV amounts to (1.80 ± 0.2) classical dipole sums.

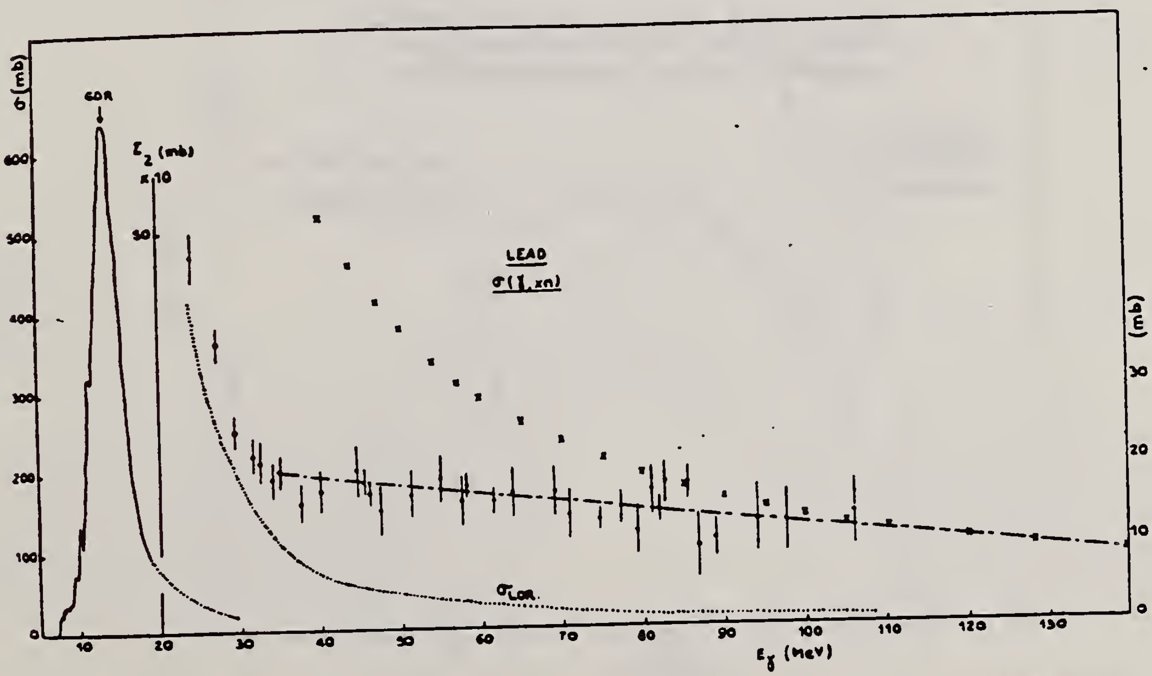

Fig. 2. Photoneutron cross sections of Pb. (1) The experimental points give $\Sigma_2 \approx \Sigma_{x=2}^{\infty}\sigma(\gamma,xn)$. (2) The dot–dash line represents a least-squares fit to the experimental Σ_2 values from 35 to 106 MeV with an rms error of 2 mb. (3) Old Saclay data, covering the giant dipole resonance up to 30 MeV [6], are shown as a solid line. (4) The dotted line represents a Lorentz line fit to the experimental σ_t data in the giant dipole resonance region [6] with σ_0 = 640 mb, E_0 = 13.4 MeV and Γ = 4.05 MeV. (5) Crosses represent the quasi-deuteron cross section σ_{QD} = $4.6(NZ/A)\sigma_D$.

over

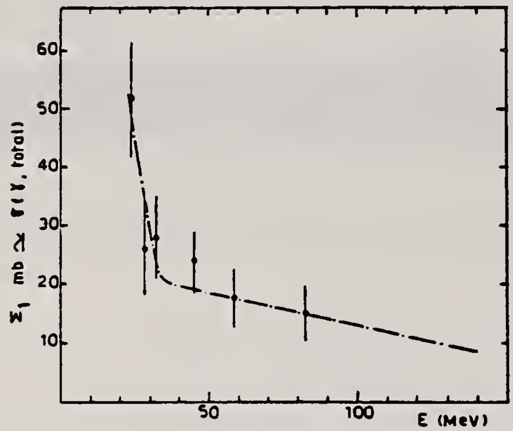

Fig. 1. Measured $\Sigma_1 = \Sigma_{x=1}^{\infty} \sigma(\gamma, xn) \approx \sigma_t$ values for Pb. The average $\Sigma_2 = \Sigma_{x=2}^{\infty} \sigma(\gamma, xn)$ results, taken from fig. 2 and represented by a dotted line, are also given for comparison.

REF. J. Lichtenstadt, J. Heisenberg, C.N. Papanicolas, C.P. Sargent
A.N. Courtemanche and J.S. McCarthy
Phys. Rev. Lett. 40, 1127 (1978)

ELEM. SYM.	A	Z
Pb	208	82

METHOD

REF. NO.	
78 Li 4	rs

REACTION	RESULT	EXCITATION ENERGY	SOURCE		DETECTOR		ANGLE
			TYPE	RANGE	TYPE	RANGE	
E,E/	ABX	5- 7	D	50-335	MAG-D		DST

M12,M14 TRANSITIONS

States at 6.42-, 6.75-, and 7.06-MeV excitation have been observed in electron scattering on ^{208}Pb. The transverse character of the excitation cross section has been established. The states have been interpreted as the $\nu(i_{13/2}^{-1}j_{15/2})_{12^-,14^-}$ and the $\pi(h_{11/2}^{-1}i_{13/2})_{12^-}$ single-particle hole excitations of the ^{208}Pb ground state, on the basis of the measured momentum-transfer dependence and the magnitude of the cross section.

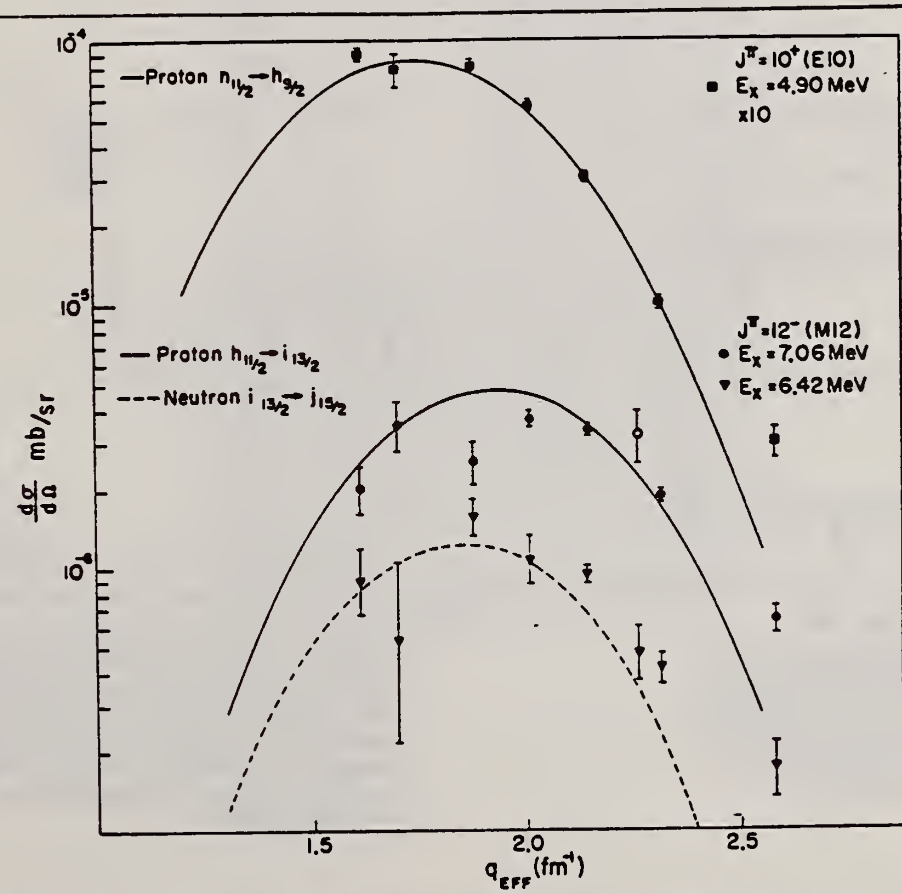

FIG. 2. Experimental cross section for the 4.90-MeV 10⁺ state, and the 6.42- and 7.06-MeV 12⁻ states. The open data points are cross sections measured at 160° multiplied by 1.5 to compensate for the different scattering angle (as discussed in text). Curves are the theoretical calculations.

REF. S. Raman, M. Mizumoto, G.G. Slaughter, and R.L. Macklin
Phys. Rev. Lett. 40, 1306 (1978)

ELEM. SYM.	A	Z
Pb	208	82

METHOD

REF. NO. 78 Ra 2 rs

REACTION	RESULT	EXCITATION ENERGY	SOURCE TYPE	SOURCE RANGE	DETECTOR TYPE	DETECTOR RANGE	ANGLE
N,G	LFT	7- 8	D	0- 1	SCD-D		UNK

Thirty-six high-energy, primary $E2$ transitions to the ^{208}Pb ground state have been identified and their radiation widths measured in a study of the reaction ^{207}Pb(n,γ). The measured $E2$ widths in the excitation energy region between 7.37 and 8.17 MeV are compared with those expected from the rising tails of giant quadrupole resonances located at 8.9 and 10.9 MeV.

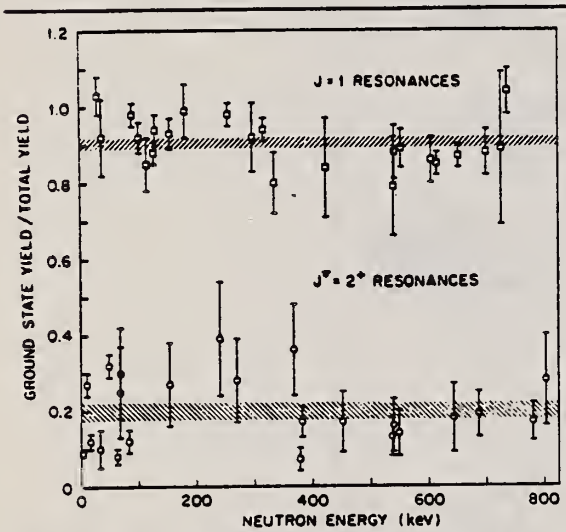

FIG. 3. Yield ratios showing clear separation into two groups leading to J^π assignments for the resonances. Ratios with error bars greater than 25% and 50% for $J = 1$ and $J^\pi = 2^+$ resonances, respectively, have been omitted for clarity. The shaded regions (eye-guides) denote unweighted averages.

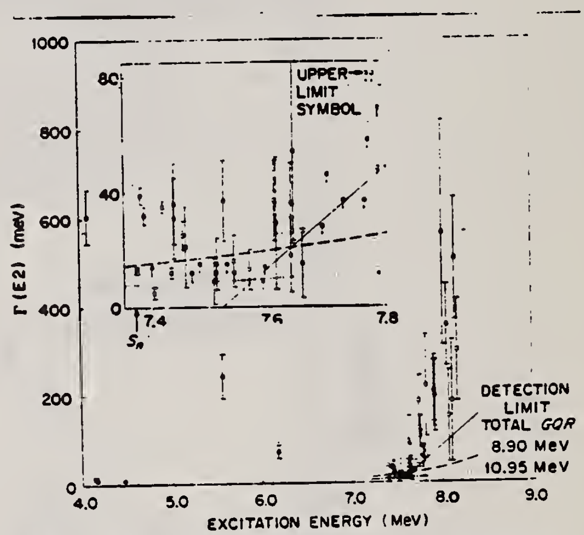

FIG. 4. Summary of $E2$ widths for individual states in ^{208}Pb. The expected widths from the tails of the giant quadrupole resonances at 10.95 and 8.90 MeV were calculated with an experimentally determined average level spacing of 5 keV for 2⁺ neutron resonances. The integrated strengths discussed in the text are more meaningful because the actual widths should exhibit fluctuations.

TABLE I. Total and ground-state radiation widths of 2^+ resonances in ^{208}Pb.

E_n[a] (keV)	Γ_γ[b] (meV)		Γ_{γ_0}[b] (meV)		E_n[a] (keV)	Γ_γ[b] (meV)		Γ_{γ_0}[b] (meV)	
3.07	145	*2*	13	*2*	(269.25)	86	*9*	18	*13*
10.19	127	*4*	39	*3*	264.75	111	*9*	36	*14*
16.17	232	*12*	32	*3*	(273.50)	128	*11*	54	*31*
(29.40)	181	*7*	<14		(288.85)	83	*13*	15	*12*
32.97	42	*2*	5	*2*	323.32	<40		<28	
45.40	93	*3*	35	*2*	(332.43)	219	*22*	<50	
62.81	118	*4*	12	*2*	359.78	<64		<40	
67.80	106	*12*	31	*14*	368.50	440	*50*	180	*60*
68.34	104	*12*	36	*14*	378.50	1240	*50*	100	*50*
83.03	186	*3*	25	*5*	382.40	601	*28*	120	*40*
87.76	65	*5*	21	*14*	395.80	296	*33*	<40	
98.41	46	*4*	<12		401.60	320	*60*	<80	
(112.10)	219	*5*	<15		402.40	<100		<60	
127.66	<240[c]		<120[c]		(411.60)	290	*40*	<80	
(136.49)	185	*5*	9	*8*	(419.50)	242	*25*	50	*40*
139.69	<20		<12		420.60	<120		<70	
(140.93)	113	*5*	15	*9*	446.30	<100		<60	
153.80	117	*9*	37	*14*	452.00	1090	*50*	220	*100*
(158.89)	102	*8*	<15		536.60	1380	*70*	210	*70*
(170.55)	31	*5*	16	*9*	539.00	1100	*60*	210	*80*
170.97	55	*10*	<12		548.60	1180	*70*	200	*80*
181.18	<500[c]		<250[c]		643.40	2700	*400*	560	*250*
(197.02)	52	*5*	13	*7*	686.50	1590	*180*	360	*90*
220.23	<16		<9		707.40	3900	*400*	150	*100*
(223.89)	82	*8*	<14		744.80	460	*110*	180	*140*
240.77	83	*9*	37	*14*	780.40	2650	*310*	510	*140*
(243.85)	290	*50*	29	*23*	803.00	940	*180*	300	*120*
249.49	253	*31*	90	*60*					

[a]Resonance energies, based on absolute neutron time of flight, are accurate to ± 0.1%. A parenthesis around an E_n value implies that the 2^+ assignment for this resonance is most probable but not certain beyond reasonable doubt. The 2^+ assignments for those resonances with quoted upper limits for the widths come from transmission and scattering measurements (Ref. 5).

[b]Total radiation width (Γ_γ) and ground-state radiation width (Γ_{γ_0}). In our notation, 145 *2* ≡ 145 ± 2, etc. The ground-state widths have been corrected for angular distribution effects.

[c]Masked by nearby strong $J = 1$ resonances. Values not shown in Fig. 4, and not included in the Porter-Thomas distribution analysis.

REF.		ELEM. SYM.	A	Z
	R. Van de Vyver, J. Devos, H. Ferdinande, R. Carchon and E. Van Camp Z. Physik A284, 91 (1978)	Pb	208	82
METHOD		REF. NO.		
		78 Va 1		egf

REACTION	RESULT	EXCITATION ENERGY	SOURCE		DETECTOR		ANGLE
			TYPE	RANGE	TYPE	RANGE	
G,N	ABX	8- 13	C	8- 13	BF3-I		4PI

The total photoneutron cross section of ^{208}Pb was measured between 8 and 13 MeV using the bremsstrahlung photon facility from a 35 MeV linac. Considerable resonance structure was observed in the cross section, of which the peak around 9 MeV, as well as the structure around 10.8 MeV may be due to $E2$ excitations.

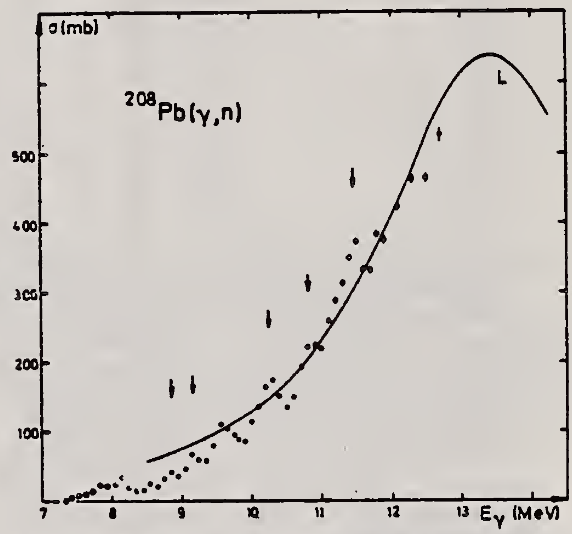

Fig. 1. The ^{208}Pb photoneutron cross section as a function of photon energy; the structure marked with an arrow is discussed in the text. The curve labeled L is determined by the Lorentz-fit parameters, as taken from the Saclay-experiment [5]

[5] Veyssiere, A., Beil, H., Bergere, R., Carlos, P., Lepretre, A.: Nucl. Phys. A159, 561 (1970)

REF.	K. Sh. Egiyan Yad. Fiz. 30, 890 (1979) Sov. J. Nucl. Phys. 30, 461 (1979)	ELEM. SYM.	A	Z
		Pb	208	82
METHOD		REF. NO.		
		79 Eg ?		hg

REACTION	RESULT	EXCITATION ENERGY	SOURCE TYPE	SOURCE RANGE	DETECTOR TYPE	DETECTOR RANGE	ANGLE
G,XP	RLY	8-250	C	130,250	MAG-D		DST

Experimental data are presented on the inclusive photoproduction of protons in the nuclei ^{12}C, ^{24}Mg, ^{63}Cu, ^{118}Sn, and ^{208}Pb irradiated by bremsstrahlung with maximum energies 0.13 and 0.25 GeV. The regions of angles 30–90° and of photoproton momenta 0.24–0.48 GeV/c were studied.

PACS numbers: 25.20. + y

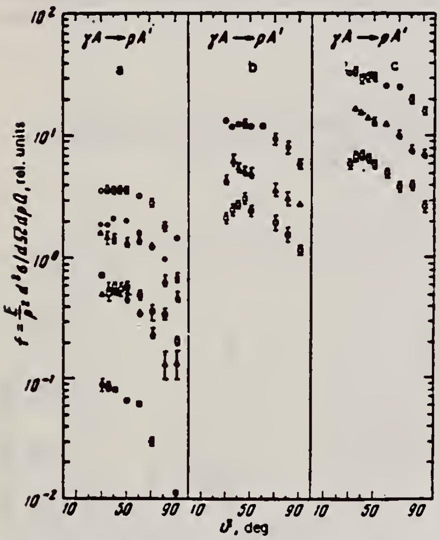

FIG. 2. Relative yields of photoprotons as a function of emission angle; experimental points: O, ●—for $p_p = 0.29$ GeV/c; △, ▲—0.34 GeV/c; □, ■—0.40 GeV/c. The hollow points are for $E_{\gamma max} = 0.25$ GeV and the solid points for $E_{\gamma max} = 0.13$ GeV: a—for ^{12}C, b—for ^{63}Cu, c—for ^{208}Pb.

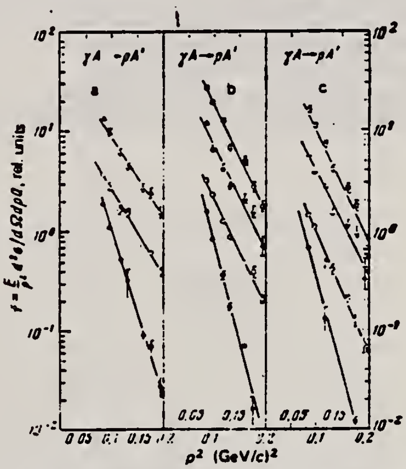

FIG. 3. Momentum spectra of protons. The experimental points are as follows: O and ●—for ^{12}C, △—for ^{63}Cu, □—for ^{208}Pb. The hollow points are for $E_{\gamma max} = 0.25$ GeV and the solid points are for $E_{\gamma max} = 0.13$ GeV; a—for $\vartheta_p = 30°$, b—for $\vartheta_p = 60°$, c—for $\vartheta_p = 90°$. The lines have been drawn through the experimental points by the method of least squares.

TABLE II. Values of the exponent n in the A^n dependence of the proton yield in reactions (2) and (3).

ϑ_p, deg	$E_\gamma = 0.25$ GeV, p_p, GeV/c: 0.29	0.34	0.40	$E_\gamma = 0.13$ GeV, p_p, GeV/c: 0.29	0.34
30	1.15±0.04	1.17±0.04	1.20±0.05	0.59±0.08	0.62±0.06
60	–	1.17±0.02	1.22±0.03	–	–
90	1.02±0.03	1.11±0.03	1.24±0.05	–	–

(over)

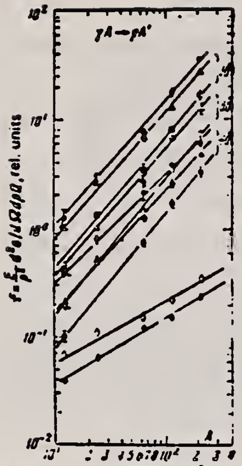

FIG. 5. A-dependence of the photoproton yield in reactions (2) and (3). Experimental points for $E_{\gamma max} = 0.25$ GeV: circles—$p_p = 0.29$ GeV/c; triangles—$p_p = 0.34$ GeV/c, squares—$p_p = 0.40$ GeV/c; half-open symbols—for $\vartheta_p = 30°$, open symbols—$\vartheta_p = 60°$, solid symbols—$\vartheta_p = 90°$, for $E_{\gamma max} = 0.13$ GeV: ◇—$p_p = 0.29$ GeV/c, $\vartheta_p = 30°$; ♦—$p_p = 0.34$ GeV/c, $\vartheta_p = 30°$. The lines have been drawn through the experimental points by the method of least squares.

REF. R.J. Holt, H.E. Jackson, R.M. Laszewski, J.R. Specht
Phys. Rev. C20, 93 (1979)

Card 1 of 2

ELEM. SYM.	A	Z
Pb	208	82

METHOD

REF. NO.	
79 Ho 1	ng

REACTION	RESULT	EXCITATION ENERGY	SOURCE TYPE	SOURCE RANGE	DETECTOR TYPE	DETECTOR RANGE	ANGLE
$ G,N	ABX	7-11	C	8-11	TOF-D		DST

The photoneutron cross section of ^{208}Pb was observed using a very high resolution time-of-flight spectrometer. The cross sections were observed in the photoneutron energy range 16 to 1000 keV and at reaction angles of 90° and 135°. The deduced ground-state radiative widths were calibrated to the well-known $^{2}H(\gamma,n)^{1}H$ reaction cross section. The 7.99-MeV resonance, previously believed to be an $M1$ excitation, is shown to be an $E1$ resonance. Current progress in the search for the collective $M1$ resonance in ^{208}Pb is reviewed. In addition, recent theoretical predictions of the properties of the giant $M1$ resonance are reviewed. Finally, the present high resolution observations in conjunction with previous photoneutron polarization measurements were employed in order to deduce the s-d-wave admixtures for eight $E1$ excitations.

POL, NONPOL N, LFT, J-PI

[NUCLEAR REACTIONS $^{208}Pb(\gamma,n)^{207}Pb$, $E_{exc}=7.4-8.4$ MeV, observed $\sigma(\theta)$, $\theta=90°$, 135°; deduced $\Gamma_{\gamma0}$, J^{π}.]

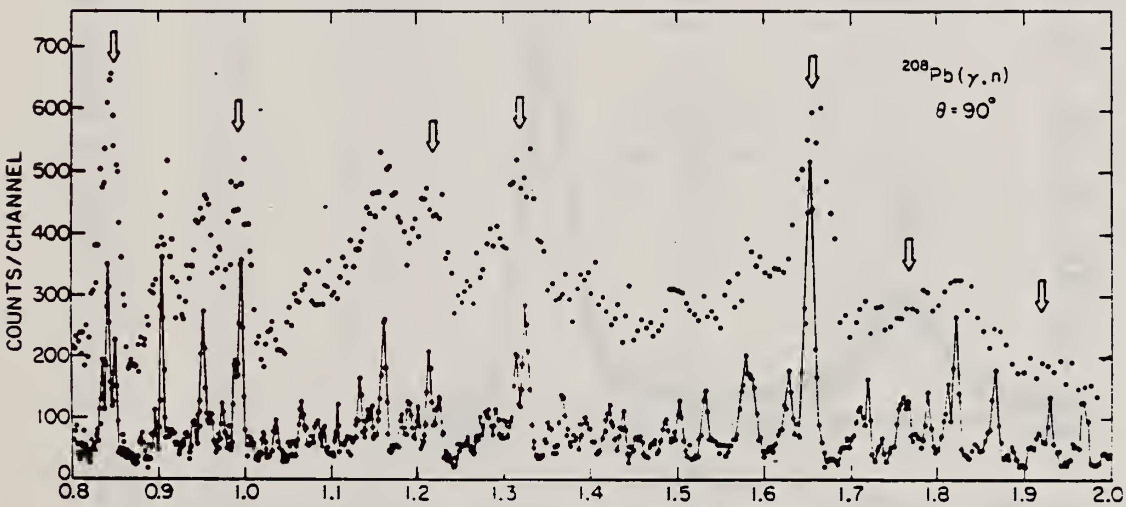

FIG. 10. The high-resolution photoneutron spectrum above 8 MeV. The arrows indicate those regions where significant nonzero (γ,n) polarizations were observed. The uppermost points represent the spectra for the polarization measurement and are compared with the high-resolution spectrum.

TABLE I. R-matrix parameters for the analysis of the 600-keV region in the $^{208}Pb(\gamma,n_0)^{207}Pb$ reaction.

E_γ (MeV)	$m\mathcal{L}$	$\Gamma_{\gamma0}$ (eV)	l_1	Γ_{n1} (keV)	l_2	Γ_{n2} (keV)
7.9731	$E1$	5.5	0	0.20	2	[illegible]
7.9828	$E1$	8.9	0	0.04	2	[illegible]
7.9838	$E2$	0.4	1	0.14	3	0.03

(over)

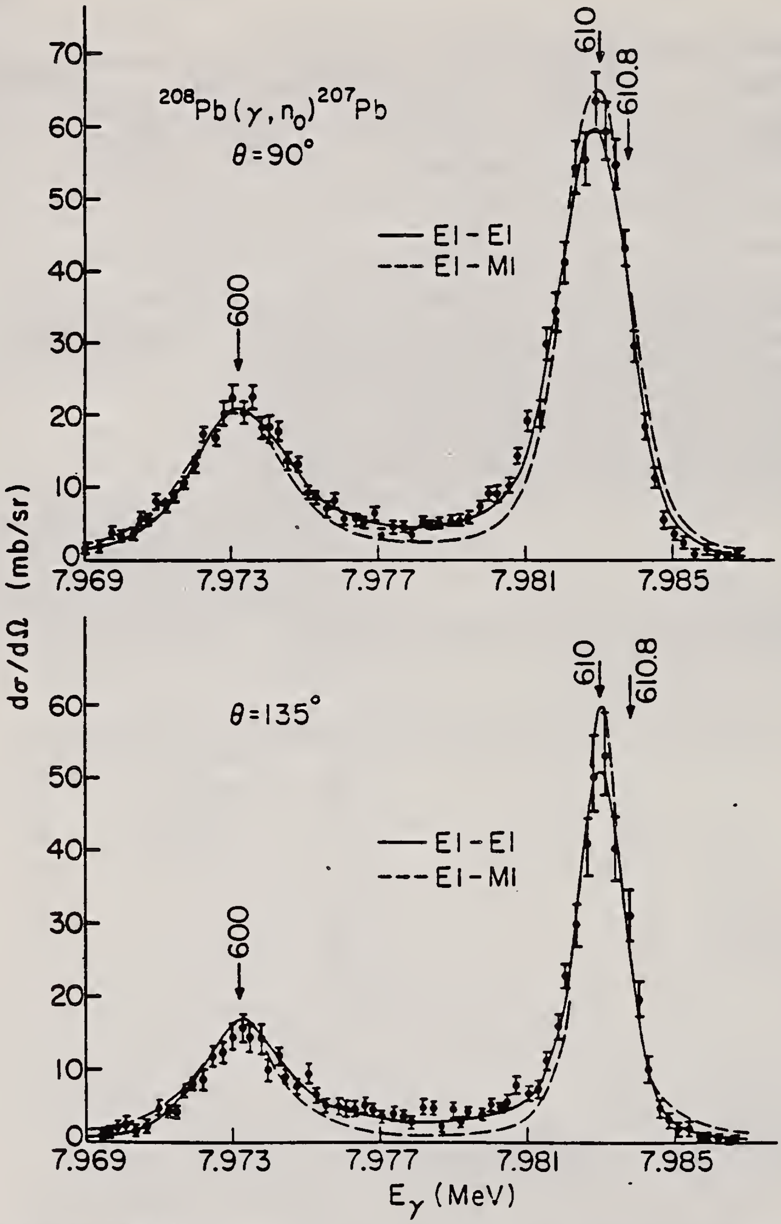

FIG. 3. Cross sections for the $^{208}Pb(\gamma,n_0)^{207}Pb$ reaction at 90° and 135° and in the vicinity of the 600- and 610-keV resonances. The solid curve represents the multilevel analysis when the two resonances are $E1$ excitations, while the dashed curve is the result when the 610-keV resonance is assumed to be an $M1$ excitation.

REF. R.J. Holt, H.E. Jackson, R.M. Laszewski, J.R. Specht
Phys. Rev. C20, 93 (1979)

ELEM. SYM.	A	Z
Pb	208	82

METHOD

REF. NO.	
79 Ho 1	hg

REACTION	RESULT	EXCITATION ENERGY	SOURCE		DETECTOR		ANGLE
			TYPE	RANGE	TYPE	RANGE	

TABLE II. Results of the present high-resolution photoneutron experiment.

E_n (keV)	E_γ (MeV)	R $\sigma(90°)/\sigma(135°)$	J^π	$g_\gamma \Gamma_{\gamma 0} \Gamma_n / \Gamma$ (eV)	$\Gamma_{\gamma 0}$ (eV)
992	8.367	1.3 ±0.12	1^{-a}	5.15	3.7
985	8.360	1.4 ±0.18	$1,2^-$	2.86	1.91, 1.15
971	8.346	1.3 ±0.2	$1,2^-$	1.43	1.0, 0.6
966	8.341	0.67 ±0.13	$1,2^-$	0.40	0.27, 0.16
947	8.322	1.53 ±0.13	1^{-a}	4.44	3.0
938	8.313	1.06 ±0.13	$1,2^-$	1.35	0.9, 0.5
921	8.295	1.48 ±0.24	$1,2^-$	0.41	0.3, 0.2
902	8.276	1.64 ±0.15	1^{-a}	2.88	1.9
891	8.265	0.75 ±0.13	$1,2^-$	0.41	0.27, 0.16
879	8.253	1.25 ±0.29	$1,2^-$	0.37	0.25, 0.15
849	8.223	1.20 ±0.12	$1,2^-$	2.61	1.7, 1.0
840	8.214	1.67 ±0.16	1^{-a}	6.17	4.1
834	8.208	1.03 ±0.11	$1,2^-$	1.69	1.1, 0.7
830	8.204	0.63 ±0.09	$1,2^-$	0.55	0.37, 0.22
813	8.187	1.18 ±0.19	$1,2^-$	0.69	0.46, 0.28
773	8.147	1.17 ±0.21	2^{+c}	0.38	0.25
731	8.105	1.29 ±0.13	1^{-a}	3.04	2.0
721	8.094	1.40 ±0.19	$1,2^-$	0.85	0.57, 0.34
694	8.067	1.44 ±0.12	$1,2^-$	3.92	3.1, 1.9
647	8.020	1.20 ±0.06	1^{-a}	10.37	6.9
638	8.011	1.16 ±0.21	2^{-a}	0.20	0.13
630	8.003	1.51 ±0.18	$1,2^-$	0.40	0.27, 0.16
610	7.983	1.57 ±0.08	1^-	13.39	8.9
600	7.973	1.46 ±0.09	1^{-a}	7.43	5.5
594	7.967	0.72 ±0.09	$1,2^-$	0.37	0.25, 0.15
548	7.921	0.73 ±0.04	$1,2^-$	3.69	2.5, 1.5
543	7.916	0.87 ±0.08	2^{-c}	0.94	0.38
537	7.910	1.23 ±0.06	1^{-a}	9.17	6.1
499	7.871	1.14 ±0.13	$1,2^-$	0.81	0.54, 0.32
488	7.860	1.03 ±0.09	$1,2$	1.91	1.3, 0.8
481	7.853	0.91 ±0.08	$1,2^-$	1.81	1.2, 0.7
449	7.821	1.2 ±0.2	$1,2^-$	4.0	2.6, 1.6
425	7.797	1.3 ±0.15	$1,2^-$	1.3	0.87, 0.52
419	7.791	1.9 ±0.2	1^{-}	0.8	0.53
332	7.704	1.2 ±0.15	1^{-a}	0.75	0.50
313.7	7.685	1.15 ±0.05	1^{-a}	9.6	6.4
295	7.666	0.99 ±0.1	1^{-a}	0.57	0.40
281.0	7.652	1.8 ±0.2	$1,2^-$	0.43	0.29, 0.17
253.6	7.625	0.98 ±0.10	1^{-a}	19.6	13.1
246	7.617	0.67 ±0.07	$1,2^-$	1.64	1.1, 0.66
179	7.550	1.51 ±0.15	1^{-a}	10.9	7.3
154.8	7.526	1.72 ±0.17	1^{-b}	0.69	0.46
129.6	7.500	1.03 ±0.10	1^{-a}	1.14	0.76
125.8	7.485	1.78 ±0.18	1^{-a}	2.1	1.4
114.1	7.494	1.49 ±0.15	1^-	1.7	1.1
101.3	7.472	1.61 ±0.16	$1,2^-$	0.23	0.15, 0.09
89.6	7.460	1.97 ±0.20	1^{-a}	2.0	1.3
47.7	7.418	0.53 ±0.05	2^{-a}	0.06	0.02
40.7	7.411	0.92 ±0.09	1^{-a}	5.2	3.5
37.2	7.407	0.67 ±0.07	1^{-a}	0.96	0.64
30.1	7.400	1.5 ±0.15	$1,2^-$	0.3	0.2, 0.12
16.6	7.307	1.3 ±0.15	1^{-a}	0.02	0.01

[a] Assignments are based on photoneutron polarization observations, Refs. 6 and 7.
[b] Assignments are taken from Refs. 9, 10, and 35.
[c] Assignments are from Ref. 36.

(over)

TABLE III. Comparison of photoneutron experiments with the present work. The values in parentheses have been renormalized to the strength of the 40.7-keV resonance determined from the present work.

E_n (keV)	Argonne R	Argonne $\Gamma_{\gamma 0}$ (eV)		Livermore R	Livermore $\Gamma_{\gamma 0}$ (eV)	Toronto R	Toronto $\Gamma_{\gamma 0}$ (eV)
30.1	1.5 ± 0.15	0.2		1.41 ± 0.2	0.2	1.10 ± 0.17	0.4
37.2	0.67 ± 0.07	0.64		0.64 ± 0.09	0.56 [a]	0.74 ± 0.14	1.0
40.7	0.92 ± 0.09	3.5		1 [b]	4.2 [c] (3.3)	0.88 ± 0.07	4.2 [c] (3.5)
89.6	1.97 ± 0.20	1.3				1.25 ± 0.09	0.9
114.1	1.49 ± 0.15	1.1		1.54 ± 0.22	1.4	1.23 ± 0.14	0.9
179	1.51 ± 0.15	7.3		1.53 ± 0.22	11.0	1.37 ± 0.05	11.8
246	0.67 ± 0.07	0.66	13.8	1.10 ± 0.15	15.3	1 [b]	17.7
253.6	0.98 ± 0.10	13.1					
295	0.99 ± 0.10	0.4				1.09 ± 0.16	1.7
313.7	1.15 ± 0.05	6.4		1.12 ± 0.16	6.7	1.10 ± 0.07	7.0
600	1.46 ± 0.09	5.5	14.4	1.81 ± 0.25	12.8	1.60 ± 0.17	21.2
610	1.57 ± 0.08	8.9					
647	1.20 ± 0.06	6.9		1.26 ± 0.18	5.5	1.24 ± 0.22	6.7
834	1.03 ± 0.11	1.1					
840	1.67 ± 0.16	4.1	6.9	1.49 ± 0.21	6.8	1.53 ± 0.37	7.3
849	1.20 ± 0.12	1.7					
	Total	62.84			64.46(53.7)		80.8(67.3)

[a] This value was obtained by assuming that this resonance is a dipole excitation.
[b] The angular distributions were normalized to unity for these resonances in Refs. 1 and 5.
[c] The values of $\Gamma_{\gamma 0}$ were normalized to the strength of the 40.7-keV resonance in Refs. 1 and 5.

TABLE IV. Comparison of present ground-state radiation widths with those of the fast-neutron capture method.

E_n (keV)	E_γ (MeV)	J^π	Argonne $\Gamma_{\gamma 0}$ (eV)	Oak Ridge $\Gamma_{\gamma 0}$ (eV)
16.6	7.397	1^+	0.01	0.07
30.1	7.410	$1,2^+$	0.2	0.64
37.2	7.417	1^+	0.64	0.76
40.7	7.421	1^-	3.5	5.07
47.7	7.418	2^+	0.02	0.035
89.6	7.470	1^+	1.3	2.01
101.3	7.481	$1,2^+$	0.15	0.32
114.1	7.494	1^+	1.1	1.55
125.8	7.496	1^+	1.4	2.59
129.6	7.510	1^+	0.76	0.95
154.8	7.535	1^+	0.46	0.66
179	7.559	1^-	7.3	15.8
253.6	7.625	1^-	13.1	21.1
295	7.666	1^+	0.40	0.71
313.7	7.685	1^-	6.4	10.1
332	7.704	1^+	0.50	1.19
419	7.791	1^+	0.53	0.58
488	7.860	$1,2^+$	1.3	1.6
537	7.910	1^-	6.1	7.2
543	7.916	2^+	0.38	0.2
600	7.973	1^-	5.5	9.9
610	7.983	1^-	8.9	14.0
638	8.011	2^+	0.13	0.56
647	8.020	1^-	6.9	9.3
694	8.067	$1,2^+$	3.1	3.2
721	8.094	$1,2^+$	0.57	1.1
731	8.105	1^-	2.0	3.1
773	8.147	2^+	0.25	0.51
840	8.214	1^-	4.1	7.0
902	8.276	1^-	1.9	4.4
947	8.322	1^-	3.0	5.4
992	8.367	1^-	3.7	5.6
		$\sum \Gamma_{\gamma 0}$	85.6	137.2

REF.	R.M. Laszewski and P. Axel Phys. Rev. C 19, 342 (1979)	ELEM. SYM.	A	Z
		Pb	208	82

METHOD	REF. NO.	
	79 La 1	hg

REACTION	RESULT	EXCITATION ENERGY	SOURCE TYPE	SOURCE RANGE	DETECTOR TYPE	DETECTOR RANGE	ANGLE
G,G	ABX	4- 8	D	4-8	NAI-D		135
		(4.5-7.4)		4.5-7.5			

Average elastic photon scattering cross sections were measured for ^{209}Bi, ^{208}Pb, ^{207}Pb, ^{206}Pb, Tl and Hg at excitation energies between 4.5 MeV and the neutron emission threshold, with an energy resolution in the range between 50 and 150 keV. This resolution was sufficient to determine the strengths of most of the strong levels in this energy region for ^{208}Pb; there are concentrations of strength in a few levels near 5.5 and 7 MeV with the sum of $B(E1)\uparrow$ values equal to about 0.84 and 0.65 e^2 fm^2, respectively; each of these two groups of levels corresponds to only about 0.63% of the electric dipole sum rule. In the neighboring isotopes, approximately the same amount of strength is distributed among many more energy levels; although this strength is spread in energy more than it is in ^{208}Pb, it remains relatively localized.

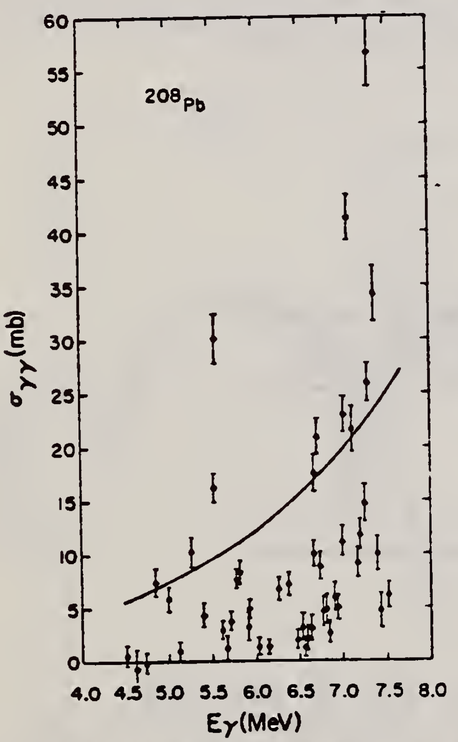

FIG. 3. ^{208}Pb (enriched to 73% 208 isotope): experimental average elastic photon scattering cross sections. The solid curve is a low energy extrapolation of the giant dipole resonance Lorentzian. Note that because the large peaks are dominated by very strong levels, the average "cross section" is governed by the tagged photon resolution; nuclear absorption effects distort the relative intensities.

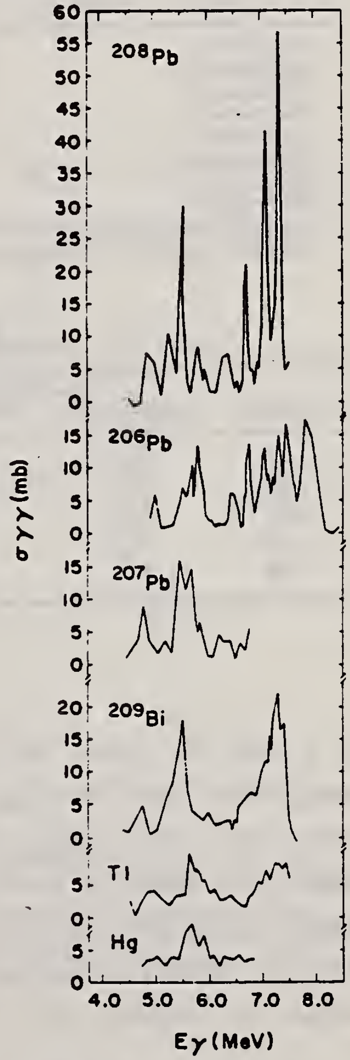

FIG. 12. Comparison of the measured cross sections of, respectively, from the top, ^{208}Pb, ^{206}Pb, ^{207}Pb, ^{209}Bi, Tl, and Hg.

over

TABLE III. Nuclear levels in ^{208}Pb (assuming $g\Gamma_0/\Gamma = 3$).

E_γ (MeV)[a]	Γ_0 (eV)	$B(E1)\uparrow$ (e^2 fm^2)
7.332	44.5 ± 2.9	0.322 ± 0.021
7.083 } 7.063 }	25.9 ± 2.1	0.209 ± 0.017
6.721	13.0 ± 1.6	0.122 ± 0.015
5.513	21.4 ± 2.2	0.366 ± 0.038
5.293	7.0 ± 1.4	0.135 ± 0.027
4.842	6.9 ± 1.4	0.174 ± 0.035

[a]References 14, 19–21.

TABLE V. Comparison of measured level widths.

Energy (MeV)	Γ_0[a] (eV)	Γ_0[b] (eV)	Γ_0[c] (eV)	Γ_0[d] (eV)	I_0 (eV)
4.842	6.9 ± 1.4	6.3	5.7		5.1[e]
5.293	7.0 ± 1.4	8.6	6.8		
5.513	21.4 ± 2.2	28	18		
5.85	4.4 ± 1.1[i]		5.6[j]		
6.262	8.9 ± 1.1[i]	4.1			
6.721	13.0 ± 1.6	15	13	14 ± 7	
7.063 }		29	24 }		31[e], 18 ± 3[f]
	25.9 ± 2.1			30 ± 13	
7.083 }		14	15 }		17[g], 16[h]
7.332	44.5 ± 2.9[i]	38	42	41 ± 10	

[a]This work.
[b]Reference 14.
[c]Reference 19.
[d]Reference 3.
[e]Reference 10.
[f]Reference 21.
[g]Reference 11.
[h]Reference 20.
[i]Possibly contains the strength of neighboring weaker levels.
[j]Reported in Ref. 19 for a level at 5.919 MeV.

TABLE VI. Transition strength comparison at 5.5 and 7 MeV.

Nucleus	5.0–6.0 MeV $\int\sigma_{\gamma\gamma}dE$ (MeV mb)	5.0–6.0 MeV %^{208}Pb strength	6.5–7.5 MeV $\int\sigma_{\gamma\gamma}dE$ (MeV mb)	6.5–7.5 MeV %^{208}Pb strength
Bi	10.4	68%	10.7	44%
^{208}Pb	15.2	100%	24.4	100%
^{207}Pb	12.6	83%	...	...
^{206}Pb	15.8	104%	20.2	83%
Tl	8.3	55%	7.8	32%
Hg	11.6	76%	...	...

[3]P. Axel, K. Min, N. Stein, and D.C. Sutton, Phys. Rev. Lett. 10, 299 (1963).
[10]C.P. Swann, Phys. Rev. Lett. 32, 1449 (1974).
[11]C.P. Swann, Nucl. Phys. A201, 534 (1973).
[14]D.F. Coope, L.E. Cannell, and M.K. Brussel, Phys. Rev. C 15, 1877 (1977).
[19]J.W. Knowles, A.M. Khan, and W.F. Mills (to be published).
[20]W. Scholz, H. Bakhra, R. Colle, and A. Li-Scholz, Phys. Rev. C 9, 1568 (1974).
[21]R.J. Sparks, H. Lancman, and C. VanDer Leun, Nucl. Phys. A259, 13 (1976).

REF. J. Lichtenstadt, J. Heisenberg, C.N. Papanicolas, C.P. Sargent, A.N. Courtemanche, J.S. McCarthy
Phys. Rev. C20, 497 (1979)

ELEM. SYM.	A	Z
Pb	208	82

METHOD

REF. NO. 79 Li 2 egf

REACTION	RESULT	EXCITATION ENERGY	SOURCE TYPE	SOURCE RANGE	DETECTOR TYPE	DETECTOR RANGE	ANGLE
E,E/	ABX	6-7	D	50-335	MAG-D		DST

6.43, 6.74, 7.06 MEV

Inelastic electron scattering cross sections for the excited states at 6.43, 6.74, and 7.06 MeV in ^{208}Pb were measured with high resolution. The measurements were done in forward and backward directions covering the momentum transfer range of $0.3 < q < 2.5$ fm^{-1}. The state at 7.06 MeV was identified as the $\pi(i_{13/2}h_{11/2}^{-1})_{12-}$ and the states at 6.74 and 6.43 MeV as the $\nu(j_{15/2}i_{13/2}^{-1})_{14-,12-}$, respectively. The identification was based on four criteria: (a) the agreement between the q dependence of the measured form factor with that of Hartree-Fock single particle-hole prediction, with no adjustment of radial parameters, (b) the absence of a longitudinal form factor, (c) the relative magnitude of the observed levels, and (d) the excitation energies being close to the single p-h energies. The measured strength of each state was found to be 50% of the single p-h prediction.

[NUCLEAR REACTIONS ^{208}Pb(e, e') $E = 50-335$ MeV; measured $\sigma(E)$, $\theta = 90°$, 160°. ^{208}Pb deduced, levels $J^\pi = 12^-$, 14^-. DWBA calculation with Hartree-Fock single particle wave functions.]

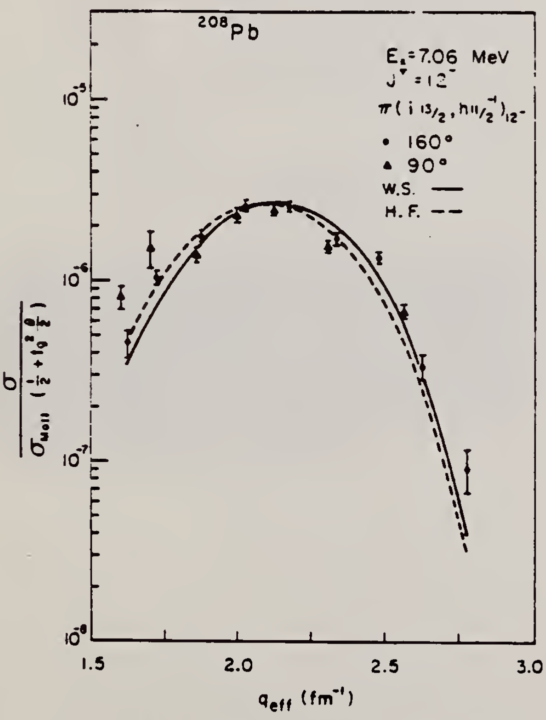

FIG. 3. Cross section of the level at 7.06 MeV with $J^\pi = 12^-$. The dashed and solid lines are single p-h predictions of the $\pi(i_{13/2}h_{11/2}^{-1})_{12^-}$ transition, using Hartree-Fock and Woods-Saxon wave functions, respectively. The curves presented are the "reduced cross sections" calculated in DWBA at 160°. The calculation at 90° is almost identical to that at 160°, to the accuracy of the graph.

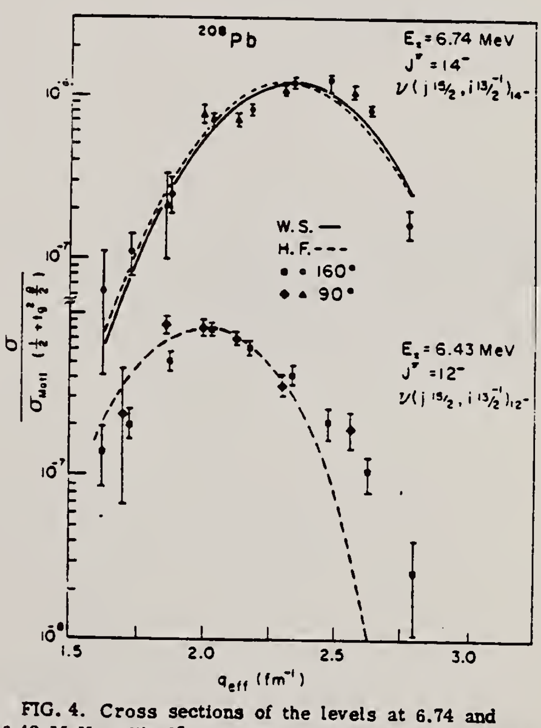

FIG. 4. Cross sections of the levels at 6.74 and 6.43 MeV, with $J^\pi = 14^-$, 12^-, respectively. The dashed and solid lines are single p-h predictions of the $\nu(j_{15/2}i_{13/2}^{-1})_{14^-,12^-}$ transitions, using Hartree-Fock and Woods-Saxon wave functions, respectively. For calculational details see text.

(over)

TABLE II. Experimental cross sections measured for the excited states at 6.43, 6.74, and 7.06 MeV. Errors are the statistical errors only. The number following *E* is the power of 10 which multiplies the preceding number ($En \equiv 10^n$).

E (MeV)	%	6.43 MeV (mb/sr)	%	6.74 MeV (mb/sr)	%	7.06 MeV (mb/sr)	%
			90°				
201.53	0.22					2.15*E*-6	15.5
213.85	0.21	5.44*E*-7	97			3.59*E*-6	22
236.85	0.15	1.60*E*-6	13.5	4.06*E*-7	54	2.58*E*-6	11
255.96	0.13	1.39*E*-6	12.5	1.26*E*-6	13.5	3.72*E*-6	7.1
273.97	0.18	9.64*E*-7	7.3	1.01*E*-6	7.6	3.46*E*-6	3.4
298.59	0.17	4.36*E*-7	14	1.30*E*-6	5.6	1.93*E*-6	5.9
335.40	0.22	2.03*E*-7	30	1.04*E*-6	12	6.96*E*-7	12
			160°				
140.69	0.11	2.56*E*-7	40	1.16*E*-7	74	8.23*E*-7	20
149.97	0.22	3.30*E*-7	21	1.84*E*-7	28	1.70*E*-6	8.9
165.29	0.12	6.61*E*-7	12	3.35*E*-7	23	2.36*E*-6	5.8
180.70	0.25	8.71*E*-7	8.2	7.90*E*-7	9.0	2.89*E*-6	4.3
195.27	0.26	5.74*E*-7	9.4	7.85*E*-7	7.6	2.43*E*-6	4.0
210.99	0.10	3.39*E*-7	13.5	9.91*E*-7	6.9	1.37*E*-6	6.0
225.12	0.17	1.53*E*-7	22	9.20*E*-7	6.8	9.64*E*-7	6.6
240.07	0.22	6.70*E*-8	24	5.33*E*-7	7.5	2.17*E*-7	14.5
255.12	0.22	1.42*E*-8	59	9.34*E*-8	19	5.09*E*-8	27

REF. A. M. Nathan, R. Starr, R. M. Laszewki,.P. Axel
Phys. Rev. Lett. 42, 221 (1979)

ELEM. SYM.	A	Z
Pb	208	82

METHOD

REF. NO.	
79Na1	hg

REACTION	RESULT	EXCITATION ENERGY	SOURCE		DETECTOR		ANGLE
			TYPE	RANGE	TYPE	RANGE	
$ G,G	JPI	5-8	C	14	NAI-D		DST
		(5.51-7.33)					

POL PHOTONS, IN,OUT

The parities of four bound $J=1$ levels in ^{208}Pb that are strongly excited by γ rays were determined by observing the elastic scattering of plane-polarized photons. The levels at 5.51, 7.06, 7.08, and 7.33 MeV are excited by electric dipole radiation, and therefore have negative parity. The 1^- assignment for the 7.06-MeV level is of particular significance because this level had previously been thought to contain about 36% of the $M1$ strength in ^{208}Pb.

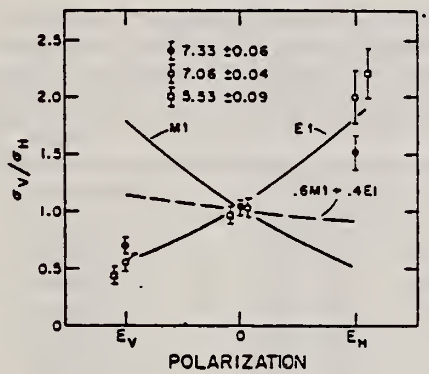

FIG. 2. A summary of the vertical-to-horizontal ratios for vertical polarization (E_V), horizontal polarization (E_H), and no polarization (0). The solid lines represent the expected results for an energy-independent partial polarization $P=0.28$. The dashed line indicates the expected result for unresolved strengths that are 60% $M1$ and 40% $E1$. The results show that all of the strong levels must be excited by $E1$.

REF.		ELEM. SYM.	A	Z
C. Woodward, G.A. Petersor Phys. Rev. C20, 2437 (1979)		Pb	208	82
METHOD		REF. NO. 79 Wo 4		hq

REACTION	RESULT	EXCITATION ENERGY	SOURCE TYPE	SOURCE RANGE	DETECTOR TYPE	DETECTOR RANGE	ANGLE
E,E/	SPC	19-26	D	60	MAG-D		180

SEARCH FOR M1 EXCIT.

A search for $2\hbar\omega$ $M1$ excitations in ^{208}Pb has been made under conditions of maximum sensitivity by means of 180° scattering of 60 MeV electrons. The results do not show the strength predicted by Speth *et al.*

[NUCLEAR REACTIONS $^{208}Pb(e,e')$, $E=60$ MeV, $\theta=180°$, measured $\sigma(E,180°)$.]

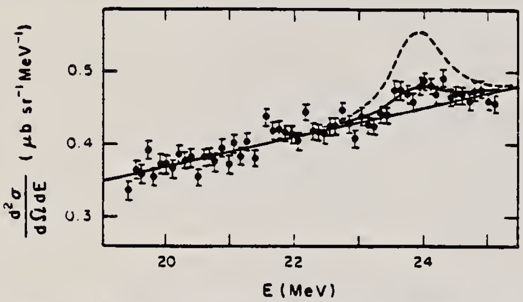

FIG. 1. Spectrum of electrons of incident energy 60 MeV scattered through 180° from ^{208}Pb in the excitation interval from 19 to 26 MeV. At 24 MeV the dashed line represents a predicted peak of cross section 180 nb/sr and the solid line the best fit of a Breit-Wigner peak of the same width, showing no firm evidence of $2\hbar\omega$ $M1$ excitations in this energy range.

REF. T. Chapuran, R. Vodhanel, M.K. Brussel
Phys. Rev. C22, 1420 (1980)

ELEM. SYM.	A	Z
Pb	208	82

METHOD

REF. NO.	
80 Ch 3	hg

REACTION	RESULT	EXCITATION ENERGY	SOURCE TYPE	SOURCE RANGE	DETECTOR TYPE	DETECTOR RANGE	ANGLE
G,G	SPC	4-8	C	7-11	SCD-D		DST
				(7-10.37)			

Resonant photon scattering from ^{206,207,208}Pb and ^{209}Bi has been measured from 4 MeV to the neutron thresholds using enriched targets, Ge(Li) detectors and bremsstrahlung beams with end-point energies of 7.0, 7.5, 7.6, 8.0, 8.5, and 10.4 MeV. Energies and values of $g\Gamma_0{}^2/\Gamma$ were obtained for many levels not observed in previous photon experiments. Spins of levels in ^{206}Pb and ^{208}Pb were determined from the angular distributions, and ground-state branching ratios were obtained from self-absorption measurements for seven transitions in ^{208}Pb. The results are compared with earlier spectroscopic studies and with lower resolution average cross-section measurements. The spectra of ^{207}Pb and ^{209}Bi are discussed in terms of the excitations of the ^{208}Pb core.

[NUCLEAR REACTIONS ^{206,207,208}Pb, ^{209}Bi(γ,γ); enriched targets; resonance fluorescence with 7.0, 7.5, 7.6, 8.0, 8.5, and 10.4 MeV bremsstrahlung. Measured E_γ, I_γ at 90° and 127°, and self-absorption; deduced $g\Gamma_0^2/\Gamma$, Γ_0/Γ, J.]

TABLE III. ^{208}Pb results. The values for Γ_0^2/Γ have been extracted assuming $J=1$ where not measured (except $J=2$ for the level at 4.085 MeV). The listed uncertainties for Γ_0/Γ include statistical errors only, while those for Γ_0^2/Γ also include the uncertainty in $N_{\rm inc}(E)\epsilon(E)$.

Energy (keV)	J	Γ_0^2/Γ (eV)	Γ_0/Γ
4085.2 ± 2.0		0.68 ± 0.15	
4841.6 ± 1.0	1	5.0 ± 0.8	$0.85^{+0.13}_{-0.08}$
5292.6 ± 2.0	1	5.1 ± 0.8	$0.78^{+0.22}_{-0.14}$
5512.2 ± 1.0	1	22.3 ± 3.4	$0.98^{+0.02}_{-0.04}$
5948.0 ± 3.0		1.0 ± 0.3	
6263.4 ± 3.0		2.6 ± 0.5	
6311.7 ± 3.0		3.2 ± 0.6	
6362.8 ± 3.0		1.6 ± 0.4	
6720.1 ± 1.5	1	7.6 ± 1.5	$1.00^{+0.00}_{-0.11}$
7063.3 ± 1.5	1	15.7 ± 2.6	$0.98^{+0.02}_{-0.07}$
7082.8 ± 1.5	1	8.8 ± 1.5	1.0[a]
7243.0 ± 4.0		1.7 ± 0.6	
7277.9 ± 4.0		1.7 ± 0.6	
7332.2 ± 1.5	1	26.9 ± 4.8	$1.00^{+0.00}_{-0.12}$

[a] See text for discussion.

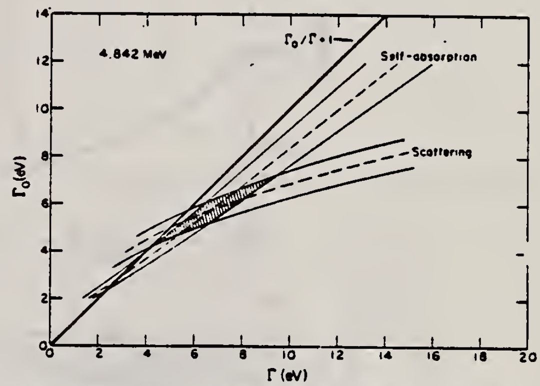

FIG. 7. Combined results of the self-absorption and scattering measurements for the 4.842 MeV level in ^{208}Pb. The dashed curves indicate combinations of Γ_0 and Γ which reproduce the experimental results; the solid curves represent the error band for each case. The shaded region contains the values of Γ_0 and Γ consistent with both experiments, and with the condition $\Gamma_0/\Gamma \leq 1$.

TABLE IV. ^{208}Pb angular distribution measurements. Listed uncertainties are statistical only.

Energy (MeV)	$W(90°)/W(127°)$	J
4.085	1.74 ± 1.10	
4.842	0.71 ± 0.07	1
5.293	0.74 ± 0.12	1
5.512	0.68 ± 0.04	1
6.720	0.71 ± 0.07	1
7.063	0.76 ± 0.05	1
7.083	0.72 ± 0.08	1
7.332	0.75 ± 0.09	1

	$W(\theta)$	$W(90°)/W(127°)$
Dipole	$1+0.500\,P_2(\cos\theta)$	0.73
Quadrupole	$1+0.357\,P_2(\cos\theta)+1.143\,P_4(\cos\theta)$	2.28[a]

[a] The experimental ratio for quadrupole scattering is reduced to 2.20 by the finite angular acceptance of the detector.

(OVER)

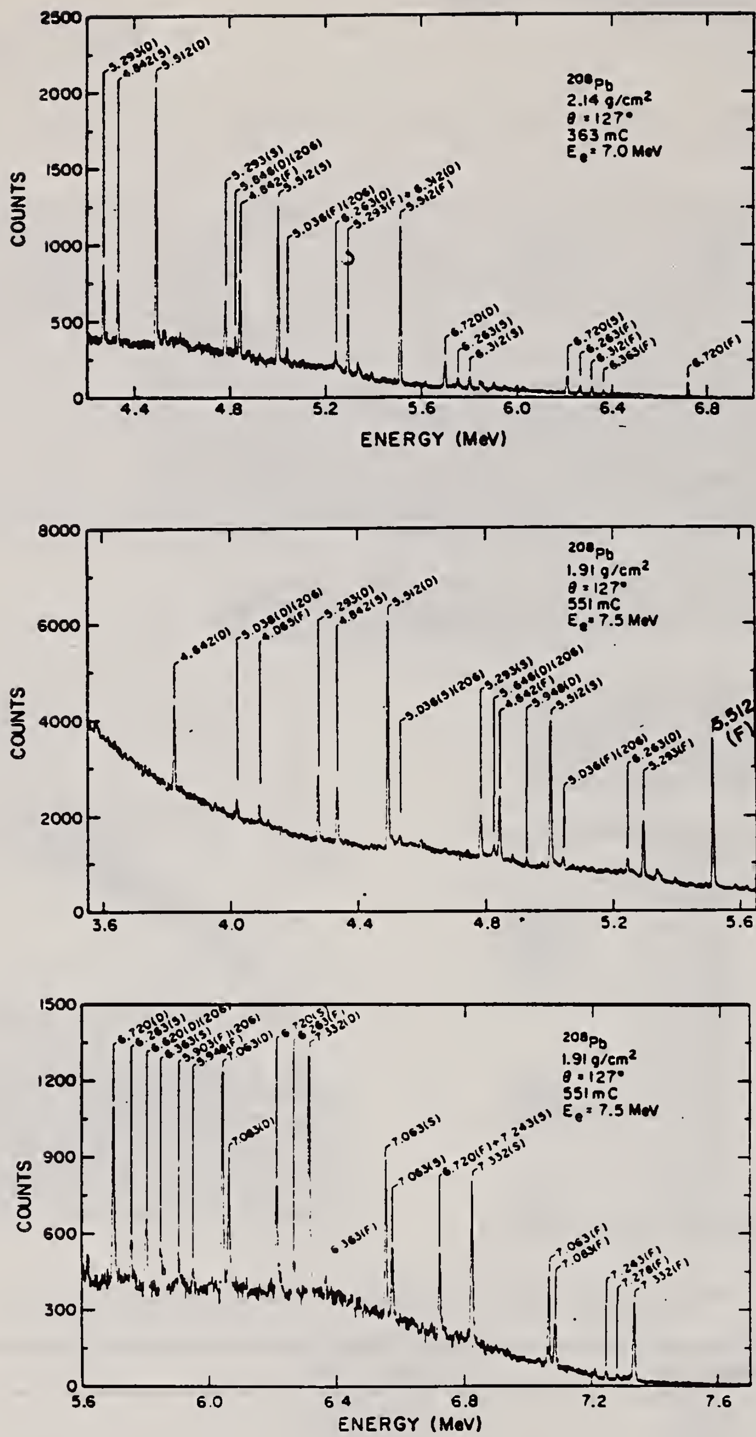

FIG. 5. Spectra for 7.0 MeV (upper figure) and 7.5 MeV (lower two figures) bremsstrahlung scattered from enriched (72.5%) ^{208}Pb targets. (*F*), (*S*), and (*D*) refer to the full energy, single-, and double-escape peaks, respectively. One channel corresponds to 1.36 keV in the 7.0 MeV spectrum, and 1.48 keV in the 7.5 MeV spectrum.

REF. D. Goutte, J.B. Bellicard, J.M. Cavedon, B. Frois, M. Huet, P. Leconte, Phan Xuan Ho, S. Platchkov, J. Heisenberg, J. Lichtenstadt, C. N. Papanicolas, I. Sick
Phys. Rev. Lett. 45, 1618 (1980)

ELEM. SYM.	A	Z
Pb	208	82

METHOD

REF. NO.	
80 Go 2	hg

REACTION	RESULT	EXCITATION ENERGY	SOURCE TYPE	SOURCE RANGE	DETECTOR TYPE	DETECTOR RANGE	ANGLE
E,E/	ABX	2	D	52-502	MAG-D		DST
		(2.615)					

Transition charge radius of 7.334±0.011 fm.
Transition probability of $6.12\times10^5 e^2.fm^6$ ±2%

BEL 2.615 MEV

The transition charge density for the octupole vibration of ^{208}Pb has been determined with an unprecedented accuracy for an inelastic transition. A comparison with some of the best theoretical calculations shows a persistent discrepancy in the interior of the nucleus which offers a measure of the limitations of the various theoretical approaches considered.

PACS numbers: 21.10.Ky, 25.30.Cg, 27.80.+w

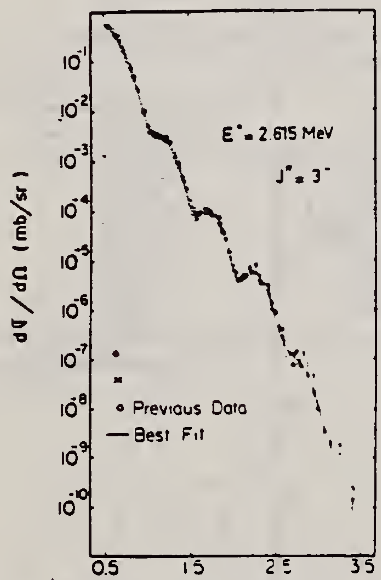

FIG. 1. Experimental cross sections recalculated to an incident energy of 502 MeV. The solid line represents the best fit obtained with the Fourier-Bessel analysis. Solid circles, new data taken at Saclay, crosses, new data taken at M.I.T.; open circles, previous data (Refs. 3–5).

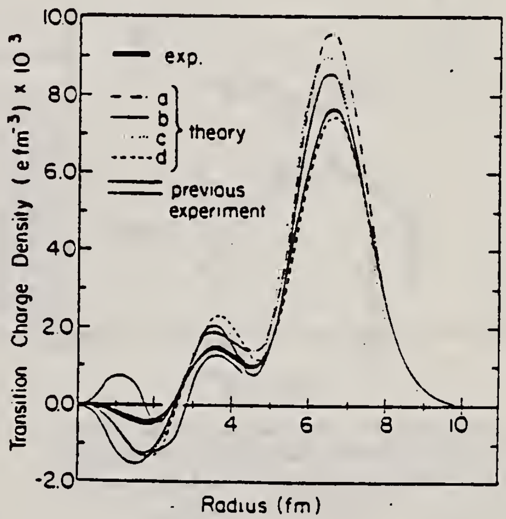

FIG. 2. Comparison of experimental transition charge density of the 3^- level at 2.615 MeV in ^{208}Pb with various theoretical predictions: curve *a*, from Ref. 15; curve *b* from Ref. 13; curve *c*, from Ref. 12; and curve *d*, with use of the Migdal interaction. The shaded area in the interior represents the experimental uncertainty from the previous analysis (Ref. 16). Note that below $r = 4.2$ fm, curves *a* and *d* are indistinguishable.

REF.	J. Lichtenstadt, C.N. Papanicolas, C.P. Sargent, J. Heisenberg, J.S. McCarthy Phys. Rev. Lett. 44, 858 (1980)	ELEM. SYM. Pb	A 208	Z 82
METHOD		REF. NO. 80 Li 1		hg

REACTION	RESULT	EXCITATION ENERGY	SOURCE TYPE	SOURCE RANGE	DETECTOR TYPE	DETECTOR RANGE	ANGLE
E,E/	ABX	4-7	D	70-335	MAG-D		DST
		(4.89-6.10)					

Natural-parity high-spin states of $J^\pi = 12^+$ (6.10 MeV) and 10^+ (4.89, 5.07, and 5.92 MeV) were observed and identified via inelastic electron scattering. Dominant single-particle-hole configurations in these excitations were deduced. The measured cross sections indicate a reduction of the transverse transition amplitude to 65% of the shell-model prediction, and the absence of an effective charge for the neutron.

4 HI-SPIN, 4.9-6.1 MEV

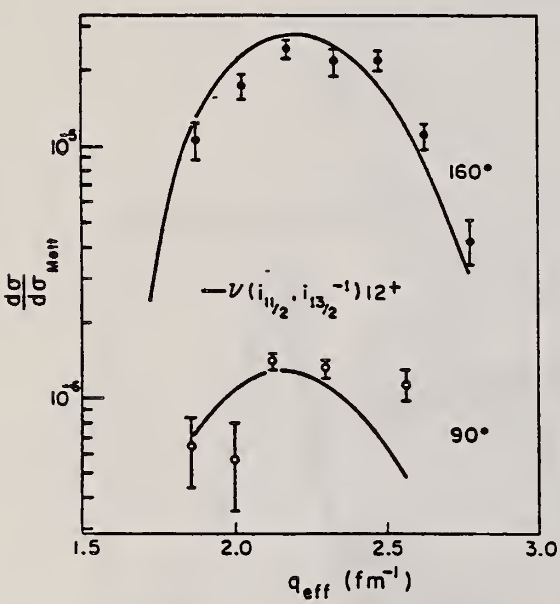

FIG. 1. Reduced (e,e') cross sections from the excited 12^+ state at 6.10 MeV, measured at 90° and 160°. Solid lines are DWBA calculation of the SPH transition $\nu(1i_{11/2}, 1i_{13/2}^{-1})_{12^+}$, scaled down by $0.65g_{free}$.

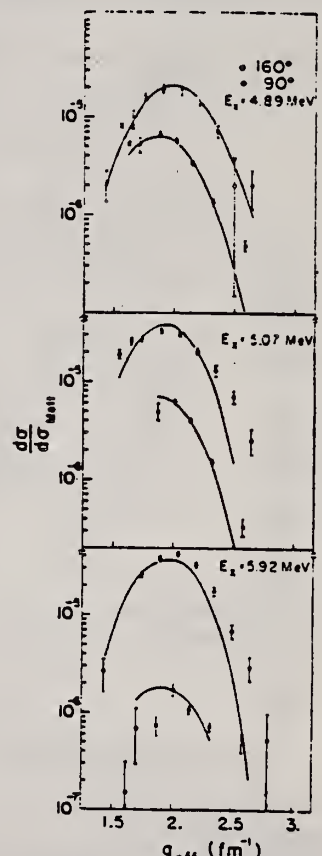

FIG. 2. Reduced (e,e') cross sections from the three 10^+ excited states. Solid lines are DWBA calculations of the following admixtures: (i) 4.89 MeV: 0.65 $\langle A\rangle$, $-0.58\langle B\rangle$, $0.30\langle C\rangle$, and $-0.17\langle D\rangle$. (ii) 5.07 MeV: 0.73 $\langle A\rangle$, $0.68\langle B\rangle$, $-0.02\langle C\rangle$, and $0.03\langle D\rangle$. (iii) 5.92 MeV: $0.12\langle A\rangle$, $-0.16\langle B\rangle$, $-0.07\langle C\rangle$, and $0.98\langle D\rangle$. Quenching factors are $0.65g_{free}$, and $0.92e(\pi)$. $\langle A\rangle \equiv \nu(2g_{9/2}, 1i_{13/2}^{-1})_{10^+}$; $\langle B\rangle \equiv \pi(1h_{9/2}, 1h_{11/2}^{-1})_{10^+}$; $\langle C\rangle \equiv \nu(1j_{15/2}, 2f_{5/2}^{-1})_{10^+}$; $\langle D\rangle \equiv \nu(1i_{11/2}, 1i_{13/2}^{-1})_{10^+}$.

REF. K. Ackermann, K. Bangert, U.E.P. Berg, G. Junghans, R.K.M. Schneider, R. Stock, K. Wienhard
Nucl. Phys. A372, 1 (1981)

ELEM. SYM.	A	Z
Pb	208	82

METHOD

REF. NO.	
81 Ac 11	hg

REACTION	RESULT	EXCITATION ENERGY	SOURCE TYPE	SOURCE RANGE	DETECTOR TYPE	DETECTOR RANGE	ANGLE
G,G	LFT	5-8	C	10	SCD-D		DST

7 LEVELS

Abstract: Nuclear resonance fluorescence measurements on ^{58}Ni with bremsstrahlung and Ge(Li) detectors were performed to search for bound state dipole excitations. Ten levels with ground state decay widths larger than 0.3 eV have been observed in the energy region between 6 and 10 MeV for which precise excitation energies, spins and lifetimes are reported. The measured transition probabilities are compared with theoretical estimates of E1 and M1 strength in ^{58}Ni. Since the ^{58}Ni(γ, γ) cross sections were determined relative to strong transitions in ^{208}Pb, the results of a separate ^{208}Pb(γ, γ) measurement are also presented.

E NUCLEAR REACTIONS ^{58}Ni(γ, γ), ^{208}Pb(γ, γ), $E < 10$ MeV; measured E_γ, $\sigma(\theta)$; deduced lifetimes, spins. Enriched targets.

TABLE 1

Comparison of ground state decay widths in ^{208}Pb

This measurement		Chapuran [b]	
E_x (keV)	Γ_0 [a] (eV)	E_x (keV)	Γ_0 [a] (eV)
5294±3	5.2±1.5	5292.6±2.0	5.1±0.8
5514±3	17.7±4.8	5512.2±1.0	22.3±3.4
6266±3	3.0±1.1	6263.4±3.0	2.6±0.5
6721±3	6.9±2.0	6720.1±1.5	7.6±1.5
7064±3	16.0±4.4	7063.3±1.5	15.7±2.6 †
7084±3	8.0±2.3	7082.8±1.5	8.8±1.5
7333±3	26.5±7.1	7332.2±1.5	26.9±4.8 †

† Used for decay widths calibration.
[a]) $\Gamma_0/\Gamma = 1$ assumed.
[b]) Ref. [13]).

REF. K.V. Alanakyan, M.Dzh. Amaryan, R.A. Demirchyan, K.Sh. Egijan, M.S. Ogandzhanyan, Yu.G. Sharabyan
Nucl. Phys. A367, 429 (1981)

ELEM. SYM.	A	Z
Pb	208	82

METHOD

REF. NO.	
81 Al 8	hg

REACTION	RESULT	EXCITATION ENERGY	SOURCE		DETECTOR		ANGLE
			TYPE	RANGE	TYPE	RANGE	
G,P	ABY	8-999	C	999	TEL-D		DST

999=4.5 GEV

Abstract: The angular dependences of proton photoproduction from the nuclei ^{12}C, ^{63}Cu and ^{208}Pb irradiated by bremsstrahlung γ-quanta with maximum energy 4.5 GeV, both in the cumulative region (i.e. in the kinematical region in which the production of protons in the collision of γ-quanta of the given energy with the quasi-free nuclear nucleon is forbidden) and in the non-cumulative region, are investigated. The experimental data obtained are compared with the results of theoretical calculations of cumulative proton photoproduction according to the following models: the "quasi-two-body" scaling model, the low-nucleon correlation model, the fluctuon model and the cluster model.

E NUCLEAR REACTIONS ^{12}C, ^{63}Cu, $^{208}Pb(\gamma, p)$, $E = 4.5$ GeV bremsstrahlung; measured $\sigma(E_p, \theta_p)$; deduced reaction mechanism. Natural target.

Fig. 5. The same as in fig. 3 for ^{208}Pb.

REF. Y. Birenbaum, Z. Berant, S. Kahane, A. Wolf, R. Moreh
Nucl. Phys. A369, 483 (1981)

ELEM. SYM.	A	Z
Pb	208	82

METHOD

REF. NO.	
81 Bi 6	hg

REACTION	RESULT	EXCITATION ENERGY	SOURCE TYPE	SOURCE RANGE	DETECTOR TYPE	DETECTOR RANGE	ANGLE
G,N	RLY	7-11	D	7 - 12	SCI-D		DST
		(7.4-11)		(7 - 11.4)			

$$I(E_\gamma,G) = \frac{a_1P_1 + a_3P_3}{1 + a_2P_2}$$

Abstract: Angular distributions of photoneutrons from the ^{207,208}Pb(γ, n_0) reactions were measured at 11 angles around θ = 90° The γ-source, E_γ = 7–11.4 MeV, contained discrete lines ($\Delta E \lesssim$ 30 eV) obtained from n-capture and was used in conjunction with a high-resolution ^{3}He spectrometer. Strong evidence for an E2 contribution and for E2-E1 and possibly E1-M1 interference was obtained in both ^{207}Pb and ^{208}Pb. The results are compared with calculations using a direct-semidirect model which involved an E1 and isoscalar E2 giant resonances The results indicate that this model could explain only certain features of the data while most of the other features remain unexplained.

E NUCLEAR REACTIONS ^{208,207}Pb(γ, n), E = 7.0–11.4 MeV; measured $\sigma(\theta)$ for θ = 40°–140°. Deduced E2-E1 and M1-E1 interference effects.

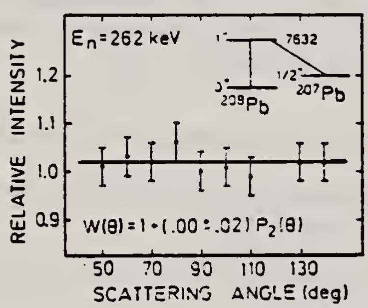

Fig. 4. Angular distribution of the 262 keV neutron group emitted by the ^{208}Pb(γ, n_0) reaction and resonantly photoexcited by the 7632 keV γ-line of the Fe(n, γ) reaction.

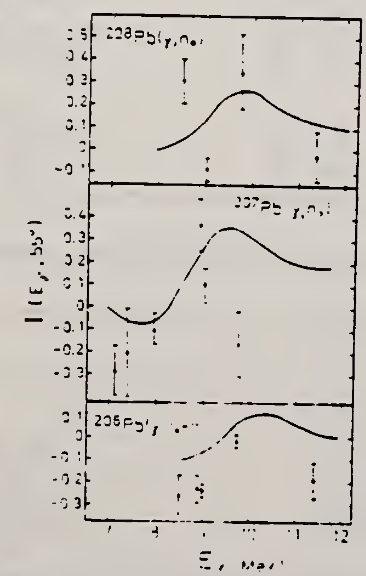

Fig. 9. Measured interference factor $I(E_\gamma, \theta)$ for the three reactions ^{206,207,208}Pb(γ, n_0). The data for the ^{206}Pb target were taken from ref. ¹). The solid curves are calculated using the DSD model.

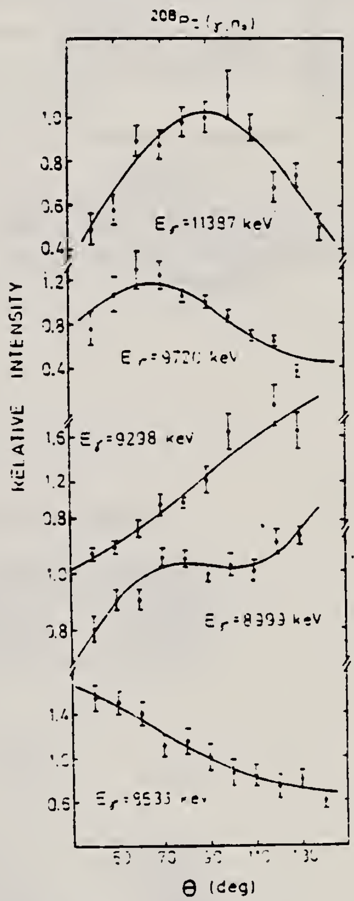

Fig. 6. Angular distributions of neutrons from the ^{208}Pb(γ, n) reaction leading to the ground state in ^{207}Pb for various incident photon energies.

(OVER)

U.S. DEPARTMENT OF COMMERCE
NATIONAL BUREAU OF STANDARDS

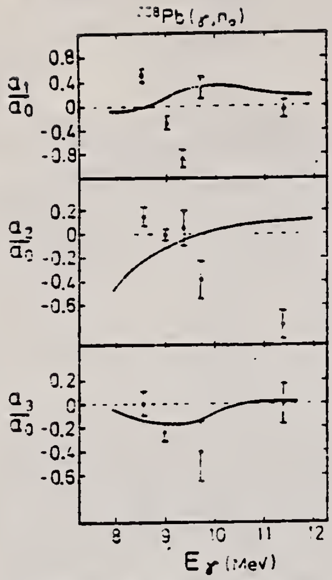

Fig. 7. Angular distribution coefficients a_1, a_2 for the (γ, n) transitions to the ^{207}Pb ground state. The solid curves are calculated using the DSD model.

REF. W. Biesiot, Ph.B. Smith
Phys. Rev. C24, 808 (1981)

ELEM. SYM.	A	Z
Pb	208	82

METHOD

REF. NO.	
81 Bi 7	hg

REACTION	RESULT	EXCITATION ENERGY	SOURCE TYPE	SOURCE RANGE	DETECTOR TYPE	DETECTOR RANGE	ANGLE
$ G,MU-T	LFT	4-7	D	4-7	NAI-D		DST
		(4.841-7.064)		(4.841-7.064)			

POL.G, AZMUTH ANG DST

Level parameters in ^{208}Pb have been determined by means of the resonance gamma-ray absorption technique and measurement of the azimuthal distribution of the elastic scattering of plane-polarized photons. The radiation was produced in suitably chosen (p,γ) reactions. The 7.1 MeV doublet was found at $E_x = 7063.5 \pm 0.2$ and 7083.3 ± 0.3 keV with ground-state radiation widths of 19.1 ± 1.5 and 9.1 ± 1.3 eV. A unique negative parity assignment could be made to both levels, in agreement with other observations. The 4.84 MeV bound level has an excitation energy $E_x = 4842.2 \pm 0.2$ keV and is most probably a $J^\pi = 1^+$ level.

[NUCLEAR REACTIONS ^{34}S$(p,\gamma)^{35}$Cl, ^{208}Pb res. abs., ^{208}Pb res. fluor., $E = 4.8$, 7.1 MeV; measured $\sigma(E,E_\gamma)$. ^{208}Pb deduced levels π, Γ, levels. Enriched lead sample.]

TABLE II. Comparison of measured level width and branching ratio for the members of the 7.1 MeV doublet in ^{208}Pb.

	Γ_0^2/Γ(7.06 MeV) (eV)	Γ_0^2/Γ(7.08 MeV) (eV)	Γ_0/Γ (7.06 MeV)	Γ_0/Γ (7.08 MeV)
This work	17.4 ± 3.3	9.1 ± 1.3		
	19.5 ± 1.7			
Sparks *et al.* (Ref. 5)	18 ± 3			
Chapuran *et al.* (Ref. 26)	15.7 ± 2.6	8.8 ± 1.5	$0.98^{+0.02}_{-0.07}$	1.0
Laszewski and Axel (Ref. 25)	25.9 ± 2.1			
Knowles *et al.* [Ref. 14(b)]	24 ± 3	15 ± 3		
Swann (Ref. 7)	31 ± 3	17 ± 2	0.8 − 1.0	0.8 − 1.0
Scholz *et al.* (Ref. 22)		16^{+6}_{-4}	0.62	0.62
Yeh and Lancman (Ref. 23)	29 ± 3	16 ± 3	$0.9^{+0.1}_{-0.4}$	$0.8^{+0.2}_{-0.3}$
Coope *et al.* (Ref. 24)	29 ± 10	14 ± 5		

TABLE III. Comparison of measured level width and branching ratio of the 4.84 MeV level in ^{208}Pb.

	Γ_0^2/Γ (eV)	Γ_0/Γ
This work	$4.3^{+[illegible]}_{-1.4}$	
Swann (Ref. 10)	5.1 ± 0.8	1
Knowles *et al.* (Ref. 14b)	6 ± 2	
Coope *et al.* (Ref. 24)	6.3 ± 2.2	
Laszewski and Axel (Ref. 25)	6.9 ± 1.4	
Chapuran *et al.* (Ref. 26)	5.0 ± 0.8	$0.85^{+0.13}_{-0.09}$
Earle *et al.* (Ref. 31)		1.0

(OVER)

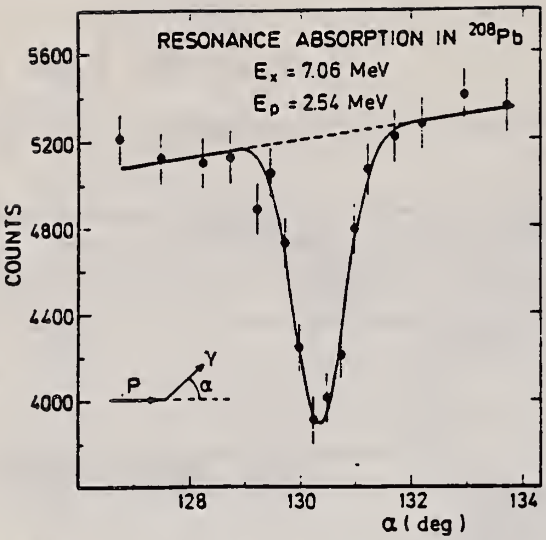

FIG. 5. The transmission curve resulting from the resonance absorption in a 7 mm thick absorber of ^{208}Pb of the 7.06 MeV ($R \to 1.76$ MeV) decay gamma of the $E_p = 2.54$ MeV resonance in $^{34}S(p,\gamma)^{35}Cl$. The ordinate represents the total number of true counts in a spectrum gate. The solid and dotted lines have the same meaning as those described in Fig. 3. The value of the normalized χ^2 for the fit is 0.65.

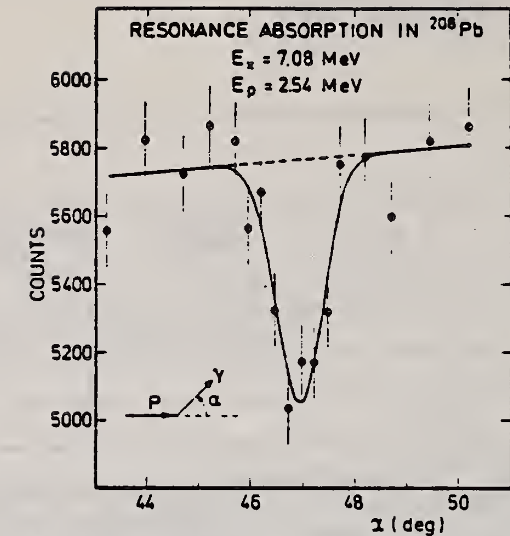

FIG. 6. The transmission curve resulting from the resonance absorption in a 7 mm thick absorber of ^{208}Pb of the 7.08 MeV ($R \to 1.76$ MeV) decay gamma of the $E_p = 2.54$ MeV resonance in $^{34}S(p,\gamma)^{35}Cl$. The layout is the same as described under Fig. 3. The value of the normalized χ^2 for the fit is 1.18.

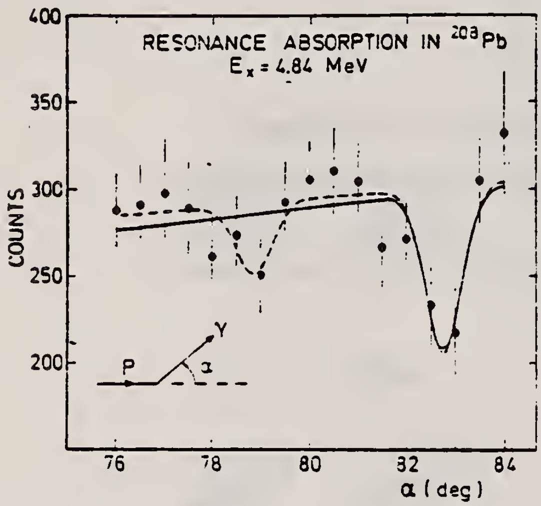

FIG. 8. The transmission curve resulting from the resonance absorption in a 30 mm thick absorber of ^{208}Pb of the 4.84 MeV ($R \to 3.16$ MeV) decay gamma of the $E_p = 1.68$ MeV resonance in $^{34}S(p,\gamma)^{35}Cl$. The ordinate represents the total number of true counts in a spectrum gate. The solid line is the best fit to the data. The dotted line represents a fit of two closely spaced resonances in ^{208}Pb to the data. The value of the normalized χ^2 for the first fit is 0.79 and for the second fit 0.53.

REF.
G. Kühner, D. Meuer, S. Müller, A. Richter, E. Spamer, O. Titze, W. Knüpfer
Phys. Lett. 104B, 189 (1981)

ELEM. SYM.	A	Z
Pb	208	82

METHOD

REF. NO.	
81 Ku 3	hg

REACTION	RESULT	EXCITATION ENERGY	SOURCE TYPE	SOURCE RANGE	DETECTOR TYPE	DETECTOR RANGE	ANGLE
E,E/	SPC	8-12	D	30-50	MAG-I		DST

E1, E2 STRENGTH

Low momentum transfer, high-resolution inelastic electron scattering on ^{208}Pb has been used to study the distribution of E1 and E2 strength in the region of excitation energy E_x = 8–12 MeV. The E1 and E2 strength is very fragmented and the EWSR strength amounts to (10^{+7}_{-6})% and (29^{+11}_{-8})% in the investigated energy region, respectively. The E2 strength found is less than most current theoretical predictions but agrees qualitatively with a 1p – 1h + 2p – 2h model calculation presented in this paper. The E2 strength is also smaller than what is known from hadron scattering and the shape of the strength distribution is also markedly different in electron and hadron scattering.

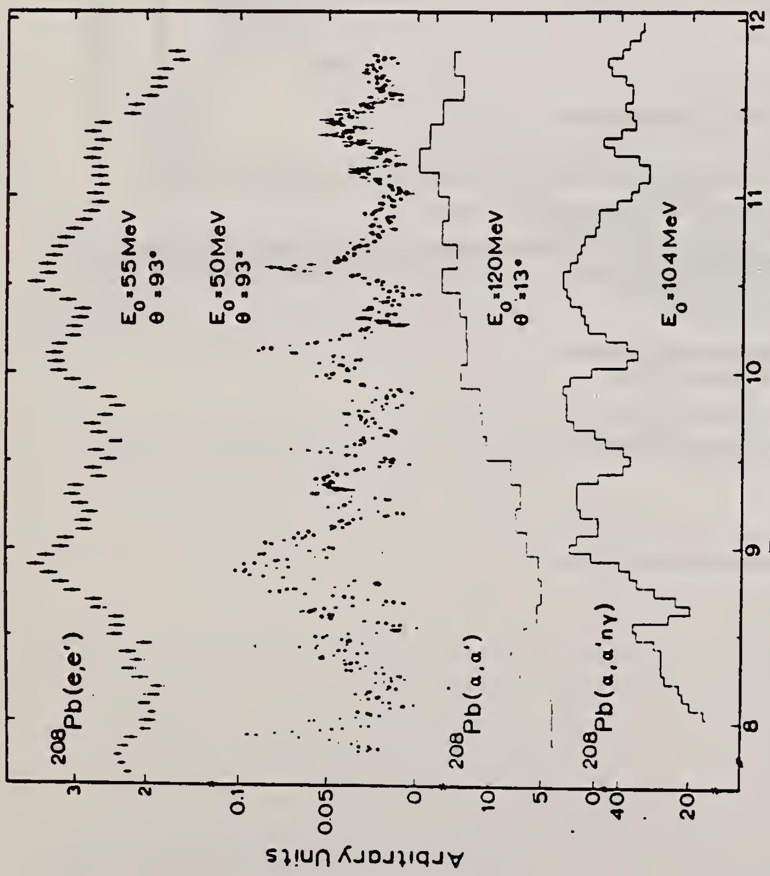

Fig. 2. Comparison of medium- and high-energy resolution (e,e') spectra from Darmstadt with (α,α') and (α,α'nγ) spectra taken at Groningen [2] and Karlsruhe [13], respectively.

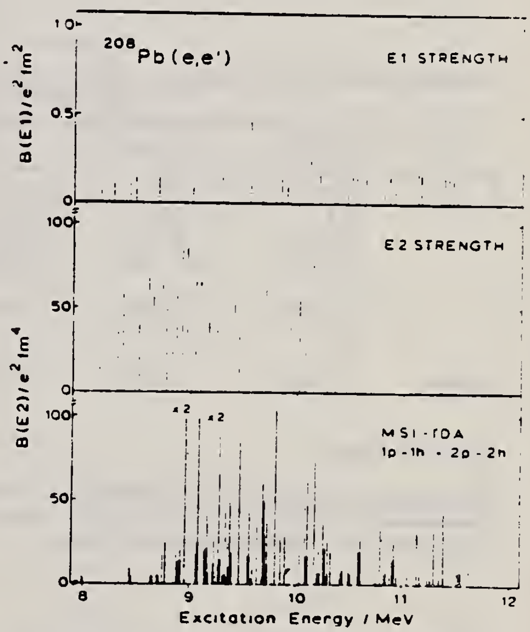

Fig. 3. Experimental E1 (upper part) and E2 (middle part) strength distributions and a theoretical E2 strength distribution (lower part) calculated as described in the main text.

REF. R. Leicht, M. Hammen, K.P. Schelhaas, B. Ziegler
Nucl. Phys. A362, 111 (1981)

ELEM. SYM.	A	Z
Pb	208	82

METHOD

REF. NO.	
81 Le 3	egf

REACTION	RESULT	EXCITATION ENERGY	SOURCE TYPE	SOURCE RANGE	DETECTOR TYPE	DETECTOR RANGE	ANGLE
G,G	ABX	10-100	D	10-100	NAI-D		DST

Figure 5 shows expanded energy region between 10 and 40 MeV

SEE 82LE3

Abstract: Experimental data on elastic scattering of photons in the energy range from 10 to 100 MeV for the nucleus ^{208}Pb are presented. These new data along with some previously published data on photoabsorption are tentatively analysed in the framework of a consistent description. Besides a value for the summed total strength, the partial strengths of some multipoles were obtained. An electric quadrupole resonance was found to be located at 24.3 MeV with a strength of 1.4 isovector sums. An experimental value was deduced for a parameter which can be regarded as a half-density radius for the spatial interaction strength density distribution, including exchange currents, in a nucleus. This radius parameter was found to be 4.9±0.15 fm, considerably smaller than the electrical charge density distributions radius (6.6 fm), as obtained by elastic electron scattering.

E

NUCLEAR REACTIONS ^{208}Pb(γ, γ), E = 10–100 MeV: measured $\sigma(E, \theta)$. ^{208}Pb deduced E2 resonance parameters, radius parameter. Enriched target.

TABLE 2

Parameters obtained from an application of eqs. (5) and (8) to experimental data on photoabsorption and scattering

	E_n (MeV)	Γ_n (MeV)	D_n	Remark
E1	11.62	1.3	0.07	lower part of giant dipole
	13.5	3.5	1.15	main giant dipole
	26 ±2	8 ±2	0.05±0.01	first harmonic dipole?
	67 ±3	105 ±10	0.75±0.02	"quasideuteron"
E2	24.3±0.4	4.5±0.5	0.05±0.015	giant quadrupole resonance 1.4 isovector E2 sums
M1 or E2	16 ±0.2	5 ±0.4	0.05±0.015	charge exchange M1? 3.2 isovector E2 sums, if E2
sum of all multipoles:			2.12	
radius parameter of 2-parameter Fermi distribution: C = 4.9±0.12 fm.				

D_n in units of the classical dipole sum (3 b · MeV).

(over)

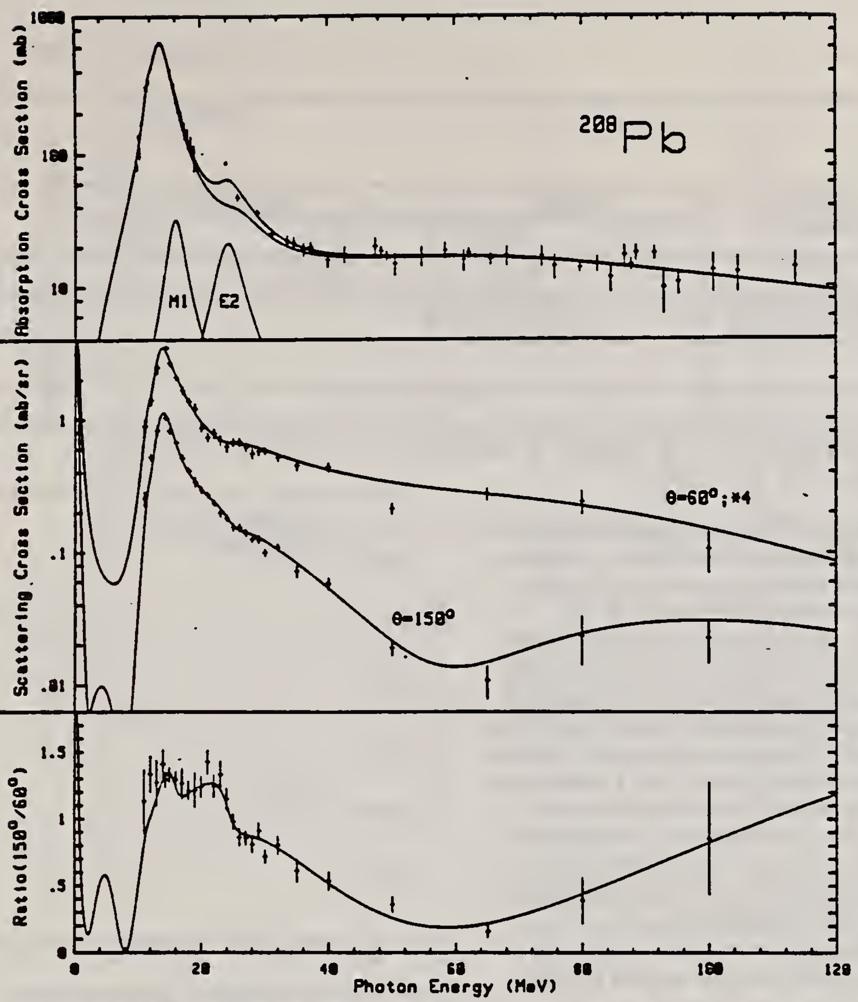

Fig. 4. In this figure all experimental information on absorption [1,2]), and scattering is summarised. The parameters, describing simultaneously absorption and scattering cross sections, are listed in table 2.

REF. Z.W. Bell, L.S. Cardman, P. Axel
Phys. Rev. C25, 791 (1982)

ELEM. SYM.	A	Z
Pb	208	82

METHOD

REF. NO.	
82 Be 2	hg

REACTION	RESULT	EXCITATION ENERGY	SOURCE TYPE	SOURCE RANGE	DETECTOR TYPE	DETECTOR RANGE	ANGLE
G,N	ABX	9-12	D	9-12	TOF-D		DST
		(9.9-11.2)		(9.9-11.2)			

Coefficients of the Legendre expression can be found in the paper in Tables III, IV, V.
Plots of coefficients are in Figs. 13, 14, 15.

The partial differential photoneutron cross sections for ^{208}Pb were measured in the energy region from 9.9 to 11.2 MeV with an energy resolution of about 100 keV. Neutrons leaving ^{207}Pb in its ground state and first two excited states were resolved, and angular distributions were determined from measurements at seven angles from 45° to 135°. These data provide more information about the fine structure observed in earlier, poorer resolution measurements of the total photoneutron cross section and strongly support the interpretation of this structure as being due to electric dipole excitations. The measured partial cross sections provide a sensitive test for models attempting to describe the photon interaction cross section and the coupling of the excited states to the continuum. Calculations using a statistical model with transmission coefficients obtained from a conventional optical model are unable to explain even the average behavior of the branching ratios with energy. The measured angular distributions show clear evidence for interference of either $E2$ or $M1$ processes with the predominant $E1$ interaction. The interference terms have a magnitude approximately equal to that predicted by a simple direct-semidirect calculation including the electric dipole and isoscalar electric quadrupole giant resonance. However, this agreement is puzzling because the average of interferences between the many compound nuclear levels in this region of excitation would be expected to reduce anisotropies about 90° toward zero.

[NUCLEAR REACTIONS ^{208}Pb(γ,n), E=9.9−11.2 MeV; tagged photon resolution 120 keV; measured $\sigma(E_n,\theta)$, θ=45°−135°; observed interference of either $E2$ or $M1$ with $E1$.]

TABLE I. Partial cross sections (mb).

E_γ (MeV)	σ_0	σ_1	σ_2	$\sigma_>$
11.20	23.6±2.5	49.2±4.5	86.4±5.5	38.4±18.9
11.08	38.2±3.0	49.9±4.6	93.0±5.3	38.4±18.9
10.84	37.7±2.4	58.8±3.9	101.4±5.0	12.5±6.3
10.70	28.1±2.3	43.4±3.7	106.6±5.7	7.9±3.9
10.60	46.5±2.2	62.9±3.6	119.7±5.0	0.5±0.6
10.48	29.5±2.3	48.5±3.6	78.7±4.9	−0.5±2.7
10.34	19.2±1.7	33.4±2.5	52.2±3.1	1.4±0.5
10.21	27.2±2.1	40.5±3.2	57.3±4.2	4.3±2.1
10.11	46.8±2.3	49.5±2.9	104.3±3.9	−0.4±2.4
10.01	58.9±2.5	40.7±3.0	76.2±4.0	0.1±0.5
9.92	33.1±2.9	38.5±3.6	36.2±4.6	−0.3±0.5

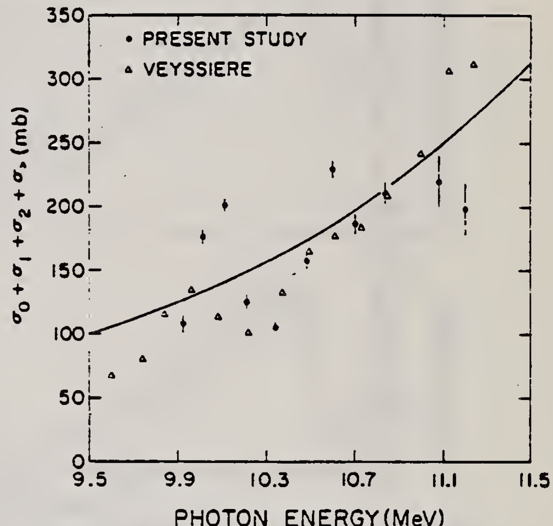

FIG. 5. The total photoneutorn cross section plotted as a function of photon energy. The triangles are the data of Ref. 1 and the solid dots are the results of the present experiment. The solid curve is the extrapolated tail of the Lorentz line fit to the giant dipole resonance data of Ref. 1.

[1]A. Veyssiere, H. Beil, R. Bergere, P. Carlos, and A. Lepretre, Nucl. Phys. A159, 561 (1970). 70 Ve 1

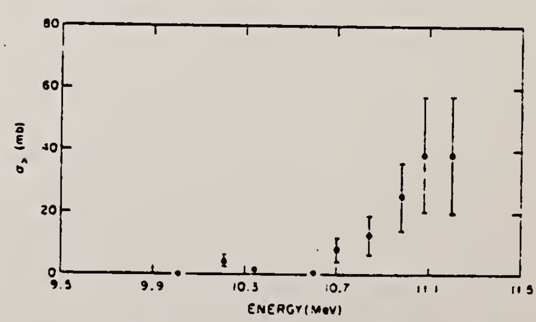

FIG. 8. The partial cross section for ^{208}Pb(γ,n) reactions leaving ^{207}Pb in excited states higher than the second plotted as a function of gamma ray energy.

(OVER)

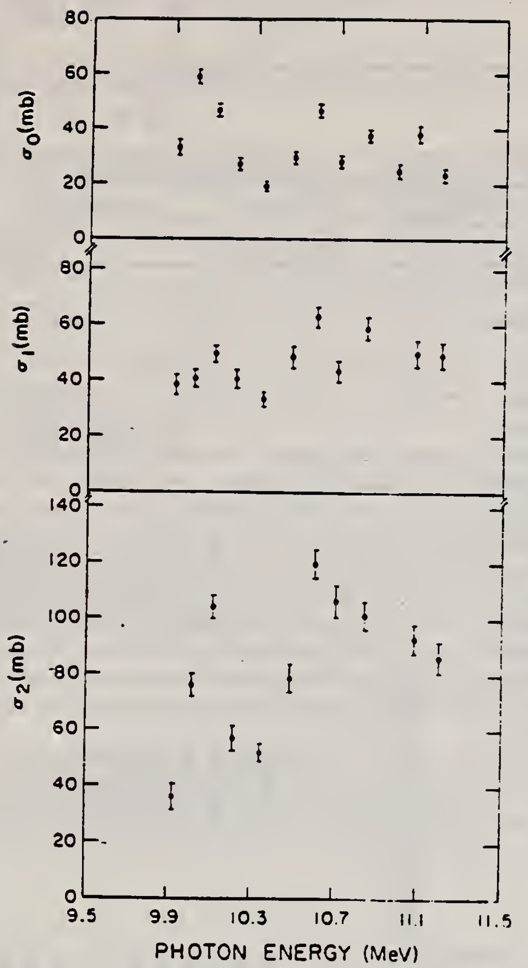

FIG. 7. The partial cross sections for $^{208}Pb(\gamma,n)$ reactions leaving ^{207}Pb in its ground state (σ_0), first excited state (σ_1), and second excited state (σ_2) plotted as a function of gamma ray energy.

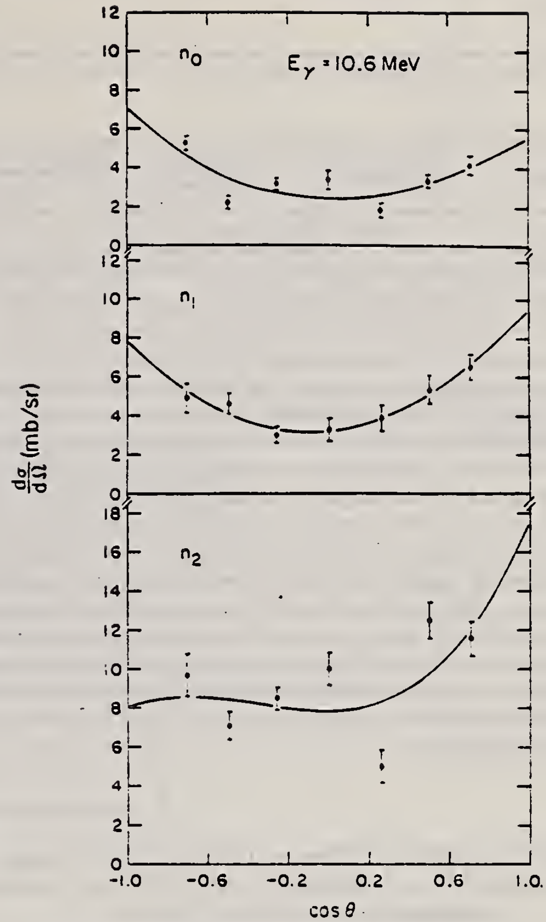

FIG. 11. A representative set of angular distributions for the three partial cross sections measured. The solid curves are the fits to the data obtained using a Legendre expansion.

REF. Z.W. Bell, L.S. Cardman, P. Axel
Phys. Rev. C25, 791 (1982)

ELEM. SYM.	A	Z
Pb	208	82

METHOD

REF. NO.	
82 Be 12	egf

REACTION	RESULT	EXCITATION ENERGY	SOURCE TYPE	SOURCE RANGE	DETECTOR TYPE	DETECTOR RANGE	ANGLE
G,N	ABX	10-11	D	10-11	TOF-D		DST

3 FINAL STATE SIGS

The partial differential photoneutron cross sections for ^{208}Pb were measured in the energy region from 9.9 to 11.2 MeV with an energy resolution of about 100 keV. Neutrons leaving ^{207}Pb in its ground state and first two excited states were resolved, and angular distributions were determined from measurements at seven angles from 45° to 135°. These data provide more information about the fine structure observed in earlier, poorer resolution measurements of the total photoneutron cross section and strongly support the interpretation of this structure as being due to electric dipole excitations. The measured partial cross sections provide a sensitive test for models attempting to describe the photon interaction cross section and the coupling of the excited states to the continuum. Calculations using a statistical model with transmission coefficients obtained from a conventional optical model are unable to explain even the average behavior of the branching ratios with energy. The measured angular distributions show clear evidence for interference of either $E2$ or $M1$ processes with the predominant $E1$ interaction. The interference terms have a magnitude approximately equal to that predicted by a simple direct-semidirect calculation including the electric dipole and isoscalar electric quadrupole giant resonance. However, this agreement is puzzling because the average of interferences between the many compound nuclear levels in this region of excitation would be expected to reduce anisotropies about 90° toward zero.

[NUCLEAR REACTIONS ^{208}Pb(γ,n), E=9.9−11.2 MeV; tagged photon resolution 120 keV; measured $\sigma(E_n,\theta)$, θ=45°−135°; observed interference of either $E2$ or $M1$ with $E1$.]

TABLE I. Partial cross sections (mb).

E_γ (MeV)	σ_0	σ_1	σ_2	$\sigma_>$
11.20	23.6±2.5	49.2±4.5	86.4±5.5	38.4±18.9
11.08	38.2±3.0	49.9±4.6	93.0±5.3	38.4±18.9
10.84	37.7±2.4	58.8±3.9	101.4±5.0	12.5±6.3
10.70	28.1±2.3	43.4±3.7	106.6±5.7	7.9±3.9
10.60	46.5±2.2	62.9±3.6	119.7±5.0	0.5±0.6
10.48	29.5±2.3	48.5±3.6	78.7±4.9	−0.5±2.7
10.34	19.2±1.7	33.4±2.5	52.2±3.1	1.4±0.5
10.21	27.2±2.1	40.5±3.2	57.3±4.2	4.3±2.1
10.11	46.8±2.3	49.5±2.9	104.3±3.9	−0.4±2.4
10.01	58.9±2.5	40.7±3.0	76.2±4.0	0.1±0.5
9.92	33.1±2.9	38.5±3.6	36.2±4.6	−0.3±0.5

TABLE II. Configuration probabilities for $E1$ states.

Configuration	$\alpha(lj)$ Harvey and Khanna (Ref. 21)	Empirical
$(s_{1/2},p_{1/2}^{-1})$	0.004	0.142
$(d_{3/2},p_{1/2}^{-1})$	0.098	0.008
$(d_{3/2},f_{5/2}^{-1})$	0.028	0.243
$(d_{5/2},f_{5/2}^{-1})$	0.000	0.008
$(g_{7/2},f_{5/2}^{-1})$	0.696	0.008
$(s_{1/2},p_{3/2}^{-1})$	0.032	0.008
$(d_{3/2},p_{3/2}^{-1})$	0.055	0.008
$(d_{5/2},p_{3/2}^{-1})$	0.089	0.567

TABLE III. Coefficients of the Legendre expansion of $d\sigma_0/d\Omega$.

E_γ (MeV)	a_{00}	a_{01}	a_{02}	a_{03}
11.20	1.88±0.20	1.10±0.36	0.22±0.56	a
11.08	2.97±0.23	1.42±0.43	0.37±0.69	a
10.84	3.00±0.19	1.77±0.55	0.35±0.61	0.06±0.98
10.70	2.17±0.18	0.83±0.34	0.01±0.53	a
10.60	3.70±0.17	−0.48±0.57	2.63±0.55	−0.24±0.79
10.48	2.35±0.18	0.15±0.58	−0.20±0.59	−1.21±0.96
10.34	1.53±0.13	0.62±0.42	−0.11±0.45	−0.47±0.69
10.21	2.16±0.17	1.04±0.31	−0.33±0.66	a
10.11	3.73±0.18	1.14±0.59	1.41±0.58	−0.78±0.89
10.01	4.69±0.20	1.36±0.61	0.60±0.65	−2.19±1.07
9.92	2.64±0.23	2.19±0.76	2.00±0.62	0.76±1.48

[a]Indicates coefficient not included in the fit.

U.S. DEPARTMENT OF COMMERCE
NATIONAL BUREAU OF STANDARDS

REF. J. Heisenberg, J. Lichtenstadt, C.N. Papanicolas, J.S. McCarthy
Phys. Rev. C25, 2292 (1982)

ELEM. SYM.	A	Z
Pb	208	82

METHOD

REF. NO.	
82 He 2	egf

REACTION	RESULT	EXCITATION ENERGY	SOURCE TYPE	SOURCE RANGE	DETECTOR TYPE	DETECTOR RANGE	ANGLE
E,E/	FMF	3-5	D	50-335	MAG-D		DST

9 LEVELS 2.6-4.6 MEV

High resolution electron scattering measurements on ^{208}Pb have been performed at 90° and 160°, which allow the spatial reconstruction of transition charge densities and for the first time, transition current densities. The measurement covering the momentum transfer range of $0.5 < q < 2.6$ fm^{-1} is supplemented by high momentum transfer data from Saclay, extending the data for some of the states up to a momentum transfer of 3.4 fm^{-1}. We report on the first three $J^\pi = 5^-$ states and the first $J^\pi = 7^-$ state. Transition charge densities have been also extracted for the lowest $J^\pi = 2^+$, 4^+, 6^+, and 8^+ states. The densities are compared to a number of theoretical calculations. Transverse electric currents are shown for the 5^- states that indicate a quenching of the magnetization current similar to observations from other states but the absence of quenching in the convection current contribution.

NUCLEAR REACTIONS ^{208}Pb(e,e') measured cross sections at 90° and 160°, $0.5 \le q \le 2.6$ fm^{-1}. Low lying $J^\pi = 2^+, 4^+, 6^+, 8^+, 5^-, 7^-$ states analyzed. Transition charge densities and current densities extracted in DWBA.

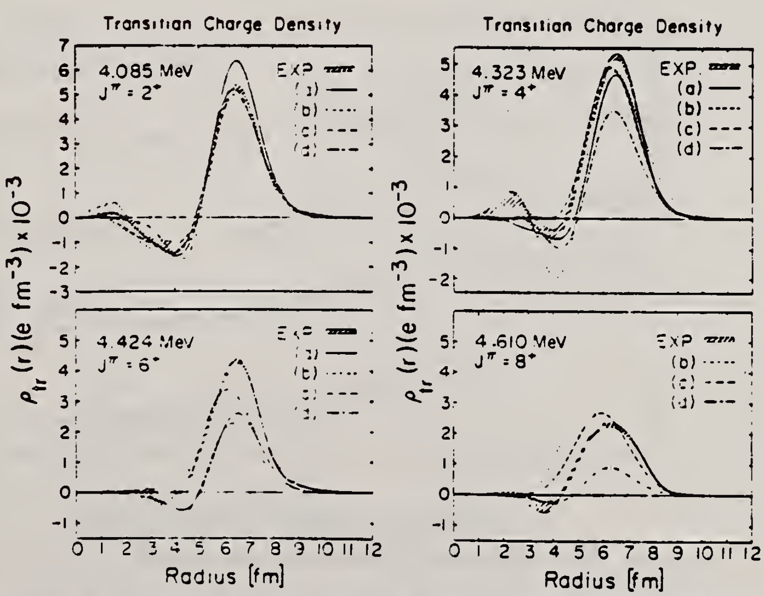

FIG. 4. Transition charge densities for the even spin natural parity states in ^{208}Pb. The theoretical curves are from: (a) Bertsch and Tsai (Ref. 21), (b) Knüpfer and Huber (Ref. 22), (c) Gogny and Decharge (Refs. 4 and 35), and (d) Heisenberg and Krewald (Ref. 23).

(OVER)

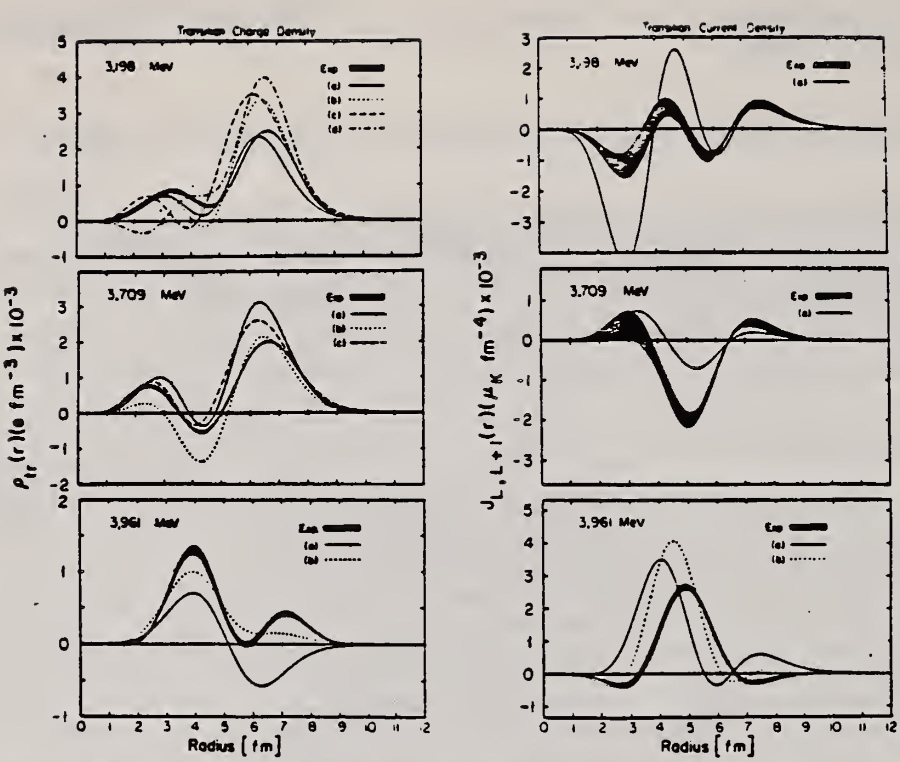

FIG. 8. Transition charge and current densities for the first three 5^- levels in ^{208}Pb. The theoretical curves are (a) from Heisenberg and Krewald (Ref. 23), (b) from Gogny (Ref. 35), (c) from Knüpfer and Huber (Ref. 22), and (d) from Bertsch and Tsai (Ref. 21). For the 3.961 MeV state curves (b) are from Ref. 23 also but calculated with a shifted $h_{9/2}$ energy.

REF. R.S. Hicks, R.L. Huffman, R.A. Lindgren, B. Parker, G.A. Peterson, S. Raman, C.P. Sargent
Phys. Rev. C26, 920 (1982)

ELEM. SYM.	A	Z
Pb	208	82

METHOD

REF. NO.	
82 Hi 1	egf

REACTION	RESULT	EXCITATION ENERGY	SOURCE TYPE	SOURCE RANGE	DETECTOR TYPE	DETECTOR RANGE	ANGLE
E,E/		2-8	D	40-75	MAG-D		180

10 LVS 2.61-7.48 MEV

Inelastic cross sections for 180° electron scattering from ^{208}Pb have been measured at incident energies of 40.5, 50.4, 60.3, and 75.2 MeV. Transverse electric form factors have been determined for the 3^- state at 2.614 MeV, the 5^- states at 3.198 and 3.708 MeV, the 2^+ states at 4.085 and 6.21 MeV, the 4^+ state at 4.323 MeV, and the 6^+ state at 4.422 MeV. The results for these natural parity states are compared to the predictions of an incompressible, irrotational current model, and of a particle-hole model. All transverse electric form factors show strong contributions from intrinsic magnetization currents. Transverse form factors were obtained for the proposed 1^+ state at 4.84 MeV, for the group of 1^+ states at 7.48 MeV, and for several proposed 2^- states. A search for $M1$ transition strength was made up to excitation energies of 19 MeV. The future of electron scattering as a tool for probing $M1$ strength in ^{208}Pb is discussed.

[NUCLEAR REACTIONS ^{208}Pb(e,e′), E=40.5, 50.4, 60.3, and 75.2 MeV, measured σ(180°). ^{208}Pb deduced levels and transverse form factors. Enriched target, magnetic spectrometer.]

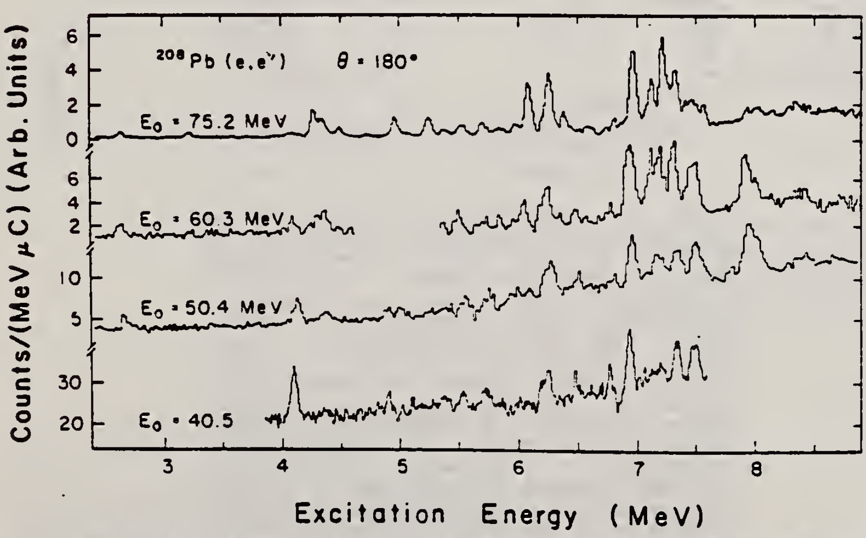

Fig. 1. Measured spectra of electrons inelastically scattered from ^{208}Pb.

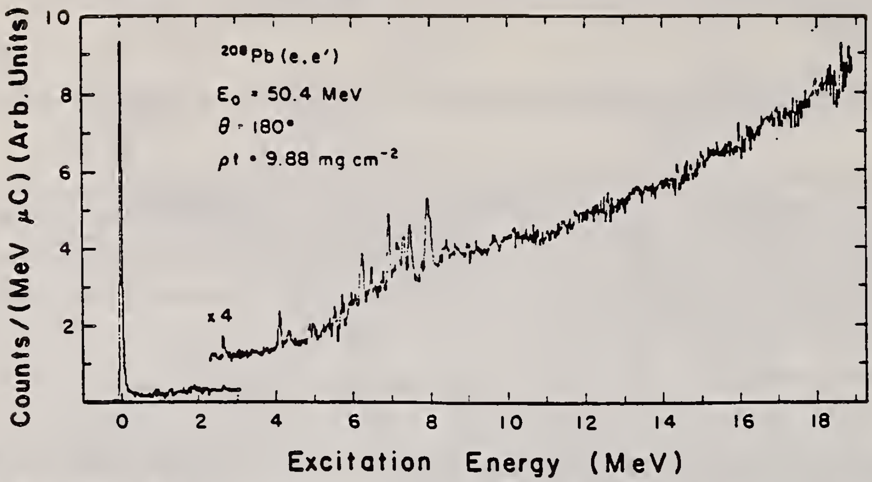

Fig. 2. Scattered electron spectrum, obtained with 50.4 MeV electrons, shows a large elastic peak and little evidence of significant sharp structure in the range E_x = 9-19 MeV.

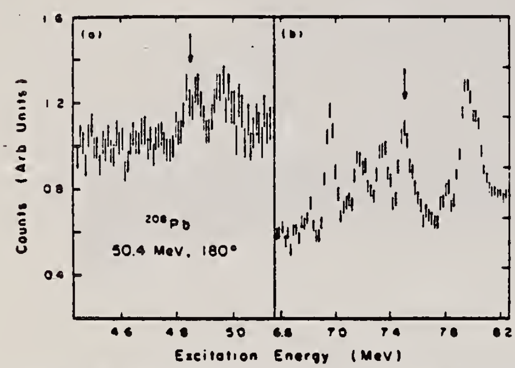

Fig. 6. Detail of an inelastic electron spectrum showing candidate M1 peaks at 4.84 and 7.48 MeV.

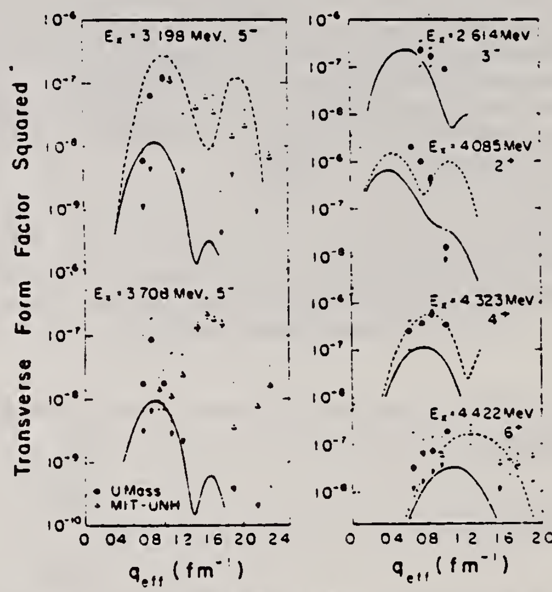

Fig. 3. Transverse (e,e′) form factors for low-lying electric transitions in ^{208}Pb. In cases where no experimental datum is explicitly shown, the error bar indicates an upper limit, i.e., the measured value plus three standard deviations. The solid curves are for irrotational, Tassie-model currents. Dashed curves include, in addition, neutron magnetization currents due to predicted strong particle-hole components, as described in the text. To facilitate the comparison of measurements taken under different kinematic conditions, the data and the DWBA calculations are plotted as a function of an effective momentum transfer defined by (see Ref. 12) $q_{eff} = q[1+(3Z\alpha/2E_iR)]$, where α is the fine structure constant, and R is the uniform density charge radius.

REF. C.N. Papanicolas, J. Heisenberg, J. Lichtenstadt, J.S. McCarthy, D. Goutte, J.M. Cavedon, B. Frois, M. Huet, P. Leconte, Phan Xuan Ho, S. Platchkov, I. Sick
Phys. Lett. 108B, 279 (1982)

ELEM. SYM.	A	Z
Pb	208	82

METHOD

REF. NO.	
82 Pa 1	egf

REACTION	RESULT	EXCITATION ENERGY	SOURCE TYPE	SOURCE RANGE	DETECTOR TYPE	DETECTOR RANGE	ANGLE
E,E/	FMF	3,4	D	350-502	MAG-D		DST

3=3.198,4=3.709 MEV

The transition charge densities for the two lowest 5⁻ states in ^{208}Pb have been determined from recent electron scattering data. The high momentum transfers achieved allow a very precise determination of their detailed structure. They are in disagreement with present theoretical calculations.

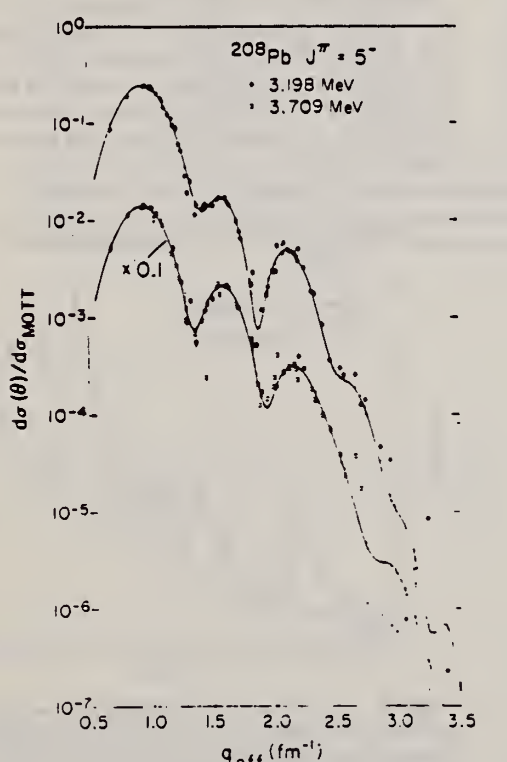

Fig. 1. Experimental values for $d\sigma(\theta)/d\sigma_{MOTT}$ for longitudinal inelastic electron scattering. The best fits obtained using phenomenological transition densities are also shown.

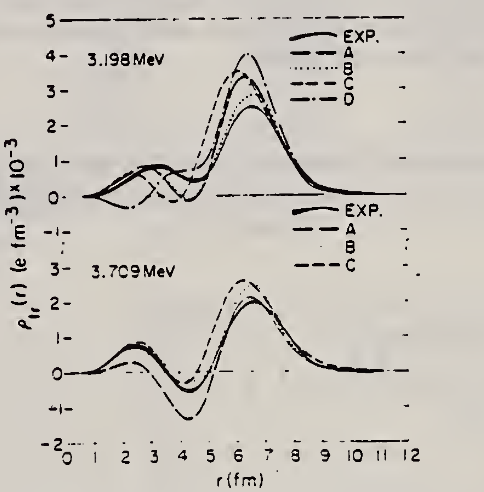

Fig. 2. Comparison of the extracted transition charge densities to a number of theoretical calculations for the lowest $J^\pi = 5^-$ states of ^{208}Pb: curve A is that of Knüpfer and Huber [9]; B is that of Khodel and Saperstein [12]; C is that of Gogny and Dechargé [10] and D is that of Bertsch and Tsai.

REF. R.D. Starr, P. Axel, L.S. Cardman
Phys. Rev. C25, 780 (1982)

ELEM. SYM.	A	Z
Pb	208	82

METHOD

REF. NO.	
'82 St 1	hg

REACTION	RESULT	EXCITATION ENERGY	SOURCE TYPE	SOURCE RANGE	DETECTOR TYPE	DETECTOR RANGE	ANGLE
G,G	ABX	9-12	D	9-12	NAI-D		DST
		(9.5-12)		(9.5-.2)			

The elastic photon scattering cross sections of ^{208}Pb and ^{206}Pb were measured at 90° and 135° in the energy range from 9.5 to 12 MeV with a tagged photon beam whose energy spread was about 125 keV. The ^{206}Pb cross section rises monotonically with energy, and is consistent with a total photon interaction cross section which has a Lorentzian energy dependence with a peak cross section of 650 mb at 13.6 MeV and a width $\Gamma \simeq 3.8$ MeV. The ^{208}Pb scattering cross section is larger and has some rapid variations with energy; there is a narrow extra peak near 10.04 MeV and there are abrupt increases in the cross section just below 10.6 and 11.3 MeV. The relative scattering observed at the two angles indicates that all of the scattering, including the rapid variations with energy, is dominated by dipole interactions. This dipole assignment for the fine structure is important for the proper interpretation of inelastic electron scattering by ^{208}Pb. Some of the observed fine structure in inelastic electron scattering must be dipole; the fine structure previously reported as being due to electric quadrupole excitation should be considered as tentative until the correct dipole contributions are included.

[NUCLEAR REACTIONS ^{206,208}Pb($\gamma\gamma$), $E = 9.5-12$ MeV; measured $\sigma(E;\theta)$; resolution 125 keV; observed fine structure; inferred dipole excitation.]

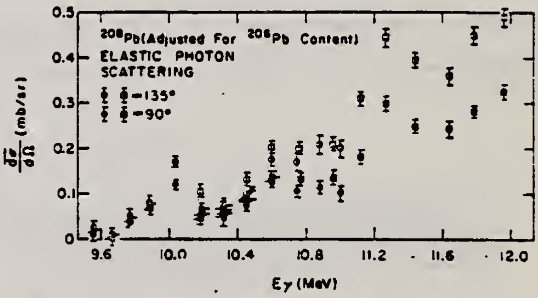

FIG. 2. Differential elastic scattering cross sections for ^{208}Pb: The open symbols give the values obtained at 135°, while the dark symbols correspond to 90°. In both cases, the circles give the data obtained in the lower energy range (run 1 in Table I), while the squares were obtained during the higher energy run. The errors are statistical.

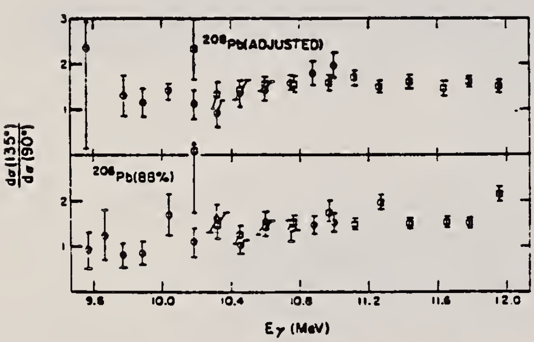

FIG. 4. The ratio of the differential scattering cross sections at 135° to those at 90°: The circles are used for the lower energy range (run 1 in Table I), while the squares correspond to the higher energy run. The ratios that are determined reliably are consistent with the value of 1.5 expected for dipole radiation.

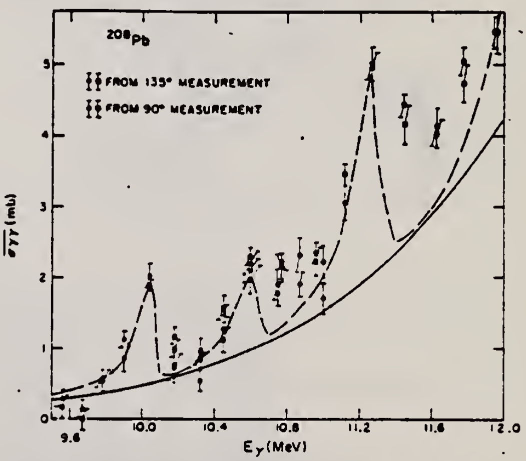

FIG. 5. The elastic photon scattering cross sections for ^{208}Pb: The values of the cross sections integrated over angle were inferred from the data at 135° (open symbols) and 90° (solid symbols) using Eq. (16). The circles correspond to the lower energy run (i.e., run 1 in Table I), while the squares correspond to run 2. The observed cross sections are well above the solid line expected if the photoabsorption were an extrapolation to low energy of the giant dipole resonance. The dashed line illustrates the scattering that would be expected if there were additional concentrations of photon absorption, as described in the text.

(over)

TABLE I. Elastic scattering cross sections.

Run No.	Counter	Energy (MeV)	^{208}Pb $\sigma_{\gamma\gamma}$[a] (mb)	^{208}Pb $\sigma_{\gamma\gamma}$[b] (mb)	^{206}Pb[c] $\sigma_{\gamma\gamma}$[a] (mb)	^{206}Pb[c] $\sigma_{\gamma\gamma}$[b] (mb)
2	1	11.95	5.46±0.23	5.46±0.30	3.44±0.12	2.38±0.15
2	2	11.78	5.05±0.20	4.72±0.25	2.71±0.10	2.68±0.13
2	3	11.64	4.03±0.20	4.12±0.28	2.33±0.10	2.30±0.13
2	4	11.45	4.43±0.17	4.16±0.28	1.98±0.08	1.98±0.12
2	5	11.27	4.98±0.19	5.01±0.23	2.04±0.09	1.59±0.10
2	6	11.12	3.45±0.16	3.05±0.25	1.54±0.07	1.57±0.10
1	1	11.00	2.22±0.22	1.71±0.20	1.37±0.09	1.37±0.17
2	7	10.96	2.35±0.15	2.23±0.20	1.33±0.08	1.12±0.10
1	2	10.87	2.32±0.25	1.91±0.18	0.98±0.07	1.02±0.13
2	8	10.77	2.23±0.12	2.16±0.18	0.96±0.06	0.96±0.08
1	3	10.75	1.92±0.23	1.78±0.18	0.86±0.08	0.96±0.15
1	4	10.60	1.98±0.21	2.11±0.18	0.75±0.07	0.75±0.12
2	9	10.60	2.30±0.12	2.21±0.18	0.82±0.06	0.85±0.08
2	10	10.46	1.50±0.12	1.64±0.18	0.58±0.06	0.70±0.08
1	5	10.45	1.12±0.19	1.27±0.17	0.61±0.06	0.92±0.12
1	6	10.32	0.52±0.16	0.87±0.12	0.63±0.06	0.59±0.10
2	11	10.32	0.86±0.11	0.96±0.18	0.47±0.06	0.49±0.08
1	7	10.19	0.73±0.19	0.99±0.13	0.38±0.06	0.52±0.12
2	12	10.19	1.17±0.12	0.75±0.20	0.41±0.06	0.20±0.08
1	8	10.04	1.91±0.07	2.03±0.17	0.49±0.06	0.44±0.10
1	9	9.90	0.87±0.20	1.12±0.13	0.23±0.04	0.42±0.10
1	10	9.78	0.56±0.16	0.64±0.13	0.31±0.06	0.59±0.17
1	11	9.67	−0.02±0.15	0.15±0.13	0.30±0.06	0.37±0.15
1	12	9.56	0.29±0.13	0.18±0.17	0.22±0.04	0.37±0.13

[a]Calculated from 135° differential cross section assuming dipole radiation.
[b]Calculated from 90° differential cross section assuming dipole radiation.
[c]Not corrected for 2.7% ^{208}Pb or 9.0% ^{207}Pb in enriched ^{206}Pb target.

REF.		ELEM. SYM.	A	Z
	K. Wienhard, K. Ackermann, K. Bangert, U.E.P. Berg, C. Bläsing, W. Naatz, A. Ruckelshausen, D. Rück, R.K.M. Schneider, R. Stock Phys. Rev. Lett. 49, 18 (1982)	Pb	208	82
METHOD		REF. NO. 82 Wi 5		egf

REACTION	RESULT	EXCITATION ENERGY	SOURCE TYPE	SOURCE RANGE	DETECTOR TYPE	DETECTOR RANGE	ANGLE
$ γ,γ	ABX	4-7	C	10	SCD-D		DST

The parities of eleven $J = 1$ levels in ^{208}Pb were determined by nuclear resonance fluorescence scattering of linearly polarized photons. A new 1^+ level at $E_x = 5.846$ MeV with $\Gamma_0^2/\Gamma = 1.2 \pm 0.4$ eV was found. This level can probably be identified with the theoretically predicted isoscalar 1^+ state in ^{208}Pb. All other bound dipole states below 7 MeV with $\Gamma_0^2/\Gamma > 1.5$ eV have negative parity. The 1^- assignment to the 4.842-MeV level is of special significance because of previous conflicting results about its parity.

$ BEAM, SCTNG ASM

PACS numbers: 21.10.Hw, 25.20.+y, 27.80.+w

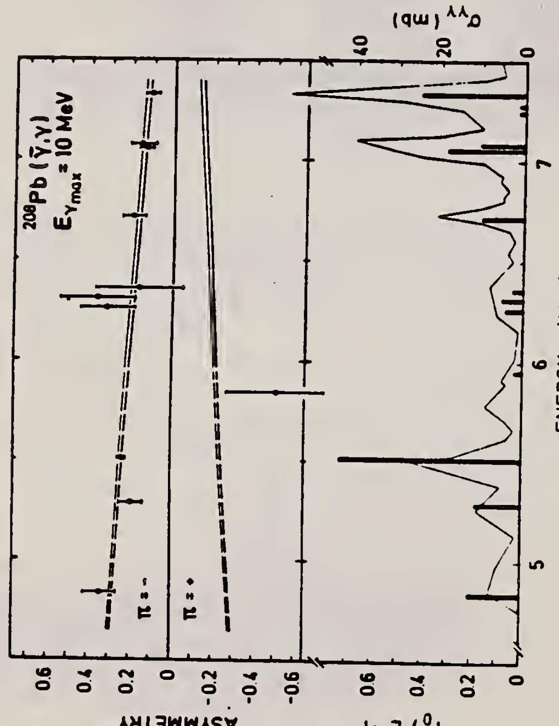

FIG. 1. A summary of the measured asymmetries for the observed γ-ray transitions is shown in the upper part. The solid and dashed lines represent the expected asymmetries for transitions with negative (π = −) and positive (π = +) parity. For comparison, in the lower part, the values $(1/E^2)\Gamma_0^2/\Gamma$ for transitions observed in unpolarized NRF scattering are drawn as vertical bars (left scale) together with the average elastic photon scattering cross section (right scale).

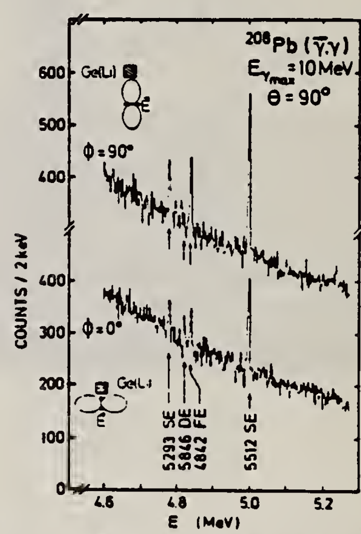

FIG. 2. Part of ^{208}Pb(γ_{pol}, γ) spectra in the 5-MeV region. In the upper part the electric vector $\vec{E}$ of the incoming photons was perpendicular and in the lower part parallel to the scattering plane as shown in the inset.

Pb
A=209

Pb
A=209

Pb
A=209

REF.

I. Bergqvist, D.M. Drake, and D.K. McDaniels
Nucl. Phys. A191, 641 (1972)

ELEM. SYM.	A	Z
Pb	209	82

METHOD

REF. NO.	
72 Be 7	egf

REACTION	RESULT	EXCITATION ENERGY	SOURCE TYPE	SOURCE RANGE	DETECTOR TYPE	DETECTOR RANGE	ANGLE
N,G	ABX	10-19	D	6-15	NAI-D		90

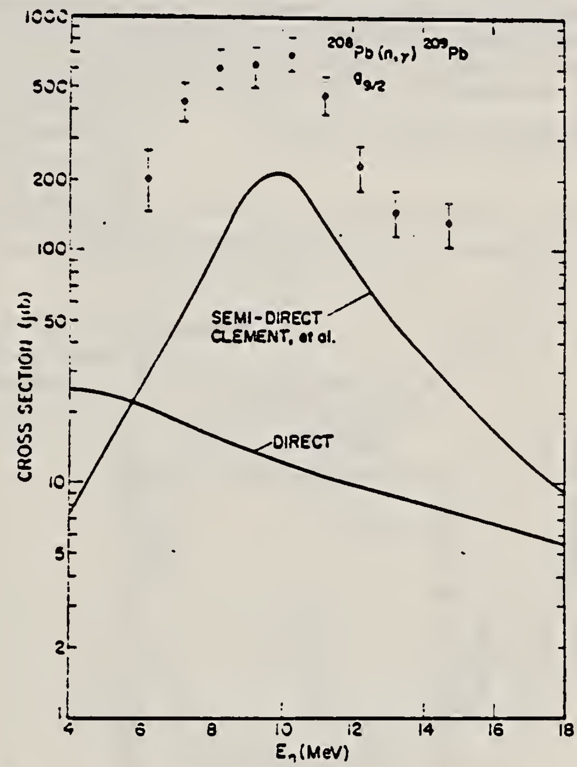

Fig. 6. Total (n,γ) cross section for the γ-ray transition to the $g_{\frac{9}{2}}$ ground state level of ^{209}Pb. The differential cross section at 90° was evaluated using eq. (4) of the text and the total cross section obtained by multiplying by 4π. The upper curve is the prediction from eq. (4) of the semi-direct theory of Clement *et al.* [8]). The lower curve is the theoretical prediction of the direct capture theory of Lane and Lynn [30]).

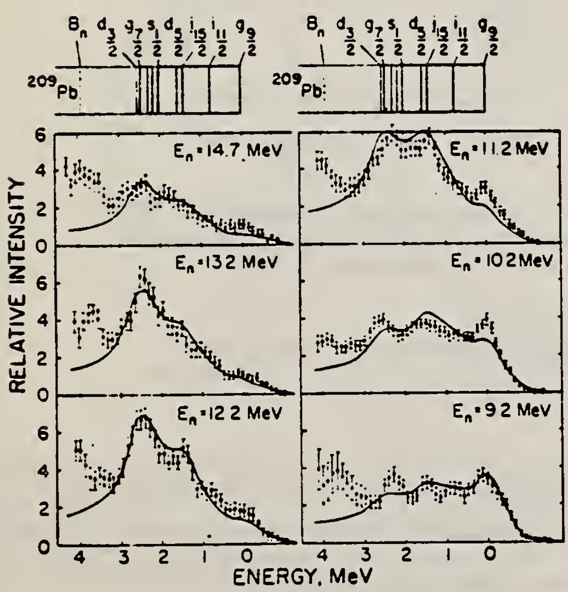

Fig. 5. Comparison of the measured spectra and those predicted from semi-direct capture theory at 6 neutron energies spanning the giant-dipole resonance. The experimental spectra were normalized to the same amount of charge and to the NaI(Tl) detector efficiency of the ground state transition. The theoretical spectra were computed using the cross-section predictions of Clement *et al.* [8]), for each γ-ray transition to a single-particle state of ^{209}Pb, folding in the measured NaI(Tl) detector line shape, and correcting for the detector γ-ray efficiency. The theoretical spectra were normalized absolutely to the measured ones by making the number of events below 2.5 MeV (excitation energy) the same in both spectra.

[8] C.F. Clement et al., Nucl. Phys. 66 (1965) 273, 293

[30] A.M. Lane et al., Nucl. Phys. 11 (1959) 646

REF.	ELEM. SYM.	A	Z
D.M. Drake, S. Joly, L. Nilsson, S.A. Wender, K. Aniol, I. Halpern, D. Storm Phys. Rev. Lett. 47, 1581 (1981)	Pb	209	82
METHOD	REF. NO. 81 Dr 4		hg

REACTION	RESULT	EXCITATION ENERGY	SOURCE TYPE	SOURCE RANGE	DETECTOR TYPE	DETECTOR RANGE	ANGLE
N,G	RLY	11-24	D	7-20	NAI-D		DST

MEAS FORE-AFT ASYMMET

The forward-to-backward asymmetry of high-energy photons emitted in the radiative capture of neutrons with energies up to 20 MeV was measured for ^{208}Pb. The asymmetry increases abruptly from small values to large ones near $E_\gamma \sim 23$ MeV supporting the location in that neighborhood of the $E2$ giant isovector resonance.

PACS numbers: 24.30.Cz, 25.40.Lw

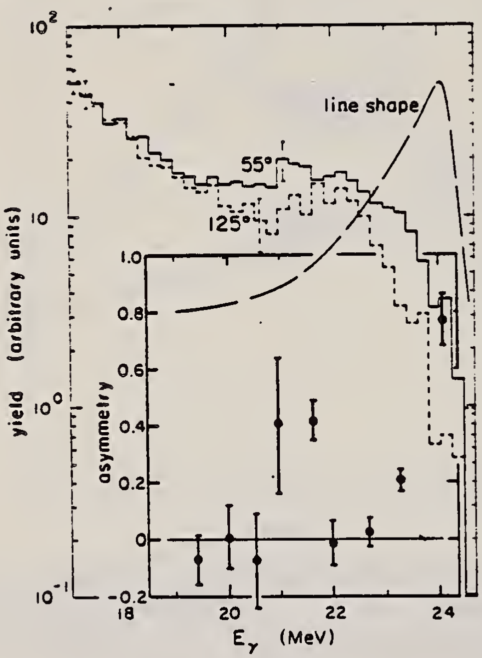

FIG. 2. The high-energy photon (photopeak) spectra measured at 55° and 125° when ^{208}Pb is bombarded with 20-MeV neutrons. These spectra have been corrected for attenuation in the target and for Doppler shift, but were not in any other way renormalized. The two spectra were individually unfolded with use of the measured line shape (shown in the figure for $E_\gamma = 24$ MeV) and the asymmetries $A(55°)$ were computed as a function of photon energy. These asymmetries were combined with the results obtained from the one-escape spectra and are plotted in the lower portion of the figure. The energies for the five points of lowest excitation correspond to known states or doublets in ^{209}Pb. The higher points were arbitrarily placed $\frac{1}{2}$ MeV apart. The unfolding was terminated at $E_\gamma = 18.8$ MeV.

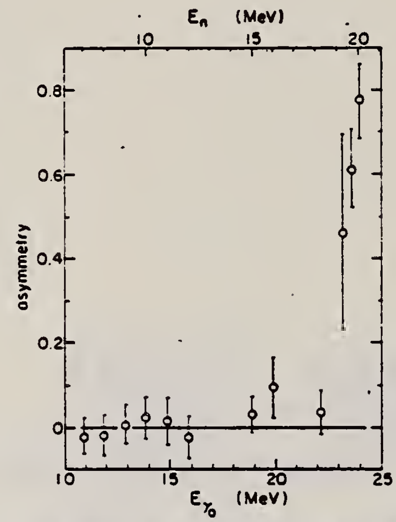

FIG. 3. The measured fore-aft asymmetry $A(55°)$ for photons emitted to the ground state of ^{209}Pb when neutrons of energy E_n are captured in ^{208}Pb.

$$A(\theta) = [Y(\theta) - Y(\pi - \theta)]/[(Y(\theta) + Y(\pi - \theta)].$$

REF. S.E. King, M. Potokar, N.R. Roberson, H.R. Weller, D.R. Tilley
Nucl. Phys. A384, 129 (1982)

ELEM. SYM.	A	Z
Pb	209	82

METHOD

REF. NO.	
82 Ki 1	egf

REACTION	RESULT	EXCITATION ENERGY	SOURCE		DETECTOR		ANGLE
			TYPE	RANGE	TYPE	RANGE	
N,GØ	ABX	10-19	D	6-15	NAI-D		DST

Abstract: The giant dipole resonance region of ^{209}Pb has been studied via the reaction ^{208}Pb(n, γ) for transitions leading to the ground and first excited states of ^{209}Pb. Measured angular distributions were used to extract a_2 coefficients at 8 energies and a_1 coefficients at 4 energies between 10 and 13 MeV. The results are compared to direct-semidirect model and pure resonance model calculations using both real and complex form factors. Absolute cross sections at 90° were measured in 200 keV steps from $E_n(E_\gamma)$ = 7.0(10.9) MeV to 13.0(16.9) MeV and are compared to previous data and to DSD and PRM calculations. The transitions to the ground and first excited states exhaust 0.39 % and 0.13 % of the classical dipole sum, respectively, between the excitation energies of 10.9 and 16.9 MeV.

E | NUCLEAR REACTIONS ^{208}Pb(n, γ), E = 7–13 MeV: measured $\sigma(\theta)$. ^{209}Pb levels deduced dipole EWSR in GDR region. Direct-semidirect, pure resonance model calculations.

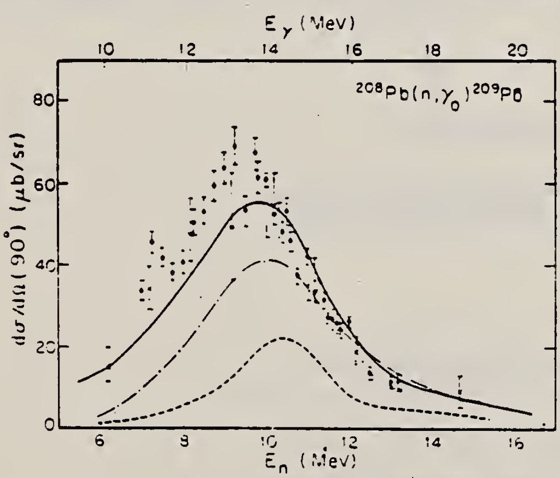

Fig. 3. Absolute 90° cross sections for ^{208}Pb(n, γ_0). The TUNL data (·) and the data from ref. [9]) (×) are compared to DSD model calculations using a real form factor (dashed line) V_1 = 75 MeV, and a complex form factor (solid line) V_1 = 75 MeV, W_1 = 125 MeV. The PRM calculations with a real form factor (dotted line) V_1 = 132 MeV, and a complex form factor (dot-dashed line) V_1 = 132 MeV, W_1 = 132 MeV are also shown. Other parameters of the calculations are given in ref. [13]). The error bars include the uncertainties due to background subtraction and stripping procedures as well as the statistical uncertainties associated with the data points.

(OVER)

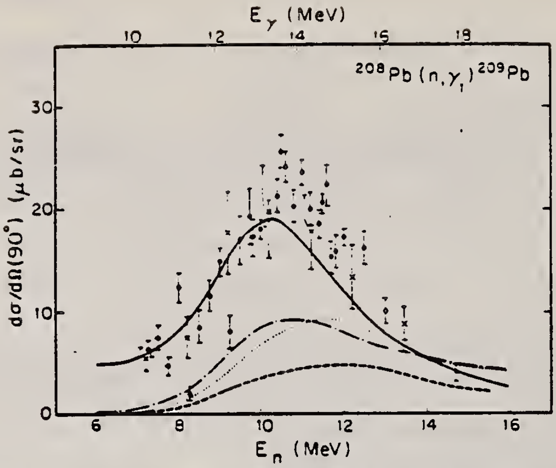

Fig. 4. The differential cross sections measured at 90° for ^{208}Pb(n, γ_1). The notation for the data and model calculations is the same as in fig. 3.

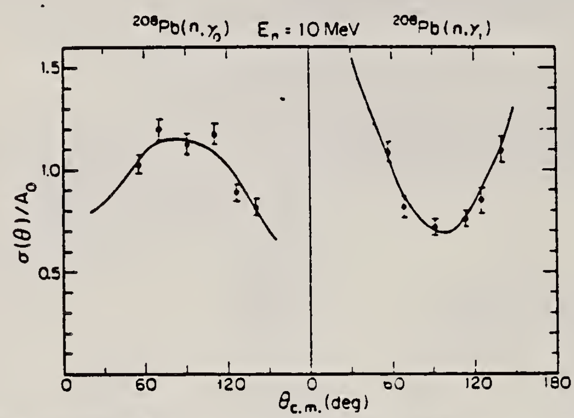

Fig. 5. Angular distributions for ^{208}Pb(n, γ) at 10.0 MeV neutron energy and fits (solid line) to the data using Legendre polynomial expansions. The angular distribution coefficients are given in table 1.

TABLE 1

Angular distribution coefficients obtained from the data. the errors are discussed in the text

E_n (MeV)	γ_0		γ_1	
	a_1	a_2	a_1	a_2
10	0.10 ± 0.06	-0.42 ± 0.12	0.15 ± 0.07	0.60 ± 0.10
10.5		-0.67 ± 0.16		0.31 ± 0.17
11	0.24 ± 0.07	-0.56 ± 0.09	0.10 ± 0.09	0.34 ± 0.10
11.5		-0.55 ± 0.12		0.33 ± 0.20
11.7		-0.39 ± 0.20		0.50 ± 0.16
12		-0.83 ± 0.14		0.43 ± 0.16
12.5	0.20 ± 0.08	-0.15 ± 0.15	0.22 ± 0.09	-0.03 ± 0.14
13	0.19 ± 0.12	-0.70 ± 0.17	-0.09 ± 0.11	-0.16 ± 0.21

# BISMUTH
Z=83

Bismuth was probably not recognized as a specific metal by the early orientals, Greeks, or Romans, but by the Middle Ages, Europeans were becoming aware of its special nature. Basil Valentine, in the Fifteenth Century referred to it as wismut (from the German Weissmuth, "white matter"). Georgus Agricola, at the end of the sixteenth Century, Latinized wismuth to bisemutum. It was not until 1739 that J. H. Pott first demonstrated the characteristic properties of bismuth.

BI
A=209

BI
A=209

Ref. F. Ferrero, A.O. Hanson, R. Malvano, C. Tribuno
Nuovo Cimento 4, 418 (1956)

Elem. Sym.	A	Z
Bi	209	83

Method

Betatron; threshold detector

Ref. No.	
56 Fe 1	EGF

Reaction	E or ΔE	E_0	Γ	$\int \sigma dE$	$J\pi$	Notes
(γ,n)	Bremss. 30					

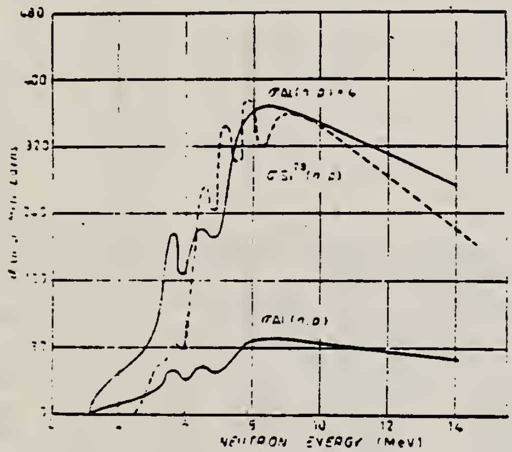

Fig. 2. (n, p) cross sections for ^{27}Al and ^{28}Si.

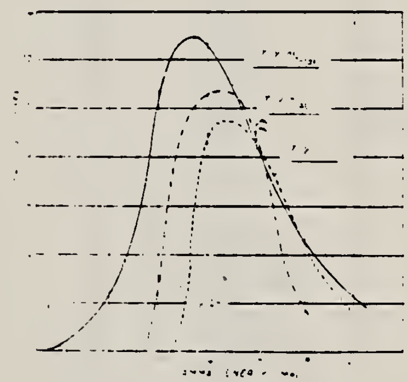

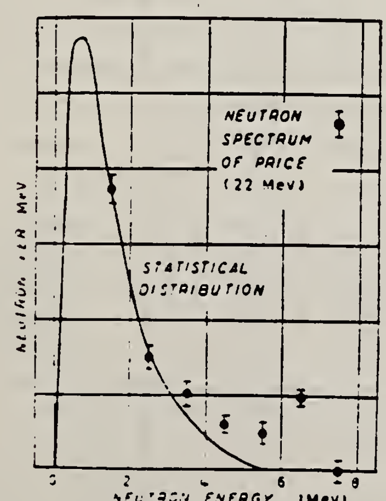

Fig. 5. Energy spectrum of the photoneutrons from bismuth at 22 MeV as observed by Price.

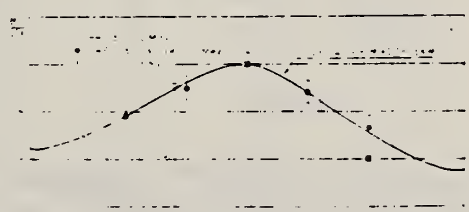

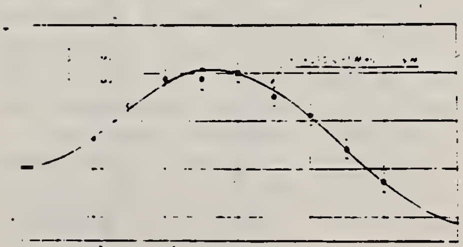

Ref. E.G. Fuller, E. Hayward
Phys. Rev. 101, 692 (1956)

Elem. Sym.	A	Z
Bi	209	83

Method
Betatron; photon scattering; NaI spectrometer

Ref. No.
56 Fu 1 | NVB

Reaction	E or ΔE	E_0	Γ	∫σdE	Jπ	Notes
$Bi^{209}(\gamma,\gamma)$	Bremss. 4-40					Detector at 120°. Cross sections given here are 13% too high due to erroneous cos θ factor in denominator of Eq. 5. [See footnote 8 in Phys. Rev. 106, 993 (1957)].

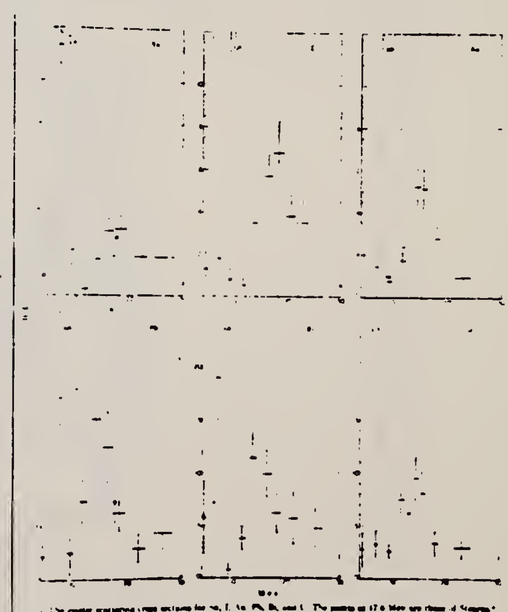

L. R. Gaerttner and G. L. Yeater, Phys. Rev. 76, 363 (194[illegible]
Dressel, Goldhaber, and Hanson, Phys. Rev. 77, 754 (1950)
M. B. Stearns, Phys. Rev. 87, 706 (1952).

B.I. Gavrilov, L.E. Lazareva
Zhur. Eksp. i Teor. Fiz. 30, 855 (1956);
Soviet Phys. JETP [illegible] 571 (1957)

Elem. Sym.	A	Z
Bi	209	83

Method: γ-Bremsstrahlung; synchrotron; BF_3 counter.

Ref. No.	
56 Ga 1	EGF

Reaction	E or ΔE	E_0	Γ	$\int \sigma dE$	Jπ	Notes 565
(γ,xn)	~ 7.5-27	13.9	5.9	3.96 MeV-b		
(μ_t)	~7.5-27	13.8	4.8	3.12 MeV-b		

TABLE I. Fundamental characteristics of photoneutron cross sections.

Element	$E_{\sigma_n\,max}$ in mev	$\sigma_{n\,max}$ in barns	Half width in mev	$\int_{E_n}^{E_0}\sigma_n(E)dE$ in mev-barns	$\int_{E_n}^{E_0}\sigma_n(E)dE:\sigma_{n\,max}$
Copper	17.2	0.126	4.3	0.93	7.4
Zinc	16.3	[illegible]	6.3	0.66	8.1
Cadmium	16.0	0.270	6.4	2.28	8.4
Iodine	15.5	0.288	6.0	2.35	8.2
Tantalum	14.5	[illegible]	6.8	3.87	8.6
Gold	14.2	0.571	6.0	4.37	7.6
Thallium	[illegible]	[illegible]	5.4	4.99	7.6
Bismuth	13.9	0.537	5.9	3.96	7.4
Thorium	14.5	0.798	5.6	6.33	8.0
Uranium	15.9	1.15	6.8	12.5	10.6

TABLE II. Threshold of photoneutron reactions (mev).

Element	(γ, n)	(γ, 2n)	(γ, 3n)	(γ, 4n)
Cadmium	6.7	14.6	23.0	>30
Iodine	9.4	16.2	26.0	32.9
Tantalum	7.6	13.9	21.6	28.2
Gold	8.1	14.9	23.9	⩾30
Thallium	7.5	14.0	22	28.8
Bismuth	7.4	14.2	22.5	29.6

TABLE III. Characteristics of the cross section of absorption of γ-quanta by nuclei.

Element	E_{res} in mev	$\sigma_\gamma(E=E_{res})$ in barns	half width in mev	$\int_{E_n}^{E_0}\sigma_\gamma dE$ in mev-barns	$\int_{E_n}^{E_0}\sigma_\gamma dE/0.06\times(ZN/A)$	$\int_{E_n}^{E_0}\sigma_\gamma(E)dE/E$	$\int_{E_n}^{E_0}\sigma_\gamma(E)dE/E^2$	$r_0\times10^{13}$ in cm
Cadmium	15.6	0.263	5.1	1.76	1.06	0.111	0.00745	1.26
Iodine	15.5	0.288	4.9	1.86	1.00	0.117	0.00768	1.16
Tantalum	13.9	0.448	4.5	2.74	1.05	0.190	0.0139	1.15
Gold	14.2	0.571	4.7	3.49	1.23	0.244	0.0182	1.23
Thallium	14.0	0.648	4.6	3.77	1.28	0.266	0.0200	1.25
Bismuth	13.8	0.537	4.9	3.12	1.04	0.230	0.0178	1.16

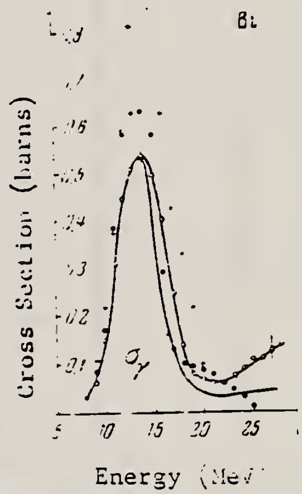

Figure 2: Photoneutron cross section σ_n, computed from the yield curves by the "photon difference method." "+" -- cross sections obtained in Reference 8 [Montalbetti, Katz and Goldemberg, Phys. Rev. 91, 659 (1959)]. For Cd, I, Ta, Au, Tl and Bi, curves are presented for the cross section of γ-quanta, computed from the statistical theory of nuclei. " " -- cross sections obtained in Ref. 9 [Nathans and Halpern, Phys. Rev. 93, 437 (1954)].

Ref. W. [illegible] Hartley, W.E. Stephens, E.J. Winhold
Phys. Rev. 104, 178 (1956)

Elem. Sym.	A	Z
Bi	209	83

Method: Li (p,γ) source, 480 kev protons; BF_3 counters

Ref. No.	
56 Ha 1	EGF

Reaction	E or ΔE	E_o	Γ	$\int \sigma dE$	Jπ	Notes
$Bi^{209}(\gamma,xn)$						Average Li cross section is 305 mb; cross section with detector response weighted for low energy neutrons, 280 mb. Assumed ratio 17.6/14.8 = 1.7. Calculated cross section at 14.8 and 17.6 MeV assuming cross section curves measured at Pennsylvania and Saskatchewan (refer Table I).

[illegible] for photoneutron [illegible] by the lithium gamma rays. The results are compared with previous data

[illegible]	Present [illegible] A	Present [illegible] B	[illegible]	Pennsylvania		Saskatchewan		[illegible]	[illegible]
[illegible]	18 mb	33 mb	37 mb			60 mb	0.5	23 mb	47 mb
[illegible]	40	4?	47	60 mb	0.5	95	0.5	30	60
[illegible]	23	25	23			40	0.7	22	32
[illegible]	56	51	55±12			95	0.6	45	75
[illegible]	48	45	48			90	0.7	38	54
[illegible]	175	170	135			240	1.0	175	175
[illegible]	200	170	180						
[illegible]	355	360	200	350	1.3	420	2.3	420 / 530	320 / 240
[illegible]	365	355	325						
[illegible]	330	295		315	1.7	480	1.9	440	235
[illegible]	365	340	290						
[illegible]	310	295	250	320	1.6	440	2.5	400 / 300	250 / 200
[illegible]	305	280	250	270	2.6	530	2.4	480	195

[illegible] 14.8 and 17.6 MeV [illegible] of the lithium gamma-ray lines.
[illegible] Ph.D. thesis, University of Pennsylvania, 1956 (unpublished).
[illegible] cross sections at 14.8 and 17.6 Mev as obtained from Group A data and 14.8/17.6 [illegible] cross-section ratios.
[illegible] 14.8/17.6 cross-section ratio from Pennsylvania [illegible] data.
[illegible] 14.8/17.6 cross-section ratio from Saskatchewan [illegible] data.

Ref. S. DeBenedetti, U. Farinelli, F. Ferrero, R. Malvano, G. Pelli, C. Tribuno
Nuovo Cimento 6, 682 (1957)

Elem. Sym.	A	Z
Bi	209	83

Method: Betatron; neutron yield; radioactivity; ion chamber

Ref. No.	
57 De 1	NVB

Reaction	E or ΔE	E_o	Γ	$\int \sigma dE$	Jπ	Notes
$Bi^{209}(\gamma,n-\gamma)$	Bremss. 10-30	1.43				E_o in energy Isomeric activity of Bi^{208} = 2.5 ms.

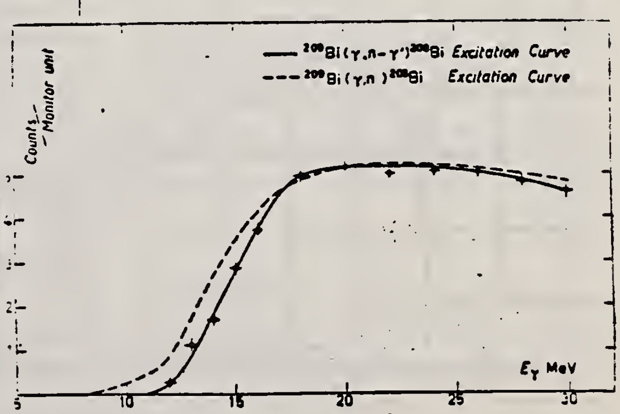

Fig. 2.

Ref. F. Ferrero, L. Gonella, R. Malvano, C. Tribuno, A.O. Hanson Nuovo Cimento $\underline{5}$, 242 (1957)	Elem. Sym. Bi	A 209	Z 83
Method 31 MeV betatron; neutron yield, angular distribution; threshold detector, $Si^{28}(n,p)Al^{27}$ reaction.	Ref. No. 57 Fe 1		EGF

Reaction	E or ΔE	E_0	Γ	$\int \sigma dE$	Jπ	Notes
Bi(γ,n!)	Bremss.					
	20					
	30					

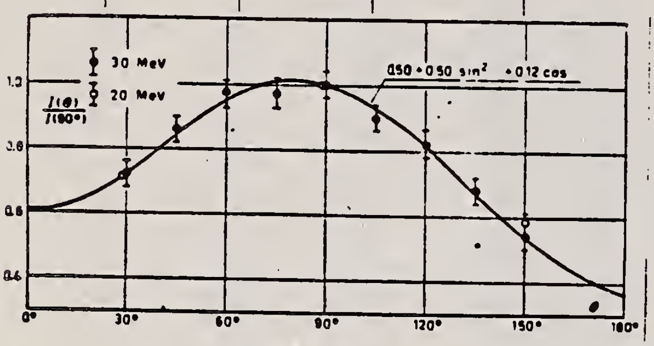

Fig. 7.

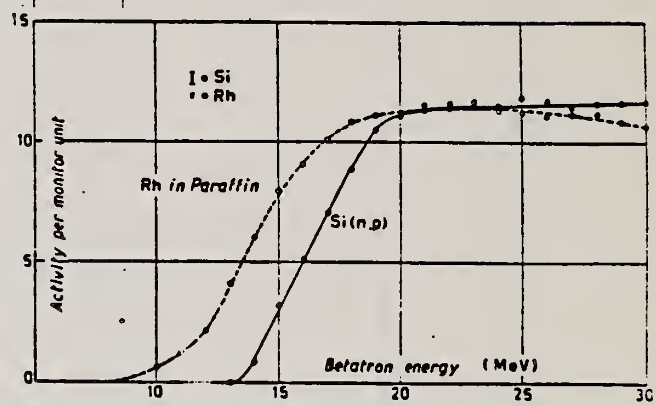

Fig. 2.

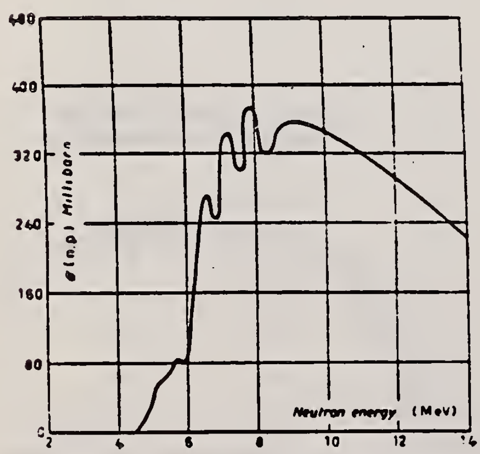

Fig. 1.

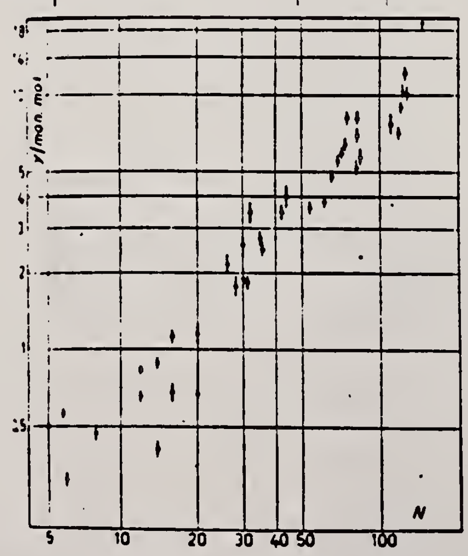

Fig. 8.

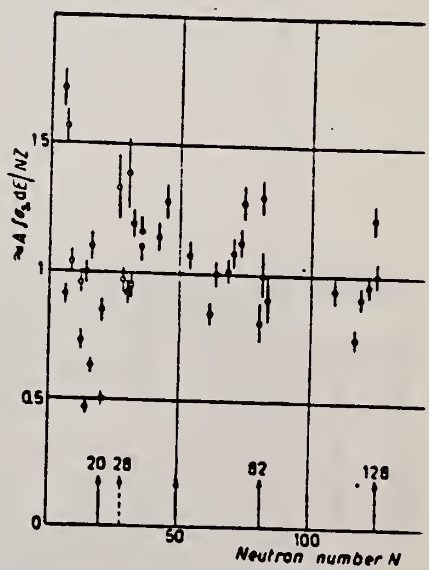

Fig. 9.

Ref.	Elem. Sym.	A	Z
G.N. Zatsepina, L.E. Lazareva, A.N. Pospelov Zhur. Eksp. i Teoret. Fiz. 32, 27 (1957); Soviet Phys. JETP 5, 21 (1957)	Bi	209	83

Method	Ref. No.	
Synchrotron; emulsions	57 Za 1	EGF

Reaction	E or ΔE	E_o	Γ	$\int \sigma dE$	$J\pi$	Notes
$Bi^{209}(\gamma,n)$	Bremss. 18.9					Neutrons measured at angles 30°, 90°, 150°.

FIG. 3. Spectrum of photoneutrons emitted from Bi at

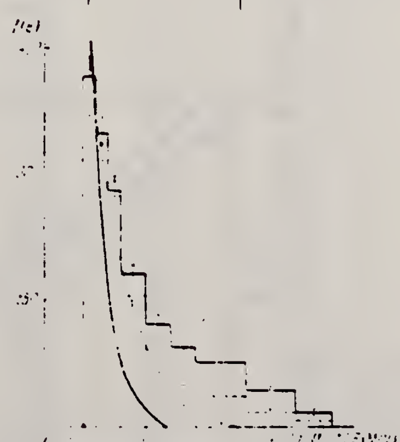

FIG. 2. Energy distribution of photoneutrons from Bi.

Relative neutron yields at different energies at 30°, 90° and 150° to the direction of the x-ray beam (per unit solid angle)*.

Energy interval, mev.	[illegible]	[illegible]	[illegible]
[illegible]	[illegible]	1 ± [illegible]	[illegible]
[illegible]	[illegible]	1 ± [illegible]	[illegible]
[illegible] – 11	[illegible]	1 ± [illegible]	[illegible]
[illegible] – 11	[illegible]	1 ± [illegible]	[illegible]
[illegible] – 11	[illegible]	1 ± [illegible]	[illegible]

* The neutron yield at 90° is taken as unity. The errors shown are statistical errors.

Ref. W. Bertozzi, F.R. Paolini, C.P. Sargent
Phys. Rev. 110, 790 (1958)

Elem. Sym.	A	Z
Bi	209	83

Method
MIT linear accelerator; time of flight

Ref. No.	
58 Be 2	EH

Reaction	E or ΔE	E_o	Γ	$\int \sigma dE$	Jπ	Notes
$Bi^{209}(\gamma,n)$	Bremss. ~ 14.3 ~ 15.8					Detector at 120°

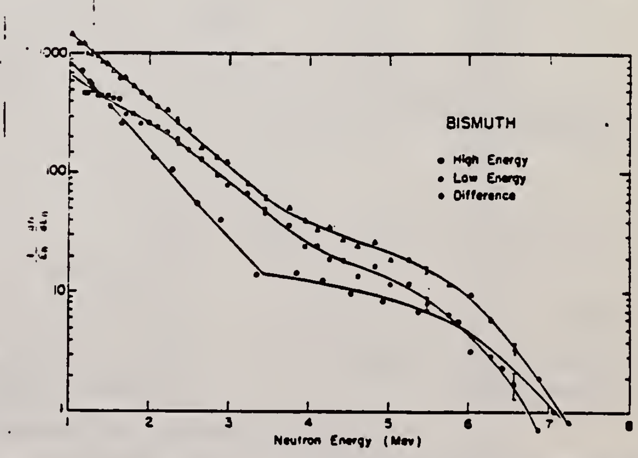

FIG. 1. Energy spectra $(1/E_n)dN/dE_n$ of photoneutrons from Bi for bremsstrahlung of maximum energies ~14.3 Mev and ~15.8 Mev, and difference spectrum.

L. Katz, G.B. Chidley
Nuclear Reactions at Low and Medium Energies (Academy of Science, USSR: 1958) 371

Bi	209	83

METHOD Betatron; neutron cross section; BF_3 counters; ion chamber monitor

REF. NO. 58 Ka 1 NVB

REACTION	RESULT	EXCITATION ENERGY	SOURCE TYPE	SOURCE RANGE	DETECTOR TYPE	DETECTOR RANGE	ANGLE
G,XN	ABX	8-22	C	8-22	BF3-I		4PI

Таблица 2

Пороги испускания фотонейтронов

Изотоп	B_n, Мэв	B_{2n}, Мэв	Изотоп	B_n, Мэв	B_{2n}, Мэв
V^{51}	11,16	20,5	L^{139}	8,81	16,1
Mn^{55}	10,14	19,2	Pr^{141}	9,46	17,6
Co^{59}	10,44	18,6	Tb^{159}	8,16	14,8
As^{75}	10,24	18,1	Ho^{165}	8,10	14,6
Y^{89}	11,82	20,7	Tm^{169}	8,00	14,7
Nb^{93}	8,86	17,1	Lu^{175}	7,77	14,2
Rh^{103}	9,46	16,8	Ta^{181}	7,66	13,8
J^{127}	9,14	16,2	Au^{197}	7,96	13,3
Cs^{133}	9,11	16,5	Bi^{209}	7,43	14,5

THRESHOLDS

не приведены, поскольку они превышают 22 *Мэв* во всех случаях, кроме золота, для которого $B_{3n}=21$ *Мэв*. Свойства сечений $\sigma_C(\gamma)$ сведены в табл. 3.

Таблица 1

Изотоп	$E_{макс}$, Мэв	$\sigma_м(E_\gamma)$, барн	Γ, Мэв	Σ^{22}, Мэв·барн	Y(22), 10^6 нейтрон/100 р·моль
V^{51}	18,4	0,062	5,2	0,33	1,62
Mn^{55}	20,2	0,060	7,0	0,39	2,01
Co^{59}	18,3	0,068	6,3	0,44	2,30
As^{75}	16,4	0,090	9,5	0,74	4,25
Y^{89}	17,1	0,172	5,2	0,93	5,33
Nb^{93}	18,0	0,156	7,5	1,17	6,80
Rh^{103}	17,5	0,160	9,4	1,40	8,28
J^{127}	15,2	0,273	6,8	1,76	11,9
Cs^{133}	16,5	0,238	7,7	1,59	10,7
La^{139}	15,5	0,325	3,8	1,55	11,2
Pr^{141}	15,0	0,320	4,9	1,93	13,1
Tb^{159}	15,6	0,274	9,8	2,49	18,1
Ho^{165}	13,5	0,305	8,9	2,52	18,7
Tm^{169}	16,4	0,250	8,4	1,91	14,9
Lu^{175}	16,0	0,225	8,4	1,90	23,0
Ta^{181}	14,5	0,380	8,5	3,15	22,0
Au^{197}	13,8	0,475	4,7	3,04	22,6
Bi^{209}	13,2	0,455	5,9	2,89	23,2

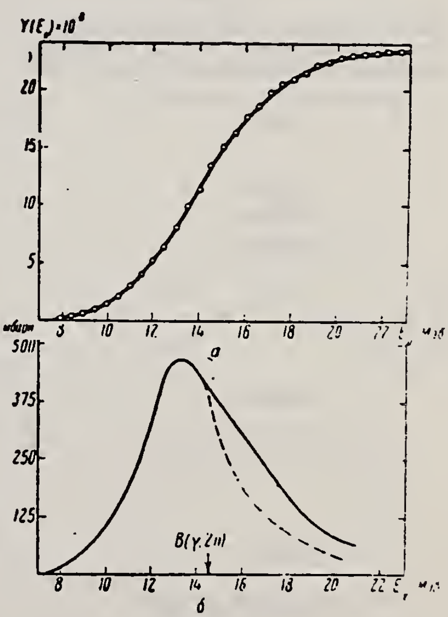

Рис. 17.

а — Выход фотонейтронов для Bi; б — $\sigma_м(E_\gamma)$ и $\sigma_C(\gamma)$ для Bi

Ref. V. Emma, C. Milone, A. Rubbino, A. Malvano Nuovo Cimento 17, 365 (1960)	Elem. Sym.	A	Z
	Bi	209	83
Method: Betatron; emulsions	Ref. No. 60 Em 1		JHH

Reaction	E or ΔE	E_0	Γ	∫σdE	Jπ	Notes
$Bi^{209}(\gamma,n)$	Bremss. 30					For $(4<E_n\leq 5)$MeV, neutron energy group, $I(\theta) = A+B \sin^2\theta$, where $B/A \simeq 0.7$

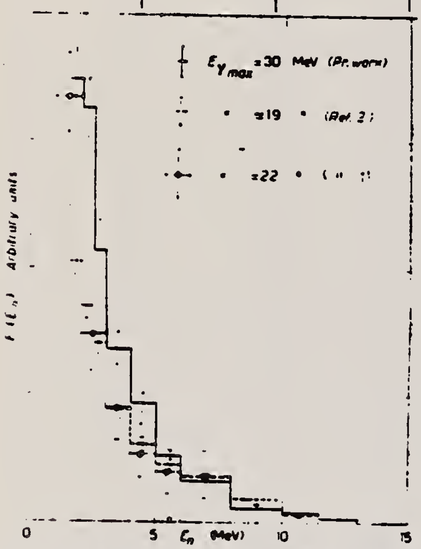

Fig. 3. - Comparison between the experimental spectra obtained at $E_{\gamma max}$=18.9 (2), 22 (4) and 30 MeV after normalization in the energy range (3 < E_n < 5) MeV

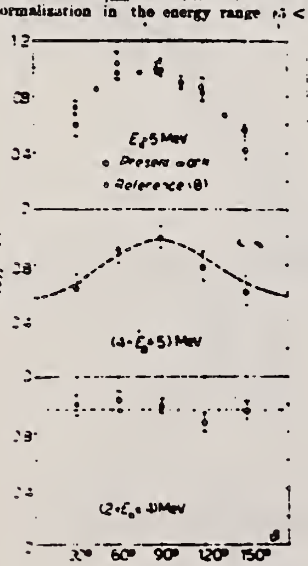

Fig. 4. - Experimental angular distribution of photoneutrons from ... for the various neutron ...

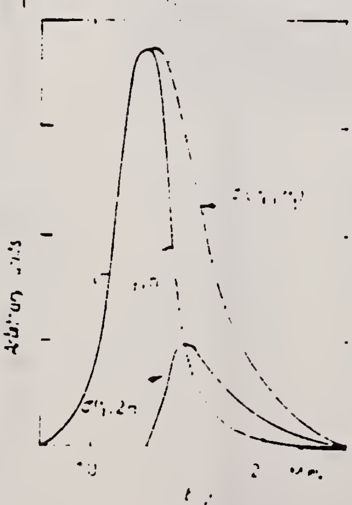

Fig. 5. - ... cross sections deduced ... photoneutron cross sections ... the statistical theory of nuclear reactions.

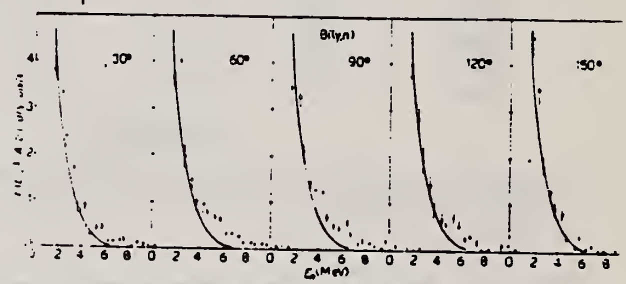

Fig. 2. - Energy spectra of the photoneutrons from Bi at angles θ=30°, 60°, 90°, 120° and 150°. The continuous curve is the calculated evaporative spectrum (see text).

TABLE III.

E. Silva, J. Goldemberg, P. B. Smith and L. Marquez: Nuovo Cim. ... (1958).
J. H. Carver and W. Turchinetz: Proc. Phys. Soc., 71, 613 (1958).
J. H. Carver and W. Turchinetz: Proc. Phys. Soc., 73, 110 (1959).
A. J. Berman and K. L. Brown: Phys. Rev., 96, 83 (1954).
F. Ferrero, R. Malvano, E. Silva, J. Goldemberg and G. Moscati: N. Phys., 10, 423 (1959).

REF.	ELEM. SYM.	A	Z
K.N. Geller, J. Halpern, E.G. Muirhead Phys. Rev. 118, 1302 (1960)	Bi	209	83

METHOD	REF. NO.	
Betatron; neutron threshold; ion chamber	60 Ge 3	NVB

REACTION	RESULT	EXCITATION ENERGY	SOURCE TYPE	SOURCE RANGE	DETECTOR TYPE	DETECTOR RANGE	ANGLE
G,N	NØX	THR	C	THR	BF3-I		4PI

THRESHØLD

TABLE I. Summary and comparison of neutron separation energies inferred from present threshold measurements with values predicted from mass data and reaction energies. All energies are expressed in the center-of-mass system in Mev.

Reaction	No. runs	Present results	Other results	Method	Reference
$Bi^{209}(\gamma,n)Bi^{208}$	42	7.432±0.010(calib)	7.430±0.050	LSA	a

a J. R. Huizenga, Physica 21, 410 (1955).

Ref. L.A. Kul'chitskii, V. Presperin
Zhur. Eksp. i Teoret. Fiz. 39, 1001 (1960);
Soviet Phys. JETP 12, 696 (1961)

Elem. Sym.	A	Z
Bi	209	83

Method

90 MeV Synchr.; proton recoil counter telescopes

Ref. No.	
60 Ku 2	JH

Reaction	E or ΔE	E_o	Γ	$\int \sigma dE$	Jπ	Notes
$Bi^{209}(\gamma,n)$	Bremss.; $E_{\gamma max}$=90MeV					Relative yields in table are per nuclear neutron.

Element	Relative neutron yield	Element	Relative neutron yield
Li	1.00±0.05	Cu	0.37±0.02
Be	1.22±0.09	Cd	0.35±0.02
O	0.74±0.05	I	0.39±0.02
Al	0.49±0.03	Bi	0.41±0.0[illegible]
Ca	0.33±0.02		

Ref. K. Reibel, A.K. Mann Phys. Rev. 118, 701 (1960)	Elem. Sym. Bi	A 209	Z 83
Method: γ's from $F^{19}(p,\alpha\gamma)$ reaction; protons from VandeGraaff; AnI.	Ref. No. 60 Re 1		JHH

Reaction	E or ΔE	E_o	Γ	∫σdE	Jπ	Notes
$Bi^{209}(\gamma,\gamma)$	$E_p = 2.05$					$\langle\bar{\sigma}\rangle = 17.5 \pm 1.3$ mb
						D (average level spacing based on J):
					7/2	3.9 ± 3.7 kev
					9/2	3.1 ± 2.9 kev
					11/2	2.6 ± 3.5 kev
						$\bar{\Gamma}_{\gamma o}/\bar{\Gamma}_{\gamma} = 0.3 \pm 0.2$
						$\bar{\Gamma}_{\gamma} = 2.5 \pm 1.5$ eV
						$\bar{\Gamma}_{\gamma o} = 0.75 \pm 0.5$ eV
	$E_p = 2.40$					$\langle\bar{\sigma}\rangle = 12 \pm 2$ mb
	$E_\gamma = 6.9$					$\langle\bar{\sigma}\rangle = 10 \pm 2$ mb
	$E_\gamma = 7.1$					$\langle\bar{\sigma}\rangle = 19 \pm 4$ mb

REF.	ELEM. SYM.	A	Z
R.G. Baker, K.G. McNeill Can. J. Phys. 39, 1158(1961)	Bi	209	83

METHOD	REF. NO.	
betatron; fast neutron yield; angular distribution; Al and Si threshold detectors; ion chamber	61 Ba 2	NVB

REACTION	RESULT	EXCITATION ENERGY	SOURCE TYPE	SOURCE RANGE	DETECTOR TYPE	DETECTOR RANGE *	ANGLE
G,XN	ABY	THR-22	C	22	THR-I	3-+	DST
G,XN	ABY	THR-22	C	22	THR-I	5-+	DST

In Tables 2 and 4:

$\bar{\sigma}$ = average cross section of detector weighted with neutron spectrum .

Φ = neutrons/100 roentgen/mole

$$W(\theta) = a_o \sum_{n=1}^{\infty} [1 + A_n P_n (\cos \theta)]$$

* "3-+" is the detector range of Aluminum and "5-+" of Silicon.

TABLE II

Normalized yields for aluminum detectors

Element	Al(n,γ) reaction 30°	90°	150°	a_0	Al(n,p) reactions 30°	60°	90°	a_0	a_1	a_2	$(\bar{\sigma}\Phi)^* \times 10^9$
Bismuth	399	567±130	620	541±85	3632	5139±290	3168	4366±185	0.06±0.06	−0.35±0.1	17.76
	478	423±130	641	484±85	2562	5353±290	2955	4144±185	−0.05±0.06	−0.53±0.1	16.87
Lead	426	312±120	725	429±77	3123	5754±260	3154	4591±166	−0.004±0.05	−0.51±0.07	18.68
Tantalum	378	367±190	688	441±122	2757	3024±425	2088	2757±275	0.14±0.14	−0.19±0.17	11.22
Lanthanum	208	222±110	330	243±70	2139	3371±250	1891	2768±160	0.05±0.07	−0.43±0.10	11.27
Arsenic	77	100±50	108	97±32	788	937±115	764	865±74	0.02±0.11	−0.16±0.14	3.52
Copper	13	65±30	70	55±20	710	748±70	569	700±45	0.11±0.08	−0.14±0.11	2.85

*$(\bar{\sigma}\Phi) = 4.07 \times 10^4 a_0$ millibarn-neutron.

TABLE IV

I Element	II a_0	III a_1	IV a_2	V $(\bar{\sigma}\Phi)\times 10^{9*}$	VI Φ_{total} (22 Mev)$\times 10^9$	VII Φ_{fast}/Φ_{total}
Vanadium	245 (1±0.06)	0.01±0.08	−0.00±0.10	6.05	0.21	0.12
Chromium	164 (1±0.03)	0.04±0.04	−0.05±0.05	4.05	0.17	0.10
Manganese	308 (1±0.02)	0.07±0.03	−0.09±0.04	7.61	0.25	0.12
Iron	200 (1±0.03)	0.05±0.04	−0.17±0.05	4.94	0.18	0.11
Cobalt	390 (1±0.02)	0.08±0.03	−0.22±0.04	9.63	0.26	0.15
Nickel	145 (1±0.05)	0.07±0.07	−0.23±0.09	3.58	0.12	0.12
Copper	347 (1±0.02)	0.05±0.03	−0.29±0.04	8.57	0.30	0.12
Arsenic	482 (1±0.03)	0.11±0.04	−0.24±0.05	11.91	0.33	0.15
Rubidium	638 (1±0.05)	0.13±0.06	−0.14±0.08	15.76		
Strontium	409 (1±0.05)	0.10±0.06	−0.17±0.08	10.10		
Yttrium	290 (1±0.10)	0.08±0.12	−0.12±0.15	7.16		
Silver	590 (1±0.04)	0.10±0.06	−0.22±0.08	14.57	0.87	0.07
Cadmium	905 (1±0.02)	0.02±0.02	−0.26±0.03	22.35		
Iodine	1133 (1±0.03)	0.04±0.04	−0.29±0.05	27.99	1.42	0.08
Barium	1048 (1±0.04)	0.10±0.06	−0.38±0.08	25.89		
Lanthanum	1595 (1±0.02)	0.02±0.03	−0.42±0.04	39.40	1.04	0.15
Cerium	1316 (1±0.05)	0.05±0.06	−0.39±0.08	32.50		
Dysprosium	1652 (1±0.08)	0.04±0.10	−0.34±0.13	40.80		
Tantalum	1558 (1±0.02)	0.04±0.03	−0.22±0.04	38.48	2.50	0.06
Tungsten	1365 (1±0.02)	−0.07±0.03	−0.24±0.04	33.71		
Mercury	1345 (1±0.02)	0.04±0.03	−0.31±0.04	33.22		
Lead	2274 (1±0.01)	0.02±0.02	−0.42±0.03	56.17	2.72	0.08
Bismuth	2162 (1±0.02)	0.05±0.03	−0.45±0.04	53.40	3.36	0.06
Thorium	3031 (1±0.04)	0.06±0.05	−0.32±0.07	74.87		
Uranium	4630 (1±0.02)	0.05±0.03	−0.17±0.04	114.36		

*$(\bar{\sigma}\Phi) = 2.47 \times 10^7 a_0$ millibarn-neutron. Errors are standard errors due to counting statistics only.

REF.

A. Bussiere de Nercy
Ann. Phys. (Paris) Third Series 6, 1379 (1961)

ELEM. SYM.	A	Z
Bi	209	83

METHOD

REF. NO.	
61 Bu 4	egf

REACTION	RESULT	EXCITATION ENERGY	SOURCE		DETECTOR		ANGLE
			TYPE	RANGE	TYPE	RANGE	
G,G	ABX	10-25	C	22	NAI-D		DST

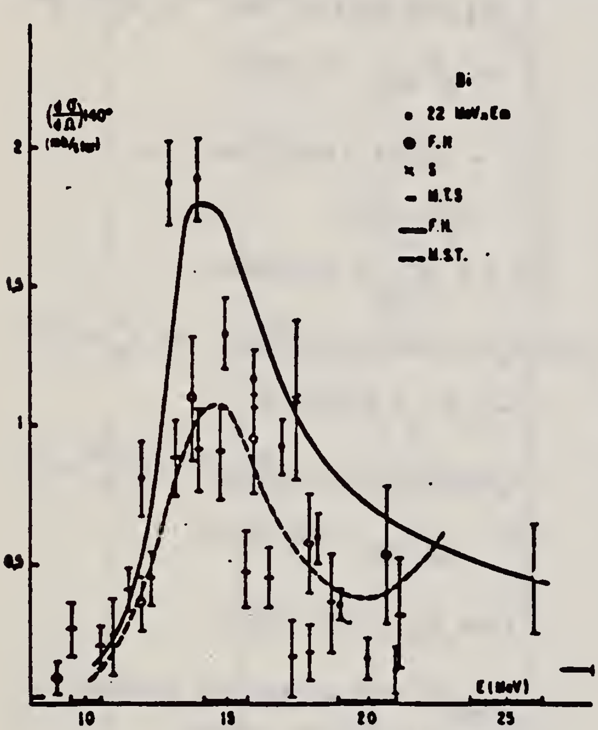

les représentent les sections efficaces prévues par la relation de dispersion.

Fig. 26. — Section efficace différentielle de diffusion (γ, γ) à 140° pour le bismuth.

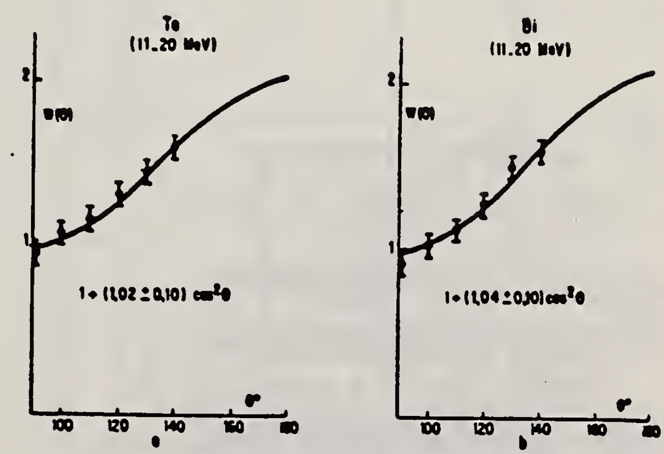

Fig. 27. — Distribution angulaire des photons diffusés par le tantale (a) et le bismuth (b) (11-20 MeV).

Ref. H.G. DeCarvalho, A. Celano, G. Cortini, R. Rinzivillo, G. Ghigo Nuovo Cimento 10, 187 (1961) | Elem. Sym. | A | Z

Ref. H. Crannell, R. Helm, H. Kendall, J. Oeser, M. Yearian
Phys. Rev. 123, 923 (1961)

Elem. Sym.	A	Z
Bi	209	83

Ref. No.	
61 Cr 1	JHH

Method Linac; Čerenkov counter telescope

Reaction	E or ΔE	E_o	Γ	$\int \sigma dE$	Jπ	Notes
$(e^-,e^{-\prime})$	183	2.60			3/2+	Measured γ transition rate Γ_m: $\Gamma_m=(1.5\pm0.47)\text{X}10^{11}\text{sec}^{-1}$ if $I_e^{E3}=\frac{15}{2}$ $G=\Gamma_m/\Gamma_{sp}=54.2\pm17.$ $\Gamma_m=(6.0\pm1.9)\text{X}10^{11}\text{sec}^{-1}$ if $I_e^{E3}=3/2$ $G=\Gamma_m/\Gamma_{sp}=110.0\pm34.$
		4.30			1/2+	$\Gamma_m=(9.74\pm3.4)\text{X}10^{8}\text{sec}^{-1}$ if $I_e^{E4}=17/2$ $G=\Gamma_m/\Gamma_{sp}=27.4\pm9.6$ $\Gamma_m=(8.75\pm3.1)\ \text{X}10^{9}\text{sec}^{-1}$ if $I_e^{E4}=1/2.$ $G=\Gamma_m/\Gamma_{sp}=269.0\pm9.5.$ Fits R_o = 1.20 fermi. (Γ_{sp} = single-particle estimate of the γ transition rate).

FIG. 17. Energy-level diagram for Bi^{209} showing the known excited states below 4.5 Mev. The spin assignments in brackets are the lowest values compatible with the assigned transition multipolarities. It is expected that the electron excitation process may excite groups of states with an energy spacing less than about 200 kev. The consequences of excitation of groups of states, unresolved in the present experiment, are not incorporated in the diagram but are described in the text.

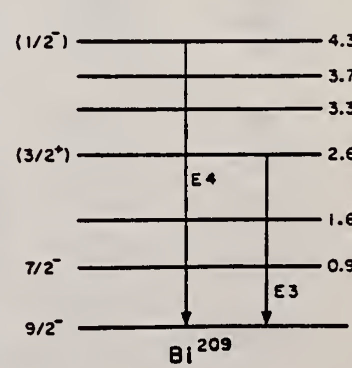

Ref. H.G. DeCarvalho, A. Celano, G. Cortini, R. Rinzivillo, G. Ghigo
Nuovo Cimento 19, 187 (1961)

Elem. Sym.	A	Z
Bi	209	83

Method Sychrotron; emulsions

Ref. No.	
61 De 2	JHH

Reaction	E or ΔE	E_o	Γ	$\int \sigma dE$	Jπ	Notes
$Bi^{209}(\gamma, f)$	300 - 1000 MeV					Slope = $\frac{d\,\sigma_Q^F}{d\ell nE}$ = 6.5×10^{-27} cm^2 ±10% over range 300-1000 MeV.

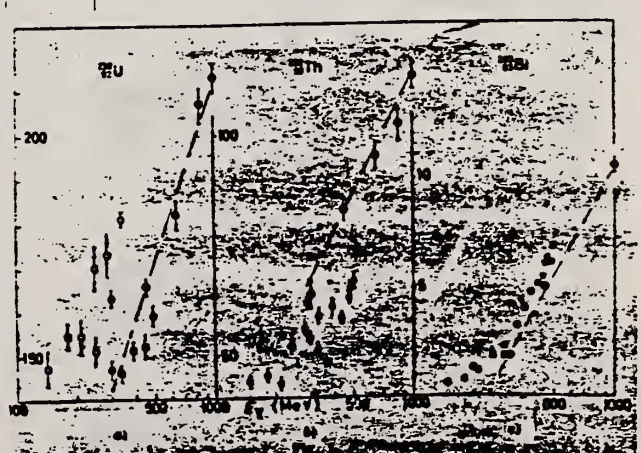

REF.	ELEM. SYM.	A	Z
J. Miller, C. Schuhl, C. Tzara J. Phys. Radium <u>22</u>, 529 (1961)	Bi	209	83

METHOD	REF. NO.	
Positron annihilation; neutron cross section; BF_3 counter; ion chamber	61 Mi 1	NVB

REACTION	RESULT	EXCITATION ENERGY	SOURCE		DETECTOR		ANGLE
			TYPE	RANGE	TYPE	RANGE	
G,G	ABX	10-21	D	10-21	NAI-D	10-22	DST
G,XN 469	ABX	8-22	D	8-22	BF3-I		4PI

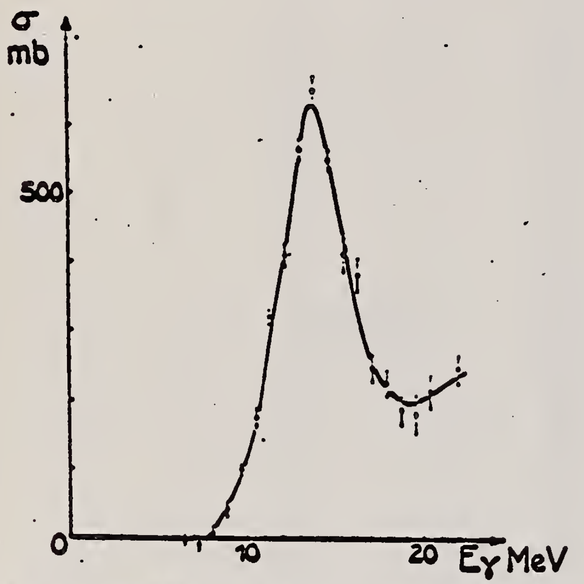

Fig. 2a. — Bismuth, $\sigma(\gamma, n) + 2\sigma(\gamma, 2n) + \sigma(\gamma, np) + \ldots$

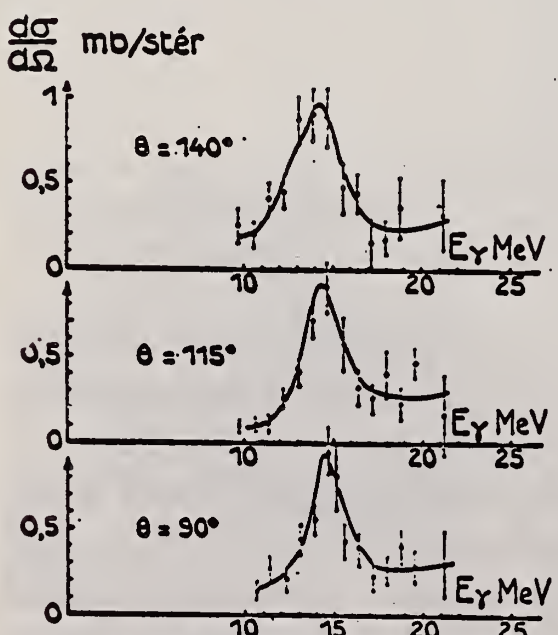

Fig. 6. — Distribution angulaire des photons diffusés élastiquement sur Bi.

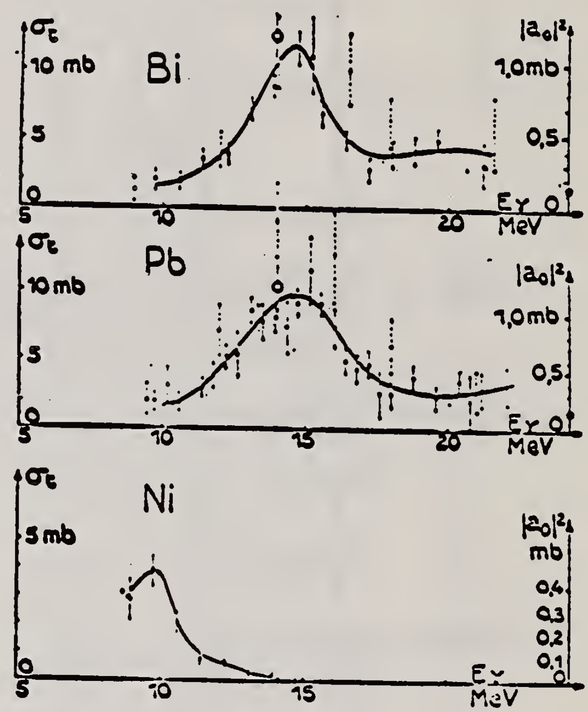

Fig. 8. — Section efficace totale de diffusion élastique et module au carré de l'amplitude de diffusion vers l'avant. Cas de Ni, Pb et Bi.

Cercles vides : module au carré des amplitudes de diffusion absorptive calculées à partir des sections efficaces $\sigma(\gamma, n) + 2\sigma(\gamma, 2n) + \sigma(\gamma, np) + \ldots$ (seule la première réaction intervient vers (14 MeV).

Cercles pleins : limites $(Ze^2/Mc^2)^2$ de la section efficace de diffusion à haute énergie. En réalité, à cause des interactions mésoniques des nucléons et de l'incertitude sur la limite à haute énergie de la diffusion, il vaudrait mieux parler de la section efficace de diffusion vers l'avant au delà de la résonance géante et avant le seuil photomésonique ; on peut montrer que l'expression

$$(Ze^2/Mc^2)^2 (1 + 0{,}8x)^2$$

où x est la fraction de force d'échange entre nucléons, est mieux appropriée.

En pointillés : résultats de Fuller et Hayward.

U.S. DEPARTMENT OF COMMERCE
NATIONAL BUREAU OF STANDARDS

Ref. F. Tagliabue, J. Goldemberg
Nuclear Phys. 23, 144 (1961)

Elem. Sym.	A	Z
Bi	209	83

Method 22 MeV betatron; $Si^{28}(n,p)Al^{28}$ threshold detector.

Ref. No.	
61 Ta 1	JHH

Reaction	E or ΔE	E_0	Γ	$\int \sigma dE$	Jπ	Notes
$Bi^{209}(\gamma,n)$	Bremss. 22					$E_n > 6$ MeV. $W(\theta_n) = A + B \sin^2\theta$ where B/A = 1.1±0.15 Consistent with detailed calculation according to Ferrero, et al [Nuovo Cimento 4, 418 (1956)] which gives $W(\theta) = 1 + 0.90 \sin^2\theta$.

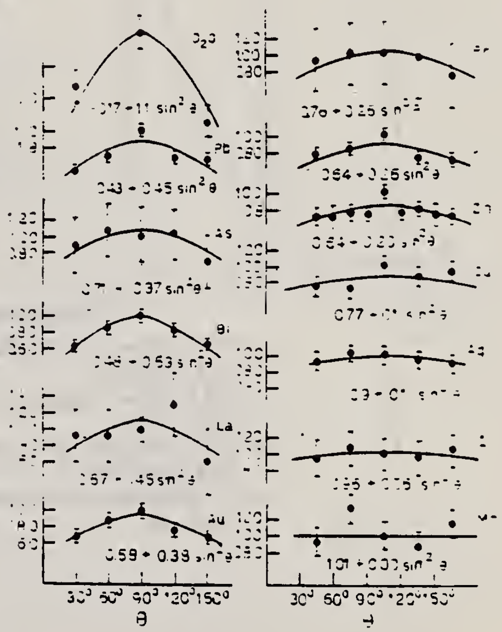

Figure 4: Angular distributions of fast photoneutrons as observed with the $Si^{28}(n,p)Al^{28}$ detector. D^A^ta normalized at 90° in each case.

Ref.	Elem. Sym.	A	Z
T. Tohei, M. Sugawara, S. Mori, M. Kimura J. Phys. Soc. Japan 16, 1657 (1961)	Bi	209	83

Method	Ref. No.	
25 MeV betatron; photon scattering; NaI(Tℓ) spectrometer; ion chamber	61 To 1	NVB

Reaction	E or ΔE	E_0	Γ	$\int \sigma dE$	Jπ	Notes
$Bi^{209}(\gamma,\gamma)$	Bremss. 5-12	8.0				Detector at 120° Table II from J. Phys. Soc. Japan 18, 17-22 (1963)

References

1) E. G. Fuller and E. Hayward: Phys. Rev. **101** (1956) 692.
2) see E. Segre: *Experimental Nuclear Physics*, vol. 1, p. 346.
3) J. S. Levin and D. J. Hughes: Phys. Rev. **101** (1956) 1328.
4) K. Reibel and A. K. Mann: Phys. Rev. **118** (1960) 701.

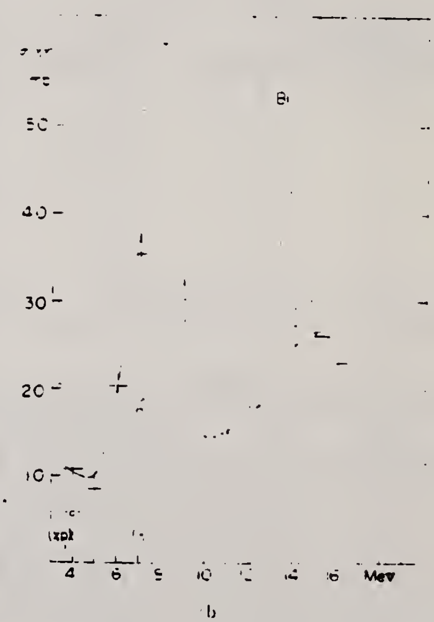

Fig. 9 The elastic scattering cross sections of photons. : data from Fuller and Hayward[1]. : data from monochromatic γ-rays[4].
a : σ(γ, γ) by Pb. The arrows indicate the positions of (γ, p) and (γ, n) threshold energies of isotopes. Numbers 1, 2 and 3 correspond to Pb, Pb and Pb.
b : σ(γ, γ) by Bi. The arrows indicate the positions of (γ, p) and (γ, n) threshold energies of Bi.

Ref. A. Wataghin, R.B. Costa, A.M. Freire, J. Goldemberg Nuovo Cimento 19, 864 (1961)	Elem. Sym. Bi	A 209	Z 83
Method: Betatron; emulsions (proton recoil tracks)	Ref. No. 61 Wa 1		JHH

Reaction	E or ΔE	E_o	Γ	$\int \sigma dE$	Jπ	Notes
$Bi^{209}(\gamma,xn)$	Bremss. 22					Neutron spectra at 30°, 90° and 150°. $I(\theta) = A + B \sin^2\theta + C \cos\theta$, where B/A, C/A are given in Table 1. B/A has peak at ~ 5.5 MeV (E_n).

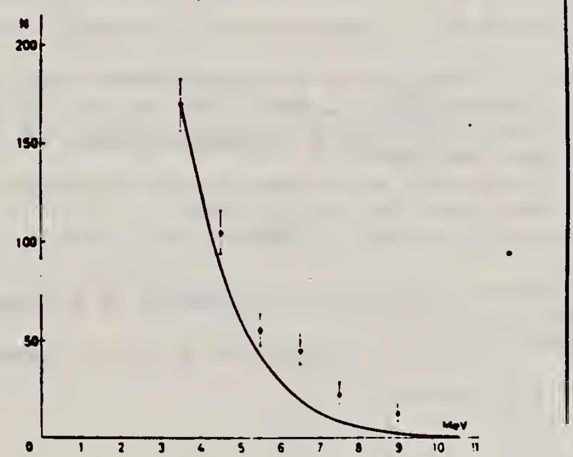

Fig. 2a. – Neutron energy spectrum for θ = [illegible]. Full line is evaporation spectrum.

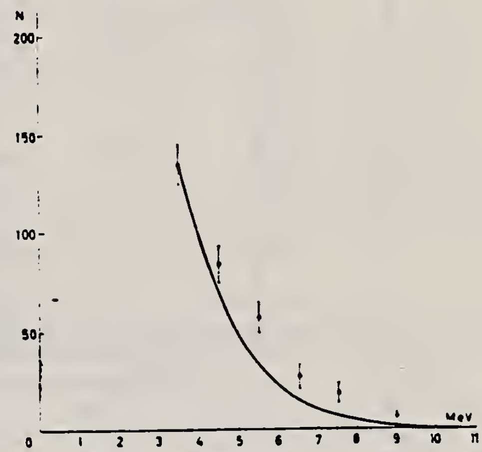

Fig. 2c. – Neutron energy spectrum for θ=150°. Full line is evaporation spectrum.

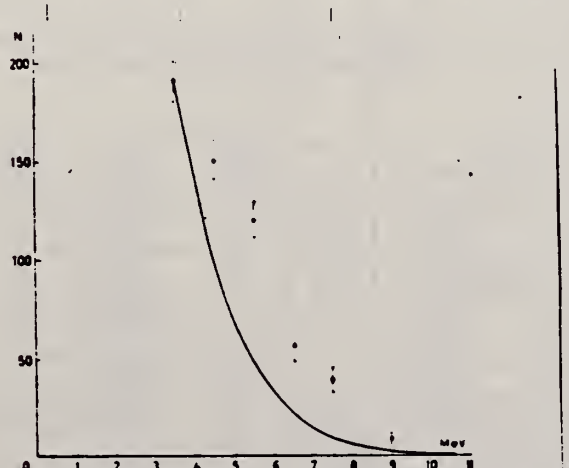

Fig. 2b. – Neutron energy spectrum for θ = [illegible]. Full line is evaporation spectrum.

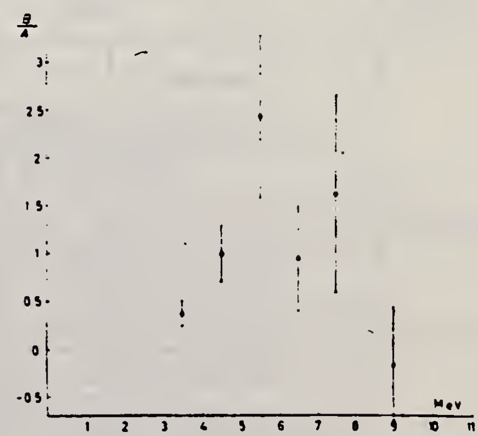

Fig. 3. – B/A as a function of the neutron energy on the assumption that the angular distribution $I(\theta)$ is described by the formula $I(\theta) = A + B \sin^2\theta + C \cos\theta$.

Ref.	PAGE 2	Elem. Sym.	A	Z
		Bi	209	83

Method

Ref. No. 61 Wa 1

Reaction	E or ΔE	E_o	Γ	∫σdE	Jπ	Notes

TABLE I. – *Number of events corrected and normalized.*

[illegible]

TABLE II. – *Measurements of B/A.*

E_{max}	Neutron energy interval (MeV)	B/A	Detector	Reference
22.6	> 3	0.86 ± 0.15	emuls.	This work
22.0	> 6	0.92 ± 0.41	emuls.	This work
18.9	> 4	2.0	emuls.	[illegible]
18.9	> 1.5	0.47	emuls.	[illegible]
20.0	> 6	6.9 ± 0.1	^{28}Si(n, p)^{28}Al	[illegible]
22	> 6	5.6	^{28}Si(n, p)^{28}Al	[illegible]
22	> 6	1.1 ± 0.15	^{28}Si(n, p)^{28}Al	[illegible]
30	> 6	1.0 ± 0.1	^{28}Si(n, p)^{28}Al	[illegible]
20	> 4	1.9 ± 0.5	^{27}Al(n, p)^{27}Mg	[illegible]
22	> 4	0.90 ± 0.10	^{27}Al(n, p)^{27}Mg	[illegible]
30	> 4	0.67 ± 0.1	^{27}Al(n, p)^{27}Mg	[illegible]
30	4÷5	~ 0.7	emuls.	(11)

(1) H. L. Poss: *Phys. Rev.*, 79, 539 (1950).

(2) F. Ferrero, A. O. Hanson, R. Malvano and C. Tribuno: *Nuovo Cimento*, 4, 418 (1956).

(3) G. N. Zatsepina, L. E. Lazareva and A. N. Pospelov: *Soviet. Phys. J.E.T.P.* 5, 21 (1957).

(4) V. Emma, C. Milone and R. Rinzivillo: *Nuovo Cimento*, 14, 1149 (1959).

(5) V. F. Weisskopf and D. H. Ewing: *Phys. Rev.*, 57, 472 (1940).

(6) R. S. White: Section 2-*D*, in *Fast Neutron Physics*, J. B. Marion and J. L. Fowler ed. (New York, 1960).

(7) F. Tagliabue and J. Goldenberg: private communication.

(8) G. A. Price: *Phys. Rev.*, 93, 1279 (1954).

(9) G. Cortini, C. Milone, A. Rubbino and F. Ferrero: *Nuovo Cimento*. 9, 85 (1958).

(10) B. B. Kinsey: of *Encyclopedia of Physics*, ed. by S. Flügge (Berlin, 1957), vol. 11 p. 296.

(11) V. Emma, C. Milone, A. Rubbino and R. Malvano: private communication,

Ref. O. Borello, F. Ferrero, R. Malvano, A. Molinari
Nuclear Phys. 31, 53 (1962)

Elem. Sym.	A	Z
Bi	209	83

Method
31 MeV betatron; threshold detectors: Aℓ(n,α), Si(n,p)

Ref. No.	
62 Bo 5	JHH

Reaction	E or ΔE	E_0	Γ	$\int \sigma dE$	Jπ	Notes
$Bi^{209}(\gamma,n)$	Bremss. 30					

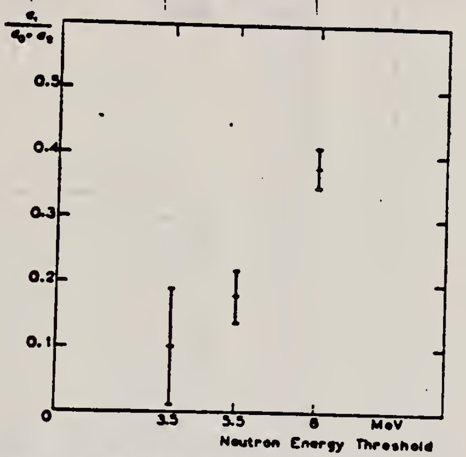

Fig. 1. The weighted means of the ratio $a_1/(a_0+a_2)$.

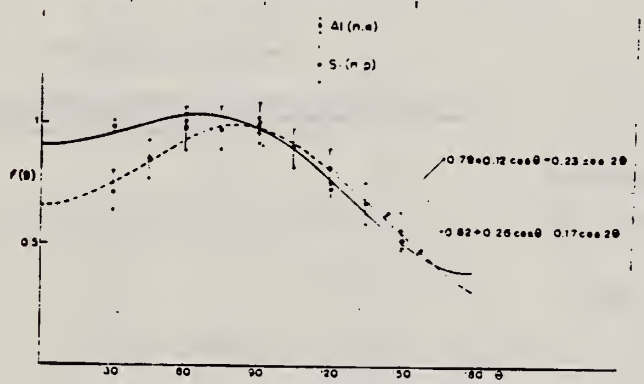

Fig. 3. The neutron angular distribution normalized at 90°

TABLE 1
Summary of experimental data

Ref.	Case	Maximum energy (MeV)	Fast neutron detectors	Neutron energies E_n (MeV)	B/A	$A+B\cos^2\theta+(C\cos\theta)$
[illegible]	a	[illegible]	$Al^{27}(n,p)Mg^{27}$	[illegible] 3.5	3.0 ±0.3	1 −3.0 cos²θ
[illegible]	b	[illegible]	$Si^{28}(n,p)Al^{28}$	≥3.5	3.0	1 −3.0 cos²θ
	c	[illegible]	$Al^{27}(n,p)Mg^{27}$	3.5	[illegible] ±0.1	1 [illegible] cos²θ
	d	10	$Al^{27}(n,p)Mg^{27}$	≥3.5		
[illegible]	e	[illegible]	$Si^{28}(n,p)Al^{28}$	≥3.5	[illegible] ±0.1	1 [illegible] cos²θ
	f	[illegible]	$Si^{28}(n,p)Al^{28}$	≥5.5	1.0 ±0.1	[illegible] cos²θ +0.13 cos θ
	g	[illegible]	$Al^{27}(n,p)Mg^{27}$	≥3.5	0.07 ±0.1	[illegible] cos²θ [illegible] cos θ
[illegible]	h	10.0	nuclear emulsions	≥1.3	0.4	1 [illegible] cos²θ
	i	10.0	nuclear emulsions	>6	2.0	1 −2.0 cos²θ
	j	10.0	nuclear emulsions	>7	2.1	1 −2.1 cos²θ
[illegible]	k	[illegible]	nuclear emulsions	$3 < E_n < 11$	1.33	[illegible] cos²θ [illegible] cos θ
[illegible]	l	[illegible]	nuclear emulsions	$3 < E_n <$ [illegible]		symmetry
	m	[illegible]	nuclear emulsions	$3 < E_n <$ [illegible]	0.7	1 +0.7 cos²θ
	n	[illegible]	nuclear emulsions	>6	[illegible]	[illegible] cos²θ −0.13 cos θ
[illegible]	o	[illegible]	$Si^{28}(n,p)Al^{28}$	≥5.5	1.4 ±0.15	1 +1.1 cos²θ
[illegible]	p	[illegible]	nuclear emulsions	>6	[illegible] ±0.15	1 +1.1 cos²θ +0.155 cos θ
[illegible]	q	[illegible]	$Si^{28}(n,p)Al^{28}$	≥5.5	angular distribution anisotropic and marked forward asymmetry	
Present work		[illegible]	$Al^{27}(n,p)Mg^{27}$	≥8	[illegible] ±0.05	[illegible] cos²θ [illegible] cos θ

TABLE 2
Values of $f(\theta)$

Refs.	Case	Neutron energy E_n (MeV)	$\frac{a_1}{a_0-a_2}$	$f(\theta)=a_0-a_1\cos\theta-a_2\cos 2\theta$
[illegible]	c	≥ 3.5	0.35±0.07	0.72 −0.16 cos θ −0.26 cos 2θ
[illegible]	g	≥ 3.5	0.05±0.03	0.78 −0.03 cos θ −0.19 cos 2θ
[illegible]	e	≥ 5.5	0.23 ±0.06	0.77 −0.07 cos θ −0.23 cos 2θ
[illegible]	f	≥ 5.5	0.14 ±0.11	0.76 −0.12 cos θ −0.23 cos 2θ
[illegible]	k	$3 < E_n < 11$	1.1 ±3.00	0.54 −0.09 cos θ −0.46 cos 2θ
[illegible]	n	> 3	0.35±0.18	0.71 −0.12 cos θ −0.37 cos 2θ
[illegible]	o	≥ 5.5	−0.02±0.09	0.75 −0.01 cos θ −0.22 cos 2θ
[illegible]	p	> 3	0.31 ±0.25	0.76 −0.16 cos θ −0.24 cos 2θ
Present work		≥ 8	0.38 ±0.03	0.82 −0.26 cos θ −0.17 cos 2θ

TABLE 3
Values of the weighted mean for the ratio $a_1/(a_0+a_2)$

Neutron energy (MeV) E_n	$\left(\frac{a_1}{a_0+a_2}\right)_{mean}$
≧ 3.5	0.10±0.09
≧ 5.5	0.18±0.04
≧ 8	0.38±0.03

References

1) V. de Sabbata, Nuovo Cim. 11 (1959) 225
2) S. Fujii and O. Sugimoto, Nuovo Cim. 12 (1959) 513
3) T. Ericson and V. Strutinsky, Nuclear Physics 8 (1958) 284
4) A. Molinari, Nuovo Cim. 18 (1960) 1296
5) H. L. Poss, Phys. Rev. 79 (1950) 539
6) G. A. Price, Phys. Rev. 93 (1954) 1279
7) F. Ferrero, O. A. Hanson, R. Malvano and C. Tribuno, Nuovo Cim. 4 (1956)
8) G. N. Zatsepina, L. E. Lazareva and A. N. Pospelov, JETP (Soviet Physics)5 (1957) 21
9) G. N. Zatsepina, V. V. Igonin, L. E. Lazareva and A. I. Lepestkin, Compt. Rend. du Congrès International de Physique Nucléaire 1958 (Dunod, Paris) p. 156
10) V. Emma and C. Milone, Nuovo Cim. 17 (1960) 365
11) F. Tagliabue and J. Goldemberg, Nuclear Physics 23 (1961) 144
12) A. Wataghin, R. B. Costa and J. Goldemberg, Nuovo Cim. 19 (1961) 864
13) G. C. Reinhardt and W. D. Whitehead, Bull. Amer. Phys. Soc. 6 (1961) 251
14) Whittaker and Robinson, The Calculus of Observations (Blackie and Son Ltd, London, 1958)
15) A. G. de Pinho Filho, Nuclear Physics 16 (1960) 271
16) J. Goldemberg, P. Dyal and J. O'Connell, private communication (1960)
17) J. Eichler and H. A. Weidenmuller, Z. für Phys. 152 (1958) 261
18) J. Sawicki, Nuclear Physics 6 (1958) 525
19) L. A. Kul'chitskii and V. Presperin, JETP (Soviet Physics) 12 (1961) 696
20) G. E. Brown and M. Bolsterly, Phys. Rev. Lett. 3 (1959) 472
21) H. W. Schmitt and J. Halperin, Phys. Rev. 121 (1961) 827
22) Baker and McNeill, Can. J. of Phys. 39 (1961) 1158
23) Reinhardt and Whitehead, private communication

Ref.		Elem. Sym.	A	Z
	E.G. Fuller, E. Hayward Nuclear Phys. 33, 431 (1962)	Bi	209	83

Method	Ref. No.	
50 MeV betatron; BF_3, NaI counters	62 Fu 4	JHH

Reaction	E or ΔE	E_0	Γ	$\int \sigma dE$	Jπ	Notes
$Bi^{209}(\gamma,\gamma)$	4.5-8.5					$\int$ corrected for multiple neutron production.
$Bi^{209}(\gamma,xn)$				$\int^{185} = 3.93$ MeV-b		Self-absorption measurements made at 7 MeV.

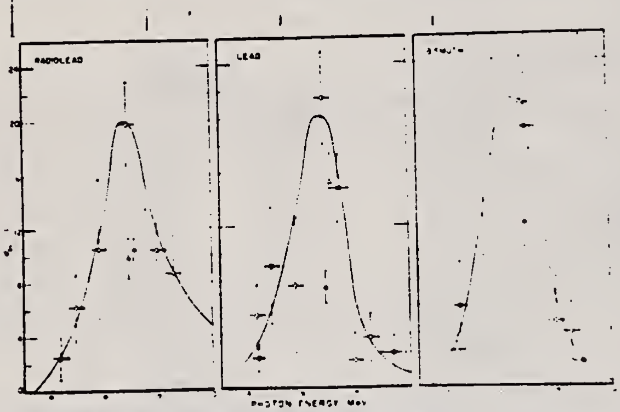

Fig. 1. The elastic scattering cross sections for lead, radiolead and bismuth. The indicated errors are based only on the number of counts. The [illegible] data obtained in an earlier experiment 3). The points [illegible] by triangles at [illegible] and [illegible] MeV are the results of Reibel and Mann 5).

Ref 3: Fuller & Hayward - Phys. Rev. 101, 692 (1956)

Ref 5: Reibel & Mann - Phys. Rev. 118, 701 (1960)

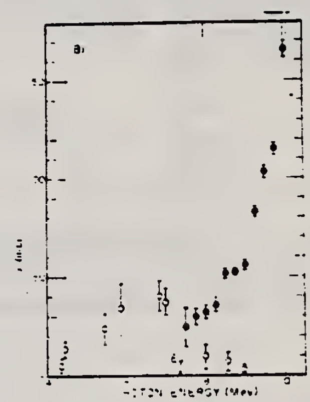

Fig. 9. The total absorption cross section for bismuth in the threshold region. The closed circles represent the (γ, n) cross section. The estimated total scattering cross section points are the open circles and the arrow indicates the (γ, n) threshold.

Table 1

Observed transmissions corrected for electronic absorption

Absorber	Thickness (g/cm²)	Targets: [illegible]	[illegible]	[illegible]
[illegible]	[illegible]			[illegible]
	[illegible]	[illegible]	[illegible]	
		[illegible]		
[illegible]	11.2	[illegible]	[illegible]	[illegible]
			[illegible]	
[illegible]	[illegible]	[illegible]	[illegible]	[illegible]
				[illegible]
[illegible]	[illegible]	[illegible]		[illegible]
[illegible]	[illegible]	[illegible]		[illegible]
[illegible]	[illegible]	[illegible]		[illegible]
[illegible]	[illegible]			[illegible]
[illegible]	[illegible]			[illegible]

*) Measured with both target and absorber at liquid nitrogen temperature

Table 3

Average level parameters at 6 MeV

	Lead	Radiolead	Bismuth
[illegible]	1.0	1 - 400	[illegible]
[illegible]	24—38	20—205	10—[illegible]
Γ (eV)	[illegible]	[illegible]	[illegible]
σ (max) (b)	[illegible]	205	[illegible]
[illegible]	0.1[illegible] - 0.21	0.14 - 1.0	0.2 - [illegible]
[illegible] MeV) (mb)	21	20	21
$\int$ σdE (MeV · mb)	42	40	48

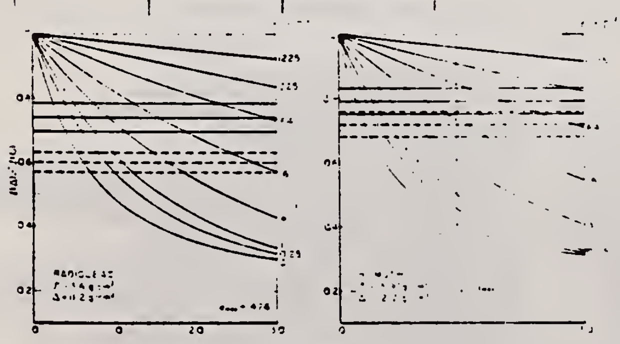

Fig. 5. Self-absorption attenuation curves for radio-lead and bismuth. The ratio [illegible] as defined in the text [illegible] has been evaluated as a function of the peak absorption cross section [illegible] for the target and absorber thicknesses used in the experiments. The horizontal lines represent the measured attenuations and their uncertainties for the experiments performed at room temperature (solid lines) and liquid nitrogen temperature (dashed lines). The quantity [illegible] is the maximum possible value of the average peak absorption cross section at 6 MeV [illegible] times the electronic absorption cross section. This maximum value assumes electric dipole scattering and represents an average over all possible spins for the excited states.

Ref. J. Miller, C. Schuhl, C. Tzara
Nuclear Phys. 32, 236 (1962)

Elem. Sym.	A	Z
Bi	209	83

Method
Linac; monoergic photons by e^{+} annihilation in flight; NaI

Ref. No.	
62 Mi 3	JHH

Reaction	E or ΔE	E_o	Γ	$\int \sigma dE$	Jπ	Notes
$Bi^{209}(\gamma, xn)$	8-22	14.0±0.5		$\int_0^{22} = 3.73\pm0.06$ MeV-b		

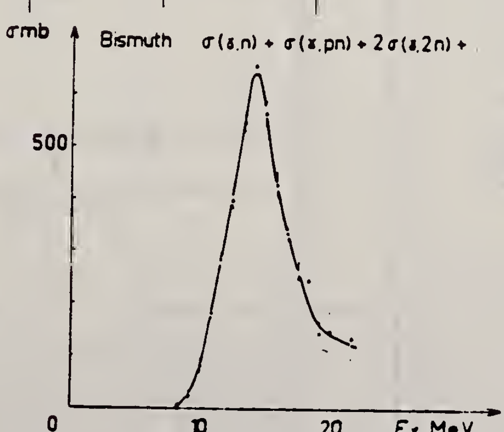

Fig. 12. Section efficace
$\sigma = \sigma(\gamma, n) + \sigma(\gamma, np) + 2\sigma(\gamma, 2n) + \ldots$ pour le bismuth.

Résultats expérimentaux

[illegible]								
209	12	14.0 ± 0.5	3.73 ± 0.06	1.21 ± 0.02	[illegible]	[illegible]	[illegible]	

[illegible]

Ref. G.C. Reinhardt, W.D. Whitehead
Nuclear Phys. 30, 201 (1962)

Elem. Sym.	A	Z
Bi	209	83

Method 55 MeV betatron; synchrotron; $Si^{28}(n,p)Al^{28}$ activity; $Cu^{63}(\gamma,n)Cu^{62}$ monitor.

Ref. No. 62 Re 1 — EGF

Reaction	E or ΔE	E_o	Γ	$\int \sigma dE$	Jπ	Notes
$Bi^{209}(\gamma,n)$	Bremss. 55					

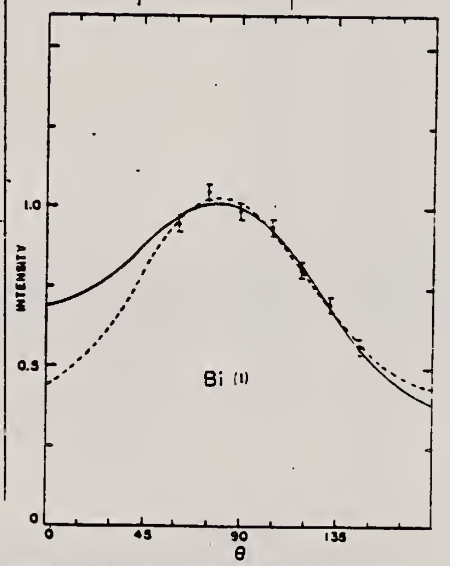

Fig. 5. Angular distribution of fast neutrons from bismuth with target 1. Dotted curve is of form $a_0 + a_1\cos\theta + a_2\cos^2\theta + a_3\cos^3\theta$. Solid curve is of form $a_0 + a_1\cos\theta + a_2\cos^2\theta$. Errors on points are statistical errors in counting only

Parameters of the fit [illegible]

	Bi(1)	Bi(2)	Pb	Au	[illegible]	[illegible]	[illegible]
a_0	1.00 ± 0.02	1.00 ± 0.02	1.00 ± 0.02	1.00 ± 0.02	1.00 ± [illegible]	1.00 ± 0.02	1.00 ± 0.01
a_1	0.15 ± 0.03	0.18 ± 0.04	0.17 ± 0.01	0.14 ± 0.01	[illegible]	[illegible]	0.14 ± 0.03
a_2	0.47 ± 0.06	0.10 ± 0.08	0.41 ± 0.09	0.21 ± 0.07	[illegible] ± 0.11	[illegible]	0.39 ± 0.06
[illegible]	0.18 ± 0.04	0.21 ± 0.05	0.20 ± 0.05	[illegible]	[illegible]	[illegible]	0.16 ± 0.03
A_2*	0.37 ± 0.05	0.34 ± 0.06	0.32 ± 0.07	[illegible]	[illegible]	[illegible]	0.30 ± 0.04
[illegible]	0.53 ± [illegible]	[illegible]	0.59 ± [illegible]	0.79 ± [illegible]	[illegible]	[illegible]	[illegible]
	0.47 ± 0.06	0.10 ± 0.08	0.41 ± 0.09	0.21 ± 0.07	[illegible] ± 0.11	0.14 ± 0.06	[illegible] ± 0.06
	0.15 ± 0.03	0.18 ± 0.04	0.17 ± 0.04	0.14 ± 0.03	0.17 ± [illegible]	0.12 ± 0.03	0.14 ± 0.03

* Renormalized so that $A_0 = 1$

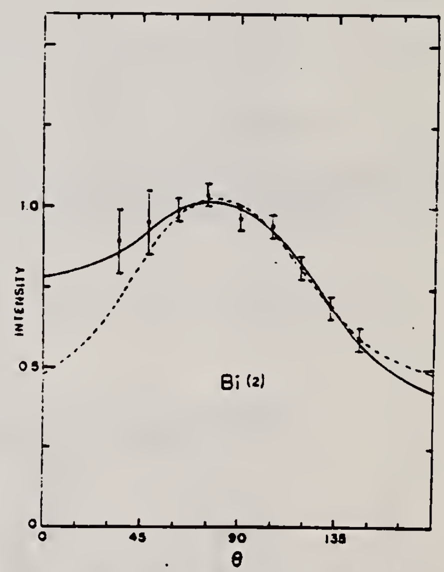

Fig. 6. Angular distribution of fast neutrons from bismuth with target 2. See fig. 5.

Table 4

Parameters of the fit (3) for the expressions $a_0 + a_1\cos\theta + a_2\cos^2\theta + a_3\cos^3\theta$, $1 + A_1P_1 + A_2P_2 + A_3P_3$

	Bi(1)	Bi(2)	Pb	Au	W	Ho	La
a_0	1.01 ± 0.02	1.00 ± 0.02	1.01 ± 0.03	0.98 ± 0.02	1.00 ± 0.03	1.00 ± 0.02	1.01 ± 0.02
a_1	0.19 ± 0.05	0.17 ± 0.07	0.21 ± 0.07	0.07 ± 0.06	0.16 ± 0.09	0.12 ± 0.05	0.17 ± 0.05
a_2	0.38 ± 0.11	0.37 ± 0.15	0.50 ± 0.16	0.05 ± 0.12	0.13 ± 0.20	0.33 ± 0.12	0.47 ± 0.11
a_3	−0.17 ± 0.18	0.05 ± 0.24	−0.17 ± 0.25	0.31 ± 0.19	0.05 ± 0.32	0.03 ± 0.19	−0.17 ± 0.17
A_1*	0.11 ± 0.15	0.23 ± 0.18	0.13 ± 0.20	0.27 ± 0.13	0.20 ± 0.22	0.15 ± 0.14	0.09 ± 0.13
A_2*	0.45 ± 0.09	0.28 ± 0.11	0.33 ± 0.12	0.03 ± 0.08	0.09 ± 0.14	0.21 ± 0.09	0.37 ± 0.09
A_3*	−0.08 ± 0.09	0.02 ± 0.11	−0.08 ± 0.12	0.13 ± 0.08	0.02 ± 0.13	0.01 ± 0.08	−0.08 ± 0.08

* Renormalized so that $A_0 = 1$

Ref. P.Axel, K.Min, N.Stein, D.C.Sutton

Phys.Rev.Letters 10, 299 (1963)

Elem. Sym.	A	Z
Bi	209	83

Method: Bremsstrahlung monochromator

Ref. No. 63Ax1 BG

Reaction	E or ΔE	E_o	Γ	$\int \sigma dE$	Jπ	Notes
(γ,γ)		5.45	(350 KeV)			Quasi-elastic scattering - poor resolution of photon; detector did not separate high energy inelastic scattering from elastic scattering. Fig. 135° quasi-elastic cross section. Optical model considered.

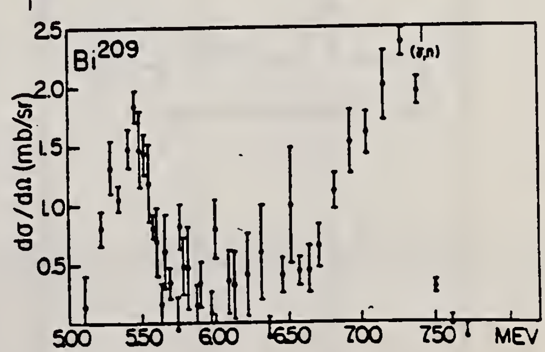

Ref. W.C. Barber, J. Goldemberg, G.A. Peterson, Y. Torizuka
Nuclear Phys. 41, 461 (1963)

Elem. Sym.	A	Z
Bi	209	83

Method Linac (Standford Mark II); counter telescope

Ref. No. 63 Ba 1 — BG

Reaction	E or ΔE	E_o	Γ	$\int \sigma dE$	Jπ	Notes
$Bi^{209}(e,e')$	41.5					Ground state $9/2^-$ No resonances. Detector at 180°

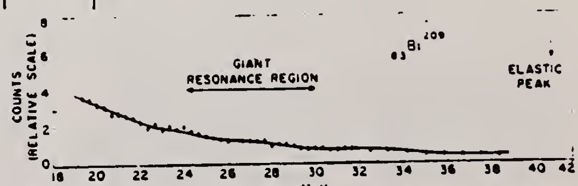

Fig. 19. Spectrum of 41.5 MeV inelastically scattered electrons from a Bi^{209} target.

Ref.	Elem. Sym.	A	Z
M. Sugawara, S. Mori, A. Ono, A. Hotta, M. Kimura J. Phys. Soc. Japan 18, 17 (1963)	Bi	209	83
Method 25 MeV betatron; photon scattering; NaI spectrometer; NBS chamber	**Ref. No.** 63 Su 1		NVB

Reaction	E or ΔE	E_o	Γ	$\int \sigma dE$	Jπ	Notes
$Bi^{209}(\gamma,\gamma)$	Bremss. 4-14					Detector at 120° σ_{max} = 8 mb [Corrects results in J. Phys. Soc. Japan 16, 1657 (1961)]

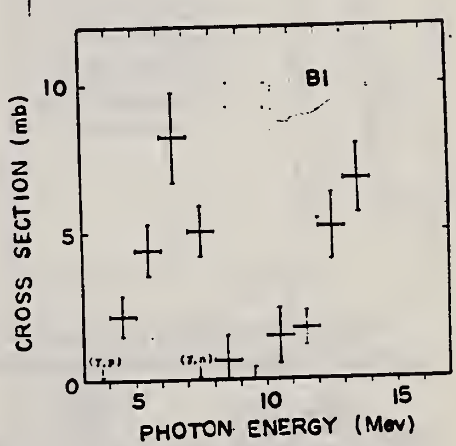

(g)

Ref.	Elem. Sym.	A	Z
C.S. Young, D.J. Donahue Phys. Rev. 132, 1724 (1963)	Bi	209	83

Method	Ref. No.	
200 kW pool reactor; monoergic γ's from (n,γ) in Mn, Fe and Cu;NaI	63 Yo 1	JHH

Reaction	E or ΔE	E_o	Γ	$\int \sigma dE$	$J\pi$	Notes
$Bi^{209}(\gamma,\gamma)$	6.0-8.2					Measured σ (elastic scattering) values in Table II; interpolated to 7 MeV in Table V.

TABLE II. Total elastic scattering cross sections (mb).

Source element	Energy interval (MeV)	Source energy (MeV)	Target (thickness in cm) Ta(1.3)	Hg(3)	Pb(0.6)	Bi(1.3)
Tl	5.0–7.0	6.41 6.75			0.6 ± 0.4	
Mn	6.0–7.5	7.26 7.15 7.05	<0.3	0.5 ±0.3	0.9 ± 0.5	0.8 ±0.4
Fe	6.0–7.6	7.64 7.28	0.7 ±0.4	2.4 ±1.3	125 ±20[a]	2.0 ±1.1
Cu	7.6–8.2	7.91.	<0.2	<0.4	<0.2	<0.2

[a] Calculated using the intensity of 7.64-MeV γ rays produced by neutron capture in iron.

TABLE V. Cross sections at about 7 MeV (mb).

	This work	Ref. 2	Ref. 1[a]	Ref. 3	Ref. 4[b]
Ta	<0.3		2		
Hg	0.5±0.3	3.5			
Pb	0.9±0.5	15	17	60	55
Bi	0.8±0.4	17.5	19	35	17

[a] See also E. G. Fuller and Evans Hayward, Phys. Rev. Letters 1, 465 (1958).
[b] Differential cross sections at 135° were multiplied by 11.2.

[1] E. G. Fuller and Evans Hayward, Phys. Rev. 101, 692 (1956); Nucl. Phys. 33, 431 (1962).
[2] K. Riebal and A. K. Mann, Phys. Rev. 118, 701 (1960).
[3] Tsutomu Tohei, Masumi Sugawara, Shigeki Mori, and Motohara Kimara, J. Phys. Soc. Japan 16, 1657 (1961).
[4] P. Axel, K. Min, N. Stein, and D. C. Sutton, Phys. Rev. Letters 10, 299 (1963).

Ref.	G.N. Zatsepina, V.V. Igonin, L.E. Lazareva, A.I. Lespestkin Zhur. Eksp. i Teoret. Fiz. 44, 1787 (1963) Soviet Phys. JETP 17, 1200 (1963)	Elem. Sym. Bi	A 209	Z 83
Method	Synchrotron; neutron spectra, angular distribution data; emulsions; ion chamber monitor	Ref. No. 63 Za 1		JHH

Reaction	E or ΔE	E_0	Γ	∫σdE	Jπ	Notes
$Bi^{209}(\gamma,n)$	Bremss. 14 19					

FIG. 4. Integral spectrum of photoneutrons from bismuth for $(h\nu)_{max}$ = 19 MeV. Histogram 1 – summary neutron spectrum $N_\Sigma(\epsilon_n)$ for 30, 90, 150, and 270°; curve 2 – calculated spectrum $N_d(\epsilon_n)$ of the "direct" neutrons; histogram 3 – difference $N_\Sigma(\epsilon_n) - N_d(\epsilon_n)$; curve 4 – calculated evaporation-neutron spectrum.

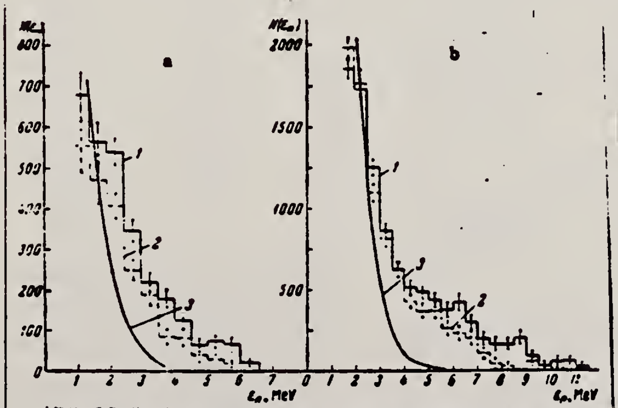

FIG. 2. Energy distributions of photoneutrons from bismuth irradiated by x-rays with maximum energy $(h\nu)_{max}$ = 14 MeV (a) and 19 MeV (b) for different emission angles: histogram 1 – $N_{90°} + N_{270°}$, histogram 2 – $N_{30°} + N_{150°}$. Curve 3 – neutron spectrum calculated in accordance with the evaporation model.

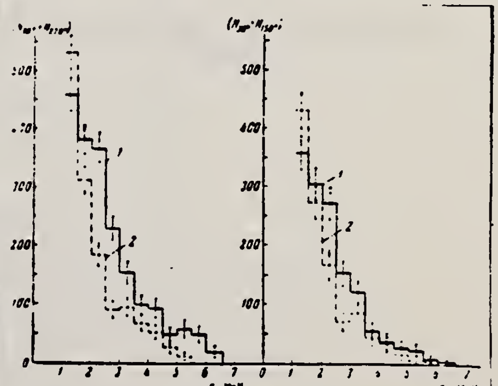

FIG. 6. Comparison of the spectra of photoneutrons from bismuth (1) and gold (2) for different emission angles at $(h\nu)_{max}$ = 14 MeV.

REF.	ELEM. SYM.	A	Z
F.R. Allum, T.W. Quirk, B.M. Spicer Aust. J. Phys. 17, 420 (1964)	Bi	209	83

METHOD	REF. NO.	
Synchrotron; r-chamber	64 Al 4	NVB

REACTION	RESULT	EXCITATION ENERGY	SOURCE TYPE	SOURCE RANGE	DETECTOR TYPE	DETECTOR RANGE	ANGLE
G,N	NØX	THR-18	C	18	SCI-I	4-	DST
				(17.5)		(4.5-)	

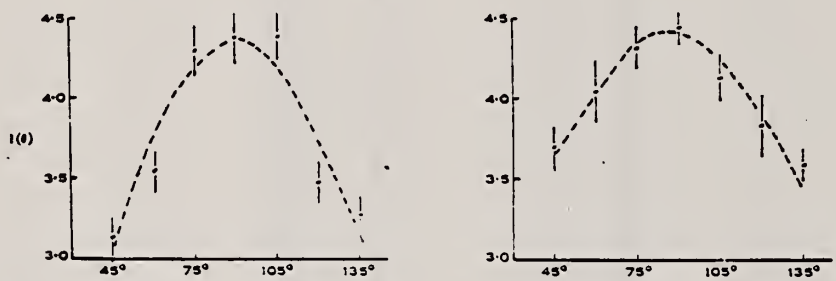

(a) (b)

Fig. 1.—Fast photoneutron ($>4 \cdot 5$ MeV) angular distributions from bismuth and lead. (*a*) Bismuth, $I(\theta) = 4 \cdot 36 - 0 \cdot 04 \cos\theta - 2 \cdot 52 \cos^2\theta$ (dotted line); (*b*) lead, $I(\theta) = 4 \cdot 40 + 0 \cdot 14 \cos\theta - 1 \cdot 71 \cos^2\theta$ (dotted line).

No asymmetry about 90°.

REF.	ELEM. SYM.	A	Z
F.R. Allum, T.W. Quirk, and B.M. Spicer Nucl. Phys. 53, 545 (1964)	Bi	209	83

METHOD	REF. NO.	
	64 Al 5	JOC

REACTION	RESULT	EXCITATION ENERGY	SOURCE TYPE	SOURCE RANGE	DETECTOR TYPE	DETECTOR RANGE	ANGLE
G,XN	NØX	THR-34	C	34	THR-I	6-	DST

Table 1

Summary of present experimental data at 34 MeV bremsstrahlung

Element		$-\frac{a_2}{a_0}$	$\frac{a_1}{a_0}$
$_4$Be		0.43±0.02	0.05±0.0
$_6$C		0.61±0.04	0.09±0.0
$_{13}$Al		0.39±0.03	0.05±0.0
$_{22}$Ti		0.34±0.02	0.06±0.0
$_{24}$Cr	34 MeV	0.33±0.02	0.02±0.0
	22 MeV	0.13±0.07	−0.02±0.0
$_{29}$Cu		0.36±0.02	0.10±0.0
$_{50}$Sn		0.38±0.02	0.11±0.0
$_{56}$Ba		0.39±0.03	0.11±0.0
$_{73}$Ta	Before installation of iron shielding	0.26±0.04	0.13±0.0
	After installation of iron shielding	0.27±0.02	0.12±0.0
$_{82}$Pb	target diameter 3.0 cm	0.39±0.03	0.15±0.0
	target diameter 1.5 cm	0.40±0.03	0.19±0.0
$_{83}$Bi		0.42±0.03	0.17±0.0

$Y = a_0 + a_1 \cos\theta + a_2 \cos^2\theta$

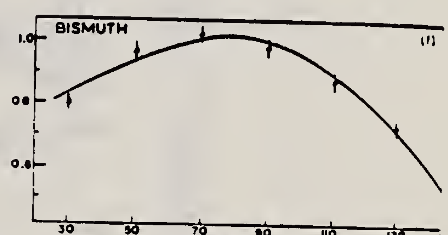

REF.	ELEM. SYM.	A	Z
E.S. Anashkina Zhur. Eksp. i Teoret. Fiz. 45, 404 (1963); Soviet Phys. JETP 18, 279 (1964)	Bi	209	83

METHOD	REF. NO.	
Neutron angular distribution; nuclear emulsion	63 An 3	NVB

REACTION	RESULT	EXCITATION ENERGY	SOURCE TYPE	SOURCE RANGE	DETECTOR TYPE	DETECTOR RANGE	ANGLE
G,XN	ABY	9-85	C	85	EMU-D	1-12	DST
						(1.5 - 11.5)	

For 1.5 MeV $\leq E_n \leq$ 11.5 MeV,

$$\text{yield} = (3.7 \pm 0.8)\ 10^{-3}\ \frac{\text{neutrons}}{\text{mole MeV/cm}^2}$$

Angular Distributions:

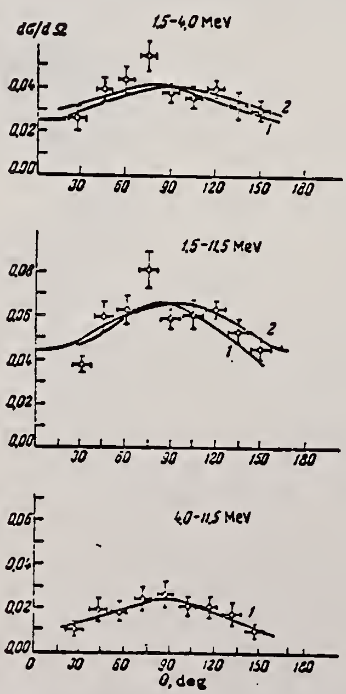

The curves 1 in the figure correspond to least-square fitting. It is possible to represent them by the following formulas:

1.5 — 4.0 MeV : $(1.00 \pm 0.08) + (0.10 \pm 0.08) \cos\theta - (0.4 \pm 0.1) \cos^2\theta$,

4.0 — 11.5 MeV : $(1.00 \pm 0.08) + (0.02 \pm 0.08) \cos\theta - (0.7 \pm 0.2) \cos^2\theta$,

1.5 — 11.5 MeV : $(1.00 \pm 0.05) + (0.07 \pm 0.05) \cos\theta - (0.5 \pm 0.1) \cos^2\theta$.

REF.	ELEM. SYM.	A	Z
B. Arad (Huebschmann), G. Ben-David (Davis), I. Pelah, Y. Schlesinger Phys. Rev. 133, B684-700 (1964)	Bi	209	83

METHOD	REF. NO.	
Reactor, (n,γ) reactions source	64 Ar 1	NVB

REACTION	RESULT	EXCITATION ENERGY	SOURCE		DETECTOR		ANGLE
			TYPE	RANGE	TYPE	RANGE	
G,G	ABX	7	D	7	NAI-D		135
		(6.996)		(6.996)			

TABLE II. Capture gamma-ray sources and their properties.[a]

Source	Chemical composition	Mass kg	Principal γ rays (in MeV)
Al	Metal	1.640	7.73
Cl	polyvinyl Chloride	0.380	8.55, 7.78, 7.41, 6.96, 6.64, 6.12, 5.72
Co	CoO	0.230	7.49, 7.20, 6.98, 6.87, 6.68, 6.48, 5.97, 5.67
Cr	Metallic powder	0.480	9.72, 8.88, 8.49, 7.93, 7.09, 6.65, 5.60
Cu	Metal	1.860	7.91, 7.63, 7.29, 7.14, 7.00, 6.63
Fe	Metallic powder	0.440	9.30, 7.64, 7.28, 6.03
Hg	$Hg_2(NO_3)_2 \cdot 2H_2O$	0.310	6.44, 6.31, 5.99, 5.67, 5.44
Mn	MnO_2	0.240	7.26, 7.15, 7.04, 6.96, 6.79, 6.10, 5.76
Ni	Metal	0.900	9.00, 8.50, 8.10, 7.83, 7.58, 6.84, 6.64
Ti	TiO_2	0.210	6.75, 6.56, 6.42
V	V_2O_5	0.120	7.30, 7.16, 6.86, 6.51, 6.46, 5.87, 5.73
Y	Y_2O_3	0.200	6.07, 5.63

[a] For more detailed information, additional lines, intensities, etc., see Ref. 6.

TABLE III. Effective cross sections.

γ source	Energy (MeV)	Scatterer Element	Protons	Neutrons	$\langle\sigma_{\gamma\gamma}\rangle$ (mb)	Notes
Hg	5.44	Hg	80	116, 118, 119, 120, 121, 122, 124	128	
Cl	6.12	Pr^{141}	59	82	103	
V	6.508	Sn	50	62, 64–70, 72	14	a
Co	6.690	Pr^{141}	59	82	2.7	
Co	6.867	Nd	60	82, 83, 84, 85, 86, 88	22	a
Al	6.98	Pb^{208}	82	126	2900	
Cl	6.98	Pb	82	124, 125, 126	346	b
Ti	6.996	Bi^{209}	83	126	1560	a
Cu	7.01	Sn	50	62, 64–70, 72	1000	b
Ti	7.149	Pb^{208}	82	126	1000	b
Co	7.201	Pb^{208}	82	126	25	b
Mn	7.261	Pb^{208}	82	126	25	
Fe	7.285	Pb^{208}	82	126	4100	a
V	7.305	Pb^{208}	82	126	12.5	a
Hg	7.32	Pb	82	124, 125, 126	5500	
Fe	7.639	Ni	28	30, 32, 34, 36	10.5	c
Fe	7.639	Pr^{141}	59	82	10	d
Cr	8.499	Cu	29	34, 36	24.4	d
Cr	8.881	Pr^{141}	59	82	9.3	
Ni	8.997	Sm	62	82, 85–88, 90, 92	2.8	

[a] A large error could be introduced in the cross-section values because of large differences in line intensities quoted by Bartholomew and Higgs and by Groshev *et al.* (Ref. 6).
[b] Because of the low counting rate, thick scatterers were used, which will introduce a systematic error in estimating $\langle\sigma_{\gamma\gamma}\rangle$ for resonances having a high nuclear cross section.
[c] The cross section was evaluated assuming the gamma intensity to be 0.02 photons per 100 captured neutrons (see text).
[d] Reference 6 gives the 7.639 line of iron capture gamma rays as a single line. However, a recent paper by Fiebiger, Kand, and Segel [Phys. Rev. 125, 2031 (1962)] reports two different lines of equal intensities having energies of 7.647 and 7.633 MeV. The present experiment cannot resolve an energy difference of 14 keV, therefore, there is no possibility of deciding which line is responsible for the scattering.

REF.	ELEM. SYM.	A	Z
A. De Marco, R. Garfagnini, G. Piragino Phys. Letters 10, 213 (1964)	Bi	209	83

METHOD	REF. NO.	
Synchrotron; NBS ion chamber	64 De 1	JOC

REACTION	RESULT	EXCITATION ENERGY	SOURCE		DETECTOR		ANGLE
			TYPE	RANGE	TYPE	RANGE	
$ G,N	NØX	THR - 80	C	80	CCH	0-16	135

POL OF NEUTS

$P = 0.14 \mp 0.10$ for $0.4 < En \leq 4$ MeV

$P = 0.20 \mp 0.21$ for $4 < En \leq 16$ MeV

REF. H. G. De Carvalho, G. Cortini, E. Del Giudice, G. Potenza, R. Rinzivillo, and G. Ghigo Nuovo Cimento 32, 293 (1964)	ELEM. SYM. Bi	A 209	Z 83
METHOD	REF. NO. 64 De 4		HMG

REACTION	RESULT	EXCITATION ENERGY	SOURCE TYPE	SOURCE RANGE	DETECTOR TYPE	DETECTOR RANGE	ANGLE
G,F	ABX	300-999	C	300-999	EMU-D	300-999	4PI

TABLE I.

Nuclide	Bi 209	W 184	Ag
Number of runs	3	2	1
Number of atoms cm^{-3}	$\sim 2\cdot 10^{20}$	$\sim 5\cdot 10^{20}$	10^{22}
Total number of tracks	$\sim$ 6000	$\sim$ 500	$\sim$ 100
Cross-sections per equivalent quantum, σ_Q, at 1000 MeV (millibarns)	12.2 ± 0.7	1 ± 0.1	0.1
Cross-sections per photon, σ_k, between 300 and 1000 MeV (millibarns)	7.8 ± 0.8	0.65 ± 0.11	$\sim$0.05
Fissility	0.12	0.012	<0.0015

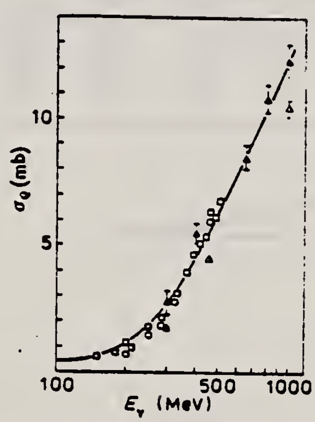

Fig. 3. – The Bi photofission cross-section per equivalent quantum, plotted againts ln E. The data from BERNARDINI *et al.* [8] (circles), from JUNGERMAN *et al.* [9] (squares) and from DE CARVALHO *et al.* [1] (open triangles) are shown, together with those obtained in the present work (full triangles).

REF.	ELEM. SYM.	A	Z
Yu.Ya. Glazunov, M.V. Savin, I.N. Safina, E.F. Fomushkin, Yu.A. Khokhlov Zhur. Eksp. i Teoret. Fiz. 46, 1906-08 (1964) Soviet Phys. JETP 19, 1284 (1964)	Bi	209	83
METHOD	REF. NO.		
Linac	64 Gl 1		NVB

REACTION	RESULT	EXCITATION ENERGY	SOURCE TYPE	SOURCE RANGE	DETECTOR TYPE	DETECTOR RANGE	ANGLE
G,N	SPC	16	D	16	TØF-D	0-5	90

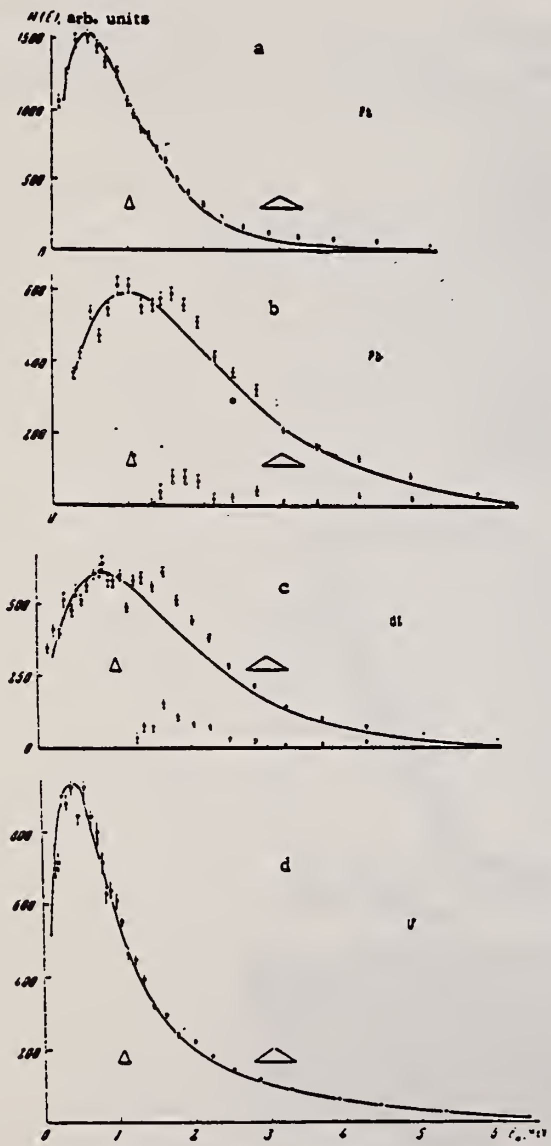

Photoneutron energy distributions.

shown in the figure. The solid curves a, b, and c are the evaporation spectra

$$N(E) \sim \frac{E}{T} \exp\left(-\frac{E}{T}\right)$$

with the temperature T = 0.48 ± 0.03 MeV for platinum, 0.84 ± 0.04 MeV for Bi, and 0.98 ± 0.04 MeV for lead.

The solid curve d is the sum of the evaporation spectrum and the fission spectrum of uranium:

$$N(E) = \alpha \frac{E}{T} \exp\left(-\frac{E}{T}\right) - (1-\alpha) \exp\left(-\frac{E}{T}\right)$$

$$\times \frac{1}{\sqrt{\pi \omega T_f}} \exp\left(-\frac{E}{T_f}\right) \sinh \frac{\sqrt{\omega E}}{T_f}$$

with the parameters: T = 0.33 ± 0.03 MeV, T_f = 1.05 ± 0.04 MeV, ω = 0.5 MeV, α = 0.49 ± 0.01.

REF.	ELEM. SYM.	A	Z
R.R. Harvey, J.T. Caldwell, R.L. Bramblett, S.C. Fultz Phys. Rev. 136, B126-31 (1964)	Bi	209	83

METHOD	REF. NO.	
Positron annihilation; ion chamber	64 Ha 2	NVB

REACTION		RESULT	EXCITATION ENERGY	SOURCE		DETECTOR		ANGLE
				TYPE	RANGE	TYPE	RANGE	
G,N	179	ABX	6-27	D	6-26	BF3-I		4PI
G,2N	180+	ABX	12-27	D	12-26	BF3-I		4PI

179+

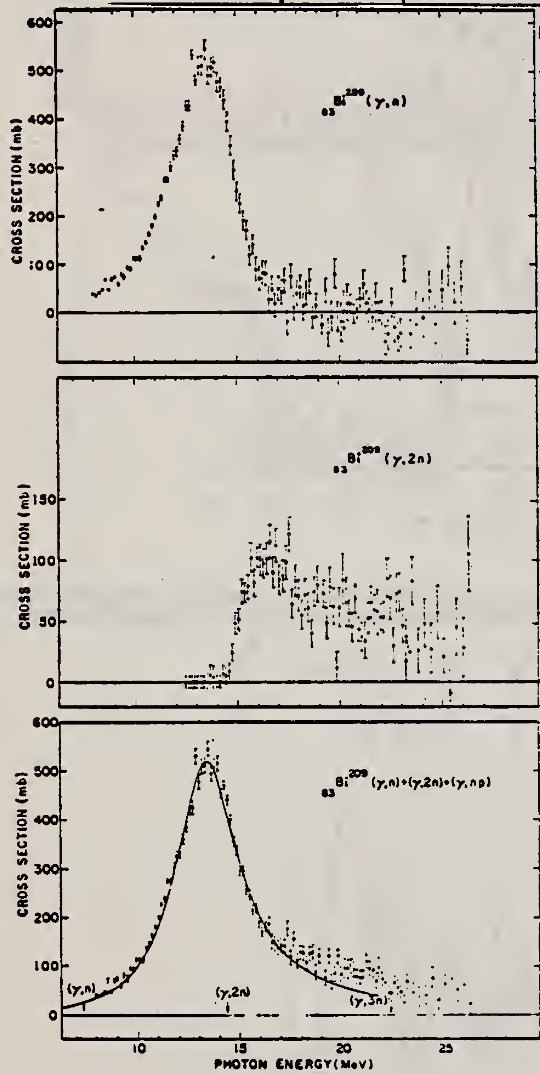

FIG. 4. Top figure shows data points for $\sigma[(\gamma,n)+(\gamma,np)]$ for Bi^{209}, obtained from single-neutron counting data. Center figure shows data for $\sigma(\gamma,2n)$ obtained from double-neutron counting data. Data points for the compound nucleus formation cross section of Bi^{209}, i.e., $\sigma[(\gamma,n)+(\gamma,np)]+\sigma(\gamma,2n)$ are shown in the bottom figure. Solid curve is a plot of a Lorentz line having the parameters given in Table II. The data are uncertain below 8 MeV owing to low beam intensities encountered.

TABLE II. Lorentz line parameters and σ_{-2} values for Pb isotopes and Bi.

Isotope	Peak σ_0 (mb)	Width Γ (MeV)	E_0 (MeV)	σ_{-2} (mb/MeV)	$0.00225A^{5/3}$ (mb/MeV)
Pb^{206}	525	3.75	13.7	15.6±1.6	16.2
Pb^{207}	485	3.87	13.6	14.5±1.5	16.3
Pb^{208}	495	3.78	13.6	14.1±1.4	16.4
Bi^{209}	520	3.83	13.5	16.6±1.7	16.6

TABLE I. Integrated cross sections in MeV-b, up to 28 MeV, for Pb isotopes and Bi.

Isotope	$\int_0^{28}\sigma(\gamma,n)dE$	$\int_0^{28}\sigma(\gamma,2n)dE$	$\int_0^{28}\sigma dE$	$\int_0^{28}\sigma dE+W$	$0.06NZ/A$
Pb^{206}	2.22	0.56	2.78±0.28	3.07±0.36	2.96
Pb^{207}	2.05	0.60	2.65±0.27	2.95±0.30	2.97
Pb^{208}	1.96	0.95	2.91±0.29	3.21±0.32	2.98
Bi^{209}	2.17	0.76	2.93±0.29	3.25±0.33	3.00

FORM NBS-418
(REV. 7-14-64)
USCOMM-DC 28010-P64

REF.	ELEM. SYM.	A	Z
I. Bergqvist, B. Lundberg, L. Nilsson, and N. Starfelt Phys. Letters 19, 670 (1966)	Bi	209	83

METHOD	REF. NO.	
Van de Graaff	66 Be 1	EGF

REACTION	RESULT	EXCITATION ENERGY	SOURCE TYPE	SOURCE RANGE	DETECTOR TYPE	DETECTOR RANGE	ANGLE
N,G	SPC	11	D	7	NAI-D	8-18	

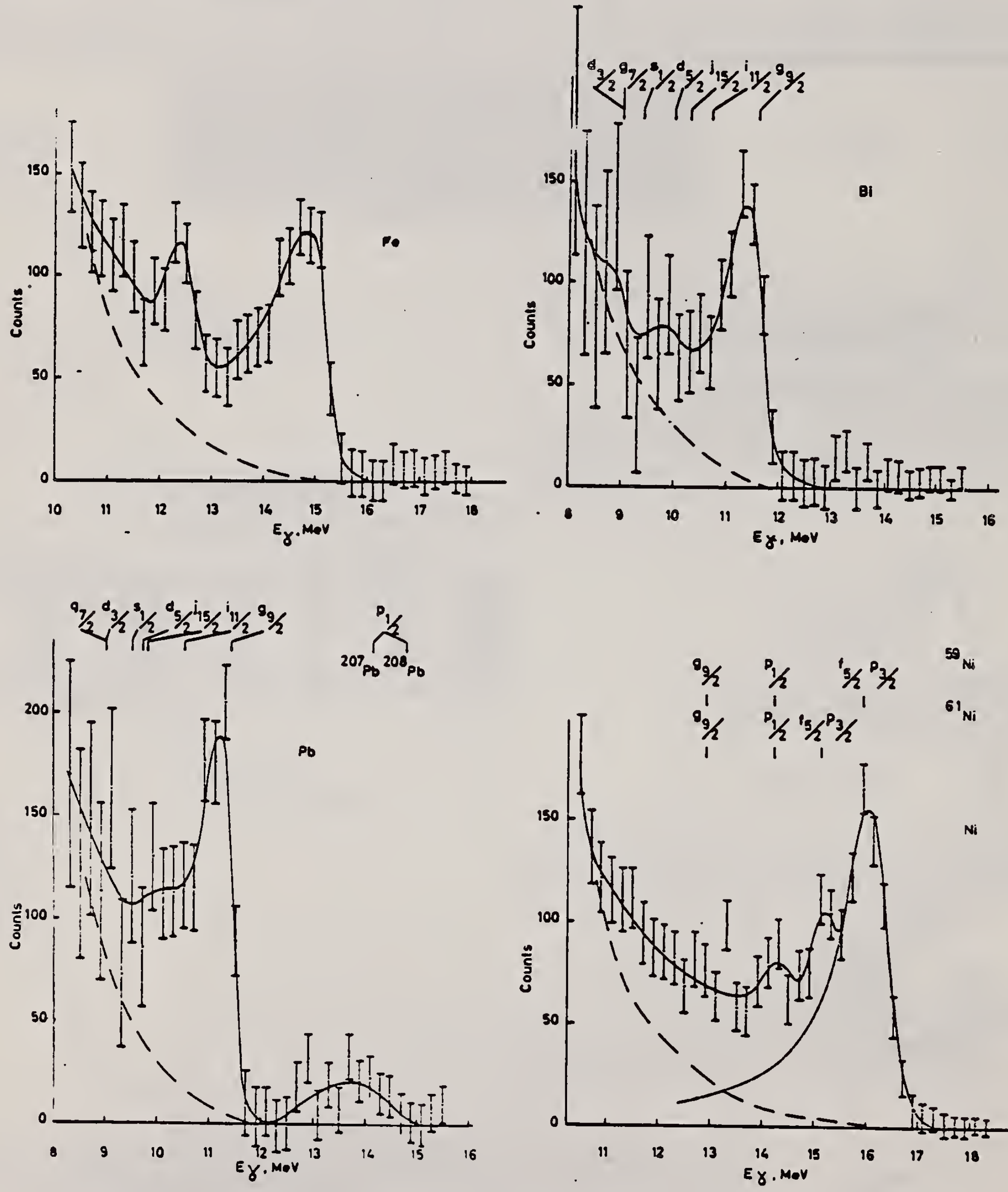

Fig. 1. Gamma-ray spectra emitted in the capture of 7.4 MeV neutrons. The dashed line is the spectrum calculated for the decay of a compound nucleus. The dot-dashed line is the response function of the gamma-ray spectrometer for 16.0 MeV γ rays. Single-particle states as determined from (d,p) reactions are shown.

REF.	ELEM. SYM.	A	Z
G. Ben-David, B. Arad, J. Balderman, and Y. Schlesinger Phys. Rev. 146, B852 (1966)	Bi	209	83

METHOD	REF. NO.	
Nuclear Resonance Scattering using N,G reactions.	66 Be 3	JDM

REACTION	RESULT	EXCITATION ENERGY	SOURCE TYPE	SOURCE RANGE	DETECTOR TYPE	DETECTOR RANGE	ANGLE
G,G	RLX	5 - 10	D	5 - 10	NAI-D	5 - 10	135

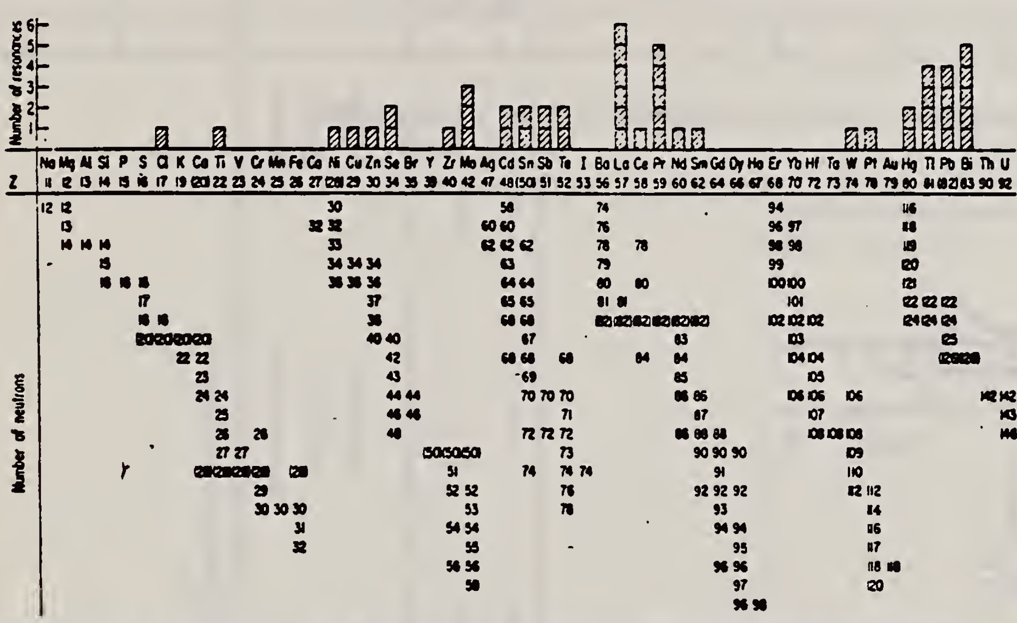

Fig. 3. Histogram of distribution of observed resonances among the different targets. The atomic number is given directly beneath the chemical symbol followed by the neutron numbers of the naturally occurring isotopes. Magic numbers are shown in brackets.

TABLE III. List of effective cross sections.

Scatterer	Energy (MeV)	Gamma source	δ (mb)	Scatterer	Energy (MeV)	Gamma source	δ (mb)
Sm^{144}	8.997	Ni	100	Sn	7.01	Cu	110
Pr^{141}	8.881	Cr	9	Nd	6.867	Co	30
La	8.532	Ni	6	Pr^{141}	6.867	Co	3
Te	8.532	Ni	3[a]	Te	6.7	Ni	...
Cu	8.499	Cr	24	La	6.54	Ag	12
Zr	8.496	Se	3050	Cd	6.474	Co	110
Zn	8.119	Ni	13	Mo	6.44	Hg	25[g]
Se	7.817	Ni	50	La	6.413	Ti	72
Se	7.76	K	90	Mo	6.413	Ti	10
Sb	7.67	V	...[b]	Tl	6.413	Ti	25
Cd	7.64	Fe	40[c]	W	~6.3	Ti	...[b]
Ni	7.64	Fe	7[c]	Sb	6.31	Hg	6[a]
Pr^{141}	7.64	Fe	12[c]	Ti	6.31	Hg	2[a]
Tl	7.64	Fe	370[c]	Sn	6.27	Ag	75
La	7.634	Cu	7	Pb^{206}	6.15	Gd	...[h]
Mo	7.634	Cu	11	Te	5.8	Ni	...[f]
Bi^{209}	7.634	Cu	4	La	6.12	Cl	35
Te	7.528	Ni	66[d]	Pr^{141}	6.12	Cl	110
Bi^{209}	7.416	Se	100	Pt	5.99	Hg	40[a,g]
Bi^{209}	7.300	As	80[e]	Tl	5.99	Hg	5[g]
Pb^{208}	7.285	Fe	4100	Pb^{208}	5.9	Sr	...[h]
Cl	7.285	Fe	34	Ce	5.646	Co	17
Pr^{141}	7.185	Se	80	Bi^{209}	5.646	Co	55
Tl	7.16	Cu	120	Pb^{206}	5.53	Ag	70
La	7.15	Mn	50	Hg	5.44	Hg	75[g]
Bi^{209}	7.149	Ti	2000	Hg	4.903	Co	385

[a] High-energy component of a complex spectrum.
[b] A broad scattered spectrum with no observable peak structure.
[c] There are actually two lines of energies 7.647 and 7.633 MeV having equal intensities in the iron capture gamma spectrum. The cross section has therefore been corrected, although there is no possibility at present of deciding which line is responsible for each resonance.
[d] Is probably an independent level in the complex spectrum of Ni γ rays on Te.
[e] Rough estimate.
[f] May be inelastic component from 7.528 level in Te.
[g] The relative line intensities in this case are due to Groshev and co-workers.
[h] No line is known for the source at this energy.
[i] Difficult to resolve among the many source lines present at this energy.

FORM NBS-418
(REV. 7-14-64)
USCOMM-DC 28010-P64

REF.	ELEM. SYM.	A	Z
B.L. Berman, G.S. Sidhu, and C.D. Bowman Phys. Rev. Letters 17, 761 (1966)	Bi	209	83

METHOD	REF. NO.	
Linac	66 Be 4	JDM

REACTION	RESULT	EXCITATION ENERGY	SOURCE TYPE	SOURCE RANGE	DETECTOR TYPE	DETECTOR RANGE	ANGLE
G,N	ABX	7	C	11	TOF-D		135

The absolute cross section might contain systematic errors of up to 50%.

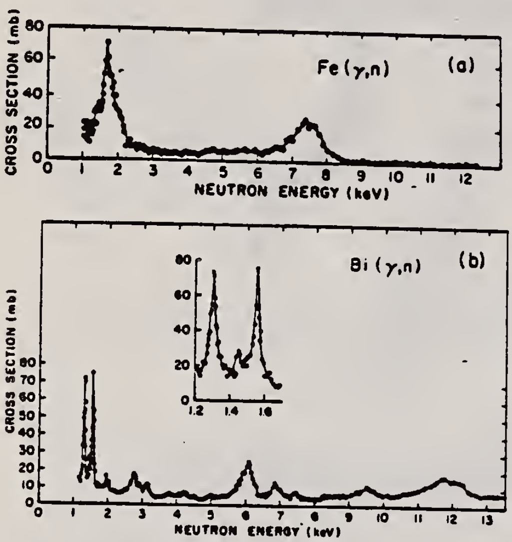

FIG. 2. Absolute cross section for threshold photoneutrons from iron and bismuth as a function of laboratory neutron energy $[\sigma = 4\pi(d\sigma/d\Omega)|_{135°}]$.

OVER

Table I. Experimental parameters.

Neutron sample	Sample thickness (in.)	$E_{thr}(\gamma,n)$ (MeV)	Bremsstrahlung target	Target thickness (in.)	E_e (MeV)	Bremsstrahlung conversion efficiency (10^{-8} photon/electron sr eV)	Ω_γ (sr)	Average beam current (μA)	W (μsec/channel)	Beam burst width (nsec)	Run time (h)
Fe	1.017	11.21[a]	Al	1.015	12.5	1.57	0.025	36.8	0.125	500	4
Bi	0.502	7.43	Ag	0.249	11.0	4.64	0.133	6.4	0.0625	40-100	34

[a] Fe^{56} (isotopic abundance 91.7%).

REF. N. De Botton, J. Miller, C. Schuhl, G. Tamas and C. Tzara
Nucl. Phys. 75, 396 (1966)

ELEM. SYM.	A	Z
Bi	209	83

METHOD
Photon Monochromator

REF. NO.
66 De 1 — JDM

REACTION	RESULT	EXCITATION ENERGY	SOURCE TYPE	SOURCE RANGE	DETECTOR TYPE	DETECTOR RANGE	ANGLE
G,G	RLX	12 - 17	D	12 - 17	NAI-D		DST

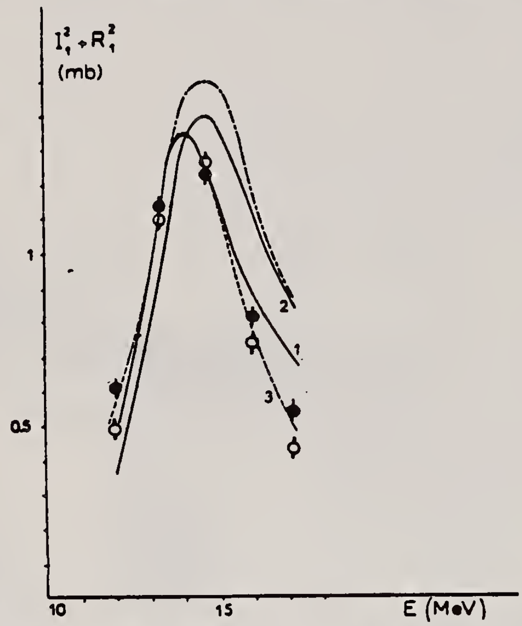

Fig. 1. Sections efficaces de diffusion dipolaire vers l'avant. Résultats déduits de raies de Lorentz: 1) maximum à 13.3 MeV, 2) maximum à 14 MeV, 3) résultat expérimental. – courbe en traits mixtes: déduite de l'absorption mesurée – cercles pleins et vides: points déduits des résultats expérimentaux de diffusion, relatifs au Pb et Bi respectivement.

TABLEAU 1
Donnés expérimentales

E_γ (MeV)	dσ/dΩ (μb/sr) Pb $\theta = 90°$	Pb 135°	Bi 90°	Bi 135°
12	305±20	348±25	246±15	252±15
13.33	570±20	690±30	550±20	692±30
14.67	602±20	910±25	635±20	925±30
16.00	407±20	648±30	369±20	540±30
17.17	270±15	412±20	215±15	412±15

TABLEAU 2
Section efficace et terme d'interférence à $\theta = 0$

E (MeV)	$X = I_1^2+R_1^2$ (mb) Pb	Bi	$Y = I_1 I_2+R_1 R_2$ (mb) Pb	Bi
12.00	0.61±0.04	0.49±0.03	0.15 ±0.05	0.17±0.03
13.33	1.14±0.04	1.10±0.04	0.26 ±0.05	0.19±0.05
14.67	1.20±0.04	1.27±0.04	−0.008±0.04	0.04±0.05
16.00	0.81±0.04	0.74±0.04	−0.054±0.05	0.02±0.04
17.17	0.54±0.04	0.43±0.03	−0.010±0.035	−0.12±0.03

REF.
A. De Marco, R. Garfagnini and G. Piragino
Nuovo Cimento 44B, 172 (1966)

ELEM. SYM.	A	Z
Bi	209	83

METHOD

REF. NO.	
66 De 2	JDM

REACTION	RESULT	EXCITATION ENERGY	SOURCE		DETECTOR		ANGLE
			TYPE	RANGE	TYPE	RANGE	
G,N	SPC	THR - 80	C	THR - 80	CCH-D	0 - 15	135

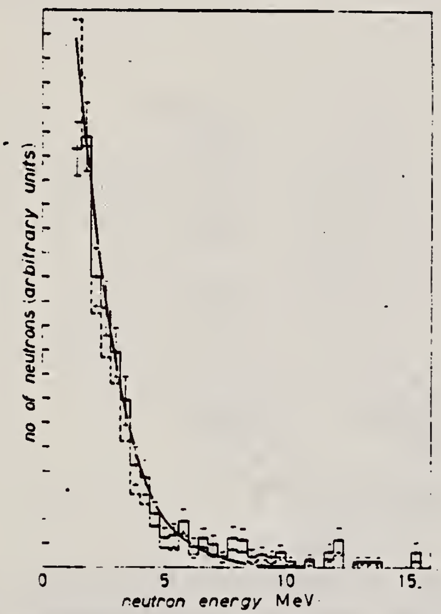

Fig. 2. – Energy distribution of photoneutrons from Bi. The dashed and the full-line histogram represent respectively the uncorrected and the corrected spectrum. The full-line curve corresponds to the expression given by LE COUTEUR and LANG (15) to represent the neutron energy distribution (see the text for the normalization chosen).

REF.		ELEM. SYM.	A	Z
J. F. Ziegler and G. A. Peterson Proc. Gatlinburg Conference 319 (1966)		Bi	209	83
METHOD		REF. NO. 66 Zi 2		hmg

REACTION	RESULT	EXCITATION ENERGY	SOURCE TYPE	SOURCE RANGE	DETECTOR TYPE	DETECTOR RANGE	ANGLE
E,E/	RLX		D	28-70	MAG-D		DST

(B(EL)

TABLE 1

Values of B(E3↑)

Isotope	Energy level	B(E3↑) (e^2b^3)
^{209}Bi	2.58	0.527 ± .012
	2.58} 2.73}	0.773 ± .020
^{208}Pb	2.615	0.788 ± .028
^{207}Pb	2.62} 2.66}	0.740 ± .012
^{206}Pb	2.60	0.702 ± .032

2. Tuan, S. T., and Wright, L. E., Bull. Am. Phys. Soc. 11, 338 (1966); Reynolds, J. T., Ph. D. Thesis, Duke University; Onley, D. S., private communications.
3. Elton, L. R. B., "Nuclear Sizes," Oxford Univ. Press, London, 1961); Hofstadter, R., private communication.

REF.

G. P. Antropov, I. E. Mitrofanov, V. S. Russkikh
Izv. Akad. Nauk SSR Fiz. 31, 336 (1967)
Bull. Acad. Sci. USSR 31, 320 (1967)

ELEM. SYM.	A	Z
Bi	209	83

METHOD

REF. NO.	
67 An 2	egf

REACTION	RESULT	EXCITATION ENERGY	SOURCE TYPE	SOURCE RANGE	DETECTOR TYPE	DETECTOR RANGE	ANGLE
G,XN	ABX	THR-20	C	8-20	BF3-I		4PI

712

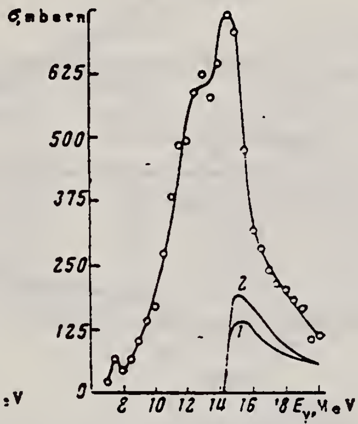

Fig.7

Fig.7. Experimentally determined cross section $\sigma_{(\gamma,n)} + 2\sigma_{(\gamma,2n)}$ of Bi. The lower curves representing $\sigma_{(\gamma,2n)}$ were calculated on two assumptions: 1 - a = 10.2 and 2 - a = 20.9.

REF.	ELEM. SYM.	A	Z
M. Giannini, P. Oliva, D. Prosperi and G. Toumbev Nucl. Phys. A101, 145 (1967)	Bi	209	83
METHOD	REF. NO. 67 Gi 1		egf

REACTION	RESULT	EXCITATION ENERGY	SOURCE TYPE	SOURCE RANGE	DETECTOR TYPE	DETECTOR RANGE	ANGLE
G,G	LFT	7	D	6-8	NAI-D	4-8	DST

Note: Varied Doppler Width

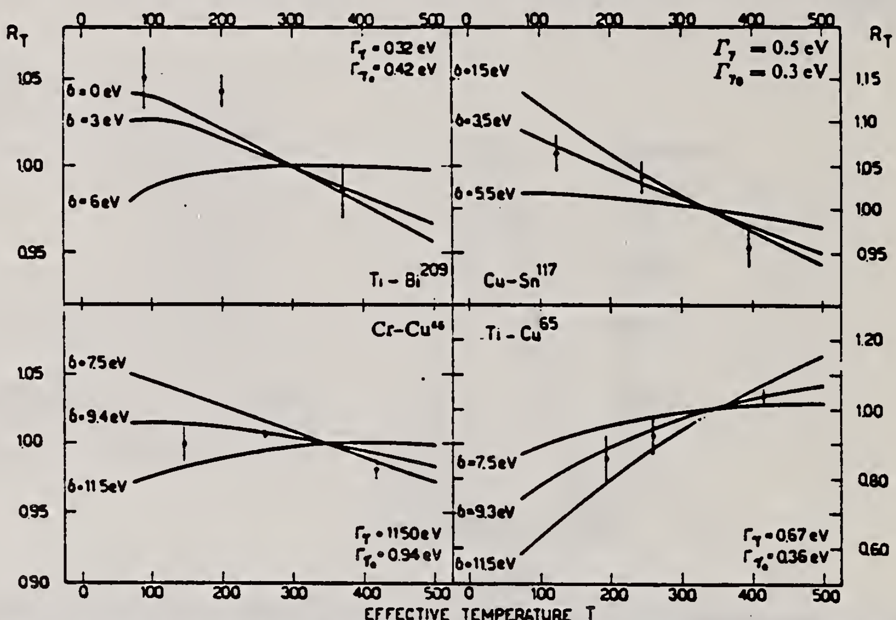

Fig. 7. Calculated variation in resonant scattering cross section as a function of scatterer temperature for different values of δ. Eq. (11) defines R_T.

TABLE 3
Angular distribution results

Resonant isotope	Resonant level energy (MeV)	Ground state spin	Resonant level spin	Statistical factor g	A_2^{exp}	A_2^{th}
Bi	7.15	$\frac{9}{2}$	$\frac{11}{2}$	1.2		0.09
			$\frac{9}{2}$	1.0	0.15±0.04	0.19
			$\frac{7}{2}$	0.8		0.03
Sn	7.01	$\frac{1}{2}$	$\frac{1}{2}$	1.0		0
			$\frac{3}{2}$	2.0	0.24±0.04	0.25
Cu	8.50	$\frac{3}{2}$	$\frac{1}{2}$	0.5	0.00±0.05	0
			$\frac{3}{2}$	1.0		0.16
			$\frac{5}{2}$	1.5		0.14
Cu	6.07	$\frac{3}{2}$	$\frac{1}{2}$	0.5		0
			$\frac{3}{2}$	1.0	0.20±0.04	0.16
			$\frac{5}{2}$	1.5		0.14

[over]

TABLE 4

Experimental results

Source-scatterer	Energy (MeV)	Γ_γ (eV)	$\Gamma_{\gamma 0}$ (eV)	$\Gamma_{\gamma 0}/\Gamma_\gamma$	δ (eV)	$\langle\sigma_{\gamma\gamma}\rangle$ (b)	$\bar{\sigma}_{r_a}$ (b)
Ti-^{209}Bi	7.15	0.32 ± 0.23	0.42 ± 0.14	> 0.68	< 2	2.6 ± 0.8	3.6 ± 1.2
Cu-^{117}Sn	7.01	0.5 ± 1.1	0.3 ± 0.3		3.6 ± 0.7	1.2 ± 0.4	3.4 ± 3.5
Cr-^{65}Cu	8.50	11.5 ± 8.0	0.94 ± 0.29	0.08 ± 0.04	9.4 ± 0.7	$(4.2 \pm 1.3) \cdot 10^{-2}$	0.64 ± 0.20
{Ti-^{65}Cu	6.07	0.67 ± 0.35	0.36 ± 0.07	0.54 ± 0.19	9.3 ± 0.8	0.44 ± 0.13	2.0 ± 0.4
{Ti-^{63}Cu	6.07	0.32 ± 0.18	0.16 ± 0.03	0.51 ± 0.18	9.2 ± 0.8	0.20 ± 0.06	0.92 ± 0.19

In the last two columns, $\langle\sigma_{\gamma\gamma}\rangle$ and $\bar{\sigma}_{r_a}$ are effective cross sections measured at temperature $T_s = 300°$ K.

REF.	ELEM. SYM.	A	Z
R. R. Hurst and D. J. Donahue Nucl. Phys. A91, 365 (1967)	Bi	209	83

METHOD	REF. NO.	
Neutron capture gamma rays	67 Hu 1	EGF

REACTION	RESULT	EXCITATION ENERGY	SOURCE TYPE	SOURCE RANGE	DETECTOR TYPE	DETECTOR RANGE	ANGLE
G,N	ABX	9-11	D	9-11	BF3-I		4PI

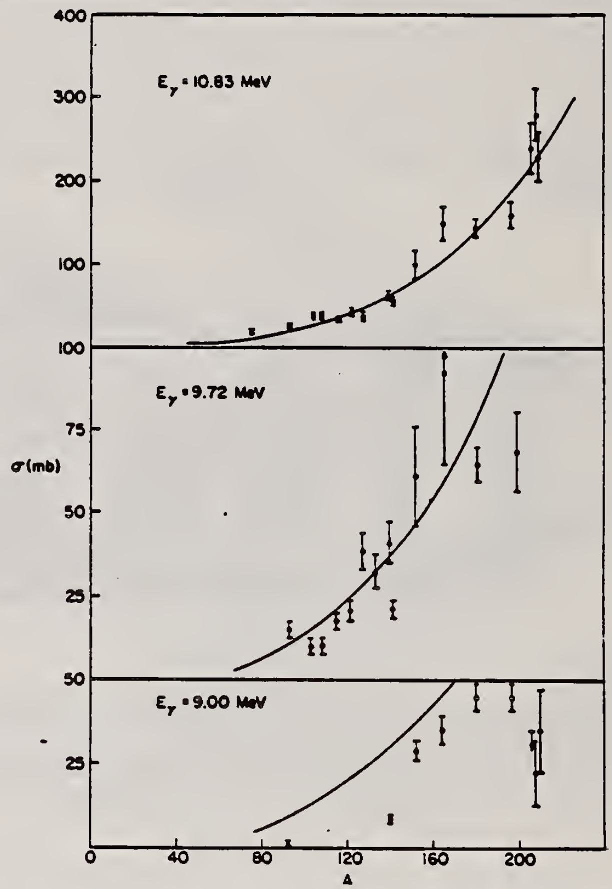

Fig. 1. Cross section (in mb) versus mass number of the target for gamma-ray energies of 9.00, 9.72 and 10.83 MeV. The solid lines are plots of eq. (1) in the text.

TABLE 1

Photoneutron cross sections (mb)

Target	7.72 MeV	9.00 MeV	9.72 MeV	10.83 MeV
^{59}Co				9.0 ± 0.8
^{75}As				20.4 ± 1.7
^{93}Nb		0.53 ± 0.10	14.6 ± 2.2	25.8 ± 2.1
^{103}Rh			10.6 ± 1.7	38.8 ± 3.1
^{107}Ag, ^{109}Ag			10.0 ± 1.5	37.6 ± 2.9
^{115}In			17.1 ± 2.6	33.3 ± 2.7
^{121}Sb, ^{123}Sb			20.7 ± 3.1	42.5 ± 3.6
^{127}I			38.7 ± 5.8	38.8 ± 3.1
^{133}Cs			31.7 ± 4.8	52.5 ± 3.8
^{139}La		8.61 ± 0.86	40.8 ± 6.5	63.0 ± 5.0
^{141}Pr			21.5 ± 3.2	58.3 ± 4.1
^{151}Eu, ^{153}Eu		28.9 ± 3.2	61.3 ± 14.7	102 ± 18
^{165}Ho		35.6 ± 4.3	92.2 ± 27.6	150 ± 20
^{181}Ta	4.14 ± 0.36	45.4 ± 3.7	65.0 ± 5.5	146 ± 12
^{197}Au		44.5 ± 3.6	68.4 ± 13.5	160 ± 15
^{206}Pb		<34.3		238 ± 29
^{208}Pb		22.6 ± 11.3		280 ± 31
^{209}Bi		36.1 ± 12.0		226 ± 27

REF.	ELEM. SYM.	A	Z
F. T. Kuchnir, P. Axel, L. Criegee, D. M. Drake, A. O. Hanson and D. C. Sutton Phys. Rev. 161, 1236 (1967)	Bi	209	83

METHOD	REF. NO.	
	67 Ku 1	HMG

REACTION	RESULT	EXCITATION ENERGY	SOURCE TYPE	SOURCE RANGE	DETECTOR TYPE	DETECTOR RANGE	ANGLE
G,N	SPC	12-16	D	12-16	TOF	0-8	115

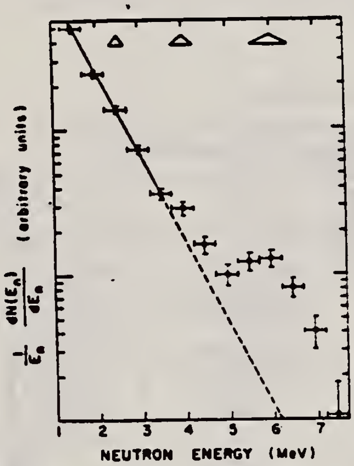

Fig. 4. Semilogarithmic plot of the spectrum resulting from the data shown in Fig. 3 after dividing by the neutron energy and correcting for the detector efficiency (solid line in Fig. 2). Triangles represent the neutron-energy resolution. The solid line extrapolated to higher neutron energies is the result of a least-squares fit to the five lowest-energy points. The apparent nuclear temperature represents only a lower limit since the line-shape correction has not been included.

REF.
A. V. Mitrofanova, Yu. N. Ranyuk, and P. V. Sorokin
J. Nucl. Phys. (USSR) 6, 703 (1967)
Sov. J. Nucl. Phys. 6, 512 (1968)

ELEM. SYM.	A	Z
Bi	209	83

METHOD

REF. NO.	
67 Mi 1	HMG

REACTION	RESULT	EXCITATION ENERGY	SOURCE TYPE	SOURCE RANGE	DETECTOR TYPE	DETECTOR RANGE	ANGLE
G,F	ABX	300-999		300-999	TRK-I		

Detector: Fission fragment tracks in glass.

999 = 1600 MEV

Angular distribution measured for Pb was found isotropic; for other elements it was assumed isotropic.

Nucleus	Fissionability D	Cross section σ_K, $\mu\beta$	Nucleus	Fissionability D	Cross section σ_K, $\mu\beta$
Bi	0.11±0.01	7.8±0.6	Os	0.0058±0.0005	0.37±0.04
Pb	0.050±0.004	3.4±0.3	Re	0.0056±0.0006	0.35±0.04
Tl	0.031±0.003	2.1±0.2	Ta	0.0045±0.0005	0.27±0.03
Au	0.019±0.002	1.25±0.10	Hf	0.0042±0.0004	0.25±0.03
Pt	0.012±0.002	0.80±0.08			

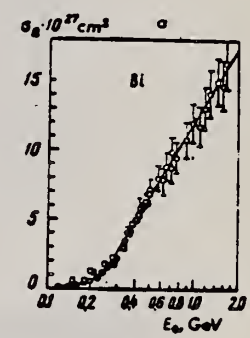

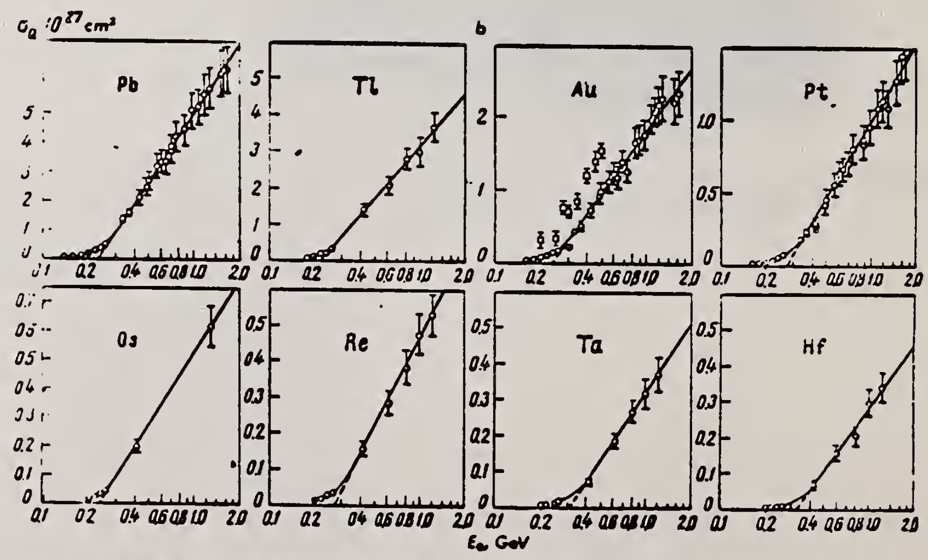

Fig. 1. Photofission fragment yields. O-present work; □-Jungerman and Steiner.[11] The curves were plotted through the experimental points.

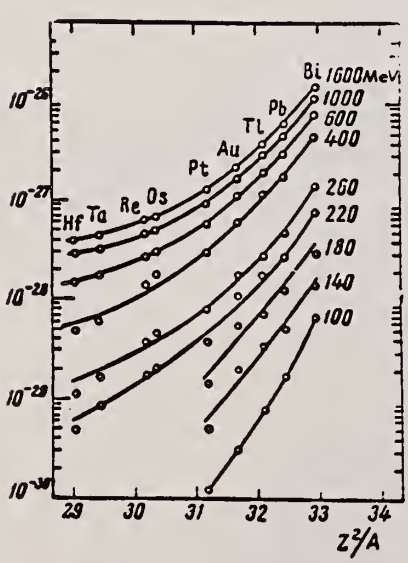

Fig. 2. Photofission fragment yields as a function of Z^2/A. The ordinates are values of σ_Q in units of cm².

REF.	ELEM. SYM.	A	Z
Yu. N. Ranyuk and P. V. Sorokin J. Nucl. Phys. (USSR) 5, 37 (1967) Sov. J. Nucl. Phys. 5, 26 (1967)	Bi	209	83

METHOD	REF. NO.	
	67 Ra 2	HMG

REACTION	RESULT	EXCITATION ENERGY	SOURCE TYPE	SOURCE RANGE	DETECTOR TYPE	DETECTOR RANGE	ANGLE
G,F	ABX	THR-260	C	100-260	EMU-I		DST

Angular distribution isotropic to 5%.

Table II

$E_{\gamma max}$, MeV	Cross section per equivalent γ quantum, 10^{-27} cm²			
	Bi	Pb	Au	Pt
100	0.07±0,005	0.017±0.002	0.003±0.0005	0.0012±0.0002
120	0.15±0.01	0.032±0.003	0.014±0.001	0.0035±0.0003
140	0.20±0.01	0.054±0.004	0.020±0.001	0.0053±0.0006
150 *	0,61±0.12	—	—	—
160	0.31±0.01	0.096±0.005	0.037±0.001	0.012±0.0005
180	0.46±0.02	0.13±0.01	0.055±0.001	0.015±0.001
180 *	0.68±0,09	—	—	—
200	0.62±0.02	0.20±0.01	0.082±0.002	0.031±0.001
200 *	1.3 ±0.24	—	0.31±0.09	—
200 **	0.7	—	—	—
220	0.83±0,03	0.28±0.01	0.108±0.003	0.039±0.001
240	1.22±0.03	0.36±0.01	0.146±0.003	0.063±0.001
240 **	1.5	—	—	—
250 *	1.78±0.22	—	0.33 ±0.07	—
260	1.50±0,04	0.50±0.02	0.180±0.004	0.085±0.002

*From [20].
**From [11].

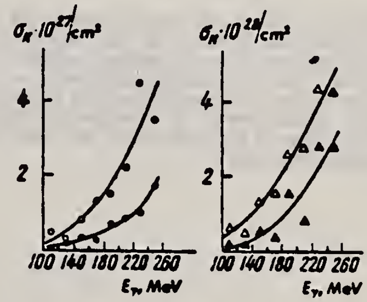

Fig. 3. Photofission cross sections. ○ – Bi, ● – Pb, △ – Au, ▲ – Pt. The curves were calculated from smoothed yield curves.

REF.	ELEM. SYM.	A	Z
J. M. Wyckoff Phys. Rev. 159, 953 (1967)	Bi	209	83

METHOD	REF. NO.	
	67 Wy 1	HMG

REACTION		RESULT	EXCITATION ENERGY	SOURCE		DETECTOR		ANGLE
				TYPE	RANGE	TYPE	RANGE	
G,4NP	G,8NP	RLI	THR-137	C	137	ACT-I		4PI
G,5NP								
G,6NP								
G,7NP								

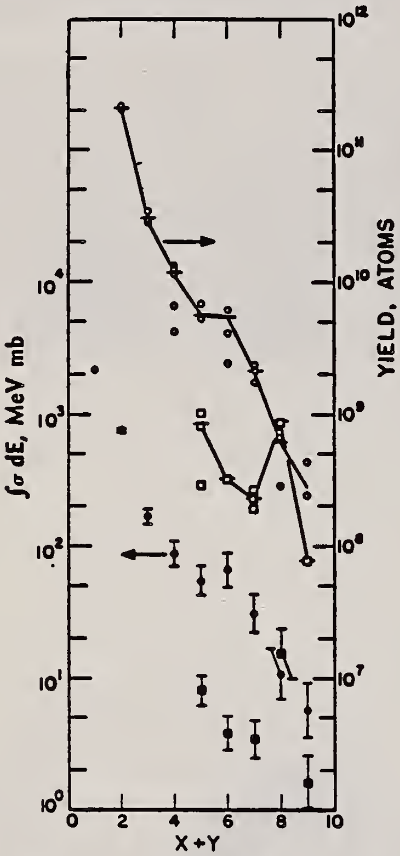

FIG. 1. The plotted points in the upper portion of this graph represent the relative yield in atoms of each nuclide plotted against the sum of the neutrons x and protons y emitted. Circles are for bismuth and squares for lead nuclides with $y=1$. The points in the lower portion of the graph are cross sections integrated to 137-MeV photon energy. Uncertainties indicated are deduced from the scatter of the yield points and thick target bremsstrahlung shape uncertainty.

TABLE I. Integrated cross sections and mean yield for production of $^{200-208}$Bi and $^{200-204}$Pb.

Process	Nuclide produced	Mean yield	$\int\sigma\,dE$ MeV-mb
(γ,n)	^{208}Bi	...	2170
$(\gamma,2n)$	^{207}Bi	2.08×10^{11}	760 ±38
$(\gamma,3n)$	^{206}Bi	3.09×10^{10}	168 ±25
$(\gamma,4n)$	^{205}Bi	1.19×10^{10}	88 ±22
$(\gamma,5n)$	^{204}Bi	5.63×10^{9}	55 ±16
$(\gamma,6n)$	^{203}Bi	5.43×10^{9}	66 ±23
$(\gamma,7n)$	^{202}Bi	2.10×10^{9}	31 ±12
$(\gamma,8n)$	^{201}Bi	6.01×10^{8}	10.7 ± 5.9
$(\gamma,9n)$	^{200}Bi	2.76×10^{8}	5.7 ± 3.4
$(\gamma,4np)$	^{204}Pb	8.25×10^{8}	8.0 ± 2.4
$(\gamma,5np)$	^{203}Pb	3.12×10^{8}	3.8 ± 1.3
$(\gamma,6np)$	^{202}Pb	2.28×10^{8}	3.4 ± 1.3
$(\gamma,7np)$	^{201}Pb	8.57×10^{7}	15.3 ± 8.4
$(\gamma,8np)$	^{200}Pb	7.8×10^{7}	1.62 ± 0.97

REF.		ELEM. SYM.	A	Z
J. M. Wyckoff Phys. Rev. 159, 953 (1967)		Bi	209	83
METHOD		REF. NO.		
		67 Wy 1		HMG

REACTION		RESULT	EXCITATION ENERGY	SOURCE		DETECTOR		ANGLE
				TYPE	RANGE	TYPE	RANGE	
G,3N	G,7N	RLI	THR-137	C	137	ACT-I		4PI
G,4N	G,8N							
G,5N	G,9N							
G,6N								

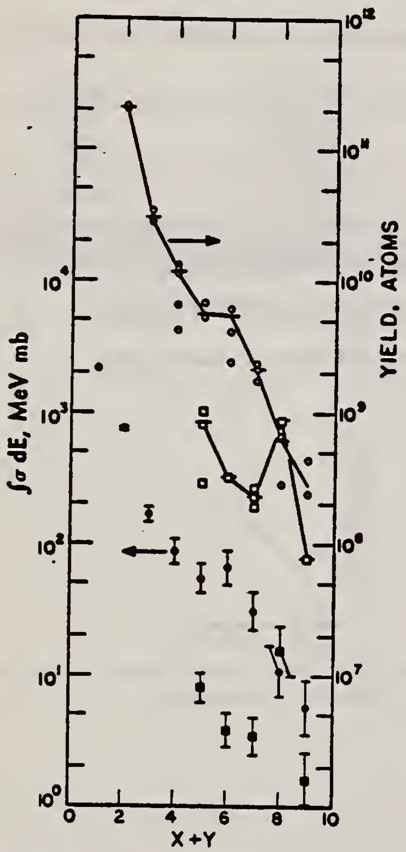

FIG. 1. The plotted points in the upper portion of this graph represent the relative yield in atoms of each nuclide plotted against the sum of the neutrons x and protons y emitted. Circles are for bismuth and squares for lead nuclides with $y=1$. The points in the lower portion of the graph are cross sections integrated to 137-MeV photon energy. Uncertainties indicated are deduced from the scatter of the yield points and thick target bremsstrahlung shape uncertainty.

TABLE I. Integrated cross sections and mean yield for production of $^{200-208}$Bi and $^{200-204}$Pb.

Process	Nuclide produced	Mean yield	$\int\sigma\, dE$ MeV-mb
(γ,n)	^{208}Bi	...	2170
$(\gamma,2n)$	^{207}Bi	2.08×10^{11}	760 ±38
$(\gamma,3n)$	^{206}Bi	3.09×10^{10}	168 ±25
$(\gamma,4n)$	^{205}Bi	1.19×10^{10}	88 ±22
$(\gamma,5n)$	^{204}Bi	5.63×10^{10}	55 ±16
$(\gamma,6n)$	^{203}Bi	5.43×10^{9}	66 ±23
$(\gamma,7n)$	^{202}Bi	2.10×10^{9}	31 ±12
$(\gamma,8n)$	^{201}Bi	6.01×10^{8}	10.7 ± 5.9
$(\gamma,9n)$	^{200}Bi	2.76×10^{8}	5.7 ± 3.4
$(\gamma,4np)$	^{204}Pb	8.25×10^{8}	8.0 ± 2.4
$(\gamma,5np)$	^{203}Pb	3.12×10^{8}	3.8 ± 1.3
$(\gamma,6np)$	^{202}Pb	2.28×10^{8}	3.4 ± 1.3
$(\gamma,7np)$	^{201}Pb	8.57×10^{8}	15.3 ± 8.4
$(\gamma,8np)$	^{200}Pb	7.8×10^{7}	1.62 ± 0.97

REF. A. V. Babchenko, V. V. Petrenko, Yu. N. Ranyuk, P. V. Sorokin Ukr. Fiz. Zhur. 13, 863 (1968) Ukr. Phys. J. 13, 615 (1968)	ELEM. SYM.	A	Z
	Bi	209	83
METHOD	REF. NO. 68 Ba 2		egf

REACTION	RESULT	EXCITATION ENERGY	SOURCE TYPE	SOURCE RANGE	DETECTOR TYPE	DETECTOR RANGE	ANGLE
E,F	ABX	THR-999	D	200-999	FRG-I		4PI

999=1.5 GEV

σ_e = electron induced fission

σ_Q = cross section per equivalent photon for photofission

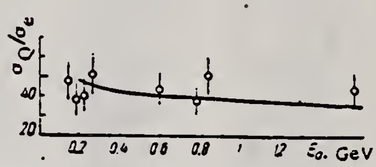

Fig. 2. σ_Q/σ_e as a function of electron energy.

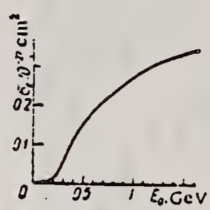

Fig. 3. Cross section for the fission of bismuth by electrons as function of electron energy.

REF. H. R. Bowman, R. C. Gatti, R. C. Jared, G. Kilian, L. G. Moretto, S. G. Thompson, M. R. Croissiaux, J. H. Heisenberg, R. Hofstadter, L. M. Middleman, and M. R. Yearian
Phys. Rev. 168, 1396 (1968)

ELEM. SYM.	A	Z
Bi	209	83

METHOD

REF. NO. 68 Bo 1 — HMG

REACTION	RESULT	EXCITATION ENERGY	SOURCE TYPE	SOURCE RANGE	DETECTOR TYPE	DETECTOR RANGE	ANGLE
E,F	ABI		D	250,500	EMU-I		4PI
					(MICA)		

TABLE I. Experimental results.

Target	Thickness	Method used	Fission cross section 250 MeV e^- (cm^2)	Fission cross section 500 MeV e^- (cm^2)
$_{92}U^{235}$ [a]	85 $\mu g/cm^2$	Mica	$(6.0\pm1.2)\times10^{-27}$	$(9.4\pm1.9)\times10^{-27}$
$_{92}U^{238}$	162 $\mu g/cm^2$	Counter	$(5.0\pm1.0)\times10^{-27}$	$(7.0\pm1.4)\times10^{-27}$
$_{83}Bi^{209}$	1 mg/cm^2	Mica	$(2.3\pm0.5)\times10^{-29}$	$(1.4\pm0.3)\times10^{-29}$
$_{73}Ta^{181}$	4 mg/cm^2	Mica		3.9×10^{-31} [b]

[a] U^{235}/U^{238} was 1.12×10^{-3} in target sample.
[b] Not corrected for photofission contribution [see (4) in text].

REF. N. N. Kaushal, E. J. Winhold, P. F. Yergin, H. A. Medicus and R. H. Augustson Phys. Rev. 175, 1330 (1968)	ELEM. SYM.	A	Z
	Bi	209	83

METHOD	REF. NO.	
	68 Ka 1	HMG

REACTION	RESULT	EXCITATION ENERGY	SOURCE		DETECTOR		ANGLE
			TYPE	RANGE	TYPE	RANGE	
G,N	ABX	50-85	C	55,85	TOF-D	10-85	67
							(67.5)

NEUT ENGY SPEC

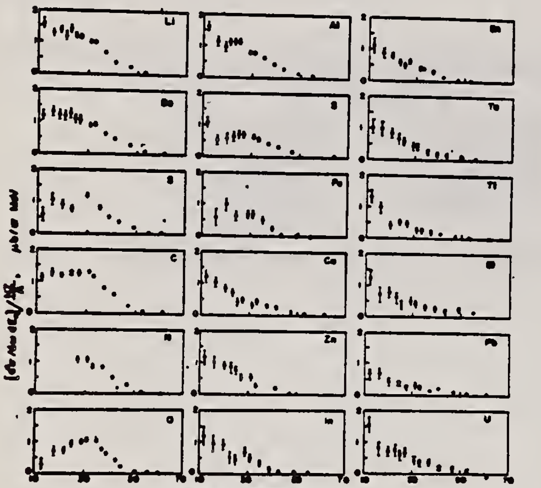

FIG. 6. Observed neutron spectra due to 55–85-MeV difference photon spectra. The effective cross sections have been divided by NZ/A.

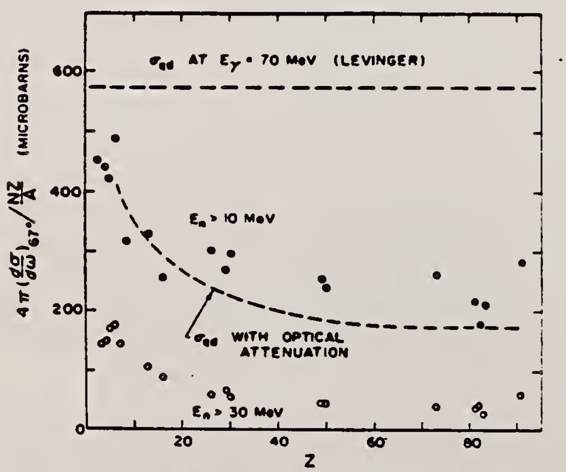

FIG. 7. Effective cross sections for production of fast neutrons with energies greater than 10 MeV (solid circles) and 30 MeV (open circles) by the 55–85-MeV photon difference spectrum. The dashed curves are modified quasideuteron model predictions as discussed in the text.

TABLE I. Comparison of present cross-section values in mb for production of high-energy photoneutrons by 55–85-MeV photons with measured cross sections $\sigma(\gamma,Tn)$, also in mb, for total photoneutron production. The present cross-section values are uncertain by 8 to 10% because of counting statistics and normalization errors; in addition all values depend on an absolute normalization in terms of the deuteron photodisintegration cross section, which is known to about 10% at these energies.

Target	$4\pi(d\sigma/d\omega)_{67°}$ (E_n > 10 MeV) [Present experiment]	$\sigma(\gamma,Tn)$ Jones and Terwilliger[a]	$\sigma(\gamma,Tn)$ Costa *et al.*[b]	Other results
Li	0.75		1.0	
Be	1.0	2.7	2.3	2.3[c]
B	1.0		1.4	
C	1.5	1.3	1.4	2.4[d]
O	1.3		1.6	
Al	2.8	5.5	4.6	8[d]
S	2.1		4.4	6.5[d]
Fe	4.2	16	12	
Cu	4.3	20	19	
Zn	4.4		15	
In	7.4			
Sn	7.0			
Ta	10.7	95		
Tl	10.7			
Pb	8.3	100		
Bi	13			
U	16	65		

[a] Average cross sections between 55 and 85 MeV, as read from Figs. 4 and 5 of Ref. 4.
[b] $\int_{5}^{85}\sigma dE - \int_{5}^{55}\sigma dE/30$, as taken from Fig. 4 of Ref. 5 and Table I of Ref. 6.
[c] S. Costa, L. Pasqualini, G. Piragino, and L. Roasio, Nuovo Cimento 42, 306 (1966).
[d] G. Bishop, S. Costa, S. Ferroni, R. Malvano, and G. Ricco, Nuovo Cimento 42, 148 (1966).

REF.			
A. I. Lepestkin Yad. Fiz. 8, 433 (1968) Sov. J. Nucl. Phys. 8, 251 (1969)	Bi	209	83
METHOD	REF. NO. 68 Le 1		HMG

REACTION	RESULT	EXCITATION ENERGY	SOURCE		DETECTOR		ANGLE
			TYPE	RANGE	TYPE	RANGE	
G,N	SPC	7-20	C	20	EMU-D	0-13	DST

FIG. 1. Energy distribution of photoneutrons from Bi for $E_{\gamma\,max}$ = 20 MeV for an angle of 90°.

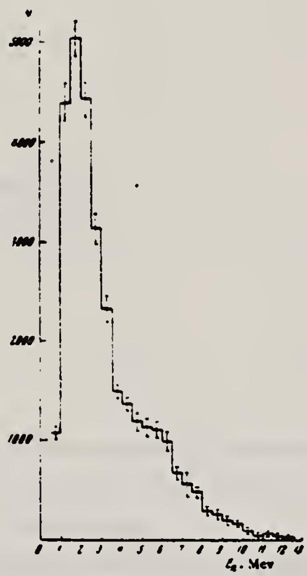

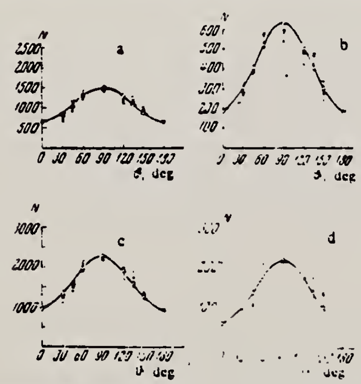

FIG. 2. Angular distributions of photoneutrons from Bi for $E_{\gamma\,max}$ = 20 MeV: a – 5 < E_n ≤ 7 MeV, b – 7 < E_n ≤ 9 MeV, c – 5 < E_n ≤ 12.6 MeV, d – 9 < E_n ≤ 12.6 MeV. X – Experimental points (the statistical errors are shown). O – points from a curve calculated by the method of least squares (solid line).

REF.	ELEM. SYM.	A	Z
R.V. Warnock and R.C. Jensen J. Inorg. Nucl. Chem. 30, 2011 (1968)	Bi	209	83

METHOD	REF. NO.	
	68 Wa 1	egf

REACTION	RESULT	EXCITATION ENERGY	SOURCE TYPE	SOURCE RANGE	DETECTOR TYPE	DETECTOR RANGE	ANGLE
G,F	ABX	30-40	C	30-40	ACT-I		4PI

FRAGMENT YIELDS

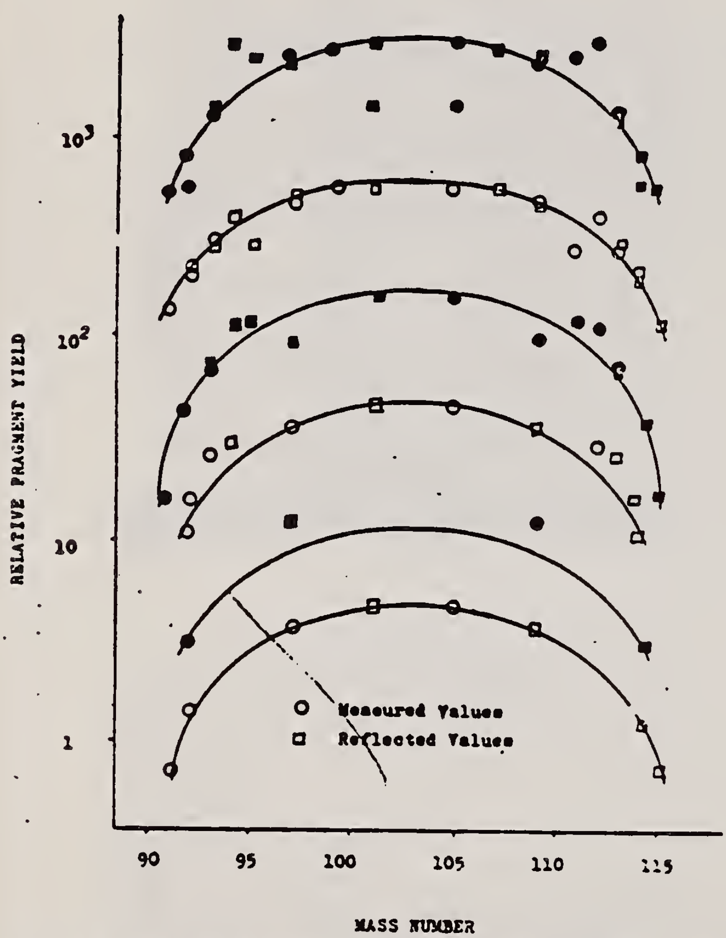

Fig. 2. Fragment yield per saturated copper activity as a function of mass number and peak bremsstrahlung energy.

(over)

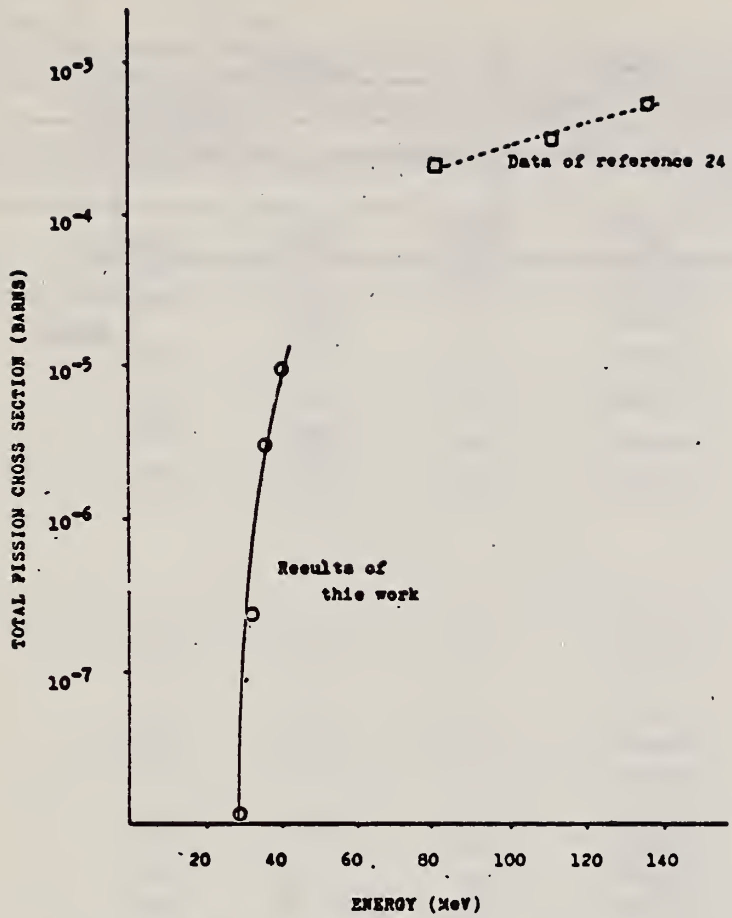

Fig. 3. Total fission cross-section as a function of photon energy.

REF.	ELEM. SYM.	A	Z
J. F. Ziegler and G. A. Peterson Phys. Rev. 165, 1337 (1968)	Bi	209	83

METHOD	REF. NO.	
	68 Zi 1	HMG

REACTION	RESULT	EXCITATION ENERGY	SOURCE TYPE	SOURCE RANGE	DETECTOR TYPE	DETECTOR RANGE	ANGLE
E,E/	FMF	2-3	D	28-73	MAG-D	28-73	100

B(EL)

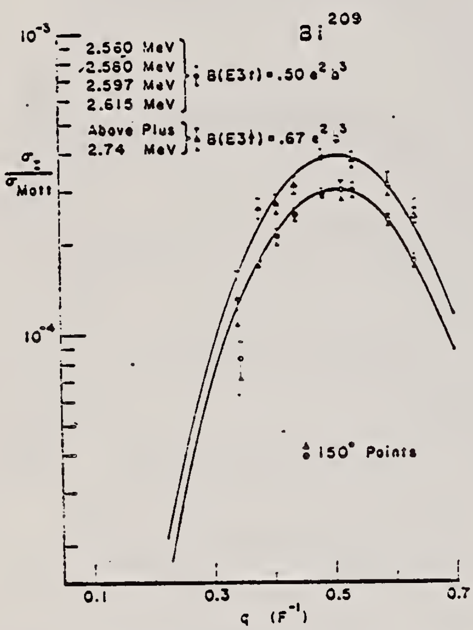

FIG. 15. Experimental relative cross section versus momentum transferred to the nucleus Bi^{209} normalized to an initial electron energy of 70 MeV for the group of excitations at about 2.6 MeV. The solid curves are the best fits of the GBROW calculation assuming the Tassie hydrodynamical model for an $L=3$ transition.

OVER

TABLE II. Experimental values of reduced nuclear transition probabilities $B(EL)$ for the excitation of a nucleus from its ground state to an excited state as determined by the electron scattering methods of this experiment and by other methods. The units of $B(EL)$ are e^2b^L where e is the electron charge, b is 10^{-24} cm² (1 b), and L is the multipolarity of the transition. $B(EL)_{sp}$ is the single-particle estimate of Eq. (10).

Nuclide	Level (MeV)	Transition character	This experiment $B(EL, 0 \to L)$ e^2b^L	This experiment $G = \frac{B(EL)}{B(EL)_{sp}}$	Ref.	Other experiments $B(EL, 0 \to L)$ e^2b^L
Pb^{206}	4.09	$E2$	0.23±0.02	6.2	a	(p,p')0.20
Pb^{207}	4.090[b] 4.125[b]	$E2$	0.26±0.02	7.0	c d	(α,α')0.33 (p,p')0.18
Pb^{208}	4.07	$E2$	0.30±0.02	8.1	c e	(α,α')0.33 (p,p')0.17
Pb^{206}	2.65	$E3$	0.64±0.04	35	a	(p,p')0.33
Pb^{207}	2.625[b] 2.664[b]	$E3$	0.67±0.04	37	c d	(α,α')0.56 (p,p')0.32
Pb^{208}	2.614	$E3$	0.72±0.04	39.5	c f g e h i j k	(α,α')0.57 (e,e')0.55 (p,p')0.67 (p,p')0.36 $(C^{12},C^{12\prime}\gamma)$0.83 (p,p')0.84 (p,p')0.97 (n,n')0.71
Bi^{209}	2.6[l]	$E3$	0.67±0.05	37	c i m	(α,α')0.57 (e,e')0.55 (p,p')0.65
Pb^{206}	4.32	$E4$	0.22±0.02	25	a	(p,p')0.058
Pb^{207}	4.29	$E4$	0.21±0.03	24	c	(α,α')0.12
Pb^{208}	4.31	$E4$	0.23±0.02	26	c f e	(α,α')0.13 (e,e')0.24 (p,p')0.057
Pb^{208}	5.25	$E3$ $(E4)$	0.13±0.03 0.14±0.07	7.2 16		
Pb^{208}	5.6	$E3$	0.09±0.03	5	c	(α,α')0.16
Pb^{208}	6.2	$E2$ $(E0)$	0.07±0.02	2		
Pb^{208}	3.2	$E5$	0.06±0.02	14	c e	(α,α')0.03 (p,p')0.034

[a] G. Vallois, J. Saudinos, and O. Beer, Phys. Letters 24, 512 (1967).
[b] Peaks were not resolved in this experiment. Energies taken from J. C. Hafele and R. Woods, Phys. Letters 24, 579 (1966).
[c] J. Alster, Phys. Rev. 141, 1138 (1966); Phys. Letters 25B 459 (1967).
[d] G. Vallois, J. Saudinos, O. Beer, M. Gendrot, and P. Lopato, Phys. Letters 22, 659 (1966).
[e] J. Saudinos, G. Vallois, O. Beer, M. Gendrot, and P. Lopato, Phys. Letters 22, 492 (1966).
[f] H. Crannell, R. Helm, H. Kendall, J. Oeser, and M. Yearian, Phys. Rev. 123, 923 (1961); and H. W. Kendall and J. Oeser, *ibid.* 130, 245 (1963).
[g] A. Scott and M. P. Fricke, Phys. Letters 20, 654 (1966).
[h] A. Z. Hrynkiewicz, S. Kopta, S. Szymczyk, and T. Walczak, Nucl. Phys. 79, 495 (1966), references cited therein, and see text of this section.
[i] G. R. Satchler, R. H. Bassel, and R. M. Drisko, Phys. Letters 5, 256 (1963).
[j] T. Stovall and N. M. Hintz, Phys. Rev. 135, B330 (1964).
[k] P. H. Stelson *et al.*, Nucl. Phys. 68, 97 (1965).
[l] Approximate energy of seven unresolved peaks, J. C. Hafele and R. Woods, Phys. Letter 24, 579 (1966).
[m] S. Hinds, H. Marchant, J. H. Bjerregaard, and O. Nathan, Phys. Letters 20, 674 (1966.

REF.

R. B. Begzhanov and S. M. Akhrarov
ZhETP Pis. Red. 10, 39 (1969)
JETP Letters 10, 26 (1969)

ELEM. SYM.	A	Z
Bi	209	83

METHOD

REF. NO.	
69 Be 7	hmg

REACTION	RESULT	EXCITATION ENERGY	SOURCE TYPE	SOURCE RANGE	DETECTOR TYPE	DETECTOR RANGE	ANGLE
G,G	LFT	7.0	D	7.0	D		DST
		(7.15)		(7.15)			(90,135)

7.15 MEV

Self-Absorption.

Results of determination of the resonance-level parameters

Source-scatterer	E_γ, MeV	$<\sigma_{pp}>$, mb	Γ_{γ_0}, eV	D, keV	Reference
Pb → Zn^{64}	7.38	33±4.5	0.58±0.12	53.70±10.13	This work
Ti → Mo^{96}	6.413	11.2 ±1.4	0.11±0.02	8.68± 1.57	"
Ti → La^{139}	6.413	16 04±2.10	0.28±0.05	8.03± 1.42	"
Ti → Bi^{209}	7.15	1200±230	0.32 ±0.07	1.84± 0.40	"
	6.996	1550	–	–	[1]
	7.15	2600±800	0.42±0.14	–	[5]
Ti → Cu^{65}	6.07	423 ±108	0.34±0.06	99.1±17.4	This work
	6.07	440±130	0.36±0.07		[5]
Ti → Cu^{63}	6.07	215± 71	0.18 ±0.04	57.14±12.70	This work
	6.07	200± 60	0.16± 0.03	–	[6]
Cr → Cu^{63}	8.50	22 ± 7	0.25±0.08	130±40	This work
	8.499	35	75	–	[1]
	8.50	19 ±6	0.28±0.09	–	[6]
Cr → Cu^{65}	8.50	36 ± 9	0.47±0.10	21.36±4.54	This work
	8.499	80	10.5	–	[1]
	8.50	42 ±13	0.94±0.29	–	[6]
Cu → Sn^{117}	7.01	1150±240	0.15±0.04	0.44 ±0.12	This work
	7.01	1000	–	–	[1]
	7.01	1200±400	0.3 ±0.3	–	[5]
Hg → Mo^{96}	6.44	201 ±37	0.12 ±0.04	0.23 ±3.07	This work

REF.

R. Cesareo, M. Giannini, P. Oliva, D. Prosperi and M. C. Ramorino
Nucl. Phys. A132, 512 (1969)

Bi	209	83

METHOD

REF. NO. 69 Ce 1 — egf

REACTION	RESULT	EXCITATION ENERGY	SOURCE		DETECTOR		ANGLE
			TYPE	RANGE	TYPE	RANGE	
G,G	NOX	6-8	D	6-8	SCD-D	0-8	DST

3.2. THE 7637 keV RESONANCE IN Bi

The spectrum of the photons scattered from natural Bi is shown in fig. 6. Elastic transitions at 7637, 7172 and 6392 keV are evident. The energies and the relative intensities are given in table 2 together with the energies of the capture γ-ray lines for comparison purposes. The angular distribution on the 7637 keV transition, measured at 90° and 135° with the Ge(Li) detector, gives the result

$$N(135°)/N(90°) = 1.19^{+0.12}_{-0.08}.$$

For the angular distribution sequences $\frac{9}{2}(1)\frac{9}{2}(1)\frac{9}{2}$, $\frac{9}{2}(1)\frac{11}{2}(1)\frac{9}{2}$, $\frac{9}{2}(1)\frac{7}{2}(1)\frac{9}{2}$, such a ratio is equal to 1.16, 1.06 and 1.002 respectively. The spin of the 7637 keV level then probably has the value $\frac{9}{2}$.

TABLE 2

Energies and relative intensities of the photons resonantly scattered from a Bi target

E_γ(keV)	I_γ(rel)	$E_\gamma(n,\gamma)_{Cu}$ [a])	$I_\gamma(n,\gamma)_{Cu}$ [a])
6392 ± 8	23 ± 6	6393.4	1.1
7172 ± 4	20 ± 4	7176.1	2.4
7637	100	7637.0	14.5

[a]) Ref. [11]).

REF.

R. Garfagnini, G. Piragino & A. Zanini
Atti Accad. Naz. Lincei, Rend.
Cl. Sci. Fis. Mat. Natur. 47, 33 (1969)

ELEM. SYM.	A	Z
Bi	209	83

METHOD

REF. NO.	
69 Ga 3	egf

REACTION	RESULT	EXCITATION ENERGY	SOURCE TYPE	SOURCE RANGE	DETECTOR TYPE	DETECTOR RANGE	ANGLE
G,XN	SPC	8-85	C	85	CCH-D		135

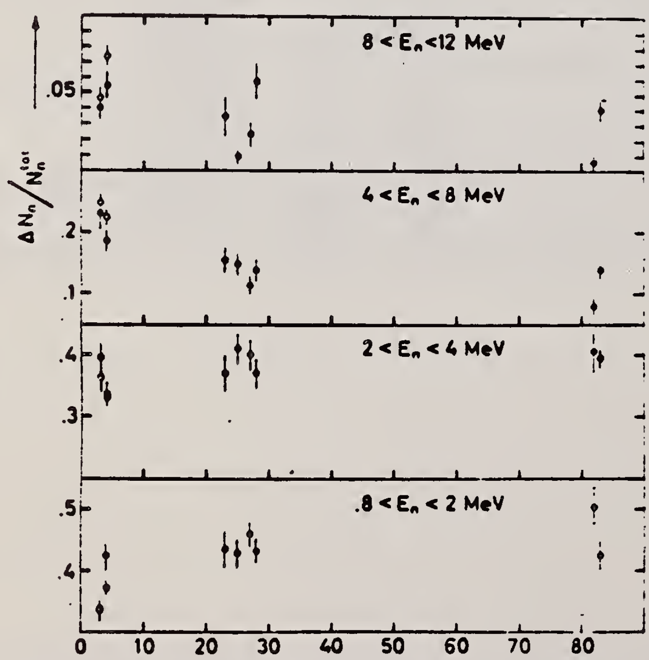

Fig. 1. – Percentage of the photoneutrons emitted at 135°, in the respective energy interval as a function of Z, by a γ-ray bremsstrahlung beam with $E_{\gamma max}$ ≃ 85 MeV. The open circles represent the values obtained at 90° for ^{7}Li and ^{9}Be.

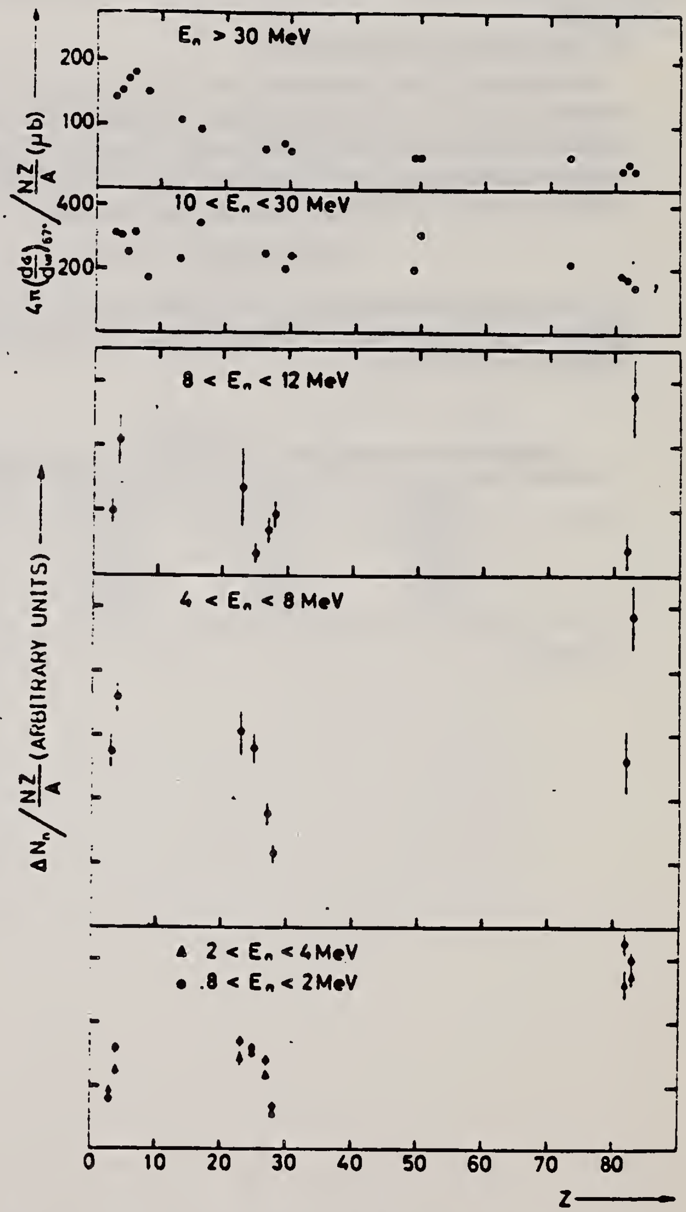

Fig. 2. – Number of photoneutrons emitted at 135°, normalized to the sum rule factor NZ/A, as a function of Z. In the upper part is reported the effective cross section divided by NZ/A for photoproduction of fast neutrons by 55–85 MeV bremsstrahlung photons as deduced by Kaushal *et al.* [1].

[1] N.N. Kaushal et al., Phys. Rev. 175, 1330 (1968).

REF.		ELEM. SYM.	A	Z
	A. P. Komar, B. A. Bochagov, A. A. Kotov, Yu. N. Ranyuk, G. G. Semenchuk, G. E. Solyakin, and P. V. Sorokin Yad. Fiz. 10, 51 (1969) Sov. J. Nucl. Phys. 10, 30 (1970)	Bi	209	83

METHOD	REF. NO.	
	69 Ko 2	egf

REACTION	RESULT	EXCITATION ENERGY	SOURCE		DETECTOR		ANGLE
			TYPE	RANGE	TYPE	RANGE	
G,F	SPC	THR-999	C	250-999	SCD-D		DST
		(1000)		(1000)			

999 = 1000 MEV

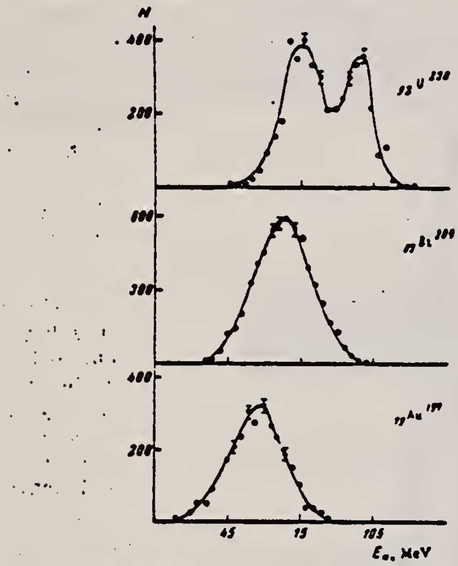

FIG. 2. Single-ended energy spectra of fragments from photofission of $_{92}U^{238}$, $_{83}Bi^{209}$, and $_{79}Au^{197}$.

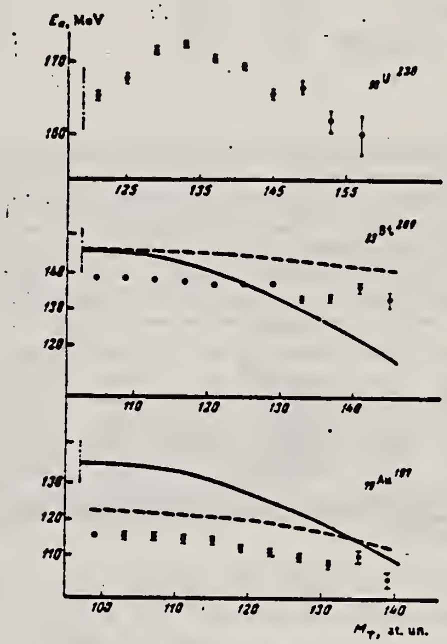

FIG. 4. Average total kinetic energies $\bar{E}_K$ of fragments from photofission of $_{92}U^{238}$, $_{83}Bi^{209}$, and $_{79}Au^{197}$, as a function of the heavy fragment mass. Points—experiment; solid curves—theory; dashed curves—experiment with inclusion of a correction for neutron emission from the fragments.

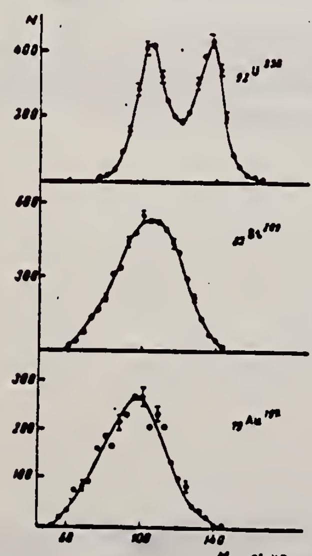

FIG. 3. Fragment mass distributions from photofission of $_{92}U^{238}$, $_{83}Bi^{209}$, and $_{79}Au^{197}$.

REF.		ELEM. SYM.	A	Z
L.E. Lazareva and A.I. Lepestkin Yad. Fiz. 10, 266 (1969) Sov. J. Nucl. Phys. 11, 149 (1970)		Bi	209	83
METHOD		REF. NO.		
		69 La 2		hmg

REACTION	RESULT	EXCITATION ENERGY	SOURCE TYPE	SOURCE RANGE	DETECTOR TYPE	DETECTOR RANGE	ANGLE
G,N	SPC	29	C	29	EMU-D	4-	DST
		(28.5)		(28.5)			

E_n	b/a	A/a
>3.5	.48	.13
>8	1.53	.98
$3.5<E_n\leq 5$	.20	-.004

Asymmetry coefficients A/a in the angular distributions of the type $I(\vartheta) = a + b\sin^2\vartheta + A\cos\vartheta$, obtained in different investigations for photoneutrons from Bi

Reference	$E_{\gamma\,max}\sim 20$ MeV: $E_{\gamma\,max}$, MeV	E_n, MeV	A/a	Reference	$E_{\gamma\,max}\geq 30$ MeV: $E_{\gamma\,max}$, MeV	E_n, MeV	A/a
[15]*	20	>5.5	0.14±0.11	[15]*	30	>3.5	0.05±0.03
						>5.5	0.23±0.06
[14]	22	>3	0.155±0.056	[8]	30	>4	0.33±0.04
[3]	22	>5.5	0.09±0.06	[8]	55	>5.5	0.29±0.05
[8]	17.5	>4.5	−0.02±0.07	[8]	34	>8	0.29±0.05
[9]	20	>3.5	−0.08±0.04	Present work	28.5	3.5–5	−0.004±0.084
		>5	−0.03±0.07			>3.5	0.13±0.07
		>7	−0.01±0.17			>5	0.23±0.11
						>8	0.98±0.31

*More accurate values of the asymmetry coefficients, obtained from the data of [15], are given in [5].

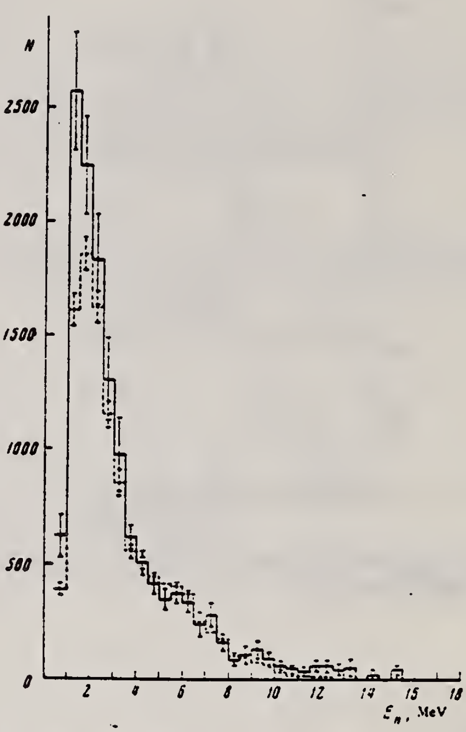

FIG. 4. Energy spectrum of photoneutrons from Bi at 90°, following irradiation by a bremsstrahlung spectrum with maximum energy $E_{\gamma max}$ = 20 MeV (dashed curve) and 28.5 MeV (solid curve). The histograms are made to coincide in the interval 4 – 4.5 MeV.

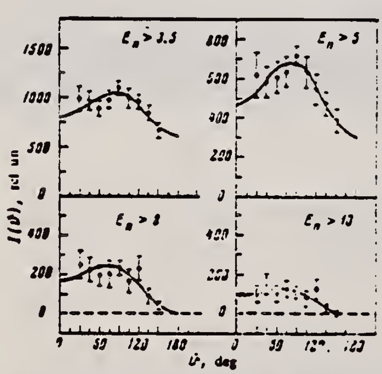

FIG. 2. Angular distributions for different integrals of the neutron energy E_n. The curves were calculated by the method of least squares ($I(\vartheta) = a + b\sin^2\vartheta + A\cos\vartheta$).

[5]O. Borello, F. Ferrero, R. Malvano, and A. Molinari, Nucl. Phys. 31, 53 (1962).

[15]F. Ferrero, A. O. Hanson, R. Malvano, and C. Tribuno, Nuovo Cimento 4, 418 (1956).

F. R. Metzger
Phys. Rev. 187, 1680 (1969)

Bi	209	83

METHOD	REF. NO.	
	69 Me 2	hmg

REACTION	RESULT	EXCITATION ENERGY	SOURCE		DETECTOR		ANGLE
			TYPE	RANGE	TYPE	RANGE	
G,G	LFT	2-3	C	3	SCD-D		127
		(2.563, 2.581,		(2.72)			
		2.598)					

2.563, 2.581, 2.598

The resonant scattering of electron bremsstrahlung by the $\frac{7}{2}^+$, $\frac{9}{2}^+$, and $\frac{11}{2}^+$ members of the 2.6-MeV septuplet in Bi^{209} has been studied. On the basis of the scattered intensities, and assuming ground-state branching ratios Γ_0/Γ of 0.5, 1.0, and 1.0, respectively, ground-state transition widths of $\Gamma_0(2.581, \frac{7}{2}^+) < 10$ meV, $\Gamma_0(2.563, \frac{9}{2}^+) = 30 \pm 5$ meV, and $\Gamma_0(2.598, \frac{11}{2}^+) = 9.0 \pm 2.4$ meV were obtained. The observed transition strengths agree well with the predictions of the particle-vibration model in the form used by Hamamoto, with $e_{eff}^2(E1) = 0.05$.

TABLE II. Bi^{209}. Summary of the widths Γ_0 obtained from the resonance-scattering experiments, and comparison of the corresponding $B(E1)$'s with the results of other experiments and of calculations (Ref. 10) based on the particle-vibration coupling model. $B(E1)_{sp} = (e^2/4\pi)(\frac{3}{4})^2 R_0^2$ was used for the single-particle reduced $E1$ transition probability.

Level energy (MeV)	Γ_0/Γ	Γ_0 (MeV)	$B(E1)_{expt}/B(E1)_{sp}$ This work	$B(E1)_{expt}/B(E1)_{sp}$ Others	$B(E1)_{theor}$[a] / $B(E1)_{sp}$
2.563	1	30±5	$(7.5 \pm 1.3) \times 10^{-4}$	$\geq 2.1 \times 10^{-4}$ [b]	5.5×10^{-4}
2.581	0.5	<10	$< 2.5 \times 10^{-4}$	6.3×10^{-6} [b]	7.5×10^{-6}
2.598	1	9.0±2.4	$(2.2 \pm 0.6) \times 10^{-4}$	$\geq 2.1 \times 10^{-4}$ [b]	3.1×10^{-4}

[a] Reference 10, using $e_{eff}^2(E1) = 0.05$.
[b] Reference 2.

[2] R. A. Broglia, J. S. Lilley, R. Perazzo, and W. R. Phillips, Univ. of Minnesota, AEC Report No. COO-1265-79 (unpublished).
[10] I. Hamamoto, Nucl. Phys. A135, 576 (1969).

REF.

L. G. Moretto, R. C. Gatti, S. G. Thompson, J. T. Routti, J. H. Heisenberg, L. M. Middleman, M. R. Yearian, R. Hofstadter
Phys. Rev. 179, 1176 (1969)

ELEM. SYM.	A	Z
Bi	209	83

METHOD

REF. NO.	
69 Mo 1	hmg

REACTION	RESULT	EXCITATION ENERGY	SOURCE TYPE	SOURCE RANGE	DETECTOR TYPE	DETECTOR RANGE	ANGLE
E,F	ABX	THR-999	D	60-999	TRK-I		DST
G,F	ABX	THR-999	C	60-999	TRK-I		DST

Tabular data given; angular distribution isotopes

999 = 1 GEV

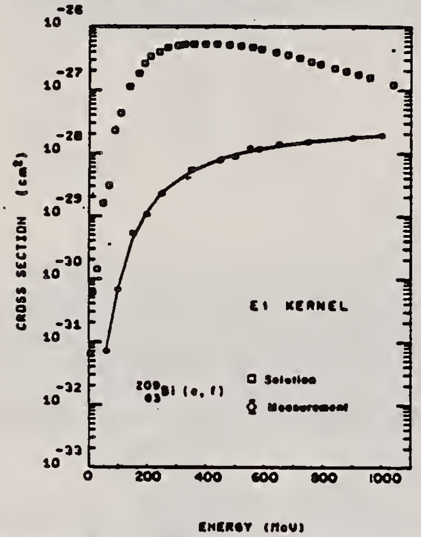

FIG. 7. Photofission cross section as a function of energy for $^{209}_{83}$Bi (open squares) as obtained by unfolding the electron-induced fission cross-section data (diamonds) with the $E1$ kernel. The solid line is the fit to the electron-induced fission cross sections which is obtained by folding back the photofission cross section into the $E1$ kernel.

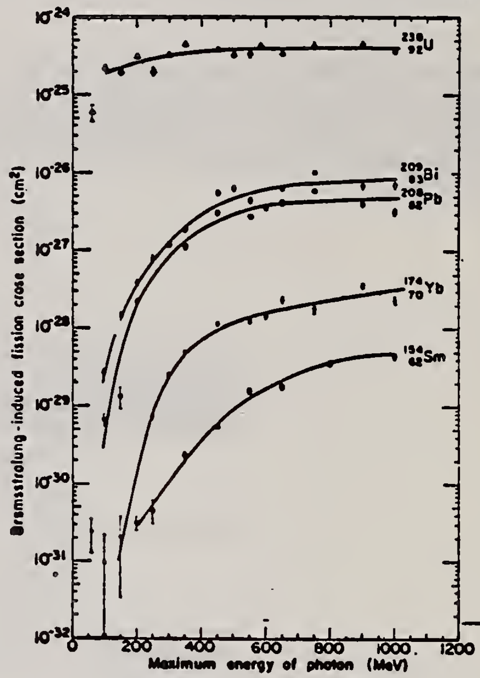

FIG. 4. Bremsstrahlung-induced fission cross section per equivalent quantum.

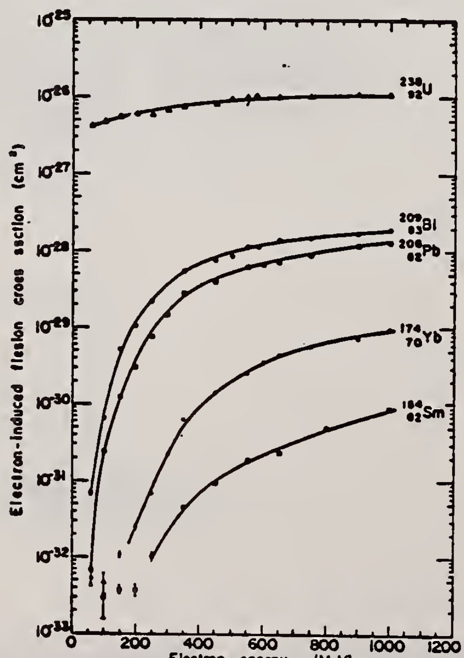

FIG. 2. Electron-induced fission cross-section data. Different symbols for the same isotope refer to different targets.

REF. S. Ramchandran and J. A. McIntyre
Phys. Rev. 179, 1153 (1969)

ELEM. SYM.	A	Z
Bi	209	83

METHOD

REF. NO.	
69 Ra 1	hmg

REACTION	RESULT	EXCITATION ENERGY	SOURCE		DETECTOR		ANGLE
			TYPE	RANGE	TYPE	RANGE	
G,G	LFT	8,8	D	8,8	NAI		DST
		(7.416)		(7.416)			
		(7.149)		(7.149)			

$W(\theta) \sim [1 + a\, P_2(\cos\theta)]$

8,8 = 7.416, 7.149

over

TABLE II. Experiment compared to theory assuming a pure dipole transition.

^{90}Zr	Cd	Sn	Hg	^{203}Tl	^{208}Pb	^{209}Bi (7.416 MeV)	^{209}Bi (7.149 MeV)	$A_2^2(J_0, J_1, L=1)$ (Theoretical)	J_0	J_1
$\alpha \pm \Delta\alpha$ (Experimental)										
0.489±0.027	0.488±0.034	0.490±0.095	0.48±0.11		0.485±0.026			0.500	0	1
	0.488±0.034	0.490±0.095	0.48±0.11	0.0017±0.0110				0.000	1/2	1/2
	0.488±0.034	0.490±0.095	0.48±0.11	0.0017±0.0110				0.250	1/2	3/2
			0.48±0.11					0.000	3/2	1/2
			0.48±0.11					0.160	3/2	3/2
			0.48±0.11					0.140	3/2	5/2
						0.195±0.033	0.184±0.074	0.024	9/2	7/2
						0.195±0.033	0.184±0.074	0.194	9/2	9/2
						0.195±0.033	0.184±0.074	0.033	9/2	11/2

TABLE V. Summary of energy-level parameters.

Element	^{90}Zr	Cd	Sn	Hg	^{203}Tl	^{208}Pb	^{209}Bi	^{209}Bi
Level energy (MeV)	8.496[a]	6.485[b]	6.988[c]	4.906[b]	7.647[d]	7.277[e]	7.416[c]	7.149[a]
γ ray source	Se	Co	Cu	Co	Fe	Fe	Se	Ti
	0→1	0→1	0→1	0→1	1/2→1/2	0→1	9/2→7/2	9/2→7/2
		(1/2→3/2)	(1/2→3/2)	3/2→5/2	(1/2→3/2)		9/2→9/2	9/2→9/2
$J_0 \to J_1$				(1/2→3/2)			9/2→11/2	9/2→11/2
				(3/2→3/2)				
Γ_0/Γ	0.8±0.2				0.85±0.17[f]	$0.95_{-0.11}^{+0.05}$	0.6±0.2	
Γ_0 (eV)	1.68±0.02				1.0[f]	0.68±0.03	0.14±0.09	
ε (eV)	5.60±0.15				11.5±0.2[f]	8.00±0.14	3.4±1.6	

[a] L. V. Groshev, V. N. Lutsenko, A. M. Demidov, and V. I. Polekov, *Atlas of Gamma Spectra from Radiative Capture of Thermal Neutrons* (Pergamon Press, Inc., New York, 1959).
[b] E. B. Shera and D. W. Hafemeister, Phys. Rev. 150, 894 (1966).
[c] H. H. Bolotin (private communication from L. M. Bollinger).
[d] R. Moreh and G. Ben-Yaacov, Nuclear Research Center—Negev Report, NRCN-180, 1967, (unpublished).
[e] L. V. Groshev, A. M. Demidov, G. A. Kotelnikov, and V. N. Lutsenko, Nucl. Phys. 58, 465 (1964); G. T. Ewan and A. J. Tavendale, Nucl. Instr. Methods 26, 183 (1964).
[f] See Ref. 24a.

REF.	ELEM. SYM.	A	Z
Yu. N. Ranyuk, V.M. Sanin, and P.V. Sorokin Ukr. Fiz. Zhur. 14, 408 (1969)	Bi	209	83

METHOD	REF. NO.	
	69 Ra 4	egf

REACTION	RESULT	EXCITATION ENERGY	SOURCE		DETECTOR		ANGLE
			TYPE	RANGE	TYPE	RANGE	
G,F	ABX	35-140	C	40-140	TRK-I		4PI

Yields of nuclear fission reaction for Bi, Au and Pt by bremsstrahlung were measured by means of solid state track detectors in the energy range from 40 to 140 MeV. The fission threshold for these nuclei is higher than the giant resonance energy which allowed total photofission cross-sections to be calculated by the yield curves.

A rapid increase of the cross-sections with the photon energy testifies to the preference of the statistical model within which the fission thresholds of target nuclei were calculated.

The results of the present experiment may be used to obtain information on the photon interaction mechanism in the energy region between the giant resonance and the threshold of meson production where this problem is still obscure.

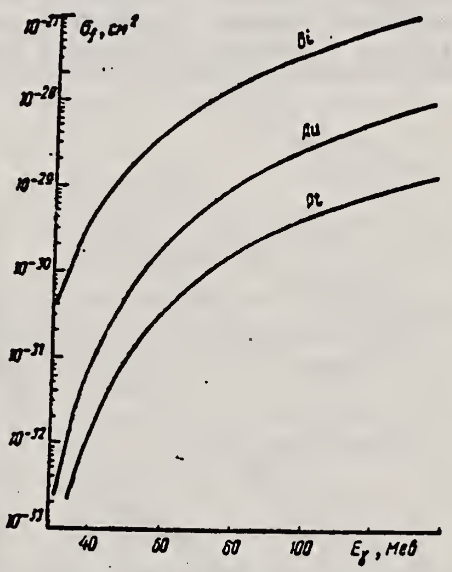

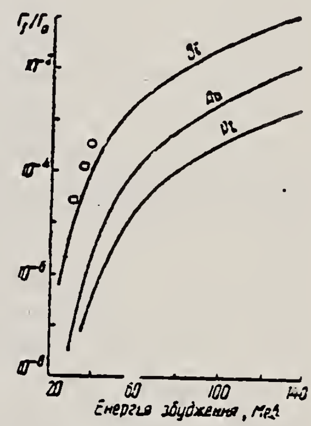

Рис. 3. Перерізи фотоподілу, розраховані на один реальний γ-квант підгонкою за формулою (4).

Рис. 4. Відношення ділильної і нейтронної ширин: □ — дані роботи [5] для суміші ізотопів Bi^{207} і Bi^{209}.

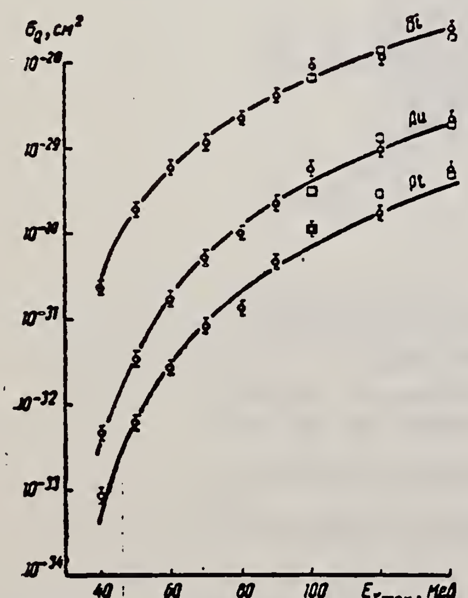

Рис. 2. Виходи уламків поділу: ○ — дані даної роботи, □ — дані роботи [3]. Суцільні криві одержані підгонкою за формулою (4).

REF.	H. Tsubota, N. Fujiwara, H. Ishimaru, E. Tanaka, T. Aizawa, M. Kanazawa and N. Mutsuro J. Phys. Soc. Japan 26, 1 (1969)	ELEM. SYM.	A	Z
		Bi	209	83

METHOD	REF. NO.	
	69 Ts 1	egf

REACTION	RESULT	EXCITATION ENERGY	SOURCE TYPE	SOURCE RANGE	DETECTOR TYPE	DETECTOR RANGE	ANGLE
G,N	NOX	15-26	C	26	SCI-D	7-	DST
				(25.5)			

Paper gives summary of angular distribution measurements.

Table I. A summary of the results.
$W(\theta)=A+B\sin^2\theta+C\cos\theta$

Target	E_{bias}(MeV)	A	B	C	B/A	C/A
Bi	7.4	0.65±0.02	0.35±0.11	0.16±0.05	0.55±0.20	0.24±0.10
	8.7	0.66±0.01	0.34±0.06	0.18±0.03	0.51±0.10	0.27±0.06
Pb	7.4	0.45±0.05	0.55±0.11	0.10±0.01	1.22±0.25	0.22±0.04
	8.7	0.75±0.03	0.26±0.03	0.17±0.03	0.22±0.03	0.22±0.03
Ta	7.4	0.69±0.02	0.32±0.03	0.03±0.01	0.46±0.05	0.05±0.02
	8.7	0.80±0.04	0.20±0.02	0.05±0.03	0.25±0.04	0.07±0.04

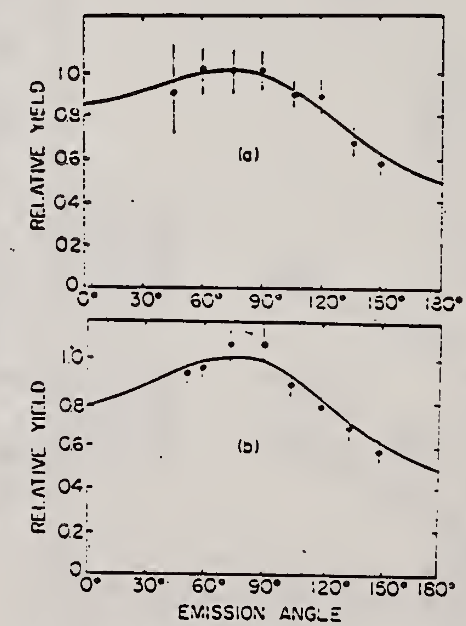

Fig. 6. The angular distributions of fast photoneutrons from Bi irradiated with 25.5 MeV bremsstrahlung.
(a) The neutron detecting bias energy is set at 8.7 MeV.
(b) The neutron detecting bias energy is set at 7.4 MeV.

REF. V. V. Verbinski and W. R. Burrus
Phys. Rev. 177, 1671 (1969)

ELEM. SYM.	A	Z
Bi	209	83

METHOD

REF. NO.	
69 Ve 1	hmg

REACTION	RESULT	EXCITATION ENERGY	SOURCE TYPE	SOURCE RANGE	DETECTOR TYPE	DETECTOR RANGE	ANGLE
G,XN	SPC	THR-33	C	33	TOF-D	0-14	DST

TABLE II. (γ,n) reactions induced by 33-MeV end-point thin-target bremsstrahlung.

Target	E_γ giant resonance peak (MeV)	θ	T[a] (MeV)	Thresholds (γ,n)	Thresholds (γ,pn)	Thresholds $(\gamma,2n)$
^{27}Al	~22	55°	3.07±0.1	13.1	19.4	24.4
		93°	3.07±0.1			
^{206}Pb	~13	90°	1.50±0.1	8.0	14.8	14.8
		141°	1.43±0.1			
^{208}Pb	~13	90°	1.52±0.1	7.4	14.8	14.1
		141°	1.52±0.1			
^{209}Bi	~13	90°	1.66±0.1	7.4	11.1	14.3
		141°	1.47±0.1			

[a] From plot of $\ln[\phi(E)/\sigma_c E^{5/11}]$ versus E.

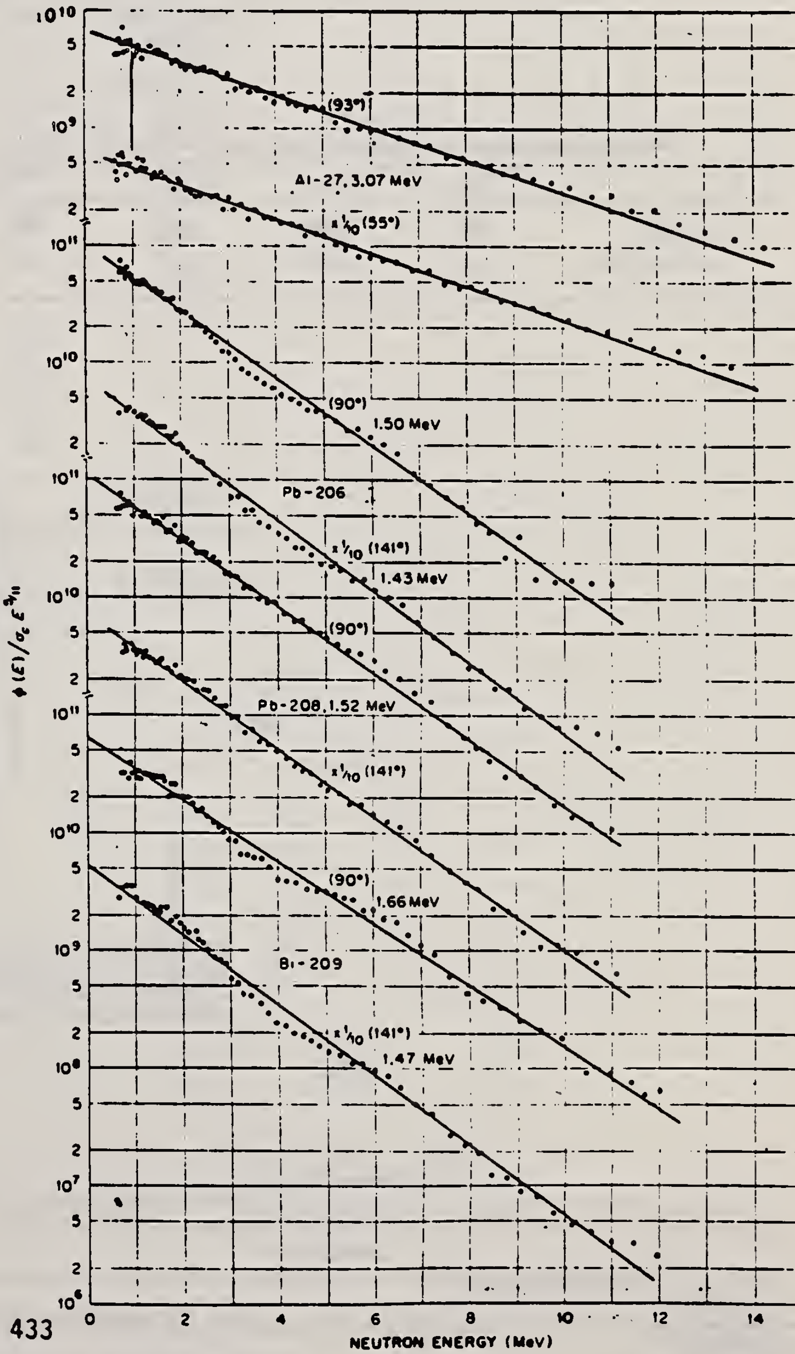

FIG. 7. Evaporation-analysis plots of neutron spectra from (γ,n) reactions. The logarithmic plots of $\phi(E)/(\sigma_c E^{5/11})$ show moderately good straight-line fits. Values of T, the magnitude of the reciprocal slope, are shown. In some cases, T is slightly higher at 90° than at 141°, indicating that a weak component of direct emissions is present. These are preferentially emitted at 90°, the direction of the electromagnetic field.

REF.	ELEM. SYM.	A	Z
L. A. Currie and R. H. Rodriguez-Pasques Nucl. Phys. A157, 49 (1970)	Bi	209	83

METHOD	REF. NO.	
	70 Cu 1	egf

REACTION	RESULT	EXCITATION ENERGY	SOURCE TYPE	SOURCE RANGE	DETECTOR TYPE	DETECTOR RANGE	ANGLE
G,T	ABY	THR-90	C	90	ACT-I		4PI

TABLE 4

Bremsstrahlung-weighted and integrated (γ, t) cross sections (90 MeV)

	^{27}Al	Zn	Sn	^{209}Bi
σ_{-1}(mb)	0.072	0.007_4	0.065	0.007_2
σ_0(MeV · mb)	4.0	0.4_2	3.8	0.4_1

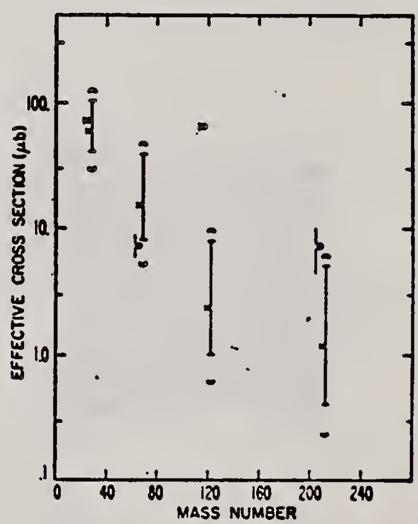

Fig. 3. Experimental (o) and statistical model (x) absolute phototriton yields (90 MeV). Yields, expressed in terms of "effective cross sections" (μb), are plotted versus mass number. Limits for the experimental yields represent ± one standard deviation; those for the calculated yields correspond to limiting values for the level density parameter (—) and for the photon absorption cross section (⊐).

B. Schrøder, G. Nydahl and B. Forkman
Nucl. Phys. A143, 449 (1970)

Bi	209	83
REF. NO. 70 Sc 1		egf

METHOD

REACTION	RESULT	EXCITATION ENERGY	SOURCE TYPE	SOURCE RANGE	DETECTOR TYPE	DETECTOR RANGE	ANGLE
G,F	RLY	THR-700	C	700	ACT-I		4PI

TABLE 3

Measured cumulative fission yields relative to $A = 91$ (^{232}Th) and $A = 105$(^{209}Bi)

Mass number	Thorium fission yield (%) 300 (MeV)	500 (MeV)	700 (MeV)	900 (MeV)	1100 (MeV)	Average	Bismuth fission yield (%) 700 MeV
85	1.3	0.98	0.70	1.4	1.4	1.1	0.46
91	5.5	5.5	5.5	5.5	5.5	5.5	2.1
92	5.3			5.2	6.0	5.5	3.2
95							4.8
97	4.4			6.2	5.2	5.3	5.1
99	3.1	4.0	4.5	5.5	5.1		4.9
103	3.1			5.2	5.8		5.1
105	3.5	4.5	5.4	6.0	6.0		5.0
112	4.6	6.2	6.8	7.5	8.3		4.0
131	1.3			2.7	3.5	2.5	
132	1.9		3.5	3.0	2.2	2.6	
133	4.0	4.1		5.5	5.0	4.7	
140	4.9			6.0	6.2	5.7	
141	4.5				5.6	5.1	
143	2.9	4.6	3.5	4.5	5.3	4.2	
detector	30 cm³	7 mm	7 mm	7 mm	30 cm³		30 cm³

it is possible to define an average curve in the regions $A \leq 97$, $A \geq 131$. The increase of yields in the valley is considerably greater than for uranium.

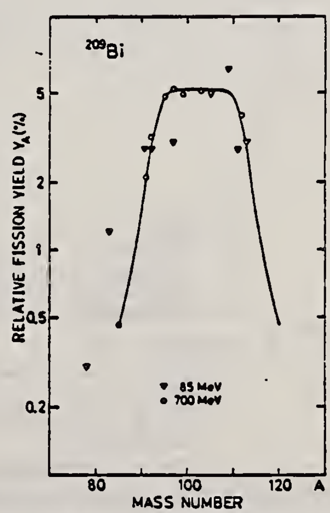

Fig. 7. Relative fission yields of ^{209}Bi at different irradiation energies. All yields normalized to $Y_{105} = 5.0$ %. Data at 85 MeV as given by Sugarman [8]). The curve is drawn through the present data points.

REF.

V. Emma, S. Lo Nigro and C. Milone
Lettere al Nuovo Cimento 2, 117 (1971)

ELEM. SYM.	A	Z
Bi	209	83

METHOD	REF. NO.	
	71 Em 1	egf

REACTION	RESULT	EXCITATION ENERGY	SOURCE TYPE	SOURCE RANGE	DETECTOR TYPE	DETECTOR RANGE	ANGLE
G,F	ABY	THR-999	C	300-999	FRAG-I		4PI

999 = 1000 MEV

TABLE I. – *Fission cross-sections per photon between* 300 *and* 1000 MeV.

	Our results		Previous results	
	σ_k (mb)	$\bar{\sigma}_k$ (mb)	σ_k (mb)	
Bi	7.6 ± 0.2	7.9 ± 1.3	7.8 ± 0.2 (3)	7.8 ± 0.8 (2)
Pb	3.3 ± 0.1	3.2 ± 1.5	3.4 ± 0.3 (3)	

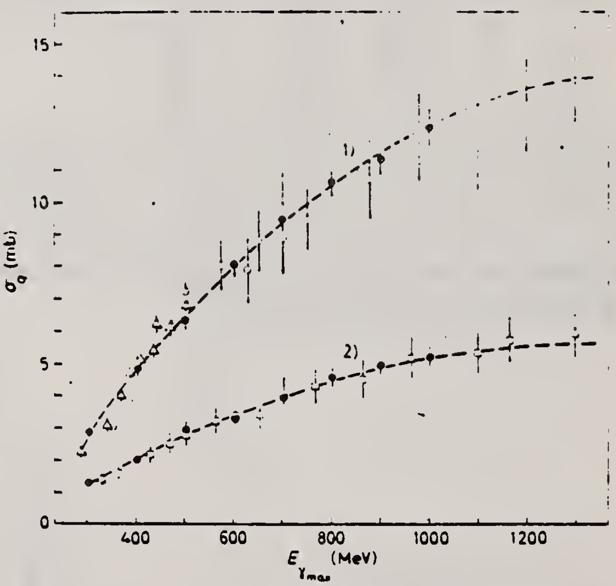

Fig. 3. – Our experimental data of the photofission cross-section per equivalent quantum for Bi and Pb compared with previous results. Experimental points: ● our data calculated as mean values of the results obtained with thin and thick targets; ▵ ref. (1); ○, □ ref. (3). The dashed lines are the best curves calculated by the least-squares method taking into account our results only. 1) Bi, 2) Pb.

(1) J. A. Jungerman and H. M. Steiner: *Phys. Rev.*, 106, 585 (1957).
(2) H. G. De Carvalho, G. Cortini, E. Del Giudice, G. Potenza and R. Rinzivillo: *Nuovo Cimento*, 32, 293 (1964).
(3) A. V. Mitrofanova, Yu. N. Ranyuk and P. V. Sorokin: *Sov. Journ. Nucl. Phys.*, 6, 512 (1968).

REF.	K. Shoda, A. Suzuki, M. Sugawara, T. Saito, H. Miyase, S. Oikawa Phys. Rev. C3, 1999 (1971)	ELEM. SYM.	A	Z
		Bi	209	83
METHOD		REF. NO.		
		71 Sh 2		hmg

REACTION	RESULT	EXCITATION ENERGY	SOURCE		DETECTOR		ANGLE
			TYPE	RANGE	TYPE	RANGE	
E,P	ABX	10-14	D	17-21	MAG-D	7-16	125
							(123.5)

The radiative widths of the $E1$ transition through the ground isobaric analog states of ^{207}Tl and ^{209}Pb in ^{207}Pb and ^{209}Bi, respectively, were determined from the cross section of the $(e,e'p)$ reaction. The results are 98 and 140 eV, respectively, after the correction for the interference from the continuous part of the reaction. They correspond to an effective charge of 0.56 and 21, respectively. The $E1$ matrix elements were determined and used for the estimation of β matrix elements $|i\xi'' \int \vec{r}''|$. The result is 0.055 in natural units ($\hbar = c = m_e = 1$) for the β-decay ^{207}Tl$(3s_{1/2}{}^{-1}) \to {}^{207}Pb(3p_{1/2}{}^{-1})$. In the case of ^{209}Pb$(2g_{9/2}) \to {}^{209}$Bi$(1h_{9/2})$, the result is 0.043, which is much larger than the theoretical estimate. For the $E1$ isobaric analog states of the first excited state of ^{209}Pb in ^{209}Bi, the radiative width and the effective charge were also determined to be 170 eV and 0.46, respectively.

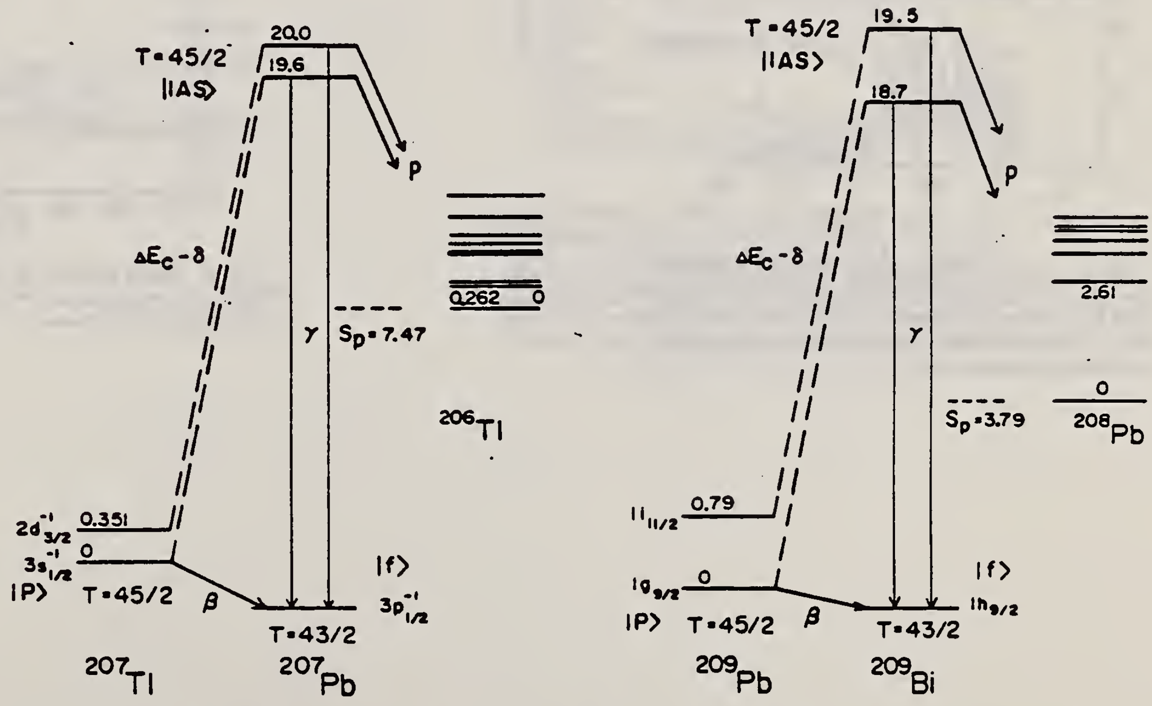

FIG. 1. The level diagram for the relations of $E1$ IAS and β decay. The energy levels are indicated in units of MeV. The single-particle configurations of the relevant states are indicated.

[over]

TABLE I. Radiative widths of $E1$ IAS in ^{207}Pb and ^{209}Bi. The errors include statistical uncertainties only.

Nucleus	Ground state	IAS	E_x (MeV)	Γ_γ^R (eV)	Γ_γ^{IAS} (eV)	$2(T+1)\Gamma_\gamma^{IAS}$ (keV)	$2(T+1)\frac{\Gamma_\gamma^{IAS}}{\Gamma_W}$	$2(T+1)\frac{\Gamma_\gamma^{IAS}}{\Gamma_{sp}}$
^{207}Pb	$\frac{1}{2}^-(3p_{1/2}^{-1})$	$\frac{1}{2}^+(3s_{1/2}^{-1})$	19.6	160±50	98±30	4.4±1.3	0.25±0.08	0.32±0.09
^{209}Bi	$\frac{9}{2}^-(1h_{9/2})$	$\frac{9}{2}^+(2g_{9/2})$	18.7	180±20	140±20	6.3±0.8	0.40±0.05	430±55
^{209}Bi	$\frac{9}{2}^-(1h_{9/2})$	$\frac{11}{2}^+(1i_{11/2})$	19.5	220±30	170±20	7.6±1.0	0.43±0.06	0.21±0.03

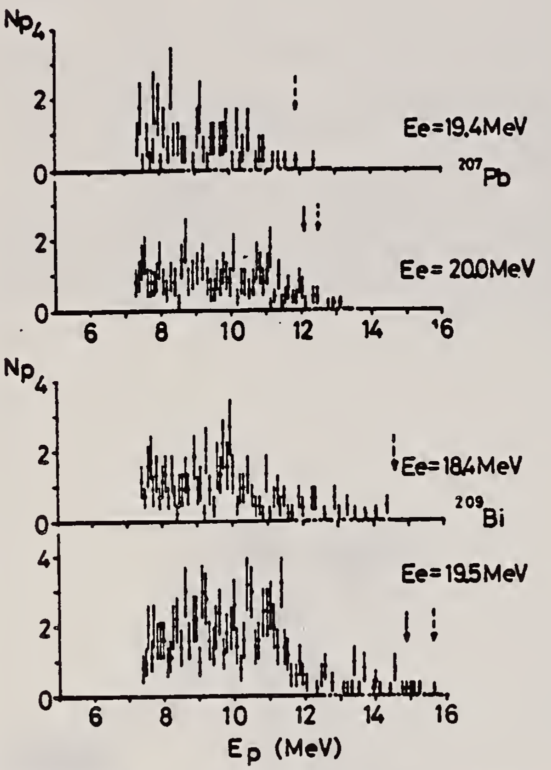

FIG. 2. Examples of the proton energy distributions. The positions expected for the maximum end-point energy of the protons are shown by the dashed vertical arrows. The solid vertical arrows indicate the position of p_0 through the ground IAS.

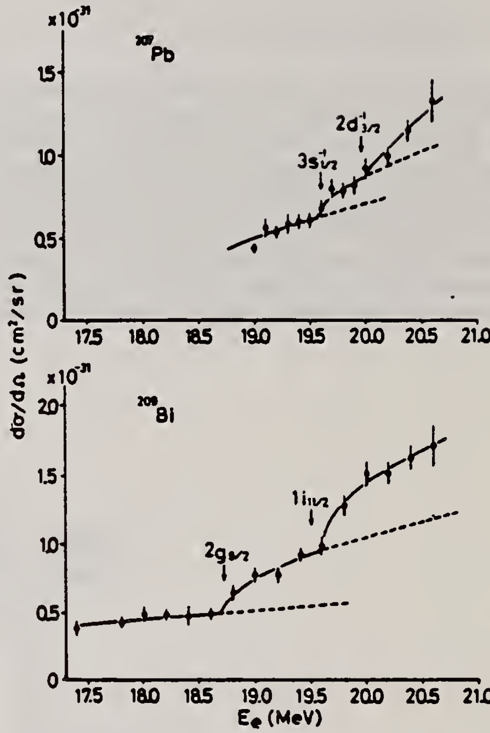

FIG. 3. Cross sections of the ^{207}Pb$(e,e'p)$ and ^{209}Bi$(e,e'p)$ reactions at $\theta=125.3°$. The positions of the IAS are shown by arrows.

REF. K. A. Snover, J. F. Amann, W. Hering and P. Paul
Phys. Letters 37B, 29 (1971)

ELEM. SYM.	A	Z
Bi	209	83

METHOD

REF. NO. 71 Sn 2 egf

REACTION	RESULT	EXCITATION ENERGY	SOURCE		DETECTOR		ANGLE
			TYPE	RANGE	TYPE	RANGE	
P,G	ABX	13-22	D	9-18	NAI-D		90

Table I
A comparison of the experimental γ-ray transition strengths Γ_γ(exp) with theoretical single-particle E1 strengths Γ_γ (th) for the analog resonances.

Transition	Γ_γ(exp)* (eV)	Γ_γ(th) (eV)	Γ_γ(exp)/Γ_γ(th)*
$2g_{9/2} \to 2f_{7/2}$	110(660)	380	0.30(1.8)
$2g_{9/2} \to 1h_{9/2}$	<10	~1	~0.33(2.0)
$1i_{11/2} \to 1h_{9/2}$	~190(1150)	565	0.20(2.2)
$3d_{5/2} \to 2f_{7/2}$	40(440)	200	0.40(1.5)
$3d_{5/2} \to 3p_{3/2}$	95(360)	240	~0.14(1.3)
$2g_{7/2} \to 1h_{9/2}$	~15(140)	105	
$2g_{7/2} \to 2f_{7/2}$	<10	20	
$(2g_{7/2} + 3d_{3/2}) \to (2f_{5/2} + 3p_{3/2})$			~0.26(1.2)**

* Values obtained from the solutions with $\Delta\phi \approx 0^\circ$, and in parenthesis, for $\Delta\phi \approx -90^\circ$.
** Ratios of experimental and theoretical resonance cross sections computed for the sum of all the possible transitions.

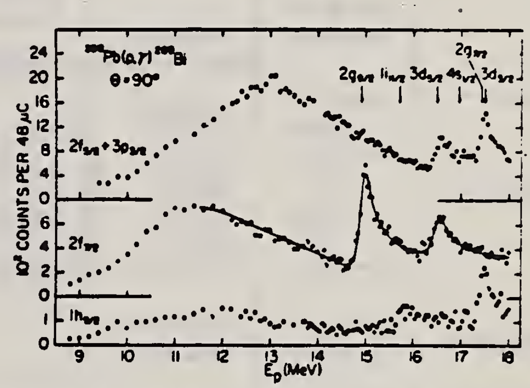

Fig.2. ^{208}Pb(p, γ)^{209}Bi excitation curves at θ = 90° for transitions to the $1h_{9/2}$, $2f_{7/2}$ and $2f_{5/2} + 3p_{3/2}$ final states. The absolute normalization for the ordinate is given by 0.94 ± 0.19 μb/sr per 100 counts/48 μC. The energies and configurations of the known single-particle analog resonances are indicated in the upper right. The solid curve represents a least-squares fit to the data, as described in the text.

REF.	ELEM. SYM.	A	Z
G.A. Vartapetyan, N.A. Demekhina, V.I. Kasilov, Yu. N. Ranyuk, P.V. Sorokin and A.G. Khudaverdyan Yad. Fiz. 14, 65 (1971) ~~Sov. J. Nucl. Phys. 14, 37 (1972)~~	Bi	209	83

METHOD	REF. NO.	
	71 Va 4	egf

REACTION	RESULT	EXCITATION ENERGY	SOURCE TYPE	SOURCE RANGE	DETECTOR TYPE	DETECTOR RANGE	ANGLE
G,F	ABX	100-999	C	100-999	TRK-I		4PI

999 = 5 GEV

$E_{\gamma\,max}$, MeV	Photofission yields per cm² per equivalent photon					
	U^{235}	U^{238}	Th^{232}	Bi^{209}	Au^{197}	Ta^{181}
100	$(226\pm20)\cdot10^{-27}$	$(120\pm12)\cdot10^{-27}$	$(50\pm5)\cdot10^{-27}$	$(0.70\pm0.08)\cdot10^{-28}$	$(3.0\pm0.4)\cdot10^{-28}$	
120				$(1.5\pm0.2)\cdot10^{-28}$	$(1.1\pm0.2)\cdot10^{-28}$	
140				$(2.6\pm0.2)\cdot10^{-28}$	$(2.0\pm0.2)\cdot10^{-28}$	
150	$(240\pm20)\cdot10^{-27}$		$(63\pm7)\cdot10^{-27}$			
160				$(3.1\pm0.3)\cdot10^{-28}$	$(3.7\pm0.4)\cdot10^{-28}$	
180				$(4.6\pm0.5)\cdot10^{-28}$	$(5.5\pm0.6)\cdot10^{-28}$	
200	$(265\pm30)\cdot10^{-27}$	$(150\pm15)\cdot10^{-27}$	$(72\pm7)\cdot10^{-27}$	$(6.1\pm0.6)\cdot10^{-28}$	$(8.2\pm0.8)\cdot10^{-28}$	$(4.9\pm0.5)\cdot10^{-28}$
220				$(8.3\pm0.8)\cdot10^{-28}$	$(1.1\pm0.1)\cdot10^{-27}$	$(8.2\pm0.8)\cdot10^{-28}$
240				$(1.2\pm0.1)\cdot10^{-27}$	$(1.5\pm0.2)\cdot10^{-27}$	$(1.2\pm0.1)\cdot10^{-27}$
245		$(156\pm16)\cdot10^{-27}$				
260				$(1.5\pm0.2)\cdot10^{-27}$	$(1.8\pm0.2)\cdot10^{-27}$	$(1.6\pm0.2)\cdot10^{-27}$
280		$(160\pm16)\cdot10^{-27}$	$(85\pm9)\cdot10^{-27}$			
300				$(2.2\pm0.2)\cdot10^{-27}$	$(2.3\pm0.2)\cdot10^{-27}$	
330				$(3.5\pm0.4)\cdot10^{-27}$	$(4.4\pm0.4)\cdot10^{-27}$	
370				$(4.2\pm0.4)\cdot10^{-27}$	[illegible]	
400	$(318\pm30)\cdot10^{-27}$	$(175\pm20)\cdot10^{-27}$				
[illegible]			$(106\pm11)\cdot10^{-27}$			$(7.0\pm0.7)\cdot10^{-27}$
[illegible]				[illegible]	[illegible]	
[illegible]				[illegible]	[illegible]	
[illegible]		[illegible]	$(115\pm12)\cdot10^{-27}$	[illegible]	[illegible]	
[illegible]				[illegible]	[illegible]	
[illegible]	$(346\pm35)\cdot10^{-27}$					
[illegible]				[illegible]	[illegible]	[illegible]
645				[illegible]	[illegible]	
[illegible]		$(200\pm20)\cdot10^{-27}$	$(120\pm12)\cdot10^{-27}$	[illegible]	[illegible]	
[illegible]				[illegible]	[illegible]	
[illegible]						$(2.4\pm0.2)\cdot10^{-27}$
[illegible]				[illegible]	[illegible]	
[illegible]		$(220\pm22)\cdot10^{-27}$	$(135\pm14)\cdot10^{-27}$			
[illegible]	$(386\pm40)\cdot10^{-27}$					
[illegible]		$(224\pm23)\cdot10^{-27}$	$(140\pm14)\cdot10^{-27}$			
[illegible]						$(2.2\pm0.2)\cdot10^{-27}$
[illegible]				$(11.3\pm1.1)\cdot10^{-27}$	$(1.9\pm0.2)\cdot10^{-27}$	
[illegible]	$(400\pm40)\cdot10^{-27}$					
[illegible]	$(390\pm40)\cdot10^{-27}$	$(217\pm23)\cdot10^{-27}$	$(136\pm14)\cdot10^{-27}$			
[illegible]				$(12.5\pm1.3)\cdot10^{-27}$	[illegible]	
[illegible]						$(3.3\pm0.3)\cdot10^{-27}$
[illegible]				$(13.5\pm1.4)\cdot10^{-27}$	[illegible]	
[illegible]	[illegible]	[illegible]	$(152\pm15)\cdot10^{-27}$			
[illegible]				$(14.3\pm1.4)\cdot10^{-27}$	$(2.0\pm0.2)\cdot10^{-27}$	
[illegible]	$(445\pm45)\cdot10^{-27}$	$(238\pm24)\cdot10^{-27}$	$(153\pm15)\cdot10^{-27}$			
[illegible]				[illegible]	[illegible]	
[illegible]				$(15.5\pm1.6)\cdot10^{-27}$	$(2.2\pm0.2)\cdot10^{-27}$	
[illegible]	[illegible]	$(207\pm21)\cdot10^{-27}$	[illegible]			
[illegible]	$(435\pm45)\cdot10^{-27}$	$(242\pm24)\cdot10^{-27}$	$(155\pm16)\cdot10^{-27}$			
[illegible]	[illegible]	$(245\pm25)\cdot10^{-27}$	$(152\pm15)\cdot10^{-27}$	[illegible]	[illegible]	
[illegible]	$(455\pm45)\cdot10^{-27}$	$(230\pm23)\cdot10^{-27}$	$(146\pm15)\cdot10^{-27}$			
[illegible]	[illegible]	$(251\pm25)\cdot10^{-27}$	[illegible]		$(3.0\pm0.3)\cdot10^{-27}$	$(6.4\pm0.6)\cdot10^{-28}$
[illegible]				[illegible]	$(3.0\pm0.3)\cdot10^{-27}$	$(6.6\pm0.7)\cdot10^{-28}$
[illegible]	[illegible]	$(254\pm27)\cdot10^{-27}$	$(154\pm18)\cdot10^{-27}$			
4000	[illegible]	[illegible]		$(20.2\pm2)\cdot10^{-27}$	$(2.8\pm0.2)\cdot10^{-27}$	$(6.8\pm0.7)\cdot10^{-28}$
[illegible]	[illegible]	[illegible]	$(206\pm21)\cdot10^{-27}$	[illegible]	[illegible]	$(6.3\pm0.6)\cdot10^{-28}$

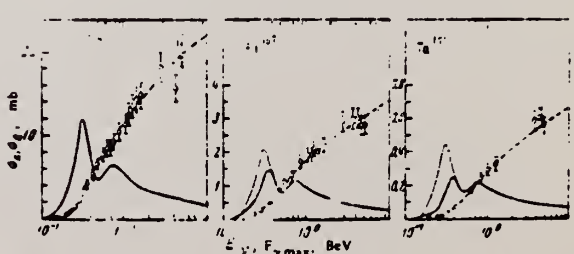

FIG. 3. Solid heavy curve–photofission cross section of Bi^{209}, Au^{197}, Ta^{181}. Dashed curve–the same cross section, integrated over the Schiff bremsstrahlung spectrum (yield per equivalent photon as a function of bremsstrahlung maximum energy). Thin line–cross section for γp interaction, multiplied by the number of nucleons in the nucleus and by the fissility.

REF.		ELEM. SYM.	A	Z
W. C. Barber, E. Hayward, J. Sazama PICNS-72, p. 313 Sendai		Bi	209	83
METHOD		REF. NO. 72 Ba 16		hvm

REACTION	RESULT	EXCITATION ENERGY	SOURCE		DETECTOR		ANGLE
			TYPE	RANGE	TYPE	RANGE	
$ G,G	RLX	15.1	D	15.1	NAI-D		90

POL G; ALSO G/

$$\eta = \frac{(d\sigma/d\Omega)_{\parallel} \text{ to polarization vector}}{(d\sigma/d\Omega)_{\perp} \text{ to polarization vector}}$$

Table 1. Results and Comparison with Theory

Target	$\frac{d\sigma}{d\Omega})_{\perp}$ (Arbitrary Units)	η(exp)	η(DCM)	η(HD)
Cd	0.39±0.05	0.09±0.08	0.19	0
Sn	0.65±0.06	0.11±0.06	0.067	0
Ta	1.74±0.14	0.14±0.07	0.180	0.155
Au	2.08±0.15	0.17±0.06	0.067	0
Bi	2.65±0.26	0.02±0.06	0	0

REF.	ELEM. SYM.	A	Z
N.A. Demekhina, V.I. Kasilov, A.V. Mitrofanova, Yu. N. Ranyuk, and P.V. Sorokin Yad. Fiz 16, 911 (1972) Sov. J. Nucl. Phys. 16, 502 (1973)	Bi	209	83
METHOD	REF. NO. 72 De 12		hmg

REACTION	RESULT	EXCITATION ENERGY	SOURCE TYPE	SOURCE RANGE	DETECTOR TYPE	DETECTOR RANGE	ANGLE
G,F	NOX	THR* 2	C	0* 2	TRK-I		DST

$d\sigma/d\Omega \sim 1+2\ v/V \cos\theta - P \sin^2\theta$

* ENERGIES IN GEV

Table II

Element	E_γ max, MeV	χ^2	$w(\chi^2-\chi_q^2)$	$a = 2v/V$	$a = 2v/V$ [16]	v, (MeV/nucleon)$^{1/2}$	ϵ, MeV
U^{238}	3000	0.16	0.99	−0.031±0.025		0.042±0.005	0.160±0.020
	3800	0.55	0.85	0.013±0.017		0.018±0.002	0.045±0.005
	5100	0.59	0.65	0.040±0.017		0.054±0.006	0.206±0.031
Bi^{209}	700	0.93	0.45	0.155±0.017		0.091±0.009	0.431±0.052
	1000	1.14	0.3	−0.085±0.017		0.047±0.005	0.229±0.023
	1200	0.76	0.6	0.094±0.020		0.055±0.006	[illegible]
	1300	0.91	0.4	0.093±0.018		0.055±0.006	[illegible]
	1480	0.62	0.85	0.034±0.018		0.020±0.002	0.040±0.004
Au^{197}	350				0.097±0.010		
	450				[illegible]±0.010		
	600				0.090±0.010		
	645	0.87	0.35	0.054±0.015		0.044±0.004	0.187±0.018
	700				0.116±0.010		
	800	0.45	0.95	0.008±0.020		0.005±0.001	0.020±0.002
	850				0.121±0.010		
	900	4.50	0.001	0.124±0.018		0.064±0.005	0.400±0.040
	1000	0.95	0.4	0.101±0.017	0.090±0.010	0.052±0.005	0.262±0.025
	1300	0.87	0.4	0.094±0.017		0.049±0.005	0.234±0.024
	1400	0.90	0.5	0.075±0.015		0.029±0.004	0.147±0.015
	3000	1.34	0.15	0.122±0.017		0.065±0.006	0.410±0.040
	3800	0.7	0.65	0.093±0.17		0.048±0.005	0.223±0.022
Ta^{181}	600	0.8	0.5	0.087±0.018		0.044±0.004	0.176±0.018
	700				0.147±0.010		
	1145	5.2	0.001	0.144±0.018		0.072±0.007	0.468±0.047
	1480	1.25	0.15	0.127±0.013		0.064±0.006	0.370±0.037
	5100	2.02	0.001	0.200±0.020		0.160±0.010	0.900±0.090

Note. χ^2 is the value of χ^2 per degree of freedom, $w(\chi^2-\chi_q^2)$ is the probability of the value of χ^2, a = 2v/V is the anisotropy coefficient, ϵ is the fissioning-nucleus kinetic energy, v is the fissioning-nucleus velocity.

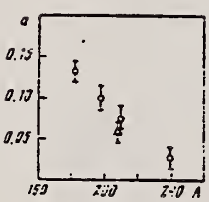

FIG. 3. Anisotropy coefficent as a function of target-nucleus atomic number. Points: O—results of the present work, Δ—results of Kroon and Forkman [16].

$$a = 2\frac{v}{V}$$

REF. V. di Napoli, A. M. Lacerenza, D. Margadonna, S. M. Terenzi
Radiochem. Radioanal. Letters 11, 99 (1972)

ELEM. SYM.	A	Z
Bi	209	83

METHOD

REF. NO.	
72 Di 10	hmg

REACTION	RESULT	EXCITATION ENERGY	SOURCE		DETECTOR		ANGLE
			TYPE	RANGE	TYPE	RANGE	
G,2N	ABY	THR-999	C	999	ACT-D		4PI
G,3N	ABY	THR-999	C	999	ACT-D		4PI
G,4N	ABY	THR-999	C	999	ACT-D		4PI
G,AU*	ABY	THR-999	C	999	ACT-D		4PI
G,SE**	ABY	THR-999	C	999	ACT-D		4PI

* 5 AU ISOTOPES OBS
** SE = SELENIUM 75

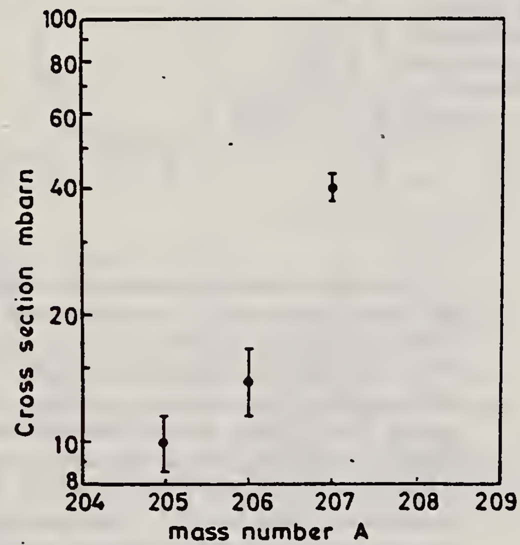

Fig.1. Cross sections per equivalent quantum of the photoproduction of ^{207}Bi, ^{206}Bi and ^{205}Bi from ^{209}Bi vs. the mass number A

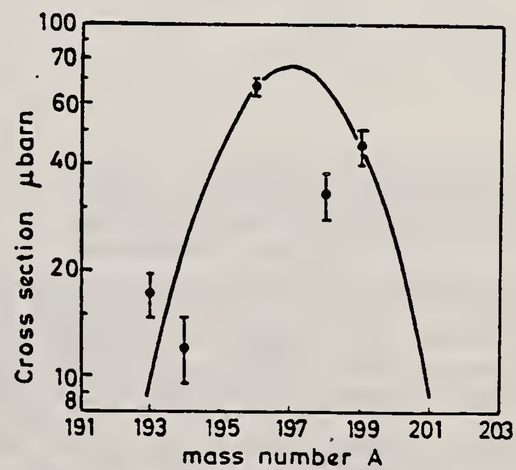

Fig.2. Cross sections per equivalent quantum of the photoproduction of gold isotopes from ^{209}Bi vs. the mass number A

REF.	ELEM. SYM.	A	Z
H. E. Jackson and K. J. Wetzel Phys. Rev. Letters 28, 513 (1972)	Bi	209	83

METHOD	REF. NO.	
	72 Ja 1	hmg

REACTION	RESULT	EXCITATION ENERGY	SOURCE		DETECTOR		ANGLE
			TYPE	RANGE	TYPE	RANGE	
G,G	RLX	10	D	10	SCD-D		90
		(10.83)		(10.83)			

RATIO: RAMAN/ELASTIC

We have measured the differential cross sections for the elastic scattering of 10.83-MeV photons by U, Th, and Bi targets and for inelastic scattering to the first excited states of the residual nuclei over a range of scattering angles. The inelastic scattering is found to be significantly weaker than predicted by currently accepted models of the giant dipole resonance.

To establish that the anomaly we observe was not limited to uranium, we repeated the measurements on a second deformed actinide target (^{232}Th) and also on a spherical nucleus (^{209}Bi) for which no observable Raman component was expected. For ^{232}Th at 90° the observed ratio is 0.7 ± 0.1, while for ^{209}Bi no inelastic scattering to the first excited state was observed; i.e., the experimental ratio is ≤ 0.1. Thus the evidence suggests that the Raman to elastic ratio we find may be characteristic of the deformed actinide nuclei.

REF.

K. Shoda, M. Sugawara, T. Saito, H. Miyase, A. Suzuki, S. Oikawa, and J. Uegaki
PICNS-72, 321 Sendai

ELEM. SYM.	A	Z
Bi	209	83

METHOD

REF. NO. 72 Sh 10 hvm

REACTION	RESULT	EXCITATION ENERGY	SOURCE TYPE	SOURCE RANGE	DETECTOR TYPE	DETECTOR RANGE	ANGLE
E,P	ABI	18- 20	C	17- 21	MAG-D		DST
E,P	SPC	19- 20	C	18- 21	MAG-D		DST

I A STATES

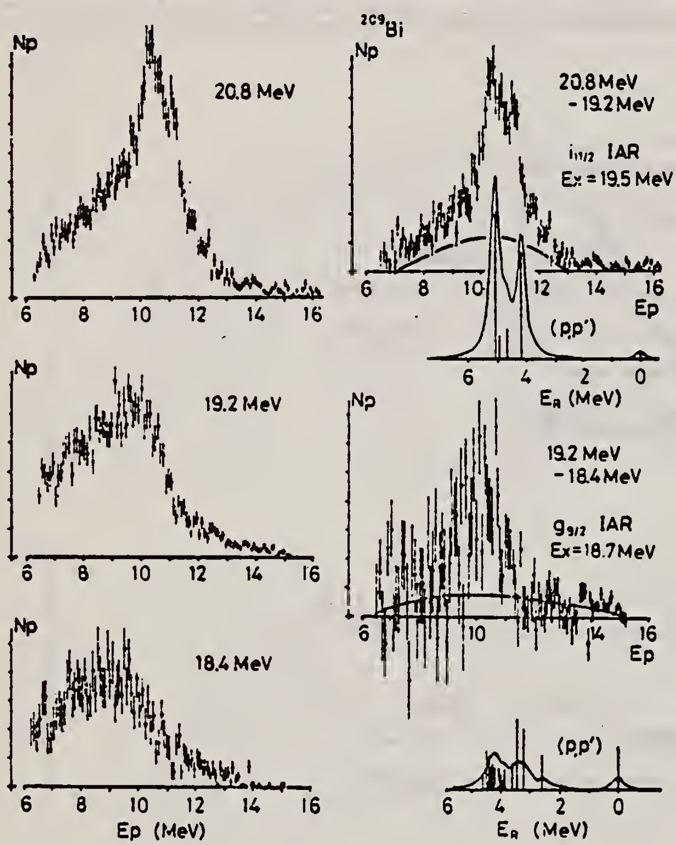

Fig. 6 Photoproton energy distributions from ^{209}Bi. Those from (e,e'p) are shown in the left hand side. Those from difference method are shown in the right hand side. The results are compared with the proton groups determined by the (p,p') results.

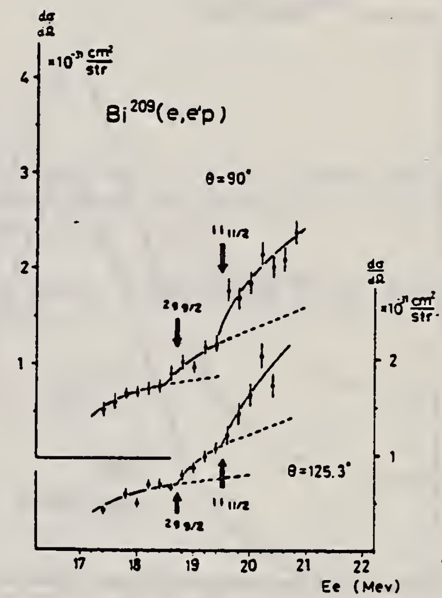

Fig. 2 The (e,e'p) cross sections of ^{209}Bi. The positions of E1 IAS are shown by arrows.

Table 1. Examples of radiative width of IAR obtained from (e,e'p) experiment in lead region. The result from ^{208}Pb(p,γ_0) are also shown with parenthesis. (Ref. (5))

Nucleus	Ground State	IAS	E_x (MeV)	Γ_γ^A (eV)	$2(T+1)\frac{\Gamma_\gamma^A}{\Gamma_W}$	$2(T+1)\frac{\Gamma_\gamma^A}{\Gamma_{sp}}$
^{207}Pb	$3p^{-1}_{1/2}$	$3s^{-1}_{1/2}$	19.6	98±30	0.25±0.08	0.32±0.09
^{209}Bi	$1h_{9/2}$	$2g_{9/2}$	18.7	140±20 (<10)	0.40±0.05	430±55 (~0.33)
^{209}Bi	$1h_{9/2}$	$1i_{11/2}$	19.5	170±20 (~190)	0.43±0.06	0.21±0.03 (0.20)

5
K.A. Snover, J.F. Amann, W. Hering, P. Paul, Phys. Letters 37B, 29 (1971).

REF.	ELEM. SYM.	A	Z
B.W. Thomas, D.M. Crawford and H. H. Thies Nucl. Phys. A196, 89 (1972)	Bi	209	83

METHOD	REF. NO.	
	72 Th 2	egf

REACTION	RESULT	EXCITATION ENERGY	SOURCE		DETECTOR		ANGLE
			TYPE	RANGE	TYPE	RANGE	
G,XN	RLX	7-20	C	6-19	BF3-I		4PI

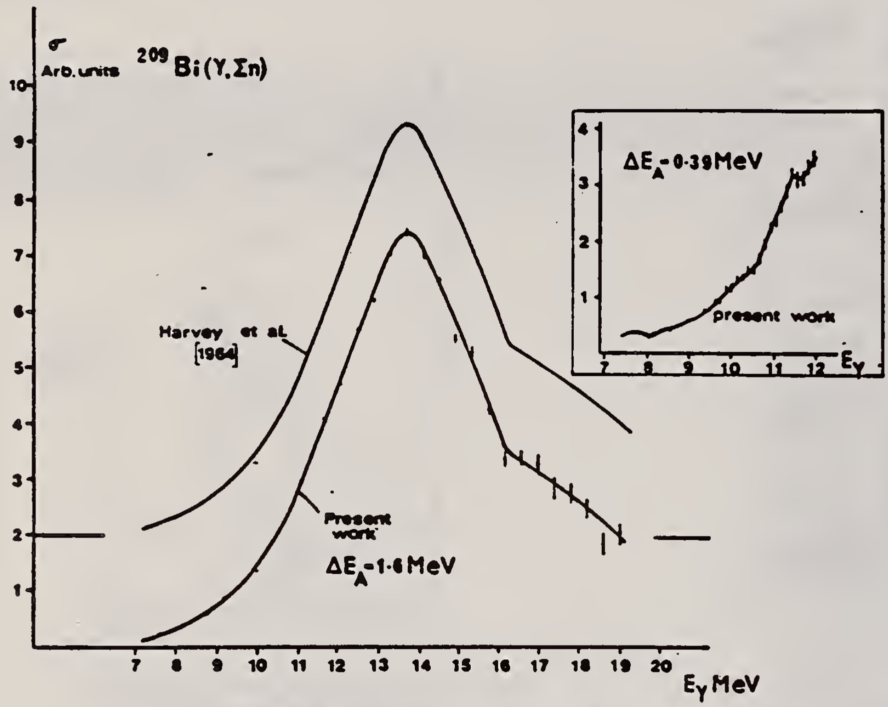

Fig. 6. Cross section for ^{209}Bi(γ, Σn).

REF.

R.F. Barrett, J.R. Birkelund, B.J. Thomas, K.S. Lam, and H.H. Thies
Nucl. Phys. A210, 355 (1973)

ELEM. SYM.	A	Z
Bi	209	83

METHOD

REF. NO.	
73 Ba 20	egf

REACTION	RESULT	EXCITATION ENERGY	SOURCE TYPE	SOURCE RANGE	DETECTOR TYPE	DETECTOR RANGE	ANGLE
G,N	NOX	THR- 27	C	10- 27	BF3-I		4PI

MEAN NEUT ENERGY

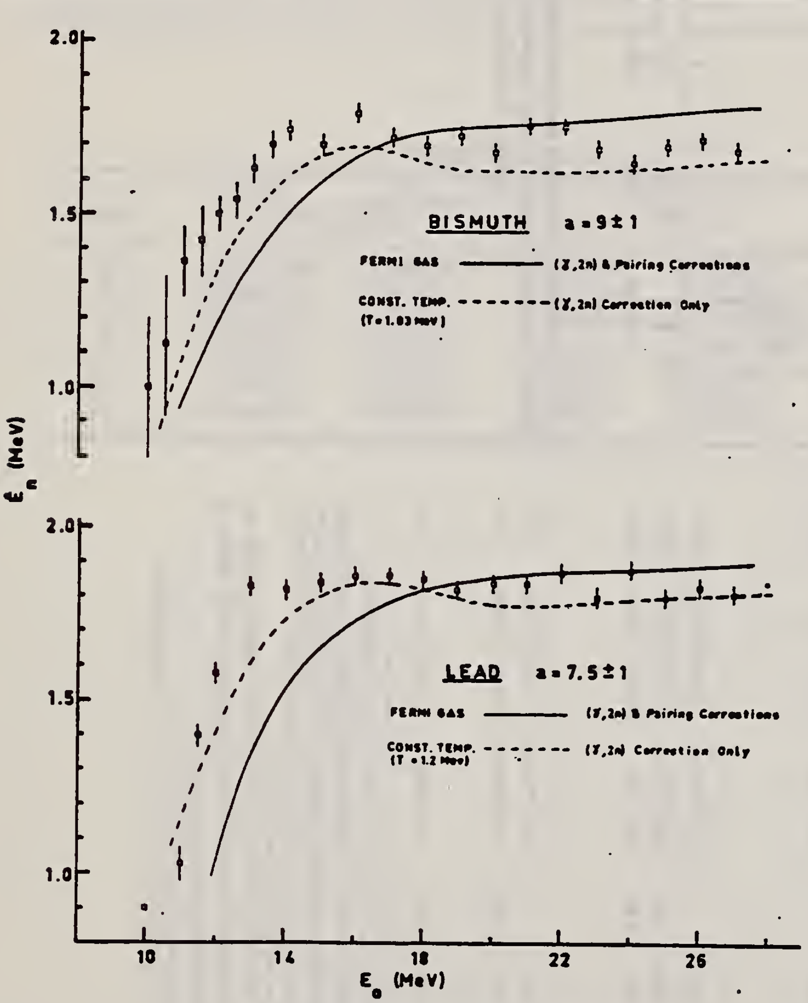

Fig. 11. Same as fig. 5, for lead and bismuth.

1
H. Baba and S. Baba, Japan Atomic Energy Research Institute report JAERI-1183 (1969).
2
H. Baba, Nucl. Phys. A159, 625 (1970).
15
T.D. Newton, Can. J. Phys. 34, 804 (1956).

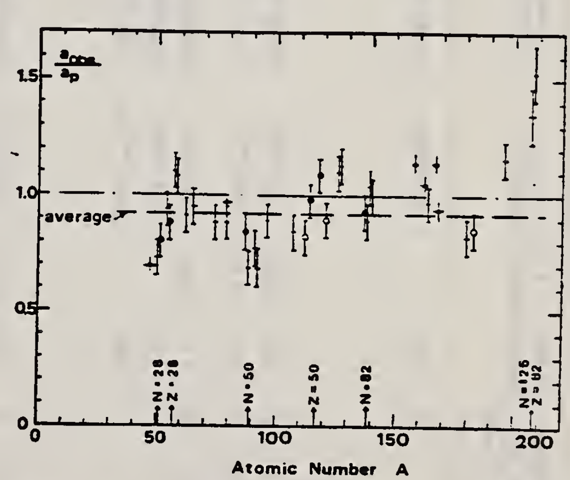

Fig. 15. Ratio a_{obs}/a_p versus atomic number A. Here a_{obs} is the level density parameter taken from the neutron resonance work of refs. [1,2]), and a_p is the level density parameter derived from the present (γ, n) work. Filled circles represent points where nuclei in the neutron resonance and in the (γ, n) experiment were the same. Open circles represent points where the respective nuclei were approximately matched. Triangles represent points which are based on measurement of neutron mean energies at two bremsstrahlung energies only.

(over)

TABLE 3 (continued)

Target	N (residual nucleus)[a]	Goodness of fit[b] no p.c.	Goodness of fit[b] with p.c.	$\hat{E}_e(24)$ (MeV)[c]	T (MeV)[d]	a_p (MeV^{-1})[e]	a_{obs} (MeV^{-1})[f]	a_{obs}/a_p
Ba	75 1%		F	1.16		16.5–^{136}Ba	15.39–^{136}Ba	0.93
	77 2%							
	78 7%							
	79 8%							
	80 11%							
	81 71%							
La	80 100%	F	F	1.25	0.72	15.5–^{138}La	13.76–^{139}La	0.89
Ce	81 89%	F	G	1.24	0.70	17.0–^{139}Ce	17.8 –^{141}Ce	1.04
	83 11%							
Pr	81 100%	G	G	1.17	0.65	17.0–^{140}Pr	17.05–^{142}Pr	1.00
Tb[g]	93 100%			1.15		19.3–^{158}Tb	21.85–^{160}Tb	1.14
Dy[g]	93 2%			1.06		20.9–$^{161.5}$Dy	21.9 –^{162}Dy	1.05
	94 19%							
	95 25%							
	96 25%							
	97 28%							
Ho	97 100%	P	G	1.06	0.56	21.4–^{164}Ho	20.66–^{166}Ho	0.97
Er[g]	95 2%			1.11		19.2–^{166}Er	21.9 –^{166}Er	1.14
	97 33%							
	98 23%							
	99 27%							
	101 15%							
Tm[g]	99 100%			1.03		24.0–^{168}Tm	22.58–^{170}Tm	0.94
Ta	107 100%		G	1.00	0.49	26.0–^{180}Ta	21.2 –^{181}Ta	0.82
W	107 26%	G	F	0.98	0.50	27.0–^{183}W	23.0 –^{183}W	0.85
	108 14%							
	109 31%							
	111 28%							
Au	117 100%		G	1.19		17.5–^{196}Au	20.24–^{198}Au	1.16
Pb ($Z = 82$)	123 24%		V.P.	1.87	1.20	7.5–^{206}Pb	10.1 –^{207}Pb	1.35
	124 23%							
	125 52%							
Bi	125 100%		F	1.65	1.03	9.0–^{208}Bi	13.8 –^{210}Bi	1.53

[a]) Neutron numbers and abundances of respective residual nuclei in (γ, n) experiments.

[b]) These give an assessment of the goodness of fit of a calculated $\hat{E}_e$ versus E_0 curve to the observed data, using the Fermi gas level density formula both without and with pairing corrections.

[c]) Bremsstrahlung photoneutron mean energies $\hat{E}_e$ for peak bremsstrahlung energy $E_0 = 24$ MeV.

[d]) Nuclear temperature from fit with constant-temperature formula.

[e]) Level density parameter a_p derived from the present (γ, n) experiment, using a Fermi gas formula plus pairing correction, and corresponding residual nucleus (the atomic weight shown is the weighted average of atomic weights of the respective isotopes present).

[f]) As column 7, but using data on n-resonance absorption from refs. [1,2]).

[g]) Measurements of $\hat{E}_e(E_0)$ for these nuclei were made only for $E_0 = 21$, 23 and 24 MeV.

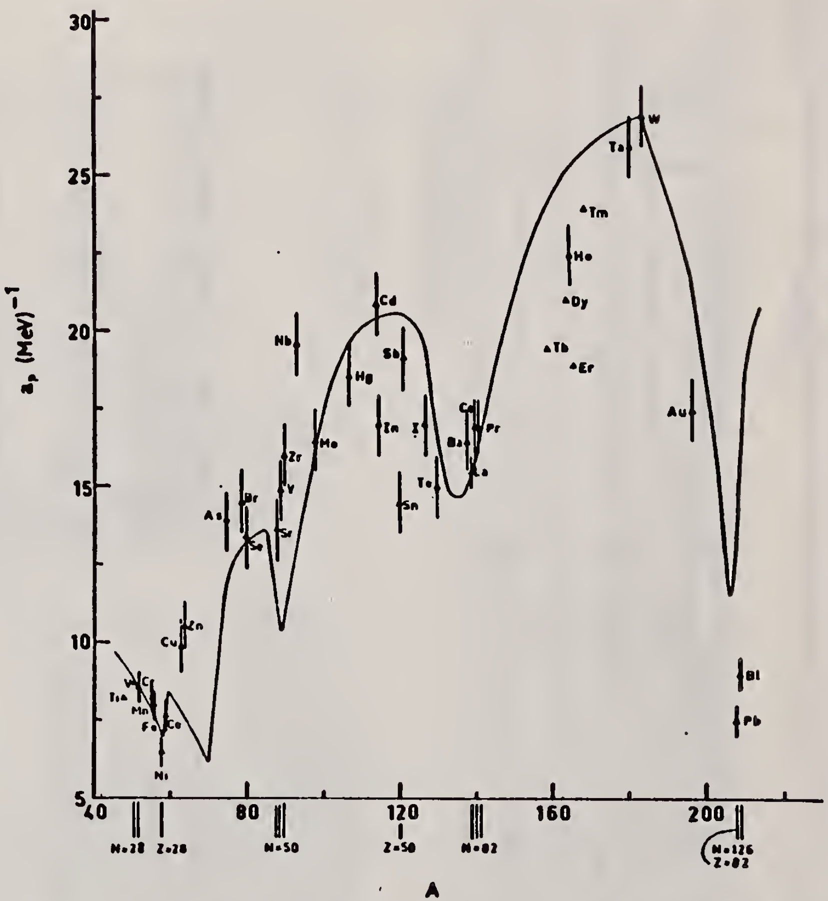

Fig. 12. Experimental values of the level density parameter a_p (Fermi gas formula plus pairing correction) versus atomic number A. The continuous curve is a least-squares fit to the data of a theoretical calculation from Newton [15]).

REF.						ELEM. SYM.	A	Z
E. Hayward, W. C. Barber, and Jed Sazama Phys. Rev. C8, 1065 (1973)						Bi	209	83
METHOD						REF. NO. 73 Ha 3		hmg

REACTION	RESULT	EXCITATION ENERGY	SOURCE TYPE	SOURCE RANGE	DETECTOR TYPE	DETECTOR RANGE	ANGLE
$G, G	RLY	15	D	15	NAI-D		90
		(15.1)		(15.1)			

POLARIZED PHOTONS

TABLE II. Results.

Target	$d\sigma^{\parallel}/d\Omega_p$ Arbitrary units	$d\sigma^{\perp}/d\Omega_p$	η_p	η	$\eta(DCM)$
Cd	0.042 ± 0.028	0.39 ± 0.05	0.11 ± 0.07	0.09 ± 0.07	0.19
Sn	0.084 ± 0.036	0.65 ± 0.06	0.13 ± 0.06	0.11 ± 0.06	0.07
Ta	0.24 ± 0.10	1.47 ± 0.14	0.16 ± 0.07	0.14 ± 0.07	0.20
W	0.52 ± 0.10	1.66 ± 0.12	0.31 ± 0.07	0.29 ± 0.07	0.20
Pt	0.23 ± 0.08	1.94 ± 0.13	0.12 ± 0.04	0.10 ± 0.04	0.08
Au	0.39 ± 0.11	2.08 ± 0.15	0.19 ± 0.06	0.17 ± 0.06	0.07
Bi	0.10 ± 0.15	2.65 ± 0.26	0.04 ± 0.06	0.02 ± 0.06	0

REF.	ELEM. SYM.	A	Z
S. Klawansky, H.W. Kendall, A.K. Kerman, and D. Isabelle Phys. Rev. C7, 795 (1973)	Bi	209	83

METHOD	REF. NO.	
	73 Kl 1	hmg

REACTION	RESULT	EXCITATION ENERGY	SOURCE TYPE	SOURCE RANGE	DETECTOR TYPE	DETECTOR RANGE	ANGLE
E,E/	FMF	0-125	D	101-245	MAG-D		DST

QUASIELASTIC

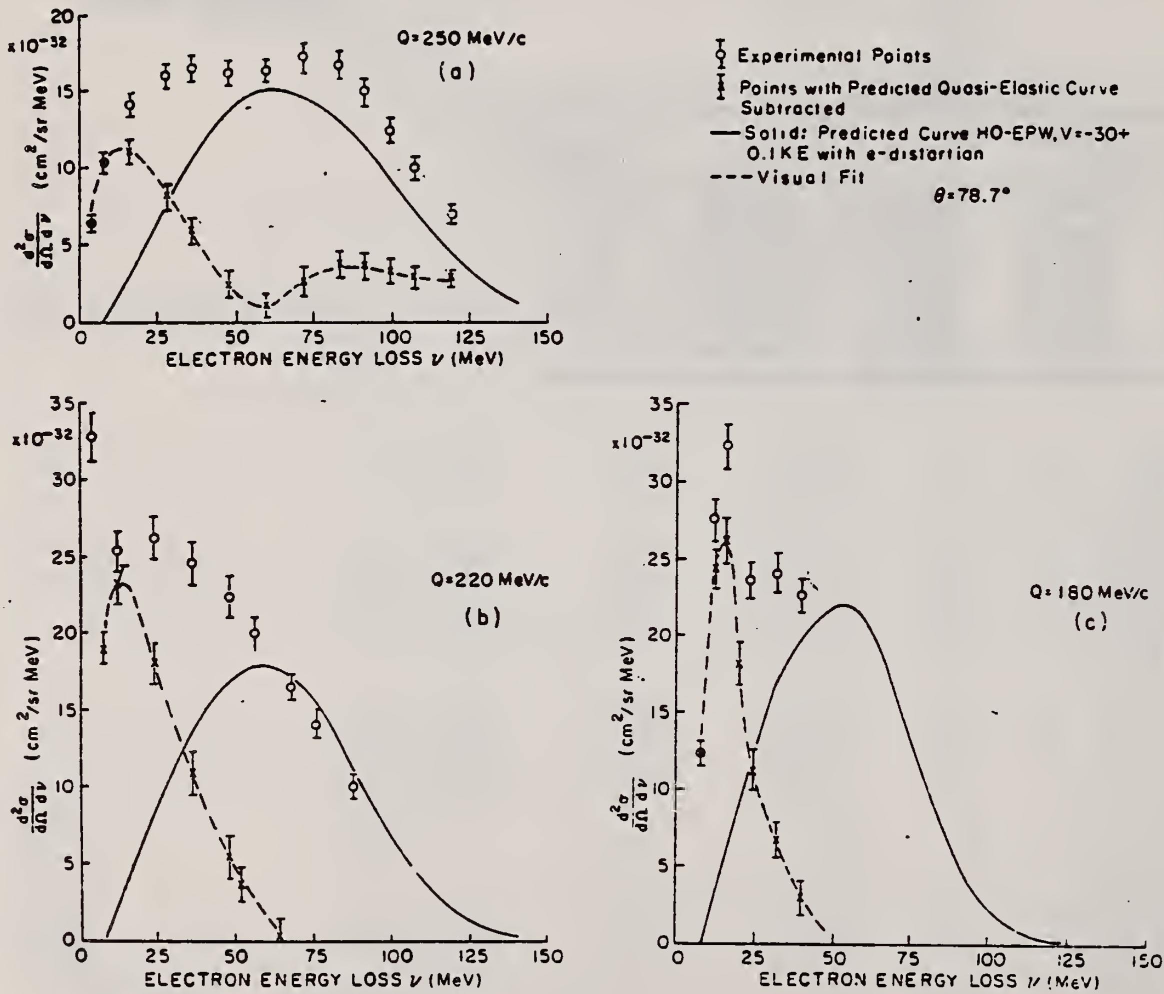

FIG. 3. Experimental points for $\theta = 78.7°$, $q = 250$ (a), 220 (b), and 180 MeV/c (c). The solid line is HO-EPW with $V = -30 + 0.1$ KE (MeV) and electron distortion. The x's represent the result of subtracting the HO-EPW result from the experimental data.

(over)

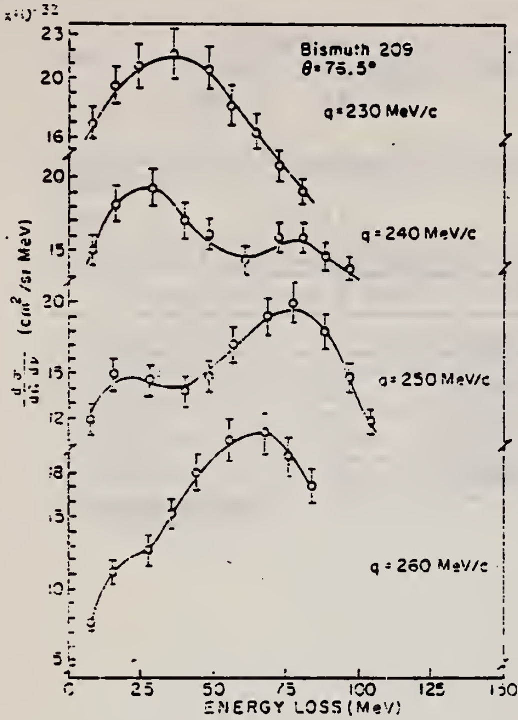

FIG. 1. Inelastic spectra for electrons on ^{209}Bi. $\theta = 76.5°$, q = 230, 240, 250, and 260 MeV/c. The data points are interpolations between measured points. See text for further discussion. Solid curves are visual fits to the points.

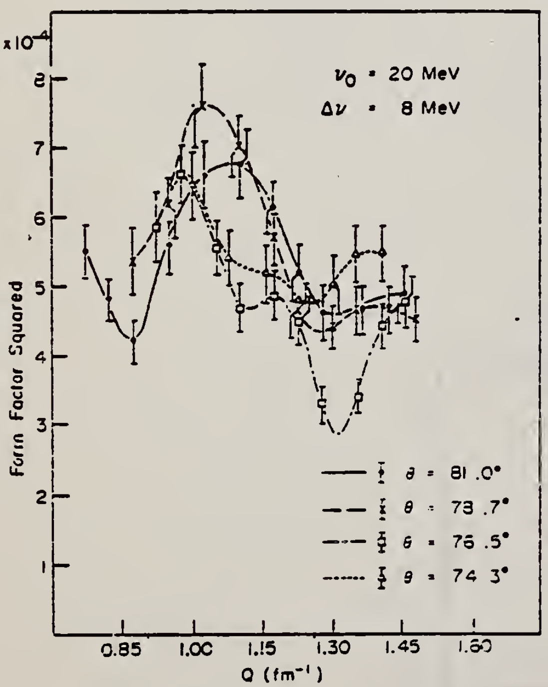

FIG. 4. Excitation form factor squared as a function of q for scattering angles $\theta = 74.3$, 76.5, 78.7, and 81.0°, obtained by using Eq. (11) with $\nu_0 = 20$ MeV, and $\Delta\nu = 8$ MeV. σ_{qe} is the HO-EPW result with $V = -30 + 0.1$ KE (MeV) and electron distortion. The errors shown are statistical only. The largest contribution to the uncertainties in the form factor arises from uncertainties in the predicted quasielastic distributions. This contribution is not included in the errors shown in the figure but is discussed in the text.

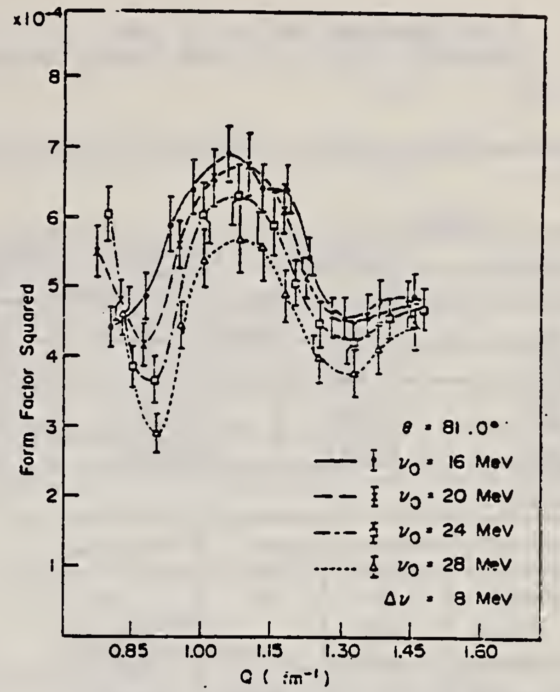

FIG. 5. Excitation form factor squared as a function of q for $\theta = 81.0°$, $\Delta\nu = 8$ MeV, $\nu_0 = 16$, 20, 24, and 28 MeV. σ_{qe} as in Fig. 4. See caption to Fig. 4 for discussion of the errors.

REF.	ELEM. SYM.	A	Z
S. M. Kocimski and B. C. Cook PICNS-73, Vol.II, p.1059 (1973) Asilomar	Bi	209	83

METHOD	REF. NO.	
	73 Ko 3	egf

REACTION	RESULT	EXCITATION ENERGY	SOURCE TYPE	SOURCE RANGE	DETECTOR TYPE	DETECTOR RANGE	ANGLE
G,N	ABI	7- 30	C	7- 58	MOD-I		4PI
G,2N	ABI	7- 30	C	7- 58	MOD-I		4PI
G,3N	ABI	7- 30	C	7- 58	MOD-I		4PI
G,4N	ABI	7- 30	C	7- 58	MOD-I		4PI

SIG SN GIVEN

References	Harvey et al.	Wyckoff	Present work
E_M (MeV)	28	137*	58
s_0 (γ,n) (mb×MeV)	2170		2830±100
s_0 (γ,2n) (mb×MeV)	760		732±30
s_0 (γ,3n) (mb×MeV)		168±25	172±40
s_0 (γ,4n) (mb×MeV)		88±22	220±100
s_0 (γ,tot) (mb×MeV)	2930±290		3954±150
60×NZ/A (mb×MeV)	3000	3000	3000
s_{-1} (mb)			263.6±25
s_{-2} (mb/MeV)	16.6±1.7		16.6±1.0

*) In this case the measurement was performed for one energy only. The cross sections were deduced from the ratio of the yields assuming the absorption.

Table 1.

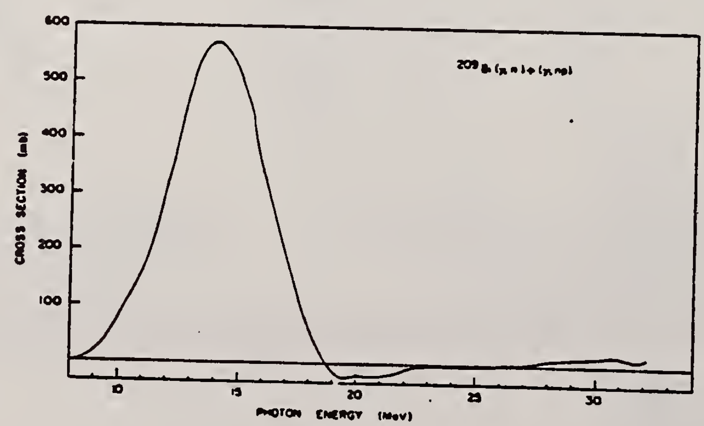

Figure 1.

REF.	S.J. Mecca and J.R. Rothamel Nucl. Phys. A201, 570 (1973)	ELEM. SYM.	A	Z
		Bi	209	83
METHOD		REF. NO.		
		73 Me 1		egf

REACTION	RESULT	EXCITATION ENERGY	SOURCE		DETECTOR		ANGLE
			TYPE	RANGE	TYPE	RANGE	
G,G	ABX	5	D	5	SCD-D		DST

5 = 5.609

TABLE 1

Resonant energy results

E_γ [a]) (MeV)	I_γ [a])	E_γ [b]) (MeV)	I_γ [b])	E'_γ (present work) (MeV)	E'_γ [c]) (MeV)
5.646±0.006	8	5.608±0.005	1.3	5.609±0.005	5.646
		5.643±0.005	1.0		
		5.663±0.005	5.4		
4.903±0.008	3	4.890±0.005	0.9		4.903
		4.908±0.005	1.1		
		4.924±0.005	0.65	4.924±0.005	

[a]) Co(n,γ) from ref. [3]).
[b]) Co(n,γ) from ref. [4]).
[c]) Ref. [1]).

TABLE 2

Effective cross-section results

Target	$\langle\sigma_{\gamma\gamma'}\rangle$ [a]) (mb)	$\langle\sigma_{\gamma\gamma'}\rangle$ [b]) (mb)	$\langle\sigma_{\gamma\gamma'}\rangle$ [c]) (mb)
^{209}Bi	55±20%	338	348±20%
^{nat}Hg	385±20%	1777	not measured

[a]) Ref. [1]).
[b]) Value from ref. [1]) adjusted using the intensity from ref. [4]), consistent with the resonance energy from the present work.
[c]) Present work.

[1]G. Ben-David, B. Arad, J. Balderman & Y. Schlesinger, Phys. Rev. 146, 852 (1966).
[4]Nucl. Data Tables A3 (1967); 1966 data.

REF.	Yu.I. Sorokin, V.A. Khrushchev, and B.A. Yur'ev Izv. Akad. Nauk SSSR Ser. Fiz. 37, 1891 (1973) Bull. Acad. Sci. USSR Phys. Ser. 37, 80 (1973)	ELEM. SYM.	A	Z
		Bi	209	83
METHOD		REF. NO.	73 So 19	hmg

REACTION	RESULT	EXCITATION ENERGY	SOURCE TYPE	SOURCE RANGE	DETECTOR TYPE	DETECTOR RANGE	ANGLE
G,XN	ABX	7- 28	C	7- 28	BF3-I		4PI

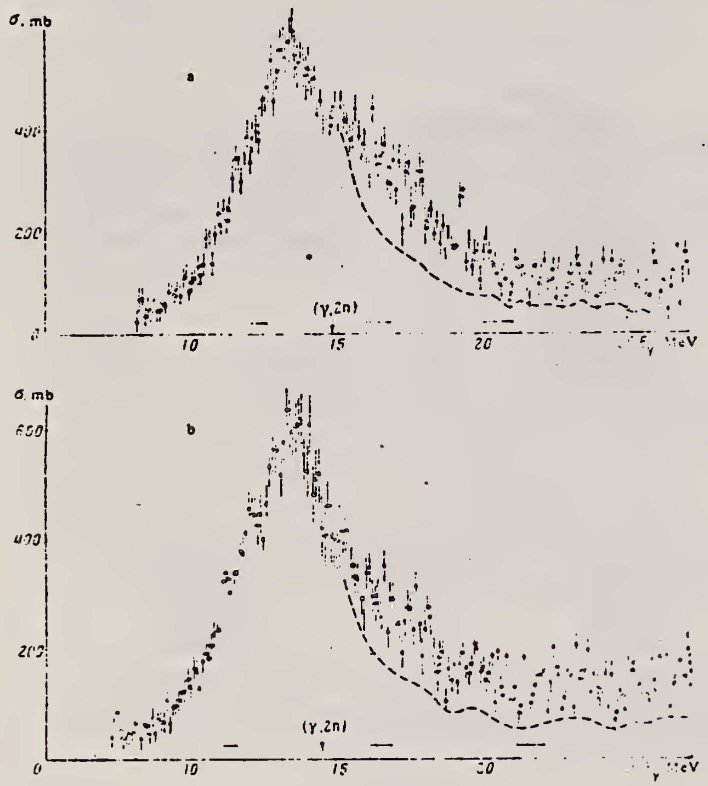

Photoneutron cross section $\sigma(\gamma,Tn)$ for ^{197}Au (a) and ^{209}Bi (b). The dashed curves gives the photo-absorption cross section σ_γ.

Photoneutron Cross Section Parameter Values for ^{197}Au and ^{209}Bi

	^{197}Au	^{209}Bi
$\sigma(\gamma,Tn)$ [E_γ < 27 MeV], MeV·b	[illegible]	[illegible]
$\sigma(\gamma,Tn)$ [E_γ < 20 MeV], MeV·b	3.37	[illegible]
$\sigma(\gamma,Tn)$ [E_γ 20 – 27 MeV], MeV·b	[illegible]	[illegible]
σ_γ [E_γ < 20 MeV], MeV·b	2.81	2.96
σ_γ [E_γ < 27 MeV], MeV·b	[illegible]	3.47
σ_γ [E_γ 20 ÷ 27 MeV], MeV·b	0.34	0.51
$\sigma(E1) = \frac{0.06\ NZ}{A}$ MeV·b	[illegible]	3.00
$\sigma(E2)$, MeV·b	0.48	0.5
σ_m, mb	[illegible]	[illegible]
E_m, MeV	13.3	13.2
G, MeV	4.3	4.0

REF.	C. P. Swann Nucl. Phys. A201, 534 (1973)	ELEM. SYM.	A	Z
		Bi	209	83
METHOD		REF. NO.		
		73 Sw 4		egf

REACTION	RESULT	EXCITATION ENERGY	SOURCE TYPE	SOURCE RANGE	DETECTOR TYPE	DETECTOR RANGE	ANGLE
G,G	LFT	7	D	7	SCD-D		UKN

7 = 7.18, 7.21

TABLE 1

Summary of observed levels in ^{208}Pb, ^{207}Pb and ^{209}Bi and some of their properties

Nucleus	E_γ (keV)	Spin	Γ_0/Γ	$g\Gamma_0^2/\Gamma$ (eV)	Γ_0 (eV) present	Γ_0 (eV) ref. [3]	Γ_0 (eV) ref. [2]	s.p. estimate (W.u.) E1	s.p. estimate (W.u.) M1
^{208}Pb	7071 ± 2	1	1		31 ± 3	15	30 ± 13	0.036	4.4
	7091 ± 2	1	1		17 ± 2	15		0.019	2.3
^{207}Pb	7186 ± 5	$\frac{1}{2}, \frac{3}{2}$		15 ± 4					
	7206 ± 5	$\frac{1}{2}, \frac{3}{2}$		25 ± 5					
^{209}Bi	7179 ± 5	$\frac{7}{2}, \frac{9}{2}, \frac{11}{2}$		24 ± 5					
	7202 ± 5	$\frac{7}{2}, \frac{9}{2}, \frac{11}{2}$		30 ± 5					

Weisskopf units given are based on our data.

REF.	C. P. Swann PICNS-73, Vol.I, p.317 Asilomar Proceedings of the International Conference on Nuclear Structure	ELEM. SYM.	A	Z
		Bi	209	83
METHOD		REF. NO.	73 Sw 13	hmg

REACTION	RESULT	EXCITATION ENERGY	SOURCE TYPE	SOURCE RANGE	DETECTOR TYPE	DETECTOR RANGE	ANGLE
G,G	LFT	2- 5	C	5	SCD-D		DST

J-PI, 10 LEVELS

Table: Properties of States Observed in $^{206,207,208}Pb$ and ^{209}Bi

Nuclei	E_γ (keV)	J^π	Γ_0/Γ	$g\Gamma_0^2/\Gamma$ (eV)	Γ_0 (eV)	G(EL)	G(M1)
^{206}Pb	3742	1	1		0.13(2)	0.001	0.12
	4114	2^+	1		0.30(6)	5	
	4326	1	1		0.90(9)	0.004	0.56
	4602	1	1		0.23(3)	0.001	0.12
^{207}Pb	3300	$1/2^+$ a)			0.039(6)		
	3928	$(3/2^-)$	1	0.68(7)			
	4104	$3/2^-$	1		0.55(6)	8	
	4140	$5/2^-$	1		0.46(5)	6	
	4627	$1/2^+$ b)	1		0.64(7)	0.003	
	4872	1/2,3/2	1	3.6(5)		∿0.01	∿1.2
	4982	1/2,3/2	1	4.0(5)		∿0.01	∿1.2
^{208}Pb	4087	2^+	1		0.49(5)	7	
	4843	1	1		5.1(5)	0.02	2.3
^{209}Bi	2826	$5/2^-$	(.63) c)		0.09(1)		
	3977	5/2--13/2		0.82(8)			
	4085	$5/2^-$--$13/2^-$		0.28(3)		∿5	
	4144	"		0.07(2)		∿1	
	4156	"		0.21(4)		∿3	
	4176	"		0.21(4)		∿3	
	4206	"		0.25(3)		∿4	
	4747	7/2--11/2		2.9(5)		∿0.013	∿1.4
	4784	"		2.7(5)		∿0.012	∿1.3
	4822	"		1.4(3)		∿0.005	∿0.7

a) see ref. 3 b) see ref. 4 c) see ref. 5

3) S.M. Smith, P.G. Roos, C. Moazed and A.M. Bernstein, Nucl. Phys. A173, 32 (1971).

4) R.A. Mayer, B.L. Cohen and R.C. Diehl, Phys. Rev. C2, 1898 (1970).

5) R.A. Broglia, J.S. Lilley, R. Perazzo and W.R. Phillips, Phys. Rev. C1, 1508 (1970).

REF.	J. Uegaki, S. Oikawa, A. Suzuki, H. Miyase, T. Saito, M. Sugawara, and K. Shoda PICNS-73, Vol.I, p.209 Asilomar Proceedings of the International Conference on Nuclear Structure	ELEM. SYM. Bi	A 209	Z 83
METHOD		REF. NO. 73 Ue 1		hmg

REACTION	RESULT	EXCITATION ENERGY	SOURCE TYPE	SOURCE RANGE	DETECTOR TYPE	DETECTOR RANGE	ANGLE
E,P	RLX	3- 40	D	40	MAG-D		DST

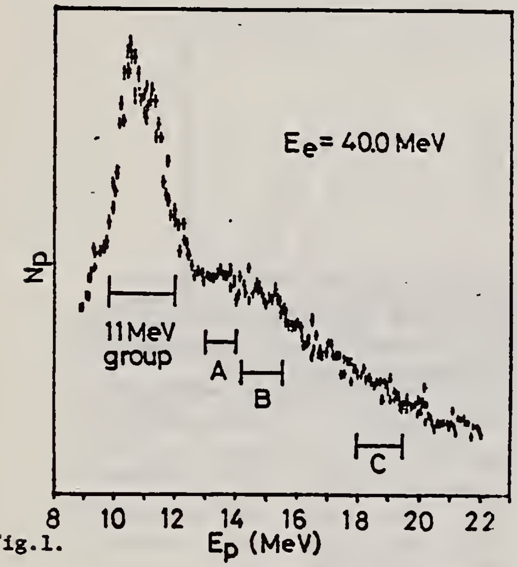

Fig.1.

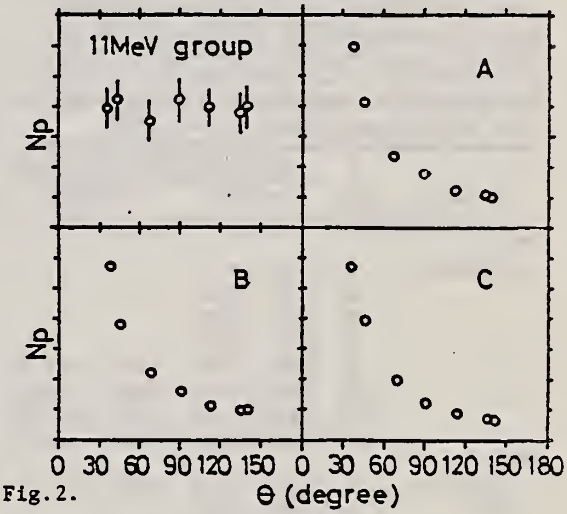

Fig.2.

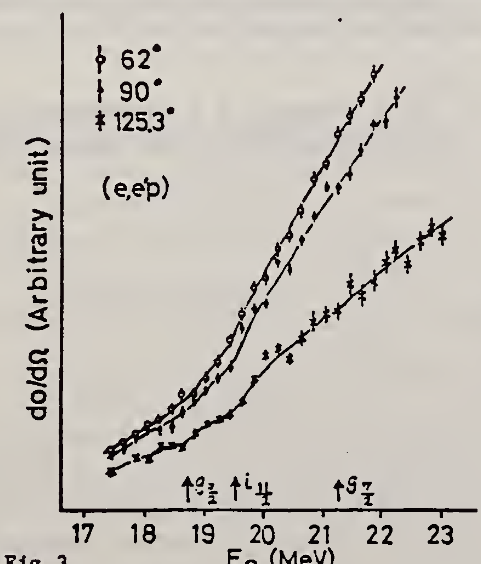

Fig.3.

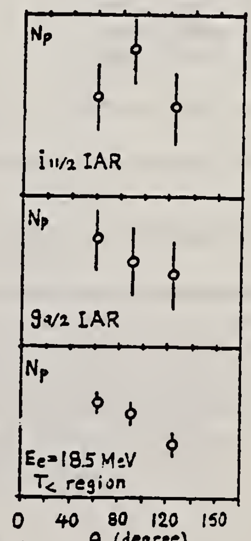

Fig.4.

REF.	ELEM. SYM.	A	Z
H.E. Jackson, G.E. Thomas, and K.J. Wetzel Phys. Rev. C9, 1153 (1974)	Bi	209	83

METHOD	REF. NO.	
	74 Ja 2	hmg

REACTION	RESULT	EXCITATION ENERGY	SOURCE TYPE	SOURCE RANGE	DETECTOR TYPE	DETECTOR RANGE	ANGLE
G,G	ABX	10	D	10	SCD-D		90
		(10.83)		(10.83)			

TABLE I. Differential cross sections measured for elastic and inelastic scattering of 10.83-MeV photons. State or states populated by inelastic scattering are indicated in parentheses below the target. The errors given result from the statistical error in the measurement of the cross section relative to the calibration value, the 90° uranium inelastic cross section.

Nucleus	θ (deg)	$d\sigma/d\omega$ (elastic) (mb/sr)	$d\sigma/d\omega$ (inelastic) (mb/sr)
^{238}U			
(2^+, 45 keV)	20	1.72 ±0.17	
	30	0.97 ±0.12	
	50	0.334 ±0.039	
	60	0.23 ±0.04	
	70	0.245 ±0.024	0.136 ±0.015
	90	0.182 ±0.017	0.154 ±0.012
	120	0.189 ±0.017	0.160 ±0.013
	150	0.303 ±0.016	0.160 ±0.015
^{232}Th			
(2^+, 45 keV)	90	0.129 ±0.015	0.103 ±0.007
Pb	20	1.28 ±0.12	
	30	0.55 ±0.07	
	50	0.289 ±0.051	
	60	0.20 ±0.04	
	70	0.087 ±0.014	
	90	0.079 ±0.005	
	120	0.060 ±0.004	
	150	0.127 ±0.008	
^{209}Bi			
($\frac{7}{2}^-$, 910 keV)	90	0.101 ±0.0062	~0
^{181}Ta			
($\frac{9}{2}^+$, 136 keV)	90	0.0370 ± 0.003	0.006 56 ± 0.0015
^{159}Tb			
($\frac{5}{2}^+$, 58 keV)	90	0.0314 ± 0.003	0.0110 ±0.0016
$\frac{7}{2}^-$, 138 keV)			0.005 11 ± 0.0011

TABLE III. Comparison of calculated and observed values of the 90° cross sections for elastic scattering and of the ratio at 90° of Raman to elastic scattering by various nuclei for 10.83-MeV photons. The parameters used in the calculations are given in Table II.

Target	$d\sigma_{elas}(90°)/d\Omega$ (mb/sr) Calc	Exp	$d\sigma^{(90°)}_{Raman}/d\sigma^{(90°)}_{elas}$ Calc	Exp
Tb	0.036	0.031 ± 0.003	0.80	0.51 ± 0.06
Ta	0.055	0.037 ± 0.003	0.28	0.18 ± 0.04
Pb	0.076	0.079 ± 0.005	0	
Bi		0.101 ± 0.006	0	~0
Th	0.128	0.129 ± 0.015	0.91	0.60 ± 0.08
U	0.157 [a]	0.182 ± 0.017	1.03	0.85 ± 0.08

[a] If the Livermore parameters (Ref. 33) for ^{235}U are used then this calculated value would be 0.210 mb/sr.

33
C.D. Bowman, G.F. Auchampaugh, and S.C. Fultz, Phys. Rev. 133, B676 (1964).

REF.

L.E. Lazareva, A.I. Lepestkin, and V.I. Sidorov
Yad. Fiz. 20, 242 (1974)
Sov. J. Nucl. Phys. 20, 128 (1975)

ELEM. SYM.	A	Z
Bi	209	83

METHOD

REF. NO.	
74 La 5	hmg

REACTION	RESULT	EXCITATION ENERGY	SOURCE TYPE	SOURCE RANGE	DETECTOR TYPE	DETECTOR RANGE	ANGLE
G,XN	SPC	7- 29	C	29	EMU-D		DST
				(28.5)			

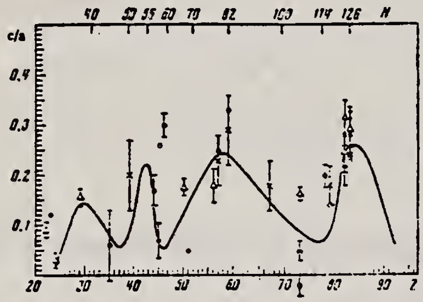

FIG. 2. Assymetry coefficients c/a obtained for nuclei with various Z in the following studies: ref. 10 – $E_{\gamma\,max}$ = 25.5 MeV, E_n > 7.4 MeV (•); ref. 11 – $E_{\gamma\,max}$ = 27–32 MeV, E_n > ~5 MeV (●); ref. 12 – $E_{\gamma\,max}$ = 34 MeV, E_n > ~8 MeV (·); ref. 13 – $E_{\gamma\,max}$ = 55 MeV, E_n > ~5 MeV (X); present work – $E_{\gamma\,max}$ = 28.5 MeV, E_n > 5 MeV (○). The smooth curve shows the coefficient b/a characterizing the photoneutron angular distribution anisotropy as a function of atomic number Z. (This has been converted from the curve given in ref. 11 and and is for the distribution $I(\vartheta) = a + b \sin^2\vartheta + c \cos\vartheta$, normalized at the points Z = 82–83.)

[11] J.W. Jury, J.S. Hewitt, K.G. McNeill, Can. J. Phys. 46, 1823 (1968).

[12] F.R. Allum, T.W. Quirk, B.M. Spicer, Nucl. Phys. 53, 545 (1964).

[13] G.C. Reinhardt and W.D. Whitehead, Nucl. Phys. 30, 201 (1962).

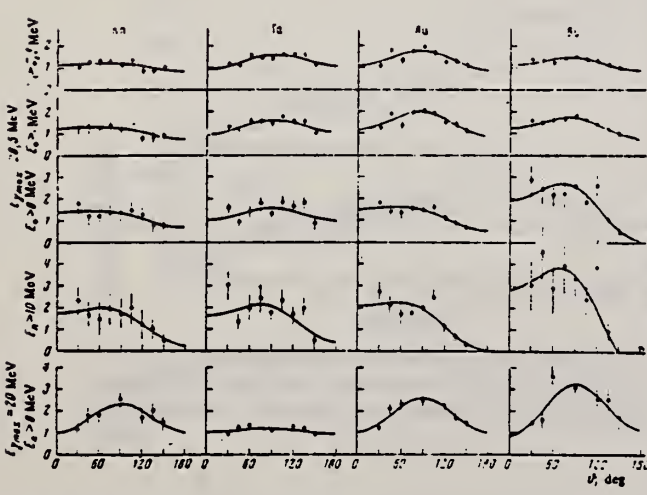

FIG. 1. Angular distributions of photoneutrons obtained in irradiation of Rh, Ta, Au, and Bi samples by bremsstrahlung with maximum energy $E_{\gamma\,max}$ = 28.5 MeV. The curves were calculated from the experimental points by the method of least squares for a distribution of the form $I(\vartheta) = a + b \sin^2\vartheta + c \cos\vartheta$ and normalized (a = 1). For comparison we have shown below the angular distributions of photoneutrons with energy E_n > 8 MeV obtained in irradiation of the same samples by bremsstrahlung with $E_{\gamma\,max}$ = 20 MeV.

(over)

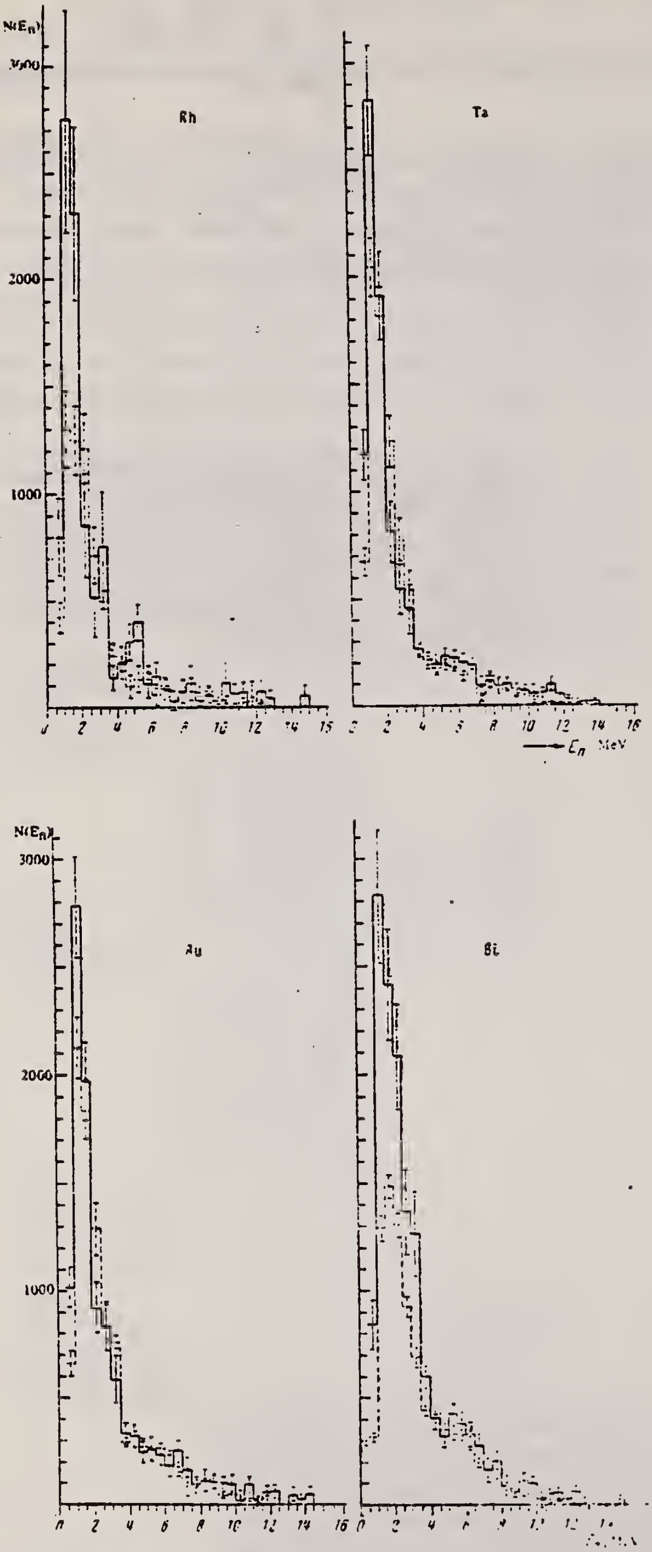

FIG. 3. Photoneutron energy spectra from Rh, Ta, Au and [illegible] radiation of the samples by bremsstrahlung with maximum [illegible] E_γ max = 20 (dashed line) and 28.5 (solid line) MeV for [illegible] maximum neutron yield. For each nucleus the histograms [illegible] E_γ max = 20 and 28.5 MeV have been combined in the [illegible] 4–4.5 MeV.

REF.

K.A. Snover, K. Ebisawa, D.R. Brown, and P. Paul
Phys. Rev. Letters 32, 317 (1974)

ELEM. SYM.	A	Z
Bi	209	83

METHOD

REF. NO.	
74 Sn 5	hmg

REACTION	RESULT	EXCITATION ENERGY	SOURCE TYPE	SOURCE RANGE	DETECTOR TYPE	DETECTOR RANGE	ANGLE
P,G	ABX	13- 29	D	17- 25	NAI-D		DST

$$Y(\theta) = \sum_{i=o}^{4} A_i P_i(\cos\theta)$$

$$\sigma = 4\pi A_o = 2\pi(Y(55^o) + Y(125^o))$$

$$A \equiv [Y(55^o) - Y(125^o)]/2P_1(\cos 55^o) = A_1 - 0.68A_3$$

$$a \equiv A/A_o$$

a and A are a measure of M1 or E2 radiation interfering with E1.

An $E2$ or $M1$ resonance is observed in the reaction $^{208}Pb(p, \gamma_0\gamma_1\gamma_2)^{209}Bi$ at $E_p \simeq 20.0$ MeV ($E_x \simeq 23.7$ MeV) with a width $\Gamma \sim 3.5$ MeV. Present evidence supports its identification as a collective $E2$ excitation.

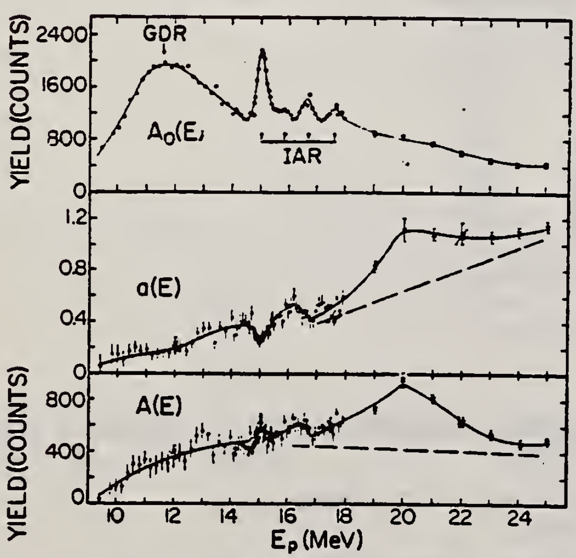

FIG. 2. Excitation curves for the reaction $^{208}Pb(p, \gamma_0\gamma_1\gamma_2)^{209}Bi$. Solid dots, data from Ref. 5; and crosses, present work. The total cross section $\sigma \simeq 4.3\ A_0\ \mu b/100$ counts.

REF.		ELEM. SYM.	A	Z
C. P. Swann J. Franklin Institute <u>298</u>, 321 (1974)		Bi	209	83
METHOD		REF. NO.	74 Sw 11	egf

REACTION	RESULT	EXCITATION ENERGY	SOURCE TYPE	SOURCE RANGE	DETECTOR TYPE	DETECTOR RANGE	ANGLE
G,G	LFT	2- 5	C	4- 5	SCD-D		UKN

10 LEVELS 2826-4822 KEV

Table II

Properties of states observed in ^{206,207,208}Pb and ^{209}Bi; G(EL) and G(M1) are the reduced transition probabilities in Weisskopf units

Nuclei	E_γ (keV)	J^π	Γ_0/Γ	$g\,\Gamma_0^2/\Gamma$ (eV)	Γ_0 (eV)	G(EL)	G(M1)
^{206}Pb	3744	1^-	1		0·13 (2)	0·001	
	4114	2^+	1		0·30 (6)	5	
	4330	1^+	1		0·90 (9)		0·56
	4606	1	1		0·23 (3)	0·001	0·12
	4974	1	1	0·8 (2)		0·003	0·32
	5038	1	1	2·3 (5)		0·007	0·90
^{207}Pb	3300	$1/2^{+}$*			0·039 (6)		
	3928	$3/2^-$	1		0·34 (4)		
	4104	$3/2^-$	1		0·55 (6)	8	
	4140	$5/2^-$	1		0·46 (5)	6	
	4627	$1/2^{+}$†	1		0·64 (7)	0·003	
	4872	$1/2^-, 3/2^-$	1	3·6 (5)			~1·2
	4982	$1/2^-, 3/2^-$	1	4·0 (5)			~1·2
^{208}Pb	4087	2^+	1		0·49 (5)	7	
	4843	1^+	1		5·1 (8)		2·3
^{209}Bi	2826	$5/2^-$	(0·63)‡		0·09 (1)		
	3977	5/2–13/2		0·82 (3)			
	4085	$5/2^-–13/2^-$		0·28 (3)		~5	
	4144	$5/2^-–13/2^-$		0·07 (2)		~1	
	4156	$5/2^-–13/2^-$		0·21 (4)		~3	
	4176	$5/2^-–13/2^-$		0·21 (4)		~3	
	4206	$5/2^-–13/2^-$		0·25 (3)		~4	
	4747	$7/2^-–11/2^-$		2·9 (5)			~1·4
	4785	$7/2^-–11/2^-$		2·7 (5)			~1·3
	4822	$7/2^-–11/2^-$		1·4 (3)			~0·7

* See Ref. (11). † See Ref. (12). ‡ See Ref. (7).

[7] C.P. Swann, Phys. Rev. Letts. 32, 1449 (1974).

[11] S.M. Smith et al., Nucl. Phys. A173, 32 (1971).

[12] R.A. Mayer et al., Phys. Rev. C 2, 1898 (1970).

REF.	ELEM. SYM.	A	Z
J. Tenenbaum, R. Moreh, and A. Nof Nucl. Phys. A218, 95 (1974)	Bi	209	83

METHOD	REF. NO.	
	74 Te 1	egf

REACTION	RESULT	EXCITATION ENERGY	SOURCE TYPE	SOURCE RANGE	DETECTOR TYPE	DETECTOR RANGE	ANGLE
G,G	LFT	5	D	4- 8	SCD-D		DST

5=5.603

TABLE 4

Values of Γ, Γ_0 and the energy separation δ (between the incident γ-line and the resonance level) as obtained from the analysis of the various experiments

Scatterer	E_γ (keV)	Γ (meV)	Γ_0 (meV)	δ (eV)	D (eV)	K_{E1} (10^{-9} MeV^{-3})	K_{M1} (10^{-9} MeV^{-3})
^{55}Mn	7491	450±250	80± 40	17 ±1			
^{140}Ce [a])	5660	13± 3	12± 2	4.7±0.3	6800	0.33	
^{141}Pr [a])	6877	85± 35	17± 9	6.7±1.5	450		116
^{142}Nd [a])	6877	340± 40	270± 20	12.4±0.3	1200	26	
^{202}Hg	4922	300± 50	260± 20	4.2±0.5	19000	3.4	
^{209}Bi [a])	5603	950±200	950±200	13 ±1	34000		160

The radiative strengths K_{E1} and K_{M1} are also given. The level spacing D refers to the excitation energy of the resonance level E_γ.

[a]) These values are slightly different from those of ref. [8]) and were obtained from a renewed analysis of the experimental results.

TABLE 2

Measured angular distribution coefficients A_2, the ratios $N_{||}/N_\perp$, the spins and parities of the ground and the resonance levels, J_0^π and J_r^π, and the character of the ground state transition

Scatterer	E_γ (keV)	A_2	$N_{\|\|}/N_\perp$	J_0^π	J_r^π	Transition
^{55}Mn	7491	0.01±0.02	1.00±0.02	$\frac{5}{2}^-$	$\frac{3}{2}$	
^{140}Ce	5660	0.51±0.02	1.14±0.04	0^+	1	E1
^{141}Pr	6877	0.11±0.02	0.95±0.03	$\frac{5}{2}^+$	$\frac{7}{2}^+$	M1
^{142}Nd	6877	0.51±0.03	1.10±0.04	0^+	1^-	E1
^{202}Hg	4922	0.51±0.02	1.18±0.03	0^+	1^-	E1
^{209}Bi	5603	0.06±0.02	0.97±0.02	$\frac{9}{2}^-$	$\frac{11}{2}^-$	M1

[8]A. Wolf, R. Moreh, A. Nof, O. Shahal, J. Tenenbaum, Phys. Rev. C6, 2276 (1972).

REF.	D. Turck, W. Ziga, and H. -G. Clerc Phys. Lett. 49B, 335 (1974)	ELEM. SYM.	A	Z
		Bi	209	83
METHOD		REF. NO.		
		74 Tu 5		egf

REACTION	RESULT	EXCITATION ENERGY	SOURCE TYPE	SOURCE RANGE	DETECTOR TYPE	DETECTOR RANGE	ANGLE
E,F	ABX	THR- 40	D	27- 40	TRK-I		4PI

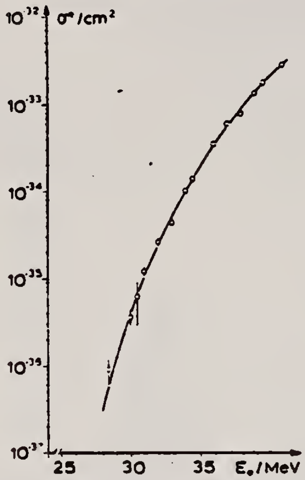

Fig. 1. Cross section σ^e for electron induced fission in ^{209}Bi as a function of electron energy E_0.

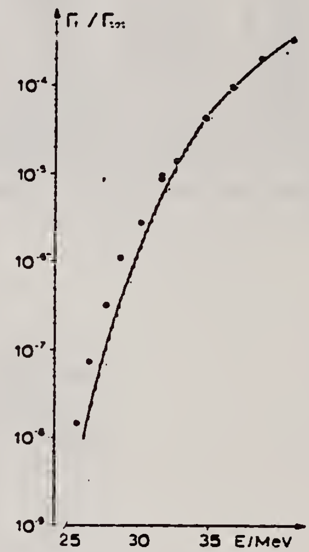

Fig. 2. Solid line: fission probability Γ_f/Γ_{tot} as a function of excitation energy E for ^{209}Bi as obtained from unfolding the electrofission cross section; the hatching indicates the statistical uncertainties. The data points are results of Khodai-Joopary [3] for the compound nucleus ^{209}Bi produced in the reaction ^{208}Pb + p.

For ^{209}Bi an electrofission cross section below 10^{-35} cm^2 was measured by the observation of correlated binary fission tracks in mica detectors. From the cross-section data between 28 and 41 MeV electron energy, a fission barrier of 25.5 ± 1.5 MeV was deduced. The method offers the possibility to measure fission barriers at low angular momentum and for nuclei not accessible otherwise.

REF.	ELEM. SYM.	A	Z
A. Wolf, R. Moreh, and O. Shahal Nucl. Phys. A227, 373 (1974)	Bi	209	83

METHOD	REF. NO.	
	74 Wo 2	egf

REACTION	RESULT	EXCITATION ENERGY	SOURCE		DETECTOR		ANGLE
			TYPE	RANGE	TYPE	RANGE	
$ G,G	LFT	6- 8	D	6- 8	SCD-D		DST

δ = Doppler width

7.168, 7.637

TABLE 4

Upper limit of Γ_0/Γ, the temperature variation ratio R_T, and the self-absorption ratio R

Scatterer (γ-source)	E_0 (MeV)	Γ_0/Γ (±15%)	R_T [a]	R(%) [b]
^{65}Cu(Ti)	6.556	0.80	0.94 ±0.02	1.1±0.5
^{69}Ga(Cu)	7.306	0.52	1.035±0.004	3.5±0.5
^{100}Mo(Cu)	7.637	0.28	1.043±0.007	0.8±0.3
^{100}Mo(Ti)	6.418	0.85	1.032±0.003	0.6±0.3
^{118}Sn(Cu)	6.988	0.84	1.020±0.009	5.7±0.2
^{126}Te(Cu)	7.915	0.4 ±0.1	0.95 ±0.05	6 ±5
^{130}Te(Cu)	7.637	0.45±0.10	0.84 ±0.05	0.9±1.5
^{139}La(Cu)	7.637	0.55	0.95 ±0.01	2.2±0.3
^{139}La(Ti)	6.418	0.78	0.968±0.008	6.4±0.8
^{141}Pr(Cu)	7.915	0.25	1.02 ±0.01	0.9±0.9
^{141}Pr(Cu)	7.252	0.51	1.005±0.003	5.9±0.4
^{144}Nd(Cu)	7.915	0.27	0.89 ±0.05	< 0.5
^{186}W(Ti)	6.418	0.31	1.030±0.004	< 0.5
^{203}Tl(Ti)	6.418	0.28	1.03 ±0.01	1.6±0.3
^{205}Tl(Cu)	7.252	0.58	1.02 ±0.01	1.6±0.7
^{209}Bi(Cu)	7.637	1.00	1.00 ±0.02	2 ±1
^{209}Bi(Ti)	7.168	1.00	0.971±0.005	28.0±0.6

[a]) The values of R_T are given for 10 g/cm^2 thick scatterers placed at an angle of 60° and a detector angle of 135°.

[b]) The values of R are given for the same scatterer-detector geometry as that of R_T and a 20 g/cm^2 thick absorber.

TABLE 7

Summary of Γ, Γ_0 and δ of resonance levels measured in the present work and in earlier works [8, 16, 17])

Isotope	Energy (MeV)	Γ (meV)	Γ_0 (meV)	δ (eV)	Ground state transition
^{65}Cu	6.556	70^{+60}_{-20}	28^{+15}_{-5}	11.2 ±0.8	
^{69}Ga [a])	7.306	105±40	48± 7	6.2 ±0.5	E1
^{100}Mo [c])	7.637	140±40	40± 5	4.5 ±0.5	E1
^{100}Mo [c])	6.418	50±35	25± 8	4.25±0.25	E1
^{118}Sn	6.988	152± 5	128± 3	5.5 ±0.5	E1
^{126}Te	7.915	12± 6	5± 2	11 ±2	M1
^{130}Te	7.637	60±30	30±10	15 ±2	E1
^{139}La [b])	7.637	170±40	47± 6	10.5 ±0.5	E1
^{139}La [b])	6.418	85^{+13}_{-7}	67± 8	9.5 ±0.5	E1
^{141}Pr [b])	7.915	7± 3	2± 1	6.6 ±1.0	M1
^{141}Pr [b])	7.252	290±30	110±10	6.4 ±0.5	E1
^{144}Nd [b])	7.915	30±10	8± 3	14.0 ±0.5	M1
^{186}W	6.418	46±35	6± 3	1 ±1	E1
^{203}Tl [b])	6.418	350±60	82±15	0.5 ±0.5	
^{205}Tl [b])	7.252	50±30	25± 6	5.2 ±1.5	M1
^{209}Bi	7.637	> 500	> 30		
^{209}Bi [b])	7.168	820±40	820±40	5.8 ±0.8	E1

[a]) Ref. [16]). [b]) Ref. [8]). [c]) Ref. [17]).

(over)

TABLE 6

Values of A_2, $N_\parallel/N_\perp$, spins, and mixing amplitudes x

Scatterer (γ-source)	E_0 (MeV)	A_2	$N_\parallel/N_\perp$	J_0^π	J^π	J_f^π	x
^{65}Cu(Ti)	6.556	0		$\frac{3}{2}^-$	$\frac{1}{2}$	$\frac{3}{2}^-$	0
^{69}Ga(Cu)	7.306	0.14 ±0.01	1.046±0.022	$\frac{3}{2}^-$	$\frac{5}{2}^+$	$\frac{3}{2}^-$	0
^{100}Mo(Cu)	7.637	0.49 ±0.05	1.17 ±0.05	0^+	1^-	0^+	0
^{100}Mo(Cu)	7.102 [a]	0.013±0.016		0^+	1^-	2^+	−0.06±0.02 [b]
^{100}Mo(Ti)	6.418	0.52 ±0.02	1.15 ±0.03	0^+	1^-	0^+	0
^{100}Mo(Ti)	5.355 [a]	0.19 ±0.08		0^+	1^-	2^+	0.21±0.12 [b]
^{118}Sn(Cu)	6.988	0.48 ±0.02	1.12 ±0.05	0^+	1^-	0^+	0
^{126}Te(Cu)	7.915	0.46 ±0.11	0.86 ±0.10	0^+	1^+	0^+	0
^{130}Te(Cu)	7.637	0.48 ±0.04	1.12 ±0.04	0^+	1^-	0^-	0
^{139}La(Cu)	7.637	0.16 ±0.02	1.024±0.015	$\frac{7}{2}^-$	$\frac{7}{2}^-$	$\frac{7}{2}^-$	0
^{139}La(Ti)	6.418	0.093±0.004	1.018±0.006	$\frac{7}{2}^+$	$\frac{7}{2}^-$	$\frac{7}{2}^+$	0
^{141}Pr(Cu)	7.915	0.41 ±0.06	0.94 ±0.03	$\frac{5}{2}^+$	$\frac{5}{2}^+$	$\frac{5}{2}^-$	$0.26^{+0.13}_{-0.08}$
^{141}Pr(Cu)	7.252	0.23 ±0.06	1.03 ±0.02	$\frac{5}{2}^+$	$\frac{3}{2}^-$	$\frac{5}{2}^+$	0
^{144}Nd(Cu)	7.915	0.50 ±0.03	0.92 ±0.09	0^+	1^-	0^+	0
^{186}W(Ti)	6.418	0.49 ±0.05	1.15 ±0.06	0^+	1^-	0^-	0
^{186}W(Ti)	6.296 [a]	−0.011±0.014		0^+	1^-	2^+	−0.10±0.03 [c]
^{203}Tl(Ti)	6.418	0	1.01 ±0.01	$\frac{1}{2}^+$	$\frac{1}{2}$	$\frac{1}{2}^-$	0
^{205}Tl(Cu)	7.252	0.71 ±0.08	0.90 ±0.02	$\frac{1}{2}^+$	$\frac{3}{2}^+$	$\frac{1}{2}^+$	−0.25±0.05
^{205}Tl(Cu)	7.047 [a]	−0.69 ±0.03		$\frac{1}{2}^+$	$\frac{3}{2}^+$	$\frac{3}{2}^+$	0.33±0.04
^{209}Bi(Cu)	7.637	0.24 ±0.04		$\frac{9}{2}^-$	($\frac{9}{2}$)	$\frac{9}{2}^-$	.
^{209}Bi(Ti)	7.168	0.20 ±0.02	1.040±0.015	$\frac{9}{2}^-$	$\frac{7}{2}^+$	$\frac{9}{2}^-$	

Errors refer to one standard deviation.
[a]) Inelastic transitions.
[b]) Ref. [17]).
[c]) Ref. [15]).

1) R. Moreh et al., Phys. Rev. C2 (1970) 1144
8) A. Wolf, et al., Phys. Rev. C6 (1972) 2276
15) R. Moreh et al., Phys. Lett. 36B (1971) 71
16) R. Moreh et al., Phys. Rev. C7 (1973) 1885
17) R. Moreh et al., Nucl. Phys. A217 (1973) 477
29) R. Moreh et al., Phys. Rev. C4 (1971) 2265
30) R. Moreh et al., Phys. Rev. 178 (1969) 1961

TABLE 8

Values of Γ_i, D, k_{E1} and k_{M1}

E1 transitions					M1 transitions				
scatterer (γ-source)	$E_0 \to E_f$ (MeV)	Γ_i (meV)	D (eV)	k_{E1} (10^{-9} MeV^{-3})	scatterer (γ-source)	$E_0 \to E_f$ (MeV)	Γ_i (meV)	D (eV)	[illegible] (10^{-9} [illegible]$^{-3}$)
^{62}Ni(Fe) [a])	7.646		12300		^{126}Te(Cu)	7.915		260	
	→ 1.172	24		0.5		→ 0.666	2.3		[illegible]
						→ 1.421	1.7		[illegible]
^{69}Ga(Cu)	7.306		660						
	→ 0.572	3.2		1.0	^{141}Pr(Cu)	7.915		90	
	→ 0.872	2.7		0.9		→ 1.298	1.3		[illegible]
						→ 1.437	0.8		[illegible]
^{100}Mo(Cu)	7.637		670			→ 1.580	1.4		[illegible]
	→ 0.535	40		7.7		→ 1.655	1.0		[illegible]
	→ 1.063	5.7		1.4					
	→ 1.461	1.4		0.4	^{141}Pr(Fe) [c])	7.632		170	
^{112}Cd(Fe) [b])	7.632		350			→ 0.145	5.6		[illegible]
	→ 0.617	11		4		→ 1.130	6.4		[illegible]
	→ 1.223	7.3		3.4		→ 1.293	0.4		[illegible]
	→ 1.429	2		1		→ 1.437	5.6		[illegible]
	→ 1.468	1.7		0.9		→ 1.451	6.8		[illegible]
						→ 1.582	1.1		[illegible]
^{130}Te(Cu)	7.637		360						
	→ 0.837	16		5.5	^{144}Nd(Cu)	7.915		350	
	→ 1.589	18		8.8		→ 0.697	13		[illegible]
^{139}La(Cu)	7.637		190			→ 1.041	2.7		[illegible]
	→ 1.384	3		2.5		→ 1.564	6.2		[illegible]
	→ 1.538	3		2.7	^{205}Tl(Cu)	7.252		1200	
						→ 0.205	4		[illegible]
^{141}Pr(Cu)	7.252		220						
	→ 0.146	82		38					
	→ 1.120	8.6		6.5					
^{186}W(Cu)	6.418		110						
	→ 0.122	12		14					

The values of D refer to an excitation energy E_0.
[a]) Ref. [1]). [b]) Ref. [29]). [c]) Ref. [30]).

REF.

M. Areskoug, B. Schroder, K. Lindgren
Nucl. Phys. A251, 418 (1975)

ELEM. SYM.	A	Z
Bi	209	83

METHOD

REF. NO.	
75 Ar 7	egf

REACTION	RESULT	EXCITATION ENERGY	SOURCE		DETECTOR		ANGLE
			TYPE	RANGE	TYPE	RANGE	
G,F	ABY	THR-600	C	600	ACT-I		4PI

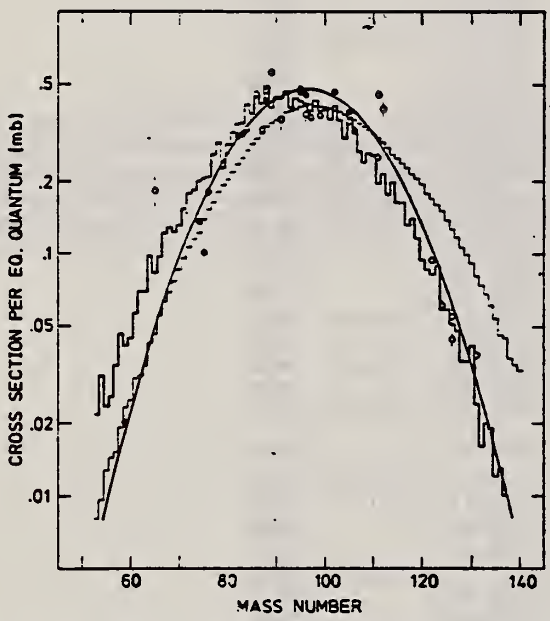

Fig. 2. Mass chain yields of fission products. Filled circles indicate measured total yields, open circles indicate total yields calculated from catcher foil yields according to eq. (2). Error bars show statistical errors. The Gaussian is the fitted mass distribution. Also shown are the primary (thin drawn histogram) and secondary (thick drawn histogram) mass distributions calculated from the liquid drop model.

(over)

TABLE 1

Formation modes (C = cumulative, I = independent), decay data and obtained values of yield σ_{tot}, range R_0 and mean charge $\langle Z \rangle$ for the fission products studied

Nuclide	Type	$T_{\frac{1}{2}}$ (d)	E_γ (keV) Intensity (%)	σ_{tot} (μb/eq. q.)	R_0 (mg/cm² of Bi)	$\langle Z \rangle$
$^{59}_{26}$Fe	C	44.6	1099(56.5), 1292(43.2)[b])	15.5±0.4	11.5±0.5	25.37
$^{65}_{30}$Zn	C	244	1116(50.75)	18.3±2.4		30.12
$^{74}_{33}$As	I	17.77	596(59.22)	29.5±0.7	9.1±1.1	33.00
$^{75}_{34}$Se	C	120.4	136(56.28), 265(57.28)	11.4±0.6	8.3±0.5	34.12
$^{76}_{33}$As	I	1.097	559(41.05)	66.6±2.5		33.00
$^{82}_{35}$Br	I	1.48	554(70.5), 698(27.9), 1044(27.8), 1317(27.5), 1475(16.7)	117.8±1.7	9.2±1.0	35.00
$^{83}_{37}$Rb	C	86.2	520(46.8), 530(30.4), 553(16.5)	52.7±0.9	8.0±0.2	37.15
$^{84}_{37}$Rb	I	33	882(73.4)	77.0±2.9		37.00
$^{86}_{37}$Rb	I	18.66	1079(8.8)	173.2±7.4		37.00
$^{87m}_{39}$Y	C	0.58	381(77)	(35.0± 1.1)		39.11
$^{87}_{39}$Y	C	3.35	388(82.5), 485(90.6)[a])	29.8± 1.5		39.11
$^{88}_{39}$Y	C	106.6	898(92)	83.9± 3.0	9.1±0.4	39.16
$^{88}_{40}$Zr	C	85	393(97)	11.4± 0.3		40.06
$^{89}_{40}$Zr	C	3.27	909(100)	35.9± 1.2		40.09
$^{90m}_{39}$Y	I	0.133	202(97)	(148.2± 5.0)		39.00
$^{91}_{38}$Sr	C	0.406	750(23.0)	134.8±13.6		37.73
$^{95}_{40}$Zr	C	65.5	724(43), 757(54.6), 766(99)[a])	242.3± 2.5	8.4±0.1	39.63
$^{95}_{41}$Nb	I	35.1	766(99)	159.3± 0.9	9.1±0.2	41.00
$^{96}_{41}$Nb	I	0.979	460(28.2), 569(55.7), 1091(49.43)	172.1± 2.7	7.1±0.5	41.00
$^{96}_{43}$Tc	I	4.3	813(82.2), 850(97.8)	15.9± 1.2		43.00
$^{97}_{40}$Zr	C	0.708	743(93.3)	81.2± 3.6		39.82
$^{99}_{42}$Mo	C	2.78	181(7.6)	250.2± 6.5		41.49
$^{101m}_{45}$Rh	C	4.47	309(83)	(19.1± 0.9)		45.08
$^{103}_{44}$Ru	C	39.6	497(90), 610(5.4)	370.7± 3.0	8.1±0.2	43.31
$^{105}_{44}$Ru	C	0.185	724(44.5)	174.2±15.1		43.65
$^{105}_{45}$Rh	C	1.496	319(19.6)[b])	324.8± 3.4	8.9±0.6	44.20
$^{105}_{47}$Ag	C	41	344(42)[c])	(9.8± 2.3)		47.06
$^{106}_{44}$Ru	C	367	622(9.76)[a])	110.5±23.1	6.2±1.4	43.75
$^{106m}_{47}$Ag	I	8.4	406(15), 430(16), 451(31), 616(24.3), 717(32)	(9.0± 0.3)		47.00
$^{110m}_{47}$Ag	I	253	658(93.8), 678(11.8), 885(74.7)	(61.1± 1.3)	7.5±0.4	47.00
$^{111}_{47}$Ag	C	7.47	342(4.6)	330.8±16.5		46.43
$^{111}_{49}$In	C	2.83	171(90.3)	14.3± 0.4		49.09
$^{112}_{46}$Pd	C	0.838	617(43.5)[a])	78.9± 6.1		45.83
$^{114m}_{49}$In	I	49.51	190(17.7)	(53.5± 1.3)	6.1±0.5	49.00
$^{115g}_{48}$Cd	C	2.224	528(27.5)	(44.2± 0.8)		47.66
$^{120m}_{51}$Sb	I	5.8	1023(99), 1172(100)	(20.8± 0.3)		51.00
$^{121m}_{52}$Te	C	154	212(100)[d])	(15.7± 0.7)	5.4±0.3	52.23
$^{122}_{51}$Sb	I	2.72	564(63)	34.3± 1.3		51.00
$^{124g}_{51}$Sb	I	60.2	603(98)	(14.8± 0.5)		51.00
$^{124}_{53}$I	I	4.17	603(62)	18.3± 0.8		53.00
$^{126}_{51}$Sb	I	12.4	415(88), 695(100), 697(32)	3.2± 0.4		51.00
$^{126}_{53}$I	I	13.0	389(34.9), 666(32.4)	18.0± 1.3		53.00
$^{131}_{56}$Ba	C	11.7	124(14)	13.1± 0.7		56.24

σ_{tot} values within parentheses were not used in the yield distribution fit.

a) Gamma radiation from daughter nucleus.

b) σ_{TB} not measured. R calculated according to $R = 2W_F(\sigma_F+\sigma_B)/(\sigma_F+\sigma_{TF})$.

c) Only σ_F measured. σ_B estimated according to $\sigma_F/\sigma_B = 1.06$.

d) Intensity unknown. Adopted value 100%.

REF.		ELEM. SYM.	A	Z
	V. S. Evseev, T. N. Mamedov, O. V. Selyugin Yad. Fiz. 21, 245 (1975) Sov. J. Nucl. Phys. 21, 129 (1975)	Bi	209	83
METHOD		REF. NO.		
		75 Ev 1		hmg

REACTION	RESULT	EXCITATION ENERGY	SOURCE TYPE	SOURCE RANGE	DETECTOR TYPE	DETECTOR RANGE	ANGLE
G,N	SPC	7- 31	C	31	SCI-D		140

Neutron energy spectra have been measured in the energy range $2 \leq E_n \leq 5$ MeV for photoexcitation of the nuclei Ta, Pb, Bi, and Th by bremsstrahlung with maximum energy 31 MeV. From the neutron spectra we have determined values of the nuclear temperature $\bar{T}$ after emission of the first neutron: 1.01 ± 0.04, 1.12 ± 0.04, 1.11 ± 0.04, and 1.25 ± 0.05 MeV respectively for Ta, Pb, Bi, and Th. Comparison of the values obtained for the nuclear level-density parameter with the predictions of the statistical theory of nuclear reactions shows that this theory does not describe the decay of collective nuclear states of the giant dipole resonance type.

REF.

Yu. I. Sorokin and B. A. Yur'ev
Izv. Akad. Nauk SSSR. Ser. Fiz. 39, 114 (1975)
Bull. Acad. Sci. (USSR) Phys. Ser. 39, 98 (1975)

ELEM. SYM.	A	Z
Bi	209	83

METHOD

REF. NO.	
75 So 12	hmg

REACTION	RESULT	EXCITATION ENERGY	SOURCE TYPE	SOURCE RANGE	DETECTOR TYPE	DETECTOR RANGE	ANGLE
G,XN	ABI	7- 27	C	7- 27	BF3-I		4PI

SEE 73 SO19

Table 1

Element	A	σ_0, (γ, Tn) MeV · b, to 27 MeV		$\sigma_{0\gamma}$, MeV · b, to 20 MeV	$\sigma_{0\gamma}$, MeV · b, 20–27 MeV	σ_{-1}, mb	σ_{-2}, mb × MeV^{-1}	E_m, MeV	K, MeV	[illegible] (1.4−1), MeV^{-1}	Threshold (γ,2n), MeV	σ_0 (E1), MeV × b
Sn	112	2.23	1.90	1.49	0.41	112	6.7	15.8	20.1	10.2	19.2	1.66
	114	2.26	1.66	1.39	0.47	108	6.5	15.7	21.5	10.2	18.1	1.68
	116	2.40	1.85	1.40	0.45	110	6.6	15.6	21.7	8.1	17.1	1.71
	117	2.52	1.86	1.39	0.47	110	6.7	15.4	21.6	7.3	16.5	1.72
	118	2.46	1.92	1.53	0.39	115	7.1	15.5	20.7	7.6	16.3	1.71
	119	2.63	1.86	1.42	0.44	111	6.8	15.4	22.0	13.2	15.8	1.74
	120	2.69	2.07	1.69	0.38	127	7.9	15.3	19.1	3.6	15.6	1.75
	122	2.94	2.03	1.51	0.52	119	7.1	15.6	21.8	4.5	15.0	1.77
	124	2.90	1.93	1.44	0.49	114	6.9	15.5	23.2	5.4	14.4	1.79
W	182	3.68	2.78	2.32	0.46	184	12.5	–	24.2	5.2	14.9	2.63
	184	4.68	2.95	2.33	0.72	196	13.0	—	23.7	5.2	13.6	2.65
Au	197	4.06	3.15	2.81	0.34	226	15.5	13.3	20.9	17.1	14.8	2.84
Pb	206	3.93	3.21	2.80	0.41	225	16.1	13.5	23.1	6.6	14.8	2.96
	208	4.32	3.28	2.81	0.47	241	16.7	13.3	22.6	9.6	14.1	2.98
Bi	209	4.59	3.47	2.56	0.51	216	17.9	13.2	21.3	10.2	14.3	3.00

REF. G. Bologna, V. Bellini, V. Emma, A.S. Figuera, S. Lo Nigro
C. Milone and G.S. Pappalardo
Il Nuovo Cimento 35A, 91 (1976)

ELEM. SYM.	A	Z
Bi	209	83

METHOD

REF. NO. 76 Bo 15 egf

REACTION	RESULT	EXCITATION ENERGY	SOURCE TYPE	SOURCE RANGE	DETECTOR TYPE	DETECTOR RANGE	ANGLE
G,F	RLX	220-500	D	220-500	TRK-I		4PI

COHERENT BREMS

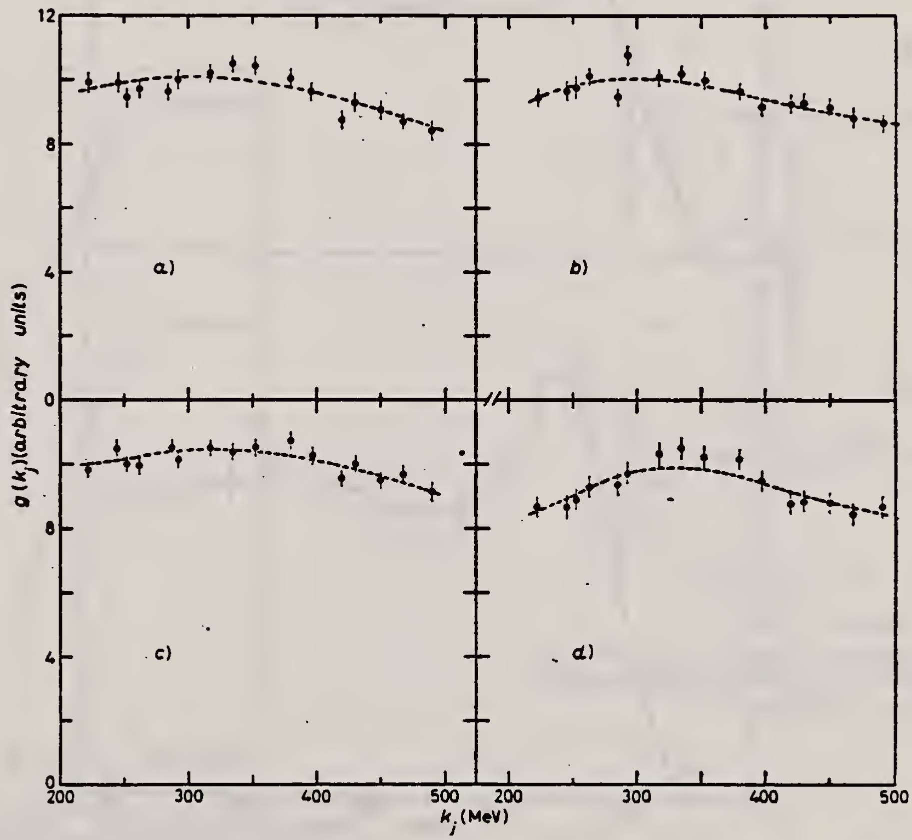

Fig. 6. – Photofission yields per equivalent quantum of Bi, Pb, Au and Pt as a function of the first peak energy k_j of photons. The dots are the experimental data; the dashed curves represent the yield functions estimated as described in sect. 5. *a*) Bi (γ, f), *b*) Pb (γ, f), *c*) Au (γ, f), *d*) Pt (γ, f).

over

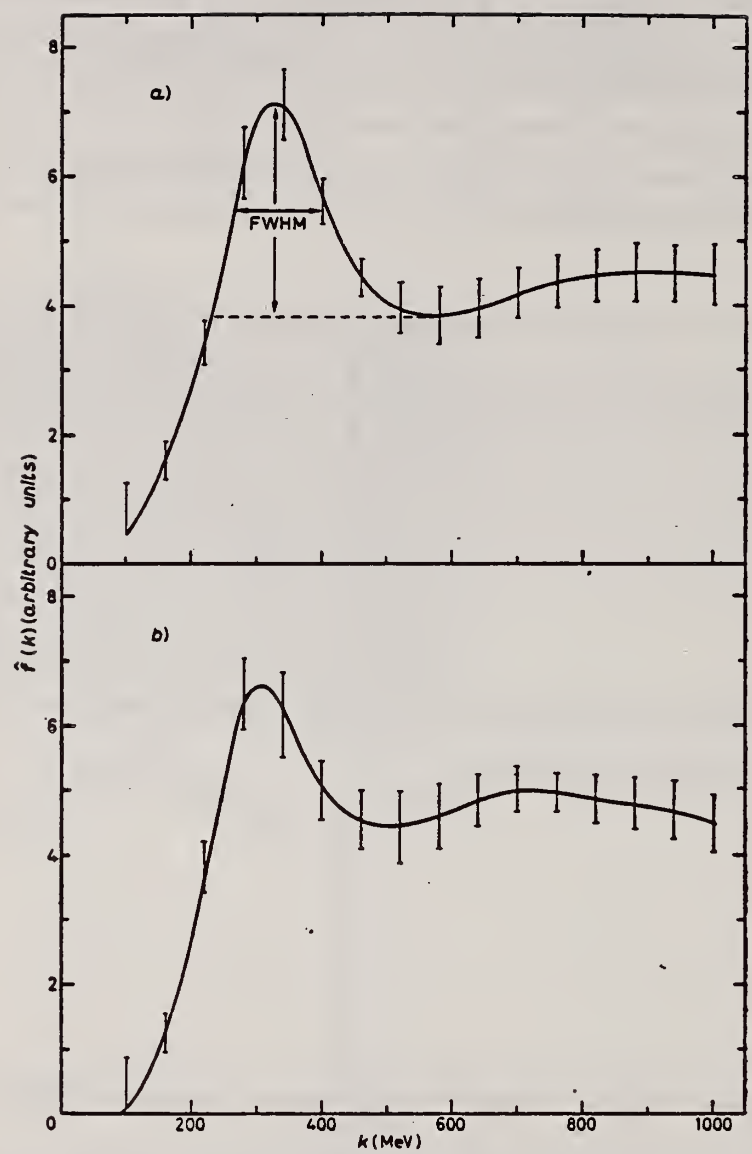

Fig. 7. – Photofission cross-section estimated by our unfolding method. For Bi the procedure used to deduce the FWHM of the first maximum is indicated. *a*) Bi (γ, f), *b*) Pb (γ, f).

REF.	ELEM. SYM.	A	Z
T. E. Drake, H. L. Pai, I. Nascimento Nucl. Phys. A259, 317 (1976)	Bi	209	83

METHOD	REF. NO.	
.	76 Dr 1	egf

REACTION	RESULT	EXCITATION ENERGY	SOURCE TYPE	SOURCE RANGE	DETECTOR TYPE	DETECTOR RANGE	ANGLE
E,F	ABX	25- 45	D	25- 45	TRK-I		DST

Abstract: The fission yields from the electrofission of ^{208}Pb and ^{209}Bi confirm the theoretically predicted large difference in the fission barrier energies of these nuclei. In addition the level density parameters at the fission saddle point were measured for ^{208}Pb and ^{209}Bi.

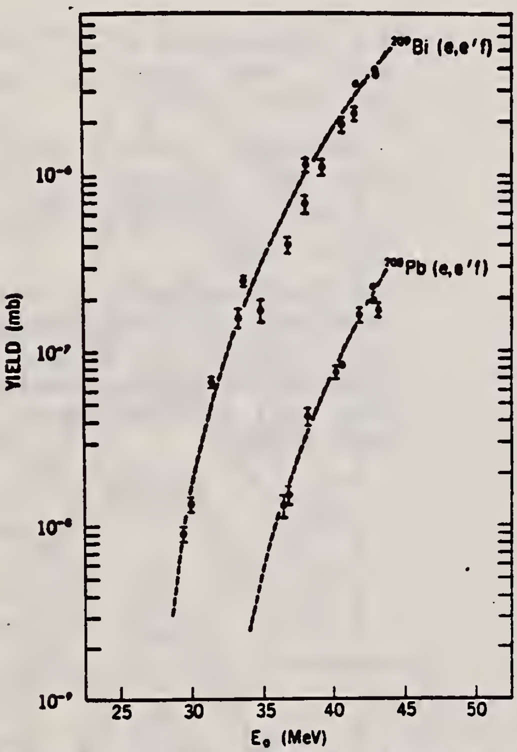

Fig. 3. The yield curves are shown for ^{209}Bi and ^{208}Pb. The data points are shown with the error bars and the theoretical fit as a dashed curve.

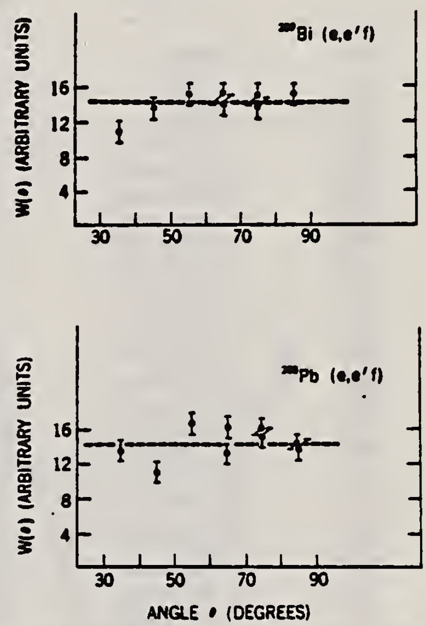

Fig. 2. The angular distribution of fission fragments from ^{209}Bi (top) and ^{208}Pb with respect to the direction of the incident electron beam of energy 43.1 and 42.8 MeV respectively.

TABLE 1

The measured level density parameters and the fission barrier energies for ^{208}Pb and ^{209}Bi

	^{208}Pb	^{209}Bi
a_n (MeV^{-1})	8.1±1	10.2±1
a_f (MeV^{-1})	10.8±1	13.0±1
B_f (MeV)	27.6±0.5 ^{a})	23.4±0.5
Δ_n (MeV)	0.6	

^{a}) This value of the fission barrier B_f includes the pairing energy Δ_f.

REF.	ELEM. SYM.	A	Z
V. Emma, S. Lo Nigro, C. Milone Nucl. Phys. A257, 438 (1976)	Bi	209	83

METHOD	REF. NO.	
	76 Em 2	egf

REACTION	RESULT	EXCITATION ENERGY	SOURCE TYPE	SOURCE RANGE	DETECTOR TYPE	DETECTOR RANGE	ANGLE
G,F	ABY	THR-999	C	999	TRK-I		4PI

999 = 1 GEV

TABLE 1

Measured values of σ_q at $E = 1000$ MeV and deduced values of σ_k assumed constant from E_0 to 1000 MeV

Element	Z^2/A	σ_q (mb)	E_0 (MeV)	σ_k (mb)
Bi	32.96	12.3±0.6	200	7.6±0.6
Pb	32.45	5.4±0.4	220	3.6±0.3
Tl	32.10	4.1±0.3	230	2.8±0.3
Au	31.68	2.0±0.15	240	1.4±0.2
Pt	31.18	1.1±0.08	255	$(8\ \pm0.7)\times10^{-1}$
Re	30.21	$(3.7\pm0.3)\times10^{-1}$	280	$(2.9\pm0.3)\times10^{-1}$
W	29.78	$(3.5\pm0.3)\times10^{-1}$	290	$(2.8\pm0.3)\times10^{-1}$
Ta	29.45	$(3.3\pm0.3)\times10^{-1}$	300	$(2.7\pm0.3)\times10^{-1}$
Hf	29.04	$(1.7\pm0.2)\times10^{-1}$	310	$(1.4\pm0.2)\times10^{-1}$
Yb	28.31	$(1.3\pm0.1)\times10^{-1}$	330	$(1.2\pm0.1)\times10^{-1}$
Tm	28.18	$(7.5\pm0.8)\times10^{-2}$	335	$(6.8\pm0.8)\times10^{-2}$
Ho	27.21	$(3.6\pm0.4)\times10^{-2}$	355	$(3.5\pm0.4)\times10^{-2}$
Dy	26.80	$(2.6\pm0.3)\times10^{-2}$	360	$(2.5\pm0.3)\times10^{-2}$
Tb	26.58	$(2.5\pm0.3)\times10^{-2}$	370	$(2.5\pm0.3)\times10^{-2}$
Gd	26.04	$(1.6\pm0.2)\times10^{-2}$	380	$(1.7\pm0.2)\times10^{-2}$
Sm	25.56	$(1.3\pm0.2)\times10^{-2}$	390	$(1.4\pm0.2)\times10^{-2}$
Nd	24.96	$(9.2\pm0.9)\times10^{-3}$	405	$(1\ \pm0.1)\times10^{-2}$
Ce	24.00	$(8\ \pm0.9)\times10^{-3}$	420	$(9\ \pm1\ )\times10^{-3}$
La	23.39	$(8.4\pm0.9)\times10^{-3}$	430	$(1\ \pm0.1)\times10^{-3}$
Sb	21.36	$(1.2\pm0.2)\times10^{-2}$	460	$(1.5\pm0.3)\times10^{-2}$
Te	21.19	$(8.8\pm1\ )\times10^{-3}$	465	$(1.2\pm0.2)\times10^{-2}$
Sn	21.06	$(1.3\pm0.2)\times10^{-2}$	465	$(1.7\pm0.3)\times10^{-2}$
Cd	20.49	$(1.7\pm0.3)\times10^{-2}$	470	$(2.2\pm0.4)\times10^{-2}$
Ag	20.47	$(2\ \pm0.3)\times10^{-2}$	470	$(2.6\pm0.4)\times10^{-2}$
Zn	13.76	$(2\ \pm0.4)\times10^{-1}$	515	$(3\ \pm0.6)\times10^{-1}$
Cu	13.44	$(2.4\pm0.5)\times10^{-1}$	515	$(3.6\pm0.8)\times10^{-1}$
Ni	13.35	$(2.4\pm0.5)\times10^{-1}$	510	$(3.6\pm0.8)\times10^{-1}$
Fe	12.10	$(3\ \pm0.6)\times10^{-1}$	510	$(4.4\pm0.9)\times10^{-1}$

[4] A.V. Mitrofanova et al. Sov. J. Nucl. Phys. 6, 512 (1968).

[7] T. Methasiri et al., Nucl. Phys. A167, 97 (1971).

[12] J.R. Nix et al., Nucl. Phys. 81, 61 (1966).

[20] N.A. Perifilov et al., JETP (Sov. Phys.) 14, 623 (1962); Proc. Symp. on the physics & chemistry of fission, Salzburg 1965, vol. 2 (IAEA) Vienna, 1965, p.283.

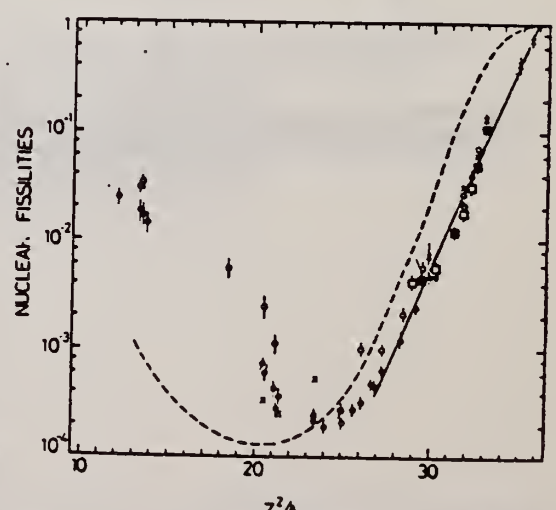

Fig. 2. Nuclear fissilities as a function of Z^2/A. Experimental points: solid circles represent our data; squares, the data from ref. [4]); open circles, the data from ref. [7]); and crosses, the data from (p,f) experiments[20]). The straight line is the best fit calculated from our data for $Z^2/A > 26$. The dashed curve is the curve VI calculated by Nix and Sassi[12]).

REF.		ELEM. SYM.	A	Z
	G. M. Gurevich, L. E. Lazareva, V. M. Mazur and G. B. Solodukhov JETP Lett. 23, 370 (1976) Pis'ma Zh. Eksp. Teor. Fiz. 23, 411 (1976)	Bi	209	83
METHOD		REF. NO. 76 Gu 5		hmg

REACTION	RESULT	EXCITATION ENERGY	SOURCE TYPE	SOURCE RANGE	DETECTOR TYPE	DETECTOR RANGE	ANGLE
G,MU-T	ABX	8- 21	C	35	NAI-D		4PI

We measured the total cross section for the absorption of rays in the region of $E1$ resonance for the nuclei ^{165}Ho, ^{178}Hf, ^{180}Hf, ^{181}Ta, ^{182}W, ^{197}Au, and ^{209}Bi. The singularity in the behavior of the resonance widths, observed in the region $160 < A < 185$, is apparently due to the influence of the neutron subshell $N = 108$.

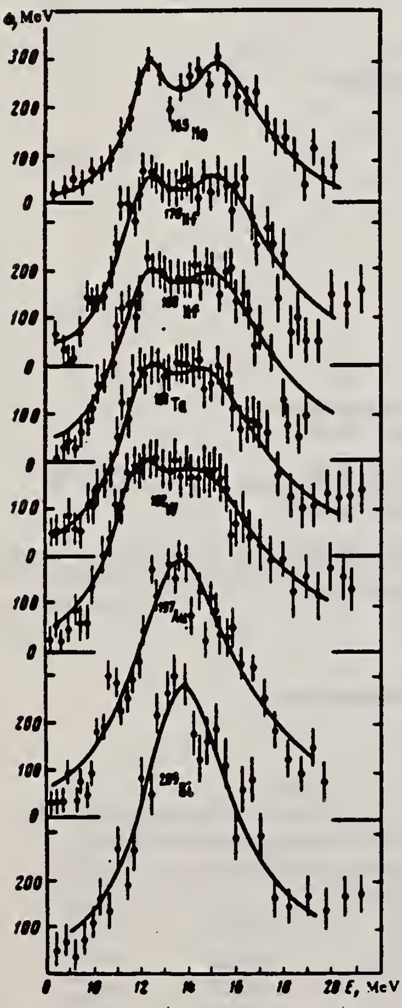

FIG. 1. Total photoabsorption cross sections for the nuclei ^{165}Ho, ^{178}Hf, ^{180}Hf, ^{181}Ta, ^{182}W, ^{197}Au, ^{209}Bi.

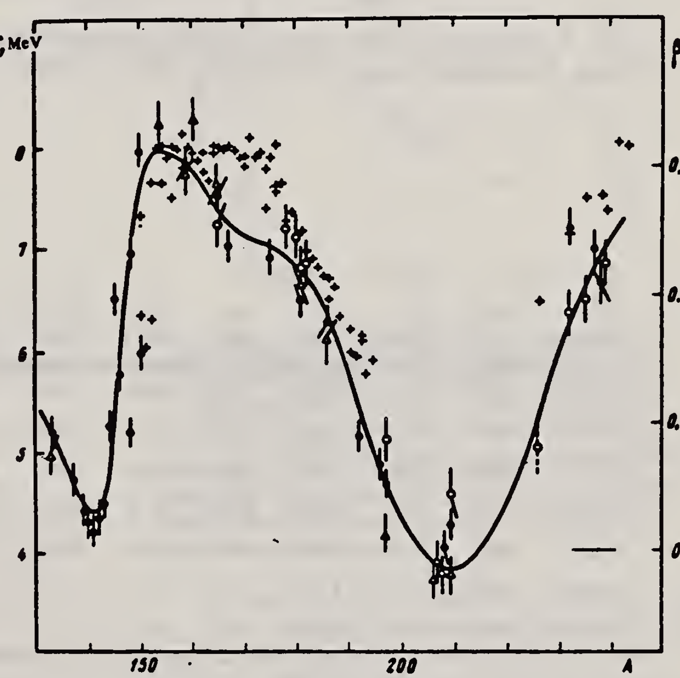

FIG. 2. Widths Γ of $E1$ giant resonance in the region of nuclei with $A > 150$ according to the data of Saclay (●), Livermore (Δ), and the Institute of Nuclear Research of the USSR Academy of Sciences (○). The crosses mark the deformation parameters β.

over

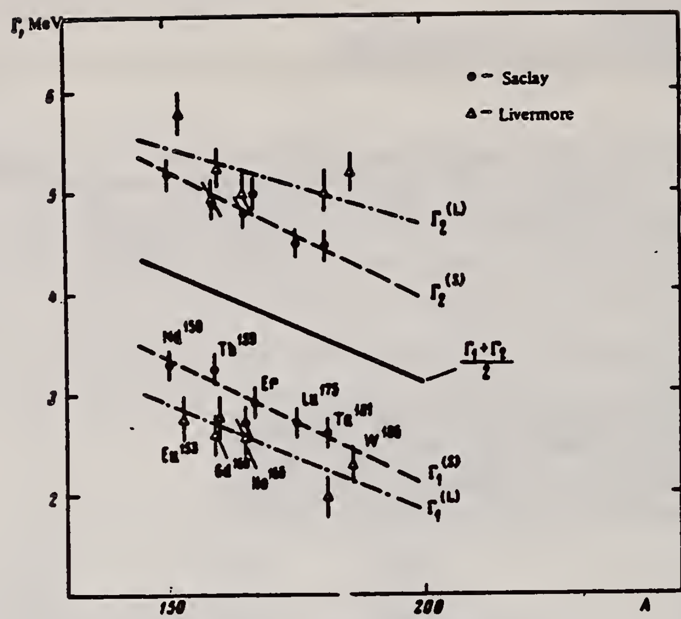

FIG. 3. Width of Lorentz lines approximating the photoabsorption cross sections, for deformed nuclei in the region $150 < A < 185$.

Nucleus	σ_1 mb	Γ_1 MeV	E_1 MeV	σ_2 mb	Γ_2 MeV	E_2 MeV	$\frac{\sigma_2\Gamma_2}{\sigma_1\Gamma_1}$	Q_0 b	β
Ho-165	235	2.0	12.2	272	4.0	15.5	2.3	6.8±0.8	0.29
Hf-178	291	3.1	12.2	334	4.9	15.5	1.8	7.5±0.8	0.28
Hf-180	286	3.2	12.2	324	5.1	15.3	1.8	7.2±0.8	0.27
Ta-181	272	3.0	12.1	316	5.1	15.0	2.0	6.8±0.8	0.26
W-182	267	3.2	11.9	303	5.6	14.8	2.0	7.2±0.8	0.26
Au-197	535	5.2	13.7	...	...	...	...	...	...
Bi-209	600	4.6	13.8	...	...	...	...	...	...

REF. D. Turck, H.-G. Clerc, H. Trager
Phys. Lett. 63B, 283 (1976)

ELEM. SYM.	A	Z
Bi	209	83

METHOD

REF. NO.	
76 Tu 2	egf

REACTION	RESULT	EXCITATION ENERGY	SOURCE		DETECTOR		ANGLE
			TYPE	RANGE	TYPE	RANGE	
E,F	ABX	24- 50	D	38- 50	TRK-I		4PI

FISSION BARRIER

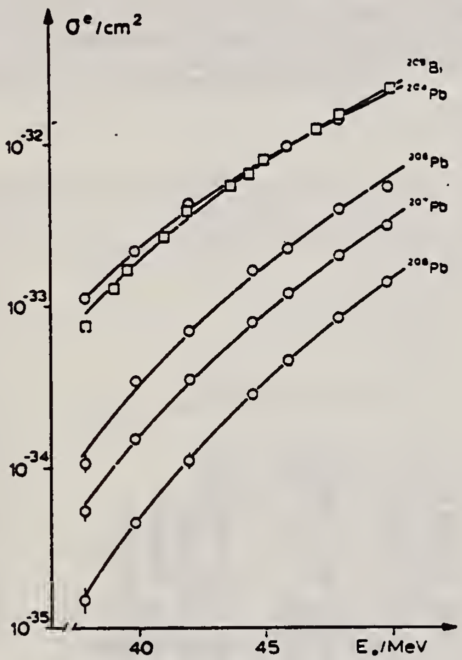

Fig. 1. Cross section σ^e for electron induced fission in ^{204,206,207,208}Pb and ^{209}Bi as a function of the incident electron energy E_0.

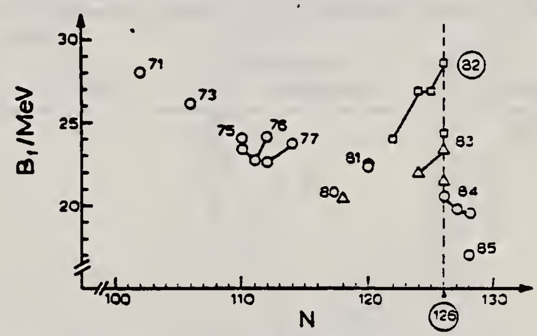

Fig. 2. Summary of fission barrier heights obtained from fits to experimental fission cross sections for nuclei with $Z \leq 85$. o: α-induced fission [12]. For ^{201}Tl, the value of 22.5±1.5 of ref. [3] is also included; △: proton-induced fission [12]; □: electron induced fission (present work). Values for different isotopes of the same element are connected by straight lines. The nuclear charge numbers are indicated. The erors are ± 1.0 MeV for proton and α-induced fission [12] and ± 1.5 MeV for electron induced fission.

[1] U. Mosel, Phys. Rev. C6 (1972) 971.
[3] D.S. Burnett et al., Phys. Rev. B134 (1964) 952.
[12] L.G. Moretto et al., Phys. Lett. B38 (1972) 471.

Table 2
Fission barriers B_f as determined from electron induced fission. In the last column theoretical fission barriers according to ref. [1] with surface independent pairing strength are listed.

isotope	B_f (MeV)	$B_f^{theor.}$ (MeV)
^{204}Pb	24.0±1.5	24.0
^{206}Pb	26.8±1.5	26.2
^{207}Pb	26.9±1.5	
^{208}Pb	28.6±1.5	28.1
^{209}Pb	24.3±1.5	

D.F. Coope, L.E. Cannell, and M.K. Brussel
Phys. Rev. C 15, 1977 (1977)

ELEM. SYM.	A	Z
Bi	209	83

METHOD	REF. NO.	
	77 Co 3	hmg

REACTION	RESULT	EXCITATION ENERGY	SOURCE TYPE	SOURCE RANGE	DETECTOR TYPE	DETECTOR RANGE	ANGLE
G,G	LFT	4 - 7	C	6,10	SCD-D		125
		(4.228-5.549)		(6.6,9.7)			

11 LEVELS 4.2-5.5 MeV

Using bremsstrahlung produced with 6.6 and 9.7 MeV beams, nuclear resonance fluorescence measurements were made on targets of ^{206,207,208}Pb and ^{209}Bi. Ground state transition widths for previously unknown energy levels with widths ≥ 1 eV were obtained. An interpretation of several of these levels in terms of a particle-core weak coupling model is suggested.

TABLE IV. Observed levels and their strengths. *The value for Γ_0 assumes $g\Gamma_0/\Gamma = 3$ for ^{206}Pb and ^{208}Pb, and $g\Gamma_0/\Gamma = 1$ for ^{207}Pb and ^{209}Bi.* Values in parentheses have uncertainties in excess of 50%. Statistical uncertainties are given for well-defined peaks. Total uncertainties include uncertainties in flux calibration. Energy values are believed to be accurate to ±3 keV for the starred (★) ^{208}Pb levels and to ±5 keV for the other levels.

Energy (MeV)	Nucleus	Γ_0 (eV)	Uncertainty (%) Statistical	Uncertainty (%) Total	Other measurements $g\Gamma_0^2/\Gamma$ (eV)	Other measurements Γ_0 (eV)	References
6.54	(Pb) 206	7.4		40			
6.73		5.5		40			
5.902		4.4	15	40			
5.854		(3.0)					
5.796		(1.0)					
5.639		(0.5)					
5.615		(1.0)					
5.577		(0.5)					
5.039		1.6	15	40			
4.974		0.8		40			
6.753	(Pb) 207	(<10)					
5.716		(3)					
5.600		(8)					
5.490		(12)					
5.223		(8)					
5.209		(8)					
4.950		(7)			4.0 $\Gamma_0/\Gamma = 1$		12
4.875 }		(13)			3.6 $\Gamma_0/\Gamma = 1$		12
4.847 }							12
7.332★	(Pb) 208	38	10	35		35,41	11,10
7.083★		14	10	35		15,17 ± 2	11,5
7.063★		29	10	35		15,31 ± 3	11,5
6.721★		15	20	40		15,14	11,10
6.357		(0.5)					
6.305		(1.0)					
6.262		4.1		45			
5.513★		28	2	35		15	11
5.293★		8.6	5	35		5	11
4.842★		6.3	5	35	$J^\pi = 1^+$	5.1 ± 0.8	12
4.085★		0.51		40	$J^\pi = 2^+$	0.5 ± 0.1	12
5.549	(Bi) 209	6.6		40			
5.522 }							
5.509 }		17	5	35			
5.498 }							
5.422		8.3		45			
5.293		12	15	40			
4.845 }					1.4		12
4.803 }		(10)			2.7		12
4.771 }					2.9		12
4.501		(3)					
4.228		(3)					

[5] C.P. Swann, Nucl. Phys. A201, 534 (1973)
[10] P. Axel, K. Min, N. Stein, and D.C. Sutton, Phys. Rev. Lett. 10, 299 (1963)
[11] A.M. Khan and J.W. Knowles, Bull. Am. Phys. Soc. 12, 538 (1967); J.W. Knowles, A.M. Khan, and W.F. Mills (unpublished)
[12] C.P. Swann, Proceedings of the International Conference on Photonuclear Reactions and Applications, (U.S. Atomic Energy Commission Office of Information Services, Oak Ridge, Tennessee, 1975), p.317

REF. V. di Napoli, M.L. Terranova, H.G. de Carvalho, J.B. Martins, J.D. Pinheiro Filho and O.A.P. Tavares
J. Inorg. Nucl. Chem. 39, 1727 (1977)

ELEM. SYM.	A	Z
Bi	209	83

METHOD

REF. NO.	
77 Di 6	egf

REACTION	RESULT	EXCITATION ENERGY	SOURCE TYPE	SOURCE RANGE	DETECTOR TYPE	DETECTOR RANGE	ANGLE
G,2N	ABY	THR-999	C	300-999	ACT-I		4PI
G,3N	ABY	THR-999	C	300-999	ACT-I		4PI
G,4N	ABY	THR-999	C	300-999	ACT-I		4PI

Abstract—Cross sections per equivalent quantum, in the energy range 0.3–1.0 GeV, have been measured for ^{209}Bi(γ, 2n), ^{209}Bi(γ, 3n), ^{209}Bi(γ, 4n), ^{59}Co(γ, 2n), ^{59}Co(γ, 3n), ^{59}Co(γ, 4n) and ^{51}V(γ, 3n) reactions. From the calculated mean absolute cross sections and the data already available in literature for (γ, xn) reactions ($x \geq 1$), a cross-section formula has been deduced which reproduces, within a factor of two, most of the experimental cross sections for target nuclei ranging between ^{9}Be and ^{238}U.

999=1 GeV

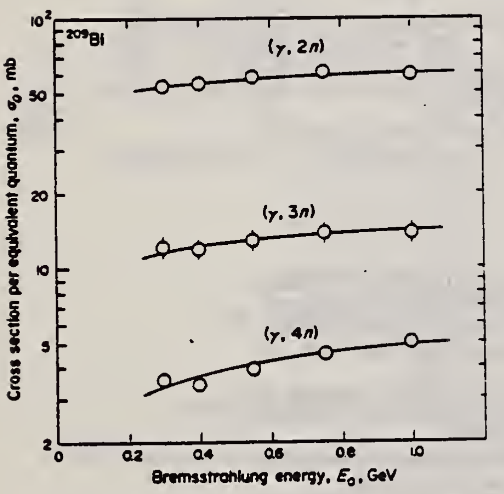

Fig. 3. The same as in Fig. 2 for the ^{209}Bi(γ, xn) reactions ($1 < x < 5$).

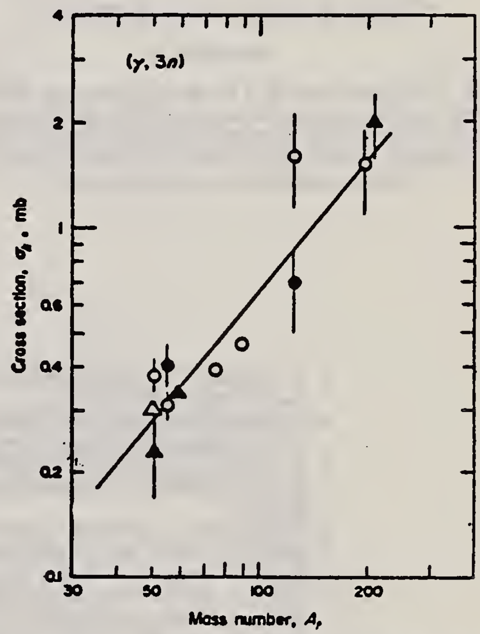

Fig. 5. The same as in Fig. 4 for the (γ, 3n) reactions. Filled circles are taken from our earlier experiments: ^{55}Mn, Ref. [7]; ^{127}I, Ref. [3]. Open circles: ^{51}V, Ref. [17]; ^{55}Mn, Ref. [11]; ^{75}As, Ref. [12]; ^{89}Y, Ref. [14]; ^{127}I, Ref. [9, 10, 13]; ^{197}Au, Ref. [15]. Open triangle: ^{51}V, Ref. [18]. Filled triangles are the results of the present work for ^{51}V, ^{59}Co and ^{209}Bi. The straight line is a least-squares fit of the experimental points.

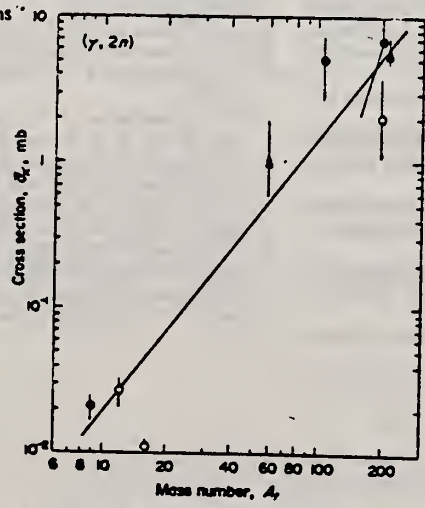

Fig. 4. Experimentally determined mean absolute cross sections, $\bar{\sigma}_k$, for the (γ, 2n) reactions vs the mass number, A_t, of the target nucleus. Filled circles are taken from our earlier experiments: ^{9}Be, Ref. [8]; ^{103}Rh, Ref. [4, 6]; ^{197}Au, Ref. [5]. Open circles: ^{12}C and ^{16}O, Ref. [16]; ^{197}Au, Ref. [15]. Filled triangles are the results of the present work for ^{59}Co and ^{209}Bi. The straight line is a least-squares fit of the experimental points.

over

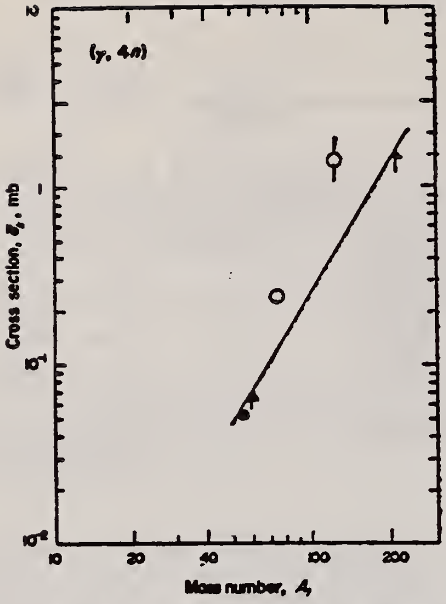

Fig. 6. The same as in Fig. 4 for the (γ, 4n) reactions. Filled circle is taken from our earlier experiment: ^{55}Mn, Ref. [7]. Open circles: ^{75}As, Ref. [12]; ^{127}I, Ref. [9, 10, 13]. Filled triangles are the results of the present work for ^{59}Co and ^{209}Bi. The straight line is a least-squares fit of the experimental points.

Table 2. Mean absolute cross sections for the (γ, xn) reactions, with $1 < x < 5$, in complex nuclei at intermediate energies.

Target nucleus	Reaction	Energy-range (GeV)	Ref.	Cross section, $\bar{\sigma}_k$(mb) (Experimental)	(Calc.†)
^{9}Be	(γ, 2n)	0.3–1.0	8	0.021 ± 0.002	0.007
^{12}C	(γ, 2n)	0.2–0.8	16	0.0277 ± 0.0004	0.025
^{16}O	(γ, 2n)	0.2–0.8	16	0.0113 ± 0.0003	0.072
^{51}V	(γ, 3n)	0.3–1.0	This work	0.23 ± 0.06	0.268
		0.25–0.60	17	0.38 ± 0.04	0.268
		0.25–0.80	18	0.307 ± 0.012	0.268
^{55}Mn	(γ, 3n)	0.3–1.0	7	0.41 ± 0.05	0.33
		0.3–0.8	11	0.311 ± 0.016	0.33
	(γ, 4n)	0.3–1.0	7	0.053 ± 0.004	0.079
^{59}Co	(γ, 2n)	0.4–1.0	This work	1 ± 1	1.3
	(γ, 3n)	0.3–1.0	This work	0.337 ± 0.007	0.4
	(γ, 4n)	0.3–1.0	This work	0.06 ± 0.01	0.1
^{75}As	(γ, 3n)	0.2–0.9	12	0.39	0.7
	(γ, 4n)	0.2–0.9	12	0.24	0.24
^{89}Y	(γ, 3n)	0.25–1.0	14	0.47	1.0
^{103}Rh	(γ, 2n)	0.4–0.9	4, 6	5.1 ± 2.4	2.7
^{127}I	(γ, 2n)	0.1–0.8	9	7.4‡	3.4
		0.3–1.0	3	20 ± 7	3.4
	(γ, 3n)	0.3–1.0	3	0.7 ± 0.2	1.9
		0.25–0.9	9, 10, 13	1.6 ± 0.5	1.9
	(γ, 4n)	0.25–0.9	9, 10, 13	1.4 ± 0.4	1.0
^{197}Au	(γ, 2n)	0.3–0.9	15	2 ± 2	5.2
		0.3–1.0	5	7 ± 5	5.2
	(γ, 3n)	0.3–0.9	15	1.5 ± 0.4	3.6
^{209}Bi	(γ, 2n)	0.3–1.0	This work	6 ± 1	5.5
	(γ, 3n)	0.3–1.0	This work	2.0 ± 0.4	3.8
	(γ, 4n)	0.3–1.0	This work	1.3 ± 0.2	2.5

†Calculated values according to eqn (12)
‡Deduced value from the interpolated σ_Q curve as indicated in Ref. [9].

3. V. di Napoli, F. Dobici, F. Salvetti and H. G. de Carvalho, *Nuovo Cimento* **48B**, 1 (1967).
4. V. di Napoli, D. Margadonna, F. Salvetti, H. G. de Carvalho and J. B. Martins, *Lett. Nuovo Cimento* **1**, 308 (1969).
5. V. di Napoli, A. M. Lacerenza, D. Margadonna, F. Salvetti, H. G. de Carvalho and J. B. Martins, *Lett. Nuovo Cimento* **1**, 65 (1971).
6. C. Aurisicchio, V. di Napoli, F. Salvetti and M. L. Terranova, *Gazz. Chim. Ital.* **102**, 378 (1972).
7. H. G. de Carvalho, J. B. Martins, O. A. P. Tavares, V. di Napoli, F. Salvetti, *Proceedings of the International Conference on Photonuclear Reactions and Applications*, Pacific Grove, Cal., Sect 8C5-1 (1973); V. di Napoli, J. B. Martins, G. Persichelli and M. L. Terranova, *Lett. Nuovo Cimento* **11**, 179 (1974).
8. V. di Napoli, M. L. Terranova, H. G. de Carvalho and J. B. Martins, *Gazz. Chim. Ital.* **104**, 463 (1974).
9. G. G. Jonsson and B. Forkman, *Nucl. Phys.* **A107**, 52 (1968).
10. G. G. Jonsson, B. Forkman and K. Lindgren, *Phys. Lett.* **26B**, 508 (1968).
11. G. Andersson, B. Forkman and B. Friberg, Report LUNP 6901, Lund Institute of Technology, Lund University, p. 4, Sect. 8, 1969 (unpublished).
12. G. Andersson and B. Forkman, Annual Report, University of Lund, Lund Institute of Technology, p. 48, (1970) (unpublished).
13. G. G. Jonsson and B. Persson, *Nucl. Phys.* **A153**, 32 (1970).
14. J. Sternby, Report LUNP 7011, Lund Institute of Technology, Lund University, September 1970 (unpublished). Also quoted in G. G. Jonsson and K. Lindgren, *Phys. Scr.* **7**, 49 (1973).
15. K. Lindgren and G. G. Jonsson, *Nucl. Phys.* **A166**, 643, (1971).
16. B. Johnsson, M. Nilsson and K. Lindgren, University of Lund Report LUNFD6/NFFR-3005/1-18/, LUTFD 6/(TFKF-3003/1-18/, October (1976).
17. I. Blomqvist, P. Janeček, G. G. Jonsson, R. Petersson, H. Dinter and K. Tesch, *Z. Physik* **A278**, 83 (1976).
18. B. Bülow, B. Johnsson, M. Nilsson and B. Forkman, *Z. Physik* **A278**, 89 (1976).
19. G. G. Jonsson and K. Lindgren, *Phys. Scr.* **7**, 49 (1973).
20. G. G. Jonsson and K. Lindgren, *Nucl. Phys.* **A141**, 355 (1970).
21. T. A. Gabriel and R. G. Alsmiller, Jr., *Phys. Rev.* **182**, 1035 (1969).
22. V. S. Barashenkov, F. G. Gereghi, A. S. Iljinov, G. G. Jonsson, and V. D. Toneev, *Nucl. Phys.* **A231**, 462 (1974).
23. V. di Napoli, D. Margadonna, F. Salvetti, H. G. de Carvalho, and J. B. Martins, *Nucl. Instr. Methods* **93**, 77 (1971).
24. C. M. Lederer, J. B. Hollander and I. Perlman, *Table of Isotopes*. Wiley, New York (1967).
25. V. di Napoli, F. Salvetti, M. L. Terranova, H. G. de Carvalho and J. B. Martins, *Phys. Rev.* **C8**, 206 (1973); V. di Napoli, A. M. Lacerenza, F. Salvetti, S. M. Terenzi, H. G. de Carvalho and J. B. Martins, *J. Inorg. Nucl. Chem.* **35**, 1419 (1973).

REF.		ELEM. SYM.	A	Z
	I. Jacob, R. Moreh and A. Wolf Nucl. Phys. A291, 1 (1977)	Bi	209	83
METHOD		REF. NO. 77 Ja 4		egf

REACTION	RESULT	EXCITATION ENERGY	SOURCE TYPE	SOURCE RANGE	DETECTOR TYPE	DETECTOR RANGE	ANGLE
G,MUT	LFT	7	D	7	NAI-D		0
		(7.29,7.632)		(7.29,7.632)			

7.28,7.63MeV,RES ABS

Abstract: A variable-energy γ-source is obtained by nuclear resonance scattering of neutron-capture γ-rays through various scattering angles. An energy resolution of less than 10^{-6} is obtained. Pb and Cd targets were employed to scatter the 7.279 and 7.632 MeV photons, respectively, of the neutron capture γ-rays of Fe. Variation of the angle of the resonantly scattered photons between 60°–150° permits an energy scan of ≈ 370 eV (for Pb) and ≈ 760 eV (for Cd) in any absorber. Thus nuclear energy levels in ^{139}La, Ce, Cd and ^{209}Bi absorbers were photoexcited and the corresponding values of $g\Gamma_0^2$ were extracted from the measured absorption curve.

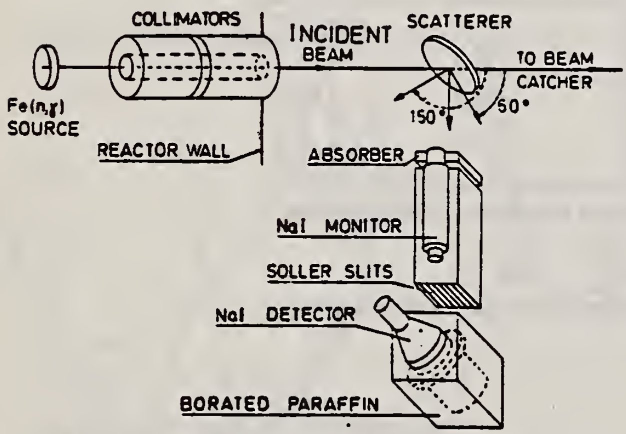

Fig. 1. Schematic diagram of the experimental arrangement.

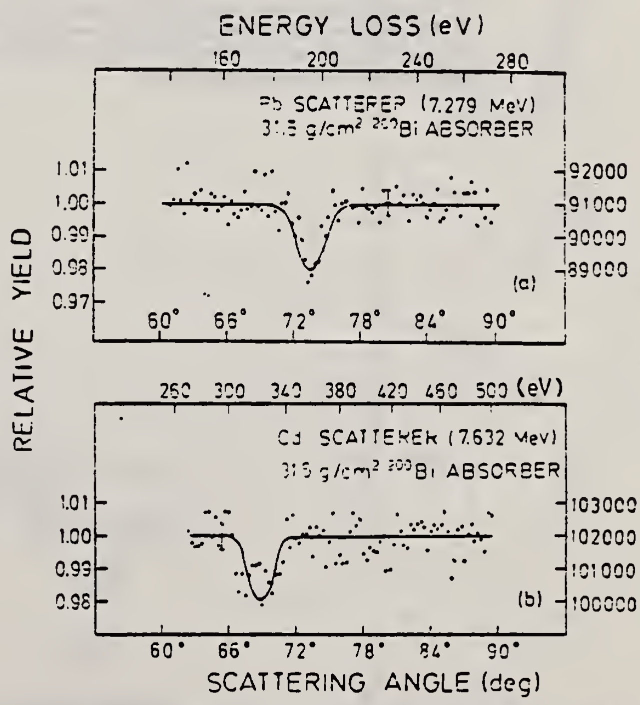

Fig. 4. (a) Normalized absorption spectrum of a ^{209}Bi absorber obtained by using a Pb scatterer of the 7.279 MeV γ-line. (b) Another absorption spectrum usng the same absorber and a Cd scatterer of the 7.632 MeV γ-line.

over

TABLE 2

Summary of experimental data and measured values of $g\Gamma_0$ obtained using the γ-monochromator

Isotope	Thickness (g/cm^2)	Angle of dip (deg)	ΔE [c] (eV)	Effect (%)	$g\Gamma_0$ (meV)
^{112}Cd [a])	35	128.0	505	3.5	150 ± 20
^{139}La	28.2	80.0	225	0.40	8.0 ± 2.0
^{139}La	18.2	100.5	322	0.27	7.1 ± 1.9
^{139}La	18.2	104.8	345	0.22	5.5 ± 1.8
^{140}Ce [b])	26.5	90.0	273	1.3	25 ± 3
^{209}Bi	31.5	73.5	196	2.0	43 ± 8
$^{209}Bi^*$	31.5	68.8	404	1.8	92 ± 12

The asterisk denotes a level at 7.632 MeV photoexcited by a Cd scatterer. All other levels are at 7.279 MeV and were photoexcited by a Pb scatterer.

[a]) The absorbing isotope was arbitrarily assumed to be ^{112}Cd.

[b]) The absorbing isotope was arbitrarily assumed to be ^{140}Ce.

[c]) Here ΔE is the energy difference between the incident γ-line and the resonance level (assuming no recoil correction in the absorbing nucleus).

REF.	R.M. Laszewski and P. Axel Phys. Rev. C 19, 342 (1979)	ELEM. SYM.	A	Z
		Bi	209	83
METHOD		REF. NO.		
		79 La 1		hg

REACTION	RESULT	EXCITATION ENERGY	SOURCE TYPE	SOURCE RANGE	DETECTOR TYPE	DETECTOR RANGE	ANGLE
G,G	ABX	4- 8	D	4-8	NAI-D		135
		(4.5-7.5)		4.5-7.5			

Average elastic photon scattering cross sections were measured for ^{209}Bi, ^{208}Pb, ^{207}Pb, ^{206}Pb, Tl and Hg at excitation energies between 4.5 MeV and the neutron emission threshold, with an energy resolution in the range between 50 and 150 keV. This resolution was sufficient to determine the strengths of most of the strong levels in this energy region for ^{208}Pb; there are concentrations of strength in a few levels near 5.5 and 7 MeV with the sum of $B(E1)\uparrow$ values equal to about 0.84 and 0.65 e^2 fm^2, respectively; each of these two groups of levels corresponds to only about 0.63% of the electric dipole sum rule. In the neighboring isotopes, approximately the same amount of strength is distributed among many more energy levels; although this strength is spread in energy more than it is in ^{208}Pb, it remains relatively localized.

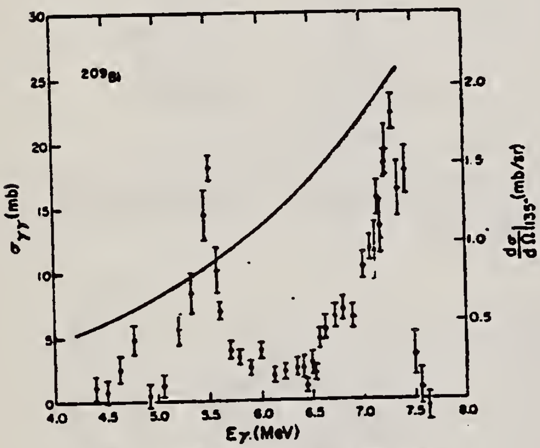

FIG. 6. ^{209}Bi: See Caption of Fig. 4.

TABLE VI. Transition strength comparison at 5.5 and 7 MeV.

Nucleus	5.0–6.0 MeV $\int\sigma_{\gamma\gamma}dE$ (MeV mb)	5.0–6.0 MeV %^{208}Pb strength	6.5–7.5 MeV $\int\sigma_{\gamma\gamma}dE$ (MeV mb)	6.5–7.5 MeV %^{208}Pb strength
Bi	10.4	68%	10.7	44%
^{208}Pb	15.2	100%	24.4	100%
^{207}Pb	12.6	83%	···	···
^{206}Pb	15.8	104%	20.2	83%
Tl	8.3	55%	7.8	32%
Hg	11.6	76%	···	···

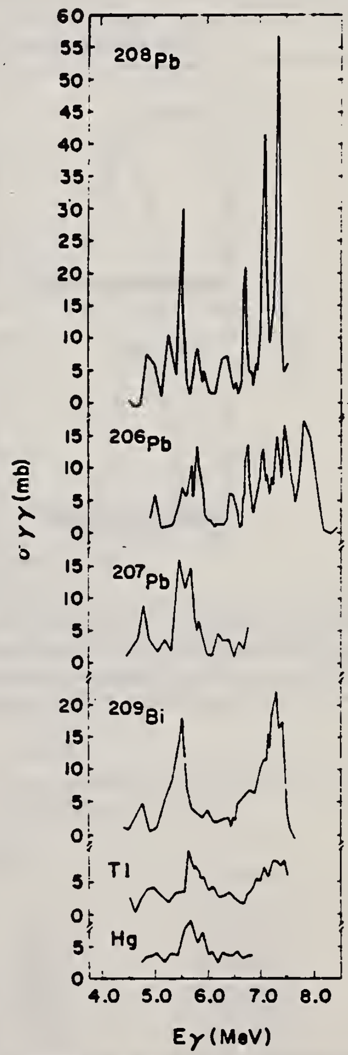

FIG. 12. Comparison of the measured cross sections of, respectively, from the top, ^{208}Pb, ^{206}Pb, ^{207}Pb, ^{209}Bi, Tl, and Hg.

REF. J. C. McGeorge, A. C. Shotter, D. Branford, J. M. Reid
Nucl. Phys. A326, 108 (1979)

ELEM. SYM.	A	Z
Bi	209	83

METHOD

REF. NO.	
79Mc2	hg

REACTION	RESULT	EXCITATION ENERGY	SOURCE TYPE	SOURCE RANGE	DETECTOR TYPE	DETECTOR RANGE	ANGLE
E,F	NOX	THR-110	D	110	SCD-D	105-170	90

Abstract: Fission of ^{232}Th, ^{237}Np, ^{209}Bi, ^{235}U and ^{238}U induced by 110 MeV electrons has been studied by means of surface barrier detectors. The resulting mass and kinetic energy distributions are presented. Comparison with the liquid drop model predictions shows reasonable agreement in the case of ^{209}Bi. The data are analysed in terms of a two component model of fission and the mean total kinetic energies of the components are shown to depend linearly on $Z_1Z_2(A_1^{1/3}+A_2^{1/3})$. Interesting differences are found when the present results are compared with the recent photofission experiments of Areskoug *et al.* and features in both sets of data correlate with changes of fragment deformation implied by the calculations of Wilkins *et al.*

MASS AND EGY DISTRIB

E NUCLEAR REACTIONS ^{237}Np, ^{232}Th, ^{209}Bi; ^{238}U, ^{235}U(e, f), E = 110 MeV; measured fission fragment E, deduced mass.

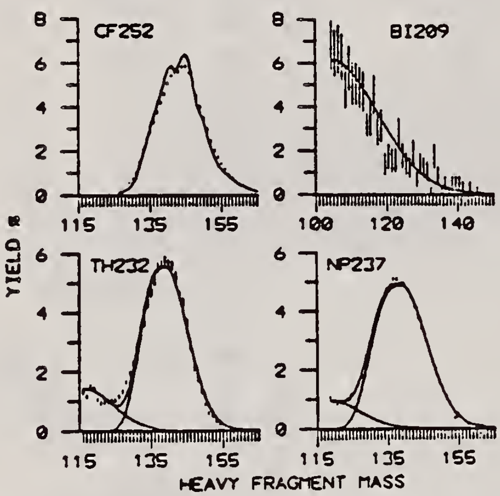

Fig. 1. The HFM yield distributions for electrofission of ^{209}Bi, ^{232}Th and ^{237}Np and spontaneous fission of ^{252}Cf. Statistical uncertainties are shown where larger than the size of the points in this and succeeding diagrams. The solid line in the ^{252}Cf case represents the experimental results of Schmidt *et al.* [12]). In the ^{209}Bi case the solid line represents a Gaussian fit to the data while the solid lines in the other two cases are the result of a two component analysis (see text).

TABLE 2

Target	Mean total KE (MeV) present work	semi-empirical [ref. [14])] a)	b)	Width present work
^{238}U	171.8 ± 3.4	168.5	169.4	11.6 ± 0.1
^{235}U	171.3 ± 3.4	169.1	170.1	10.8 ± 0.1
^{232}Th	167.0 ± 3.3	163.4	163.5	9.6 ± 0.1
^{237}Np	174.3 ± 3.0	171.9	173.3	11.5 ± 0.1
^{209}Bi	140 ± 4	146.5	143.9	11.5 ± 0.4

a) $0.1071Z^2/A^{1/3}+22.2$.
b) $0.1240Z^2/A^{1/3}$.

OVER

(REV. 7-14-64)
USCOMM-NBS-DC

U.S. DEPARTMENT OF COMMERCE
NATIONAL BUREAU OF STANDARDS

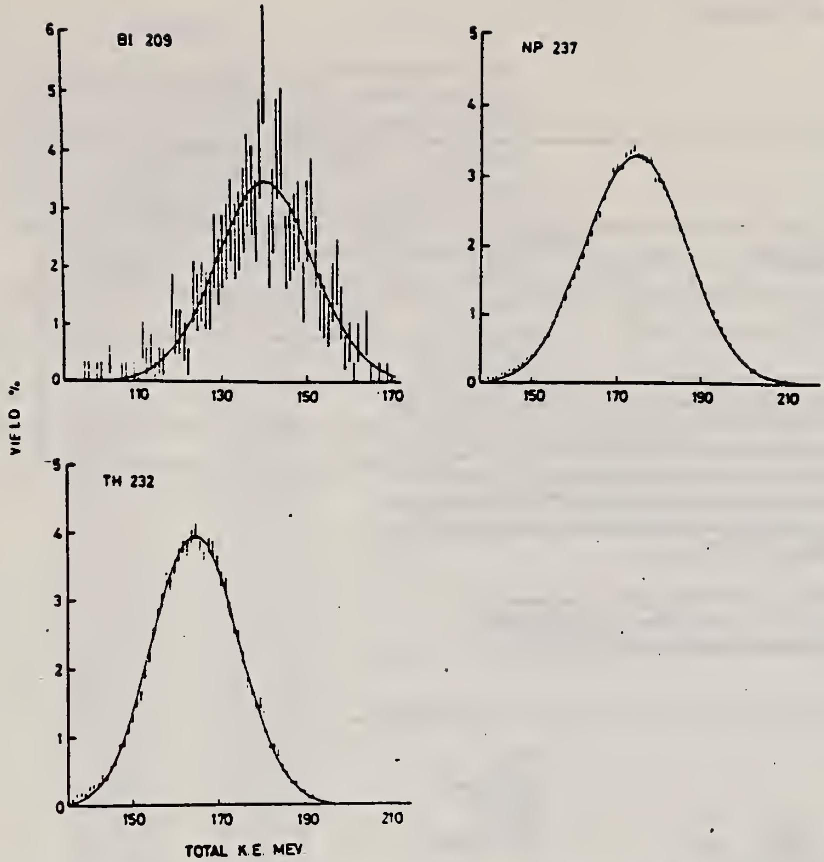

Fig. 2. Total fragment kinetic energy distributions in the electrofission of ^{209}Bi, ^{237}Np and ^{232}Th. The solid lines result from fitting a single Gaussian to the data in the ^{209}Bi case and a double Gaussian in the other cases.

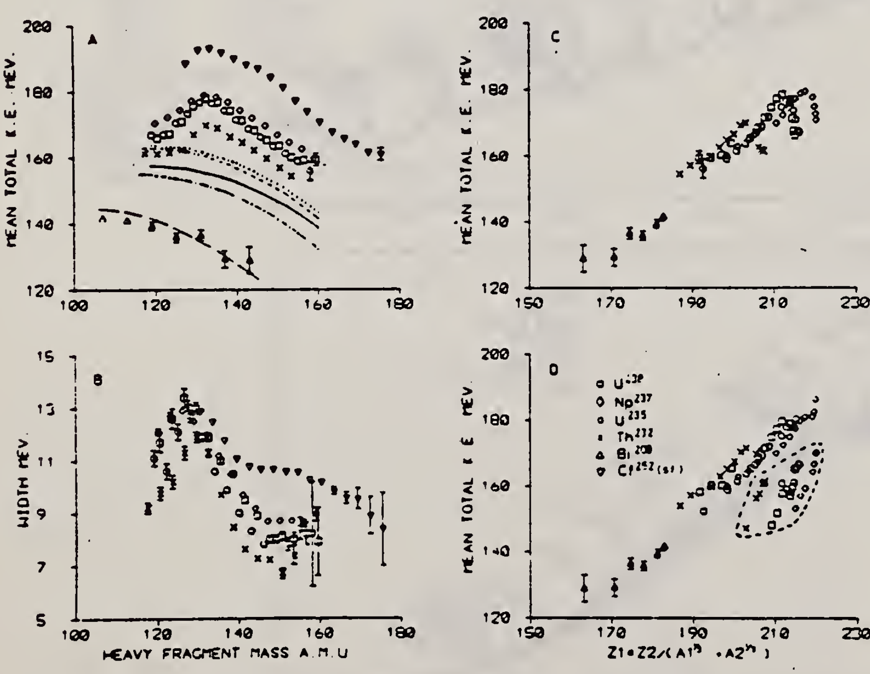

Fig. 3. Total fragment kinetic energy data from electrofission of ^{238}U, ^{235}U, ^{237}Np, ^{232}Th, ^{209}Bi and for spontaneous fission of ^{252}Cf. (A) Mean TKE versus HFM. The lines represent the LDM calculations of Nix and Swiatecki [13]) - solid ^{238}U, short dash ^{235}U, long dash ^{209}Bi, dot ^{237}Np and dot dash ^{232}Th. (B) Width of the TKE distribution versus heavy fragment mass. (C) Mean total fragment kinetic energy versus $Z_1Z_2/(A_1^{1/3}+A_2^{1/3})$. (D) Mean total fragment kinetic energy of the symmetric (enclosed by the dashed line) and asymmetric components versus $Z_1Z_2/(A_1^{1/3}+A_2^{1/3})$. In (A)(C) and (D) the relative uncertainties between targets are ± 3 MeV and the absolute uncertainties are ± 4 MeV.

REF. T. Chapuran, R. Vodhanel, M.K. Brussel
Phys. Rev. C22, 1420 (1980)

ELEM. SYM.	A	Z
Bi	209	83

METHOD

REF. NO.	
80 Ch 3	hg

REACTION	RESULT	EXCITATION ENERGY	SOURCE		DETECTOR		ANGLE
			TYPE	RANGE	TYPE	RANGE	
G,G	SPC	4-8	C	8	SCD-D		127
				(7.65)			

Resonant photon scattering from ^{206,207,208}Pb and ^{209}Bi has been measured from 4 MeV to the neutron thresholds using enriched targets, Ge(Li) detectors and bremsstrahlung beams with end-point energies of 7.0, 7.5, 7.6, 8.0, 8.5, and 10.4 MeV. Energies and values of $g\Gamma_0{}^2/\Gamma$ were obtained for many levels not observed in previous photon experiments. Spins of levels in ^{206}Pb and ^{208}Pb were determined from the angular distributions, and ground-state branching ratios were obtained from self-absorption measurements for seven transitions in ^{208}Pb. The results are compared with earlier spectroscopic studies and with lower resolution average cross-section measurements. The spectra of ^{207}Pb and ^{209}Bi are discussed in terms of the excitations of the ^{208}Pb core.

[NUCLEAR REACTIONS ^{206,207,208}Pb, ^{209}Bi(γ,γ); enriched targets; resonance fluorescence with 7.0, 7.5, 7.6, 8.0, 8.5, and 10.4 MeV bremsstrahlung. Measured E_γ, I_γ at 90° and 127°, and self-absorption; deduced $g\Gamma_0^2/\Gamma$, Γ_0/Γ, J.]

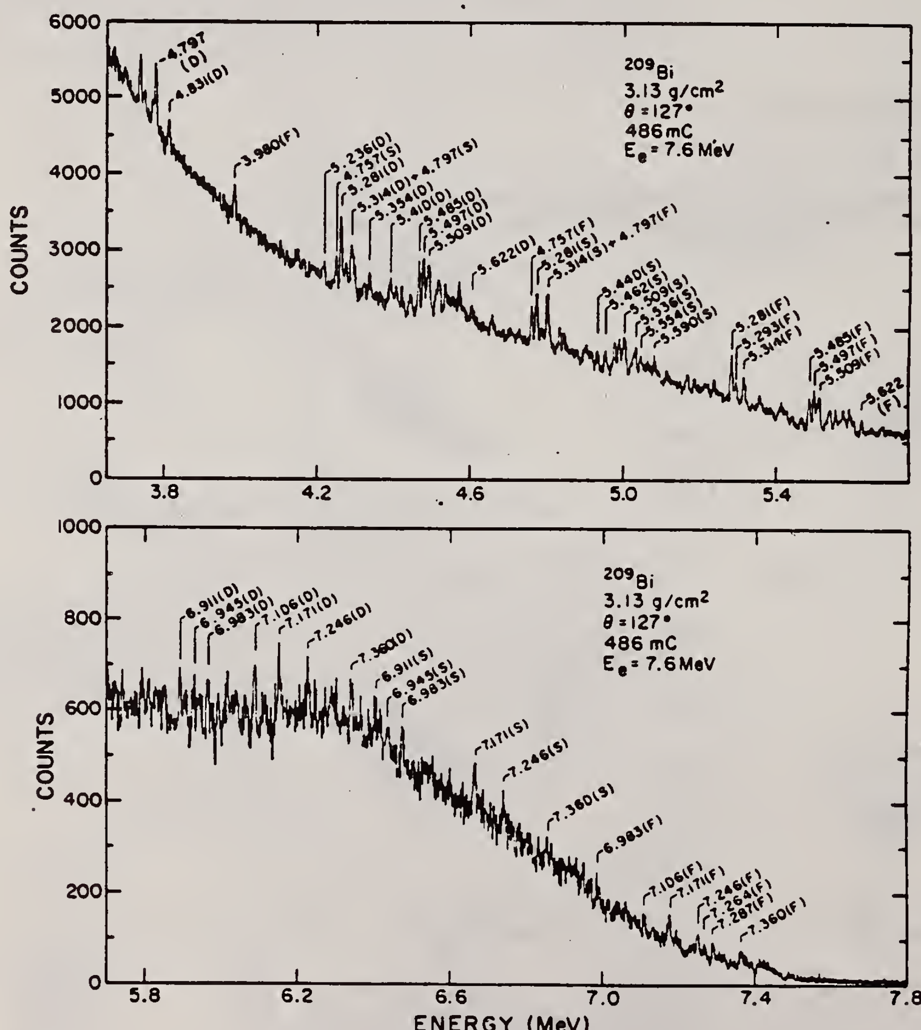

FIG. 10. Spectrum for 7.6 MeV bremsstrahlung scattered at 127° from a natural bismuth target (100% ^{209}Bi). One channel corresponds to 1.42 keV.

OVER

TABLE VIII. Comparison of measured level widths for ^{209}Bi. Values of $g\Gamma_0^2/\Gamma$ were extracted from the present experiment assuming dipole angular distributions; uncertainties include statistical and calibration errors. Parentheses indicate tentative assignments; levels in brackets are probably unresolved multiplets.

Energy[a] (MeV ± keV)	$g\Gamma_0^2/\Gamma$[a] (eV)	$g\Gamma_0^2/\Gamma$[b] (eV)	$g\Gamma_0^2/\Gamma$[c] (eV)
3.980 ± 4	0.88 ± 0.31		0.82 ± 0.08
4.757 ± 2	2.7 ± 0.7		2.9 ± 0.5
4.797 ± 2	3.5 ± 0.9	10[d]	2.7 ± 0.5
4.831 ± 2	1.5 ± 0.3		1.4 ± 0.3
(5.183 ± 4)	0.9 ± 0.3		
5.236 ± 2	1.4 ± 0.3		
5.281 ± 2	5.5 ± 1.1	12 ± 5	
5.293 ± 2	2.2 ± 0.6		
5.314 ± 2	3.0 ± 0.9		
5.354 ± 4	3.3 ± 0.8		
{5.410}	3.3 ± 0.8	8.3 ± 3.7	
(5.424 ± 4)	1.7 ± 0.5		
5.440 ± 4	1.6 ± 0.5		
5.462 ± 4	1.4 ± 0.4		
5.485 ± 2	4.0 ± 0.8		
5.497 ± 2	4.8 ± 0.9	17 ± 6	
{5.509}	6.8 ± 1.2		
{5.536}	4.4 ± 1.0	6.6 ± 2.6	
5.554 ± 2	2.6 ± 0.8		
5.573 ± 4	1.7 ± 1.0		
5.590 ± 2	3.2 ± 0.9		
5.662 ± 2	1.6 ± 0.4		
(6.911 ± 4)	2.4 ± 0.5		
(6.945 ± 4)	2.1 ± 0.6		
6.983 ± 4	2.6 ± 0.5		
(7.106 ± 4)	1.0 ± 0.3		
7.171 ± 4	4.7 ± 1.0		
7.246 ± 4	3.7 ± 0.8		
7.264 ± 4	2.4 ± 0.9		
7.287 ± 4	2.6 ± 0.7		
7.360 ± 4	4.3 ± 1.1		

[a] This work.
[b] Reference 10.
[c] Reference 36.
[d] Uncertainty reported "in excess of 50%."

REF. H.-D. Lemke, B. Ziegler, M. Mutterer, J.P. Theobald, N. Carjan
Nucl. Phys. A342, 37 (1980)

ELEM. SYM.	A	Z
Bi	209	83

METHOD

REF. NO.	
80 Le 3	hg

REACTION	RESULT	EXCITATION ENERGY	SOURCE		DETECTOR		ANGLE
			TYPE	RANGE	TYPE	RANGE	
G,F	ABX	40-65	D	40-65	ION-I		4PI

Abstract: The absolute photofission cross section of ^{209}Bi has been measured with monoenergetic γ-radiation between 40 and 65 MeV photon energy. Cross-section data have been obtained with an accuracy between 9 and 20%. The experimental result is compared with the excitation function calculated on the basis of the statistical model. In order to reproduce the measured data on $\sigma_{\gamma f}$, the (γ, n) cross section must decrease with increasing photon energy faster than the experimental total (γ, n) cross section. This behaviour can possibly be explained by the assumption that after photon absorption a compound nucleus is formed only for a small, and with photon energy decreasing, fraction of all decays.

E | PHOTOFISSION ^{209}Bi(γ, f), E = 40–65 MeV; measured σ; deduced total photoabsorption σ for compound nucleus formation.

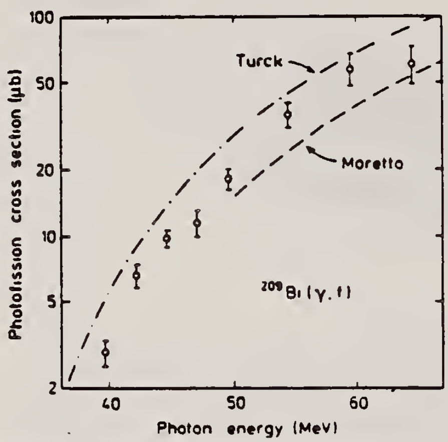

Fig. 9. The result of the present measurement. The dashed curve represents data of Moretto *et al.* [1]), the dashed-dotted curve data of Türck *et al.* [4]).

TABLE I

Summary of data with monochromatic photons

E^+ (MeV)	E_0 (MeV)	N_0 (10^{10})	$N_{\gamma,f}$	$\sigma_{\gamma,f}$ (10^{-30} cm^2)
65	64.45	1.70	234 ± 47	61.5 ± 12.2
60	59.49	1.41	188 ± 33	59.4 ± 10.3
55	54.52	3.88	314 ± 39	36.1 ± 4.4
50	49.55	9.95	407 ± 42	18.2 ± 1.9
47.5	47.07	10.40	263 ± 37	11.4 ± 1.6
45	44.59	30.50	664 ± 58	9.7 ± 0.8
42.5	42.10	16.29	243 ± 29	6.6 ± 0.8
40	39.60	32.92	208 ± 31	2.9 ± 0.4

E^+ is the kinetic energy of the positron (MeV); E_0 is the c.m. energy of the annihilation line (MeV); N_0 is the total number of monochromatic photons for that energy, $N_{\gamma,f}$ is the total number of fission events produced by N_0 and $\sigma_{\gamma,f}$ is the fission cross section deduced from N_0 and $N_{\gamma,f}$.

REF.	N.K. Sherman, C.K. Ross, K.H. Lokan Phys. Rev. C21, 2328 (1980)	ELEM. SYM.	A	Z
		Bi	209	83
METHOD		REF. NO.	80 Sh 10	egf

REACTION	RESULT	EXCITATION ENERGY	SOURCE TYPE	SOURCE RANGE	DETECTOR TYPE	DETECTOR RANGE	ANGLE
G,MUT	ABX	3-30	C	42	TOF-D		4PI

D(G,N) SPECTROMETER

Photon absorption by Al, Ta, and Bi between 3 and 30 MeV was measured using as a photon spectrometer a photoneutron time-of-flight detector and a liquid deuterium target. The atomic cross sections of Ta and Bi at the lowest energies (and of Al at higher energies) agree with calculated values appearing in published tabulations but exceed them at 25 MeV by about 2% in Ta and 3% in Bi. Calculations by others using empirical Coulomb corrections and improved screening corrections to the cross section for pair production by the nucleus agree with experiment to within $(0.5 \pm 0.4)\%$. Best experimental values of the combined correction for Bi are given.

[NUCLEAR REACTIONS ^{27}Al, ^{181}Ta, ^{209}Bi; measured total photon absorption $\sigma_\gamma(E)$; observed GDR; deduced electron pair production $\sigma_K(E)$; $E = 3.0$ to 30.0 MeV; resolution 500 keV; deduced experimental values for Bi of the combined Coulomb and screening correction; ^{2}H(γ,n) LD_2/TOF spectrometer.]

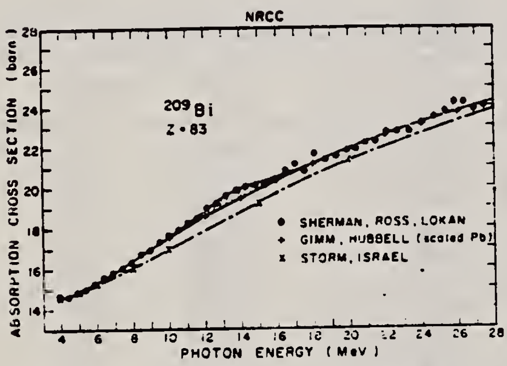

FIG. 2. The measured Bi photon absorption cross section is plotted (solid circles) against photon energy. The bars represent statistical error. The hatched area, the total (γ,n) cross section (Refs. 14 and 15), approximates the total photonuclear absorption. The crosses (+) represent the calculated (Ref. 6) atomic cross section of Pb scaled up to $Z = 83$. Previous calculations (Ref. 5) are denoted by (X).

(OVER)

TABLE IV. Measured values σ_{exp}(Bi) of the absorption cross section of bismuth and their statistical errors ϵ_{σ} are listed against photon energy ω along with the atomic cross sections σ_Z(Bi) and nuclear pair cross sections σ_K(Bi) obtained from them. The amounts $\delta\sigma_Z$ and $\delta\sigma_K$ by which σ_Z(Bi) and σ_K(Bi) exceed the calculated[a] values σ_Z(calc) and σ_K(calc) are also given.

ω (MeV)	σ_{exp}(Bi) (b)	ϵ_{σ} (mb)	σ_Z(Bi)[b] (b)	$\delta\sigma_Z$ (mb)	σ_K(Bi) (b)	σ_K(calc) (b)	$\delta\sigma_K$ (b)
3.869	14.846	±76.5	14.841	+103	5.854	5.80	+0.05
4.327	14.781	44.5	14.775	−25	6.500	6.52	−0.02
4.830	14.927	33.5	14.919	−6	7.282	7.30	−0.02
5.333	15.091	30.5	15.081	−54	7.961	8.00	−0.04
5.837	15.324	29.5	15.311	−39	8.649	8.70	−0.05
6.348	15.624	31	15.606	+36	9.311	9.28	+0.03
6.870	15.878	32	15.856	+44	9.919	9.85	+0.07
7.404	16.100	33.5	16.072	−15	10.422	10.42	0
7.936	16.412	37	16.377	+27	10.987	10.96	+0.03
8.382	16.810	39	16.763	+158	11.613	11.48	+0.13
8.936	17.013	42.5	16.953	+63	12.028	11.96	+0.07
9.476	17.402	45	17.324	+174	12.574	12.42	+0.15
9.992	17.673	47.5	17.571	+166	13.004	12.92	+0.08
10.514	17.945	50	17.807	+132	13.407	13.30	+0.11
11.039	18.293	54	18.105	+145	13.880	13.75	+0.13
11.557	18.583	58.5	18.316	+91	14.229	14.12	+0.11
12.088	19.137	60.5	18.770	+283	14.803	14.55	+0.25
12.629	19.244	66	18.744	−6	14.919	14.92	0
13.174	19.669	68.5	19.049	+49	15.334	15.33	0
13.715	19.861	76.5	19.219	−46	15.619	15.66	−0.04
14.253	20.095	80.5	19.575	+40	16.088	16.02	+0.07
14.780	20.165	89	19.695	−90	16.280	16.32	−0.04
15.293	20.299	90.5	19.922	−90	16.585	16.64	−0.06
15.840	20.428	93	20.143	−92	16.893	16.95	−0.06
16.422	20.738	94.5	20.523	+58	17.343	17.24	+0.10
16.977	21.082	108.5	20.910	+223	17.805	17.56	+0.24
17.500	20.972	112	20.830	−70	17.785	17.85	−0.10
18.078	21.532	116	21.413	+303	18.438	18.14	+0.30
18.665	21.395	118	21.295	−30	18.385	18.41	+0.03
19.286	21.513	122	21.428	−117	18.578	18.69	−0.11
19.856	21.905	146.5	21.833	+78	19.033	18.96	+0.07
20.370	22.147	148.5	22.086	+156	19.341	19.17	+0.17
20.907	22.286	154	22.232	+122	19.532	19.41	+0.12
21.468	22.247	157	22.198	−87	19.553	19.62	+0.07
22.055	22.589	161	22.544	+57	19.944	19.87	+0.07
22.670	22.862	167.5	22.822	-157	20.277	20.08	+0.20
23.314	22.906	170.5	22.871	+4	20.384	20.34	+0.04
23.989	23.098	173	23.067	+2	20.630	20.60	+0.03
24.697	23.348	182	23.318	+48	20.923	20.85	+0.07
25.312	23.504	229.5	23.476	+26	21.126	21.08	+0.05
25.825	24.074	239.5	24.049	+462	21.724	21.27	+0.45
26.355	24.281	242	24.258	+521	21.958	21.45	+0.50
26.903	23.803	247	23.782	−108	21.502	21.62	−0.12
27.470	24.142	251	24.122	+62	21.852	21.80	+0.05

[a] Calculated atomic cross section values σ_Z(calc) were obtained by interpolation of tables compiled by J. H. Hubbell, H. A. Gimm, and I. Øverbø (private communication).

[b] Obtained by subtracting the total photoneutron cross section measured (Ref. 15) by L. M. Young from σ_{exp}(Bi). See also Ref. 14.

REF.		ELEM. SYM.	A	Z
M. Schumacher, F. Smend, W. Mückenheim, P. Rullhusen, H.G. Börner Z. Phys. A300, 193 (1981)		Bi	209	83

METHOD	REF. NO.	
	81 Sc 6	egf

REACTION	RESULT	EXCITATION ENERGY	SOURCE TYPE	SOURCE RANGE	DETECTOR TYPE	DETECTOR RANGE	ANGLE
G,G	ABX	2-7		2-7	SCD-D		90

2.60-7.168 MEV

Elastic scattering by nuclei in the range of mass numbers between 64 and 238 has been studied with monochromatic photons in the energy range between 2 and 8 MeV. These photons were provided either by a Ti(n,γ) source installed in the tangential through channel of the Grenoble high flux reactor, or by ^{24}Na and ^{56}Co sources produced by deuteron bombardment of Al or Fe at the Göttingen cyclotron. The photoexcitation of 23 nuclear levels has been observed and the decay properties and groundstate widths of the majority of these levels have been determined. For the lead scattering target the coherent elastic differential cross section has been studied in detail. There is evidence that below the photo-neutron threshold the elastic scattering via virtual photoexcitation of the nucleus can be approximated by extrapolating the real part of the Giant Dipole Resonance amplitude along a Lorentzian curve. Coulomb corrections to Delbrück scattering seem to play a small role at 6.5 MeV.

Table 1. Differential cross sections for elastic scattering $(d\sigma/d\Omega)^{exp}$ of photons from ^{56}Co and ^{24}Na sources by different scattering targets, in units of μb/sr. Errors in the last digits are given in parentheses.

θ deg	Scattering targets	2.599[a] (MeV)	2.754[b] (MeV)	3.010[a] (MeV)	3.202[a] (MeV)	3.254[a] (MeV)	3.273[a] (MeV)	3.452[a] (MeV)
90	^{238}U	52.7(25)	57.5(25)[c]	56(16)	47(4)	456 (10)[c]	34(6)	49(14)
	^{209}Bi	33.1(30)	32 (2)	33(11)	32(4)	25.6(20)	29(6)	33(15)
	^{nat}Pb	31.5(23)	31.0(16)	35 (8)	27(3)	26.6(22)	25(4)	23 (8)
	^{nat}Tl	31.5(33)	-	27(12)	32(5)	24 (3)	22(7)	34(15)
	^{nat}Hg	30.0(27)	-	24(10)	28(5)	25.5(18)	26(8)	20 (8)
	^{nat}W	22.5(11)	-	17 (7)	19(3)	18.4(15)	18(5)	21 (6)
	^{181}Ta	20.0(15)	19.2 (6)	193(20)[c]	20(4)	17.3(21)	18(5)	21 (8)
	^{165}Ho	15.9(13)	-	17(10)	13(6)	15.6(20)	18(8)	-
	^{nat}Nd	11.4 (7)	14.2 (5)[d]	15 (7)	14(3)	24.2(12)[d]	13(3)	9 (6)
	^{nat}Ce	11.1 (9)	11.0 (5)	-	11(3)	9.5(13)	8(4)	-
	^{127}J	8.4(10)	8.6 (5)	-	9(2)	7 (1)	5(3)	-
	^{nat}Sb	8.0(11)	-	-	10(4)	6.8(19)	-	1,270(50)[c]
	^{nat}Sn	6.5 (7)	7.0 (5)	-	5(2)	7.6 (8)	6(3)	-
	^{nat}Cd	6.2 (5)	-	-	6(2)	6.6 (8)	7(3)	-
120	^{238}U	55.1(25)	64 (4)[c]	43(15)	55(5)	574 (10)[c]	48(5)	48(11)
	^{181}Ta	27.5(15)	25.0 (9)	227(20)[c]	22(5)	21 (2)	22(8)	-
	^{nat}Nd	17.9(30)	17.0 (9)[d]	-	-	29.8(47)[d]	-	-

[a] ^{56}Co source in Fe lattice [b] ^{24}Na source in Al lattice (part of data have been published elsewhere)
[c] Transitions to excited states observed in addition to the ground-state transition
[d] Photoexcitation of nuclear level identified from the size of the differential cross section

(OVER)

Table 2. Elastic differential cross sections $d\sigma/d\Omega(\Theta=90°)$ in μb sr measured with the Ti(n,γ) source and compared with theoretical predictions. n: predicted number of levels in a $\Delta E=25$ eV interval at 6.5 MeV. Errors in the last digits are given in parentheses

Scattering target	6.418 MeV		6.555 MeV		6.759 MeV		7.168 MeV		n
	exp.	th.	exp.	th.	exp.	th.	exp.	th.	
^{238}U	23 (12)	10.3	-	-	-	-	-	-	45
^{209}Bi	-	-	219(39)[b,c]	8.0	12 (4)	7.4	1.5(3)·10^5 [b,c]	5.7	0.1
^{nat}Pb	7.0(15)	8.6	-	-	6.5(11)	7.4	-	-	0.05
^{nat}Tl	2,586 (92)[a,c]	7.5	-	-	13 (3)[b]	6.0	-	-	0.4
^{nat}Hg	12 (3)	7.8	74(17)[b]	6.5	6.7(15)	6.4	-	-	3.4
^{nat}W	159 (10)[a,c]	6.6	306(33)[a,c]	6.3	20 (2)[a,c]	5.6	-	-	13
^{181}Ta	68 (4)[a,c]	6.3	-	-	10.1(12)[b,c]	5.3	-	-	28
^{165}Ho	15 (3)[b]	4.7	-	-	9.5(14)[b]	3.9	-	-	18
^{nat}Ce	4.1(21)	4.1	-	-	17 (1)[b,c]	3.6	-	-	0.04
^{nat}Sn	4.2(13)	3.0	-	-	2.5 (5)	2.7	-	-	1.9
^{nat}Mo	1,474 (44)[a,c]	2.5	407(39)[a,c]	2.5	8.5(15)[b,c]	2.3	817(258)[b,c]	2.0	0.5
^{nat}Zn	2.4 (8)	1.6	-	-	1.8 (5)	1.5	-	-	0.3

[a] Transitions to excited states observed [b] Photoexcitation identified from size of differential cross section
[c] Photoexcitation reported in [11]

Table 4. Properties of levels observed by photoexcitation. $(d\sigma/d\Omega)^{NR+}$: experimental differential cross section per identified isotope or element for resonance scattering through $\Theta=90°$. I^π: spin-parity of excited level; $W(\Theta)$: angular correlation function; $g=(2I_{ex}+1)/(2I_g+1)$; Γ_0: radiative groundstate transition width, Γ: total level width. Errors in the last digits are given in parentheses

Isotope	E_γ (MeV)	$(d\sigma/d\Omega)^{NR+}$ (μb/sr)	I^π	Γ_0/Γ[e]	$W(\Theta)g\Gamma_0^2/\Gamma$ (meV)	Γ_0^f (meV)	Γ_0^g (meV)
^{238}U	2.754	13 (4)	(1)	0.77	0.145	0.084	-
^{238}U	3.254	421 (5)	1$^-$	0.24	0.83	1.5	0.52(15)[d]
^{209}Bi	6.555	2.1 (4)·10^2	-	-	0.74	0.74[b]	-
^{209}Bi	7.168	1.7 (3)·10^5	9/2^{+a}	1.00	710	786	820 (40)[a]
^{203}Tl	6.418	8.75(30)·10^3	1/2[a]	0.28	30	102	82 (15)[a]
Tl	6.759	7 (3)	-	-	-	-	-
Hg	6.555	68 (17)	-	-	-	-	-
^{186}W	6.418	5.2 (3)·10^2	1^{-a}	0.32	1.75	2.4	-
^{184}W	6.555	9.8 (10)·10^2	(1)	0.52	3.44	2.9	-
^{184}W	6.759	46 (10)	(1)	0.58	0.17	0.13	-
^{181}Ta	3.010	174 (17)	-	0.72	0.42	0.59	-
^{181}Ta	6.418	62 (4)	-	0.73	0.2	0.27[c]	-
^{181}Ta	6.759	4.8 (12)	-	-	0.018	0.018[b]	-
^{165}Ho	6.418	10.3 (30)	-	-	0.035	0.035[b]	-
^{165}Ho	6.759	5.6 (14)	-	-	0.021	0.021[b]	-
Nd	2.754	2.6 (5)	-	-	-	-	-
Nd	3.254	14.0 (10)	-	-	-	-	-
Ce	6.759	13.4 (10)	-	-	-	-	-
^{121}Sb	3.452	2.20 (5)·10^3	-	0.60	2.9	4.9[b]	-
^{100}Mo	6.418	1.53 (4)·10^4	1^{-a}	0.88	52	26	25 (8)[a]
^{94}Mo	6.555	4.4 (4)·10^3	(1)	0.33	15	21	-
Mo	6.759	6.2 (15)	-	-	-	-	-
Mo	7.168	8.2 (26)·10^2	-	-	-	-	-

[a] [11] [b] $W(\Theta)g\Gamma_0$, $\Gamma=1$ assumed [c] $W(\Theta)g=1$ assumed
[d] [28] (a small correction has been applied to the data of [28])
[e] Upper limits in case not all the transitions to lower levels were observed
[f] Present work [g] Previous work

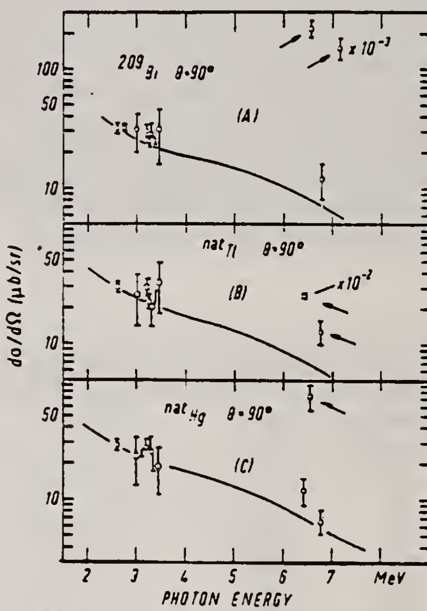

Fig. 9. Differential cross sections for elastic scattering of photons by (A) ^{209}Bi, (B) ^{nat}Tl and (C) ^{nat}Hg through $\Theta=90°$. Solid lines: calculated including R, T, lowest-order D, and N (Lorentzian shape) scattering

REF. J. Uegaki, K. Shoda, M. Sugawara, T. Saito, H. Tsubota
Nucl. Phys. A371, 93 (1981)

ELEM. SYM.	A	Z
Bi	209	83

METHOD

REF. NO.	
81 Ue 2	hg

REACTION	RESULT	EXCITATION ENERGY	SOURCE TYPE	SOURCE RANGE	DETECTOR TYPE	DETECTOR RANGE	ANGLE
E,P	ABX	4-23	D	17-23	MAG-D		DST
G,P	RLX	4-21	C	18-21	MAG-D		DST

Bremsstrahlung protron yields curves and photoproton spectra are given in Figs. 4 & 5. Subtracted proton spectra are given in Figs. 8 thru 11.

Abstract: Differential cross sections at several scattering angles and proton spectra around the $g_{9/2}$ spin-flip and $i_{11/2}$ non-spin-flip IAR in ^{209}Bi were measured with the (e, p) reaction using a broad-range magnetic spectrometer and 100 solid-state detectors. Experiments on the (γ, p) reaction using bremsstrahlung were also performed on the same subjects using the same detector system and geometry as for the (e, p) reaction experiments. Both data agree well with each other when the virtual photon theory is used. Strengths deduced for the resonance at the $g_{9/2}$ IAS at θ^{lab} = 125.3° are in basic agreement with previous data which are in contradiction with the results of the (p, γ_0) reaction and β-decay. Proton decay modes of these resonances were deduced by the photon-difference method. Proton groups emitted through the $i_{11/2}$ IAR are found to have a decay mode typical of the IAS and leave the residual nucleus in neutron 1p-1h states. The decay mode at the $g_{9/2}$ IAR shows an anomalous reaction process as do previous data on the $f_{7/2}$ spin-flip IAR in ^{139}La.

E

NUCLEAR REACTIONS ^{209}Bi(e, p), (γ, p), E = 17-23 MeV bremsstrahlung; measured $\sigma(\theta)$, E_e, E_p. ^{209}Bi deduced decay modes for IAR. Natural target.

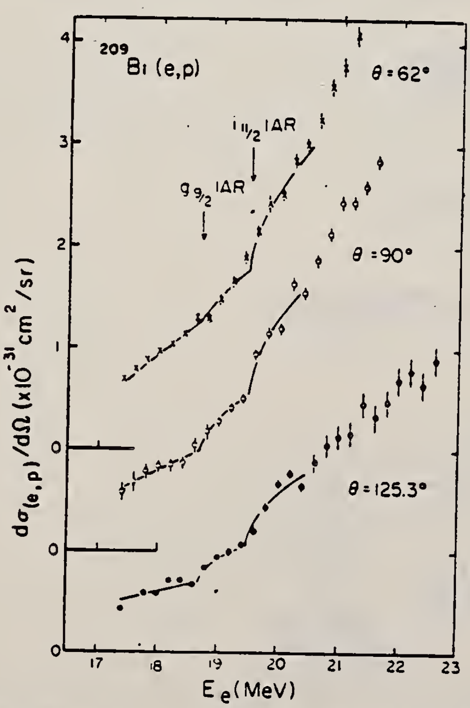

Fig. 1. ^{209}Bi(e, p) cross sections at θ^{lab} = 62°, 90° and 125.3°. The excitation energies of the $g_{9/2}$ and $i_{11/2}$ IAS are shown by arrows. Solid lines show the best fit curves with eq. (7).

(OVER)

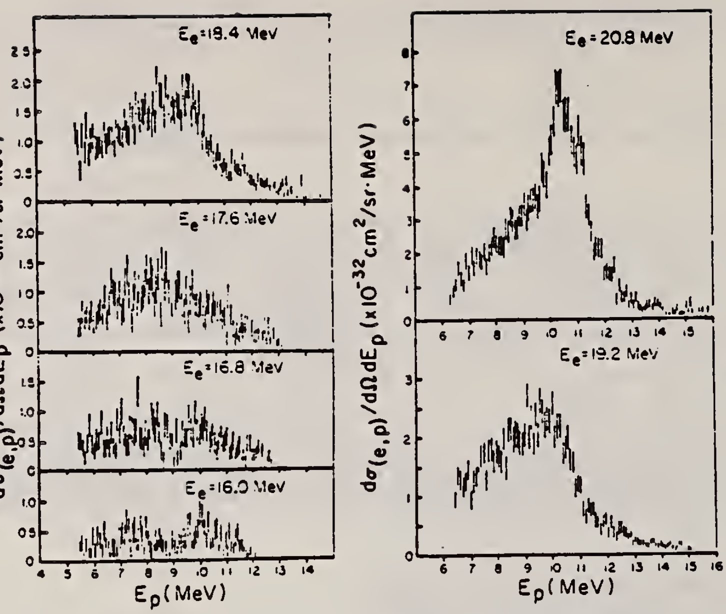

Fig. 2. Proton spectra for the ^{209}Bi(e, p) reactions at θ^{lab} = 125.3°. Incident electron energies are E_e = 20.8, 19.2, 18.4, 17.6, 16.8 and 16.0 MeV. Only the statistical errors are shown in the spectra.

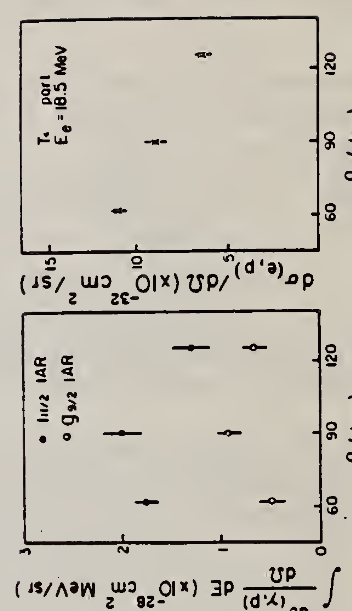

Fig. 6. Angular distributions of the $i_{11/2}$ (closed circles) and the $g_{9/2}$ (open circles) resonance strength, and the proton yield (× marks) at the $T_<$ continuum excited region.

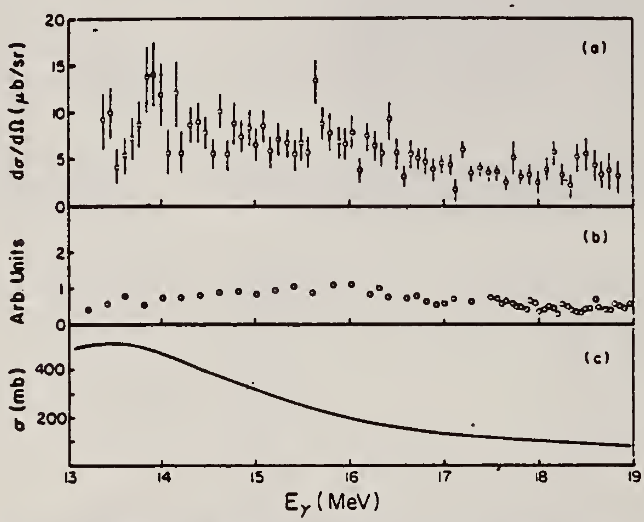

Fig. 7. (a) ^{209}Bi(γ, p_0) differential cross section at θ^{lab} = 125.3° (present results). (b) ^{209}Bi(γ, p_0) cross section calculated by the principle of detailed balance from the ^{208}Pb(p, γ_0) data at θ^{lab} = 90° [ref. [7])]. (c) ^{209}Bi(γ, n) cross section [ref. [14])].

TABLE 1

Resonance parameters for the $g_{9/2}$ and $i_{11/2}$ IAR on ^{209}Bi

IAS	Reaction	E_R (MeV)	$\int\sigma^R_{(\gamma,p)}dE$ (μb · MeV)	$\int\sigma^{IAS}_{(\gamma,p)}dE$ (μb · MeV)	Γ^{IAS}_γ (eV)	$\Gamma^{IAS}_\gamma/\Gamma^{theor}_\gamma$	Ref.
$g_{9/2}$	(p, p′)	18.645 ± 0.006					[9,10])
	(p, γ_0)	18.657 ± 0.030 [a])			< 10	~ 0.33	[7])
	(e, p)	18.7			140 ± 20	430 ± 55	[4])
	(e, p)	18.7 ± 0.1	840 ± 150	510 ± 90	68 ± 15	210 ± 41	present work
	(γ_{brem}, p)	18.7 ± 0.1					present work
$i_{11/2}$	(p, p′)	19.439 ± 0.010					[9,10])
	(p, γ_0)				~ 190	0.20	[7])
	(e,p)	19.5			170 ± 20	0.21 ± 0.03	[4])
	(e, p)	19.5 ± 0.1	1600 ± 250	1060 ± 160	170 ± 26	0.21 ± 0.03	present work
	(γ_{brem}, p)	19.5 ± 0.1					present work

[a]) This value was given by the (p, γ) reaction [7]).

Bi
A=210

Bi
A=210

Bi
A=210

REF.

I. Bergqvist, B. Lundberg, L. Nilsson, and N. Starfelt
Phys. Letters 19, 670 (1966)

ELEM. SYM.	A	Z
Bi	210	83

METHOD

Van de Graaff

REF. NO.	
66 Be 1	EGF

REACTION	RESULT	EXCITATION ENERGY	SOURCE TYPE	SOURCE RANGE	DETECTOR TYPE	DETECTOR RANGE	ANGLE
N,G	SPC	11	D	7	NAI-D	8-18	

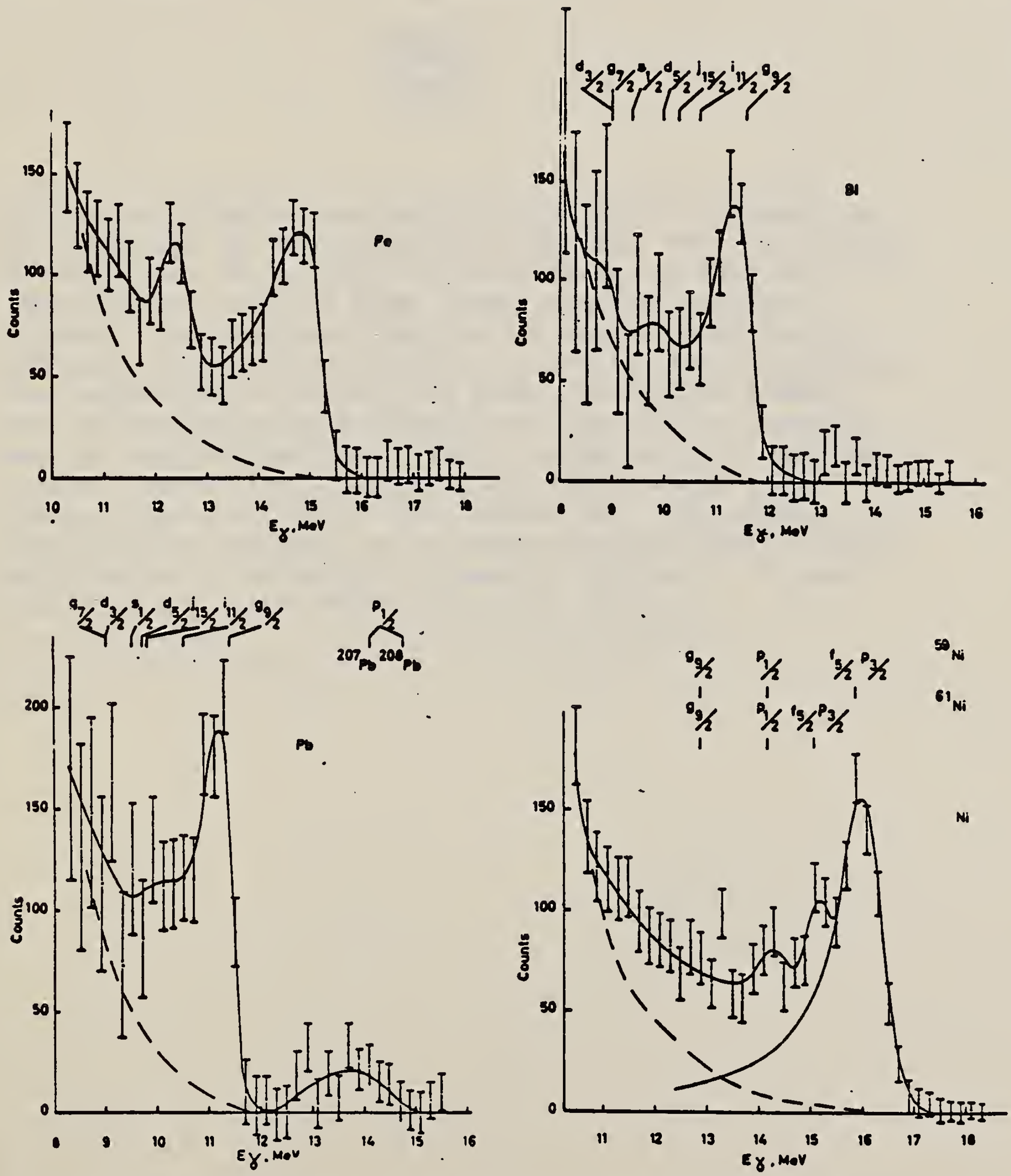

Fig. 1. Gamma-ray spectra emitted in the capture of 7.4 MeV neutrons. The dashed line is the spectrum calculated for the decay of a compound nucleus. The dot-dashed line is the response function of the gamma-ray spectrometer for 16.0 MeV γ rays. Single-particle states as determined from (d,p) reactions are shown.

RADIUM
Z=88

Radium and polonium were the first radioactive elements to be discovered by the radiochemical method. Marie Curie had observed that the activity of pitchblende was four or five times greater than one might expect from its uranium content. She concluded that the ore must contain another radioactive element in addititon to uranium and that, since the composition of the ore was known, the active element must be present in an extremely small amount and therefore must by very radioactive. Pierre and Marie Curie obtained several tons of the pitchblende and made elaborate and tedious fractionations of the complex ore. Mme. Curie exmained each fraction and in barium chloride found a white salt, radium chloride, that glowed in the dark. The new substance was named *radium*, the giver of rays.

REF. E. A. Zhagrov, Yu. A. Nemilov, and Yu. A. Selitskii
Yad. Fiz. 7, 264 (1968)
Sov. J. Nucl. Phys. 7, 183 (1968)

ELEM. SYM.	A	Z
Ra	226	88

METHOD

REF. NO.	
68 Zh 1	hmg

REACTION	RESULT	EXCITATION ENERGY	SOURCE		DETECTOR		ANGLE
			TYPE	RANGE	TYPE	RANGE	
G,F	RLY	THR-25	C	9-25	TRK-I		DST

$^{226}Ra(\gamma,f)$ threshold was found to be 8.5±.5 MeV.

$W(\theta) = 1 + a\sin^2\theta$.

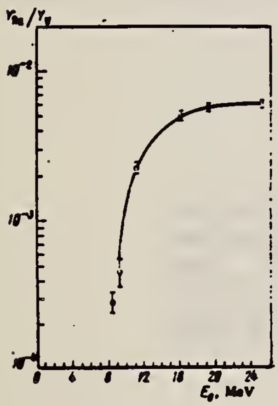

FIG. 1. Relative yield of photofission of Ra^{226} as a function of the bremsstrahlung end-point energy; light symbols—measured with a linear accelerator; filled symbols—measured with a betratron.

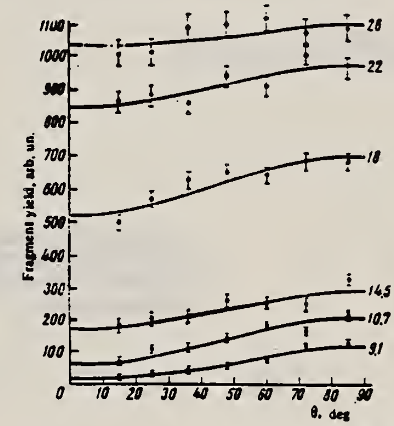

FIG. 3. Angular distributions of the emission of Ra^{226} photofission fragments relative to the direction of the bremsstrahlung beam. The curves were plotted by least squares.

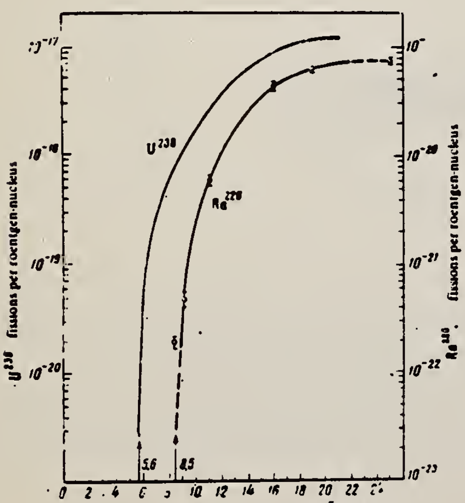

FIG. 2. Photofission yield per roentgen-nucleus for U^{238} and Ra^{226}. The arrows denote the positions of the thresholds.

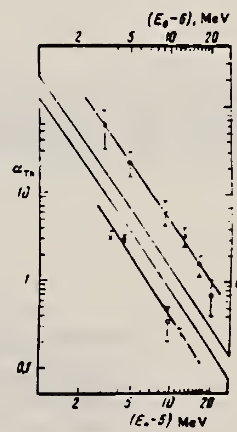

FIG. 4. Anisotropy coefficient α vs. the quantity $(E_0 - T)$, where E_0 is the end-point energy and T is a constant equal to 5 for Th^{232} and to 6 for Ra^{226}. The filled points pertain to Ra^{226} and the light ones to Th^{232}

REF.
E.A. Zhagrov, Yu. A. Nemilov, N.V. Nikitina, Yu. A. Selitskii
Yad. Fiz. 13, 934 (1971)
Sov. J. Nucl. Phys. 13, 537 (1971)

ELEM. SYM.	A	Z
Ra	226	88

METHOD

REF. NO.	
71 Zh 1	hmg

REACTION	RESULT	EXCITATION ENERGY	SOURCE		DETECTOR		ANGLE
			TYPE	RANGE	TYPE	RANGE	
G,F	ABX	9-20	C	9-20	TRK		4PI

N/F EMISSION WIDTH

$$\frac{\Gamma_n}{\Gamma_f} = 570$$

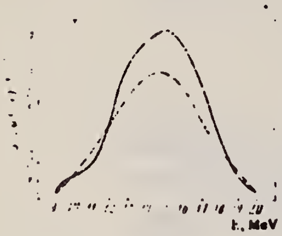

FIG. 3. Ra^{226} photofission cross sections. Solid curve—absolute measurements; dashed curve—relative measurements.

Nucleus	$\sigma_{f\,max}$, b	E_{max}, MeV	Γ, MeV	$\int_0^{16}\sigma_f dE$, MeV-b
U	1.1·10[illegible]	14.0	6.4	7.6·10[illegible]
Th	4.8·10[illegible]	14.5	6.0	3.2·10[illegible]
Ra	9.4·10[illegible]	15.0	5.5	5.2·10[illegible]

The photofission cross section of Ra^{226} is measured in the energy range 9–20 MeV as a basis for determining the ratio of the neutron emission width to the fission width. The value obtained for Γ_n/Γ_f is compared with a calculation based on the statistical model.

REF.	ELEM. SYM.	A	Z
E.A. Zhagrov, Yu.A. Nemilov, V.A. Nikolaev, Yu.A. Selitskii, and Yu.M. Tsipenyuk ZhETF Pis. Red. 20, 220 (1974) JETP Lett. 20, 95 (1974)	Ra	226	88
METHOD	REF. NO. 74 Zh 1		hmg

REACTION	RESULT	EXCITATION ENERGY	SOURCE TYPE	SOURCE RANGE	DETECTOR TYPE	DETECTOR RANGE	ANGLE
G,F	RLY	10- 15	C	11- 15	TRK-I		DST

SYM AND ASYM YIELDS

We measured the yields and angular anisotropy of the symmetrical and antisymmetrical components in the fission of ^{226}Ra in the range of bremsstrahlung limiting energies 11-15 MeV. In this energy interval, the two components have practically the same angular distribution.

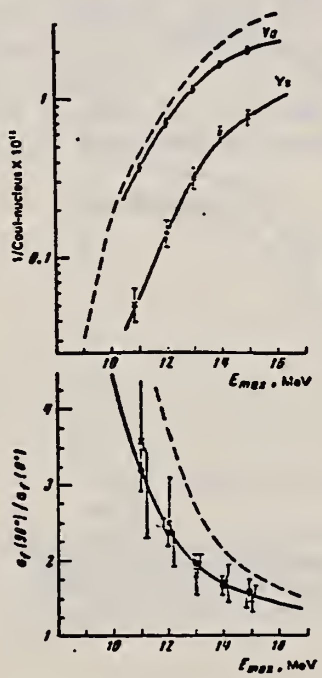

FIG. 2. Top—integral yields of symmetrical (Ys) and asymmetrical (Ya) fission components; the dashed curve shows the fragment yield in the photofission of ^{226}Ra.[8] Bottom—angular anisotropy of the fragment emission for the symmetrical (x) and asymmetrical (•) components. Solid curve—data on the anisotropy of all the fragments,[8] dashed—the same curve shifted 1.5 MeV towards higher energies.

[8] E.A. Zhagrov et al., Yad. Fiz. 7, 264 (1968); Sov. J. Nucl. Phys. 7, 203 (1968).

REF.			ELEM. SYM.	A	Z
E.B. Bazhanov, E.A. Zhagrov, Yu.A. Nemilov, V.A. Nikolaev, Yu.A. Selitskii, and Yu.M. Tsipenyuk Yad. Fiz. 22, 36 (1975) Sov. J. Nucl. Phys. 22, 17 (1975)			Ra	226	88
METHOD			REF. NO.		
			75 Ba 9		hmg

REACTION	RESULT	EXCITATION ENERGY	SOURCE		DETECTOR		ANGLE
			TYPE	RANGE	TYPE	RANGE	
G,F	RLY	THR- 28	C	11- 28	TRK-I		DST

We measured the distributions, with respect to the fragment track diameters in glass detectors, in the photofission of ^{226}Ra in the range of bremsstrahlung γ-quantum limiting energies E_0 from 11 to 28 MeV. The components of the symmetrical and asymmetrical fission are separated, and yield and anisotropy curves are obtained as functions of E_0. At all excitation energies, the anisotropies of the symmetrical and asymmetrical fission coincide within the limits of errors. Near the fission barrier, ^{226}Ra is fissioned predominantly asymmetrically, just as the heavier nuclei.

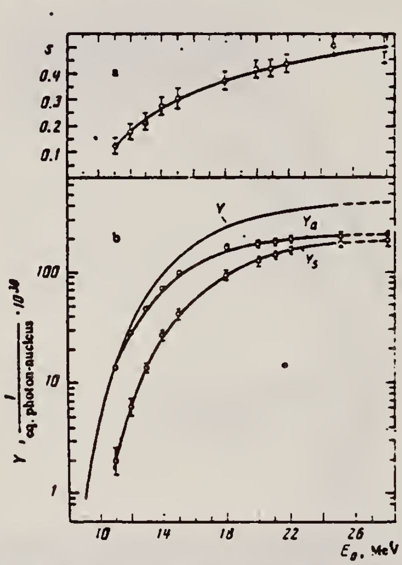

FIG. 3. Relative yield of the component of the symmetrical fission as a function of the end-point energy of the γ-ray bremsstrahlung spectrum (a). Resolution of the total photofission yield (Y) of ^{226}Ra [9,10] into symmetrical (Y_S) and asymmetrical (Y_a) components (b).

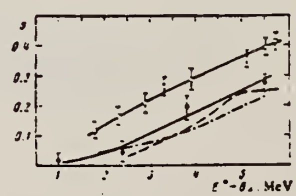

FIG. 4

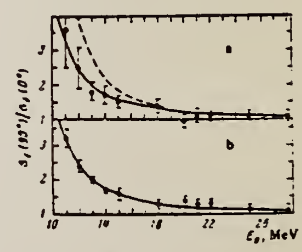

FIG. 5

FIG. 4. Dependence of the relative yield of the photofission symmetrical component on the excitation energy in excess of the fission barrier: light circles ^{226}Ra (present work), dark circles—^{227}Ra [2], dash-dot curve—^{227}Ac, dashed curve—^{228}Ac [3].

FIG. 5. Dependence of the anisotropy of the symmetrical (a) and asymmetrical (b) fission of ^{226}Ra on the end-point energy of the bremsstrahlung γ spectrum. Solid curve—anisotropy without resolution into components [10]; the dashed curve is the same line shifted by 1.5 MeV.

[2] E.A. Zhagrov et al., Nucl. Phys. A213, 436 (1973).

[3] E. Konecny et al., Phys. Lett. 45B, 329 (1973).

[9] E.A. Zhagrov et al., Yad. Fiz. 13, 934 (1971); Sov. J. Nucl. Phys. 13, 520 (1971).

[10] E.A. Zhagrov et al., Yad. Fiz. 7, 264 (1968); Sov. J. Nucl. Phys. 7, 203 (1968).

# ACTINIUM
Z=89

A metalic element named after the Greek word *aktinos*, meaning "ray". It was discovered by A. Debierne in 1899 and independently by F. O. Giesel in 1902. The isotope discovered, Ac^{227}, can be isolated in pure form from uranium ores only with difficulty. Actinium is colorless and closely resembles the lanthanide elements in its chemical properties and is regarded as the prototype for the 14 following rare-earthlike (actinide) elements of atomic numbers 90-103 inclusive.

Ac
A=227

Ac
A=227

REF.	ELEM. SYM.	A	Z
V.E. Zhuchko, Yu.A. Selitskii, V.B. Funshtein, S.V. Khlebnikov & Yu.M. Tsipenyuk Yad. Fiz. 27, 301 (1978) Sov. J. Nucl. Phys. 27, 163 (1978)	Ac	227	89
METHOD	REF. NO. 78 Zh 4		hmg

REACTION	RESULT	EXCITATION ENERGY	SOURCE		DETECTOR		ANGLE
			TYPE	RANGE	TYPE	RANGE	
G,F	ABX	THR-17	C	7-16	TRK-I		2PI
				(7.5)			

The cross section for photofission of ^{227}Ac by bremsstrahlung is obtained in the energy range 7–16 MeV from measurements of the integrated yields of fragments. The giant resonance has two peaks characteristic of a deformed nucleus with deformation parameter $\beta = 0.14$. The dependence of the deformation of the ground state of nuclei in the actinide region on the number of nucleons is discussed. The fissility of the ^{227}Ac nucleus is analyzed. The ^{227}Ac fission barrier is 7.6 ± 0.2 MeV.

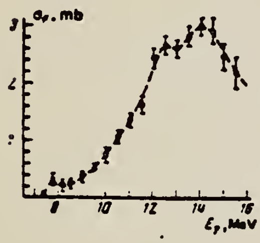

FIG. 1. Cross section for photofission of ^{227}Ac. Only the statistical errors are shown.

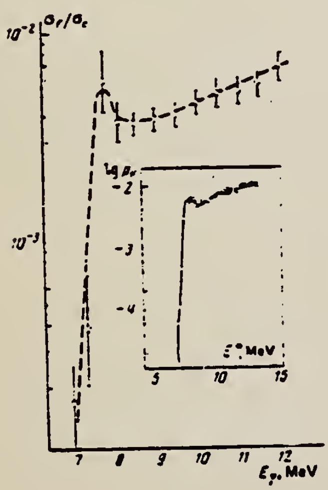

FIG. 3. Fissility of ^{227}Ac near the barrier. In the insert we have shown for comparison the results of Ref. 20 obtained in the reaction ^{226}Ra(^{3}He,df)^{227}Ac.

σ_c taken to be average of absorption cross section for Au and Th (Probably used (γ,sn) data)

DEFINITIONS OF ABBREVIATIONS AND SYMBOLS

Note: In this list definitions are given for various photoneutron reactions in which the following symbols are used: N, NL, nN, SN and XN. Corresponding definitions apply for reactions involving other nuclear particles where the symbols N (neutron) is replaced by, e.g. P, D, T, HE, A etc. Where unknown reactions result in the production of a specific radionuclide, the chemical symbol and mass number is listed as the reaction product, e.g. a G,NA22 reaction in ^{59}Co.

A	alpha particle
ANAL	analysis
ABI	absolute integrated cross-section data
ABX	absolute cross-section data
ABY	absolute yield data. Often means cross-section per equivalent quantum is listed.
ACT	measurement of induced radio-activity of the target
ASM	asymmetric, asymmetry
AVG	average
BBL	bubble chamber
BEL B(EL)	reduced electric radiative transition probability
BF3	BF_3 neutron counter with moderator e.g., Halpern detector, long counter
BML	reduced magnetic radiative transition probability, B(ML)
BREAKS	levels located by "breaks" in the yield curve
BRKUP	breakup
BRMS	bremsstrahlung
BTW	between
C	continuous. Used to describe a photon source or a detector response function. Contrast with D = discrete.
CCH	cloud chamber
CF	compared with
CHRGD	charged
CMPT	Compton
COIN COINC	coincidence, coincide
COH	coherent
CK	Cerenkov
D	deuteron or discrete. When discrete, it is used to describe a photon source or a detector response function. Contrast with C = continuous.
DLTE	energy loss
DLTQ	momentum transfer
DST	distribution
DT BAL	detailed balance
E	electron
E/	inelastically scattered electron
E+	positron
EDST	energy distribution or spectrum
E/N	used only to indicate a coincidence experiment as in (E,E/N).

	N stands for any outgoing particle measured in coincidence with an inelastically scattered electron. Distinguish from eg., (E,N) which is used to represent an electron induced reaction when only the outgoing particle N is detected.
EMU	emulsions (photographic plates)
EXCIT	excited
F	fission
FMF	form factor
FM-1	inverse femtometers
FRAG	fragment
G	photon
G/	inelastically scattered photon
G-WIDTH	gamma-ray transition width
HAD	hadrons, hadron production
HE He3	^{3}He particle
INT	interaction, integral, intensity
INC	includes
ION	ionization chamber
ISOB	isobaric
ISM	isomer
J	multiplicity of particle defined by following symbol e.g. (G,PJN) with remark J = 2,3,5,7
JPI J-PI	spin and parity of a nuclear state
K	second multiplicity index, e.g. (G,JPKN) with both J & K positive integers greater than 1
KE	kinetic energy
L	may be an integer or zero that always follows a reaction product symbol. This is used to indicate transitions to specific states in the residual nuclide. When the letter is used as in (G,NL) the cross section given is that for the sum of transitions to two or more specific final states.
LFT	excited state lifetime
LIM	limit
LV,LVS	level, levels
LQD	liquid
MAG	magnetic spectrometer
MEAS	measurement(s)
MGC	magnetic Compton spectrometer
MGP	magnetic pair spectrometer
MOD	moderated neutron detector <u>not</u> employing a BF_3 counter, e.g. rhodium foil, Szilard-Chalmers reaction, ^{3}He, ^{6}Li reactions, GD loaded liquid scintillator, etc.
MSP	mass spectrometer
MULT	multiple, multipole, multiplicity
MU-T	used only in combination with G to indicate a total photon absorption cross section measurement, i.e. (G,MU-T)
N	neutron (see also XN and SN). The notation (G,N) is used to indicate a reaction in which only a single neutron is emitted, i.e. the reaction that can, in many cases, be measured by observing the radioactive decay of the residual nuclide.

nN	where n is any integer. (G,nN) indicates the sum over all reaction cross sections in which n neutrons are emitted.
NAI	NaI(Tl) spectrometer
NEUT	neutron(s)
NOX	no cross-section data
P	proton (see also XP)
PART	particle(s)
PHOT	photon(s)
PI	pion, usually written as PI+, PI-, PI0 to indicate charge
POL	polarized or polarization
Q-SQUAR	momentum transfer squared (q^2)
RCL	recoil
REL	relative
RLI	relative integrated cross-section data
RLX	relative cross-section data
RSP	reaction spectrometer
RLY	relative yield data
SCTD	scattered
SCD	semiconductor (solid state) detector
SCI	scintillator detector other than NaI, e.g., CsI, KI, organic (liquid or solid), stilbene, He
SEP	separation
SEP ISOTP	separated isotope used
SIG	SIGMA (cross section)
SN	sum of neutron producing reactions, $\sigma(\gamma,SN)=\sigma(\gamma,N) + \sigma(\gamma,NP) + \sigma(\gamma,2N) + \sigma(\gamma,3N)$ + etc.
SPC	photon or particle energy spectrum
SPK	spark chamber
SPL	spallation
STAT	statistical
SYM	symetric, symmetry
T	triton
TEL	counter telescope
THR	threshold for reaction or threshold detector, e.g., $^{29}Si(n,p)^{29}Al$.
TOF	time-of-flight detector
TRK	tracks of particles or fragments observed in solid materials (glass, mylar, etc.)
TRNS	transition
UKN UNK	unknown
VIB	vibrational
VIR PHOT	virtual photon(s)
XN	all neutrons, total neutron yield, $\sigma(\gamma,XN) = \sigma(\gamma,N) + 2\sigma(\gamma,2N) + 3\sigma(\gamma,3N) + \sigma(\gamma,NP)$ + etc.
XP	all protons, total proton yield $\sigma(\gamma,XP) = \sigma(\gamma,P) + \sigma(\gamma,NP) + 2\sigma(\gamma,2P)$ + etc.
XX XXX	reaction products defined in REMARKS
YLD	yield

4PI — a 4π geometry was used or a method like radioactivity or a total absorption measurement

999 — energy defined in REMARKS

$ — indicates the measurement involved beams or targets that were either polarized or aligned, or that the polarization of the reaction products was determined. The polarized particle is indicated in REMARKS.

* or @ — symbols used to indicate that the units associated with the numerals on one or both sides of the symbol in a specific column are not MeV. The units are defined in REMARKS.

NBS-114A (REV. 2-8C)

U.S. DEPT. OF COMM. BIBLIOGRAPHIC DATA SHEET (See instructions)	1. PUBLICATION OR REPORT NO.	2. Performing Organ. Report No.	3. Publication Date

4. TITLE AND SUBTITLE

Photonuclear Data-Abstract Sheets 1955-1982

5. AUTHOR(S)

E.G. Fuller and Henry Gerstenberg

6. PERFORMING ORGANIZATION (If joint or other than NBS, see instructions)

NATIONAL BUREAU OF STANDARDS
DEPARTMENT OF COMMERCE
WASHINGTON, D.C. 20234

7. Contract/Grant No.

8. Type of Report & Period Covered

9. SPONSORING ORGANIZATION NAME AND COMPLETE ADDRESS (Street, City, State, ZIP)

10. SUPPLEMENTARY NOTES

☐ Document describes a computer program; SF-185, FIPS Software Summary, is attached.

11. ABSTRACT (A 200-word or less factual summary of most significant information. If document includes a significant bibliography or literature survey, mention it here)

These abstract sheets cover most classes of experimental photonuclear data leading to information of the electromagnetic matrix element between the ground and excited states of a given nucleus. This fifteen volume work contains nearly 7200 abstract sheets and covers 89 chemical elements from hydrogen through americium. It represents a twenty-seven year history of the study of electromagnetic interactions. The sheets are ordered by target element, target isotope, and by an assigned bibliographic reference code. Information is given on the type of measurement, excitation energies studied, source type and energies, detector type, and angular ranges covered in the measurement. For a given reference, the relevant figures and tables are mounted on a separate sheet for each nuclide studied.

12. KEY WORDS (Six to twelve entries; alphabetical order; capitalize only proper names; and separate key words by semicolons)

data-abstract sheets, elements, experimental, isotopes, nuclear physics, photonuclear reactions

13. AVAILABILITY

☐ Unlimited
☒ For Official Distribution. Do Not Release to NTIS
☐ Order From Superintendent of Documents, U.S. Government Printing Office, Washington, D.C. 20402.
☐ Order From National Technical Information Service (NTIS), Springfield, VA. 22161

14. NO. OF PRINTED PAGES

15. Price